UNIVERSITY OF SOUTHAMPTON

FACULTY OF PHYSICAL AND APPLIED SCIENCES

Electronics and Computer Science

Dielectric Properties of Modified Epoxy Resin Systems: A Novel Approach for Developing Materials for New Generation Technologies

by

Istebreq Saeedi

Thesis for the degree of Doctor of Philosophy

February 2020

ABSTRACT

FACULTY OF PHYSICAL AND APPLIED SCIENCES

Electronics and Computer Science

Doctor of Philosophy

by Istebreq Saeedi

Epoxy resins are thermosetting polymers that features attractive electrical, thermal and mechanical properties, which made them widely used as a primary insulating material in many electrical applications. Over the past decade, the increase in the energy demands led to increase in the size and change in the operation conditions of the electrical equipments, where their insulating materials are expected to withstand the continuous shift in the operation conditions. Consequently, polymer nanocomposite materials were introduced as a potential solution for producing high-performance insulators, and tailor the properties that effect field distribution in epoxy based materials. Later on, it was reported that some of the fillers are suggested to cause deterred properties, for example, some nano-fillers were difficult to disperse in the host material, which limited the advantages of these nanocomposites. An alternative and/or complementary approach is to use liquid functional network modifiers FNM. These FNM contains epoxide groups within their chemical structure which allows the FNM to contribute to the curing process, thus, the FNM modifier become incorporated in the cured network structure of the modified systems and influence the final properties of the system.

This research was set out to provide insights into the effect of functional network modifiers on the properties of epoxy resin systems with the hope of engineering novel epoxy based insulating material for the future. While using liquid functional network modifiers FNM approach has previously been used as a means for altering the mechanical properties of epoxy resins. This research investigated this approach in depth, and also the first study that explores this approach as means of integrating different functional groups into a thermosetting polymers, in order to effectively customise its properties.

The research started by providing a background for epoxy curing mechanisms and the method used for modifying the properties of epoxy resin systems reported in the literature. In addition to review of studies investigated the concept of voltage stabilisers that is based on which an explanation or interpretation was provided for the body of knowledge about FNM behaviour.

Prior to investigating the effect of any FNM on the properties of the modified systems, the effect of the of the FNM on the stoichiometric ratio of epoxy resins was established by running a series of experiments (FTIR, DSC, dielectric properties and AC breakdown strength of the modified systems). These experiments were carried out on a simple amine

cured epoxy resin system by using compensated and uncompensated systems. In the compensated systems, the FNM was added by precisely calculating the number of the epoxide groups being supplied by the FNM, where the equivalent number of epoxide groups provided by the resin are removed, ensuring the same number of epoxide groups present in the system after the addition of the FNM. While, in the uncompensated systems the FNM was added without changing the stoichiometry of the system. By comparing the variation in the properties of the compensated and uncompensated systems, it was concluded that the stoichiometric ratio of the FNM plays a vital role in determining the properties of the final material. In addition, the effect of the FNM on the T_g, dielectric spectroscopy and the breakdown strength is found to be attributed to several factors. In these experiments, the most dominant factor was the structure of the functional groups of the FNM.

By investigating the effect of the chemical structure of the FNM on the FTIR, DSC, dielectric properties, AC breakdown strength and DC conductivity of epoxy resin systems modified by the inclusion of varied concentrations of different FNM modifiers, it was found that the properties of the modified systems are influenced by both the chemical structure of the functional groups and the concentration of the FNM in the system. For example, the use of liquid epoxy resin and low concentration FNM (4%) suggested to produce FNM modified epoxy resins with improved properties compared to that of the neat epoxy, which is suggested to offer a new means of engineering novel materials to meet current and future needs in an adaptable way.

This research also investigated the effect of the curing mechanisms on the behaviour of the modified systems. It was found that the presence of the functional network modifier influenced the chemical, thermal and electrical properties of the amine and anhydride cured systems. This was followed by a a detailed analysis study of the molecular origin and the activation energy of each relaxation process. This analysis was needed because of the lack detailed analysis of the dielectric behaviour of anhydride cured resins in literature. Also, the presence of the FNM made prediction of the behaviour more challenging. The study analysed the temperature dependent dielectric properties along with Havriliak-Negami deconvoluted peaks, as well as the Arrhenius plots and the associated activation energies of the different molecular relaxations. It was concluded that the type of the functional group of the FNM plays a vital role in determining the network topology and the dielectric molecular dynamics of the final material.

The work reported in this research proves that functional network modifiers constitute a complementary and alternative approach for nanotechnology for designing materials with controlled dielectric properties. The systems researched, combined with the applied research method and the described experimental setup provides a complete guide for future studies to replicate the results and experiment with different FNM combinations.

Contents

List of Figures

List of Tables

Nomenclature

AC	Alternating Current
ACBD	AC breakdown
ASTM	American Society for Testing and Materials
DC	Direct current
DGEBA	Diglycidyl ether of bisphenol A
DSC	Differential scanning calorimetry
ER	Epoxy resins
FNM	Functional network modifers
FTIR	Fourier transform infrared
GHE	Glycidyl hexadecyl ether
GNPE	Glycidyl 4-Nonylphenyl ether
GPOSS	Glycidyl polyhedral oligomeric silsesquioxane
HDPE	High density polyethylene
LDPE	Low density polyethylene
OH	Hydroxyl group
PE	Polyethylene
PS	Polystyrene
PVC	Polyvinyl chloride
RMS	Root mean square
SEM	Scanning electron microscopy
Tanδ	Dielectric loss tangent
TGA	Thermogravimetric analysis
TTE	Trimethylolpropane triglycidyl ether
XLPE	Cross linked polyethylene

Symbols

α	Weibull Distribution Scale Parameter
β	Weibull Distribution Shape Parameter
ε_0	Permittivity of free space
$\varepsilon*$	Complex relative permittivity
ε'	Real Relative Permittivity
ε"	Imaginary Relative Permittivity
σ	Electrical conductivity
E	Electric field
E_a	Activation energy
I	Current
K	Boltzmann constant
T_g	Glass transition temperature
V	Voltage
w	Angular frequency

Author's Declaration

I, Istebreq Abdualla Hamad Saeedi, declare that this thesis entitled 'Dielectric Properties of Modified Epoxy Resin Systems: A Novel Approach for Developing Materials for New Generation Technologies' and the work presented in it are my own and has been generated by me as the result of my own original research.

I confirm that:

1. This work was done wholly or mainly while in candidature for a research degree at this University;
2. Where any part of this thesis has previously been submitted for a degree or any other qualification at this University or any other institution, this has been clearly stated;
3. Where I have consulted the published work of others, this is always clearly attributed;
4. Where I have quoted from the work of others, the source is always given. With the exception of such quotations, this thesis is entirely my own work;
5. I have acknowledged all main sources of help;
6. Where the thesis is based on work done by myself jointly with others, I have made clear exactly what was done by others and what I have contributed myself;
7. Parts of this work have been published in the following:

   (i) Istebreq A. Saeedi, Alun S. Vaughan and T. Andritsch, Modification of Epoxy Network Structure Using Reactive Diluent, in *The ninth UHVnet Colloquium, United Kingdom, 2016.*

   (ii) Istebreq A. Saeedi, Alun S. Vaughan and T. Andritsch, On the dielectric performance of modified epoxy networks, in *The second IEEE International Conference on Dielectrics (ICD), France, 2016, pp. 1044-1047.*

   (iii) Istebreq A. Saeedi, Alun S. Vaughan, T. Andritsch and S. Virtanen, The effect of curing conditions on the electrical properties of an epoxy

RESIN, in *The 2016 IEEE Conference on Electrical Insulation and Dielectric Phenomena (CEIDP), Canada, 2016, pp. 461-464.*

(iv) Istebreq A. Saeedi, Alun S. Vaughan, and T. Andritsch, CHANGE IN THE ELECTRICAL PROPERTIES DUE TO MODIFICATION OF THE EPOXY NETWORK STRUCTURE USING REACTIVE DILUENTS, in *2016 IEEE Conference on Electrical Insulation and Dielectric Phenomena (CEIDP), Canada, 2016, pp. 663-666.*

(v) Istebreq A. Saeedi, T. Andritsch and Alun S. Vaughan, MODIFICATION OF RESIN/HARDENER STOICHIOMETRY USING POSS AND ITS EFFECT ON THE DIELECTRIC PROPERTIES OF EPOXY RESIN SYSTEM, in *The 2017 IEEE International Symposium on Electrical Insulating Materials (ISEIM) IEEE, Japan , 2017, pp. 366-369.* Paper DOI: doi.org/10.5258/SOTON/D0105.

(vi) Istebreq A. Saeedi, Alun S. Vaughan, T. Andritsch and Orestis Vryonis, INVESTIGATION OF THE MOLECULAR DYNAMICS IN EPOXY RESIN SYSTEMS USING THE EFFECT OF DIFFERENT FUNCTIONAL GROUPS ON THE DYNAMICS OF MICROMOLECULAR NETWORKS, in *The 2017 IEEE International Symposium on Electrical Insulating Materials (ISEIM), Japan, 2017, pp. 723-726.* Paper DOI: doi.org/10.5258/SOTON/D0105.

(vii) Istebreq A. Saeedi, T. Andritsch, Alun S. Vaughan and D. J. Salter, THE INFLUENCE OF THE MOLECULAR ARCHITECTURE ON THE THERMAL AND THE DIELECTRIC PROPERTIES OF EPOXY RESIN NETWORKS, in *The* 12^{th} *IEEE International Conference on the Properties and Applications of Dielectric Materials (ICPADM), China, 2018, pp. 328-331.*

(viii) Istebreq A. Saeedi, T. Andritsch and Alun S. Vaughan, ON THE DESIGN OF THE STRUCTURE OF EPOXY RESIN NETWORKS, in *The second IEEE International Conference on Dielectrics (ICD), Hungary, 2018, pp. 1-4.*

(ix) Istebreq A. Saeedi, Alun S. Vaughan and T. Andritsch, FUNCTIONAL DESIGN OF EPOXY-BASED NETWORKS: TAILORING ADVANCED DIELECTRICS FOR NEXT-GENERATION ENERGY SYSTEMS, in *Journal of physics D: Applied Physics*, vol. 52, 2019. Paper DOI: doi.org/10.1088/1361-6463/ab09be.

(x) Istebreq A. Saeedi, T. Andritsch and Alun S. Vaughan, ON THE DIELECTRIC BEHAVIOR OF AMINE AND ANHYDRIDE CURED EPOXY RESINS MODIFIED USING MULTI-TERMINAL EPOXY FUNCTIONAL NETWORK MODIFIER, in *Polymers*, vol 11, 2019. Paper DOI: doi:10.3390

(xi) Istebreq A. Saeedi, Sunny Chaudhary, Alun S. Vaughan, T. Andritsch, THE EFFECT OF THE STOICHIOMETRIC RATIO ON THE DESIGN OF EPOXY RESIN NETWORKS, *Journal of Material Science*, Manuscript Under Preparation, 2019.

(xii) Istebreq A. Saeedi, Sunny Chaudhary, Alun S. Vaughan, T. Andritsch, Len Dissado and Nikola Chalashkanov, ON MOLECULAR DYNAMICS AND CHARGE

TRANSPORT IN FUNCTIONALLY MODIFIED EPOXY NETWORKS, in *Journal of Material Science*, Manuscript Written, 2019.

Acknowledgements

I would like to express my sincere gratitude to my supervisors Professor Alun Vaughan and Dr Thomas Andritsch for their guidance, motivation and endless patience. I am grateful for all their invaluable expertise, without their continued support and critical discussion this thesis would not have been possible. I would also like to thank Professor George Chen for his insightful comments and feedback, which helped in shaping my research.

A very special gratitude goes out to all down at the Tony Davies High Voltage Laboratory for providing great support during my experimental work. I am also grateful to my colleagues at the university of Southampton, Dr Orestis Vryonis, Dr Somyot Tantipattarakul, Dr Bo Huang, Dr Allison Shaw and Dr Sijun Wu for their help and support during my postgraduate study. A special thanks also go to Professor Leonard Dissado who provided advice and interesting discussion during my research.

I would like to acknowledge the Schlumberger Foundation Faculty for the Future for the financial support to the majority of this thesis. Thanks for all the ladies in the Schlumberger Foundation for the support at the international level.

I would like to thank my dear friend, consultant and husband Dr Nawfal Al Hashimy for his patience, unconditional support and for always being there for me no matter where I am during my good and bad times.

I am also indebted to my friend Dr Evelyne El Masri for the emotional support, amazing time, great food and unforgettable memories in Southampton without you all these tough years would not have been the same.

Last but not least, with boundless love and appreciation, I would like to acknowledge with gratitude, the support and patience of my father Professor Abdullah Al Dabash, my mother Mrs Azhar Hatahet, my brothers Dr Ahmed Saeedi and Mr Omer Saeedi. A special thanks go to my sister Sara Saeedi for always been the source that stimulate all "creative" ideas that kept me going over the past couple of years.

اهداء الى سر سعادتي و نجاحي.....
عائلتي الحبيبة

Chapter 1

Introduction

The availability of polymeric insulating materials for electrical industry become increasingly apparent during and after the second World War. Perhaps the first commercial introduction for epoxy resins was as a material used for cast insulation for transformers by Pierre Castan in Switzerland in early 1940s [2], this was followed by another commercial product by S.O Greenlee in the United States in late 1940s [3]. Later on, the technology of resins grew steadily and spread world wide until, it become well established. Epoxy resins used in contemporary technologies are produced with a wide range of thermal, electrical and mechanical properties. The essential parts of the resin are liquid at the processing temperature, therefore a number of manufacturing processes can be utilised to produce the solid final product. These manufacturing processes include dipping, casting (pouring the resin and hardener mixture into a mould, that is designed with the shape of the product) and potting (the mould contains the components to be encapsulated and forms part of the product). Factors such as viscosity, shrinkage, chemical resistance, and thermal stability are considered in the manufacturing process of resin based equipment. The importance of epoxy resins originates from the wide variety of formulations and reactions, that enables them to be produced with different properties. Consequently, epoxy resins have been used in several applications including bushings and cast resin transformers.

Over past decades, world consumption of energy has grown continuously and it is projected that between 2012 and 2040 global energy consumption will increase by 48 % due to factors such as an increase in world population and the growth of the worldwide economy [4]. Most historical and current primary energy demands have been met using fossil fuels, but it is now broadly accepted that alternative solutions will need to be adopted going forward. The reasons for this include: combustion of fossil fuels leads to environmental effects, with CO_2 emissions being generally believed to be a major cause of climate change; price instability and the nature of the fossil fuels make it impossible for these to be considered as an inexhaustible energy supply. In contrast, renewable energy derived from solar, wind and hydro are effectively infinite, relatively clean and potentially capable of producing the energy required to meet global demands. In the last three decades, considerable energy has been generated using solar panels and wind turbines and growing acceptability plus reduced costs have promoted rapid growth in the deployment of such renewable energy technologies. For example, in Uruguay and Denmark, the share of renewables reached 33 % (in 2015) and 26 % (in 2016) respectively of the total primary energy supply [5, 6]. However, on a global scale, the power

produced using renewable energy technologies still represent a relatively small fraction of the total world energy consumption.

There are several challenges facing the large-scale implementation of renewable energy technologies. For example, suitable locations for harvesting wind energy, which is widely used for generating electricity, are not evenly distributed. In many countries, offshore wind farms are more efficient compared to onshore wind turbines [7, 8] and, consequently, such sites of power generation are usually located far away from centres of demand. The same can often be said of major hydroelectric stations. Thus, the generated energy must be transmitted over long distances. In addition, the nature of wind and solar power makes such sources inherently intermittent, which can make their integration into power grids somewhat challenging [8]. In summary, the large scale utilisation of electrical power produced using such sustainable resources will require new technologically advanced electrical equipment, such as power converters and high voltage direct current (HVDC) cables. As the demands placed on such components by elevated power densities and operating voltages increase, so the development of novel material systems capable of withstanding the consequent operating conditions becomes a key enabling technology.

Since the first introduction of electrical power systems in the nineteenth century, their insulating materials have been subjected to progressive refinement. Vast research effort have been undertaken globally to explore the potential of nanotechnology to develop novel insulation systems. Lewis in 1994 [9] was one of the first scientists to articulate the concept of nanotechnology. Lewis speculated the possible consequences of the interfacial phenomena significantly influencimg bulk macroscopic behaviour. Nanofiller can take various forms and involve a variety of chemicals, so that the incorporation of nanofiller into a matrix material can influence a wide range of properties. For instance, the thermal properties of polymeric composite was altered through the incorporation of carbon nanotubes (CNT) [10], layered clay nano-fillers [11], graphene and graphene oxide nano-platelets [12–14], carbide derived nanowires [15], and aluminium nanoparticles [16]. Fillers such as aluminium flakes [17],nano-silica particles [18], titanium dioxide TiO_2 and barium titanate $BaTiO_3$ [19, 20], have been utilised to improve the dielectric properties of epoxy resins systems. In addition, nano-filler are used to enhance the dielectric properties of transformer oils [21–23]. The progressive growth in operating voltage was key to the evolution of power systems, 1 MV HVDC transformers are proven technology [24]. The ability of such applications to withstand an electric field is governed by the dielectric breakdown strength of its insulating material.

In the case of epoxy resin based insulation systems, several studies have reported improved breakdown strength of epoxy nanocomposite. For example, the inclusion of 5 wt% of nano-alumina (Al_2O_3), nano-barium titanate, and alumina resulted in an increase in the dielectric breakdown strength of the epoxy nanocomposite by about 5 % [25], 12 % [26] and 25 % [27, 28] respectively. However, the positive effects of the addition of nanofillers are far from universal, with numerous other studies that either report

insignificant or poor performance [29–35]. A possible explanation for the deteriorated performance of polymeric nanocomposite, is due to the fact that some nanoparticles have a strong tendency to agglomerate resulting from inadequate processing.

From the examples cited above it is clear that although the inclusion of nanofillers seems to be promising, problems of reproductivity, scalability, and quality assurance, may pose challenges from a technological point of view.

1.1 Functional Network Modifiers FNM: emergence and prospective

There is still poor understanding of the fundamental mechanisms by which presence of nanofillers influence the breakdown strength in a polymeric nanocomposite. Lewis [36] proposed that, nanofillers lead to the formation of interphase zones, the properties of these zones differ from those of the bulk component, and the corresponding interphase volume is sufficiently large that their properties significantly influence the system's overall behaviour. Tanaka et al. [37], presented a multicored model for interfacial areas in which factors such as molecular dynamism, chain configurations and chemical conditions varied from area to another. While the model proposed by Tanaka et al. received broad acceptance over the past few years, there is lack in quantitative verification of such model. However, recent alternative hypotheses have been suggested based on the influence of nanofillers on how the local density of electronic states is thus modified inside a system, rather than on structural factors [38, 39]. This means that the changes in electrical behaviour in the material is due to the changes in local electrical factors.

If changes in the local density of electronic states is the mechanism through which nanoparticles influence the electrical response of nanocomposites, an alternative method may be used to engineer materials with equivalent effect to that of nanofillers, where this new method will not involve the processing problems generally faced when seeking to introduce nanoparticles. Specifically, this alternative method utilies reactive moieties, referred to as functional network modifiers (FNM), as a mean of altering the network architecture of epoxy resin systems. FNM liquid additives, which are introduced to the resin and hardener mixture in the initial mixing process. The chemical structure of FNM features reactive groups, which contribute to the curing process, resulting in integration of these modifiers within the network structure of the resin. Consequently, this eliminates the dispersion issues associated with the modification using nanoparticles. In addition to the reactive part, the structure of FNM contain functional groups, which alter the local electronic traps producing an effect comparable to that the impact of the inclusion of nanofillers.

1.2 Research Motivation

Epoxy resins are generally used in casting, coating and encapsulation processes procedure for wide variety of applications in different industries, including electrical (in cast resin transformers, cable termination and as insulators to detect the presence of voltage on phase line in switchgears), electronics (encapsulation of individual component such as capacitors, transistors and coils), and aerospace (adhesives and matrices for aerospace laminating applications). Epoxy resins have proven to provide properties such as electrical insulation, mechanical and chemical resistance, which are fundamental for the operation of these application. The development of these industries, poses a challenge to the chemistry of the epoxy resin. For example, the increasing need for energy led to increase in the scale of electrical generation and transmission devices which resulted in a vast growth in the electrical sector [40]. Therefore, power equipment and, specifically high voltage insulating materials are a crucial part of the development of the electrical sector.

Consequently, numerous studies have been interested in lowering the cost and improving the properties of epoxy resin insulators to suit particular application [41–43]. Most of these studies adopted the approach of using nanotechnology through the introducing of nano- and micro-sized fillers to epoxy system to enhance its mechanical, electrical and/or thermal properties. Other studies used the approach of adding reactive modifier to modify the network structure of epoxy resin, much of the studies used reactive modifiers were focused on generating epoxy based material with improved mechanical and/or thermal properties [44–46]. However, the effect of modifying epoxy resin network using reactive modifiers on the thermal properties of the final composite is still poorly understood. In addition, there has been no detailed investigation about the effect of the FNMs on the electrical properties of epoxy resins and the mechanism behind the unusual behaviour of the modified systems. Finally, to date, only few studies investigate the association between the electrical and thermal properties of epoxy resin network modified using functional network modifiers. All these issues need to be addressed, and the underlying physics and chemistry which drive the behaviour need to be understood, in order to enable engineering novel, high-performance epoxy insulators, and tailor the properties that effect field distribution in epoxy based materials.

1.3 Research Objectives

The goal of this research is to give insights into the effect of functional network modifiers on the properties of epoxy resin systems with the hope of engineering novel epoxy based insulating material for the future. Four types of FNM were selected to alter the network

structure of the epoxy resin system, where the effect these FNMs on thermal and electrical properties was established. The main objectives of this thesis can be summarised as follows:

- Investigation of the FNM loading on the stoichiometric ratio of epoxy resins and consequently their dielectric properties.

  Hypothesis 1: The effect of the functional network modifiers on the dielectric properties relies on the number of the reactive moieties, which contribute to the chemical curing reactions.

- Investigation of the effect of functional network modifiers on the electrical properties of epoxy resin systems.

  Hypothesis 2: The inclusion of FNM in the resin system leads to changes in the network architecture of an epoxy system and therefore alters the electrical properties in an effect equivalent to the mechanisms by which nanoparticles influence the electrical response of nanocomposites.

- Investigation of the effect of different curing mechanisms on the dielectric properties of modified epoxy resin systems.

  Hypothesis 3: Changing the type of hardener (amine or anhydride) leads to changes in the curing mechanism, which would significantly affect the dielectric behaviour of the system. This is also the case when the system is altered in a systematic way, using functional network modifiers.

- Investigation of the effect of the functional network modifiers on the molecular dynamics of complex epoxy resin systems.

  Hypothesis 4: Modification of the resin structure affect the molecular dynamics. The γ and β relaxations are associated with terminal groups, while α relaxation is related to segmental movement of main-chains, the consequent dipole relaxation activate charge transport above T_g.

1.4 Research Contribution

In this project, the original contributions are as follows:

1. Modifying the properties of epoxy resin systems using different functional network modifiers is proven possible and comparable to the effect that have been reported when introducing nano-fillers to epoxy resin systems.

2. This novel method has been shown to overcome a severe limitation of fillers, usually ceramic fillers and organic polymer hosts are inherently incompatible, to compensate for this, long manufacturing processes are required which takes time and cost.

3. Different functional network modifiers with four varied functional groups were successfully introduced to the network architecture of the amine cured epoxy resins at different weight loadings.

4. Detailed analysis of the dielectric response of the modified systems was carried out, where the dipole relaxation and charge transport dynamics were associated to their molecular origins,

5. The importance of the stoichiometry to show the effect of FNM was highlighted.

6. The change in the properties of the modified system is shown to be correlated to the chemical composition of the functional groups of the functional network modifier.

7. The new approach for altering the properties of amine cured epoxy resins was successfully applied for anhydride cured resins, which proves generality of the effect of the functional network modifiers.

1.5 Thesis Outline

After this introductory chapter, a critical review of literature is presented to provide the reader with background knowledge for theories related to epoxy resin curing mechanisms, methods used to modify the breakdown strength, dielectric properties and thermal behaviour of epoxy resin systems. Chapter 2 also introduces the concept of voltage stabilisers, to help explaining the electrical behaviour of the modified systems. Details of the procedures used to manufacture the samples, including the FNM selection process, stoichiometric calculation and curing schedule are presented in chapter 3. Then, chapter 4 highlights the characterisation methods and explains the experimental techniques used to test the samples. Chapter 5 focuses on investigation of the effect of the stoichiometric ratio of the modifier on the dielectric properties of epoxy resin systems. Since the FNM contributes to the curing process, the number of active molecules of the FNM is critical factor. This chapter discusses the experimental results of two sets of samples which comprises of materials calculated using two different methods. In one set the epoxide groups of the FNM were compensated by removing equivalent number of epoxide groups from the resin, while in the other set of samples the FNM was added as a weight percentage of the total weight without changing the stoichiometry of the system. An investigation of the effect of functional network modifiers on the electrical properties of epoxy resin systems is presented in Chapter 6. The results and the associated discussion of Chapter 6 test hypothesis 2, which suggests that the inclusion of FNM in the resin system leads to change in the network architecture of an epoxy system and therefore alters the electrical properties in an effect equivalent to the mechanisms by which nanoparticles influence the electrical response of nanocomposites. Chapter 7 concentrates on investigating the

effect of different curing mechanisms on the electrical properties of modified epoxy resin systems. Amine and anhydride cured epoxy resin systems were modified using various concentrations of FNM and the manufactured samples were studied at low temperatures. The results test hypothesis 3, which suggests that changing the type of hardener (amine and anhydride) leads to changes in the curing mechanisms, which influence the dielectric behaviour of the system. Chapter 8 investigates the effect of the functional network modifiers on the molecular dynamics of epoxy resin systems, where the results discuss the molecular origin of the dipole relaxation and charge transport dynamics in FNM modified epoxy resins systems which test hypothesis 4. Finally, the thesis ends with conclusions and outlines future work summarised in Chapter 9, while details of some of the experimental data and the associated supporting figures are located in the appendices.

Chapter 2

Literature Review

2.1 Introduction to Epoxy Resins

In a broad sense, the term epoxy resins (ER) refers to polymeric materials containing one or more epoxide groups (also known as oxirane rings or ethylene oxide) situated internally or terminally within the ER molecular structure [2, 3, 47]. These epoxide groups are three-membered rings, comprise of one oxygen and two carbon atoms. There is a large variety of epoxy resins, the classification of the different types of epoxy resins are not always distinctly clear from literature. However, a broad classification of ER can be made according to the method used to synthesise the resin. Hence epoxy resins can be divided into two main types, namely non-glycidyl and glycidyl based epoxy resins, as shown in Figure 2.1 [3, 48]. The molecular structure of the main classes of ER is shown in Figure 2.2.

Since the first commercial application of epoxy resins in late 1940s, glycidyl based epoxy resins were the most important type of ER. Glycidyl ether based ER currently represents 95% of the resins used in commercial applications, while glycidyl ester and glycidyl amine resins failed to find a significant market share, because they have been reported as being self-polymerisable and unstable materials [2], which is also the case for linear aliphatics. However, cycloaliphatic resins are getting a lot of attention recently [49–53]. Since glycidyl ether based epoxy resins are the topic of interest in this work, other types of ER are considered out of the scope. ChemDraw professional software

Epoxy resins are thermosetting polymers. The chemical reaction involved in the curing process of the resin results in an irreversible transformation from a viscous liquid to an amorphous cross-linked network. The molecular chains have restricted freedom of movement and retain a specific shape. Therefore, thermosets cannot be recycled and once cured become unable to be reshaped; typically when excessive heat is applied to thermosetting polymers the network undergos thermal degradation and chain scission.

2.2 Epoxy Resin Curing Mechanisms

In general, the conversion process of a liquid resin into a cured, three-dimensional structure, occurs through the reaction of the epoxide groups within the molecular structure

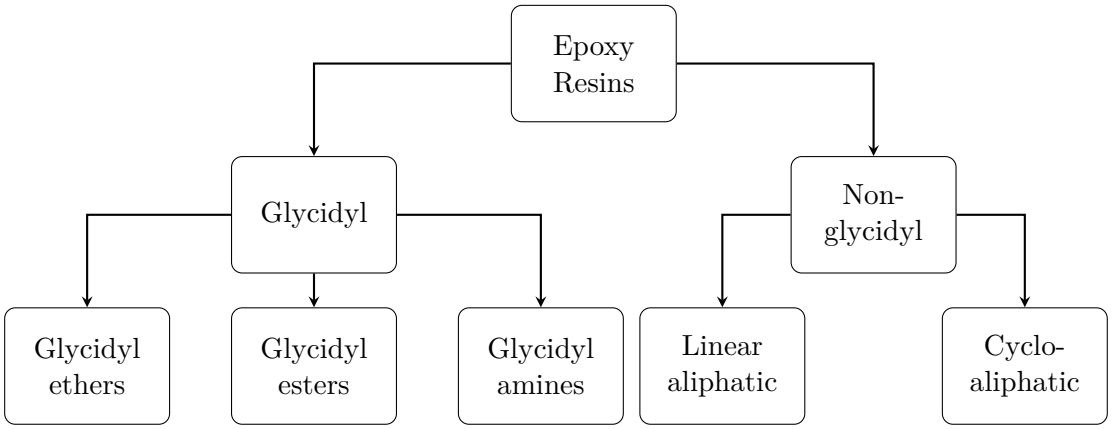

Figure 2.1: Classification of epoxy resins according to synthesis method.

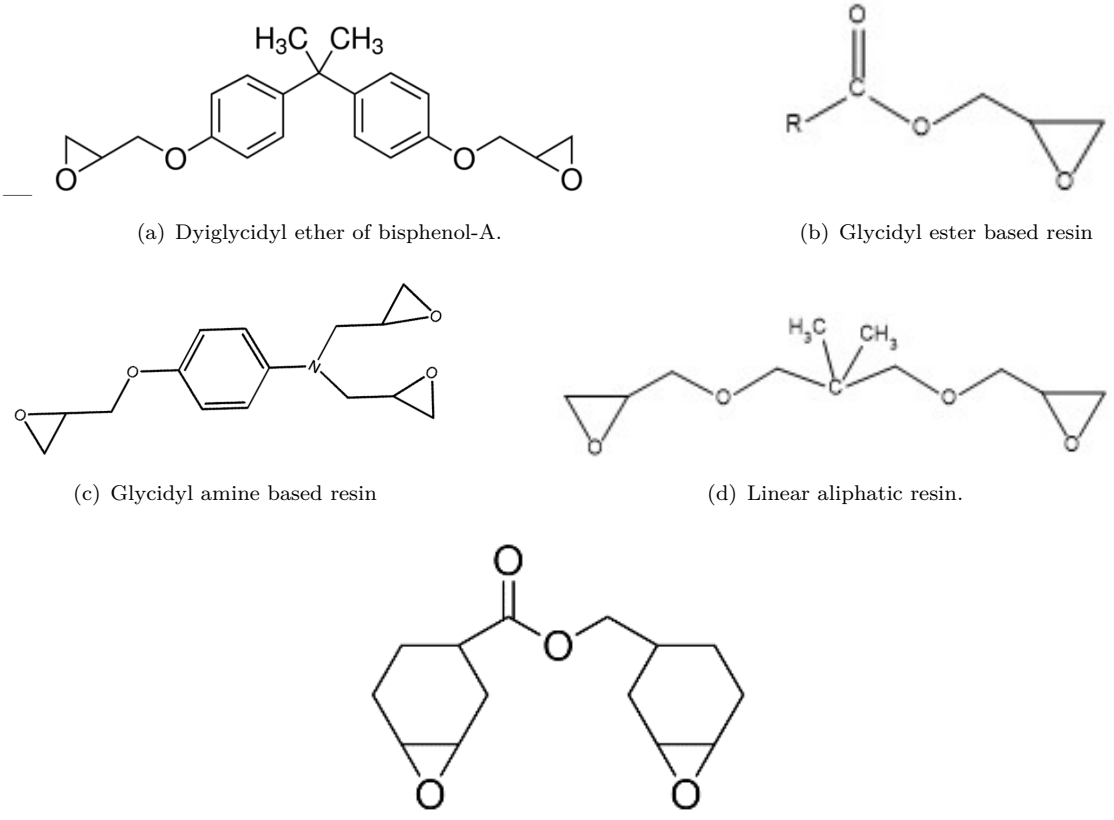

(a) Dyiglycidyl ether of bisphenol-A.

(b) Glycidyl ester based resin

(c) Glycidyl amine based resin

(d) Linear aliphatic resin.

(e) Cycloaliphatic resin.

Figure 2.2: Chemical structure of different epoxy resins.

of the resin, with the active species from the curing agent (also called hardener). Commonly, curing of the resin is accomplished through the use of amines or anhydrides, in concert with a catalyst or accelerator. The curing reactions of an epoxy resin with a hardener is a complex mechanism that involves a number of cross-linking reactions. However, several studies have discussed the principle chemical reactions that defines the resin curing mechanism in detail [3, 47, 54]. For example, the addition of an amine hardener to an epoxy based resin results in a reaction between the epoxide groups of the resin and an amine group from the hardener, which is often a primary type amine group. This reaction results in creating a secondary amine and a hydroxyl group. The secondary amine groups may later react with an epoxide group available in the system. This reaction results in forming another hydroxyl group and a tertiary type amine group, generating a cross-linked system. A schematic diagram which illustrates the curing reactions is plotted with the assistance of ChemDraw software package is presented in Figure 2.3.

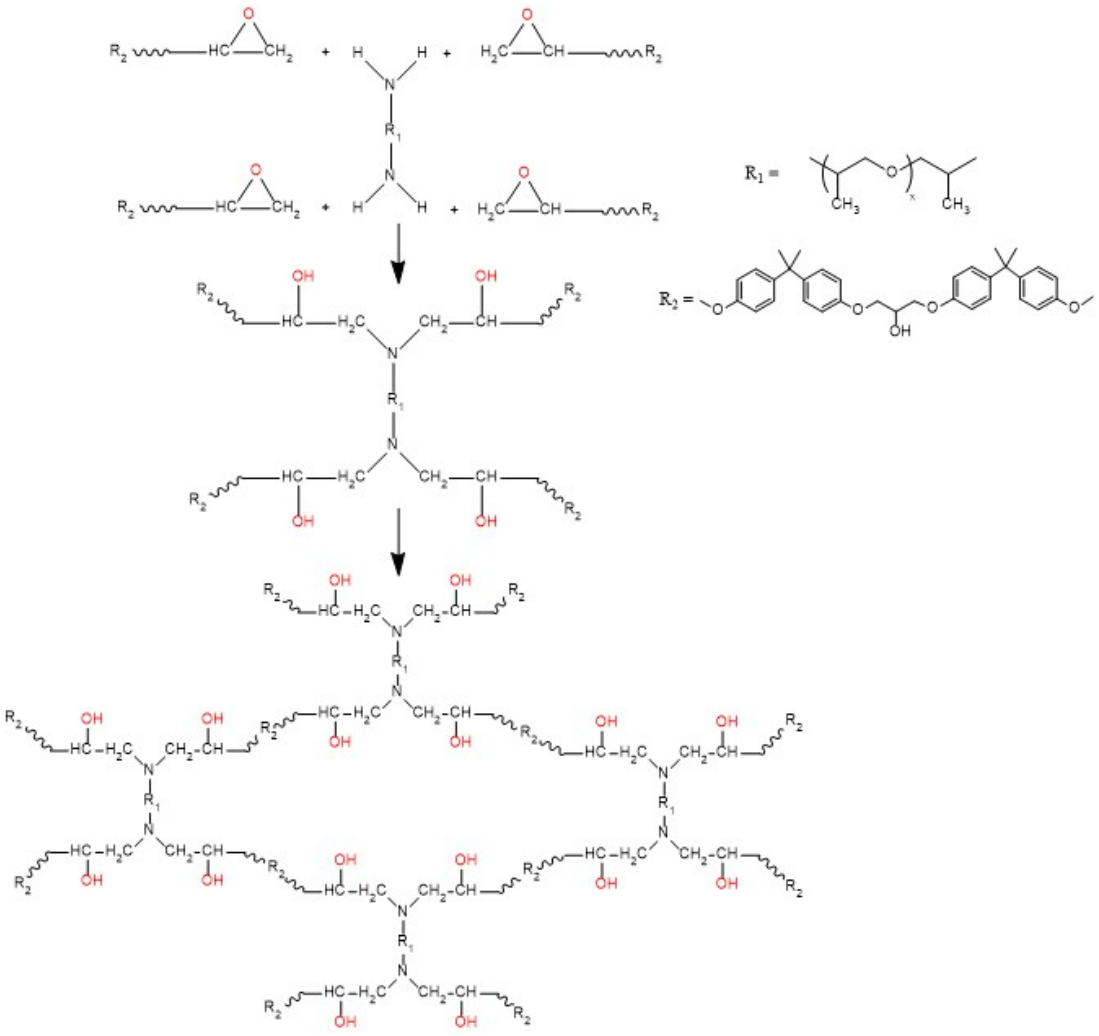

Figure 2.3: Reactions between an epoxide group and an amine group from amine hardener

In principle, the reactions between the epoxide groups and the amine groups continues until all the active groups available in the system have contributed to a cross-linking reaction. In practice, however, vitrification means that it is unlikely to consume all the reactive groups in the system.

When an anhydride hardener is used, the curing reactions are more complex compared to the cross-linking reactions of amine cured systems. This is because anhydride hardeners are not capable of reacting directly with the epoxide groups, without initiation reaction. In the anhydride initiation reaction, the anhydride rings reacts with a OH groups available in the system, creating a monoester containing a carboxylic acid. The consequent carboxylic acid group react with an epoxide groups from the resin. This reaction results in forming a hydroxyl group and an ester linkage; hence the reaction of the intermediate carboxylic acid group (active group of the anhydride hardener) and the epoxide group of the resin is referred to as esterification reaction [55–57], which is schematically presented in Figure 2.4. In addition to the reactions mentioned above, the hydroxyl groups available in the system may react with the epoxide groups of the resin, producing an ether link. If these epoxide groups originate from the backbone of the resin, the reaction is referred to as homopolymerisation.

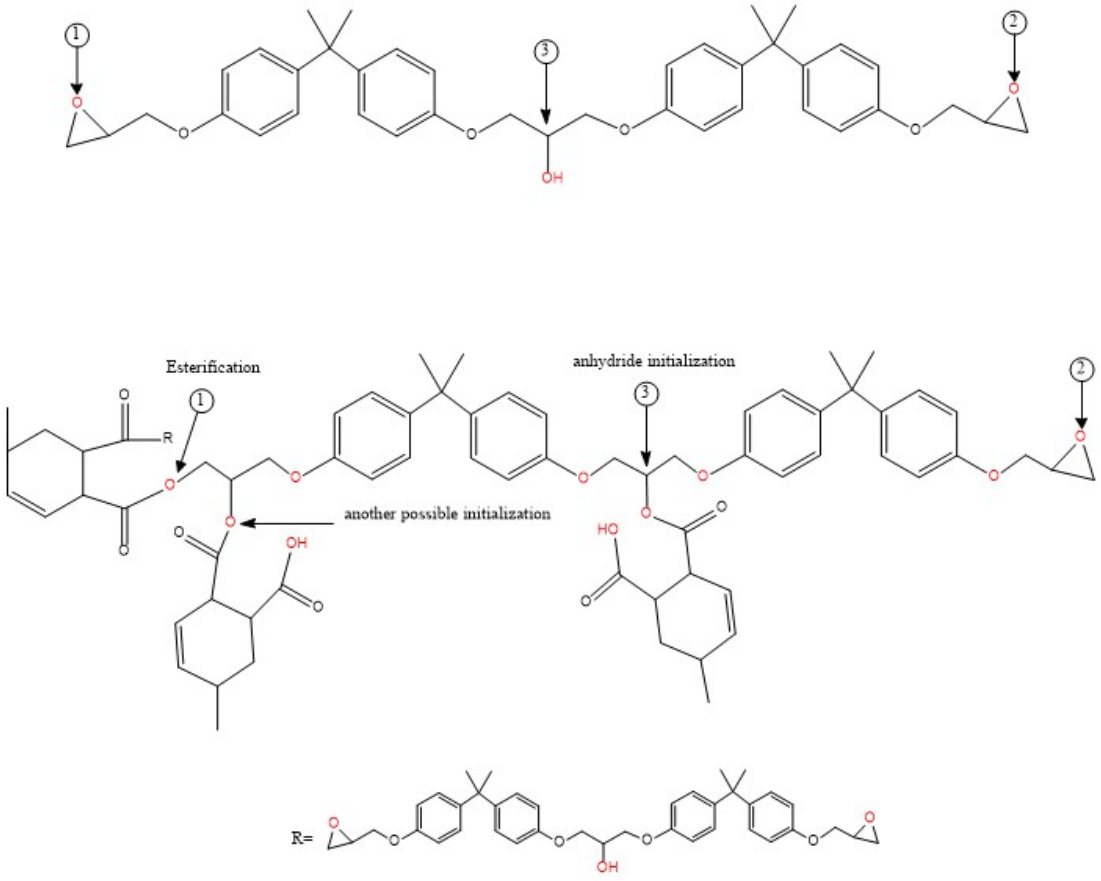

Figure 2.4: Possible curing reactions between DGEBA epoxy resin and an anhydride hardener.

Whereas, in the case of the hydroxyl groups are a consequent of a previous reaction between the resin and the hardener, the reaction is commonly referred to as etherification. It is important to point out that both reactions (homopolymerisation and etherification) may occur in anhydride and amine cured systems, where their probability increases as the curing/post-curing temperature increase [2]. Figure 2.5 present a schematic diagram for the idealised structure of the neat and FNM modified epoxy resin systems.

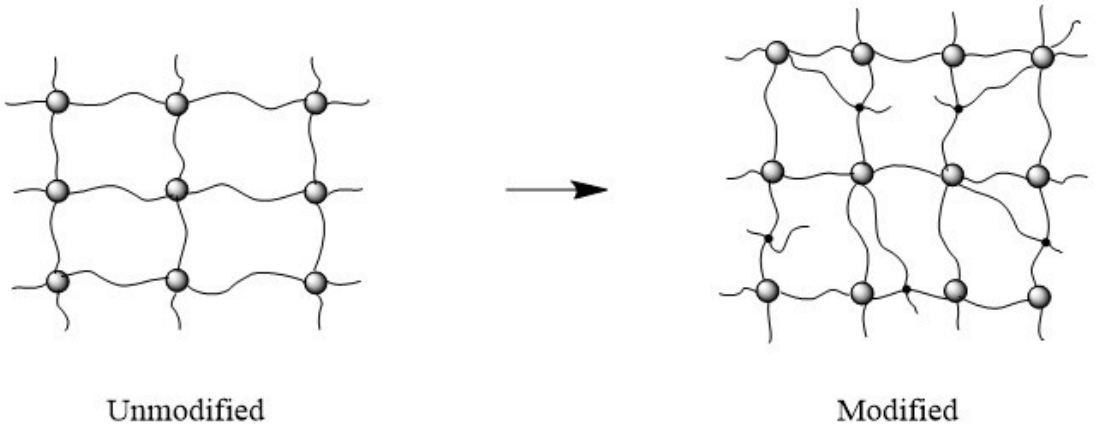

Figure 2.5: Idealised 2D schematic diagram showing the effect of the FNM on the structure of the resin.

As can be seen from the above discussion, the type of the hardener (based on it its chemical structure) defines the curing reactions, which impact the formed network structure. The primary process when using an amine hardener requires two active epoxide rings from the resin and the hardener's amine groups. However, when an anhydride hardener is used, both the terminal epoxide groups and the hydroxyl groups from the backbone of the resin may contribute to the curing process. Therefore, the curing mechanisms are directly associated with the type of the hardener, where the reactivity of the resin may vary accordingly. A comparison between the behaviour of a DGEBA resin in the presence of an amine and an anhydride hardener, in addition to, an idealised network structure assuming optimum stoichiometry is illustrated in Figure 2.6.

2.3 Methods for Modifying the Properties of Epoxy Resins

Depending on the number of the repeated units in the chemical composition of the resin, ER can be produced with different viscosities which gives manufacturing flexibility. These properties make epoxy resins an excellent thermosetting material, suitable for a wide variety of applications, from medical diagnostic equipment (MRI machines and ultrasound devices), to adhesives in aerospace applications, encapsulation of electronic devices and casting for high voltage transformers [3, 48]. The properties of epoxy resin used in each application are different. For example, according to Vryonis et al., epoxy

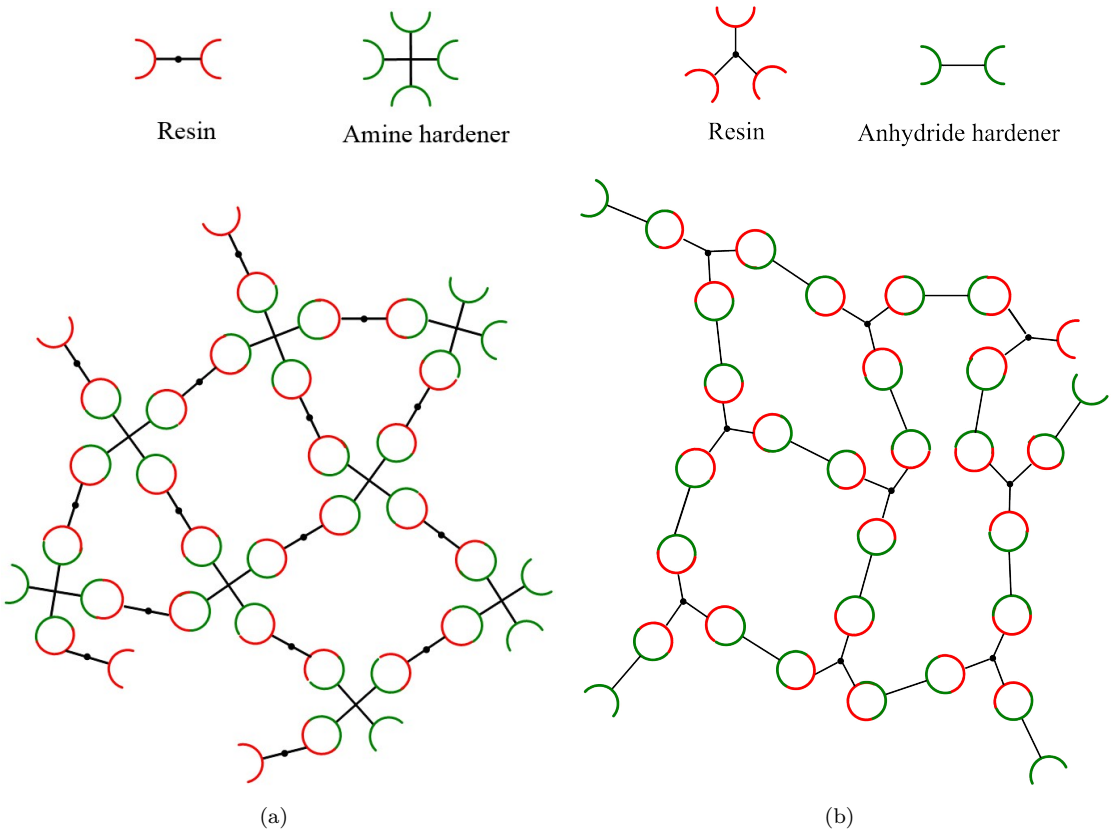

Figure 2.6: Schematic diagram showing the expected reactivity behaviour of the DGEBA resin in (a) unmodified amine cured, (b) unmodified anhydride cured. Etherification process was neglected

resin used for coating the blades of wind turbines need to enable electrical discharge to ground by increasing the surface conductivity, to protect wind turbines from damage due to lightning strikes [58]. Thus, these ER are required to have high electrical conductivity [59]. On the opposite side of the spectrum, epoxy resin with high electrical insulation properties are required for high voltage solid insulated switchgear, to insulate between the disconnect switch and earthing [3]. Consequently, to support the vast variety of applications, epoxy resins are engineered to generate specific combinations of electrical, thermal and mechanical properties. A growing number of research has been undertaken to investigate the different methods of generating ER with varied properties. There have been several studies in literature that reported the different types of modifiers, which are able to impact the electrical and thermal properties of epoxy resin systems. A broad classification of epoxy resin modifiers can be made according to the method used to introduce the modifier to the base epoxy system. Hence epoxy resin modifiers can be divided to two main types namely: fillers (nano and micro sized particles) and network modifiers (mainly liquid additives which are introduced to change the viscosity or alter the resin network on the molecular level). A critical review of literature focused on these methods is presented in the next sections of this chapter.

2.3.1 Fillers

Fillers are small grained particles that are added to a host material, in order to change its properties. Fillers could be organic or inorganic, with varied sizes, forms and shapes [60–62]. The sizes of the fillers are nowadays used to define the category of the filler. For example, fillers with size between 100 nm and 500 nm are referred to as meso-sized fillers, while fillers with size of less than 100 nm or exceeds 500 nm are known as nano-sized and micro-sized fillers, respectively [63, 64]. The physical form of fillers includes cubes, spheres, flakes, plates and fibres [65]. These fillers are added to epoxy resins to alter a number of properties of the ER systems including the mechanical, thermal and electrical properties of the composite. Throughout this work the review of the epoxy resin fillers will be focused on fillers which are introduced to epoxy resin systems for the purpose of studying the thermal, electrical and mechanical properties. Other types of fillers, for example, fillers used as antioxidant additives and colouring fillers (pigments and dyes) are studied and reviewed elsewhere [66, 67], and will not be repeated here.

2.3.1.1 Breakdown Strength in Filled Epoxy Systems

Since their first remarkable advances in the 20^{th} century, nano-dielectric materials have attracted considerable attention due to their ability to alter the electrical properties of insulating materials. Several studies have reported promising positive effect of nano sized fillers on the breakdown strength of polymeric materials [68–71]. However, not all fillers give improved breakdown strength. Contradictory results are reported in literature, where unfilled epoxy resins show better performance in breakdown test than ER system filled with certain nano-fillers. For example, Tsekmes et al. [72] conducted a study to investigate the effect of nano-fillers on the AC breakdown strength of epoxy resin systems. Varied concentrations of boron nitride nano-fillers were used to test the breakdown strength of filled epoxy resin and evaluate the reproducibility of the experimental results. The data indicated that samples with 5 wt% of boron nitride filler content have deteriorated breakdown strength compared to the breakdown strength of the unfilled epoxy systems. Tsekmes et al. [72] suggested that their results are reproducible and concluded that the breakdown strength of the filled systems depends on the filler loading rather than the method used to synthesise the composite. While the results might be valid, the interpretation of the data could have been better if they would have investigated the breakdown strength behaviour at the interaction region between the filler and the host material i.e. the effect of filler size on charge distribution at the interphase and filler surface functionality.

In a study conducted by Andritsch et al [73], the effect of different size of boron nitride on the breakdown strength of epoxy resin systems was investigated. Contrary to the findings of Tsekmes et al. [72], the data presented by Andritsch et al. [73] indicated an

increase of about 6 %, 11 %, 21 % and 42 % in the breakdown strength of composites with filler size 5 μm, 1.5 μm, 0.5 μm and 70 nm respectively. Andritsch et al. suggested that the noticed breakdown behaviour is attributed to the size of the interface associated to each filler size.

In a study by Zhe et al, it was reported that the addition of 5 wt% of Al_2O_3 nano fillers to an epoxy resin is suggested to result in 5 % increase in the breakdown strength of the filled epoxy system compared to the breakdown strength measured for the reference unfilled resin [25]. Zhe et al suggested that the filler size (micro or nano) is the factor that drives the breakdown strength of the filled epoxy resins [25]. In addition, the results of Zhe et al indicated that the inclusion of a comparable loading (5 wt%) of micro sized Al_2O_3 to the same epoxy resin would results in 56 % decrease in the breakdown strength of epoxy micro-composite compared to the behaviour of the breakdown strength, where the decrease in the breakdown strength for the materials filled with micro sized fillers was associated with voids introduced into the polymeric network during the manufacturing process. Furthermore, Zhe et al suggested that the electric tree grow rapidly at the surface of the micro filler compared to the surface of nano filler, which they associated with the noticed reduction in the breakdown strength for the micro filled systems. This statement may not be accurate since the ratio of surface to material size is greater in nano fillers [63]. Besides, the two fillers (micro and nano) were not prepared using the same method as the surface of the nano fillers was modified to ensure efficient dispersion, this procedure was not applied for surface of the micro fillers. Therefore, as the interface surface of the fillers plays a vital role in defining the final properties of the composite [9], the comparison between the influence of the nano and micro fillers on the breakdowns strength of epoxy resin systems used by Zhe et al. in [25] with only one filler modified is not accurate.

The effect of the electric field on the breakdown strength of epoxy resin systems filled with different types of nano-fillers was investigated by Iami et al [30]. The study tested epoxy resin systems filled with TiO_2, SiO_2 and layered silica nano-fillers under homogeneous and divergent AC electric fields. The results of Iami et al [30] showed that under a homogenous electric field, epoxy resin systems filled with comparable concentration of both TiO_2 and layered silica nano-fillers exhibit lower AC breakdown strength compared to that of unfilled epoxy system, while the opposite was reported for the same sample compositions tested under divergent electric field. Iami et al [30] suggested that the noticed decrease in the breakdown strength of the TiO_2 and silica filled systems reported under homogenous electric field is attributed to the high relative permittivity of these fillers compared to the permittivity of the neat epoxy resin. The study also explained that the permittivity of TiO_2 filled systems is higher than the permittivity of all other tested composites. Iami et al did not provide any experimental data or literature to support their interpretation. In addition, no explanation was provided for the behaviour of the filled epoxy system under divergent electric field. Perhaps, the behaviour noticed by

Iami et al is related to factors such as the nature of the filler surface and the interaction between the filler and the polymer, where the surface modification of TiO_2 nano-filler is reported to influence the breakdown behaviour of epoxy nanocomposite under divergent field [74].

Although several studies have presented the beneficial effects of adding fillers to polymers, it can be seen from the above discussion that not all fillers improve the breakdown strength of epoxy composites. Where several factors affect negatively the performance of the composite, these factors may includes: the filler size, type, surface functionality and dispersion.

2.3.1.2 Complex Permittivity in Filled Epoxy Systems

A growing number of studies have investigated the permittivity of epoxy resin systems filled with different fillers. However, the published literature is contradictory, and there is no clear definite explanation for the behaviour of all filled epoxy resin systems.

For instance, in a study on the effect of filler size on the dielectric properties of epoxy resin, Iyer et al [75] prepared epoxy resins filled with micro, nano and mixed size silica fillers. The study reported that samples filled with nano sized filler are suggested to show low permittivity compared to the permittivity measured for the other samples (filled with micro and mixed size fillers). Iyer et al [75] suggested that the reduced permittivity of the nano-filled systems is associated with the interaction between the filler particle and the epoxy resin, where it was claimed that large interaction between the nano-fillers and epoxy resin is present in the nano-filled systems compare to systems filled with micro size fillers.

The results of Iyer et al [75] are in contrast with the findings reported by a study of the influence of the interface region for epoxy resin system filled with similar nano-fillers conducted by Sun et al [76]. The results of Sun et al [76] showed that at low frequencies, silica nano-composite have higher permittivity compared to the permittivity measured for epoxy systems filled with micro sized fillers. Sun et al [76] stated that the variation in the dielectric behaviour of the filled system is associated with contamination through the synthesis method used to produce the fillers, as moieties retained in the system could have enhanced the ionic conductivity of the nano-filled systems, which resulted in the noted increased dielectric loss. One can question their main explanation, as it was based on the contamination during the synthesise method, while only the supplier was mentioned in the experiment section of the study and no information were provided regarding the method used to synthesis the fillers.

In a study by Singha and Thomas, the dielectric properties of epoxy systems filled with different types of fillers have been compared [29]. Varied concentrations of different types of fillers, such as TiO_2, ZnO and Al_2O_3, were used in both micro and nano

sizes. The general trend showed that the real part of complex permittivity of TiO_2 is significantly higher than that of ZnO, and at certain concentrations both fillers have higher real permittivity compared to the neat epoxy. Perhaps the most interesting reported permittivity is that of epoxy samples filled with 10 wt% TiO_2 nano-filler, as these samples were reported to have high real permittivity relative to the unfilled system. These results contradict the findings reported by Nelson and Fothergill in [77]. In their study, Nelson and Fothergill used epoxy resin systems filled with 10 wt% of TiO_2 nano-filler, which is similar to the filler and sample composition used by Singha and Thomas [29]. The results of Nelson and Fothergil [77] suggested that samples with 10 wt% of TiO_2 nano-fillers have low relative permittivity compared to that of neat epoxy systems. The hypothesis of the authors was that the presence of the nano-fillers would restrict the dipole movement, while micro sized fillers would undergo Maxwell-Wagner polarisation.

Maity et al [78] stated that the interface region between the filler and the base epoxy plays a vital role in defining the dielectric properties of the final composite, which is similar to the suggestions of Iyer et al [75]. In contrast, the work of Sun et al [76] gave more emphasis on the chemical structure of the filler and synthesis method, whilst Nelson and Fothergill [77] suggested that the size of the filler contributes to the dielectric behaviour of an epoxy nanocomposite.

It can be seen from the above discussion that the permittivity of the epoxy composite is sensitive to several factors, which influence the final behaviour of the composite. These factors could be the filler dispersion, the base material formulation, the interface area, the concentration and surface functionalisation of the filler. It may also be that a combination of any of these factors could have resulted in the contradictions found in the literature regarding the complex permittivity of epoxy filled systems.

2.3.1.3 Glass Transition Temperature Behaviour in Filled Epoxy Resin Systems

The thermal properties of epoxy resin systems are reported to be affected by the inclusion of fillers. The aim of this section is to review studies reported in literature that have been conducted to modify the thermal properties of epoxy resin systems by the inclusion of fillers. The review will emphasis on the modification of the glass transition temperature as it is relevant to the research conducted in this thesis. In a study conducted by Nishanth et al [79], the effect of adding carbon nanotube CNT on the thermal properties of epoxy resin nanocomposite was investigated. The data showed that the introduction of up to 4 wt% of CNT, resulted in 5 % increase in T_g, compared to that of the T_g measured for the neat epoxy. However, higher filler loading (above 4 wt%) shifted T_g to lower values of temperature. Nishanth et al [79] provided no explanation for the physical phenomenon of the observed behaviour of T_g. In a similar work, Kosmidou et al [80] investigated the effect of different concentrations of carbon black nano-fillers on the T_g of

epoxy resin systems. Kosmidou et al [80]considered two sets of curing schedules, where a group of samples were only cured at 60 °C for 20 h, while the other group of samples were cured for the same time and temperature as the first group, then post-cured for 2 h at 150 °C. The results showed that for low loadings of nano-carbon black fillers (below 0.7 wt%), the glass transition temperature of the epoxy nanocomposite is higher than the T_g of the neat system; However, after adding a certain concentrations of the nano-filler (above 0.7 wt%), the T_g start to decrease significantly. Kosmidou et al [80] suggested that the variation in the T_g is associated with the domination of one of two mechanisms, namely interfacial constrains and free volume. They also proposed that the free volume effect is based on the extra space generated inside the molecular matrix due to the introduction of the nano-fillers, which rises as the filler concentration increase. Whilst the interfacial concept is based on several complicated effects that occur at the surface of the nano-fillers. These were suggested to modify the molecular kinetics in this region, and constrain the chain entropy, which results in T_g shifted to a higher value. Kosmidou et al proposed that the reason for the noted rise in the T_g is associated with the interfacial constraint mechanism, which is proposed to be dominat at low filler concentration, while the free volume mechanism would dominate at 0.7 wt% and higher filler loading [80]. Kosmidou et al stated that the reason for the domination of a certain mechanism at specific concentration is attributed to agglomeration of the nano-fillers. Finally, the results of Kosmidou et al [80] indicated that the post-cured systems featured comparable behaviour to that of the non-post-cured systems, but with higher T_g values. While the explanation for the free volume and the interfacial surface constraint sounds reasonable, the sample preparation method appears to be questionable. Curing of epoxy resin plays a vital role in defining the properties of the bulk material. Kosmidou et al [80] provided no justification for using the selected curing and post curing time and temperatures, while other studies used similar hardener with DGEBA recommended the use of three stages of curing [81, 82].

In other work, the glass transition temperature of different types of ER systems filled with layered clay nano-filler has been shown to decrease monotonically, and inversely proportional to the filler loading. The decrease in the T_g was reported to be 20 °C for DGEBA and below 15 °C for all other tested resins [11]. Becker et al [11] assumed that there are several factors which affect the behaviour of the T_g in epoxy nanocomposite, where determining the impact of each factor separately may not be possible.

Sun et al [16] investigated the effect of micro and nano-sized fillers on the T_g of ER system filled with silica, silver and aluminium nano-fillers. Their results indicated that, generally, epoxy samples filled with nano-sized fillers showed lower T_g temperatures compared to the T_g of systems filled with micro fillers. Sun et al [16] explained the noted decrease in the T_g is due to a combination of the increase in both the free volume and the increase in the material to interfacial area, which significantly alter chain kinetics and causes shift of the T_g to lower values. In contrast to the findings of Kosmidou et al

[80], Sun et al [16] proposed that both mechanism occur at the same time. Other studies on the effect of fillers on T_g reported no significant effect of the corporation of fillers on the glass transition temperature of polymeric composites [83, 84]; therefore, the above discussion proves another contradiction in literature.

2.3.1.4 Mechanical Properties in Filled Epoxy Resin Systems

Fully cured epoxy resin are brittle in nature and lack sufficient toughness to be compatible with a wide range of applications. Most of the reported improvements in the mechanical properties of epoxy resin were associated with the addition of varied loadings of fillers, that featured different sizes and shapes. In a study conducted by McGrath et al [85], the effect of adding alumina (α-Al_2O_3) fillers on the mechanical properties of DGEBA epoxy resin cured with Jeffamine (D230) was investigated. The fillers were introduced to the base epoxy material using several methods, so that the produced samples can be evaluated according to four parameters, which are: particles loading, shape, size and cross-linking density. The results of fracture toughness testing indicated that the filler loading and the cross-linking density significantly affect the mechanical properties of the samples. Whereas the particles size and shape had no substantial effects [85]. Similar conclusions were reported by Radford [86], where the elastic modulus increased with increasing the filler loading, independent of the particles size. Comparable findings were suggested for phenolic resin filled with different size of $CaCO_3$ fillers [87], and for DGEBA resin filled with alumina nano-fillers [88]. However, Nakamara et al [89] claimed that the size of nano-particles has significant effect on the mechanical properties of silica filled epoxy-based resins and that the decrease in the size of silica particles within the range (2 - 47 μm) would increase the elastic modulus and the tensile strength of the material. Nakamara et al [89] provided no explanation for the reported behaviour.

While most literature is in agreement that the size of the fillers only slightly affects the mechanical properties of the epoxy nanocomposite, the shape of the particles is a more controversial parameter. The study of Lim et al [88] compared the mechanical properties of epoxy resin samples filled with rod and platelet shaped alumina particles. The results indicated that the elastic modulus increased by 30 % after the introduction of 5 wt% of the platelet-shaped particles, while the addition of the rod-shaped particles enhanced the modulus by only 17 % for the same wt%. The results of Lim et al. were explained by the fact that platelet-shaped particles features high area for the same volume compared to the rod-shaped particles, which allows transferring the mechanical stress to larger area of the particles. McGrath et al [85] disagree with the findings of Lim et al [88], where the former proved that the addition of alumina nano-fillers to DGEBA resin had an insignificant effect on the elastic modulus and the tensile strength of the alumina-filled resin, with no specific explanation. It can be seen that, Lim et al [88] used platelet and rod alumina shaped particles for the comparison, while McGrath et al

[85] utilised spherical and angular alumina shaped particles. Platelet shapes have high surface area compared to rod shapes for the same volume, while the area of spherical and angular shapes are quite similar. Therefore, both shapes spherical and angular might transfer similar mechanical stress, which would have resulted in the slight influence of the particles shape on the mechanical properties reported by McGrath et al [85]. Hence, the conclusion stated by McGrath et al in [85] about the particles shape is inaccurate due to weak comparison and should not be generalised.

Adding poly-phenylene-oxide PPO to DGEBA resin resulted in linear increase in fracture toughness of the material as a function of filler loading [90]. Similar findings reported for different systems with varied fillers [86, 87].

From the above discussion, it is possible to suggests that most published literature agrees that the cross-link density, the size distribution and the filler loading are the most important parameters in determining the mechanical properties of a nano-composite.

2.3.2 Network Modifiers

Network modifiers are liquids or solids with low melting point, used, traditionally, to control the viscosity of epoxy resin systems without causing significant changes to the behaviour of the material [48, 91, 92]. Network modifiers are usually added to epoxy resin mixture in liquid phase before curing to facilitate casting and improve the embedding of other additives [91]. There are several different types of network modifiers, which can be generally classified in two main categories according to their ability to bond with the epoxy resin network [47, 91, 93], these modifiers are namely, non-reactive and reactive network modifiers, as illustrated in Figure 2.7.

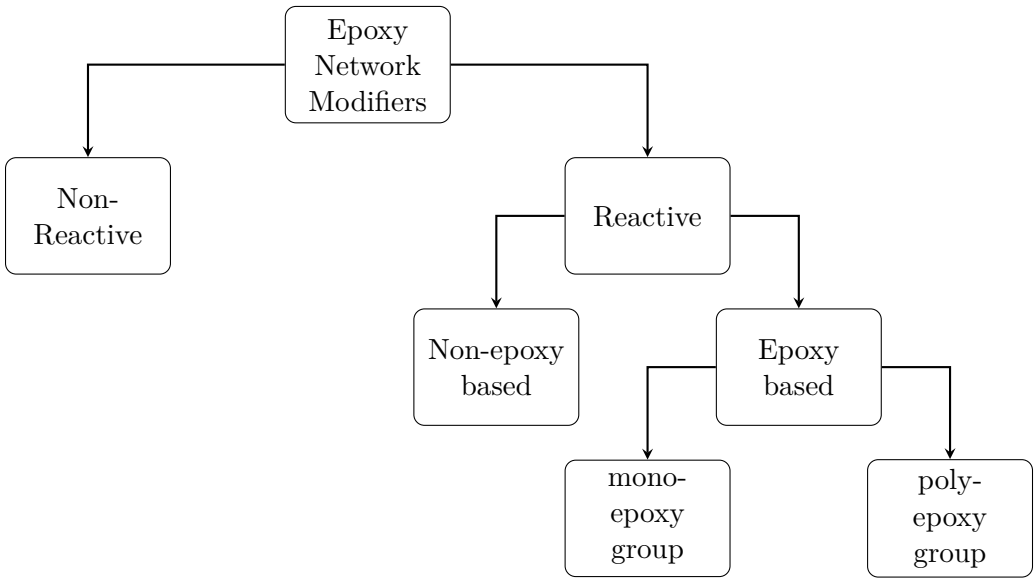

Figure 2.7: Classification of epoxy network modifiers.

In this work, single and multiple epoxy based reactive network modifiers are utilised to alter the network structure of the epoxy resin, these are referred to in the context of this thesis as functional network modifiers, FNM. Other modifiers, such as the non-reactive and reactive non-epoxy based modifiers, will be reviewed in this section; however, they have not been used in the experimental section as they are out of the scope of this work.

2.3.2.1 Non-Reactive Modifiers

Non-reactive modifiers are chemicals which are employed mainly to control the viscosity of epoxy resin systems [93]. Solvents such as toluene, xylene, acetone and castor oils are examples of non-reactive modifiers [91]. These compounds, by nature, cannot react and bond with the network of the epoxy resin and are assumed to have negligible influence on the ultimate properties of the material [3]. Non-reactive modifiers commonly used are volatile substances, which escape the system after degassing and curing, as they have low flash point, that prevent them from surviving the curing process [93]. The addition of non-reactive modifier might enhance the cross linking of the epoxy resin system, resulted from the increased freedom of movement of the molecules due to the initial reduced viscosity [91].

Liao et al [94] investigated the effect of adding acetone (as a non-reactive modifier) on the dispersion of CNT fillers in epoxy resin systems. The results showed enhanced dispersion of fillers due to the controlled viscosity achieved by the non-reactive modifier. The results of Liao et al [94] also indicated, that samples produced with the addition of acetone have significantly reduced glass transition temperature, compared to samples fabricated without acetone, although the acetone was removed from the sample mixture before curing. They provided no explanation for the effect of acetone on T_g. In addition, Liao et al [94] provided no evidence for the presence of acetone in their tested samples. Since the sample mixture was degassed, the acetone solvent might have already left the samples by the time they have conducted the T_g measurements. Indeed, one can argue that factors other than the acetone are likely resulted in the noted decrease of T_g, it would have been beneficial if the authors investigated the chemical structure of the samples using techniques such as fourier transform infrared spectroscopy to develop a clear understanding of the chemical composition of the tested materials. On the other hand, Loos et al [95] investigated the effect of residual acetone used for enhancing the dispersion of nano-fillers on the curing process and the mechanical properties of epoxy resins. They used both FTIR and thermogravimetric analysis (TGA) to support the existence of acetone in the tested samples. Loos et al [95] concluded that acetone is beneficial solvent for filler dispersion, which would have no effect on the mechanical and thermal properties of the epoxy resin system if removed before curing. This was explained by the increased viscosity of the mixture provided by the acetone, which would have modified the cross-linking density of the epoxy network before the molecules become immobile.

In another study, Hong and Wu [96] examined the effect of tetra-hydrofuran, toluene and acetone on the curing behaviour of epoxy resin systems. The results indicated that if the non-reactive modifiers are present in the cured epoxy resin systems, the functional groups of the modifiers reduce the T_g in order related to the boiling temperature of the modifier [96]. The findings of Hong and Wu are similar to the findings of Loos et al [95], as both studies concluded that non-reactive modifiers can have negative affect on the properties of the epoxy system present in the fully cured composite. Usually, the resin mixture is degassed long enough to ensure no bubbles exist in the system. The degassing process would allow volatile non-reactive molecules to escape and hence their effect can be neglected.

2.3.2.2 Reactive Network Modifiers

Reactive network modifiers in this context are generally any solvent or chemical added to the epoxy and hardener mixture which can react with the mixture and become part of the matrix and thus influence the properties of the composite [78, 81]. Reactive network modifiers, can be divided into two main types: non-epoxy based and epoxy based network modifiers, according to the functional group within its chemical structure.

a. Non-Epoxy Based Network Modifiers

Any solvent used for controlling the viscosity of the epoxy resin, combined with changing some of the properties of the system without containing epoxide groups within its chemical structure, can be consider as non-epoxy based network modifiers [91]. This class of modifiers comprises of compounds that can react with the hardener or the resin, but not considered as curing agents. Reactive non-epoxy based network modifiers which have been reported in literature include triphenyl phosphite, divinyl ethers, short chain polyols, lauric acid and lactone compounds [47, 48].

It has been suggested in several studies that reactive non-epoxy network modifiers can alter the mechanical properties of epoxy resin systems. For example, Harani et al [97] investigated the effect of hydroxyl-terminated polyester on the mechanical properties of diglycidyl ether of bisphenol A. Fourier transform infrared (FTIR) technique was used to characterise the samples which contained different concentrations of the network modifier. Harani et al [97] utilised network modifiers with two chemical structures; slightly branched and branched polyester. The results indicated that the introduction of the reactive network modifiers increased the impact strength of the modified samples. In addition, certain concentration of long chains, low branched, high molecular weight reactive network modifiers lead to significant improvement in the mechanical properties of modified system.

In another study, Tang et al [98] synthesised a polyurethane-based reactive network modifier which was used to modify an anhydride cured DGEBA resin. Two structures of network modifiers were compared, one with polyurethane while the other modifier featured short-chains imbedded between the nodes. The network modifiers shifted T_g of the cured samples to lower values and decreased the viscosity in the liquid phase. The used modifier was capable of reacting with the resin. In addition, the network modifiers improved the impact strength of the modified material. Similarly, the bending strength of liquid crystalline polyurethane-imide (PUI) modified epoxy resin increased by 32 % compared to the neat epoxy resin [99].

A more detailed study of the mechanical properties of polyurethane modified epoxy resin was conducted by Bakar et al [100]. It was found that the addition of 20 wt% of polyurethane-imide loading resulted in a maximum improvement in the impact strength, while the tensile strength reached the maximum value at 15 wt%. In addition, the measured T_g value was decreased by about 50 °C and the elastic modulus was reduced by 50 % compared to the unmodified samples.

Studies of epoxy systems modified with compounds considered as non-epoxy based network modifiers also reported change in the thermal properties of the modified systems. For instance, Dougherty and Vara [101] have shown that the addition of divinyl ethers increase the T_g of epoxy resin systems, and Pan et al [102] reported a significant increase in the T_g of the modified systems which was associated with the addition of barbituric acid. Most studies have only reported the effect of the non-epoxy reactive network modifiers on the cure kinetics, thermal and mechanical properties of epoxy resin systems [97, 101, 103]. The effect of reactive non-epoxy based modifiers on the electrical properties has not been well studied. This may be due to the low effectiveness of non-epoxy based network modifiers, compared to the epoxy based network modifiers.

b. Epoxy Based Reactive Network Modifiers

Epoxy based reactive modifiers (functional network modifiers FNM) are chemicals containing one or more epoxide groups within their chemical structure [47, 91]. Epoxy-based reactive modifiers can be sub-categoried into mono-epoxy and poly-epoxy based modifiers, according to the number of epoxide groups in the molecular structure. Mono-epoxy based reactive modifiers refer to modifiers containing only one epoxide group. An example of reactive mono-epoxy based modifiers are materials containing aromatic or aliphatic chemical structures such as ethyl glycidyl ethers and glycidyl 2-methylphenyl ether shown in Figure 2.8. Accordingly, poly-epoxy have more than one epoxy group in their molecular structure, such as diglycidyl ether and diglycidyl 1,2-cyclohexanedicarboxylate shown in Figure2.8.

Epoxy based reactive network modifiers contribute to the curing process through their epoxide groups. The reaction of these modifiers with the hardener during the curing process is similar to that of the base epoxy resin (as discussed in section 2.2). Therefore,

the reactive modifiers and the associated R-group become part of the three-dimensional network of the cured resin. Consequently, epoxy based modifiers contribute to the physical, thermal and electrical properties of the epoxy material.

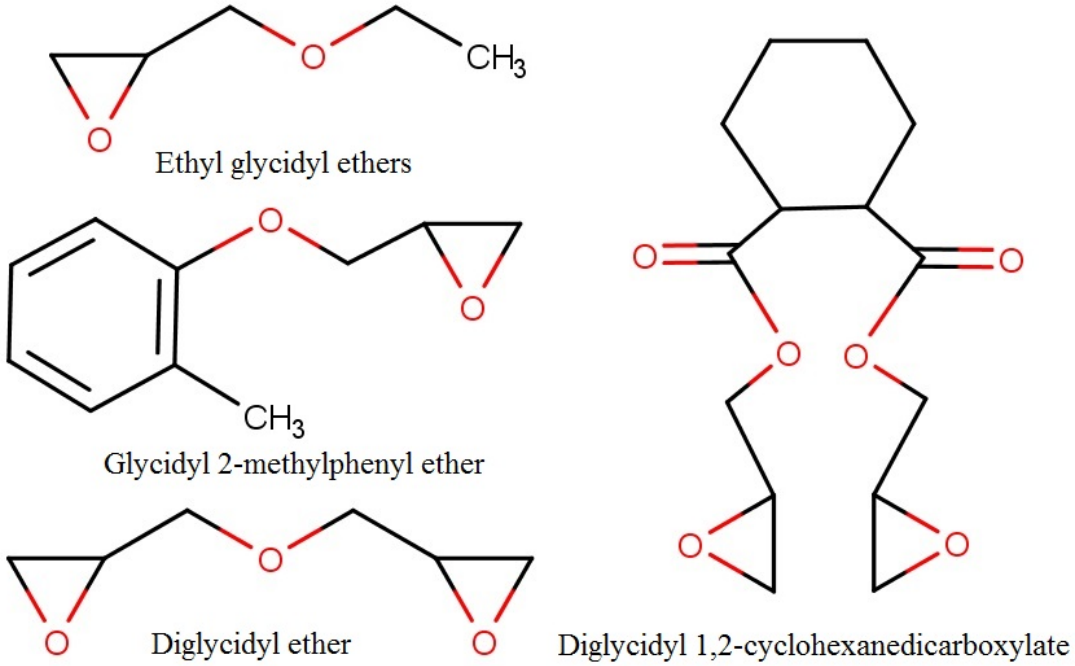

Figure 2.8: Examples of aliphatic and aromatic structures of monoepoxies and polyepoxies epoxy based reactive modifiers.

Several studies have investigated the effects of epoxy based network modifiers on the thermal and mechanical properties of epoxy resin systems. Chen et al [104] synthesised a polyepoxies reactive modifier and used it to study the thermal and mechanical properties of modified petroleum-based epoxy resin. To ensure the presence of the modifier, which was polyepoxide cardanol glycidyl ether, Chen et al [104] characterised the cured samples using FTIR. The results of Chen et al [104] indicated that the addition of up to 20 wt% of the functional modifier would improve the heat resistance and mechanical properties of the modified epoxy systems. In another study, the activation energy of an ER system modified using 1,2-cyclohexanediol diglycidyl ether (polyepoxide modifier) was measured [105]. It was reported that the introduction of 20 % by mass of the reactive modifier results in 20 % reduction in the activation energy. The authors suggested that the reason for the reduction in the activation energy is due to the ease of reaction between the amine groups of the hardener and the epoxy groups of the reactive network modifier, compared to the epoxide groups from the base resin. The authors present no proof why epoxy groups of a reactive modifier would react easier with the hardener compared to epoxy groups of the resins and this claim was not reported elsewhere in literature.

Nunez-Regueira et al [106] investigated the curing behaviour and the glass transition temperature of DGEBA epoxy resin modified using vinylcyclohexene dioxide, which is

a poly-epoxy epoxy based reactive modifier. DSC was used to measure T_g for samples with varied concentrations of the network modifier. Nunez-Regueira et al [106] stated that 15 % is a critical mass percentage beyond which the modifier has no considerable effect on the thermal properties or the degree of curing. Their results indicated that the introduction of an epoxy based reactive modifier shifts the curing peaks to higher temperature values. In addition, the study [106] showed that the measured T_g is inversely proportional to the added weight of the network modifier. The variation in the thermal properties was explained due to the shortage in the diamine hardener. In the samples used by Nunez-Regueira et al [106], there are two sources of epoxide groups (the resin and the modifier), both should be considered in the calculation of the sample stoichiometric ratio. In the case of no compensation for the amine groups consumed by the modifier, the produced samples will have an excess of epoxide groups, which affect the thermal properties of the systems. Similar behaviour of T_g was reported by Montserrat et al [107] and Pineda et al [108] for DGEBA resin modified with aliphatic diglycidyl ether and 1,4-butanediol diglycidyl ether reactive modifier respectively. Montserrat et al [107] explained the decrease in the T_g as a result of the increase in the freedom of mobility of the molecules. This is sensible, as the reactive modifiers are embedded in the resin's network, which changes the chemical structure and introduces possible free space within the epoxy matrix. Consequently, the glass transition temperature shifted to lower values.

Few studies investigated the effect of epoxy based network modifiers (specifically POSS based modifiers) on the breakdown strength of epoxy resin systems [109–112]. In all these studies, the modified system was treated as nano-structured epoxy composite without accounting for the curing reactions associated with the epoxide groups of the modifier and varying the stoichiometric ratio of the mixture accordingly to prevent unbalanced mixture (excess resin or excess hardener). In both [109] and [110] the reported enhancement in the dielectric properties can be challenged as no evidence of the chemical composition of the tested samples was provided.

According to Alhabil et al [113], altering the resin to hardener ratio results in creating network structures with varied retained chemical functionalities. Alhabil et al [113] suggested that the T_g of epoxy resin systems is greatly influenced by the precise network topology, residual amines markedly increased the conductivity of amine cured systems, leading to a consequent reduction in DC breakdown strength. Similarly, Nguyen et al [114], considered the effect of variations in stoichiometry on AC breakdown of anhydride cured epoxies and suggested reduced breakdown strength for systems with excess hardener. Therefore, it is important to consider a correct stoichiometric ratio when seeking to alter the properties of an epoxy resin using epoxy-based reactive network modifiers.

Perhaps the most relevant article is the investigation of the influence of octyl/decyl glycidyl ether modifiers on the dielectric properties and the breakdown strength of modified epoxy resins conducted by Liu et al [115]. The dielectric measurements of Liu et al [115] indicated insignificant variation in the real part of complex permittivity for samples

with up to 10 % of epoxide groups from the reactive modifier. However, at frequency below 10 Hz, the real permittivity of the 10 % sample, starts to increase. On the other hand, the imaginary part of the complex permittivity indicated increase in both $\beta-$ and $\alpha-$ relaxations. In [115], the variation in the permittivity was explained due to the decreased T_g of the modified sample. All measurements were conducted at 25 °C, while T_g of the 45 % sample was well below room temperature. The decrease in T_g was attributed to the increased free volume in the system associated with the increased percentage of the modifier. In addition, Liu et al [115] found that the introduction of 5 % of the epoxide groups from the reactive network modifier would increase the breakdown strength by about 5 % compared to the unmodified reference [115]. It was suggested that the introduction of the alkyl reactive modifier has altered the network structure, by introducing branches into the ER network, which are assumed to alter the electrical performance of the modified systems. While it may be argued that the improvement in the breakdown strength of about 5 % is marginal, it has been shown that comparable improvement in the electrical properties have been translated into significant advantage under technologically relevant electric fields [116, 117].

From the above discussion it can be seen that the introduction of epoxy based reactive network modifiers alters the mechanical properties and reduces the glass transition temperature of the epoxy resin system. There has been no detailed investigation on the impact of the reactive modifiers on the breakdown strength of epoxy resins systems and the mechanism behind the unusual behaviour of the modified materials. Recent work suggests that the introduction of epoxy based reactive modifiers, even when no electroactive character is present in their chemical structure can enhance the electrical properties of the modified system. It would be interesting to investigate the ability of epoxy based reactive modifier to function as voltage stabilisers for epoxy resins as a mean for designing the epoxy resin materials to suit particular applications.

2.4 The Concept of Voltage Stabilisers

Voltage stabilisers are additives which are used to enhance the electrical properties of polymer based high voltage insulators [118]. Perhaps the first time the term voltage stabiliser was used in the mid 1960s by Simplex Wire & Cable Company. They have patented a chemical agent featuring an aromatic structure, with the claim it would reduce the occurrence of electrical faults in cable insulations. A further investigation on voltage stabilisers was conducted later on by Ashcraft et al [119]. The authors explained that the voltage stabilising mechanism of a material depends on its ability to give and/or receive electrons, which they referred to as donor-accepter functionality. Ashcraft et al [119] also suggested that the stabilising efficiency is associated with the ionisation energy of the material. Although the concept of voltage stabilisers seemed to be promising at that time, voltage stabilisers were not applied in commercial cables at that time. This is

because the synthesised voltage stabilisers were soluble additives which are added at an early stage of the manufacturing into the polymeric insulator. After high temperature cross linking and degassing, the added voltage stabiliser would react with radicals, which results in a loss of their donor-accepter functionality [120]. To overcome this limitation, in 2004 Martinotto et al [118], synthesised benzophenone based voltage stabilisers, based on the positive effect of alkyl chains on the electrical properties of polyolefin reported previously by Takahashi et al in [121]. The voltage stabilisers manufactured by Martinotto et al [118] are benzophenone compounds that contains an alkyl chain attached to the phenyl ring of the benzophenone. Martinotto et al [118] suggested that the alkyl chain may comprise of a different number of CH_2 groups (different length) and these chains could be attached to the phenyl ring of benzophenone compound directly and/or through multiple oxygen bridges. The voltage stabilisers produced by Martinotto et al [118] were proved to be capable of retaining their functionality after cross linking and degassing. The voltage stabilisers patented by Martinotto et al [118] have taken the field voltage stabilising addetives to a new level, where most of the voltage stabilisers produced afterwards were based on the concept developed by Martinotto et al in [118].

In an attempt to increase the efficiency of voltage stabilisers additives used in cross linked polyethylene XLPE, Englund et al [122] tested a set of voltage stabilisers that comprises of an alkyl chain (C_8H_{17}) linked to benzophenone derivatives. Englund et al [122] found that the addition of low amounts of the stabiliser (about 0.76 wt%) to cross linked polyethylene would increase the resistance of XLPE to electrical treeing by about 18.4 %, compared to that of neat XLPE. Englund et al [122] concluded that the presence of the aromatic structures in the benzophenone derivatives are the main factor influencing the efficiency of the tested additives. This conclusion was further investigated in [123], where Englund et al studied the effect of the number of the aromatic rings in the chemical structure of the voltage stabiliser on the efficiency of the voltage stabilisers. The voltage stabilisers used comprised of two, three and four aromatic rings within their chemical structure, where an alkyl chain (C_8H_{17}) was attached to the phenyl ring either through oxygen or via a nitrogen bond. The results of Englund et al [123] indicated a rise of up to 50 % in the electric tree inception field of XLPE at a voltage stabilisers loading of 0.4 wt%.

More recently, Jarvid [120] studied the effect of benzil-based voltage stabilisers on the inception voltage of electrical treeing in XLPE. The tested voltage stabilisers were also based on the concept of Martinotto et al [118], where the synthesised stabilisers contained a compound featured an aromatic structure (benzil derivatives) and varied length of alkyl chains. These alkyl chains were connected to the phenyl ring of the benzil group through amine, ester and ether groups. Jarvid [120] concluded that amine based voltage stabilisers were considered as the most effective compounds tested, as these additives suggested to indicate the highest measured increase in the inception voltage of electrical treeing in the tested XLPE systems. These findings support the results reported by

Englund et al [123], where amine containing voltage stabilisers were suggested to be the most efficient additives. In addition, Jarvid et al [124] showed that an increase of up to 70 % in the dielectric strength of XLPE can be achieved using benzil based voltage stabilisers that contains methyl group bonded to the core phenyl through tertiary amine or ester.

An explanation for the mechanism of voltage stabilising of aromatic based voltage stabilisers was discussed by Jarvid et al [120] and recently in [125]. It was suggested that the voltage stabilising effect of the additives discussed above is based on either the reduction in ionisation potential (difference in the ionisation potential between the additives and the host polymer) or the high electron affinity of the added voltage stabilisers.

The evolution of voltage stabilisers from the first introduced unstable agents in mid 1960s to agents with reported 70 wt% increase in dielectric strength was achieved by developing understanding of the effect of *functional groups*. The presence of functional groups such as alkyl chains and aromatic groups promoted the positive effect of voltage stabilisers and increased their efficiency. Since the functional groups of the reactive epoxy based modifiers (FNMs) may feature chemical structure similar to that of the voltage stabilisers (such as the alkyl chains and aromatic rings), it is possible to utilise these functional groups which were reported to have positive effect on the dielectric properties while attached to other agents such as in the voltage stabiliser case discussed above. The concept of voltage stabilisers reported here will be used in explaining the impact of the functional groups of the FNM on the electrical breakdown strength of the modified systems discussed in sections 6.1.5 and 6.2.5 of chapter 6.

2.5 Summary

Epoxy resins have been used in several applications. The performance of these application is governed by the efficiency of their insulating material. The curing process of ER occur through chemical reactions between the epoxide groups of the resin and the active molecule of the hardener. The process is more complicated when anhydride hardeners are used, where the curing process involves anhydride initiation, esterification and possible etherification reactions.

Two main approached are reported to alter the thermal, electrical and mechanical properties of epoxy resin systems, which are namely, fillers and modifiers. Nano and micro sized fillers are widely explored technology for modifying the properties of epoxy resins. A large number of studies have presented the beneficial effects of introducing fillers to ER. However, there are several factors such as the filler size, type and dispersion which may negatively affect the behaviour of resin composite. Contradictions were reported in literature regarding the beneficial effect of some types of fillers. Nanotechnology have been used to improve the properties of polymeric materials for decades. Nanocomposite

based improvement methods, using nano and micro fillers, are pushed to the limited, where even if the technology is promising, the technical process involved is becoming complicated.

As an alternative method to the use of fillers is to employ network modifiers. Additive modifiers have been used, mainly, to later the viscosity of epoxy resin systems. There are different types of resin modifiers including, reactive and non-reactive network modifiers. Epoxy-based network modifiers can alter the thermal and mechanical properties of the resins. Researches of the influence of epoxy based reactive modifiers on the electrical properties of epoxy resins are not well studied. Only few studies of the effect of epoxy based network modifiers on the electrical properties of the final material and in all of these studies the FNMs were treated as fillers without taking into account the ability of the FNM to react/consume the hardener through their epoxide groups i.e. change the stoichometry. The stoichiometric ratio is an important factor in designing the network structure using FNM, as it alters the network structure and the retained functional groups, which affect the properties of the material. By studying the effect of the FNM on the network structure on the epoxy resin, altering the architecture of the resin structure might be possible. This can be achieved by adapting the behaviour of some functional groups reported in literature such as the functional groups of voltage stabiliser.

Chapter 3

Material Processing and Samples Preparation

3.1 Introduction

Engineering a novel insulating material requires an understanding of the current technology. This will aid in achieving the objectives of the research and allow us to gauge the applicability of the results. The properties of the epoxy resin network are affected by the curing mechanisms. Epoxy resin systems cured using amine and anhydride hardeners have significantly different thermal, electrical and mechanical properties. The difference in the behaviour of amine and anhydride cured system is associated with the variation in the curing mechanisms related to each system, where the final cross-liked network would also change accordingly. Therefore, it is importance to study the effect of modifying the structure of cured resins using both amine and anhydride hardeners. The aim of this chapter is to introduce the basic materials (resin, FNMs and hardeners) used in this project in addition to the preparation methods utilised to manufacture the investigated samples.

3.2 Basic Materials

The basic material used in this research is a diglycidyl ether of bisphenol DGEBA based epoxy resin DER 332 supplied by Sigma Aldrich. The epoxide equivalent weight of the DER 332 is 172 - 176 g mol^{-1}, while the value of n= 0.026. The molecular structure of DER 332 features two terminal epoxide groups, one at each end of the chain, as shown in Figure 3.1.

The resin was cured using two hardeners: one amine based and one anhydride based hardener. The amine hardener used in this work is a polyetheramine material, obtained from Huntsman, which is commercially referred to as Jeffamine D-230. The chemical structure of Jeffamin is shown in Figure 3.2a. The amine hydrogen equivalent weight of Jeffamine is 60 g mol^{-1}. The anhydride hardener used is methyltetrahydrophthalic anhydride material, also supplied by Huntsman, with the commercial name Aradur HY925. The chemical structure of the anhydride hardener is shown in Figure 3.2b.

In addition to the resin and the hardeners, a third material is added to alter the structure of the epoxy system, which is the functional network modifier. The FNM used here are epoxy based modifiers, which can contribute in the curing process through their reactive

epoxide groups. The selection process of the FNM was based on several factors, such as the safety of the material, chemical composition, physical properties and tracked history in reviewed literature. The details of the selection process of the FNM used in this work is discussed in Appendix A.

Based on the FNM selection process, five different compounds were selected as the potential FNM to cover the applicable range of chemical groups. These potential FNM materials are:

- Glycidyl hexadecyl ether (GHE), which represents long chain alkyl functional groups.
- Glycidyl 4-nonylphenyl ether (GNPE), shows the effect of materials with aromatic structure.
- Trimethylolpropane triglycidyl ether (TTE), to demonstrate the effect of multiple terminal epoxide groups.
- Glycidyl polyhedral oligomeric silsesquioxane (GPOSS), to illustrate the impact of materials with POSS molecules.
- 1,2-Epoxycyclododecane (ECD), to show the impact of cyclic groups.

The chemical structure of FNM used in this thesis are presented in Figure 3.3, while the EEW, number of epoxide groups per molecule and the suppliers, are listed in Table 3.1. After the selection process, the five materials were used to alter the structure of amine and anhydride cured epoxy resins. The manufactured samples were then characterised using the different techniques (FTIR, DSC, dielectric spectroscopy, AC breakdown strength and DC conductivity described in chapter 4). The effect of ECD functional network modifier on the permittivity, the glass transition temperature, the conductivity and the AC breakdown strength of modified epoxy resin systems is reported in Appendix A section A.2.The data indicates that the cyclic groups introduced by the inclusion of ECD have no effect on the electrical properties of the modified system, consequently ECD modified systems were excluded. Therefore, this work will demonstrate the effect of modifying the structure of amine and anhydride cured resins using FNM containing alkyl, aromatic, POSS and multi-terminal epoxide groups.

3.3 Stoichiometric Formulation

The chemical structure of the amine hardener (Jeffamine) and the anhydride hardener (Aradur HY925) are presented in Figure 3.2. From the figure, it can be seen that the Jeffamine features two primary amine groups within its chemical composition, each secondary amine group can react with one epoxide group in the system, as was explained in

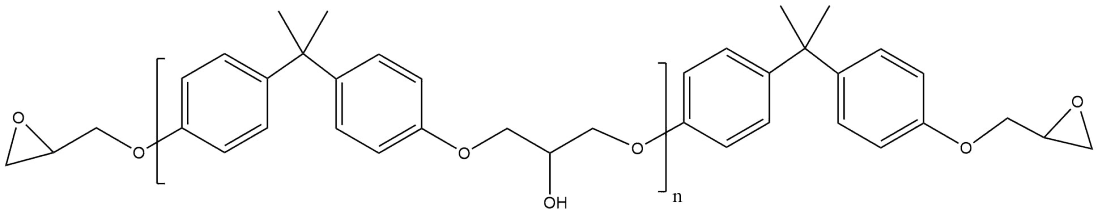

Figure 3.1: The chemical structure of a diglycidyl ether of bisphenol DGEBA based epoxy resin DER 332.

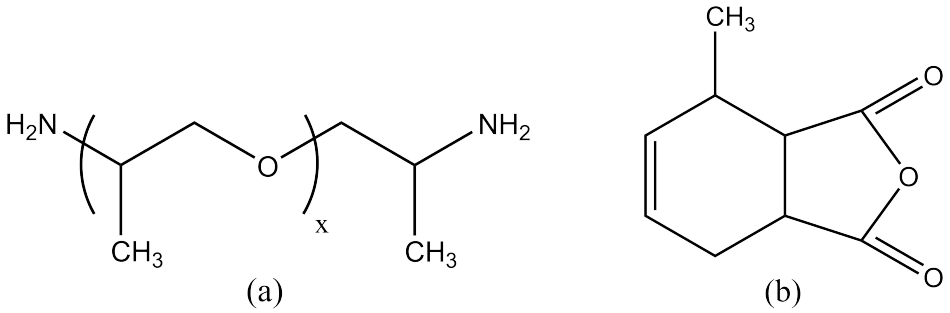

Figure 3.2: The chemical structure of the hardeners used in this thesis where (a) is the structure of a polyetheramine (Jeffamine D230, amine hardener) and (b) is methyltetrahydrophthalic anhydride (Aradur HY925, anhydride hardener)

Table 3.1: Key parameter of the functional network modifiers

FNM	Name Code	EEW ($g.mol^{-1}$)	Epoxy groups	Supplier
Glycidyl hexadecyl ether	GHE	298.50	1	Sigma Aldrich
Glycidyl 4-Nonylphenyl ether	GNPE	276.41	1	Sigma Aldrich
Trimethylolpropane triglycidyl ether	TTE	100.79	3	Sigma Aldrich
Glycidyl polyhedral oligomeric silsesquioxane	GPOSS	167.23	8	Hybrid Plastics
1,2-Epoxycyclododecane	ECD	182.30	1	Sigma Aldrich

the epoxy curing mechanisms section in chapter 2. Similarly after opening the anhydride ring and the formation of a carboxylic group, the intermediate compound, reacts with one epoxide group present in the system. Therefore, in both the amine and anhydride cured systems, there must be one epoxide group for each active group of the hardener. In the case of the neat (reference) samples, the only source of the epoxide groups is the DER 332 resin (which contains two terminal epoxide groups). Whereas, in the FNM modified systems, in addition to the epoxide groups of the resin, one or more epoxide groups are supplied by the functional network modifier. Therefore, to ensure that the

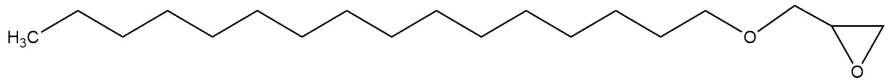

(a) Glycidyl hexadecyl ether (GHE)

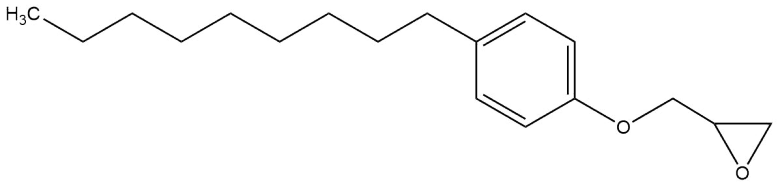

(b) Glycidyl 4-nonylphenyl ether (GNPE)

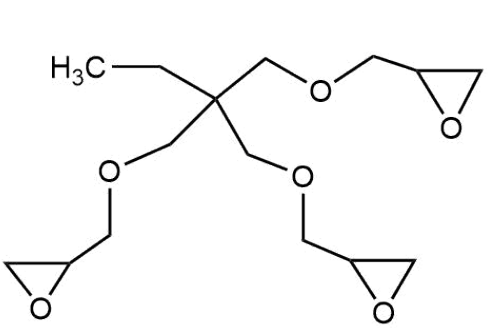

(c) Trimethylolpropane triglycidyl ether (TTE)

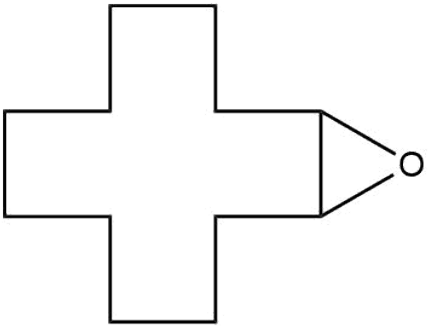

(d) 1,2-EpoxyCycloDodecane (ECD)

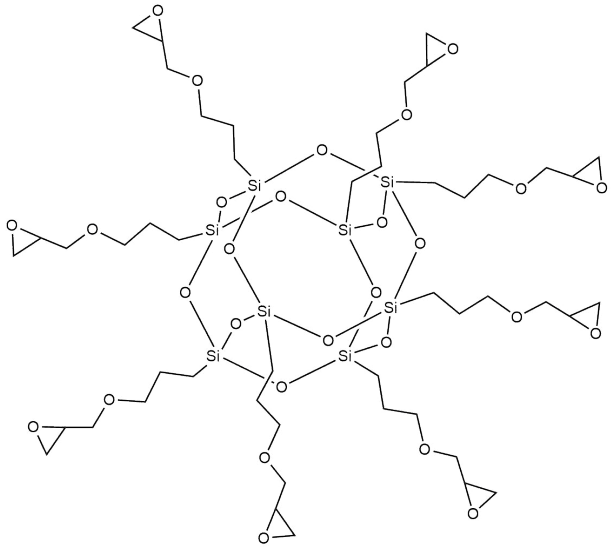

(e) Glycidyl polyhedral oligomeric silsesquioxane (GPOSS)

Figure 3.3: The chemical structure of the functional network modifiers.

number of epoxide groups (supplied by both the resin and the FNM) equals to the number of active groups of the hardener, the stoichiometric ratio of the samples has been calculated as follows:

- If the molar mass of DER 332 resins is M_e and the required resin mass is m_e, then the number of mols of epoxide from the resin N_e can be calculated by using 3.1.

$$N_e = m_e/M_e \tag{3.1}$$

- If the molar mass of the functional network modifier is M_r and the required FNM mass is m_r, then the number of mols of epoxide from the FNM N_r can be calculated by using 3.2.

$$N_r = m_r/M_r \tag{3.2}$$

- The total number of mols of epoxide groups is 3.3.

$$N_t = N_e + N_r \tag{3.3}$$

- The hardener with amine or anhydride molar mass of M_h has total number of moles of active groups N_h. For complete reaction, theoretically, all active groups from the hardener must react with all epoxide groups in the system i.e. N_h equals N_t. Then the required mass of hardener is calculated by using 3.4

$$m_h = M_h * N_t \tag{3.4}$$

3.4 Sample Preparation

The DER 332 has relatively high viscosity at room temperature (4000 mPa.s - 6000 mPa.s), therefore, it was recommended by the manufacturer to preheat the resin at 50 °C for at least one hour to reduce its viscosity. Thus, the first step to manufacture the samples was to preheat the resin. Then, the required mass of resin, modifier and hardener was weighed out, as calculated based on the method explained in the previous section. The resin and functional network modifiers were first mixed together using a magnetic stirrer. After 5 min of mixing, the hardener was added and mixing was continued for another 5 min, before the resultant mixture was degassed and cast into steel moulds. Finally, the mould was placed in a fan oven, where the sample was left to cure at specific curing regime according to the type of the hardener used to cure the system, where:

- The amine systems were cured at 80 °C for 2 h, then post-cured at 125 °C for 3 h, based on previous study [126].

- The anhydride hardened systems were cured, initially at 90 °C for 2 h, then at 150 °C for 4 h, as recommended by the manufacturer.

The produced samples, nominally 200 μm in thickness, were stored in vacuum (at about 1100 mbar) until use.

3.5 Sample Coding

The different formulation of samples were referred to according to Equation 3.5.

$$X(a)FNM \tag{3.5}$$

where X represents the molar percentage of epoxide groups in the system, which was derived from the relative FNM, the letter (a) signifies anhydride curing and FNM indicates the appropriate modifier. For example, 30AGHE is an anhydride cured resin, which has been modified by using 30 % of the epoxide groups from the GHE, while 30GHE code refers to amine cured systems with 30 % of the epoxide groups were supplied by the GHE modifier.

Chapter 4

Characterization and Experimental Techniques

To characterise and study the chemical, thermal, and electrical properties of the manufactured samples, six different techniques were used. These methods and techniques are, namely, fourier-transform infrared spectroscopy (FTIR), differential scanning calorimetry (DSC), dielectric spectroscopy, AC breakdown test, rheology test and DC conductivity. This chapter is set out to describe the experimental techniques used in this study, where the theory and data analyse are discussed.

4.1 Fourier-Transform Infrared Spectroscopy (FTIR)

4.1.1 FTIR Measurements Settings

FTIR spectroscopy is a technique used to characterise the chemical composition of a material by utilising the infrared part of the electromagnetic radiation. The concept of the infrared spectrometer is based on the change in dipole moment of the molecule which allows the material to become active in the infrared IR range, i.e the molecules in the system absorb a fraction of the incident IR beam [127]. The IR absorbance take place at specific characteristic frequencies. Thus, determination of the frequency of absorbance allows obtaining information about the molecule structure. In FTIR spectroscopy, the IR beam is subjected to a beam splitter which permits the generation of two identical beams. The two beams are then reflected through stationary and moving mirrors, where the aim of using the moving mirror is to generate a difference in the path length of the beams. Then the two beams are combined to yield an interferogram. The interferogram signal is passed through the sample and then collected by the detector. A time domain is generated for the signal by the detector, which was absorbed (reduced in intensity) by passing through the sample. Finally, Fourier transformation is used to decode the information to produce the spectra. The method used in this study is based on Attenuated Total Reflectance ATR-FTIR. In this approach, instead of using a beam splitter to divide the beam, an internal reflection element (a crystal) is used to apply the internal reflection phenomena. This means that the IR beam is passed through the crystal at an angle. The crystal is placed in contact with the sample of interest. The beam reflected from the internal surface of the crystal is directed to the detector.

In this work, ATR-FTIR iD7 Nicolet iS5 from Thermo-Scientific was used to obtain the FTIR spectra of the samples in transmission mode. A background check is first

conducted, which is then subtracted from the spectra of the sample.The aim of obtaining the FTIR spectrum is to assess the presence of the functional network modifier in the final system, i.e to ensure that the FNM have reacted with resin/hardener and survived the high temperature curing and post curing processes to become part of the final epoxy resin system.

4.1.2 FTIR Data Analysis

The OMNIC software package was used to collect the FTIR spectra. The collected data were normalised using, standard normal variate (SNV) method. The main reason for selecting the SNV method, is due to the fact that the ideal spectra for the modified systems is unknown, where the SNV can be used as a reference independent technique. Other methods which are frequently used for spectra normalisation, such as the internal standard method, require a non-changing peak available in all the samples to be used as a reference to track the variation in the absorbance [128]. In the case of the FNM modified systems, the presence of the FNM, reaction of the FNM with the hardener, the FNM loading (1 % to 30 %), and the removal of the epoxide groups after the inclusion of the FNM, are all factors that ensures variation in an FTIR absorbance peaks for the associated groups. This means that selecting a single reference peak associated with a certain chemical group, which feature the same absorbance peak in all the samples (neat and samples modified with 1 % to 30 % FNM) is not possible. Therefore, the use of methods based on internal reference peak (a peak that is common between all the samples) is not a feasible approach.

In the SNV method, the spectrum is subtracted from the average value and divided by the standard deviation. Equation 4.1 is the formula used in the SNV method, where x_{org} is the raw data, a_0 is the mean value of the spectrum and a_1 is the standard deviation. The SNV method removes the variations in the spectra associated with the thickness effect and the baseline curvature. Figure 4.1 shows a comparison between the raw data and the SNV normalised spectra.

$$X_{corr} = \frac{x_{org} - a_0}{a_1} \tag{4.1}$$

4.2 Glass Transition Temperature (DSC)

4.2.1 DSC Measurements Settings

Differential scanning calorimetry technique was used to, mainly, study the glass transition temperature of the manufactured samples. The principle of operation of the DSC

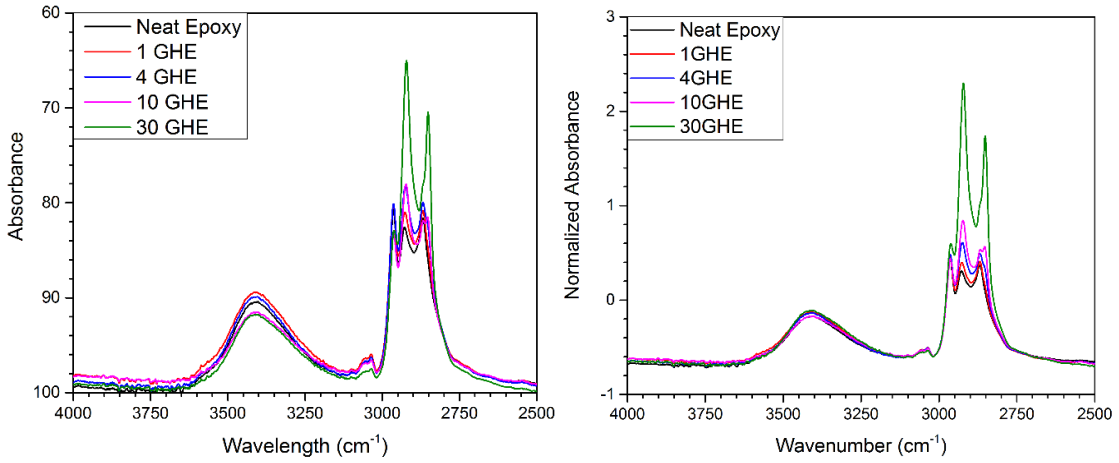

(a) Raw data

(b) SNV normalized spectra.

Figure 4.1: SNV normalisation of FTIR spectra for neat and modified samples

is based on measuring the difference in the heat flow through two materials, one of them has known thermal properties [129]. In the present work, a Perkin-Elmer DSC7 was used to measure the T_g of the samples. A mass of about 10 mg of a sample was weighted out and placed in an aluminium can, which was sealed and placed inside the equipment. Before placing the sample in the DSC, the device was calibrated. Standard calibration procedure was used each time before conducting the experiment. A reference material, which is a high purity indium with mass of about 4.5 mg and melting temperature of 156.6 °C is placed on one side of the DSC7 and an empty can on the other. A heating rate of 10 °C/min was applied for the calibration, which was later used for characterising the samples. After calibration, the indium is replaced by the sealed sample and the behaviour of the heat flow through the sample was recorded. Both the calibration and the experiments were conducted under nitrogen atmosphere to enhance heating/-cooling capabilities, avoid condensation at low temperatures and prevent oxidisation in high temperature measurements. Each sample was characterised using two heating scans with the same heating rate (10 °C/min), with the aim of the first scan to heat the sample above its T_g to remove the thermal history (effect of previous heating/cooling rate on the T_g of the material). Removing the thermal history for the samples ensure reproducible thermal characteristics.

4.2.2 DSC Data Analysis

The glass transition temperature (T_g) is defined as the range of temperatures where the segmental motion of a polymeric chain become active, which was limited to vibrational motion below the T_g. It can also be defined as the temperatures at which the material phase transforms from a glassy state (noncrystalline, rigid and mechanically solid) to a rubbery state [130]. The glass transition temperature is important, as it defines the

thermal operation limit of the epoxy based material and its application. The glass transition temperature can be determined using the heat flow through the material measured by DSC, and can also be seen in the dielectric relaxation of the material. Since the T_g is a thermo-dynamic transition, a heat capacity jump take place around the glass transition temperature in the heat flow data. There are several methods, which can be used to calculate the T_g from the temperature scan data obtained by the DSC, the most commonly used techniques to find the value of T_g are:

- Half-height of the heat capacity method. In this technique, the value of the T_g is defined as the middle point at the heat capacity jump in the temperature scan.
- Inflection point method. In this approach, the T_g is the determined by the peak point in the derivative of the temperature scan.
- The T_g may be defined as the average value of the range of temperatures along the heat capacity jump in the DSC data.

All these methods are valid but might produce slightly different values. In this work, the value of the glass transition temperature was determined by using the inflection point method. The inflection point method was selected because the T_g corresponds to the peak of the first derivative of the temperature scan data, while other parameters such as the width of the glass transition process (which is sample dependent) has limited impact on the T_g.

4.3 Dielectric Spectroscopy

The dielectric spectroscopy (DS) of the material represents a powerful method for monitoring dipole movement and molecular chain behaviour. The dielectric response can be measured as a function of time, frequency and/or temperature. Therefore, dielectric spectroscopy can be used to observe a wide range of the dynamic properties of the material [129]. The dielectric spectra are a measure of the interaction between the applied electric field and material's dipole moment, which is usually expressed as the complex permittivity. The measured permittivity is a complex term with real part (in phase with the electric field) and imaginary part (90° lagging the electric field) which can be expressed by Equation 4.2.

$$\varepsilon^* = \varepsilon' - j\varepsilon'' \tag{4.2}$$

The term ε' is the real part of the complex permittivity which represents the energy storage, and is usually known as the relative permittivity of the material. The imaginary ε'' part of the complex permittivity characterises the energy losses in the dielectric

material. In addition to the real and imaginary parts of complex permittivity, the loss tangent $\tan(\delta)$, is derived from the two parts of the complex permittivity, which is also known as dissipation factor, as can be expressed according to Equation 4.3.

$$\tan(\delta) = \frac{\varepsilon''}{\varepsilon'} \tag{4.3}$$

The dipole movement depends on the frequency of the external electric field. The dielectric spectroscopy measurements of an epoxy resin system may allow observing three different types of relaxation processes, namely, α, β and γ relaxations. The behaviour and molecular origin of the α, β and γ relaxations will be discussed in details through out the dielectric spectroscopy sections in each chapter of this thesis.

4.3.1 Room Temperature Measurements

In this work, the dielectric response of the samples was measured using SI 1260 impedance / gain-phase analyser and 1296 Solartron Dielectric Interface combined with a test cell. An equivalent circuit diagram of the experimental setup is shown in 4.2, while the equations associated with the setup which were used to calculate the impedance ($Z_s^*(w)$) of the samples are presented in equations 4.4 to 4.6. The dielectric measurements were conducted at room temperature using parallel electrodes with 30 mm diameter, which incorporates a guard ring. The studied samples were with 200 μm thickness. In order to improve the contact between the sample and the electrode, the samples were gold coated. An EMITECH K550X coater was used to sputter 30 mm diameter gold electrodes on two opposing surface of each sample. The deposition current was set at 25 mA for 3 min, which generated a gold layer with resistance about 10 Ω [131]. Samples dimensions are measured manually and entered in software package called SMART. The experimental setup was programmed to collect the dielectric response for frequencies ranging from 10^{-1} Hz to 10^6 Hz. The applied AC signal have an amplitude of 1 V_{rms}, which was found to produce low experimental noise. Before conducting the experiment, the equipment was left to warm up for about 60 min and a reference sample of fused silica was used to ensure that the equipment is running within the accuracy of <0.2 %. The value of the equipment accuracy was established using the impedance chart of the Solartron, obtained from the device data-sheet provided by the manufacturer.

$$I_s = \frac{V_2(w)}{R} \tag{4.4}$$

$$w = 2\pi * f \tag{4.5}$$

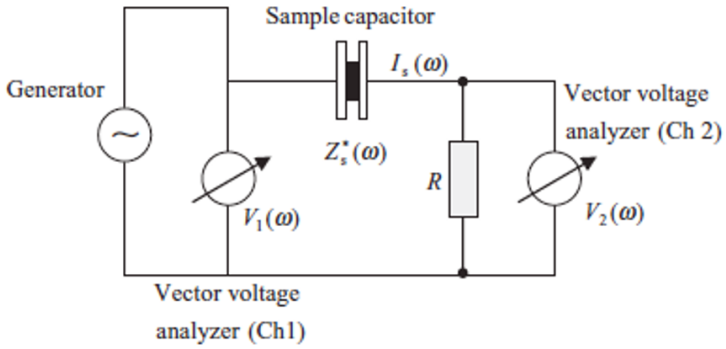

Figure 4.2: Equivalent circuit diagram of the dielectric spectroscopy setup.

$$\varepsilon^*(w) = \frac{-i}{wZ^*(w)C_0} \tag{4.6}$$

4.3.2 Temperature Dependent Measurements

In addition to the room temperature measurements, a cryostat test cell was connected to the SI 1260 impedance/gain-phase analyser via the 1296 Solartron Dielectric Interface to study the temperature dependent behaviour of the samples. The Janis-Research STVP-200-XG cryostat test cell includes a sample holder which is kept in a chamber with controlled temperature and pressure. The chamber's wall consists of two layers, the inner layer acts as a temperature exchanger area, cooled through liquid nitrogen. The temperature of the chamber is controlled through thermal radiation. In addition, two thermocouples are located inside the chamber at the sample mount. These thermocouples are used to maintain the temperature inside the chamber within the set values. Usually the chamber is filled with helium gas for measurements below 20 °C to prevent condensation of air. The measurements in this work was conducted for temperatures between -160 °C and 200 °C.

4.3.3 Dielectric Spectroscopy Data Analysis

The frequency-dependent dielectric susceptibility of materials at a given temperature, T (in kelvin), can be described by the product of a real amplitude factor and a complex shape function, with the imaginary (loss) component $X''(\omega,\mathrm{T})$ being given [132] by Equation 4.7.

$$X''(\omega, T) = X(0, T)F[\frac{\omega}{\omega_P(T)}] \tag{4.7}$$

In the above Equation 4.7, $X(0,T)$ is the susceptibility amplitude factor, $F(\frac{\omega}{\omega_P(T)})$ is the frequency-dependent imaginary component shape function with w being the angular frequency (2πf) and $w_p(T)$ the temperature dependent characteristic relaxation frequency (which corresponds to the frequency of the peak in the imaginary response component). Because the frequency appears in the shape function relative to the characteristic relaxation frequency, the time-temperature superposition principle can be used to normalise the dielectric data and facilitate the calculation of activation energy values of the different relaxation processes. In this method, the real and imaginary parts of the complex permittivity were first plotted using a log-log representation, with temperature as a parameter. A convenient reference point (X) on the frequency axis was then selected on a reference plot at a chosen temperature. Then, the frequency spectra of the next temperature is brought into alignment with the reference plot and the new coordinates corresponding to the point X are marked. This procedure is repeated for all the temperature plots, where the position of X is recorded for each temperature. The outcome is a master curve of the imaginary component of the susceptibility, where the frequency is scaled relative to $w_p(T)$ and the shift in position of X along the frequency axis, known as the translation or shift factor, given by Equation 4.8, where T_r is the chosen reference temperature.

$$logw_p(T_r)/w_p(T) \tag{4.8}$$

This is used to determine the temperature dependence of the characteristic relaxation frequency without having to identify a feature of the loss functions such as a peak, which may be very difficult for peaks with a broad frequency dependence. A similar procedure using the amplitude axis can be used to obtain the temperature dependence of the amplitude factor $w(0,T)$. The values obtained for Equation 4.9, are plotted against $1/T$, and the final shape of the graph is then assessed to check its compliance with Arrhenius behaviour. Finally, the Arrhenius Equation 4.10:

$$w_p(T)/w_p(T_r) \tag{4.9}$$

$$w_p(T) = v_0 exp(-E_a/kT) \tag{4.10}$$

where E_a is the activation energy, v_0 is the Arrhenius frequency factor and k is the Boltzmann constant, is used to determine the activation energy of any characteristic active process.

4.4 AC Breakdown Strength

4.4.1 Breakdown Measurements Settings

The AC breakdown (ACBD) test is a measure of the withstand voltage of an insulating material. The breakdown strength voltage is the potential difference which generates enough electric stress to cause dielectric failure in the insulating material. In this work, the breakdown strength of the epoxy resin was measured by applying an increasing amplitude of an AC voltage at 500 V/s rate of rise at constant frequency of 50 Hz. The ACBD strength was measured using Phenix Type 600C according to the ASTM D149-87 standard. The test cell has two steel spherical shaped ball bearing electrodes, each have a diameter of 6.32 mm. The electrodes were placed opposite to each other and held horizontally, immersed in silicon oil, to prevent surface flashover throughout the experiment. These electrodes were changed every 10 tests to prevent pitting from effecting the measurements.

4.4.2 Breakdown Data Analysis

Since the breakdown phenomenon is statistically distributed by nature, where there is no single value represents the breakdown strength of a test. The data obtained from the breakdown test require analysis using statistical distribution function. Weibull distribution is often used to provide an in depth analysis of the breakdown data. The Weibull probability distribution function can be mathematically expressed by Equation 4.11 [133].

$$F(E,\eta,\beta) = 1 - e^{-(\frac{E}{\eta})^{\beta}} \tag{4.11}$$

where E is the electric field, η is the scale parameter and β is the shape parameter. $F(E,\eta,\beta)$ is the cumulative probability of failure at E, identified by using two parameter (scale and shape), assuming the location parameter to be zero, hence referred to as two parameter Weibull distribution. The Weibull distribution is commonly used with 90 % or 95 % confidence bounds [134]. The scale parameter η related to value of the field where the probability of failure is $1 - e^{-1}$ or 63.2 %, where the parameter β describes the shape of the breakdown strength data. As the description of the data using values is quite complicated, the breakdown strength data are usually visualised by plotting the Weibull distribution data after reformatting Equation 4.11 as expressed in Equation 4.12

$$log\lceil -ln(1 - F(E))\rceil = \beta log(E) - \beta log(\eta) \tag{4.12}$$

Generally, Bernard's approximation 4.13 is applied to the data obtained from the cumulative probability for approximation, where n the total number of breakdown tests and i is the rank of each data point [133].

$$F(E_i) = \frac{i - 0.3}{n + 0.4} \tag{4.13}$$

where i is the order of the breakdown field sorted in an ascending order, and n is the number of tests performed. The breakdown strength data analysed used two parameter Weibull distribution with 90% confidence bounds, where the confidence bounds provide more accurate description for the probability of material breakdown.

4.5 Viscosity Measurements

A rheometer with a cylindrical cup was used to measure the viscosity of the epoxy resin samples in the liquid phase. To check that the equipment is running correctly, the test was first conducted for a material with a known viscosity. Then, the FNM was weighted out, where the total mass of the component was calculated and kept at 20 ml. Next, the FNM was added to the resin, both mixed for 5 min using a magnetic stirrer before adding the hardener. After another 5 min of mixing, the three element mixture was poured into the sample holder cell of the rotational viscometer. The measurements were conducted at room temperature using a Reholab MC 1 rheometer. The rotation was first set to ramp from 1 to 20 Pa, then the rotation speed was kept constant for 20 s, after that the speed was set to ramp down to zero according to standard ASTM D1084-16.

4.6 Electrical Conductivity

The conductivity of the materials were characterised using simple two-probe test methods. The coated samples were placed between two parallel electrodes fixed in horizontal position, where the voltage was applied perpendicular to the plane of the samples. An equivalent circuit diagram of the DC conductivity experiment set up is shown in Figure 4.3.

The electrodes were two aluminium disks, 50 mm in diameter, connected to a constant DC power supply. The samples holder incorporates a guard ring. A Keithley 485 current meter was connected in series with the sample. In addition, in case of sample failure to ensure that the applied current does not exceed the maximum limit of the current meter, protection resistor (90 MΩ) is connected to maintain the current below 20 mA. An electric field of 40 kV/mm was applied to measure the conductivity of the samples. All the measurements were time dependent and were conducted according to the standard ASTM D257-07 at room temperature.

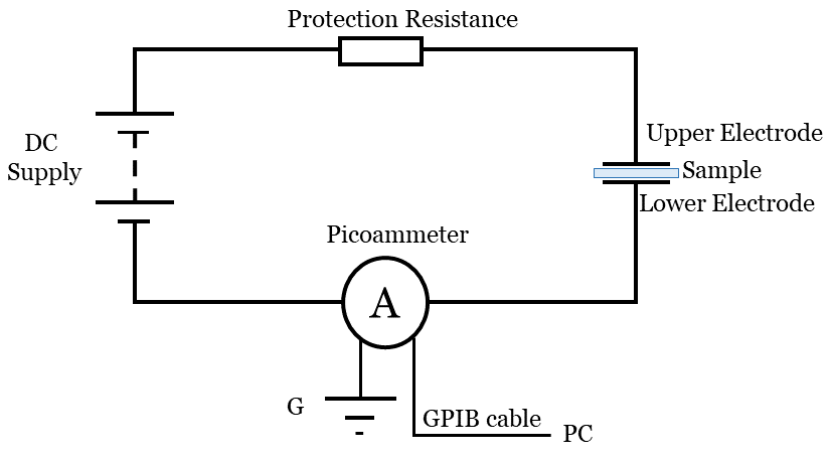

Figure 4.3: Equivalent circuit diagram of the conductivity experiment setup.

Chapter 5

Investigation of the FNM loading on the stoichiometric ratio of epoxy resins and their dielectric properties

Generally, the properties of an epoxy resin system are governed by the structure of its amorphous network. In this research, the network structure of epoxy resin systems was varied by introducing functional modifiers, which can contribute to the curing process and become part of the resin network through their epoxide groups. This chapter, investigates the effect of the stoichiometric ratio of FNM modified epoxy resins on the dielectric properties. Subsequently, an FNM was introduced into a simple amine cured epoxy resin system by using two methods. In the first approach, the FNM was added by considering and precisely calculating the number of the epoxide groups being supplied by the FNM, where the equivalent number of epoxide groups provided by the resin are removed, ensuring the same number of epoxide groups present in the system after the addition of the FNM. The samples were manufactured with different loading of epoxide groups supplied by the GPOSS (1 EG%, 4 EG%, 10 EG% and 30 EG%). The stoichiometric ratio of these samples were calculated such that each active group from the hardener would react with one epoxide group available in the system (supplied by either the resin or the GPOSS).

In the second approach for studying the influence of the stoichiometry of FNM, the GPOSS was added by weight percent (1 wt%, 4 wt%, 10 wt% and 30 wt%) without changing the stoichiometry of the resin system. In this method, the samples were modified with GPOSS where the reactive epoxide groups of the GPOSS were not included in the stoichiometric calculation of the samples. The system with epoxide groups replaced with reactive parts of the GPOSS are referred to as *epoxide compensated* systems, while the samples with GPOSS added without changing the stoichiometry of the system are called *epoxide uncompensated* systems.

The *epoxide compensated* systems are referred to as xEG% GPOSS, where x is the number of epoxide groups supplied by the GPOSS. The *epoxide uncompensated* systems are referred to as xwt% GPOSS, where x is the weight precent of the GPOSS.

Testing the hypothesis, which states that the effect of the functional network modifiers on the different properties relies on the calculation of the reactive moieties, which contribute to the chemical curing reactions. The chemical composition for both epoxide compensated and uncompensated systems was investigated using FTIR spectroscopy. Then, the influence of the stoichiometry on the glass transition temperature was established. The AC breakdown strength of the two systems of interest were discussed. The results of the dielectric spectroscopy of the epoxide compensated and uncompensated

resins was evaluated. Finally, an investigation was conducted to test the hypothesis regarding the appropriate number of the epoxide groups in the GPOSS.

5.1 FTIR Spectroscopy

The FTIR measurements were obtained to show the changes on the molecular level over the accessible range from 4000 cm^{-1} to 500 cm^{-1}. The FTIR spectra of interest for all the samples are presented in Figure 5.1. In addition, a detailed comparison is presented in the sections of Figure 5.2, while the complete FTIR spectra for all the systems are shown in Figure C.1 in Appendix C. From Figure 5.1, it can be seen that the addition of GPOSS resulted in variations in the absorbance levels of the modified systems compared to the reference material. In these spectra, there are three main regions of particular interest, which are around 3400 cm^{-1}, from 1140 cm^{-1} to 1080 cm^{-1} and from 970 cm^{-1} to 915 cm^{-1}, which are associated with hydroxyl OH groups [135–137], Si-O-Si stretch [111, 138–143] and epoxy group deformation [144–148].

In the curing process, epoxide groups from both the resin and the FNM react with primary/secondary amines of the hardener. This curing reactions generates an OH groups and a secondary/tertiary amine group. After the addition of the GPOSS, the intensity of the band associated with OH groups appears to be affected by the stoichiometric ratio of the system. In the case of the compensated systems, the compensation of the epoxide groups with similar groups from the resin resulted in an insignificant variation in the extent of the band associated with OH groups, as shown in Figure 5.2(a). On the other hand, in the case of the uncompensated system, the extent of the band related to OH groups decreases as the loading of the GPOSS increases, as shown in Figure 5.2(b). This decrease in OH contents might be associated with the reduced cross-linking reactions between the epoxide groups and the hardener such that fewer OH groups are generated.

The spectral region from 1140 cm^{-1} to 1080 cm^{-1} is associated with the presence of Si-O-Si groups, where the addition of GPOSS resulted in increased absorbance in the region for both compensated and uncompensated systems as shown in Figure 5.2(c) to Figure 5.2(f). Generally, the addition of the GPOSS resulted in inclusion of Si-O-Si groups into the modified structures, which can be clearly seen from the associated FTIR bands.

Figure 5.2(g) and Figure 5.2(h), show the spectral range for the epoxy hydrogen bonding interacting region. The spectra of the systems with compensated stoichiometry showed insignificant variation in the epoxide groups after the addition of GPOSS. While, the introduction of GPOSS to the system without changing the stoichiometric ratio resulted in an increase in the number of unreacted epoxide groups.

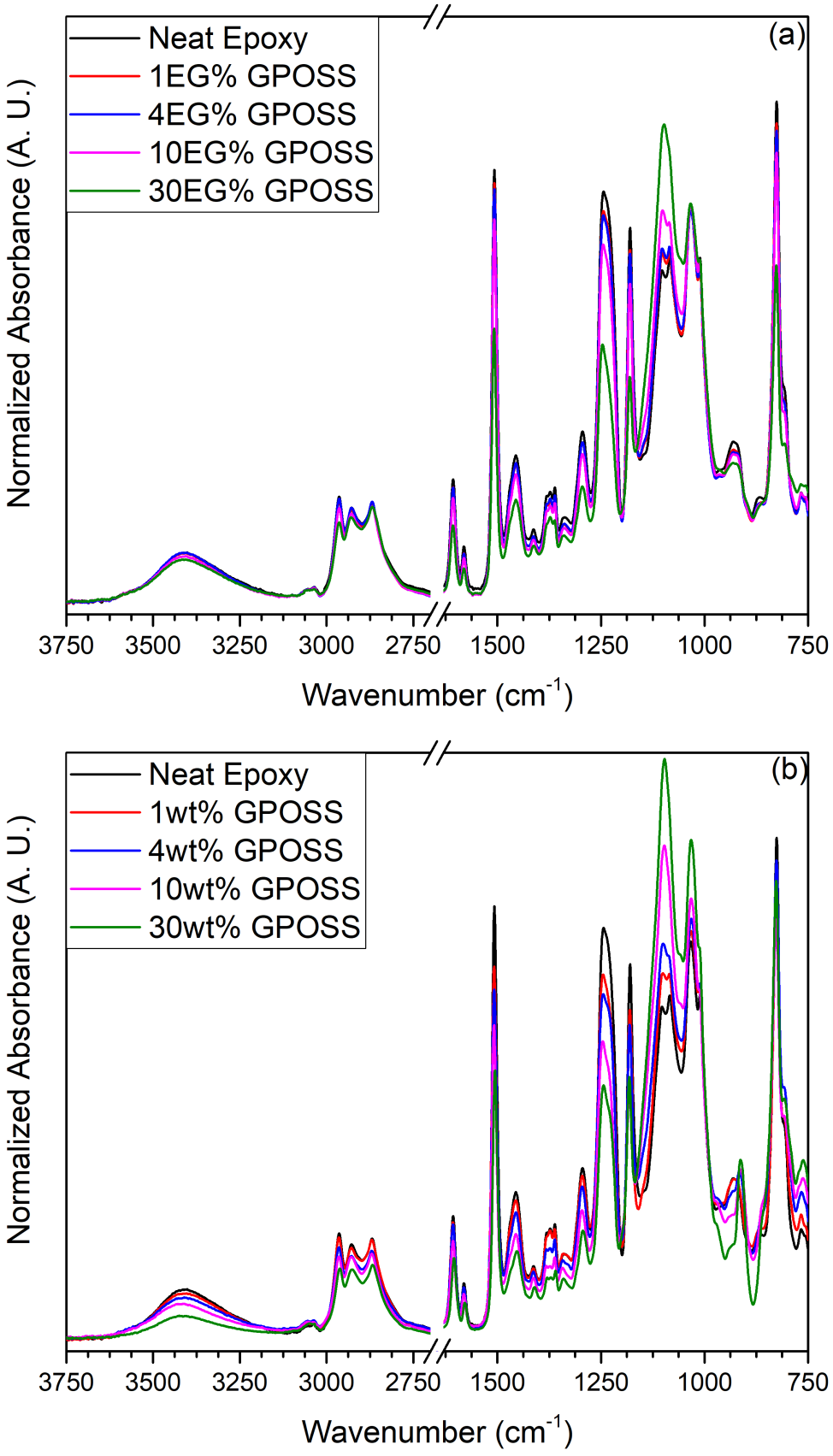

Figure 5.1: FTIR spectra of reference and GPOSS modified systems with (a) compensated stoichiometry, and (b) uncompensated stoichiometry.

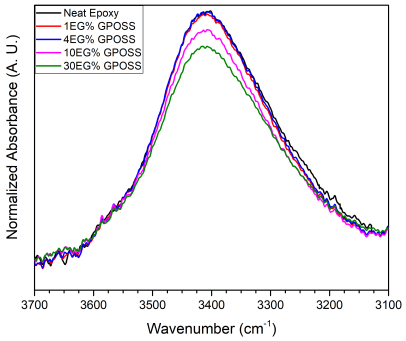

(a) Hydroxyl OH absorbance region for GPOSS compensated systems

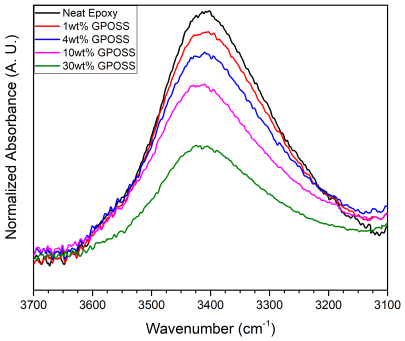

(b) Hydroxyl OH absorbance region for GPOSS uncompensated systems

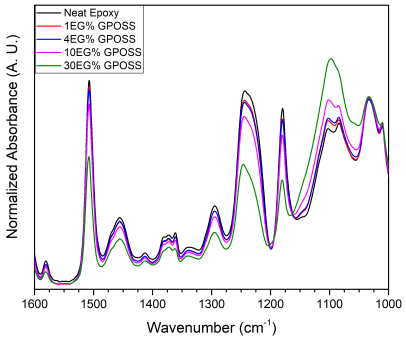

(c) Absorbance from 1600 cm^{-1} to 1000 cm^{-1} for GPOSS compensated

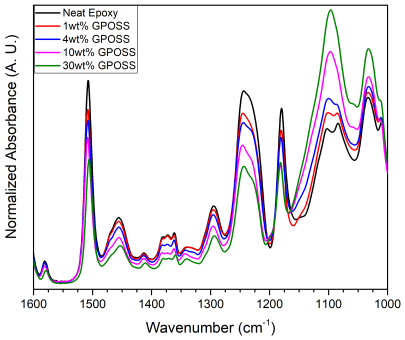

(d) Absorbance from 1600 cm^{-1} to 1000 cm^{-1} for GPOSS uncompensated

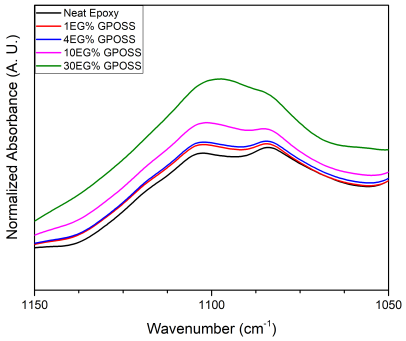

(e) Ether peaks for GPOSS compensated systems

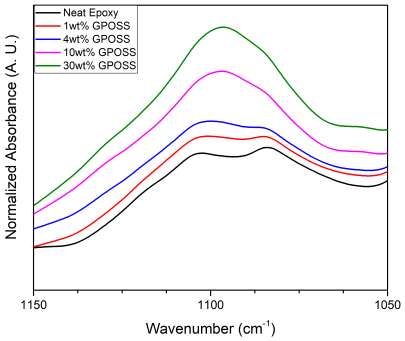

(f) Ether peaks for GPOSS uncompensated systems

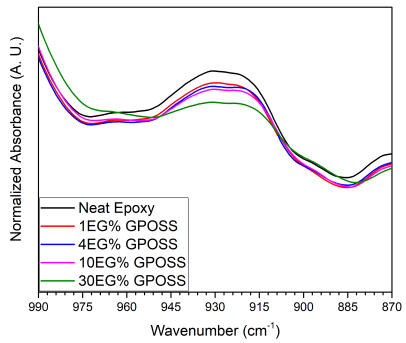

(g) Epoxy region for GPOSS compensated systems

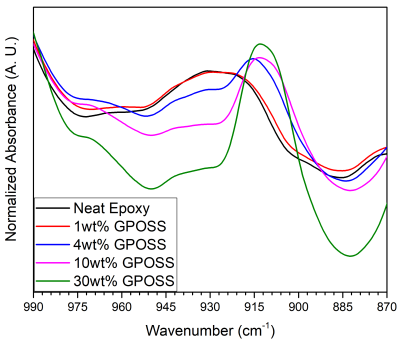

(h) Epoxy region for GPOSS uncompensated systems

Figure 5.2: Main regions of the FTIR spectra for reference and GPOSS modified systems.

To sum up, the FTIR spectra of compensated systems indicated that the addition of the GPOSS resulted in insignificant variation in both the hydroxyl groups and the epoxide groups, in addition to an increase in the Si-O-Si absorbance band. In the case of the uncompensated systems, the inclusion of the GPOSS resulted in producing a system with high number of unreacted epoxide groups and low cross-link density indicated by the reduced hydroxyl groups.

Table 5.1: Formulation of the reference and GPOSS modified systems.

Material System	Resin (g)	FNM (g)	Hardener (g)	FNM wt%[1]
Neat Epoxy	7.45	0.00	2.55	0
1 EG%	7.38	0.07	2.55	0.7
4 EG%	7.15	0.29	2.56	2.9
10 EG%	6.73	0.71	2.56	7.6
30 EG%	5.26	2.16	2.58	27.6
1 wt%	7.45	0.10	2.55	1
4 wt%	7.45	0.40	2.55	4
10 wt%	7.45	1.00	2.55	10
30 wt%	7.45	3.00	2.55	30
6GGPOSS	4.91	2.68	2.41	36.6
8GGPOSS	5.26	2.16	2.58	27.6
10GGPOSS	5.51	1.80	2.69	22

[1] FNM wt% is calculated by considering the mass of the GPOSS with respect to the total mass of polymer (resin mass and hardener mass).

5.2 Differential Scanning Calorimetry

The influence of the stoichiometric ratio on the glass transition temperature of the GPOSS modified systems is recorded by means of DSC. Figure 5.3 presents the DSC traces of epoxy resin systems modified by the addition of GPOSS, where in Figure D.5(a) the reactive groups of the GPOSS were considered when calculating the theoretical stoichiometric ratio of the sample, while in Figure D.5(b) the data obtained for the samples where the GPOSS was added on top of the theoretical ratio of the reference systems by weight percent. The different formulations used to produce the reference and GPOSS modified systems studied in this chapter are listed in Table 5.1. In addition, the values of the T_g calculated by the inflection point of the DSC traces (the transition point in the derivative of the heat flow curve) for both compensated and uncompensated GPOSS modified systems are listed in Table 5.2. The DSC data indicates that the width of the glass transition region is varied affected by the sample composition. Therefore, it was necessary to calculate the width of the T_g of the compensated and uncompensated systems, as presented in Table 5.2.

In the case of the compensates systems, it can be seen that the addition of 1%, 4%, 10% and 30% of the epoxide groups from the GPOSS, resulted in decrease in T_g by about

0.4 °C, 0.9 °C, 5.2 °C and 9.6 °C respectively, compared to the T_g of the neat epoxy. While the addition of comparable weight percentages (1%, 4%, 10% and 30%) of the GPOSS without chaining the stoichiometric ratio resulted in shifting T_g to lower values by about 2.1 °C, 3.7 °C, 6.7 °C and 27.8 °C respectively, compared to T_g of the neat epoxy.

The chemical structure of the GPOSS comprises of arm chains terminated with epoxide groups radiating from a central core of polyhedral oligomeric silsesquioxane (POSS). Therefore, the GPOSS contributes to the curing process through its epoxide groups, where after the cross-linking, the GPOSS become integrated into the resin matrix. As the epoxide groups of the GPOSS reacts, the non-reactive functional groups (POSS cage-like structure) become retained within the system generating network nodes incorporated into the molecular structure, which would consequently impact the network topology.

In the case of the compensated systems, the variation in the T_g resulted from the inclusion of the GPOSS modifier may be associated with a number of factors. The first factor could be the free volume in the system, where a significant amount of work has been reported in the literature concerning the relationship between the T_g and the free volume in the resin network [47, 100, 149, 150]. In the current study, the inclusion of the GPOSS modifier resulted in forming a branched network structure, where the POSS functional groups become retained within the network. These branches and nodes may have altered the network topology and the associated free volume in the system. Therefore, it may be suggested that the T_g of the modified systems may be related to the change in the free volume in the system. However, Hao et al. [151] suggested that the presence of POSS molecules in POSS-rich polymeric network would result in reduced free volume in the networks, while Raftopoulos et al [152] concluded that POSS molecules influence the T_g of the host polymer by performing as immobile units in the system rather than introducing free volume. Therefore, it can be suggested that the variation in the T_g reported here for the GPOSS modified systems may be influenced by factors other than the free volume in the system. These findings are in good agreement with the behaviour of the T_g reported for epoxy resin systems modified by the inclusion of different POSS based modifier (Triglycidylisobutyl-POSS (TGIB-POSS) [110], octaepoxy-POSS [111] and octa(aminophenyl)silsesquioxane [153].

The data of the compensated systems presented in Table 5.2 indicates that systems containing 1 % to 10 % of the epoxide groups from the GPOSS exhibited T_g comparable to the T_g of the neat systems (up to 5 ±2 °C). However, the addition of 30 % of the epoxide groups from the GPOSS resulted in a significant reduction in T_g (9.6 ± 2 °C). For low GPOSS loading, Lee and Lichtenhan [154] reported improved T_g of modified resin systems, which they associated with the presence of the cage-like structures of the POSS, while Liu et al [143] suggested that the POSS molecules can improve the thermal stability of the resin system by restricting the chain mobility. On the other hand, Heid et al [109] suggested that high loadings of GPOSS (about 20 wt%) were reported to shift

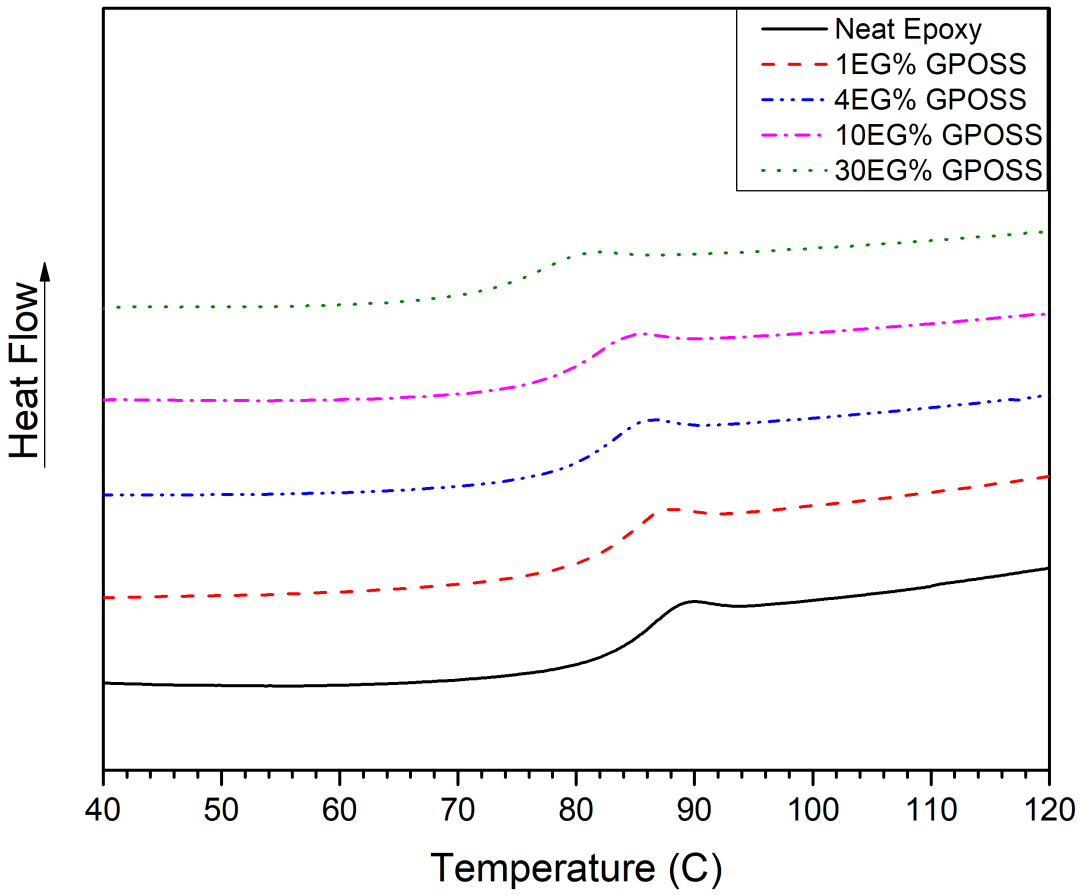

(a) DSC data for reference and GPOSS modified epoxide compensated systems.

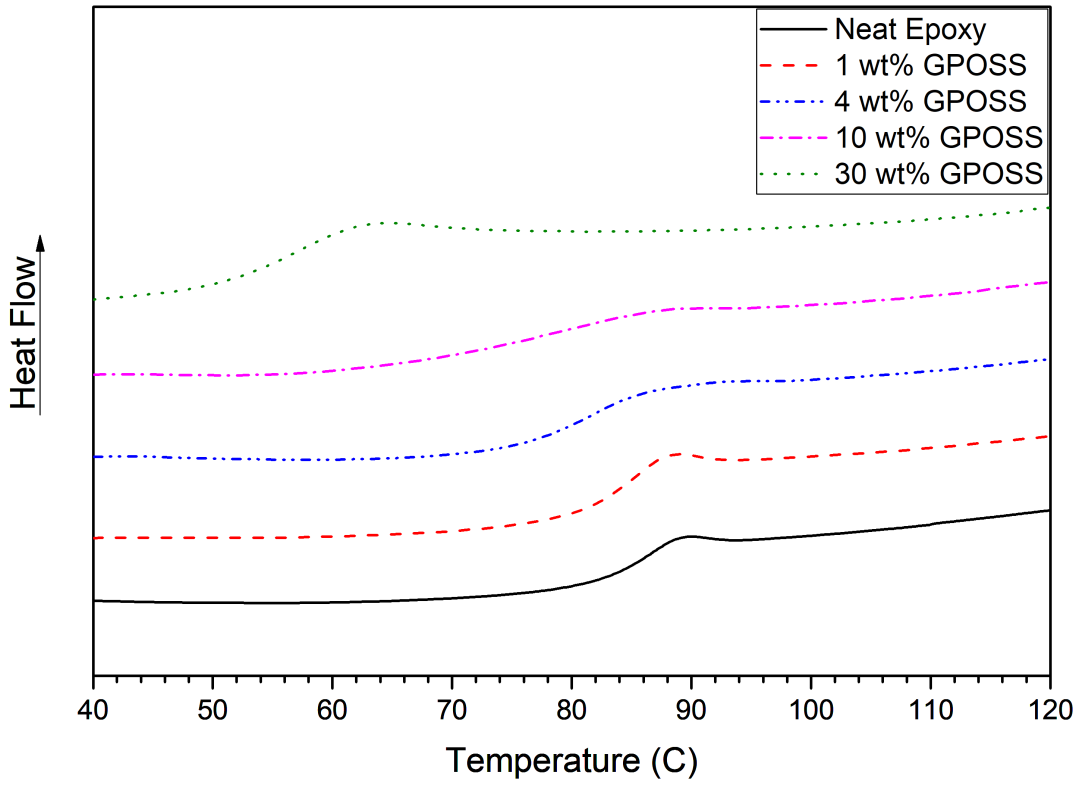

(b) DSC data for reference and GPOSS modified epoxide uncompensated systems

Figure 5.3: DSC traces for reference and GPOSS modified systems.

Table 5.2: DSC measurements for reference and GPOSS modified epoxy systems..

Sample	Compensated systems		Uncompensated systems	
	T_g(°C)	Width of T_g (°C)	T_g(°C)	Width of T_g (°C)
Reference	85.3	18	85.3	18
1%	84.9	19	83.2	21
4%	84.4	20	81.6	28
10%	80.1	22	78.6	41
30%	75.7	24	57.5	45

Error in Tg = ±2 °C

T_g to lower values (reduced by 7 °C). The reduction in the T_g noticed by Heid et al [109] was explained by the high chain mobility resulted from the reduced cross-linking density of the modified systems, where the inclusion of high loading of GPOSS suggested to generate regions at which the POSS molecules may have reacted with each other which resulted in the present of local crystalline regions. Similarly, Florea et al [155] proposed that in a system with sufficient number of POSS molecules, POSS groups would interact with each other forming localised agglomeration regions. From the above account, it is possible to suggest that the variation in the T_g of the compensated systems may be related to two competing processes, which are, namely, the effect of the POSS molecule of the thermal behaviour of the material and the variation in the cross-linking density caused by the interaction between the POSS molecules. At low GPOSS contents, the effect of the POSS retained functional groups dominate; However, the inclusion of high concentration of GPOSS promotes the probability of the interaction between its POSS functional groups.

It should be pointed out that in producing the compensated systems, the addition of the GPOSS modifier is combined by removal of the relative number epoxide groups from the resin with their associated aromatic groups (as illustrated in Table 5.1). In a DGEBA molecule there is about, one aromatic ring per epoxide group. According to Neville and Lee [3], aromatic groups influence the glass transition temperature of the epoxy resin, where systems with reduced aromatic contents are reported to have deteriorated thermal behaviour. Bacosca et al. [156] suggested that the glass transition temperature is related to the number of aromatic rings available in the system, while Ramirez et al [111] explained that the presence of aromatic groups in the polymeric structure hinders the segmental rotation motion during the glass transition process, which would shift T_g to higher temperatures. From the above studies, it can be suggested that the aromatic contents in the system is another factor that contributes to the variation in the glass transition process reported here, where in the current study, compensating the epoxide groups of the GPOSS resulted in indirectly removing the aromatic groups of the resin, it can be proposed that the variation in the aromatic content of the modified systems could have contributed to the notice change in T_g.

In the case of the uncompensated systems, the DSC data suggests that T_g decreases with increasing concentration of the GPOSS, where the glass transition process broadened significantly for the uncompensated systems. For instance, by comparing the compensated and uncompensated systems, the width of T_g for the 30 EG% and 30 wt% increased by 6 °C and 27 °C, respectively. In the uncompensated systems, the curing process is unbalanced, as the number of epoxide groups (being supplied by both the resin and the GPSS) is larger than the number of reactive groups provided by the hardener. In this inhomogeneous system and under standard curing condition, the curing reactions may proceed until, ideally, all active groups of the hardener are reacted. As such there will always be unreacted epoxide groups in these systems. The presence of unreacted epoxide groups can be evident from the FTIR spectra, as shown in Figure 5.2(h). Where the rising peak at 915 cm^{-1} is associated with the presence of the epoxide groups in the material, as it was discussed in the previous section. These unreacted epoxide groups will be present in the form of chain ends. Consequently, this would create a system with branched network and retain unreacted epoxide groups. Hence the inclusion of increased GPOSS percentage would increase the probability of producing resin matrix with such segmented topology and varied free volume. In addition, the width of the glass transition process indicates that a number of molecular species are in a rearranging movement in the glass transition region [157]. Furthermore, as explained above, at high concentrations of POSS, the POSS molecules tends to react with each other generating crystalline zones which impact the cross link density [155]. Therefore, the reduction in the T_g of the uncompensated GPOSS modified systems may be ascribed to the proposed variation in the cross-link density and the inhomogeneous network topology.

From the above discussion, it can be summarised that the T_g of modified epoxy resin systems can be affected by a combination of factors, such as, the structure of the modifier (in this case the presence of the POSS cage structure), the influence of the functional group of the modifier on the cross-link density, the resultant network topology, the reactivity of the retained groups and the free volume introduced by the functional modifier.

5.3 AC Breakdown Strength

To evaluate the AC breakdown strength of the samples, the data obtained from the AC breakdown testing were analysed using 2-parameter Weibull distribution, as presented in Figure 5.4, while the derived values of the scale (α) and shape (β) parameters along with the percent of change in the values of the α parameter of the breakdown strength of the modified systems compared to the values of the α parameter of the reference samples are listed in Table 5.3.

For the compensated systems, the inclusion of 1%, 4%, 10% and 30% of the epoxide groups from the GPOSS resulted in improvements in the breakdown strength by about

Table 5.3: AC breakdown strength data of the compensated and uncompensated GPOSS modified epoxy resin systems.

Sample	Compensated systems Weibull parameter			Uncompensated systems Weibull parameter		
	α (kV/mm)	β	%BD	α (kV/mm)	β	%BD
Reference	121.89	26.64	100	121.89	26.64	100
1%	141.81	54.77	116	130.06	26.98	107
4%	148.63	56.35	122	122.31	20.35	100.3
10%	142.85	22.05	117	116.49	14.77	96
30%	136.52	25.92	112	103.23	13.42	85

16%, 22%, 17% and 12% respectively, compared to the neat system. On the other hand, the breakdown strength was increased by only 7 % for the 1 wt% uncompensated system, while the other uncompensated systems either showed insignificant change (such as the 4 wt% which increased the breakdown strength by 0.3 %), or revealed decrease in the breakdown (the breakdown strength of the 10 wt% and 30 wt% decreased by 4 % and 15 %, respectively).

It has been suggested in several studies that the POSS molecule facilitates localised charge motion within the resin system [109, 110, 112, 158]. This implies that the POSS molecules may, to a certain extent, minimise the accumulation of free charges in the bulk resulting in a homogeneous electric field across the system. Consequently, as the external electric field increases, the internal field is kept uniform by the POSS through a process referred to by Takala et al [112] as *temporary charge scavenging*. This process would continue until all the system breaks. It is therefore concluded that the presence of the POSS allowed the modified system to withstand high field, which consequently resulted in the increased breakdown strength noticed here. However, the improvement in the breakdown strength reported here does not increase linearly with the loading of the GPOSS. The data indicates that the breakdown strength of the 10 EG% and 30 EG% compensated systems are lower than that of the 4 EG%, while the breakdown strength of most of the uncompensated systems (apart from the 1 wt% samples) falls below that values of the neat epoxy.

The above account implies that the effect of GPOSS on the charge distribution is not the only factor influencing the electrical performance of the GPOSS modified resin system. The inclusion of the GPOSS is suggested to create branches and nodes integrated in the resin matrix with the POSS cage structure become retained in the network. A schematic digram for the structure of the neat and modified systems is presented in Figure 2.5. As it was explained earlier in the DSC section, in the ideal case of a homogeneous structure, these branches positively enhance the cross link density. However, as the loading of the GPOSS increases, the POSS molecules interact with each other producing an inhomogeneous network architecture. This is consistent with the findings of Heid et al [110]. The inhomogeneous structure could be the dominant factor at high loading

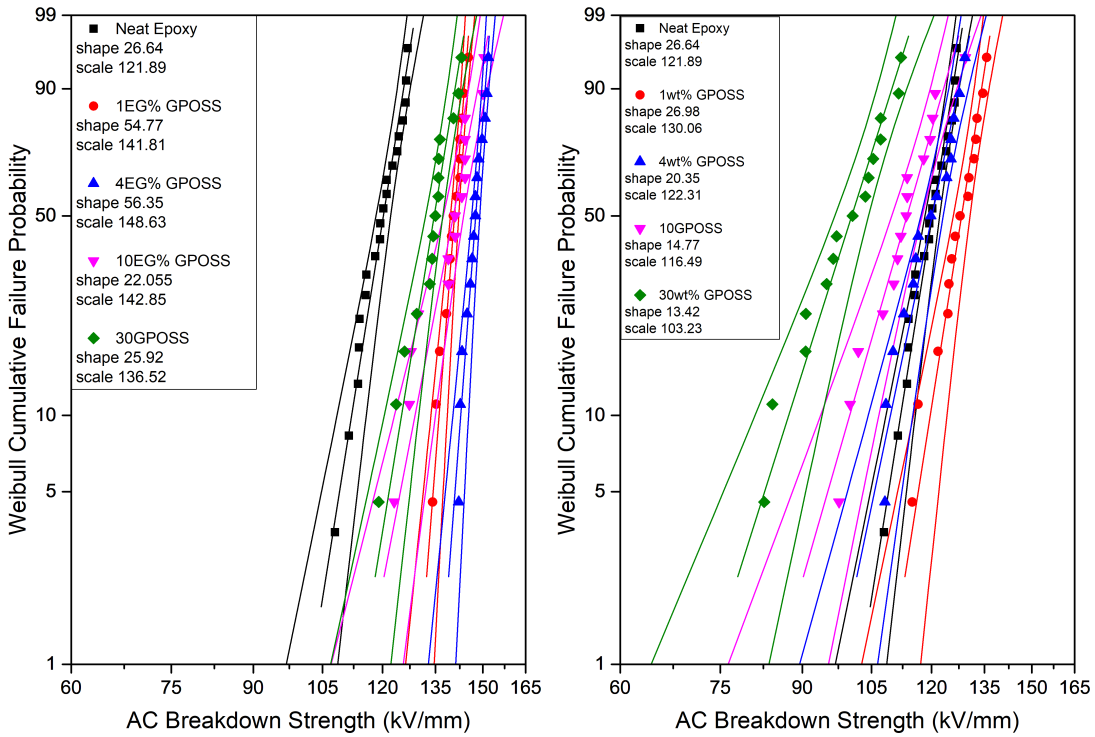

(a) AC breakdown of reference and GPOSS modified epoxide compensated systems

(b) AC breakdown of reference and GPOSS modified epoxide uncompensated systems

Figure 5.4: AC breakdown of reference and GPOSS modified systems with (a) compensated stoichiometry, and (b) uncompensated stoichiometry.

of GPOSS and hence explains the decreasing trend in the breakdown strength for the 10 EG%, 30 EG% and the uncompensated systems (apart from the 1 wt%).

In summary, the AC breakdown strength of the GPOSS modified systems is found to be influenced by the effect of the functional group of the FNM (POSS) on the charge accumulation in the bulk of the material and the probability of the GPOSS to agglomerate. The former parameter is suggested to improve the breakdown strength at low concentration of GPOSS, when the stoichiometry is compensated. While the later factor dominates at high concentrations of GPOSS for both compensated and uncompensated systems; hence reduce the breakdown strength.

5.4 Dielectric Spectroscopy

The effect of the stoichiometry on the dielectric behaviour of the GPOSS modified systems is illustrated in Figure 5.5. Generally, the real part of the complex permittivity increases with increasing the loading of the epoxide groups from the GPOSS, as shown in Figure 5.5(a) and Figure 5.5(b). This variation in the permittivity is in good agreement with the increasing trend in the real permittivity found for epoxy resins modified with 3 wt% to 4.8 wt% GPOSS reported by Takala and coauthors [112], while Huang

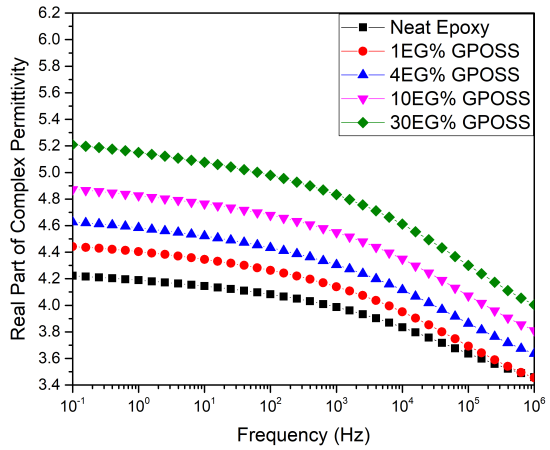

(a) Real part of permittivity of GPOSS modified epoxide compensated systems.

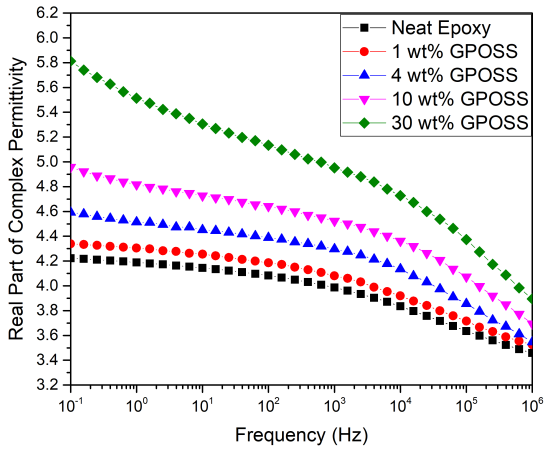

(b) Real part of permittivity of GPOSS modified epoxide uncompensated systems.

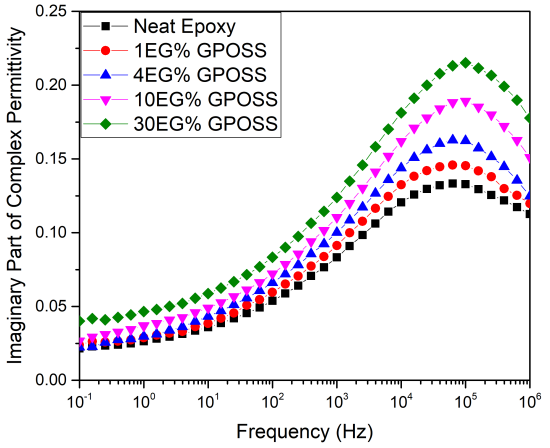

(c) Imaginary part of permittivity of GPOSS modified epoxide compensated systems.

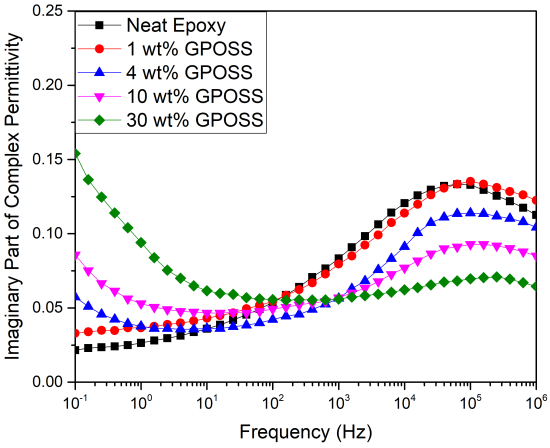

(d) Imaginary part of permittivity of GPOSS modified epoxide uncompensated systems.

Figure 5.5: Real and imaginary part of complex permittivity of reference and GPOSS modified systems.

et al [153] confirmed this dielectric behaviour at varied temperatures for POSS modified resins. Takala et al [112] associated similar dielectric behaviour with the variation in parameters other than the POSS loading, such as the size and dispersion of the POSS. However, Huang et al [153] and Heid et al [109] suggested that the inclusion of the POSS, where the inorganic part (silica) resulted in an increase in the possible mobility of charge carriers, which consequently increases the dielectric constant. Therefore, the increase in the real part of the permittivity is most likely to be attributed to the increase in the polar species resulted from the inclusion of the GPOSS.

Regarding the imaginary part of the permittivity, first consider the complex permittivity of the compensated systems shown in Figure 5.5(c). The peak in the imaginary permittivity observed at frequencies above 10^4 Hz is commonly attributed to the epoxy β relaxation [130, 149, 159–161]. In amine cured systems, the β relaxation is believed to originate from the motion of larger structural units associated with the cross-links, i.e.

due to the movements of hydroxyl (pendent groups of the cross-links) with a degree of co-operativity from the cross-links' surrounding structure [162]. The FTIR data indicated that the inclusion of the GPOSS resulted in marginal variations in the concentration of hydroxyl groups in these systems; also the epoxide absorbance peak was unaffected by the GPOSS, as shown in Figure 5.2(a). Therefore, the increase in the extent of the β relaxation observed here is attributed to the change in the molecular topology created around the cross links derived from the inclusion of the GPOSS, facilitating the mobility of the polymer chains and resulting in an increase in the strength of the β relaxation.

Consider a system that has been modified by adding GPOSS by weight percentage without compensation in the stoichiometry. The dielectric behaviour of such a system indicates variation in both the real and imaginary parts of the permittivity, as presented in Figure 5.5(b) and Figure 5.5(d). In the frequency range above 10^4 Hz, the imaginary part of the permittivity associated with the β relaxation decreases for all samples as the added percentage of the GPOSS increases. The strength of the β relaxation is associated with the number and frequency of OH groups in the system. Therefore, the noticed decrease in the strength of the β relaxation indicated in Figure 5.5(d) is consistent with the decrease in the number of hydroxyl groups evident in the FTIR spectra at OH groups presented in Figure 5.2(b).

In the frequency range below 10 Hz, the data shows that the imaginary permittivity of the modified systems increases, being sharply pronounced for the 30 wt% systems. A corresponding increase in real permittivity could also be noticed for the same frequency range of the real complex permittivity Figure 5.5(b). It may be argued that the change in the imaginary permittivity could be associated with the variation in T_g. However, this is not the case here as the measurements were conducted at room temperature and minimum measured T_g is about 57.5 °C (for the 30 wt% GPOSS systems). Indeed, Heid et al [110] have investigated the effect of POSS modifier (liquid triglycidylisobutyl POSS, which features only three terminal epoxide groups) on the dielectric properties of modified epoxy resins. Their study reported that the dielectric behaviour of the DGEBA resins modified with 5 wt% of the POSS exhibit interfacial loss peaks. This behaviour was attributed to the agglomerations of the POSS. In the current study, it is evident from the FTIR Figure 5.2(h) that there are retained unreacted epoxide groups within the structure of the uncompensated system, where it was suggested that crystalline zones could have been generated giving rise to free volume in these systems, which could have resulted in the noticed decrease in the T_g. This behaviour is consistent with the dielectric behaviour reported by Heid et al [110] and Sharma et al [163]. In the study conducted by Sharma et al [163], it was suggested that the β relaxation shifts to lower temperatures affected mainly by the free volume introduced by the inclusion of the POSS cage. Therefore, form the above discussion, the increase in the permittivity noticed at frequencies below 10 Hz in the data presented in Figure 5.5(b) and Figure 5.5(d) is may

be related to the interfacial polarisation induced by the proposed claustration of the GPOSS.

5.5 Hypothesis test of GPOSS stoichiometry

To provide a comprehensive understanding of the effect of the stoichiometry of GPOSS on the dielectric behaviour of the modified epoxy resins, an investigation was conducted to test the hypothesis regarding the appropriate number of the epoxide groups in the GPOSS. The aim is to verify if the number of the reactive epoxide groups in the GPOSS equals to eight, which was used to calculate the epoxide equivalent weight of the GPOSS. Therefore, the effect of varying the assumed number of epoxide groups in the GPOSS on the dielectric properties of the modified resins was investigated by systematically varying the assumed stoichiometry of the resin, GPOSS and the hardener. The samples were manufactured by adding 70 % of the epoxide groups from the epoxy resin, with the remaining 30 % being supplied by the GPOSS. In the 30 % epoxide groups of the GPOSS, the GPOSS was assumed to have 6 or 10 epoxide groups, where these values were selected to illustrate the behaviour above (10 groups) and below (6 groups) the nominal (8 groups). The resultant samples are referred to as xGGPOSS, where x represent the number of the epoxide groups assumed to present in the GPOSS. For example, the annotation 10GGPOSS refers to epoxy resin systems modified with 30 % of the epoxide groups from the GPOSS which was calculated assuming the GPOSS molecule contain 10 epoxide groups.

5.5.1 Differential Scanning Calorimetry

The DSC data obtained for the test samples are presented in Figure 5.6, while the T_g derived from the DSC measurements are listed in Table 5.4. As expected, compared to the neat systems which had T_g of 85.3 °C, all modified samples exhibited reduction in their glass transition temperature. The inclusion of GPOSS assuming that 6, 8 and 10 epoxide groups from the GPOSS molecule would contribute to the curing process resulted in decrease in the T_g by about 11.8 °C, 9.6 °C and 11.1 °C, respectively. These results are consistent with the findings reported by Nguyen et al [114] for epoxy resin systems investigated with varied stoichiometry. Indeed, Alhabill et al [113] reported reduced T_g for similar epoxy resin systems when there is an excess of resin in the network. On the other hand, the excess of the amine hardener is suggested to only slightly influence the thermal stability of the material. The optimum stoichiometry is correlated with the cross link density, which influences the glass transition temperature of the material. Therefore, the data obtained here suggest that the 8GGPOSS systems represents the optimum stoichiometric ratio as this system features the maximum measured T_g for the modified systems.

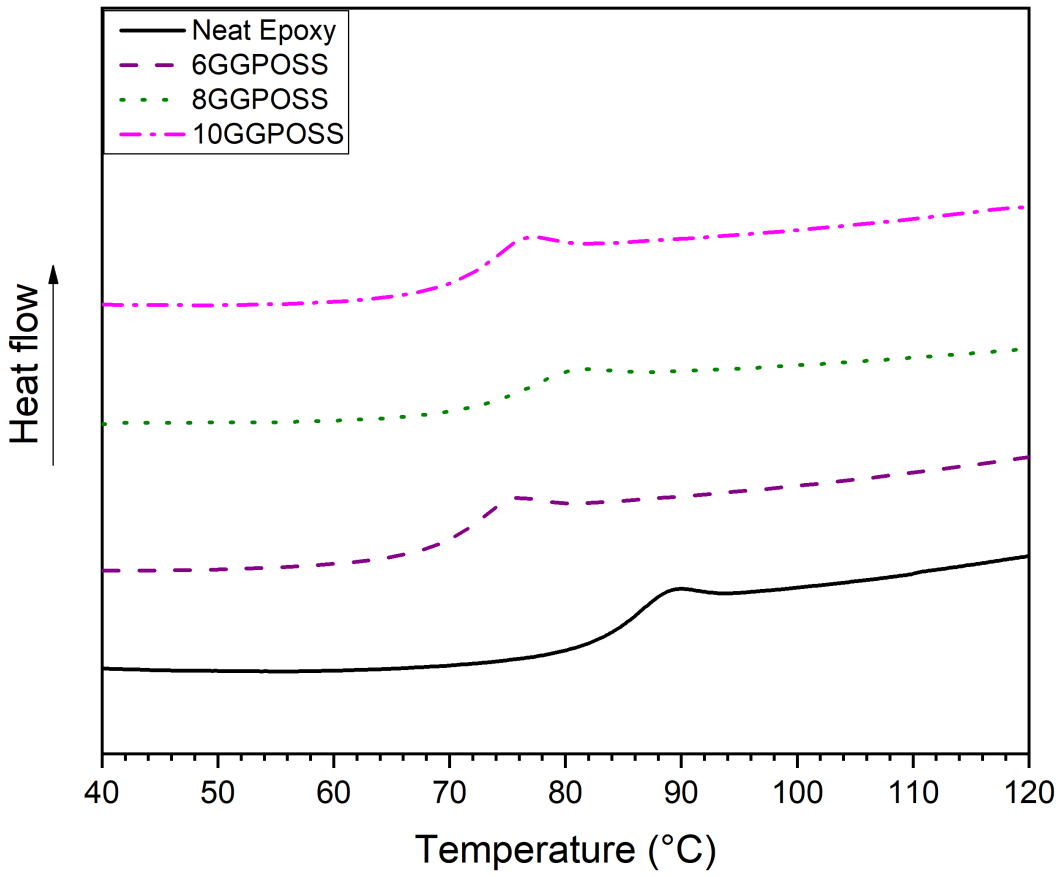

Figure 5.6: DSC of reference and GGPOSS modified epoxide compensated systems.

Table 5.4: DSC measurements for reference and GGPOSS modified systems.

Sample	T_g(°C)
Reference	85.3
6GGPOSS	73.5
8GGPOSS	75.7
10GGPOSS	74.2
Error in Tg = ±2 °C	

5.5.2 Dielectric spectroscopy

In order to evaluate the effect of the assumed interfacial chemistry of the GPOSS, the dielectric behaviour was investigated. The acquired data of the real and imaginary part of the complex permittivity for systems calculated by assuming different number of epoxide groups are presented in Figure 5.7. It was found that system that has been produced assuming the ideal number of epoxide groups of the GPOSS (8 groups) contributes to the curing process, exhibited the maximum increase in the real and imaginary part of the permittivity. The imaginary permittivity observed at frequencies above 10^4 Hz, which is associated with the β relaxation, appears as a pronounced peak for all the samples.

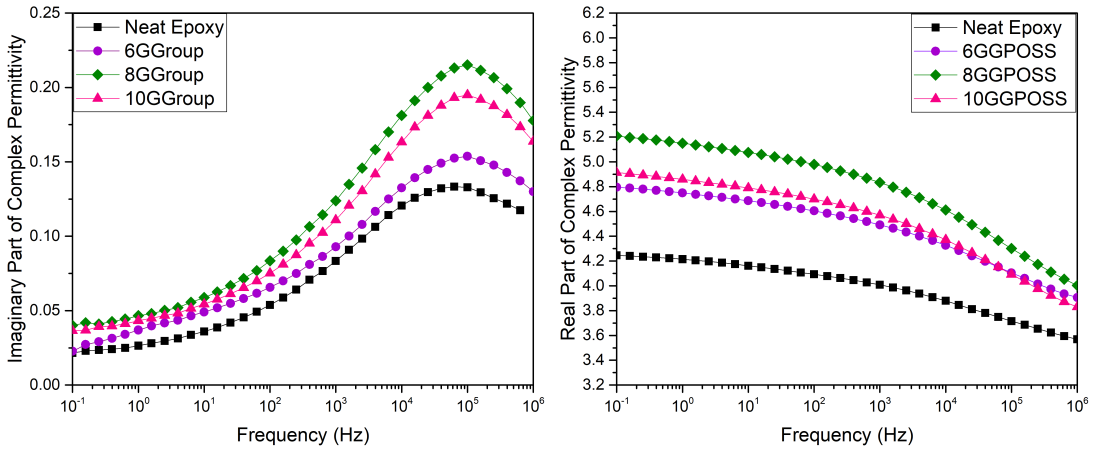

(a) Imaginary part of complex permittivity for GPOSS modified epoxide with different number reactive groups

(b) Real part of complex permittivity for GPOSS modified epoxide with different number reactive groups

Figure 5.7: Dielectric spectroscopy of reference and GPOSS modified systems with different number of epoxide groups.

With increasing the number of the assumed epoxide groups from the GPOSS to 10 groups, the strength of β relaxation decrease slightly. A reduction in the strength of the β relaxation also evident in the case if samples produced using only 6 epoxide groups, as shown in Figure 5.7. This decrease in the extent of β relaxation suggests that in the case of 6 and 10 epoxide groups, the curing reactions are unbalanced. If the hypothesis which states that each GPOSS molecules has 8 epoxide groups, were correct, then the samples produced by assuming only 10 epoxide groups would contribute to the curing process may be considered as systems with excess of hardener, while the 6GGPOSS samples are systems with excess of epoxide groups. Since the extent of β relaxation is attributed to the number of the hydroxyl groups generated during the cross linking process, therefore, the results suggests that systems with excess of hardener produced less number of hydroxyl groups, which is the same for systems with excess of resin. In both cases the curing reactions are not balanced. This effects the cross linking density which consequently alter the extent of β relaxation. As the maximum amplitude for β relaxation can be seen for the 8GGPOSS systems, it can be suggested that the optimum number of epoxide groups in the GPOSS is 8 groups.

5.6 Summary

By using two different methods (compensation and addition by weight percentage) to introduce a multi-epoxide terminated functional network modifier, a series of samples have been produced with varied structures. The properties of the manufactured systems were studied using different techniques. FTIR spectroscopy showed that the compensated GPOSS modified systems have marginal change in the hydroxyl groups, while the

OH groups decreased as the loading of the GPOSS increase in the uncompensated systems. The spectra of both systems showed similar variation in the Si-O-Si absorbance region, while the uncompensated systems featured increased number of retained unreacted epoxide groups.

Differential scanning calorimetry experiment indicated that the T_g of the modified systems is influenced by several factors such the structure of the modifier, the influence of the functional group of the modifier on the cross-link density, the network topology and the free volume introduced by the FNM.

The AC breakdown strength of the GPOSS modified epoxy resins were found to be affected by two main factors which are, namely, the functional group of the FNM and the modified network topology. Epoxy resin systems produced with theoretical stoichiometric ratio showed increased AC breakdown strength compared to that of the neat resin, due to the inclusion of the GPOSS. On the other hand, system with varied stoichiometric ratio (uncompensated) showed decreased AC breakdown strength which was attributed to the proposed agglomeration of the modifier which created an inhomogeneous network structure.

The changes in real part of the permittivity as a result of the inclusion of the GPOSS are ascribed to the presence of the inorganic silica molecules of the GPOSS in the system. Regarding the imaginary part of the complex permittivity, the β relaxation of the compensated systems increased with the increase in the concentration of the epoxide groups from the GPOSS, which is in contrast to the data obtained for the uncompensated systems. Based on the FTIR data, this behaviour can be attributed to the change in molecular topology around the cross links after the addition of the GPOSS. While in the case of the uncompensated samples, the decrease in the extent of β relaxation is associated with the decrease in the hydroxyl groups, which is evident from the FTIR.

The calculation of the compensated systems was based on the assumption that each GPOSS contribute to the curing process through 8 epoxide groups. Therefore, it was necessary to test the effect of this assumption on changing the GPOSS epoxide groups in a systematically controlled way. As it was expected, the DSC measurements (the maximum T_g) and the dielectric spectra indicated by the extent of β relaxation suggested that 8 epoxide groups from the GPOSS may contribute to the curing reactions, which is to be used to calculate the optimum stoichiometric ratio.

To sum up, it can be seen that the inclusion of the GPOSS resulted in variation in the different properties of the modified systems. The stoichiometric ratio of the GPOSS plays a vital role in determining the properties of the final material. In addition, the effect of the GPOSS on the T_g, dielectric spectroscopy and the breakdown strength is attributed to several factors where the structure of the functional groups of the GPOSS was one of the dominant factors in most of the cases. Therefore, the next chapter is set out to investigate the effect of varied percentages of different functional network

modifiers on the thermal, electrical and dielectric properties of amine cured modified epoxy resin systems.

Chapter 6

Investigation of the effect of functional network modifiers on the electrical properties of epoxy resin systems

[1] In the previous chapter, the effect of the stoichiometric ratio of FNM on the properties of modified epoxy resin systems was investigated. It was found that the stoichiometric ratio plays a vital role in determining the properties of the epoxy resin based system. In this chapter, the effect of different functional network modifiers on the glass transition temperature, permittivity, AC breakdown strength and the electrical conductivity of amine cured epoxy resin systems is explored. Here, two functional network modifiers (FNM) are used to modify the structure of a DGEBA epoxy resin, namely glycidyl hexadecyl ether (GHE) and glycidyl 4-nonylphenyl ether (GNPE). The neat and modified systems are cured using an amine based hardener (Jeffamine D230). The stoichiometric ratio of the resin, hardener and FNM is calculated so that each epoxy group (supplied by the resin and/or the FNM), reacts with an active groups from from the amine hardener in a curing mechanisms which was described in chapter 2.

6.1 GHE modified systems

The glycidyl hexadecyl ether (GHE) is a functional network modifier, which comprises a terminal epoxide group and a long alkyl chain within its chemical structure, as illustrated in Figure 3.3. The epoxide group of the GHE contributes to the curing reactions of the resin system. After curing, the epoxide group of the GHE become integrated in the resin network, while the non-reactive part of the GHE (the alkyl chain) become retained in the system. The presence of these retained molecules impacts the network structure and results in forming a system with nodes and branched chains. Consequently, the addition of the FNM impact the different properties of the final material, as it will be demonstrated in the next sections.

6.1.1 FTIR Spectroscopy

The FTIR spectra acquired for the neat and GHE modified systems is presented in Figure 6.1(a). According to Lambert et al [136], the region between wavenumbers 3000 cm^{-1}

[1] As stated in the Author's Declaration, this work was done wholly or mainly by the author of this thesis. Part of the contents of this chapter was published in item (ix) (Istebreq A. Saeedi, Alun S. Vaughan and T. Andritsch, FUNCTIONAL DESIGN OF EPOXY-BASED NETWORKS: TAILORING ADVANCED DIELECTRICS FOR NEXT-GENERATION ENERGY SYSTEMS, in *Journal of physics D: Applied Physics*, vol. 52, 2019.Paper DOI: doi.org/10.1088/1361-6463/ab09be.

and 2800 cm^{-1} is usually referred to as the CH stretching region, as this region characterises the stretching frequency of most of the CH groups. Since the GHE contains a long alkyl chain within its chemical structure ($CH_2(CH_2)_{14}CH_3$), it is important to have a detailed view of the CH stretching region of the FTIR spectra of the systems under investigation, as it is illustrated in Figure 6.1(b). From this figure, it can be observed that a new absorbance peak appears at 2851 cm^{-1}. The strength of this new absorption peak rises with the increase in the fraction of GHE present in the system. The absorption peak present at wavenumber 2927 cm^{-1} in the spectra of the neat epoxy resin is increased in strength and shifted to lower wavenumber as the loading of the GHE increases in the system.

Several studies reported that the antisymmetric stretches of CH_3 can be observed at wavenumber range from 2970 cm^{-1} to 2950 cm^{-1}, while the antisymmetric stretches of CH_2 groups often presents at wavenumber from 2940 cm^{-1} to 2915 cm^{-1} [136, 164–167]. In addition, the symmetric stretching frequencies for CH_3 and CH_2 groups are located in the wavenumber range from 2885 cm^{-1} to 2860 cm^{-1} and from wavenumber 2870 cm^{-1} to 2840 cm^{-1} respectively. This suggests that the absorbance peaks at the wavenumber 2963 cm^{-1} and 2927 cm^{-1} in the spectra shown in Figure 6.1(b), are associated with the antisymmetric stretch of CH_3 and CH_2 respectively, while the peaks at 2869 cm^{-1} and 2851 cm^{-1} are attributed to the symmetric stretch of CH_3 and CH_2 respectively.

Since the structure of GHE modifier features a long chain alkyl groups within its chemical structure, which ideally comprises of sixteen CH_2 groups and a single CH_3 group, the addition of the GHE is expected to cause significant increase in the absorbance of the overall spectra at the CH stretching region. Therefore, the shift in the antisymmetric stretch CH2 peak, the increase in intensity of the peaks at the CH region and the appearance of a new peak, are all indicators that proofs the presence of the GHE within the structure of the cured resin.

6.1.2 Differential Scanning Calorimetry

The DSC traces for the neat and GHE modified epoxy resin systems are illustrated in Figure 6.2. The values of the T_g, ΔC_p (difference in heat capacity over T_g), the onset of T_g and ΔT_g (the width of the glass transition process) are listed in Table 6.1. From Figure 6.2, it can be seen that the measurements of T_g for the 30GHE system appears as a straight line suggesting that the T_g of the 30GHE system is below the temperature range that is accessible with the used DSC equipment, thus, the T_g of the 30GHE is listed as out of the range in Table 6.1.

The glass transition temperature of the pure epoxy resin system was observed at 85.3 ±2 °C. The results indicates that the T_g decreases as the GHE content in the system

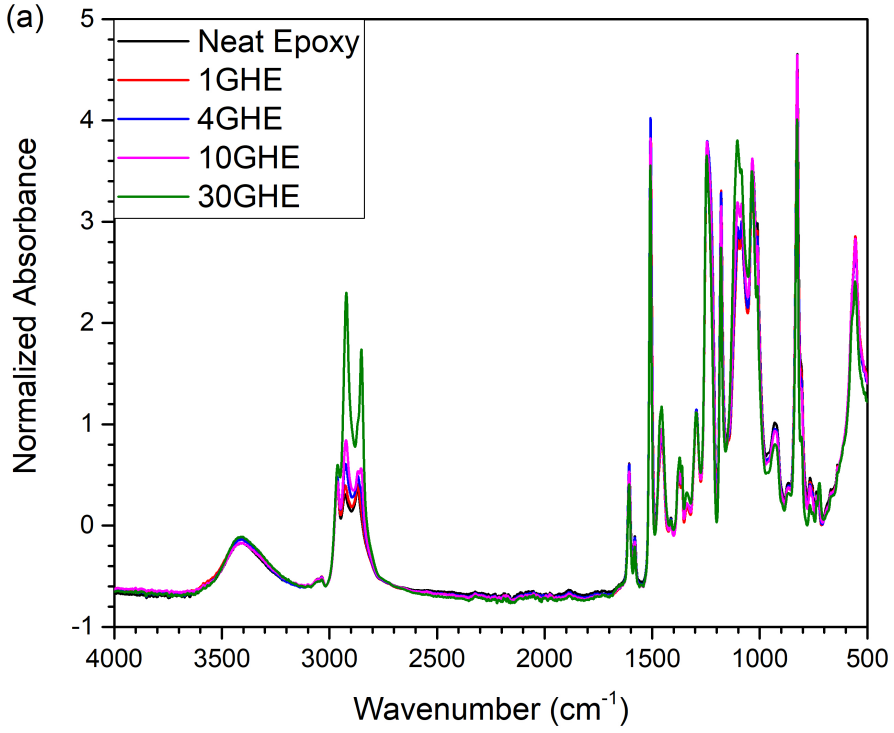

(a) complete spectra

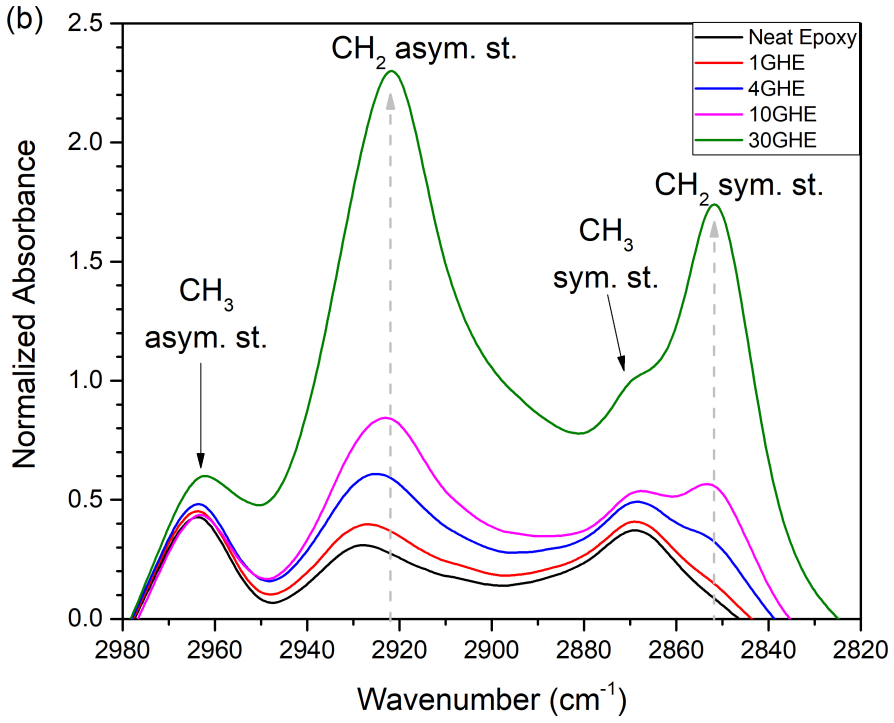

(b) FTIR spectra for wavenumber between 2980 cm^1 and 2820 cm^1

Figure 6.1: FTIR spectra of GHE modified DER 332 epoxy resin

Table 6.1: DSC data of the neat and GHE modified epoxy resins.

	T_g (°C)[a]	Onset (°C)[b]	ΔC_p J/(g.°C)	ΔT_g (°C)
Neat Epoxy	85.3	83.3	0.34	4.4
1GHE	81.7	79.6	0.32	5.5
4GHE	71.5	69.4	0.31	7.0
10GHE	54.2	50.6	0.21	15.5
30GHE	NA	NA	NA	NA

[1] Error in Tg = ±2 °C
[2] Error in onset= ±0.2 °C
[3] NA= Out of range

increase. The formulation of the different samples used in this study are listed in Table 6.2. From the latter table, it can be observed that as the GHE content increases, the required quantity of hardener is reduced, consequently, reducing the crosslink density. In addition, free volume is introduced in the system associated with the long alkyl chain of the GHE modifier. The generated free volume assists in the large-scale molecular motion, which consequently contributes to the decreases in values of the T_g. These results aline with the findings reported by Daniels and consistent with the results reported by Liu et al. for epoxy resin systems modified using a FNM containing a shorter alkyl chain with similar functional groups [115, 168].

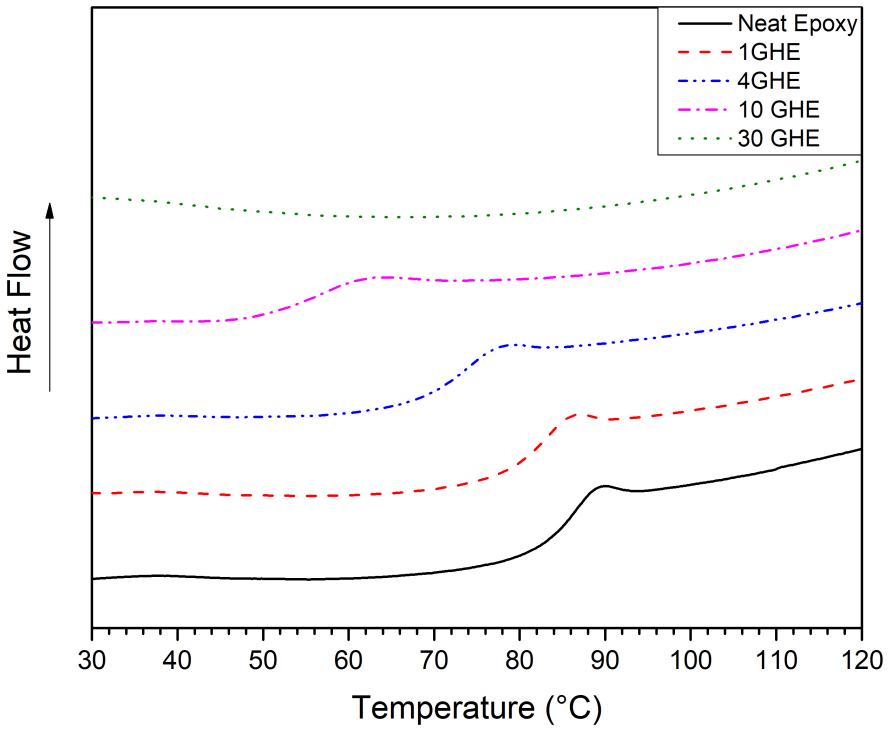

Figure 6.2: Thermal measurements for neat and GHE modified epoxy systems.

Table 6.2: Formulation of the reference and modified samples.

Material System	Resin (g)	FNM (g)	Hardener (g)
Neat Epoxy	7.45	0.00	2.55
1GHE	7.33	0.13	2.54
4GHE	7.00	0.50	2.50
10GHE	6.37	1.21	2.43
30GHE	4.50	3.49	2.21
1GNPE	7.34	0.12	2.54
4GNPE	7.03	0.46	2.52
10GNPE	6.42	1.13	2.45
30GNPE	4.62	3.12	2.26

6.1.3 Dielectric Spectroscopy

The real and imaginary part of the permittivity of the neat and GHE modified epoxy resin systems acquired at room temperature are shown in Figure 6.3. For the real part of the permittivity illustrated in Figure 6.3(a), apart from the the 30GHE system, the figure reveals that the inclusion of the GHE results in a reduction in the real permittivity, where the permittivity decrease as the contents of the GHE increase in the system. This behaviour alines with the fact that adding the GHE introduces non-polar moieties into the modified networks. In the case of the 30GHE, the dielectric spectroscopy measurements were conducted above the T_g of the system (T_g of the 30GHE system is below room temperature). The permittivity of the 30GHE was observed to increase with the decrease in the frequency, suggesting a mechanism reported in literature as ionic conductivity associated with the increase in the mobility at temperatures above T_g of the material [91].

Consider the imaginary part of the complex permittivity presented in Figure 6.3(b), the peak located at frequency from ∼100 Hz to above 10^6 Hz is attributed to the β-relaxation. Figure 6.3(b), reveals that the β-relaxation decrease in strength as the GHE contents increase in system that features T_g values above the room temperature. The strength of the β-relaxation is associated with the motion and frequency of the hydroxyl groups generated during the curing process [80, 150, 169]. Therefore, the behaviour observed here is qualitatively consistent with the variation in the glass transition temperature and the change in the composition of each system. However, by assuming a complete reaction of the epoxide groups and the active groups of the hardener in the system, a quantitative comparison between the different formulation presented in Table 6.2 and the behaviour of the β-relaxation shown in Figure 6.3(b), reveals that the strength of β-relaxation does not scale with the number of active groups of the hardener, where the strength of the β-relaxation strength decrease greater than the expected value. This suggests that a factor other than the number of the hydroxyl groups contributes to the noticed decrease in the strength of the β-relaxation. These findings are consistent with the behaviour reported by Alhabill et al [113], where the variation in the strength of the β-relaxation

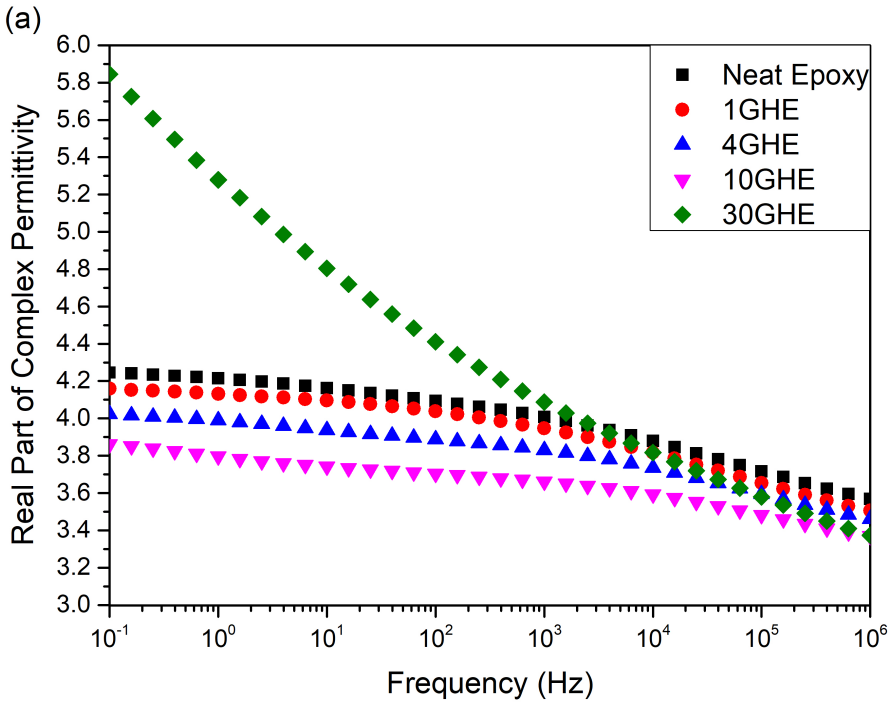

(a) Real part of complex permittivity for neat and GHE modified systems.

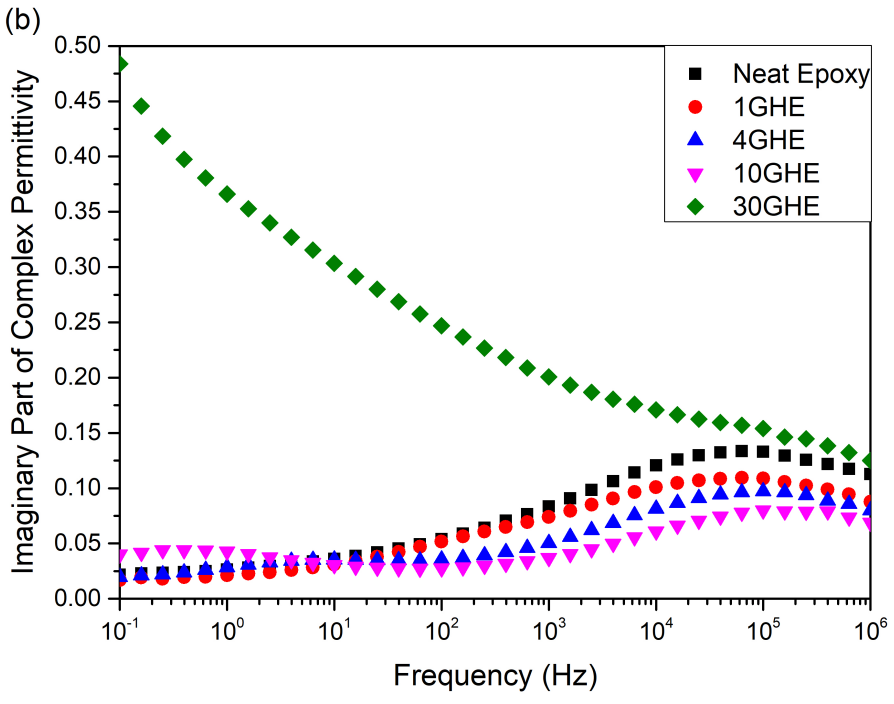

(b) Imaginary part of complex permittivity for neat and GHE modified systems.

Figure 6.3: Complex permittivity of GHE modified epoxy resin samples obtained at 20 °C

was attributed to the change in local structure of the resin network, which constrained the movement of the hydroxyl groups. In the work reported here, the inclusion of the GHE resulted in the presence of alkyl groups retained in the resin structure forming a system with branched network. These branches hindered the movement of the β associated groups, consequently, shifting the relaxation to a higher frequency that is located outside the range accessible by the equipment.

In addition to the β-relaxation, a weak relaxational peak appears at frequencies below 1 Hz in the graph of the imaginary part of the permittivity of the 10GHE system. A detailed analysis and a discussion of this peak in anhydride cured DGEBA resin systems is presented in chapter 8 of this thesis, which reveals that the peak noticed here is associated with the α-relaxation attributed to the low T_g of the 10GHE system [170–172]. As for the 30GHE, the dominant feature is a sharp increase in the imaginary part of the permittivity at the low frequency end of the measured spectra. This behaviour is anticipated as the 30GHE is above T_g at room temperature. As such, it is possible to associate the behaviour of the 30GHE with a combination of two mechanisms. The first mechanism is conduction within the network correlated to chloride ions present in the system residual from the epoxy resin manufacturing reactions [91, 173]. The other factor is that the molecular segments have a relatively high freedom of motion above T_g. From the frequency dependent permittivity of the 30GHE system, it can be suggested that the former mechanism is not dominant in these data.

6.1.4 Electrical Conductivity

The acquired DC conductivity values of the neat and GHE modified epoxy resin systems are listed in Table 6.3. Although a small increase (comparable to experimental uncertainties) in the electrical conductivity is suggested for the system with GHE content up to 10%, the data suggests that, generally, the conductivity of the GHE modified systems increase with increasing the GHE concentration. The maximum measured conductivity was reported for the 30GHE system, which suggested an increase by 3 order of magnitude compared to the conductivity of the neat system. It is possible that there are a number of factors that influence the electrical conductivity of the GHE modified systems. Based on the dielectric behaviour of the GHE modified systems discussed in the previous section, the inclusion of the GHE promotes ionic conduction in the system, which could contribute to the DC conductivity, especially in systems modified with high concentration of GHE as it was shown in the data of the 30GHE.

The network structure of the GHE modified systems comprises of retained functional groups, which increased the free volume in the system and resulted in the noticed decrease in the T_g. In case of polyethylene, where charge transport dynamics through disordered molecular conformations has been studied in details, the presence of localised regions of free volume has been shown to be an important factor in electronic conduction

Table 6.3: DC conductivity and AC breakdown measurements of neat and GHE modified samples.

Sample ID	DC Conductivity (S/cm)	Weibull α (kV/mm)	Weibull β	% BD
Neat Epoxy	$1.03 \times 10^{-17} \pm 1.01 \times 10^{-18}$	121.9 ± 1.7	26.6	100%
1GHE	$1.36 \times 10^{-17} \pm 1.04 \times 10^{-18}$	124.1 ± 2.2	20.1	102%
4GHE	$1.86 \times 10^{-17} \pm 2.15 \times 10^{-18}$	129.6 ± 1.8	24.6	106%
10GHE	$3.82 \times 10^{-17} \pm 9.12 \times 10^{-18}$	119.5 ± 1.5	26.0	98%
30GHE	$2.50 \times 10^{-14} \pm 4.15 \times 10^{-15}$	95.3 ± 3.0	11.9	78%

[174–176]. Therefore, it could be the same case here, where the free volume introduced by the GHE modifier could have affected the charge transport in the modified systems.

Finally, the addition of the GHE altered the viscosity of the system. The measured viscosity of the neat epoxy resin was 0.266 Pa.s ($\pm 4 \times 10^4$ Pa.s), which was reduced to 0.101 Pa.s($\pm 4 \times 10^4$ Pa.s) by adding 30% of the epoxide groups from the GHE modifier. The increase in viscosity is expected to increase the probability of reaction between the epoxide groups and the active groups of the hardener prior to vitrification. Therefore, the increase in the viscosity would have resulted in an increase in the cross-linking efficiency, where a homogenous system is produced. This aligns with the finding of Alhabill et al [113], where it was found that the electrical conductivity is associated with the structure of the material, systems with more homogenous structures are reported to have high electrical conductivity.

6.1.5 AC Breakdown Strength

The data obtained from the AC breakdown test for the neat and GHE modified epoxy resin systems are analysed using the Weibull distribution, where the Weibull probability distribution function and the derived parameters (the scale α and the shape β) are presented in Figure 6.4 and listed in Table 6.3. The data suggests that the breakdown strength of the modified systems increases progressively, but marginally, with the increase in the GHE content up to 4 mol.% of the GHE. Thereafter, the behaviour is reversed, where the breakdown strength decrease with increasing the GHE concentration in the system. The data of the 30GHE indicated the maximum drop in the breakdown strength, which may be correlated with the decreased T_g of the 30GHE and the influence of the ionic conduction.

The data presented in Figure 6.4 clearly demonstrates that the inclusion of the functional groups of the FNM modifies the electrical properties of the epoxy resin system. For the GHE, the retained functional groups are merely alkyl chains. These aliphatic compounds are reported to influence the electrical properties of the modified polymeric material. As it was discussed in the voltage stabilisers concept section 2.4 of chapter 2, several studies have reported the impact of alkyl groups on the electrical properties of polymeric

systems. Hunt [177], used alkyl groups as a voltage stabilising additives to manufacture polyolefins with controlled electrical properties. Similarly, Takahashi et al. employed the affect of alkyl groups on the electrical properties of the host polymeric material to produce polyolefin based polymers that features high resistance to electrical treeing [121]. Based on the findings of Hunt and Takahashi et al, Martinotto et al produced additives which were suggested to improve the electrical strength of cross-linked polyethylene [118]. The above studies ascribed the electrical behaviour of the alkyl modified system to the capability of the alkyl groups to donate / receive electrons (either high electron affinity or low ionisation potential). This would allow the alkyl groups to stabilise the internal electric field within the material. From the above account, it is possible that similar mechanisms presents in the GHE modified system, where the inclusion of alkyl groups (at concentration up to 4 wt%) functions as branches that stabilise the charge distribution in the modified resin network.

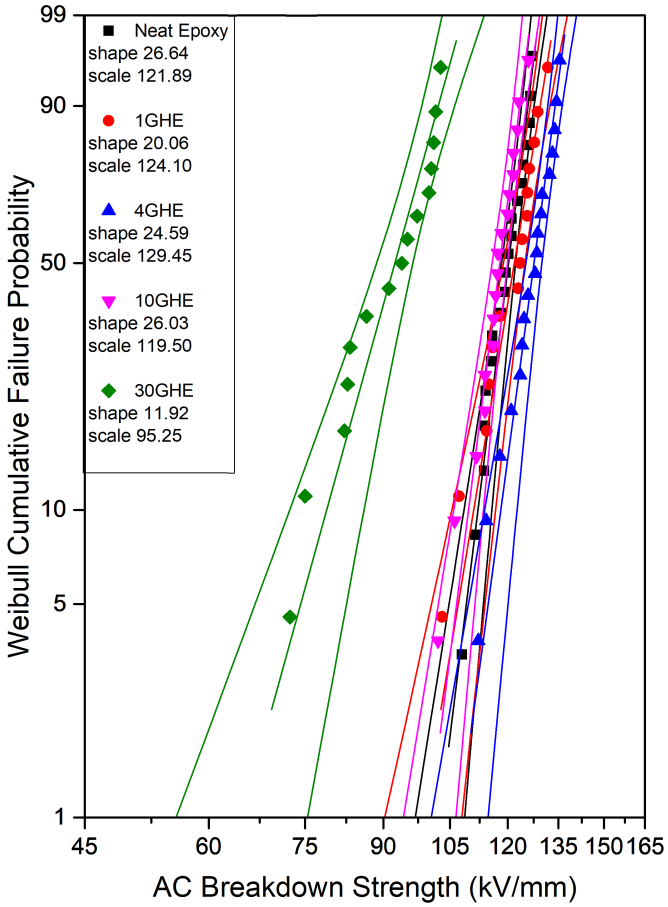

Figure 6.4: Weibull plot of the breakdown data for neat and GHE modified epoxy resin.

6.2 GNPE Modified Systems

The previous section indicated that the inclusion of the GHE (at concentration up to 4 wt%) resulted in an increase in the breakdown strength of the GHE modified systems. In this section, varied concentrations of Glycidyl 4-nonylphenyl ether (GNPE) modifier is used to alter the structure of the epoxy resin. The chemical structure of the GNPE comprises of a terminal alkyl chain (similar to the functional groups of the GHE, but the alkyl chains are shorter), in addition to an aromatic ring that is linked to a terminal epoxide group through an ether linkage. The chemical structure of the FNM is presented in Figure 3.3. The next sections provide a discussion of the data of the FTIR, DSC, permittivity measurements, AC breakdown strength and DC conductivity of the neat and GNPE modified epoxy resin systems. The investigation of the effect of the GNPE on the different properties of the resin will examine the claim that the impact of the GHE on the electrical properties is not only associated with the inclusion of the GHE, but is also attributed to the chemical structure of the functional groups of the FNM.

6.2.1 FTIR Spectroscopy

Figure 6.5(a) illustrates the FTIR spectra acquired for the neat epoxy resin and systems modified with different concentrations of GNPE. A detailed view of the CH stretching region of the FTIR spectra of the systems under investigation is presented in Figure 6.5(b). The data indicates that the increase in the contents of the GNPE modifier results in increase in the strength of the absorbance peaks located at wavenumber 2964 cm^{-1}, 2927 cm^{-1} and 2869 cm^{-1}. It can also be observed, from Figure 6.5(b), that the absorbance peak at 2964 cm^{-1} is slightly shifted to lower wavenumber proportional with the GNPE content in the system (for example, the latter peak is located at 2961 cm^{-1} for the 30GNPE system). All the above mentioned absorbance peaks are located in the CH stretching region, as it was discussed in the FTIR section of the GHE modified systems. The absorbance peaks located at wavenumber 2869 cm^{-1}, 2927 cm^{-1} and 2964 cm^{-1} are attributed to the symmetric stretch of CH_3, the antisymmetric stretch of CH_3 and CH_2 groups respectively [136]. Since the chemical structure of the GNPE comprises of an alkyl chain ($CH_2(CH_2)_7CH_3$), the addition of the GNPE is expected to cause significant increase in the absorbance of the overall spectra at the CH stretching region. Therefore, the changes in the FTIR spectra noticed in the CH region indicates the presence of the aliphatic part of the GNPE within the structure of the cured resin. However, this association between the increase in the strength of the peaks at the CH region with the increase in the GNPE contents should not be exclusively related to the aliphatic groups of the GNPE. It was reported that the carbon/carbon bonds contained within the aromatic rings also appears to stretch in this region [136].

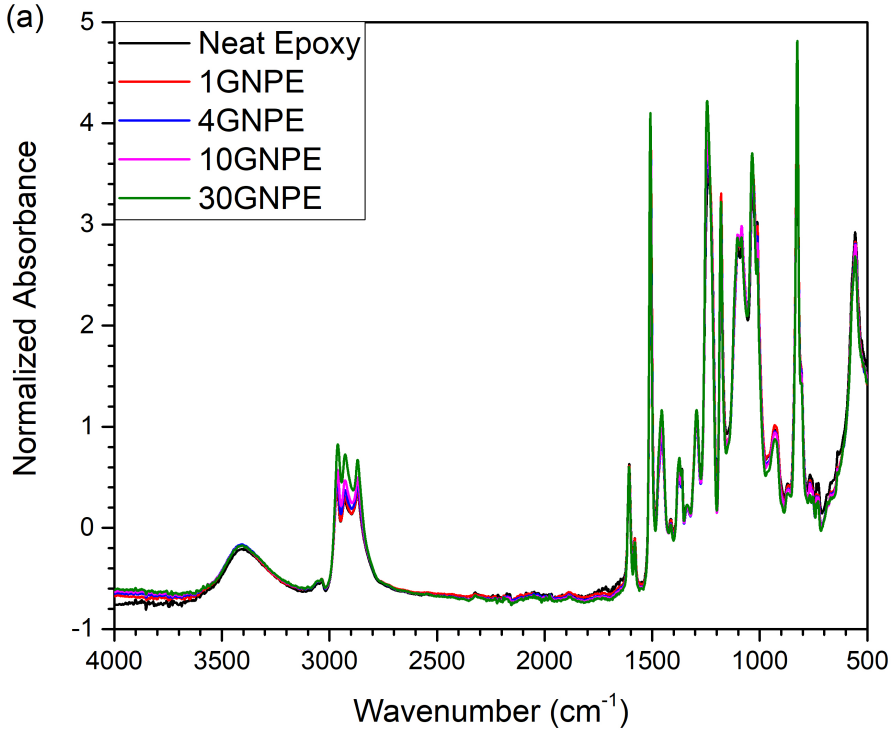

(a) The complete spectra of the neat and GNPE modified systems.

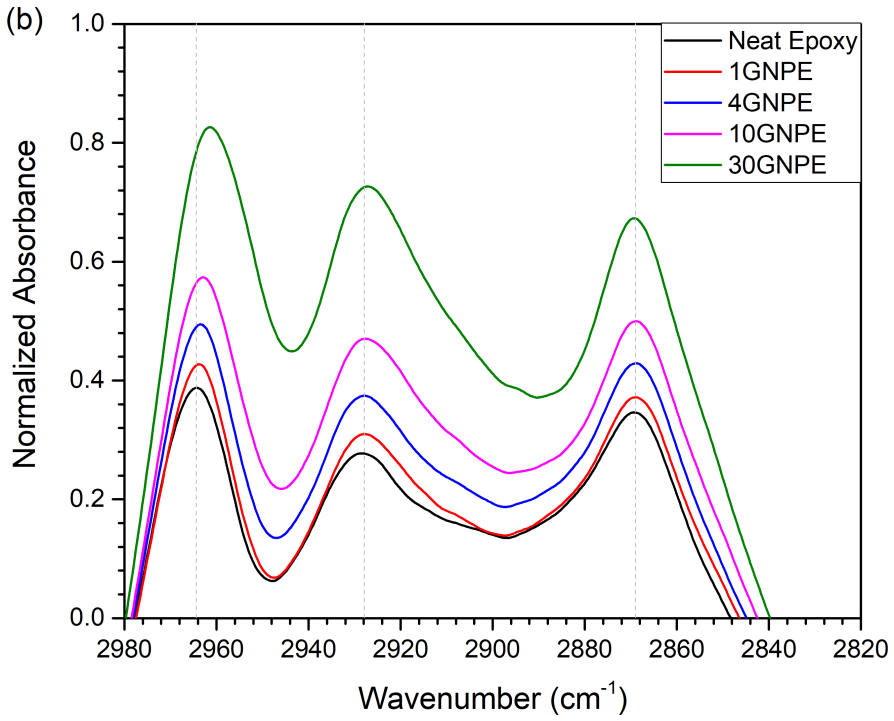

(b) FTIR spectra for wavenumber between 2980 cm^1 and 2820 cm^1.

Figure 6.5: FTIR spectra of GNPE modified DER 332 epoxy resin

The C=C stretching (also known as skeletal ring breathing modes) are reported at 1600 cm^{-1}, 1500 cm^{-1} and 1450 cm^{-1}, while the sharp strong peak presents at wavenumber from 860 cm^{-1} to 800 cm^{-1} is associated with the stretching of para disubstituted aromatic molecules [136, 137]. The FTIR spectra presented in Figure 6.6 illustrated the peaks associated with aromatic groups. Figure 6.6 presents the FTIR spectra of the neat and GNPE modified systems for the wavenumber from 1650 cm^{-1} to 450 cm^{-1}, which illustrates the stretching bands reported for the skeletal ring breathing modes and para disubstituted aromatic molecules. However, these peaks are located in the finger-print region of the spectrum [136], where most of the peak tends to overlap, which makes precise identification of a specific molecular groups quite problematical. Nevertheless, considering the complete FTIR spectra reported here suggests that the inclusion of the GNPE resulted in an increase in the strength of the absorbance peaks of the overall spectra at the CH stretching region, shift in the wavenumber of the antisymmetric stretch of the CH3 peak, and a slight variation in the absorbance peaks located in the finger-print region. All these changes in the FTIR spectra of the GNPE modified systems provides a compelling evidence for the presence of the GNPE modifier within the structure of the produced systems.

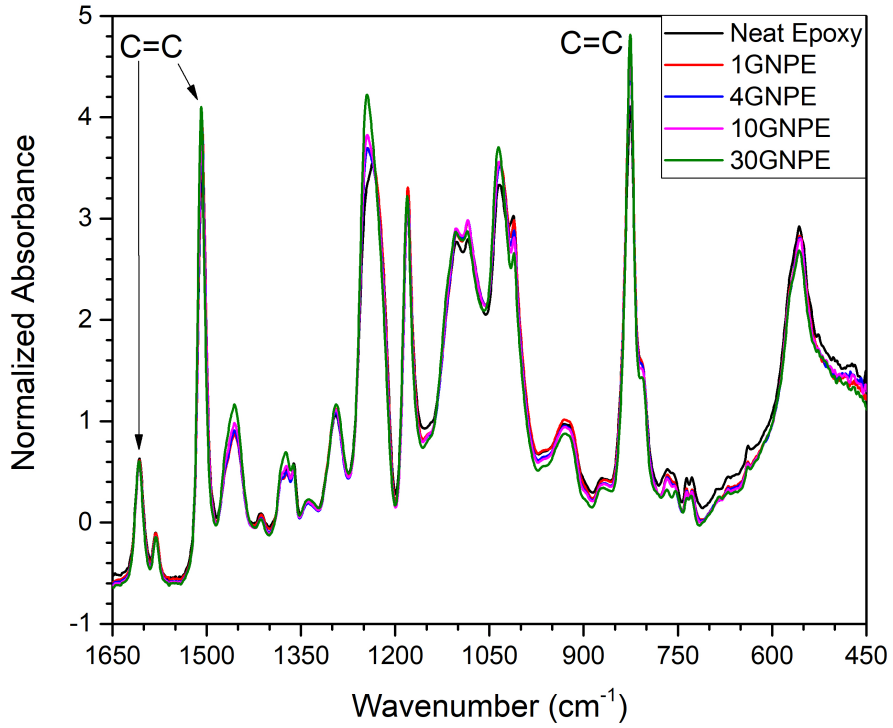

Figure 6.6: FTIR spectra of neat epoxy and GNPE modified samples for wavenumber between 1650 cm^1 and 450 cm^1.

Table 6.4: DSC data of the neat and GNPE modified epoxy resins.

	T_g (°C)[a]	Onset (°C)[b]	ΔC_p J/(g.°C)	ΔT_g (°C)
Neat Epoxy	85.3	83.3	0.34	4.43
1 GNPE	76.8	74.5	0.34	5.45
4 GNPE	75.0	72.7	0.31	7.04
10 GNPE	64.4	61.9	0.25	14.38
30 GNPE	42.5	39.2	0.27	19.36

[1] Error in Tg = ±2 °C
[2] Error in onset= ±0.2 °C

6.2.2 Differential Scanning Calorimetry

The data obtained from the DSC measurements for the neat and GNPE modified epoxy resin systems are illustrated in Figure 6.7, while the derived values of the T_g, ΔC_p, the onset of T_g and ΔT_g (the width of the glass transition process) are listed in Table 6.4. The data suggests that the inclusion of the GNPE modifier resulted in a decrease in the T_g of the modified networks as the concentration of GNPE increase in the system. For example, the measured T_g of the 30GNPE system is 42.5 ±0.2 °C, which indicates a decrease by 42.4 ±0.2 °C in the T_g of the 30GNPE compare to the T_g of the neat system (T_g of the pure system is 85.3 ±0.2 °C).

The reduction in the T_g of the GNPE modified systems is similar to the behaviour reported earlier for the systems altered using GHE modifier, where the presence of the GNPE is expected to influence the network structure and the free volume in the system in a comparable way [3, 47, 100, 149]. However, by comparing the effect of GNPE and GHE modifiers on the T_g values of the modified epoxy resins, it can be seen that the GHE modifier resulted in higher drop in T_g than GNPE for systems produced with similar FNM concentrations. For example, the T_g of the 30GHE system was reported below room temperature, while the T_g of the 30GNPE system is 42.5 ±0.2 °C. Although both GHE and GNPE resulted in shifting T_g to lower temperatures, the GNPE systems have higher glass transition temperatures than that of GHE modified system for similar FNM concentrations. The behaviour could be associated with the presence of aromatic structure within the chemical composition of the GNPE modifier. The presence of the aromatic ring is reported to environmentally constraint the molecular motion by steric hindrance, which impacts the segments arrangement associate with the glass transition process, and hence alters the T_g of the system. This process is consistent with the effect of aromatic structures on the thermal stability of epoxy resins suggested by Neville and Lee [3] and T_g reported by Babayevsky and Gillham [178]

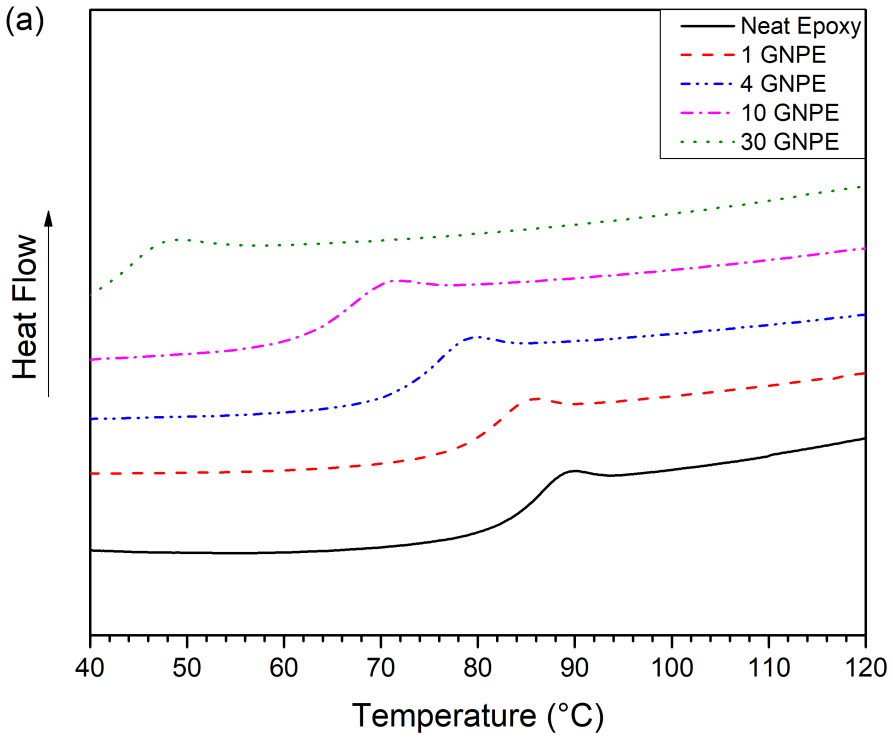

Figure 6.7: Thermal measurements for neat and GNPE modified epoxy systems.

6.2.3 Dielectric Spectroscopy

The real and imaginary part of the permittivity of the GNPE modified epoxy resin systems are shown in Figure 6.8. The data indicates that the increase in the content of the GNPE in the system, results in a general decrease in the real and imaginary parts of the permittivity. This is similar to the dielectric behaviour reported for the GHE modified systems.

In the case of the imaginary part of the permittivity of the GNPE modified systems, presented in Figure 6.8(b), the data suggests that the increase in the parts of the GNPE modifier in the system results in decrease in the strength of the β-relaxation, located at frequency around 10^5 Hz. This behaviour is quite different from the dielectric behaviour of the GHE modified systems, where in the 30GHE systems both β and α relaxation were observed. As it was discussed in the section of the dielectric behaviours of the GHE modified systems, the strength of the β-relaxation is associated with the hydroxyl groups present in the system [80, 150]. Since the addition of the GNPE resulted in reduction in the strength of the β-relaxation, it can be suggested that the addition of the GNPE modifier could have resulted in reduction in the number of hydroxyl groups generated during the curing process of the epoxy resin system. This could be a consequence of the reduction in the crosslink density and/or the change in the free volume in the system associated with the retained functional groups of the modifier. Similar effect was reported for non-stoichometric epoxy resins [113]. In addition, since the chemical formulation of

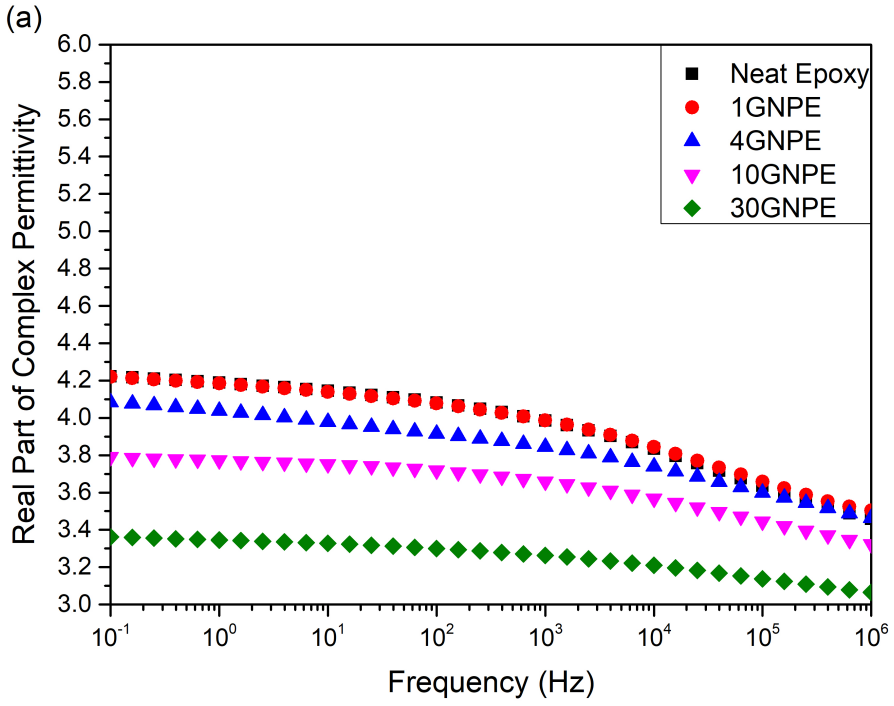

(a) Real part

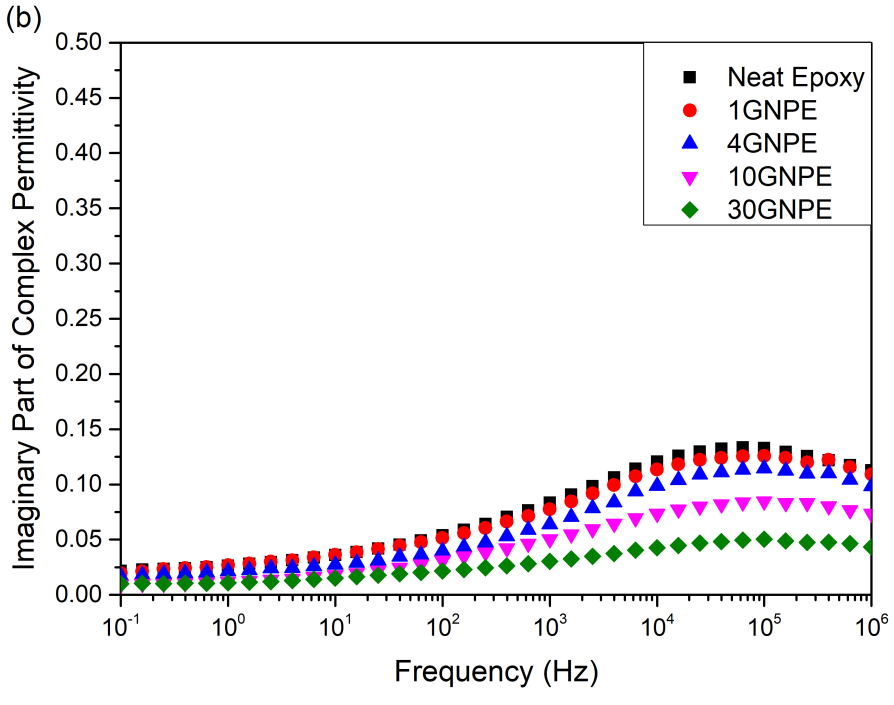

(b) Imaginary part

Figure 6.8: Complex permittivity of GNPE modified epoxy resin samples obtained at 20 °C

Table 6.5: DC conductivity and AC breakdown measurements of neat and GNPE modified samples

Sample ID	DC Conductivity (S/cm)	Weibull α (kV/mm)	Weibull β	% BD
Neat Epoxy	$1.03 \times 10^{-17} \pm 1.01 \times 10^{-18}$	121.9 ± 3	26.6	100%
1 GNPE	$1.22 \times 10^{-17} \pm 2.40 \times 10^{-17}$	134.2 ± 2	56.6	110%
4 GNPE	$4.08 \times 10^{-17} \pm 1.50 \times 10^{-17}$	135.3 ± 2	43.7	111%
10GNPE	$1.40 \times 10^{-16} \pm 7.42 \times 10^{-17}$	133.9 ± 3	43.4	110%
30GNPE	$2.22 \times 10^{-16} \pm 8.93 \times 10^{-17}$	134.8 ± 6	20.8	110%

GNPE features aromatic structure, these functional groups might have constrained the movement of the hydroxyl-ether groups. Consequently, it can be suggested that both the decrease in the number of the hydroxyl groups and the environmental constrained caused by the integration of the FNM within the structure of the epoxy resin, have contributed to the reduced β-relaxation noticed here.

6.2.4 Electrical Conductivity

The DC conductivity values obtained for the neat and GNPE modified epoxy resin systems are listed in Table 6.5. Although a small increase (comparable to experimental uncertainties) in the electrical conductivity is suggested for the system with low content of GNPE (up to 4%mol), the general trend in the data indicates that the increase in the loading of the GNPE modifier resulted in an increase in the electrical conductivity of the modified systems. This is comparable to the conductivity behaviour of the GHE modified systems. The maximum reported increase in the conductivity was measured for system modified with 30% of the epoxide groups provided by the GNPE modifier, where the DC conductivity of the 30GNPE system was found to increase by 1 order of magnitude compared to the conductivity of the neat system.

Like the GHE modified systems, the inclusion of GNPE affected the viscosity of the modified system. The measured viscosity of the neat epoxy resin was 0.266 Pa.s ($\pm 4 \times 10^4$ Pa.s), which was decreased to 0.135 Pa.s ($\pm 3 \times 10^4$ Pa.s) for the 30GNPE samples, which is anticipate to alter the cross-linking efficiency. The changes in the DC conductivity of the GNPE modified system is comparable to the behaviour of the GHE modified systems. Therefore, it is possible to propose similar explanations for behaviour of the electrical conductivity of the GNPE modified systems. It is important to point out that the DC conductivity measurements were conducted at room temperature, which below the T_g of the GNPE modified systems. Consequently, no contribution from ionic conduction is seen in the data of the 30GNPE.

6.2.5 AC Breakdown Strength

The results of the AC breakdown test for the neat and GNPE modified epoxy resin systems are analysed using the Weibull distribution as presented in Figure 6.9 and listed in Table 6.5. The figure suggests that the inclusion of the GNPE modifier resulted in a general increase in the breakdown strength of the GNPE modified systems compared to the breakdown strength of the neat resin system. By comparing the AC breakdown of the GHE (listed in Table 6.3) and the data reported for the GNPE modified systems (illustrated in Table 6.5), it can be seen that the increase in the breakdown strength resulted from the inclusion of the GNPE is greater compared to the increase in the breakdown strength reported for the GHE systems. For example, the maximum increase in the breakdown strength of the GNPE modified systems is reported for the 4GNPE, where the Weibull α parameter for the 4GNPE is 135.3 $\pm$2 kV/mm, while the neat resin system featured a lower Weibull α values (121.9 $\pm$3 kV/mm). The maximum increase in the Weibull α parameter of the GHE modified systems is reported for the 4GHE to be 129.6 $\pm$1.8 kV/mm. Furthermore, based on the data of the GHE and GNPE modified systems reported in Table 6.3 and Table 6.5 respectively, it can be suggested that the increase in the breakdown strength of the GNPE modified system is not strongly dependent on the added GNPE concentration. While it may be argued that the improvement in the breakdown strength of the FNM modified system reported here (about 10%) is small, it has been shown that comparable improvement in the electrical properties have been translated into significant advantage under technologically relevant electric fields [116, 117].

As it was highlighted in section 2.4 of chapter 2, several studies have reported the influence of aromatic rings on the breakdown strength of polymeric materials. Martinotto et al. manufactured additives that comprises of an aromatic structure (benzophenone) attached to an alkyl groups [118]. The additives produced by Martinotto et al. are suggested to feature voltage stabilising capabilities. Englund et al. [122] used additives with similar chemical structure (aromatic molecule linked to an alkyl chain), which reported improvement in the electric treeing resistance in cross-linked polyethylene. Similarly, Jarvid et al.[125] produced materials with aromatic based additives performing as voltage stabiliser and supported the results reported by Martinotto et al [118] and Englund et al. [122]. The above studies pointed out that there are two factors which are likely the cause for the noticed increase in the breakdown strength of the FNM modified systems. The high electron affinity of the aromatic-alkyl groups of the added aromatic-alkyl molecules and the difference between the ionisation potential of the functional groups compared to the ionisation potential of the host polymer [120, 125].

In the current case, the inclusion of the GNPE altered the network structure of the resin by introducing non-reactive chains, which are suggested to increase the free volume in the system, as it was seen from the T_g of the GNPE modified systems. Charge transport

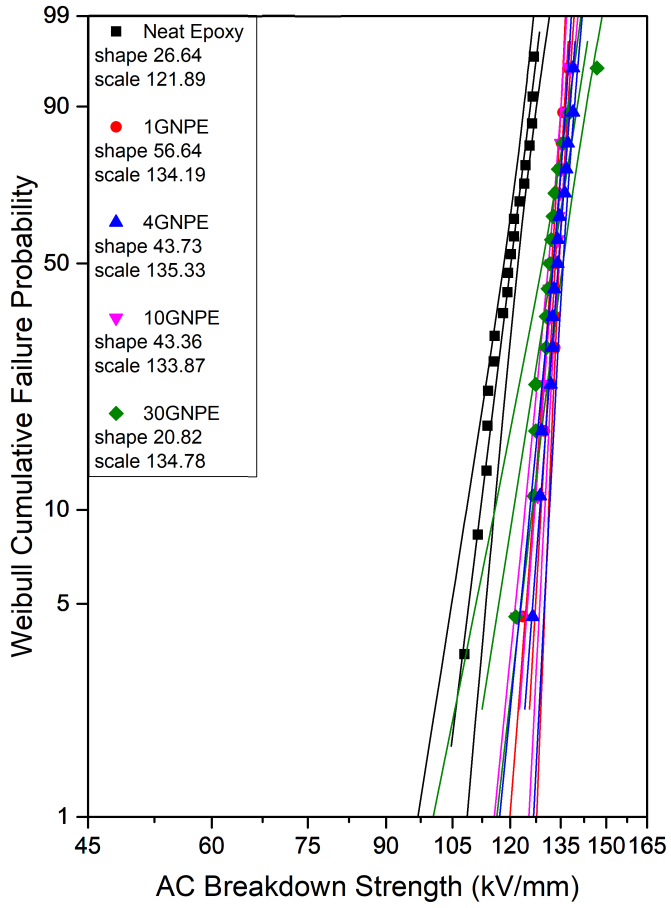

Figure 6.9: Weibull plot of breakdown data for neat and GNPE modified epoxy resin.

studies demonstrated that the free volume in the system is an important factor that influences the electrical behaviour of the polymeric network [179–181]. Consequently, the free volume introduced by the addition of the GNPE may be another factor that influenced the charge transport dynamics in the modified systems. It was shown here that the inclusion of the GNPE increases the breakdown strength of the GNPE modified systems. Since, the chemical structure of the GNPE features an aromatic structure linked to an alkyl chain, which is similar to chemical structure of the voltage stabilisers used by Martinotto et al. [118] and Jarvid et al. [120], based on the above discussion, it is possible the increased breakdown strength of the modified systems is associated with the functional groups of the FNM, where the high electron affinity of the aromatic-alkyl group, the low ionisation potential and the change in the charge transport dynamics are the factors that contributed to the improvement in the breakdown strength of the FNM modified systems.

6.3 Summary

This chapter investigated the effect of the inclusion of functional network modifiers on the different properties of epoxy resin systems. Two functional network modifiers were considered, namely, glycidyl hexadecyl ether (GHE) and glycidyl 4-nonylphenyl ether (GNPE). The studied epoxy resin samples were manufactured with varied percentages (1%, 4%, 10% and 30%) of the epoxide groups supplied by the FNM. The chapter presented and discussed the effect of introducing GHE and GNPE modifiers on the FTIR, DSC, permittivity, AC breakdown strength and DC conductivity of the neat and modified systems.

In the case of the GHE modified systems, the FTIR spectra of the neat and GHE modified systems indicated changes in the spectral regions such as shift in the antisymmetric stretch CH2 peak, increase in intensity of the peaks at the CH region and the appearance of a new peak, which are all factors associated with the chemical structure of the GHE modifier. Therefore, the FTIR measurements proofed the presence of the GHE modifier within the structure of the cured resin. Similarly, the variation in the FTIR spectra of the GNPE modified systems indicated the presence of the GNPE in the cured material.

The DSC measurements of the GHE and GNPE modified systems indicated that as the concentration of the FNM modifier increase in the system, the glass transition temperature shifts to lower values. It was not possible to measure the T_g of the 30GHE samples, because the T_g of the 30GHE is located below the temperature range that is accessible with the equipment. The variation in the T_g of the GHE and GNPE modified systems is attributed to the possible reduction in the cross-linking density and the free volume introduced as a results of the retained chains of the FNM.

The data of the real part of the permittivity of the GHE and GNPE modified systems revealed that the inclusion of both modifiers resulted in a reduction in the real permittivity as a function of the GHE in the system. This is consistent with the fact that adding the GHE and the GNPE introduces non-polar moieties into the network. The dielectric measurements were conducted at room temperature, which is above the T_g of the 30GHE system. Therefore, ionic conductivity was found to dominate the real part of the permittivity of the 30GHE. The imaginary part of the permittivity of the GHE and GNPE modified systems indicated the presence of the β- relaxation at room temperature. The variation in the strength of the β- relaxation was consistent with the T_g values of the different composition reported. The strength of the β- relaxation is associated with the motion and frequency of the hydroxyl and change in local structure of the resin network resulted from the presence of retained functional groups of the FNM. In the case of the 10GHE systems, the data of the imaginary part of the permittivity indicated the presence of the α- relaxation attributed to the low T_g of the 10GHE system. For the 30GHE, the imaginary permittivity of the 30GHE is dominated by a sharp increase

associated with the conduction correlated to residual chloride ions and the high freedom of segmental motion above T_g.

The DC conductivity measurements suggests that, generally, the conductivity of the GHE and GNPE modified systems increase with increasing the FNM concentration. The conductivity behaviour of the GHE and GNPE modified systems was attributed to a number of factors, which are (a) ionic conduction in the system, (b) presence of localised free volume regions in the structure associated with specific functional groups of the modifier, which alters charge transport dynamics in the system and (c) the reduced initial viscosity of the modified systems, which increases the cross-linking efficiency.

The AC breakdown strength of the modified systems increases with the increase in the GHE and GNPE modifier content up to 4 mol.% of the FNM. Thereafter, the behaviour is reversed. This behaviour was associated with the presence of the functional groups of the FNM retained in within the system. Two factors are suggested to explain the noticed increase in the breakdown strength of the FNM modified systems. The high electron affinity of the aromatic-alkyl groups of the added aromatic-alkyl molecules and the difference between the ionisation potential of the functional groups compared to the ionisation potential of the host polymer.

To sum up, the impact of the inclusion of GHE and GNPE modifiers reported here are found to rely on the selection of the functional group of the FNM. While a comparable technique has previously been used as a means for altering the mechanical properties of epoxy resins, this is the first time to our knowledge that this approach has been explored in depth as a means of integrating different functional groups into a thermosetting polymer in order to effectively customise its properties. While there is no doubt that some types of fillers improved the properties of thermosetting materials, the published literature has highlighted a number of problems associated with dispersion and filler agglomeration. The use of liquid and low-concentration FNM $\sim$4% suggested here appears to offer a new alternative means of engineering novel materials to meet current and future needs in an adaptable way. The work reported in this chapter is focused on providing a comprehensive understanding for the impact of FNM on the different properties of epoxy resin systems. The next chapter will discuss the impact of the different curing mechanism on the properties of the FNM modified epoxy resin systems.

Chapter 7

Investigation of the effect of different curing mechanisms on the dielectric properties of modified epoxy resin systems

[1]In the previous chapter, the effect of functional network modifiers FNM on the electrical properties of epoxy resins was discussed. In this chapter, the effect of different curing mechanisms on the electrical properties of modified epoxy resin systems is investigated. This will provide fundamental understanding of the dielectric behaviour of the modified systems which will assist in the detailed dielectric analysis explained in the next chapter. The current chapter will test the hypothesis which states that changing the type of hardener (amine or anhydride based material) leads to changes in the curing mechanism, which would significantly affect the dielectric behaviour of the resin network, this is also the case when the network is altered in a systematic way, using functional network modifiers.

For this purpose, epoxy resin samples were manufactured using 1 %, 4 %, 10 % and 30 % of the epoxide groups from the TTE functional network modifier. First, the FTIR spectra of the neat and modified samples were obtained, to illustrate the chemical composition of the samples. These samples were cured using amine and anhydride hardeners. Then, the glass transition temperature of the modified amine and anhydride cured samples, was measured. In order to investigate the effect of TTE on the dielectric response of the neat and modified systems, temperature dependent dielectric spectroscopy test was conducted for frequency range from 10^{-1} Hz to 10^{6} Hz for temperatures from -160 °C to 180 °C, using 10 °C step temperature. The temperature dependent dielectric spectroscopy measurements were conducted for the reference samples (neat amine and anhydride cured resins) and samples modified using 30 % of the epoxide groups from the TTE (which is the maximum FNM % used in this thesis, i.e provides the strength of the behaviour), while room temperature dielectric spectroscopy was conducted for the remaining samples (1 %, 4 % and 10 %), to provide understanding of the trend of the dielectric behaviour. Finally, the effect of TTE on the electrical conductivity was investigated for all the study samples. Analysing the effect of FNM on the dielectric behaviour of the modified systems give insight into the network structure and molecular dynamics. The introduction of the FNM usually results in branched networks with retained functional groups, the effect of these groups on the thermal and electrical behaviour of

[1]As stated in the Author's Declaration, this work was done wholly or mainly by the author of this thesis. Parts of the contents of this chapter was published in item (x) Istebreq A. Saeedi, T. Andritsch and Alun S. Vaughan, On the Dielectric Behavior of Amine and Anhydride Cured Epoxy Resins Modified Using Multi-Terminal Epoxy Functional Network Modifier, in *Polymers*, vol 11, 2019.Paper DOI: doi:10.3390

the modified systems is vital to design epoxy based insulating materials modified using functional network modifiers.

7.1 FTIR Spectroscopy

The FTIR spectra of neat and TTE modified amine cured epoxy resins are presented in Figure 7.1, while the spectra of the anhydride cured systems are shown in Figure 7.2. The complete spectra of amine and anhydride cured systems are shown in Figures D.1 and D.3, along with detailed spectra between 1800 cm^{-1} to 600 cm^{-1} of both systems are illustrated in Figures D.2 and D.4 in the Appendix D.

In the case of the amine cured systems, the FTIR spectra (see Figure 7.1) indicates four regions of interest. The first region, starting from the low wavenumber of the spectrum, is the epoxide groups absorbance peak which is often identified at wavenumber 915 cm^{-1} [182–184]. The second region of interest is the absorbance peak of ether groups which is present at wavenumber range from 1060 cm^{-1} to 1150 cm^{-1} [135, 145, 167]. Finally the amine and hydroxyl region at wavenumber 3300 cm^{-1} and 3400 cm^{-1} receptively [135, 137, 145, 167, 185, 186].

From Figure 7.1, it can be seen that the inclusion of the TTE affected the curing mechanism and resulted in a monotonic increase in amine contents of the modified samples. The stoichiometric ratio of the mixture (resin, FNM and hardener) used to produce the samples was calculated so that each amine group from the hardener would react with an epoxide group available in the system (supplied by the resin and/or the FNM). Since there is an increasing number of unreacted amine groups, this implies that the corresponding unreacted epoxide groups should appear in the FTIR spectra. However, the peak associated with the epoxide groups located at wavenumber 915 cm^{-1} indicates insignificant change in the number of unreacted epoxide groups in the systems after the addition of the TTE (as illustrated in Figure 7.1). On the other hand, there is a significant increase in the ether groups evident at the region 1060 cm^{-1} to 1150 cm^{-1} of the spectra. There are two main possible factors which could have resulted in the increased concentration of ether groups: the chemical structure of the components (resin and TTE) and the etherification reaction. The stoichiometry was calculated according to the number of epoxide groups, in each modified system, the % of epoxide groups from the resin is removed and substituted by the % of epoxide groups supplied by the FNM. The TTE and the resin contain ether groups within their chemical structure, with both containing one ether group per epoxide. This means that, before curing reactions starts, substituting the epoxide groups from the TTE should have negligible effect on the number of ether groups, which is not the case here. Consequently, it is possible to suggest that the second factor, etherification process which occurs at post-curing, is the

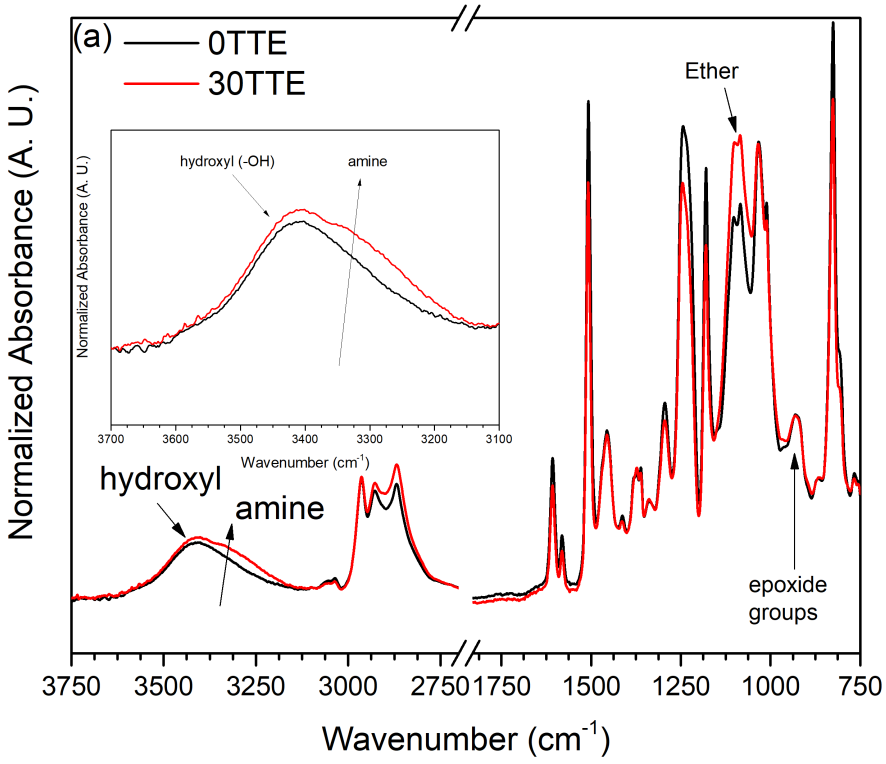

Figure 7.1: The FT-IR spectra of neat and 30TTE system.

mechanism driving the noticed increase in the absorbance peak of ether links in the modified systems, which alines with the behaviour of the epoxide peak present at 915 cm^{-1}. Similar behaviour has been reported by Vryonis et al [187], where the data proved that etherification reactions occur at the post-curing process in epoxy resin systems.

In the case of the anhydride cross-linked systems, like the amine cured samples, there are four regions of interest in the FTIR spectra of the anhydride cured systems presented in Figure 7.2. These bands includes, the absorbance peak at wavenumber range from 1060 cm^{-1} to 1150 cm^{-1} associated with the stretch of the C-O of ether groups [135, 188], the region from 1150 cm^{-1} to 1250 cm^{-1} related to the stretch of C-O bond of ester groups [189–191]. In addition to the carbonyl (C=O) peak at 1750 cm^{-1}, which is often associated with the presence of the ester groups, while the peak at 3400 cm^{-1} is the absorbance peak of the hydroxyl (OH) groups [137, 167, 185].

During the cross-linking reactions of an anhydride cured system, OH groups are both generated by the esterification process, and consumed in the anhydride initiation process (as explained in the epoxy curing mechanisms discussed in chapter 2). Therefore, the concentration of the OH groups is varied. Consequently, the absorbance peak at 3400 cm^{1} in the FTIR spectra of the anhydride cured systems associated with the hydroxyl groups does not provide a straight-forward interpretation upon which the concentration of the OH groups of the different samples may be compared. Nevertheless, the FTIR spectra of the anhydride cured systems suggests that the inclusion of the TTE

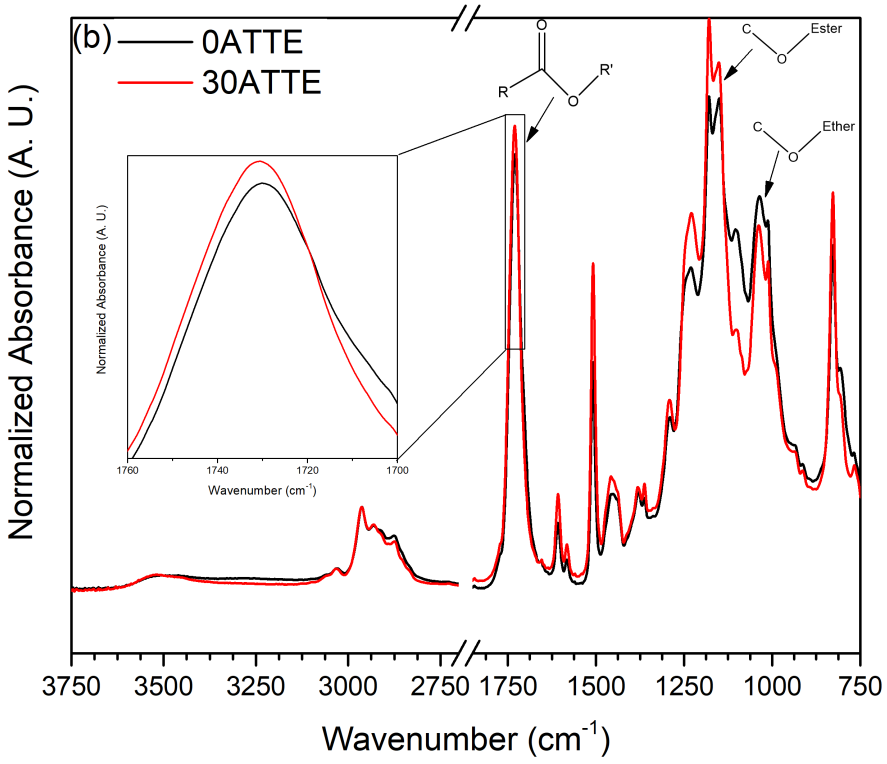

Figure 7.2: The FT-IR spectra of neat and 30ATTE system.

resulted in an increase in the ester contents of the modified systems, which is indicated by the slight increase in the ester absorbance peak and the C-O peak of the ester groups, as illustrated in Figure 7.2. In addition, the data also reveals that the introduction of the TTE resulted in decrease in the ether content of the modified samples, as implied from the C-O peak of ether groups. From the above discussion, it is possible to suggest that the presence of TTE modifier affected the relative probability of esterification and etherification/homopolymisation reactions. Consequently, the addition of the TTE influences the network topology of the modified resin systems. Such changes in T_g is often suggested to be associated with the free volume in the system.

7.2 Differential Scanning Calorimetry

The DSC data of the neat and TTE modified epoxy resin systems cured using amine and anhydride hardeners are shown in Figure 7.3 and Figure 7.4 respectively, while the derived values of the glass transition temperatures are listed in Table 7.1. In the case of the amine cured systems, the measured T_g of the neat epoxy resin system is 85.3 ±2°C, where the addition of 30% of the epoxide groups from the TTE resulted in reduce in the T_g of the modified system to 68.6 ±2°C. The data of the anhydride cured systems with similar TTE content, 30ATTE, suggested comparable reduction in T_g, where the measured T_g of the neat system was 102.9 ±2°C, which was reduced to 87.5 ±2°C for the

Table 7.1: DSC measurements for reference and modified epoxy systems.

Sample	T_g amine cured	T_g anhydride cured
Reference	85.3	102.9
1%	83.4	100.5
4%	80.1	99
10%	78.5	94.15
30%	68.6	87.5

Error in $T_g = \pm 2$ °C

30ATTE system [47, 100, 149, 150]. Since the TTE contains a non-reactive methyl group within its chemical structure (which after curing become retained within the network), the inclusion of the TTE could have altered the free volume in the modified systems. In addition, comparing the T_g values of neat samples for both amine and anhydride cured systems (listed in Table 7.1) indicates that the choice of the hardener also influences the T_g of the system. Consequently, it is possible to suggests that the changes in the T_g reported here are associated with both the choice of the hardener and the incorporation of the TTE modifier. Comparing the molecular structure of the functional group of the TTE (which is a short methyl chain) with the structure of the functional group of the GHE (which is a long chain alkyl group, as discussed in chapter 6), suggests that the functional group of the TTE is expected to have limited influence on the free volume in the system. This indicates that the T_g of the modified systems is influence by factors other than the variation in the free volume in the system introduced by the functional group of the FNM. Indeed, Alhabil et al. [192] attributed the T_g of epoxy resins to the network topology created during the curing process, while Morgan et al. [193] concluded that the network structure around the nodes imposes geometric constraints which affect T_g.

In the case of the amine cross-linked systems, the curing process involves the reaction between the epoxide groups with the amine groups of the hardener, which results in a generation of an OH group and a secondary amine. The subsequent secondary amine groups are likely to be located between the cross-links, whereas any unreacted epoxide groups will be located at the chain ends. During the samples preparation, post-curing process was conducted at constant temperature, where the change in the T_g resultant from the inclusion of the FNM increased the difference between T_g and the post-curing temperature. This behaviour may changed the relative probability of cross-linking promoting etherification/homopolymisation reactions of OH groups with epoxide chain ends. A consequence of this would be an increase in the ether contents of the system and unreacted, presumably, secondary amine groups. This is consistent with the increased strength in the absorbance peak of the ether groups evident from the FTIR spectra shown in Figure 7.1. In addition, the FTIR data also supports the interpretation that the unreacted amine groups presents in the modified systems. The

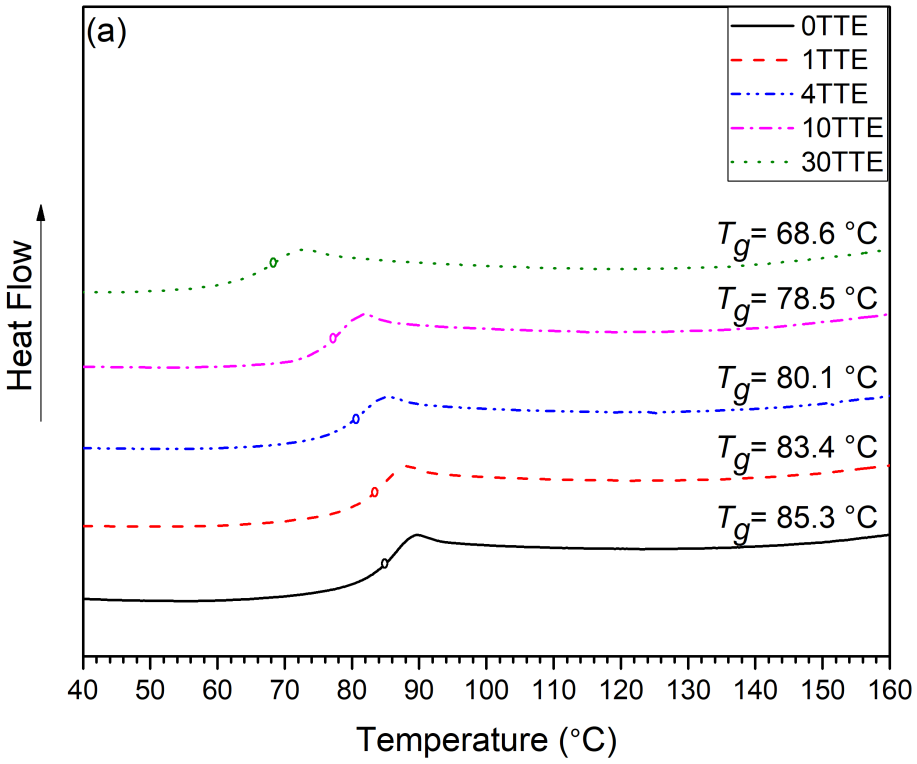

Figure 7.3: The DSC data of the neat and TTE modified amine cured epoxy resin systems.

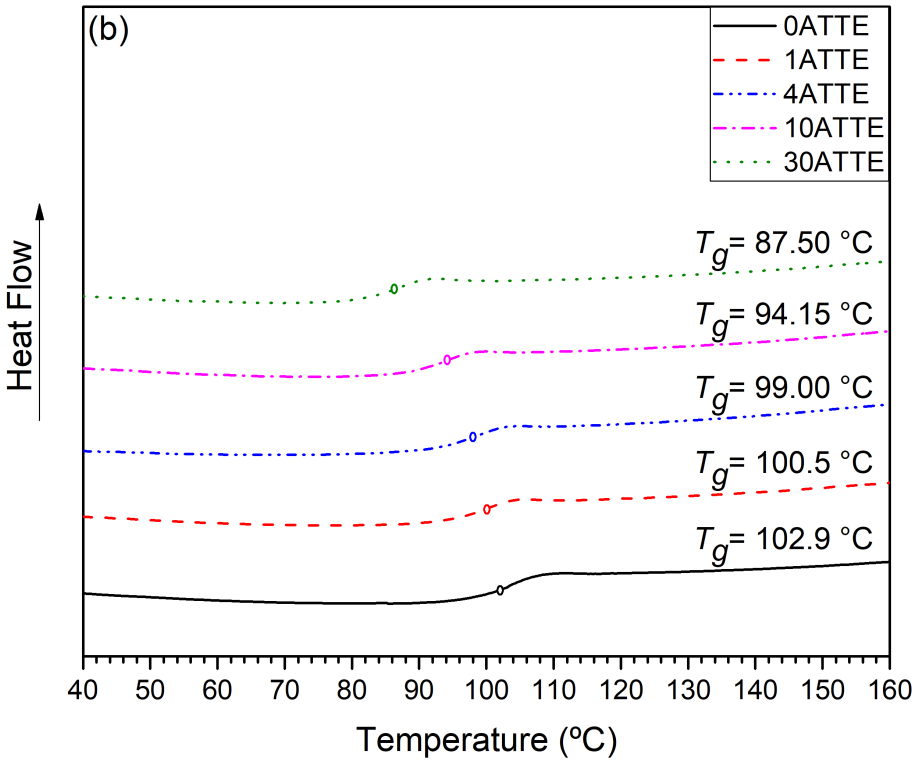

Figure 7.4: The DSC data of the neat and TTE modified anhydride cured epoxy resin systems.

presence of unreacted secondary amines in the modified systems would increase the contour length between the cross-links, which would promote chain mobility. This aligns with the decrease in the T_g for the TTE modified systems. Furthermore, substituting the epoxide groups of the resin with the epoxide groups from the TTE resulted in decreasing the composition of aromatic groups in the TTE modified systems. According to Neville and Lee [3], the aromatic groups influence glass transition process of the system. The concentration of the aromatic content in the system may be another factor that contributed to the reduction in the T_g of the amine cured TTE modified resin systems. From the above account, it is possible to suggest that the T_g of the TTE modified amine cured systems is associated with a number of factors, which occurs with no specific order, these factors are (a) variation in the network topology caused by the impact of the TTE on the probability of the cross-linking reactions, (b) the presence of unreacted amine groups which may have promoted etherification/homopolymisation reactions and (c) variation in the aromatic contents in the system resulted from the addition of the TTE modifier.

In the case of the anhydride cured systems, the curing reactions of the anhydride cross-linked systems are complex and involves a number of competing processes, this makes the association between the chemical changes observed from the FTIR spectra and the variation in the T_g quite challenging. However, the variation in the ester and ether regions (illustrated in Figure 7.2) suggests that the inclusion of the TTE modifier changed the cross-linking reaction, which resulted producing systems with different network structures.

7.3 Dielectric Spectroscopy

To provide an understanding for the relationship between the network topology, reaction pathway and the possible chemical composition of the systems, it was necessary to further examine the neat and modified systems by considering the behaviour of the molecular dynamic in these materials. Therefore, temperature dependent dielectric spectroscopy data were obtained for the studied systems. During the temperature dependent dielectric spectroscopy experiment, the dielectric behaviour was recorded at 10 °C interval, for the temperatures range from -160 °C to 180 °C. The dielectric data at the temperatures between -130 °C and -30 °C are used in this chapter, which were chosen based on the temperatures recommended by Vryonis et al [187], Ochi et al. [194, 195], Cuddihy and Moacanin [196]. The detailed temperature dependent dielectric behaviour of the neat amine cured epoxy resin systems are presented in Figures D.6, D.7 and D.8, while the data of the modified amine cured systems are shown in Figures D.9, D.10 and D.11, all located in Appendix D. Furthermore, the temperature dependent dielectric behaviour of the neat anhydride cured epoxy resin systems are shown in Figures D.12, D.13 and D.14, while the data of the TTE modified anhydride cured systems are illustrated

in Figures D.15, D.16 and D.17, in Appendix D. To indicate the extent of the dielectric behaviour, the temperature dependent dielectric measurements were conducted for the reference samples (neat amine and anhydride systems), and samples modified using 30 % of the epoxide groups from the TTE modifier, where as room temperature dielectric measurements were used to provide understanding of the general change in the dielectric behaviour for samples modified with 1 %, 4 % and 10 %. The data of the real and imaginary parts of the complex permittivity for the neat and TTE modified amine cured systems are shown in Figure D.18 and Figure D.19, while the complex permittivity of the anhydride cross-linked systems are illustrated in Figure D.20 and Figure D.21 in Appendix D.

First consider the effect of TTE on the molecular dynamics of amine cured systems, shown in Figure 7.5. At frequency range from 10^{-1} Hz to 10^{4} Hz, the γ relaxation appear as a broad peak, which implies that this relaxation originates from the motion of a number of dipolar species that are constrained by different environments. Figure 7.5 demonstrates that the strength of the γ relaxation of the modified systems is, generally, higher compared to the strength of the γ relaxation observed for the reference material. The extent of the γ relaxation is often related to the presence of different terminal groups in the system, including unreacted amine and epoxide groups [1, 149]. It is evident from the FTIR absorbance (Figure 7.1) that the TTE modified samples contains an increasing number of unreacted amine groups, which aligns with the increased strength of the γ relaxation. In a study on the dielectric properties of epoxy resins conducted by Hassan et al. [197], it was concluded that γ relaxation is associated with the motion of aminodiphenyl groups which enhance the mobility between cross-links. In addition, Jilani et al. [160] stated that ether groups are the key links that act as facilitator for the movement of the interposed molecules. In the current case, in formulating the modified samples, parts of the resin are being substituted by the TTE, consequently, reducing the number of diphenyl groups in the TTE modified samples compared to that of the neat systems. Therefore, it is possible to suggest that the increased strength of the γ relaxation noticed here is attributed to (a) the presence of unreacted dipolar molecules in the TTE modified systems; (b) the rotation of the moieties associated with the amine groups retained between the network nodes; and (c) the increase in the molecular mobility facilitated by the incorporation of a higher number of ether link and reduced aromatic content present in the modified topologies.

Regarding the β relaxation of the amine cured systems, it appears at frequency range from 0.1 Hz to 10 Hz as an increasing plateau in Figure 7.5(c) and a complete peak in Figure 7.5(d). The data suggests that the strength of the β relaxation is higher in the neat system compared to the strength of the β in the 30TTE system. For amine cured epoxy resins, it is generally accepted that the β relaxation is associated with (-CH_2-CH(OH)-CH_2-O-) hydroxylether groups formed during the cross-linking process [149, 169, 194, 197–200]. As such, the noticed decrease in the strength of the β relaxation

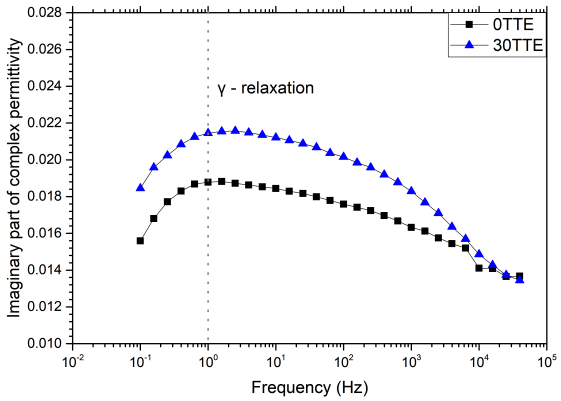

(a) -130 °C

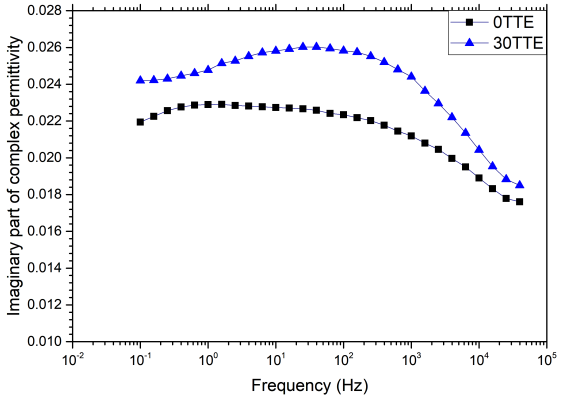

(b) -110 °C

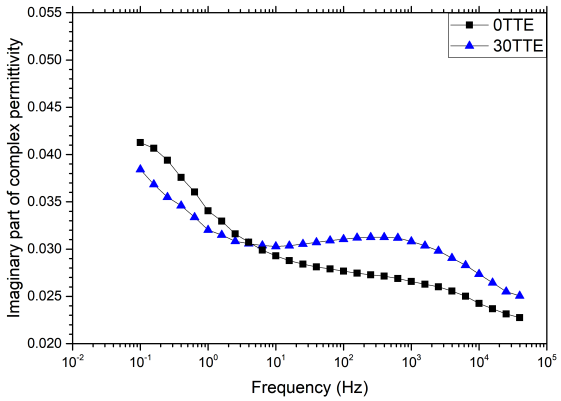

(c) -90 °C

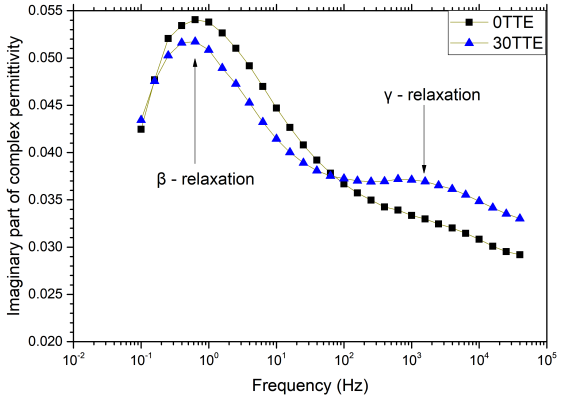

(d) -70 °C

Figure 7.5: Imaginary part of complex permittivity of reference and modified amine-cured resins at temperatures (a) -130 °C, (b) -110 °C, (c) -90 °C and (d) -70 °C.

of the 30TTE system aligns with the reported increase in the unreacted amine of the 30TTE evident from the FTIR spectra, which suggests that the modified systems have reduced cross-link density compared to that of the reference material. In addition to the β relaxation, Figure 7.5(d) features a second weaker process at frequencies above 100 Hz in the dielectric spectra of the 30TTE sample. By considering the intermediate temperatures, illustrated in Figures D.9 in Appendix D, it is possible to suggest that the noted dielectric feature is a bifurcation of the γ relaxation, which is still partially visible at -70 °C within the accessible frequency, while the comparable fraction of the γ relaxation of the neat epoxy is located at higher frequencies, thus, not apparent in the accessible frequency range. This interpretation aligns with the dielectric behaviour of the neat and 30TTE systems shown in Figure 7.5. According to Mikolajczak et al. [161], the γ and β relaxations are associated with the motion of molecules with different activation energy where each relaxation is constrained by the environment around the related dipolar species. Hassan et al. [197] suggested that variation the contour length of the molecular chains between the network nodes results in bifurcation of the dielectric relaxation. Therefore, a possible interpretation for the dielectric behaviour illustrated in Figure 7.5(d) is that there are a number of dipoles contributing to the behaviour, where the motion of each dipolar species is constrained by different environments, this would impact the contribution of the polar groups in the relaxation process and alter the temperature dependencies of the relaxation.

Turning now to the dielectric behaviour of the anhydride cured systems shown in Figure 7.6. Generally, the γ relaxation appears as a pronounced peak rather than a broad feature (compared to the γ relaxation in the case of the amine cured systems indicated in 7.5(a)). In the anhydride cross-linked reference system, the γ relaxation reached a maximum strength at frequency $\sim$40 Hz, which increases in strength and shifts to a lower frequency $\sim$5 Hz after the addition of the TTE modifier, as illustrated in Figure 7.6(a). Menczel and Prime [149] stated that the frequency displacement of a dielectric relaxation can be associated with the variation in the molecular structure and dipolar configuration in the system. Therefore, it is possible to suggest that the noticed change in the behaviour of the γ relaxation of the 30ATTE system could be attributed to the increase in the number of dipoles and the constrained environment resulted from the addition of TTE, which alines with the FTIR data presented in Figure 7.2. Indeed, increasing the temperature to -110 °C resulted in further shift in frequency and increase in the strength of the γ relaxation of both neat and TTE modified anhydride cured systems, as shown in Figure 7.6(b). The data acquired at the intermediate temperatures up to -70 °C suggests that the significantly increasing peak located at frequencies below 1 Hz is associated with β relaxation, as shown in Figure 7.6(c) (the related intermediate temperatures are shown in Figures D.12 to D.17, in Appendix D).

The FTIR spectra of the neat and 30ATTE presented in Figure 7.2, suggests variation in the proportion of the ether and ester groups. It is also evident from the FTIR data

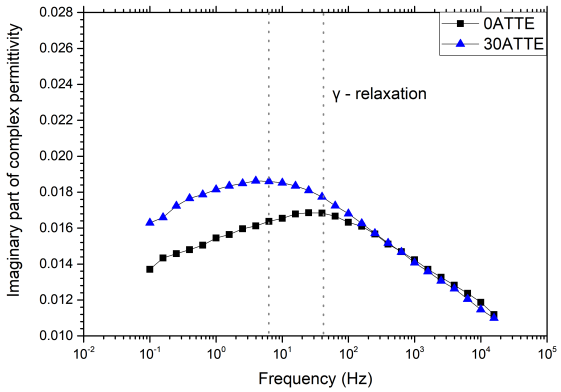

(a) -130 °C

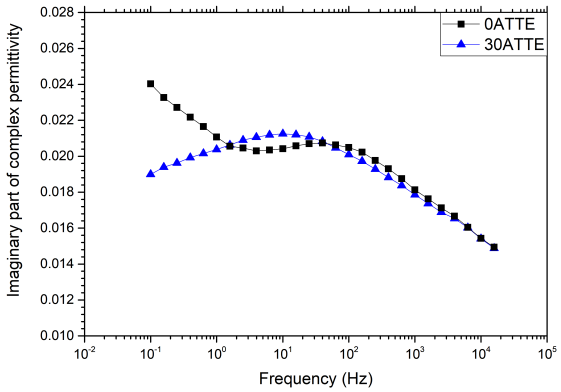

(b) -110 °C

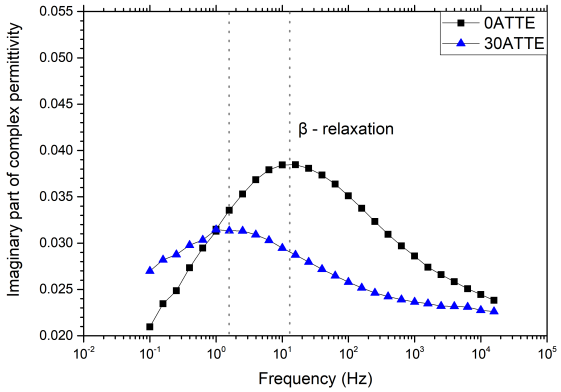

(c) -70 °C

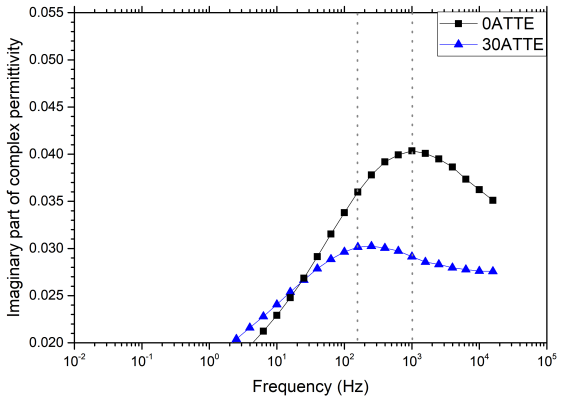

(d) -30 °C

Figure 7.6: Imaginary part of complex permittivity of reference and modified anhydride cured resins at temperatures (a) -130 °C, (b) -110 °C, (c) -70 °C and (d) -30 °C.

that the variation in the curing processes resulted from the introduction of the TTE modifier rather than change in the composition of ether groups, as both the TTE and the resin contains one ether group per epoxide groups within its chemical structure. While β relaxation of amine cured systems is investigated in a large body of literature, similar behaviour in anhydride cured systems have attracted less attention. Indeed, Cuddihy and Moacanin [196] have studied the impact of different anhydride hardeners on the curing mechanisms of epoxy resins, where it was concluded that diester segments created during the curing reactions influence the motion of interposed groups to a degree determined by local steric factors. These findings are similar to recommendation of Jilani et al. [160] reported for amine cured systems. Therefore, it can be proposed that the β relaxation of the modified system may be attributed to the conformational motion of the molecules provided by the diester links, where the strength of the β relaxation is linked to the cross linking density. In addition, based on the FTIR spectra of the anhydride cured systems shown in Figure 7.2, the data indicates that the cross-linking mechanisms were affected by the inclusion of the TTE, where the data reveals stronger ester absorbance peak for the 30ATTE system compared to that of the reference material, whereas, the ether absorbance peaks were stronger in the spectra of the neat epoxy than in the FTIR data of the 30ATTE. This increase in the ether content is a result of the the reaction of the OH groups with the epoxide groups in the system. The molecular structure of the DGEBA contains reactive hydroxyl groups, while the structure of the TTE lacks any potential OH groups. Consequently, the structure of the cured neat systems is expected to contain higher concentration of hydroxyl groups compared to that of the TTE modified systems. Therefore, the slight increase in the ether content in the neat system evident from the FTIR spectra may result from the reaction between the epoxide groups and the OH in the system in a homopolymerization reaction. From the above account, it can be seen that the data of the DSC, FTIR and dielectric spectroscopy correlates well with each other, where the high T_g of the neat systems suggest a highly cross-linked system, which aligns with the increase in the strength of the β relaxation associated with the high hydroxyl content. Where the hydroxyl are formed during both the cross-linking reactions (evident from T_g) and the additional cross links generated by homopolymerization reactions (suggested from the FTIR data).

The homopolymerization process consumes the epoxide groups retained in the system. As the same stoichiometric ratio of epoxide groups to active groups of the anhydride hardener were used in both the neat and TTE modified systems, an increase in the epoxide groups consumed through etherification and homopolymerisation (reaction of an epoxide group with an OH group), compared to the relative consumption of epoxide groups through esterification (reaction of an epoxide group with the anhydride hardener), suggests a change in the number of the related species trapped in the system. In addition, it is reasonable to suggest that some active groups may become retained in the network after vitrification, most of these residues are likely to be located at chains that ends with the unreacted epoxide and/or anhydride groups. Consequently, it is possible to suggests

that the variation in the strength of the γ relaxation (shown in Figure 7.2) is associated with changes in the number of terminal groups after the inclusion of the TTE modifier.

From the discussion presented above, it can be seen that the dielectric relaxation was explained in terms of the chemical variation observed by the FTIR data. Based on the findings of some studies [159, 198, 201, 202], it was possible to propose a relationship between the chemical species and the dielectric relaxations in the studied systems. It is suggested that the data reported here implies that the dielectric behaviour is not governed only by the dipolar species, but the environment around the dipolar units also plays an important role in determining the dielectric behaviour. Due to the complex network architecture of the epoxy cross-linked systems, molecular dynamic simulations are quite challenging and, to the time of writing this research, most of the studies that reported simulations for molecular dynamics of epoxy resin system did not consider the dielectric relaxations [203–206]. However, detailed analysis were conducted for thermoplastic materials that feature a high T_g and comprises ether links and aromatic structures. As such, these systems have parallels with the chemical structure of the neat and TTE modified systems reported here.

In the study conducted by McGonigl et al. [207], dynamic mechanical thermal analysis combined with dielectric relaxation analysis were conducted for three different polymeric materials, namely, polyethylene naphthalate (PEN), polyethylene terephthalate (PET) and a series of polyethylene terephthalate coethylene naphthalate (PETN). In this work, McGonigl et al. associated the variation in the strength of the β relaxation with the movement of dipolar units present in different local environment, where the localised chain motions associated with the β relaxation were suggested to be limited for densely packed structures. In a study conducted by Verot et al. [208] a double β relaxation was observed from the dielectric analysis of the poly(aryl ether ether ketone) (PEEK). The observed behaviour of the β relaxation was attributed to the gear rotation type motion of diphenyl ketone (DPK) groups. Specifically, these β relaxations were associated with the motion of two class of DPK units, in the first β relaxation, the units are located in a single molecule but remote from one another. While in the second β relaxation, the behaviour was related to DPK units located in closer proximity to each other but present in chain ends that described as "entangled or ball-forming" configurations. In addition, the data of Verot et al. [208] also suggested the presence of γ relaxation located at temperatures below the temperatures at which the double β relaxations were observed. Verot et al. associated the γ relaxation with the highly localised wagging of polar bridges, where the rise in the temperature would progressively transform it to β associated motion. Aurélie et al. [209], also examined the behaviour of the β and γ relaxations in PEEK, where it was reported that the γ relaxations is associated with the the localised rotational mobility of phenylene groups. Whereas, the β relaxation was attributed to the displacement of conformational defects in the system. Aurélie et al. suggested that the molecules cooperative mobility take place in all processes (γ,

β and α), where the level of intermolecular cooperative mobility increases on moving from low temperature relaxations (γ and β) to the high temperature relaxations (α process). Therefore, it is perhaps more accurate to propose the dielectric relaxations are inter-related in nature where the relaxations originate from the small dipolar unit through to larger molecular segment in the system, rather than attributing the relaxation processes exclusively with different dipolar species. Similar findings were reported for the α relaxation in amorphous materials by Rault [210], where α relaxation was claimed to originate from a number of β type processes.

To sum up, several studies have investigated the dielectric response of epoxy resin systems, where the different relaxations were suggested to originate from varied molecular origins. The association between the dipolar species and the local network structure is an important factor in determining the behaviour of the dielectric relaxation. Here, the γ relaxation was attributed to the motion of small dipolar units such as unreacted secondary amines, terminal epoxide groups and unreacted chain ends with anhydride residue. The β relaxation of the amine and anhydride cross-linked system is related to the motion of segments generated during the curing process, which are hydroxylether groups (-CH_2-CH(OH)-CH_2-O-) in the amine cured systems and diester segments in the case of the anhydride cured systems.

7.4 Electrical Conductivity

The electrical conductivity measured for the amine and anhydride cured for both neat and TTE modified systems are presented in Figure 7.7. The quoted values correspond to the average of the last one hundred measurement points obtained from three different samples of the same composition and the uncertainties correspond to the associated standard deviation. As can be seen from the Figure 7.7, prior to the inclusion of the TTE modifier, comparble DC conductivity is reported for the reference system for both the amine and the anhydride cured, about $10.3 \pm 0.5 * 10^{-18}$ S/cm and $3.4 \pm 1.3 * 10^{-18}$ S/cm respectively. This indicates that the type of the hardener has limited influence on the conductivity of the cured system. By varying the system topology, the data of the DC conductivity of the amine cured systems indicates significant variation in the electrical conductivity compared to the change in the conductivity of the modified anhydride cured systems. This behaviour could be explained by the existence of four factors, which are (a) the presence of unreacted groups from the resin and hardener (revealed by the FTIR data), (b) the inclusion of moieties explicitly present through the addition of the FNM, (c) the influence of the unreacted part of the FNM and (d) the variation in the free volume and the associated change in network topology.

The TTE modifier features three terminal epoxide groups within its chemical structure. This means that the TTE contributes to the curing process and that its functional

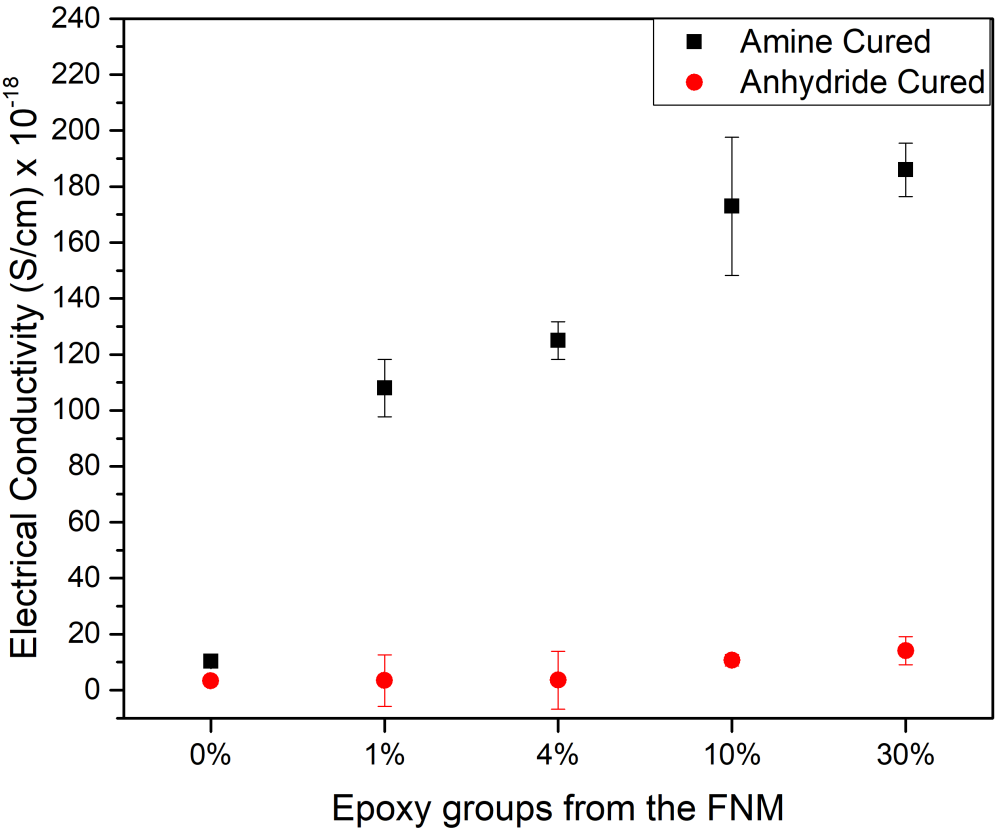

Figure 7.7: The electrical conductivity of the reference and modified amine and anhydride cured resins.

group (methyl groups) of the TTE become retained in the system after curing, which results in forming a network with branched structure. The DC conductivity of epoxy resin systems modified by the inclusion of GHE and GNPE modifiers, indicated the the presence of alkyl chains influence the electrical conductivity of the modified systems, as it was discussed in chapter 6, which is not the case here. The DC conductivity data of the anhydride cured systems reported here indicates that the inclusion of varied percentages of the TTE resulted in an insignificant variation in the the electrical conductivity of the modified systems. Consequently, the data suggests that the presence of the methyl group in the structure of the modified systems, may not be the factor that is responsible for the variation in the DC conductivity of the amine cured systems [175, 211].

Analysis of the conductivity behaviour in polyethylene with excess electrons suggested the presence of localised regions of free volume, which features electrons located in low energy states where these regions may be transformed within the network. Whereas, based on the discussion of the T_g of the amine and anhydride cured systems, it is not accurate to associate the variation in the electrical conductivity with the change in the free volume in the system. Furthermore, Cubero and Quirke [180] suggested that excess electrons become self-trapped in the system as localised polarons, where the calculated self-trapping energy was reported to be small leading to the suggestion that mechanism

such as phonon assisted hopping may be the mechanism upon which charges travel through the system. From the discussion of dielectric data presented above, it can be seen that the variation in the molecular dynamics is associated with the inclusion of the TTE modifier in both the amine and anhydride cured systems, since similar behaviour was not present in the DC conductivity measurements of the anhydride cured systems (invariant DC conductivity), it is possible to suggest that the variation in the molecular dynamics is unlikely to be the factor that influences the conductivity.

Turning now to the electrical behaviour of the amine cured systems, unlike the anhydride systems, several studies have investigated the charge transport in amine cross-linked epoxy resin systems [3, 212]. These studies suggested that the electrical conductivity of the amine cured systems is correlated with the linkage generated between the amine hardener and the epoxide groups formed during the curing reactions, while Alhabill et al reported higher DC conductivity for amine rich epoxy resin systems [113]. As was indicated from the dielectric spectroscopy data and confirmed from the FTIR spectra, unreacted secondary amine groups are present in the TTE modified amine cured systems. Therefore, it is possible to suggest that the electrical conductivity of the amine cured systems is associated with variation in the charge transport behaviour resulted from the presence of the functional groups in the modified systems. This conclusion is in good agreement with the findings of Meunier and Quirke [179], where it was suggested that the charge transport dynamics are influenced by the presence of molecules that are electrically responsive to the electric field (amine groups in the current work).

7.5 Summary

In this chapter, the dielectric behaviour of the modified amine and anhydride cured epoxy resin systems was investigated. The influence of the effect of different curing mechanisms on the FTIR, DSC, dielectric spectroscopy and DC conductivity of the modified epoxy resin systems were also examined. The FTIR spectra showed that etherification reactions resulted in an increase in the concentration of ether groups. Since the chemical structure of the TTE features one ether group per epoxide group, which is similar to the resin, the change in the chemical composition of the modifier was suggested to have insignificant influence on ether groups. In anhydride cured systems, the FTIR data suggested that the TTE modifier influences the network topology of the resin through the cross-linking reactions by promoting esterification process and reducing the probability of etherification mechanism.

The glass transition temperatures of both systems were reduced after the introduction of the FNM. The shift in T_g was associated with two factors, namely, the type of the hardener and the influence on the TTE on the network topology resulted from the variation in the curing reactions after the addition of the TTE.

The inclusion of the FNM resulted in altering the molecular dynamics of the resin. The extent of γ relaxation of the amine cured FNM modified resins were higher compared to the unmodified systems. This was correlated to three factors, the presence of retained dipolar molecules in the TTE modified systems, the rotation of the amino-diphenyl groups, and the increase in molecular mobility facilitated by the incorporation of a higher number of ether link resulted from the modified network topologies. The effect of TTE on β relaxation was interpreted by the nature of the restrained environments that constrained the dipoles after the introduction of the TTE.

In the case of the anhydride cured systems, the etherification process evident from the FTIR was used to explain the extent of β relaxation, where the later is associated with the cross linking density. On the other hand, the γ relaxation of the anhydride resins was associated with the same factors that influenced γ of the amine systems.

Finally, the electrical conductivity was suggested to be influenced by four factors, which are, the presence of unreacted functional groups from the resin and hardener or moieties explicitly introduced through the inclusion of the FNM, the influence of the unreacted part of the FNM, variation in the free volume and change in network topology.

To sum up, the presence of the functional network modifier has influenced the chemical, thermal and electrical properties of both systems. The behaviour is more complex with the anhydride cured materials as the curing mechanisms involve generation and consumption of hydroxyl groups. Literature lacks detailed analysis of the dielectric behaviour of anhydride cured resins, while the presence of the FNM makes providing unambiguous interpretation for the behaviour more challenging. Therefore, the next chapter will conduct a detailed analysis for the dielectric molecular relaxation of neat and FNM modified anhydride cured systems.

Chapter 8

Investigation of the effect of the functional network modifiers on the molecular dynamics of complex epoxy resin systems

The previous chapter has shown that the molecular dynamics in modified epoxy resin systems are related to the network topology, curing mechanism and the retained groups in the system. The influence of these factors on the molecular dynamics such as the activation energy of dipole relaxations, the molecular origins of the dielectric loss and charge transport process, remain to be understood. There is still a considerable variability in the literature regarding the origin of the molecular relaxations in epoxy resin systems (especially, β and γ relaxations). Perhaps the main reasons for the reported inconsistencies could be due to variation in the resin curing mechanism, inconsistent preparation methods and unknown percent of unreacted groups retained in the system. Most of the results reported in literature failed to address the effect of variations in the resin network architecture on the molecular dynamics, particularly, in complex systems such as anhydride cured resins where the material goes through multi complex curing mechanisms before it becomes fully cured. Due to the existence of terminal groups in epoxy resins networks, they are highly likely to affect the molecular dynamics of the resin system. While the previous chapter has shown that retained functional groups of the FNM influence the molecular dynamics in both amine and anhydride cured systems, it is hypothesised that the chemical structure of the FNM could be a detrimental factor for the affect of FNM on the dielectric properties of the tested systems. Therefore, the work described in this chapter is set out to investigate the effect of altering the network structure using different percentages of two functional network modifiers (GHE and GNPE) on the molecular dynamics of complex epoxy resin systems. The FNM considered here were chosen so as to enhance molecular mobility without directly introducing additional dipolar relaxations or charge carriers into the system. This will test the hypothesis which state that modification of the resin structure affect the molecular dynamics, and that the γ and β relaxations are associated with retained groups, while α relaxation is related to segmental movement of main-chains, the consequent dipole relaxation activates charge transport above T_g.

8.1 Differential Scanning Calorimetry

To understand the molecular dynamics of modified anhydride cured epoxy resins, samples were manufactured with 30 % of the epoxide groups supplied from GHE and GNPE modifiers.The reasons for selecting this specific percentage of the FNM is due to the

Table 8.1: DSC measurements for reference and modified epoxy systems

Sample	T_g (± 2 °C)
Reference	102
30AGNPE	52
30AGHE	36
20AGHE	50

fact that increasing the loading beyond 30 %, in most FNM such as GHE, GNPE and TTE, would result in decreasing T_g below room temperature, which makes measuring some properties and obtaining exact values quite a challenge. This especially applies for the amine cured systems where the addition of 30 % of the epoxide groups of the GHE resulted in shifting T_g out of the accessible limit of the experimental setup. Therefore, to make comparisons between the amine and anhydride cured system, whenever possible, 30 % is the maximum percentage of the epoxide groups introduced by the FNM used in this work. As will be explained later in this chapter, to understand the effect of the GHE and compare the effect of GHE functional groups with that of the GNPE, GHE modified samples were made with a certain percentage so that the T_g of GHE systems is the same as T_g of the GNPE modified materials. The required percentage of the epoxide groups from the GHE was found to be 20 %. Accordingly, in addition to the 30 % GHE and GNPE anhydride cured systems, GHE modified samples were produced with 20 % loading. The different properties of the modified samples were compared with that of the reference material, which is a neat anhydride cured DER 332 epoxy resin. The glass transition temperatures of the reference and modified anhydride cured resins are illustrated in Table 8.1.

As expected, the addition of both FNM molecules results in a general reduction in T_g. By comparing the effect of GHE and GNPE on T_g reported in Table 8.1, it can be seen that 30AGHE and 30AGNPE resulted in shifting T_g to lower temperatures by 66 ± 2 °C and 50 ± 2 °C respectively. This can be explained due to: first the alkyl chain in GHE contains sixteen carbon atoms while that in GNPE contains only nine. Consequently, additional free volume will be introduced by the GHE, which is consistent with published work on the effect of GHE on T_g [213], and FNM with long chain alkyl groups [115]. Secondly, the GNPE contains an aromatic ring within its chemical structure, these rings may interact with the aromatic rings within the backbone of the epoxy network, thereby restricting the mobility of the overall branching moiety. This process is consistent with the effect of aromatic structures on the thermal stability of epoxy resins suggested by Neville and Lee [3] and T_g reported by Babayevsky and Gillham [178]

8.2 Electrical Conductivity

The effect of the temperature on the electrical conduction in the neat and modified material systems is shown in Figure 8.1 and Figure 8.2. In the case of the unmodified systems, the current measured after 100 s falls below the equipment limit and cannot be differentiated reliably from instrumental noise. Therefore, values of the conductivity were limited to 100 s, as shown in Figure 8.1.

Generally, all the modified systems exhibited a higher conductivity compared to the reference material with behaviour varying according to the functional group of the FNM and the temperature of the measurements. For example, compare the conductivity of the unmodified specimens (all measurements were conducted below T_g which is 102 ± 2 °C) with the conductivity of 30AGHE (where the measurements were obtained above and below T_g which is 36 ± 2 °C). For the unmodified systems, the conductivity increased with increasing temperature, where similar behaviour was noticed for the 30AGHE systems in the glassy state (below T_g). When the measurements where conducted in the rubbery state at 50 °C, which is well above the measured T_g, the conductivity increased by several orders of magnitude, as shown in Figure 8.2(a). Also the inclusion of the FNM resulted in an increase in the conductivity of the modified systems and a comparable time dependence to that of the neat system.

To further illustrate the behaviour of the different material formulations, consider the values for the transient conductivity after 100 s (σ_{100}) and the initial conductivity (σ_i), as illustrated in Figure 8.3 and Figure E.1 respectively. The values of σ_i and σ_{100} are determined for each system by averaging the initial 10 data points and the final 10 data points up to 100 s. The 100 s time scale was selected based on the experimental setup explained in section 4.6 in chapter 4, where it was found that measurements conducted at high temperatures reach a stable state at about 100 s and the data obtained at low temperature measurements indicated an acceptable noise levels. While, after 100 s, the data acquired at low temperatures become dominated by noise as the obtained data falls below the accessible limit by the equipment (an example of the electrical conductivity measurements conducted at time up to 1000 s is presented in Figure E.3 located in appendix E). From Figure 8.1 and Figure 8.2, the dependence of the conductivity on the temperature for the reference and modified samples obeys Arrhenius equation. By considering σ_{100} as the rate constant, the power law equation can be represented as:

$$\sigma_{100} = Aexp\left(-\frac{E_a}{kT}\right) \tag{8.1}$$

From Figure 8.3 the following can be suggested:

- The neat system, depicted a time dependent variation in σ_{100} with low activation energy (E_a=0.1 ±0.01 eV) which results from transient conduction.

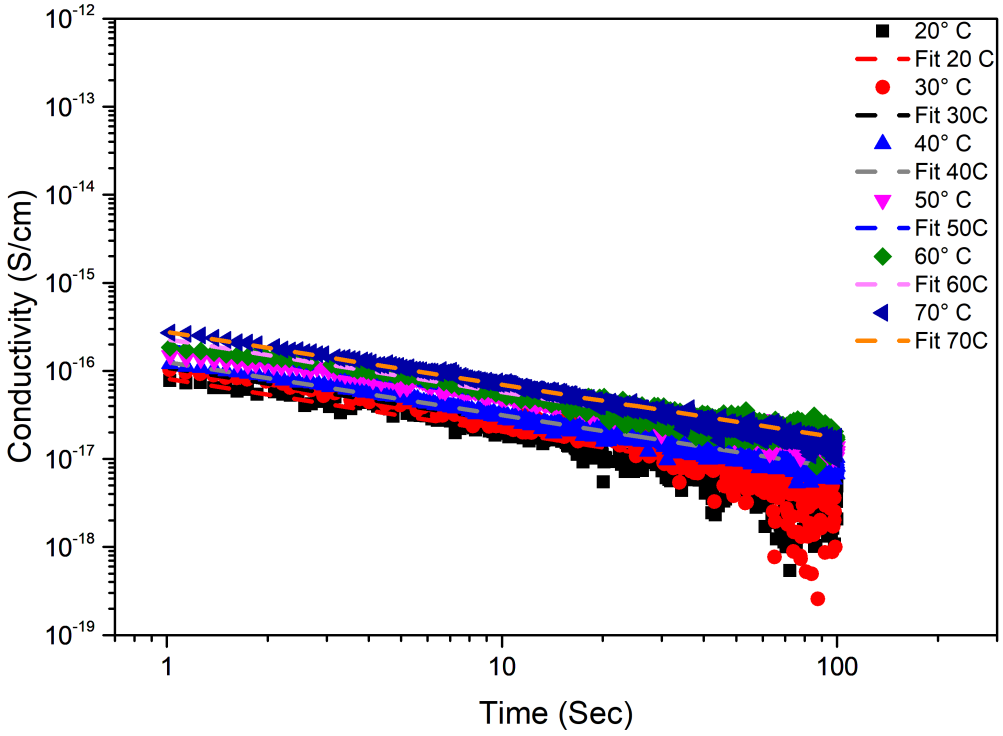

(a) Temperature dependent conductivity of reference epoxy resin system

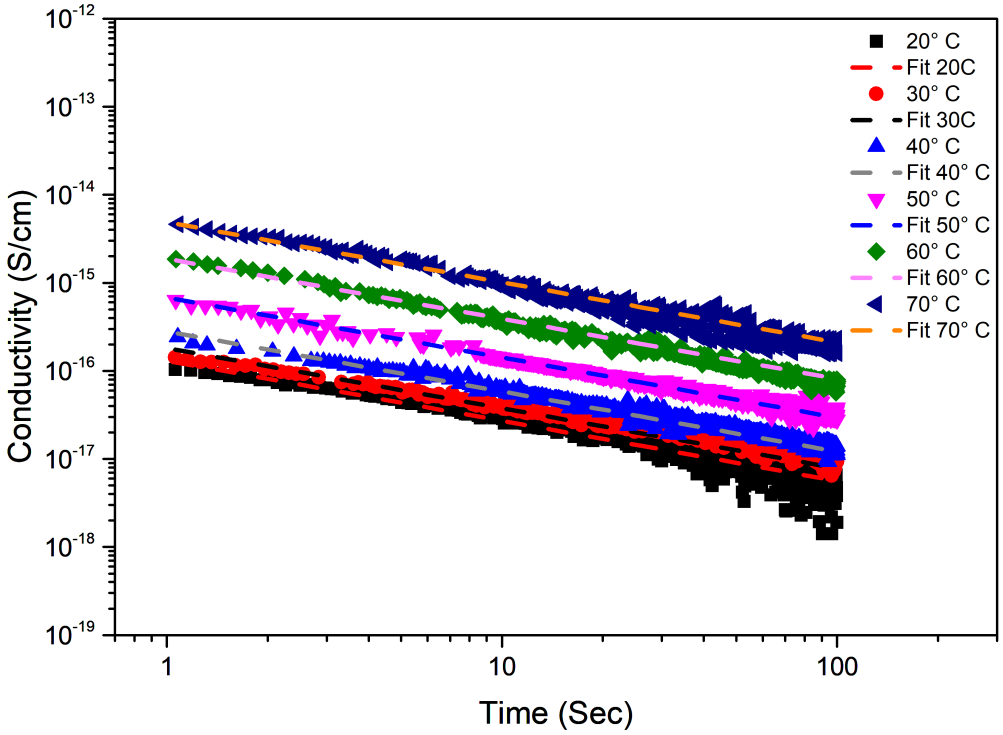

(b) Temperature dependent conductivity of 30AGNPE system

Figure 8.1: Variation of the conductivity with time at an applied field of 5.5 kV mm^{-1} from 20 °C to 70 °C for (a) the reference epoxy resin (DSC $T_g = 102 \pm 2$ °C) and (b) the 30AGNPE samples (DSC $T_g = 52 \pm 2$ °C).

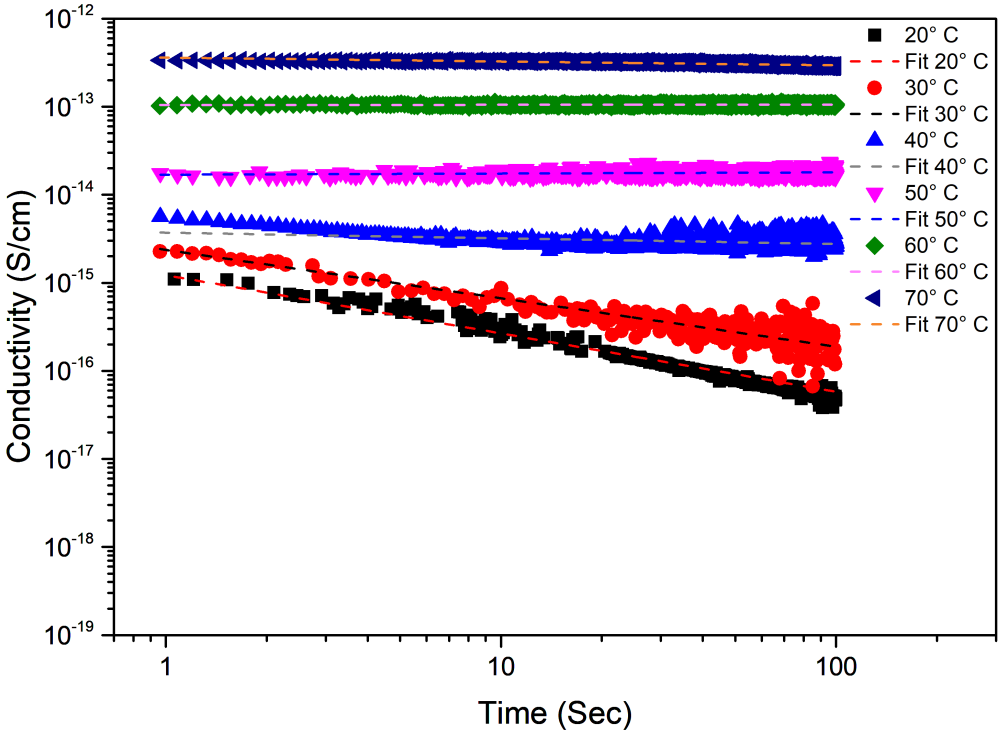

(a) Temperature dependent conductivity of 30AGHE system

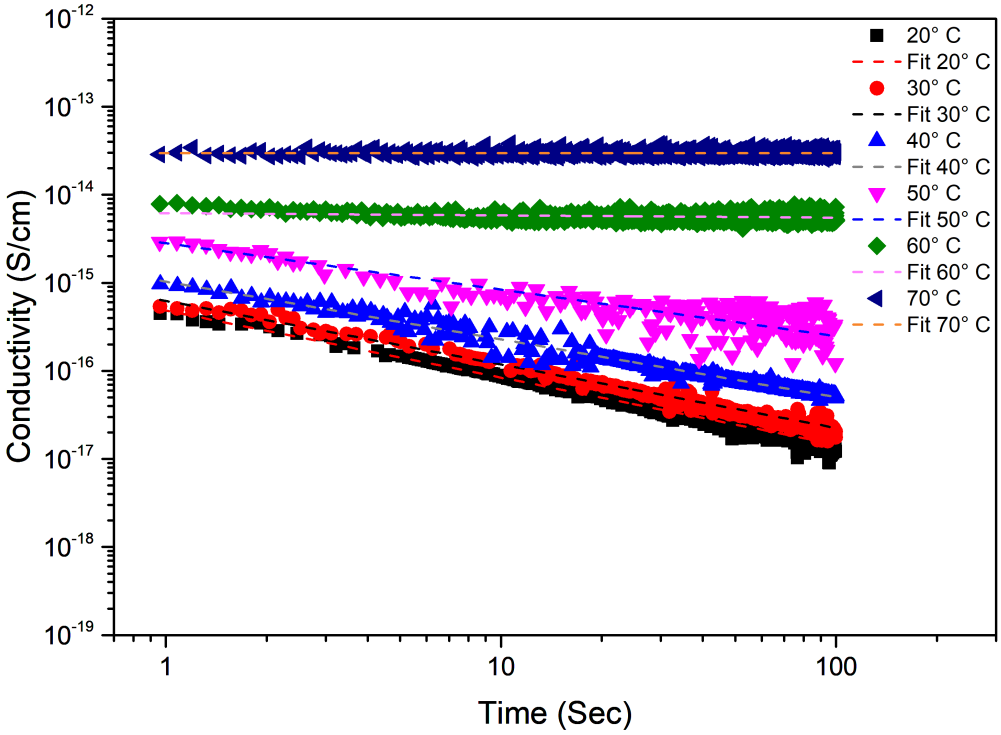

(b) Temperature dependent conductivity of 20AGHE system

Figure 8.2: Variation of the conductivity with time at an applied field of 5.5 kV mm^{-1} from 20 °C to 70 °C for (a) 30AGHE samples (DSC $T_g = 36 \pm 2$ °C) and (b) the 20AGHE samples (DSC $T_g = 50 \pm 2$ °C).

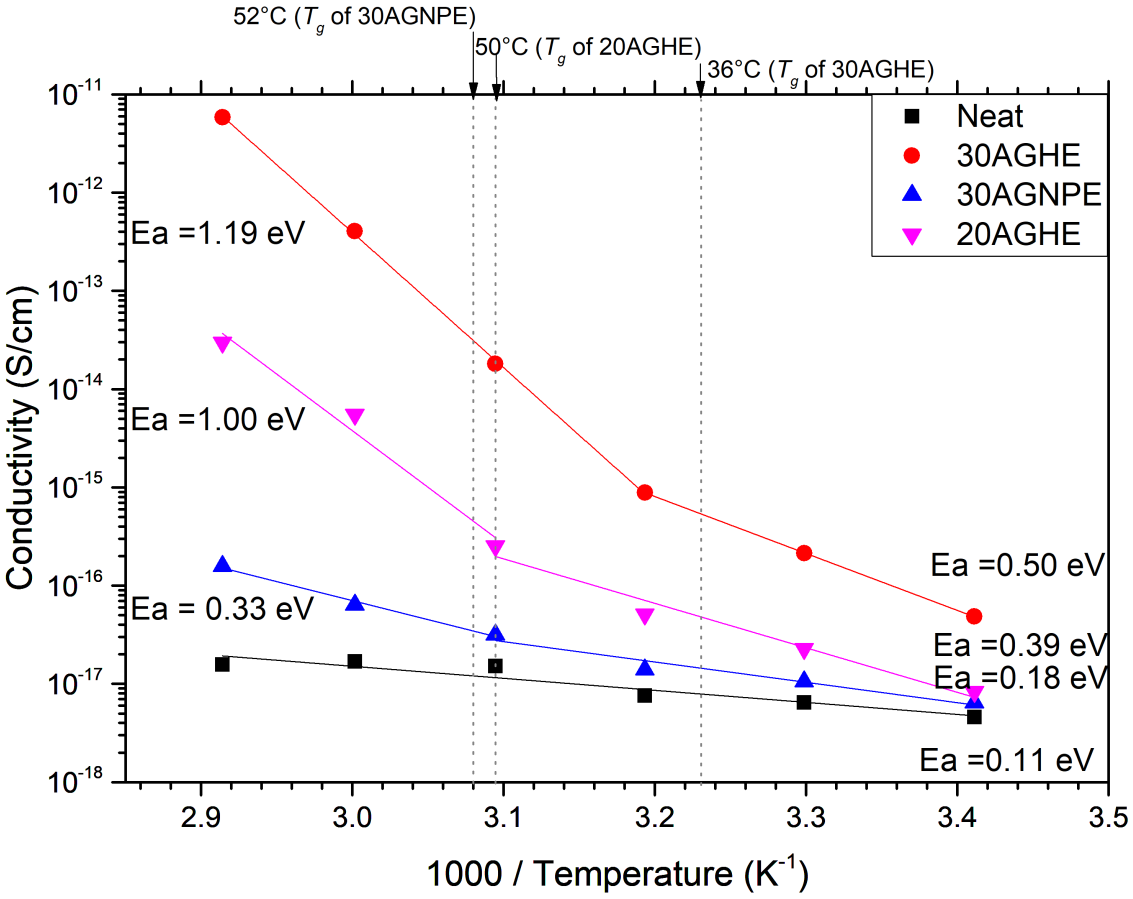

Figure 8.3: Variation of the conductivity, as represented by the quantity σ_{100}, with time at an applied field of 5.5 kV mm^{-1} from 20 °C to 70 °C for the different material formulations.

- σ_{100} of systems modified using GHE measured in the glassy state (below T_g = 36 ± 2 °C and T_g = 50 ± 2 °C for the 30AGHE and 20AGHE respectively), illustrated similar behaviour to that of the neat system with higher activation energy (E_a=0.50 ±0.02 eV and E_a=0.39 ±0.05 eV for the 30AGHE and 20AGHE respectively).

- σ_{100} of the GHE modified systems measured at the rubbery state (above T_g, at specific temperatures 40 °C for the 30AGHE and 50 °C for the 20AGHE) illustrated time independent behaviour which seems to be a DC conductivity with high activation energy (E_a=1.19 ±0.02 eV and E_a=1.00 ±0.03 eV for the 30AGHE and 20AGHE respectively).

- For the GNPE modified systems, the activation energy of σ_{100} for the process above T_g is low (E_a= 0.33 ±0.05 eV) compared to samples modified using GHE. Similarly, the increase in the conductivity resulting from the inclusion of 30% of the epoxide groups from the GNPE is lower than that of the GHE for the same

loading. This suggests that the conductivity is modified using different charge transport processes in GNPS compared to that in GHE.

The above reflects the fact that the current is produced by two different processes, DC conductivity and a transient conductivity where the transition between the two processes is governed by the glass transition temperature of the system and the functional groups of the modifier.

Now consider the variation of current with time, t, which is commonly described by the Curie-von Schweidler power law relationship [214–216].

$$I(t) = at^{-b} \tag{8.2}$$

In this equation, I is the current, t is the time after application or removal of the field, a and b are constants. Data sets of the reference and modified regimes (shown in Figure 8.1 and Figure 8.2) were initially fitted using Equation 8.2 with both a and b as free regression parameters. Figure 8.4 presents a comparison between the values of the constant a and σ_i. In this figure, parameter a was set as a free regression parameter where parameter b was set to a fixed value or a free regression parameter. The generated values for parameter a aligns perfectly with σ_i, as shown in Figure 8.4, which indicated the consistency of the method utilised. The determined values of parameter b are shown in Figure 8.5.

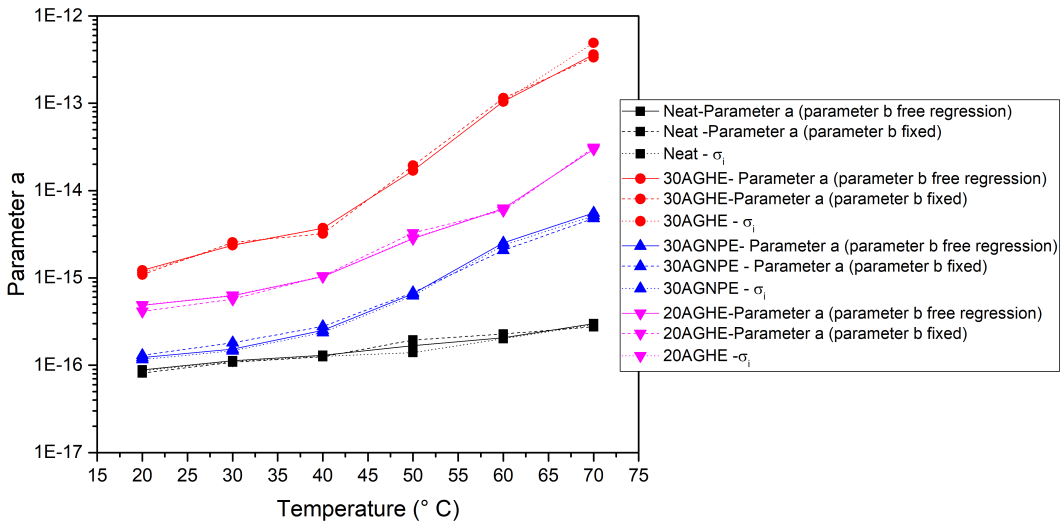

Figure 8.4: Values of parameter a compared with σ_i, illustrating the effect of altering parameter b on the values of a.

From Figure 8.5 it is evident that the data fall into two groupings: values of b around zero, which correspond to a time invariant DC conduction process and values of b between 0.50 and 0.80 corresponding to an AC conductivity that will give rise to a

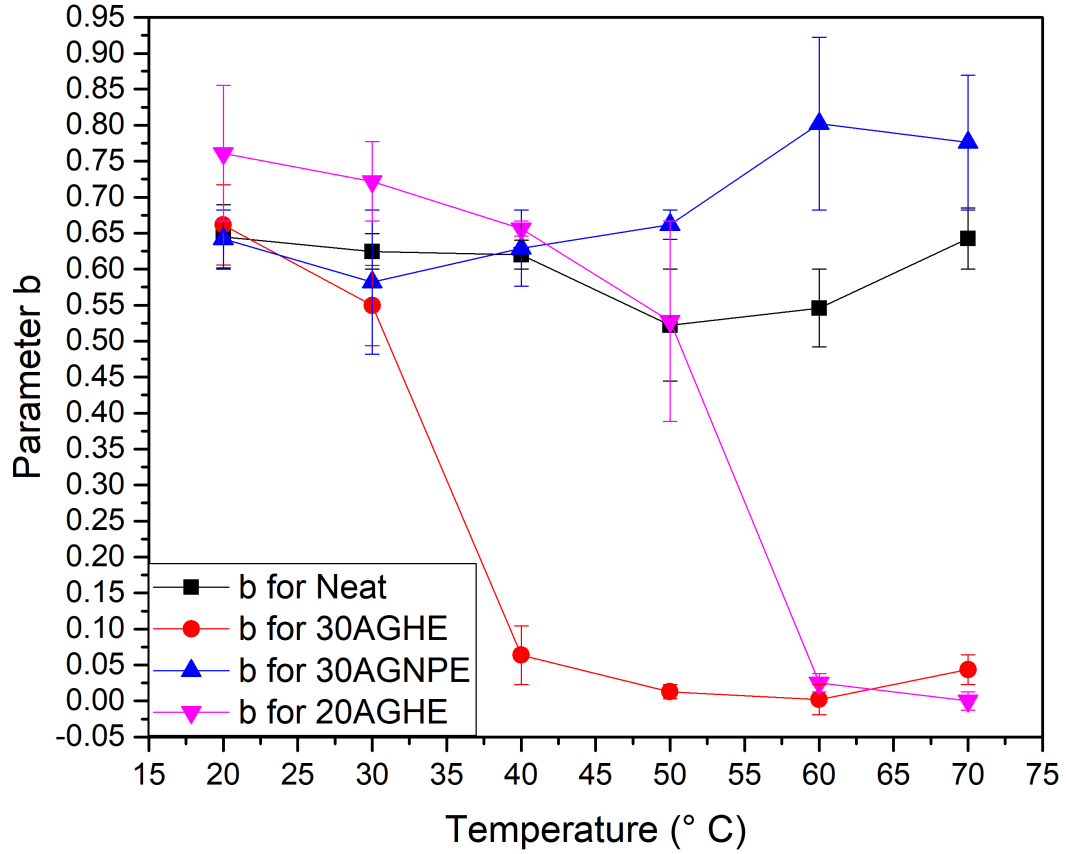

Figure 8.5: Values of fitting parameter b.

dispersion in the dielectric response. As a result, the allowable range representing the best fit estimated by taking the mean values of b is zero and 0.6 are close to what is observed which was used for the fitting. All the data of the reference epoxy presented in Figure 8.1 and Figure 8.5 correspond to systems that were in the glassy state. Similarly, when 20AGHE and 30AGHE are glassy, the conductivity varies with time in a similar manner whereas, above T_g, it becomes time invariant (b = 0). However, in the case of 30AGNPE, taking b = 0.68 both below and above T_g provides a good fit to the experimental data, suggesting that the process of charge transport is modified in different ways in systems containing GHE and GNPE (see Figure E.2).

8.3 Dielectric Spectroscopy Analysis

As the epoxy resin reacts chemically with the hardener, during the curing process, molecular diffusion decreases until no more reactions are possible, whereupon development of the structure is virtually halted. This affects the DC or ionic conductivity in the system, while the formation of the hydroxyl groups in the cross-linking process results in a

reduction in the possibility of proton conduction (subatomic particle with equal positive and negative electric charges) along the H-bonds of the resin [47].

Indeed, the formation of the cross-links also influences the number of dipoles associated with the bonding of the chemical groups (which later reach a thermally stable configuration) where the orientation and polarisation of these dipoles contribute to the permittivity of the material. Thus, in addition to the effect of the inclusion of FNM on the conductivity, the complex permittivity and molecular dynamics of the modified systems are also altered. The temperature dependent imaginary part of the complex permittivity of the neat anhydride cured epoxy resin systems and resins modified using GNPE and GHE is shown in Figures 8.7, 8.8, 8.9 and 8.10 respectively. The associated plots of the real part of the complex permittivity are illustrated in Appendix E.
Generally, there are four main features of interest in the graphs of the imaginary part of the complex permittivity. These processes (labeled as process 1 to process 4) are explained in the next section where the effects of the different functional groups of the FNM are illustrated.

In order to provide a better understanding of the effect of each FNM on the β and γ relaxations, it is necessary to examine the effect of the FNM on each relaxation separately by using a relaxation model. Functions such as Cole-Cole, Cole-Davidson, Havriliak-Negami and Dissado-Hill, are examples of models used to investigate the dielectric behvaiour and charge motion in polymeric materials. Empirical formulas (Cole-Cole, Cole-Davidson, Havriliak-Negami) provide a physical interpretation for the charge behaviour and morphology in dielectric materials, while the Dissado-Hill model also considers the effect of the interaction between the microscopic groups in the material [1, 217]. The fractal mode proposed by Dissado-Hill provides an understanding of the charge motion at low frequency and high temperature [218, 219], whereas the Havriliak-Negami describes the dielectric relaxation at lower temperatures [220]. Since the β and γ occur at low temperatures (below 0°C) the temperature dependent imaginary part of the dielectric spectroscopy for the different systems was fitted using the Havriliak-Negami (HN) fitting function. Detailed graphs of the experimental data along with their HN fit and the deconvolved peaks for the molecular relaxations of all the system are plotted in Appendix E, an example of the HN fitting of the data is shown in Figure 8.6. The temperature dependence of the β and γ peaks for the different systems deconvoluted using Havriliak–Negami fit are shown in Figures 8.7, 8.8, 8.9 and 8.10.

8.3.1 Process 1 (charge transport)

The mobility of charge carriers in a material induced via an external field results in a DC (ohmic) conductivity term contributing to the dielectric response of the system. Charge transport in an epoxy resin may be observed as an increase in the magnitude (invariant of the frequency) of the complex permittivity at the low frequency end of the dielectric

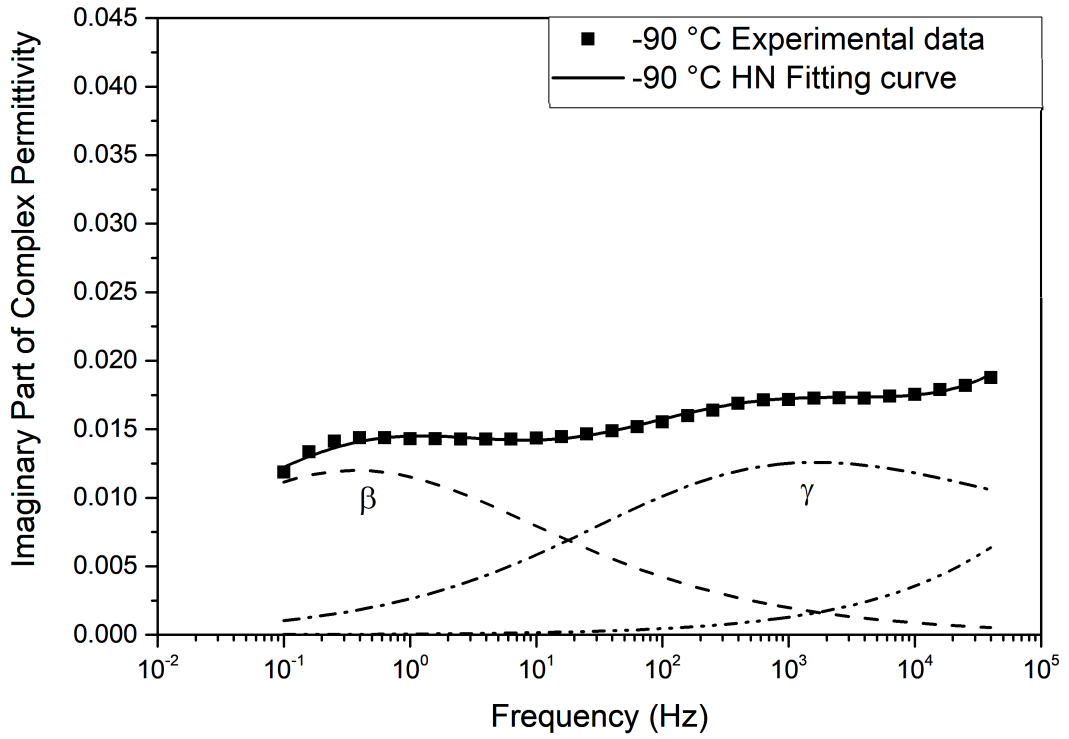

Figure 8.6: An example of Havriliak–Negami fitting showing β and γ deconvoluted peaks for the imaginary part of the complex permittivity of a 20AGHE system at -90 °C.

spectrum [1]. This process is referred to as process 1 in this study. It is important to distinguish between the conductivity contribution and the electrode polarisation process which could mask the effect of the conductivity. The electrode polarisation is the non-Ohmic barrier that results from the accumulation of charge carriers between the conductive surface of the electrode and the sample, creating a large dipole [1, 47, 130]. According to Kremer and Schonhals [1], if the real ε' and imaginary ε'' parts of the complex permittivity were plotted with temperature as a parameter, the slope of ε'' can be used to determine the type of the charge transport. Where the non-ohmic conductivity shows a slope of greater than -1 ($\text{slope}_{polrisation}$ >-1), while the ohmic DC conductivity term has a slope that equals unity (slope_{DC} = -1), as shown in Figure 8.11. The illustration suggested by Kremer and Schonhals explained above, was adopted to investigate charge transport in the neat, GNPE and GHE modified systems in this study, as shown in Figure 8.12 and Figure 8.13.

In the case of the neat epoxy resin, the slope of the imaginary part of the permittivity calculated at the maximum measured temperature (180 °C) equates to -0.97, which is accompanied by an insignificant increase in the real permittivity compared to the change in the real permittivity of the other samples (as depicted in Figure 8.12 and in more details in Figure E.4(a)). For the 30AGNPE, 30AGHE and 20AGHE systems, the slope of the imaginary permittivity at 180 °C is -0.97 ±0.004, -0.99 ±0.008 and -0.98 ±0.005

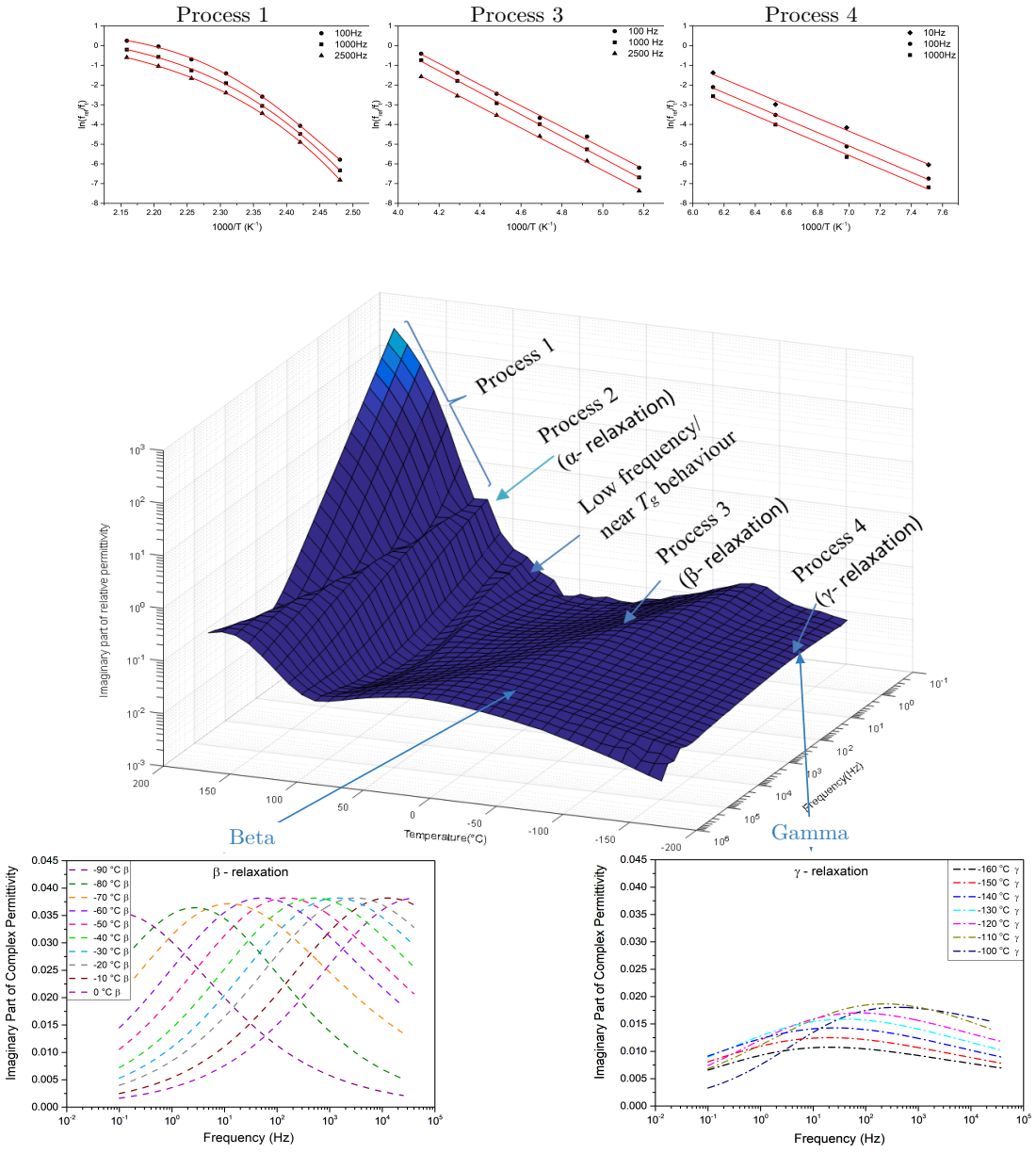

Figure 8.7: Dielectric response and analysis of the neat epoxy resin system showing 3D representation of the imaginary part of the dielectric loss, which illustrates deconvoluted temperature dependence of γ and β relaxation peaks using Havriliak–Negami fit. The top 3 are Arrhenius plot for the characteristic relaxation frequency of the different processes.

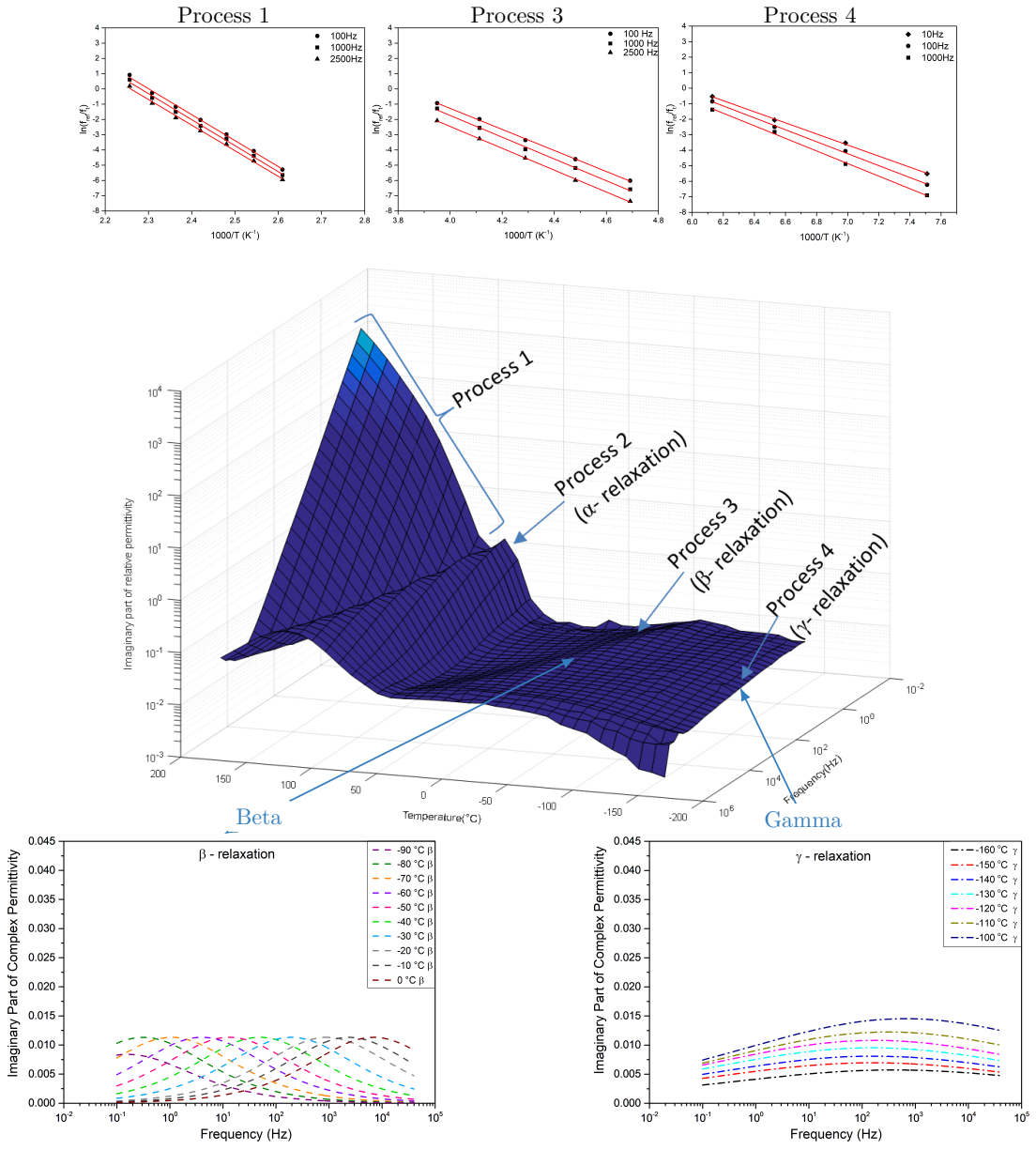

Figure 8.8: Dielectric response and analysis of the 30AGNPE epoxy resin system showing 3D representation of the imaginary part of the dielectric loss, which illustrates deconvoluted temperature dependence of γ and β relaxation peaks using Havriliak–Negami fit. The top 3 are Arrhenius plot for the characteristic relaxation frequency of the different processes.

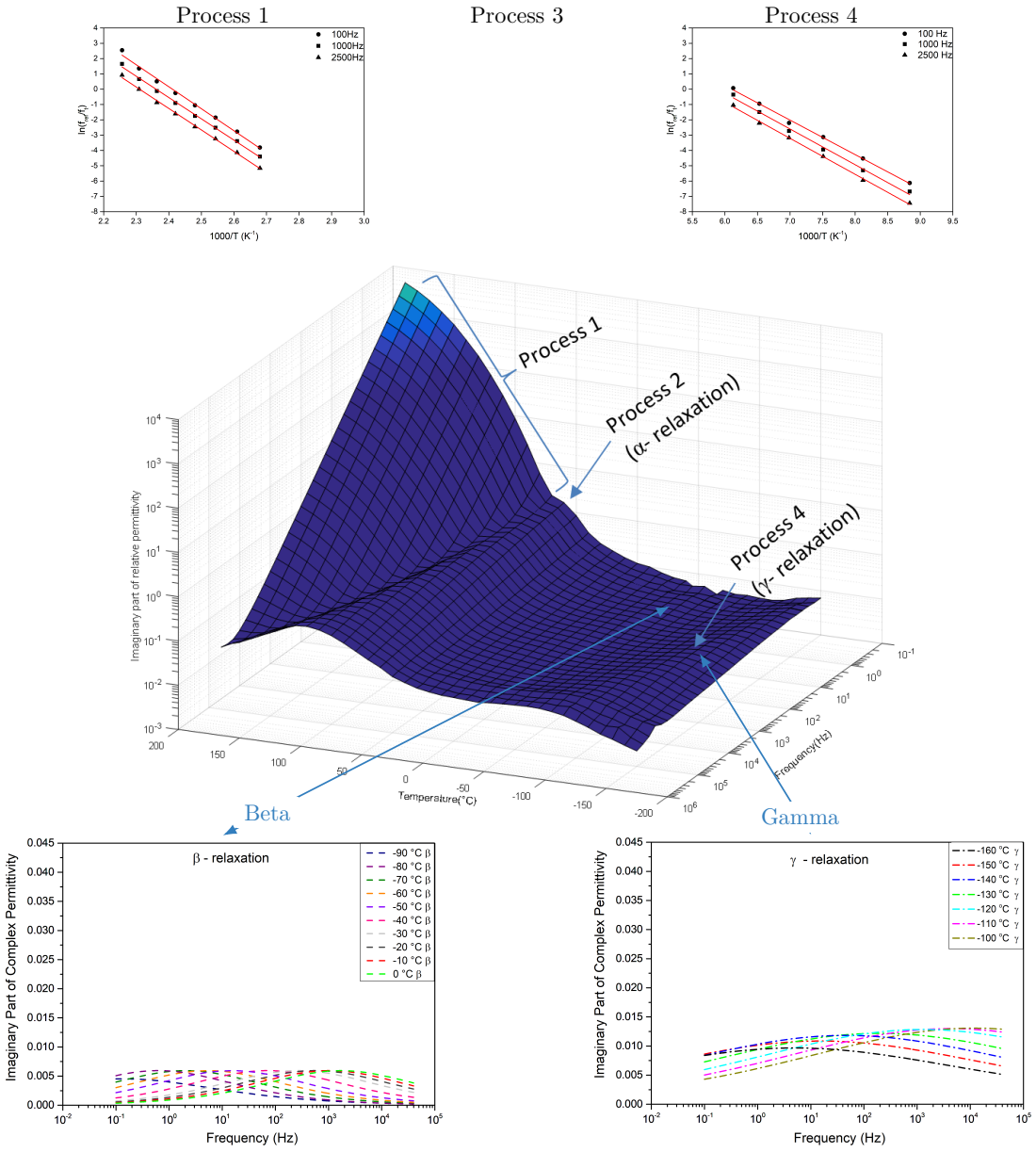

Figure 8.9: Dielectric response and analysis of the 30AGHE epoxy resin system showing 3D representation of the imaginary part of the dielectric loss, which illustrates deconvoluted temperature dependence of γ and β relaxation peaks using Havriliak–Negami fit. The top 3 are Arrhenius plot for the characteristic relaxation frequency of the different processes.

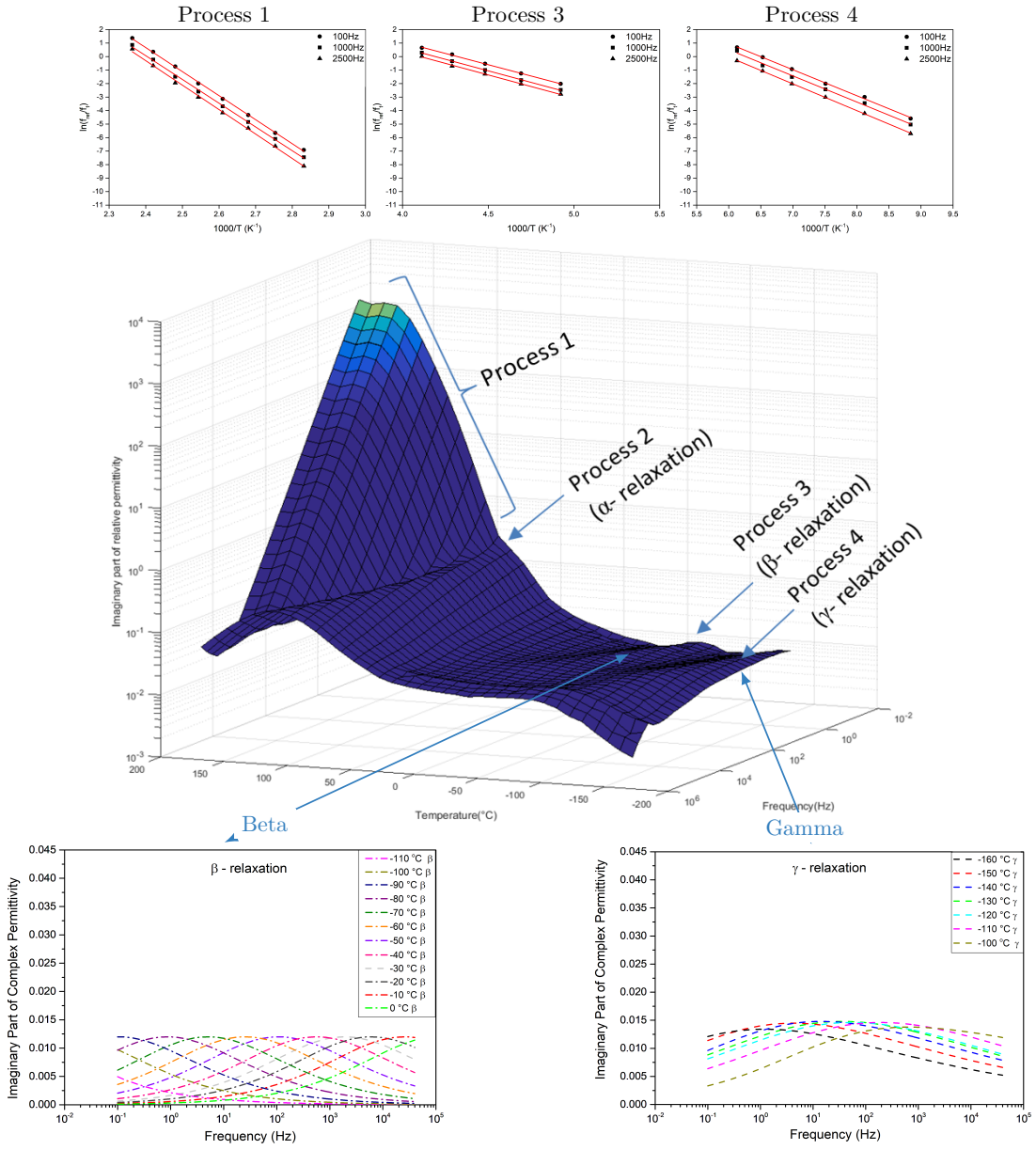

Figure 8.10: Dielectric response and analysis of the 20AGHE epoxy resin system showing 3D representation of the imaginary part of the dielectric loss, which illustrates deconvoluted temperature dependence of γ and β relaxation peaks using Havriliak–Negami fit. The top 3 are Arrhenius plot for the characteristic relaxation frequency of the different processes.

respectively. In these cases, the real part of the permittivity increased only at frequencies below 1 Hz, as shown in Figure E.4 and Figure E.5. Measurements of the imaginary permittivity in the region where the real part increases (low frequency end) were restricted to two to three data point accessible by the equipment which limited the reliability of the slope calculation. Therefore, to provide a better understanding of the behaviour, the same measurements were repeated for the neat epoxy resin at temperatures up to 250 °C, which facilitated the measurement of additional data points at the low frequency end of the imaginary permittivity where the real permittivity increased, as illustrated in Figure 8.14. The figure shows a slope equal to -1 at constant real permittivity (i.e. DC conductivity) and a slope greater than -1 (-0.85 ±0.05) in the region where the real permittivity increases (i.e. electrode polarisation), in a pattern similar to the behaviour described by Kremer and Schonhals as illustrated in Figure 8.11. The data suggests that increasing the temperature revealed more detail about the behaviour of the reference material, where both ohmic conductivity and electrode polarisation behaviours are evident in the dielectric data. The inclusion of the FNM resulted in quite similar behaviour, albeit that the onset of the DC conductivity of the modified systems was shifted to lower values. The DC term of the conductivity of the 30AGNPE, 30AGHE and 20AGHE were observed at 90 °C, 60 °C, and 70 °C respectively which are 40 °C, 70 °C and 60 °C lower than the onset of the conductivity of the neat system. In addition, the activation energy of process 1 was affected by the inclusion of the FNM, as shown in Figure 8.15 and illustrated in Table 8.2. The activation energy of process 1 for the neat system is 2.21 ± 0.02 eV, while the 30AGNPE, 30AGHE and 20AGHE modified systems were 1.46 ± 0.02 eV, 1.22 ± 0.02 eV and 1.56 ± 0.03 eV respectively. It is important to highlight that these values should not be compared with the activation energy presented in Figure 8.3, because the measurements were conducted under different conditions (field and frequency).

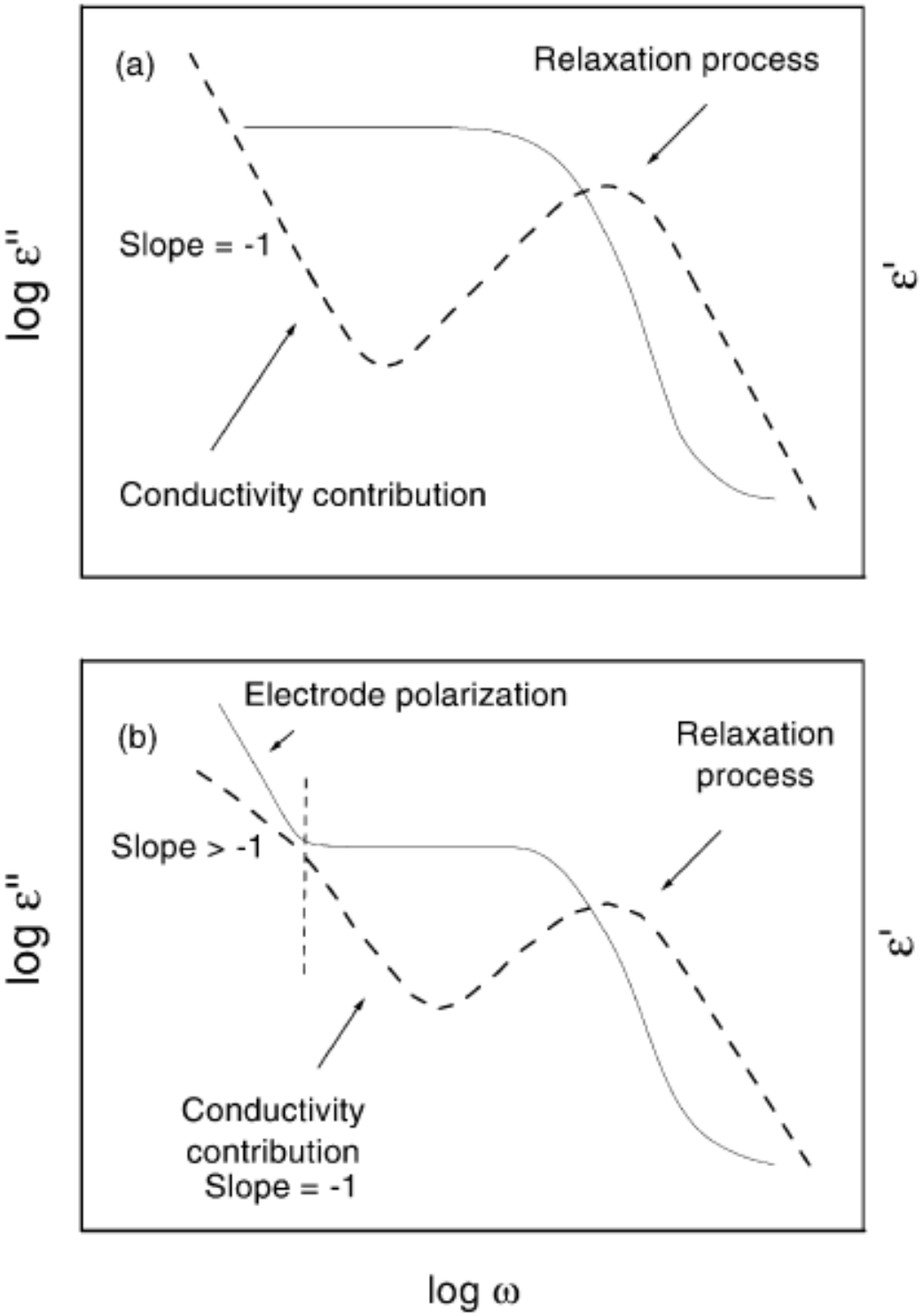

Figure 8.11: Real and imaginary part of (a) ohmic and (b) non-ohmic conductivity. The solid line represents the real permittivity, while the dashed line shows the behaviour of the imaginary part of the permittivity (reprinted from [1]).

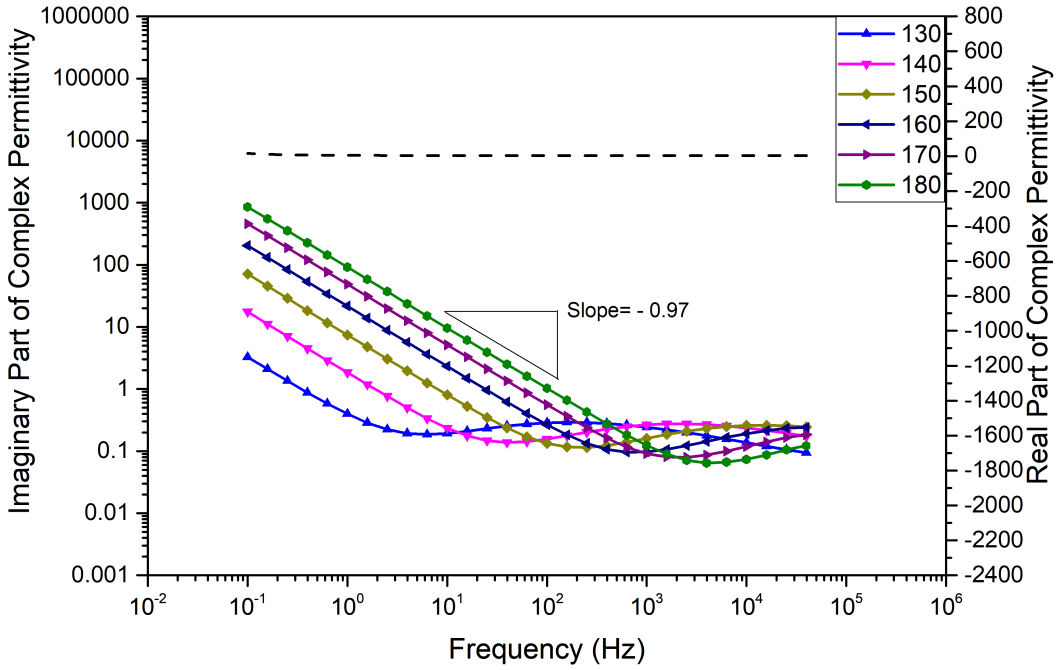

(a) Neat Epoxy

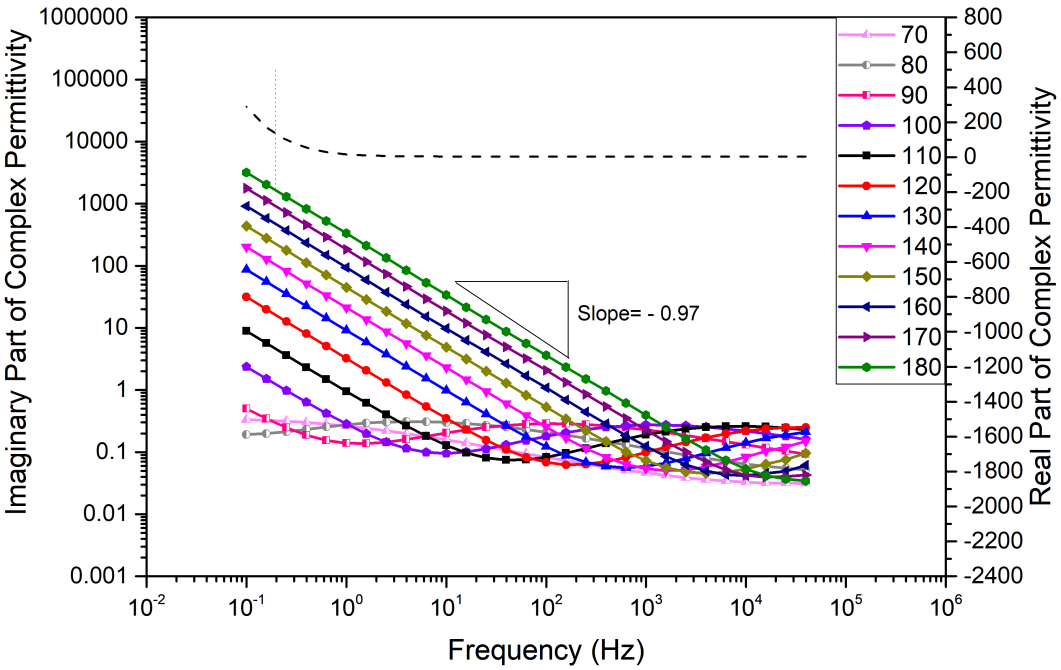

(b) 30AGNPE

Figure 8.12: Plots of the imaginary part of the dielectric permittivity against the frequency as a function of temperatures associate with Process 1 for (a) Neat epoxy and (b) 30AGHE modified systems. The grey dashed line is the real part is the real part of the permittivity at 180 °C. The legend represents the temperature in °C.

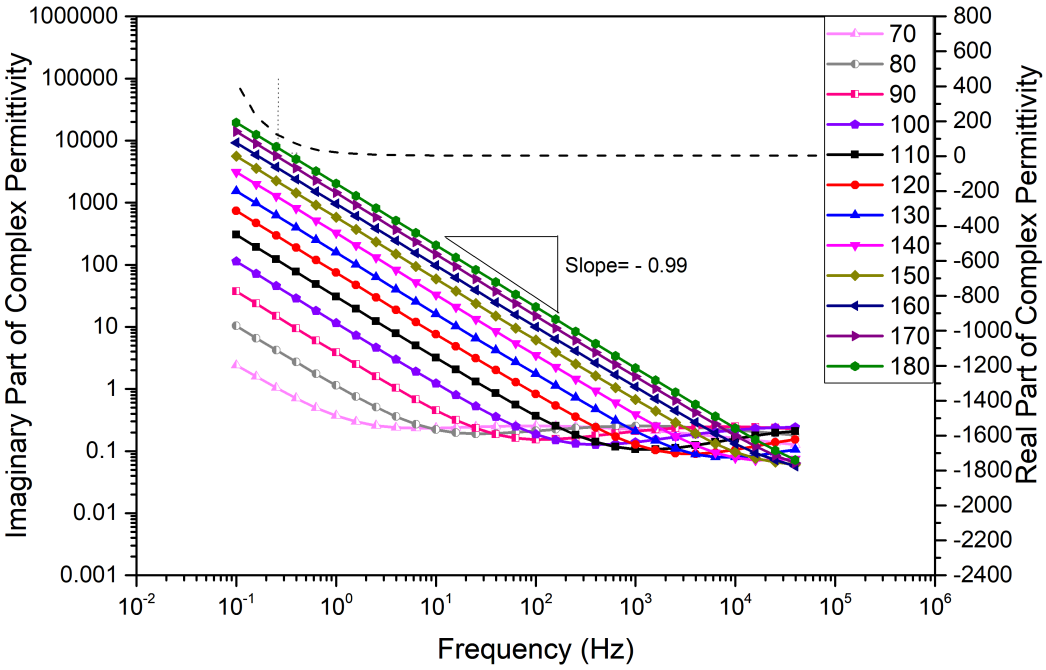

(a) 30AGHE

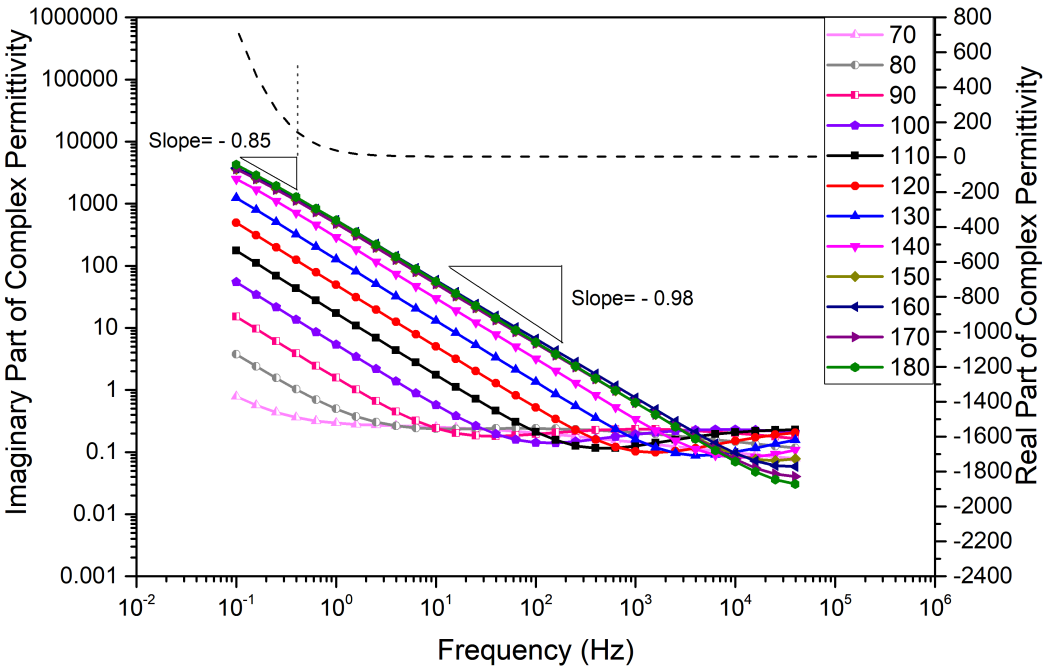

(b) 20AGHE

Figure 8.13: Plots of the imaginary part of the dielectric permittivity against the frequency as a function of temperatures associate with Process 1 for (a) 30AGHE and (b) 20AGHE modified systems. The grey dashed line is the real part is the real part of the permittivity at 180 °C. The legend represents the temperature in °C.

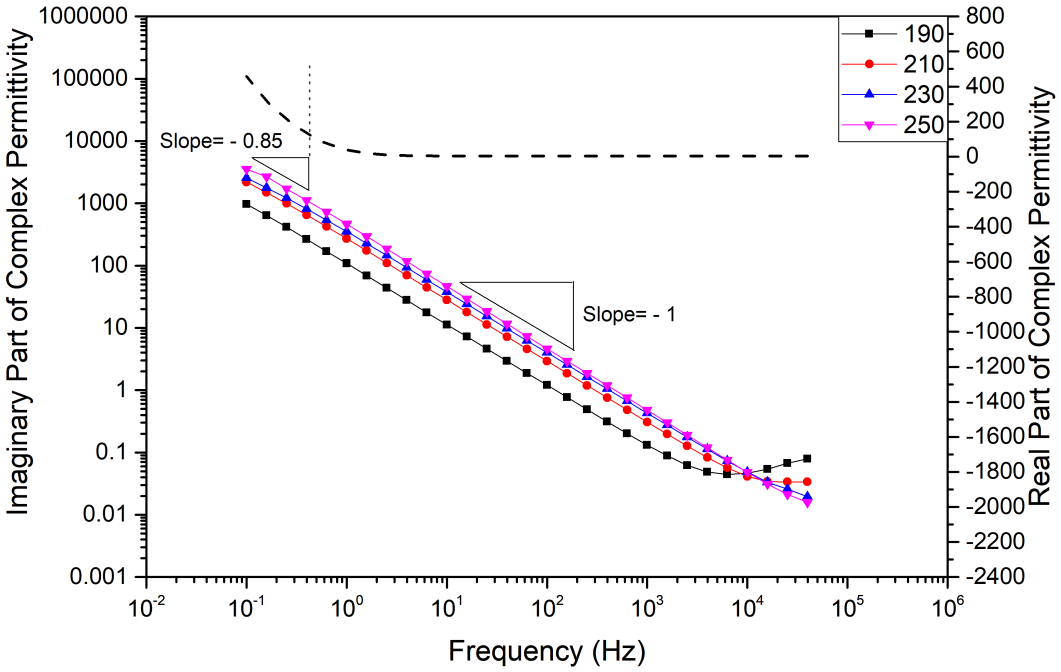

Figure 8.14: Plots of the imaginary part of the dielectric permittivity of the neat system against the frequency as a function of temperatures associate with Process 1 at temperatures up to 250 °C. The grey dashed line is the real part of the permittivity at 250 °C. The legend represents the temperature in °C.

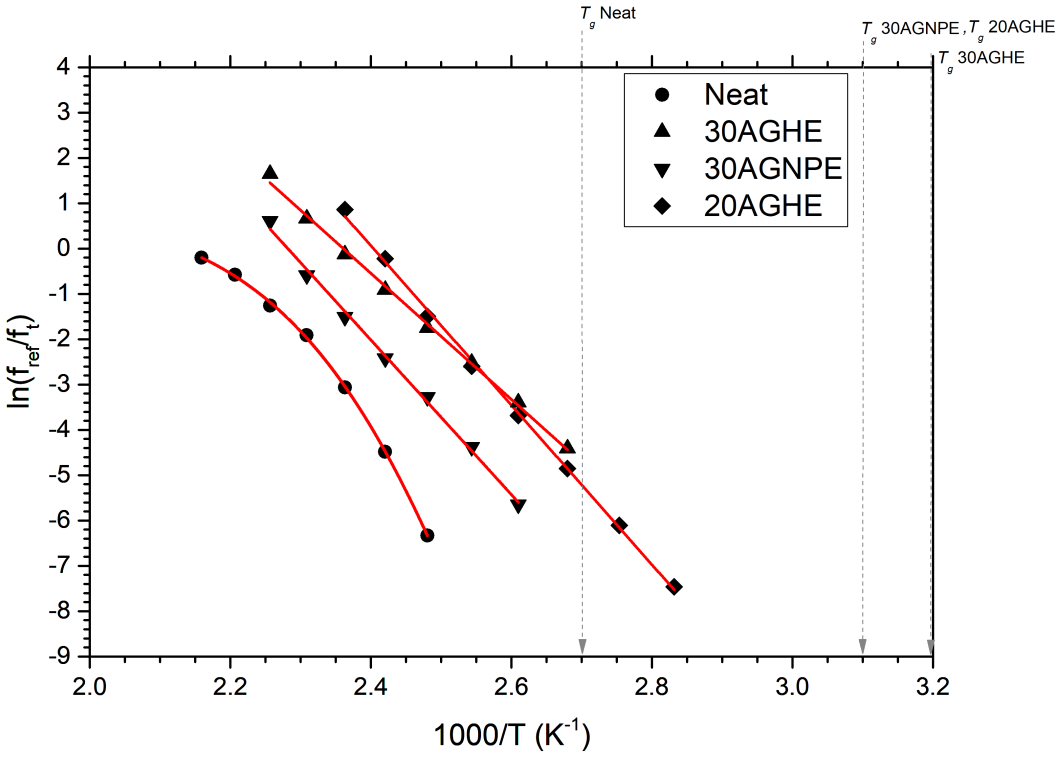

Figure 8.15: Arrhenius plot for process 1 for the studied material systems.

Table 8.2: Activation energy values for the neat and modified systems

Sample	Process 1 (charge-transport) eV	Process 3 (β- relaxation) eV	Process 4 (γ- relaxation) eV
Reference	2.21 ± 0.02	0.46 ± 0.01	0.30 ± 0.02
30%AGNPE	1.46 ± 0.02	0.61 ± 0.02	0.32 ± 0.04
30%AGHE	1.22 ± 0.02	-	0.20 ± 0.02
20%AGHE	1.56 ± 0.03	0.30 ± 0.01	0.17 ± 0.02

8.3.2 Process 2 (α- transition)

The alpha relaxation is a structural relaxation associated with the cooperative movement of chains around the glass transition of the matrix, where the material acquires sufficient thermal energy to facilitate segmental motion [130, 170, 171]. In the case of the neat epoxy resin, the onset of the α- relaxation can be seen at temperature around 90 °C, which is around 12 °C lower than the DSC measured T_g of the neat resin (T_g= 102 °C), see below Figure 8.16. For the modified systems, the onset of the 30AGNPE, 30AGHE and 20AGHE systems appears at temperatures of 40 °C, 30 °C and 40 °C respectively, as illustrated in Figure 8.16 and Figure 8.17.

The data reported here reveal the presence of a relaxation process prior to the α- relaxation. Ochi et al [221], observed two relaxational processes above the T_g of an anhydride cured system at temperatures from -70 °C to 30 °C at a frequency of 1 Hz. One of these two relaxations is the molecular β- relaxation, while the other process was associated with the weak conformational motion of the diester segments. In the current work, the data deconvoluted using Havriliak–Negami fit suggests a similar behaviour. In addition to the β- relaxation, a broad peak is evident in the deconvoluted peaks of the neat and the FNM modified systems, which is referred to as the pre-α process. Initially the pre-α process appears as a very weak peak, which steadily increases in amplitude as the temperature increase. This, presumably, is caused by the increased segmental mobility as the temperature increase. Hassan et al [159], suggested that the material topology and the free volume in the system influence the pre-α process. This is consistent with the data reported here where the onset of the pre-α process in both the neat and GNPE modified systems is at -60 °C (as illustrated in Figures E.20 and Figure E.43), while an equivalent process is present at lower temperatures (-80 °C) in the data of the GHE modified system (as illustrated in Figure E.66 and Figure E.87, which are located in Appendix E).

It is perhaps important to mention that the peak pre-α process (seen at frequency around 1 Hz) is different from the peak observed at frequencies between 100 Hz and 1000 Hz in the data deconvoluted using Havriliak–Negami fitting for the neat and the 20AGHE systems at temperature 0 °C and -20 °C respectively (as shown in Figure E.20 and Figure E.87, which located in Appendix E). The intensity and the frequency of

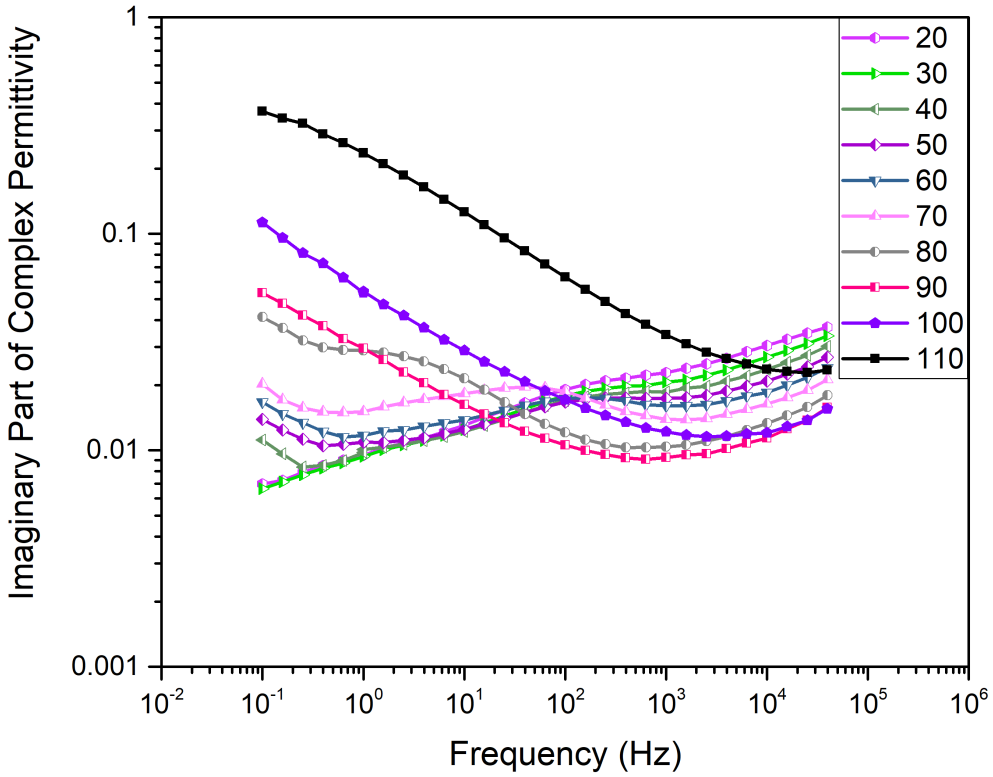

(a) Neat Epoxy

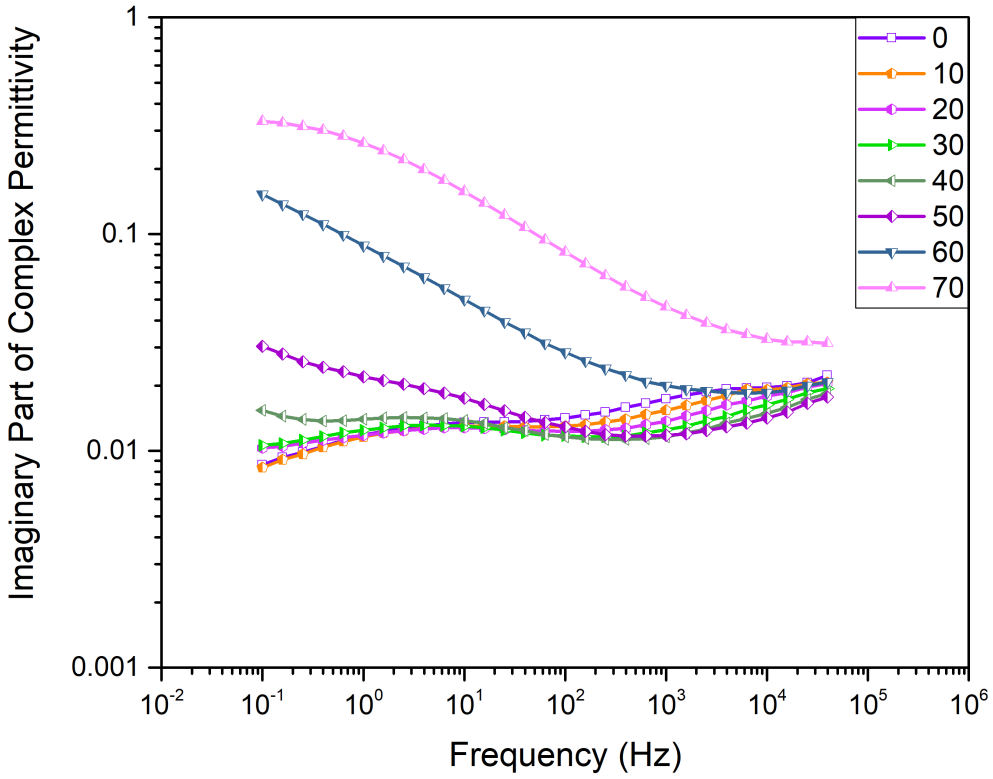

(b) 30AGNPE

Figure 8.16: Plots of the imaginary part of the dielectric permittivity against the frequency as a function of temperatures associate with Process 2 for (a) Neat epoxy and (b) 30AGNPE modified systems. The legend represents the temperature in °C.

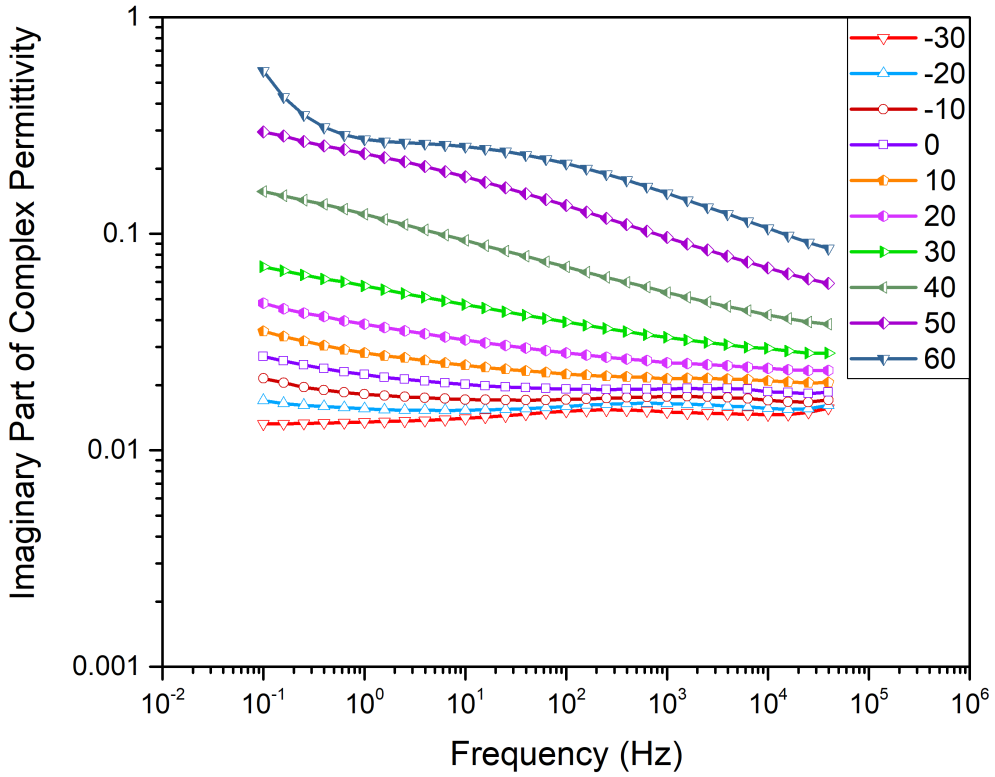

(a) 30AGHE

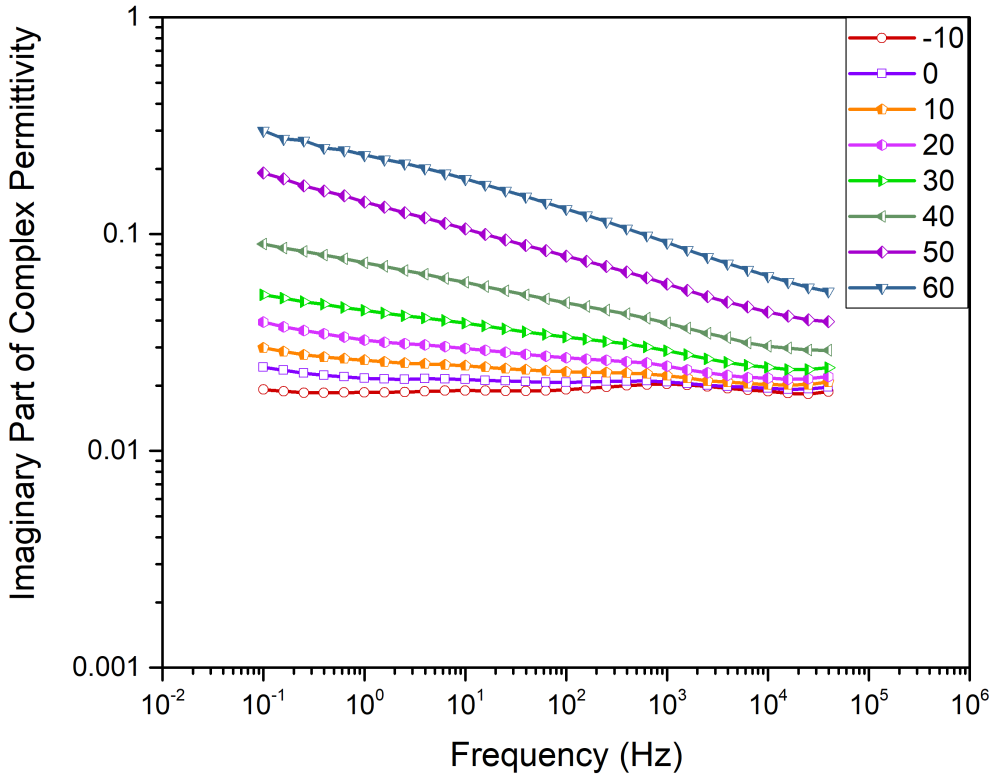

(b) 20AGHE

Figure 8.17: Plots of the imaginary part of the dielectric permittivity against the frequency as a function of temperatures associate with Process 2 for (a) 30AGHE and (b) 20AGHE modified systems. The legend represents the temperature in °C.

this secondary relaxation increase with increasing temperature. This behaviour was not present in the data of the 30AGNPE and 30AGHE systems. A detailed analysis of a similar behaviour was presented by Chao and Gary [222], where it was concluded that the behaviour is associated with moister molecules trapped and/or bonded to the resin system. Similar findings were reported by several other studies [223–225].

8.3.3 Process 3 (β- relaxation)

The beta relaxation is a thermally activated dielectric process that appears as a broad peak across the frequency sweep. The molecular β- relaxation for the neat epoxy resin is observed at temperatures from -90 °C to 0 °C, as clearly labelled in Figure 8.7. Modification of the resin by adding GNPE resulted in an insignificant change in the temperature range of the β- relaxation, while the activation energy of the relaxation increased to 0.61 ± 0.02 eV, compared to the activation energy of the neat epoxy system which is 0.46 ± 0.01 eV, Figure 8.8 and Table 8.2. This change in the activation energy is associated with the presence of the retained groups of the functional network modifier, which restrict the motion of the molecular groups, as it will be explained later in this section. Detailed graphs of process 3 are shown in Figure 8.19.

In the case of the 30AGHE system, the β- relaxation appears as a very weak process which is only visible upon expanding the vertical scale of the plot, as illustrated in Figure 8.20. The visible relaxation possess an activation energy in the typical range associated with the γ- relaxation. Therefore, to explore this issue further, samples modified with 20 % of the epoxide groups from the GHE were manufactured, where the T_g of the 20AGHE sample was chosen close to the T_g of the 30AGNPE modified systems. In addition, the data of the imaginary permittivity of the neat and modified systems were fitted and deconvoluted using Havriliak–Negami fit to provide a better understanding of the dielectric behaviour of the different systems, as illustrated in Figure 8.7, 8.8, 8.9 and 8.10.

The temperature dependent β- relaxation peaks deconvoluted using the Havriliak–Negami function for the 30AGHE systems (shown in Figure 8.9), evince a week, broad relaxation that appears across the a wide frequency range and shifts to higher frequency as the temperature increases, maintaining a constant amplitude. HN relaxation peaks with similar behaviour were suggested to describe the β- relaxation by Zhang and Stevens [222]. Since the peaks associated with the β- relaxation were very broad, it was not possible to accurately calculate the activation energy for β- relaxation of the 30AGHE.

In the case of the 20AGHE, the β- relaxation peaks deconvoluted using a Havriliak–Negami fit appear as a broad relaxation that shifts with temperature to higher frequency, where the intensity of the peaks changes, as depicted in Figure 8.10. This behaviours is quite similar to that of the 30AGNPE systems, which implies that the

presence of the GHE and GNPE restrict or impede the β- relaxation. In contrast to the GNPE, the inclusion of 20 % of the epoxide groups from the GHE resulted in a reduction in the activation energy of the β- relaxation to 0.3 $\pm$ 0.01 eV compared to that of the neat system which is 0.46 $\pm$ 0.01 eV, providing further evidence that the functional groups of the modifier is the driving parameter for the behaviour of the β-relaxation reported here.

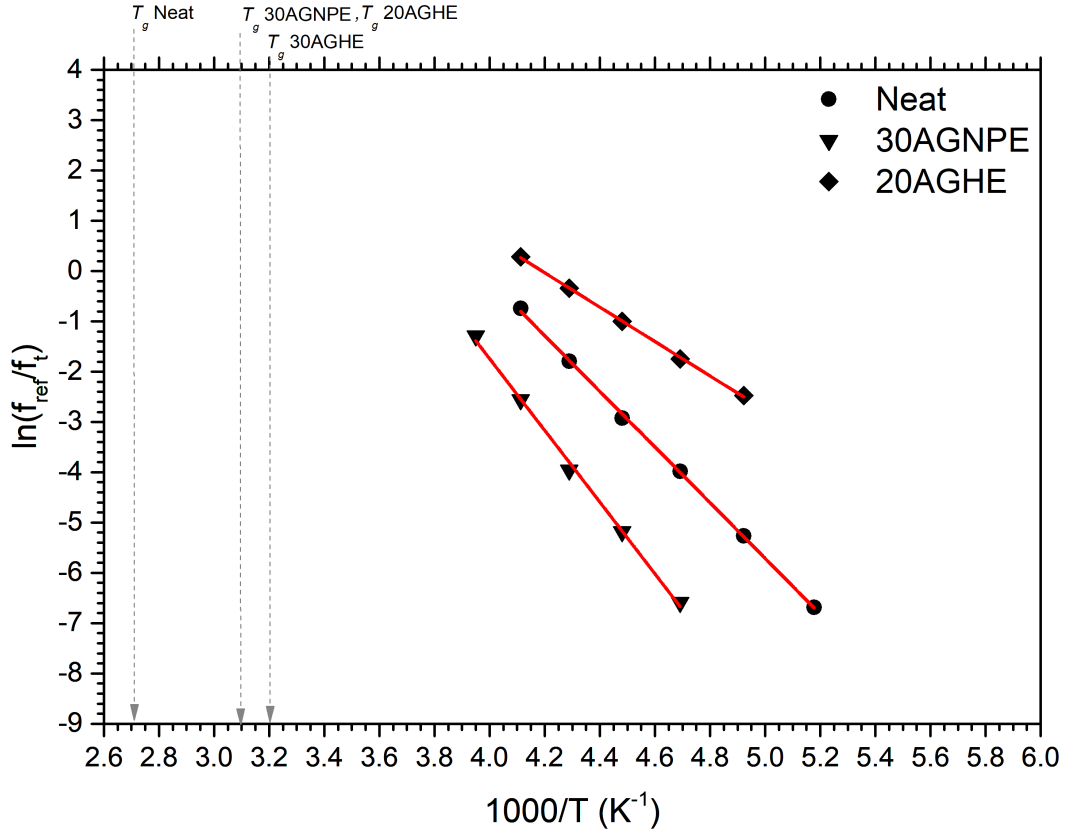

Figure 8.18: Arrhenius plot for process 3 for the study samples.

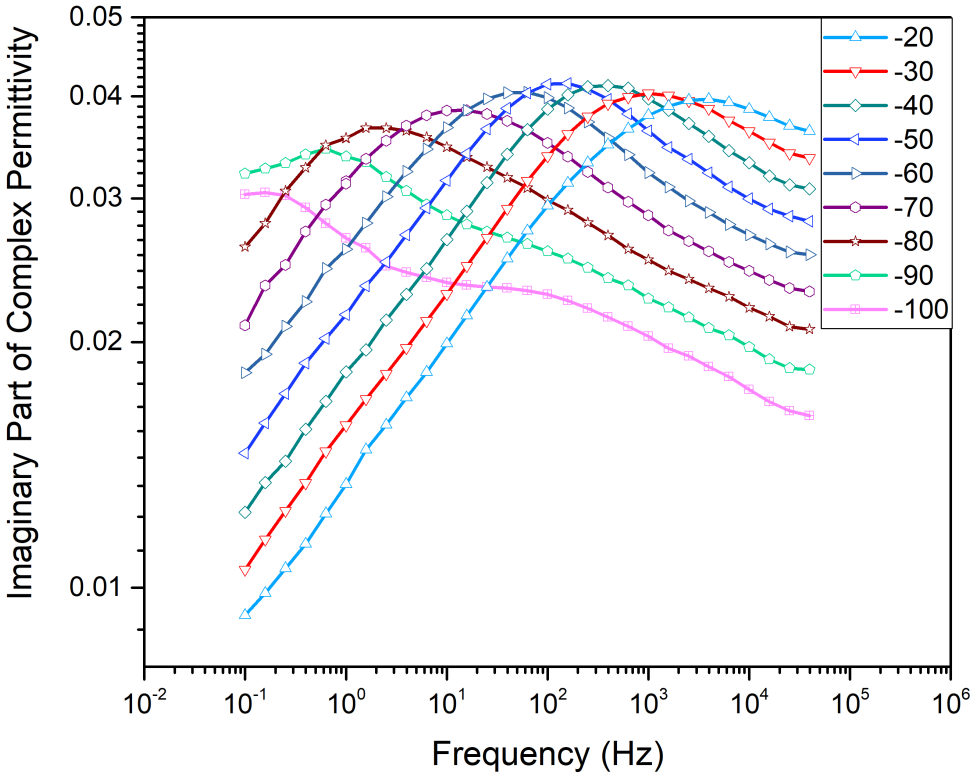

(a) Neat Epoxy

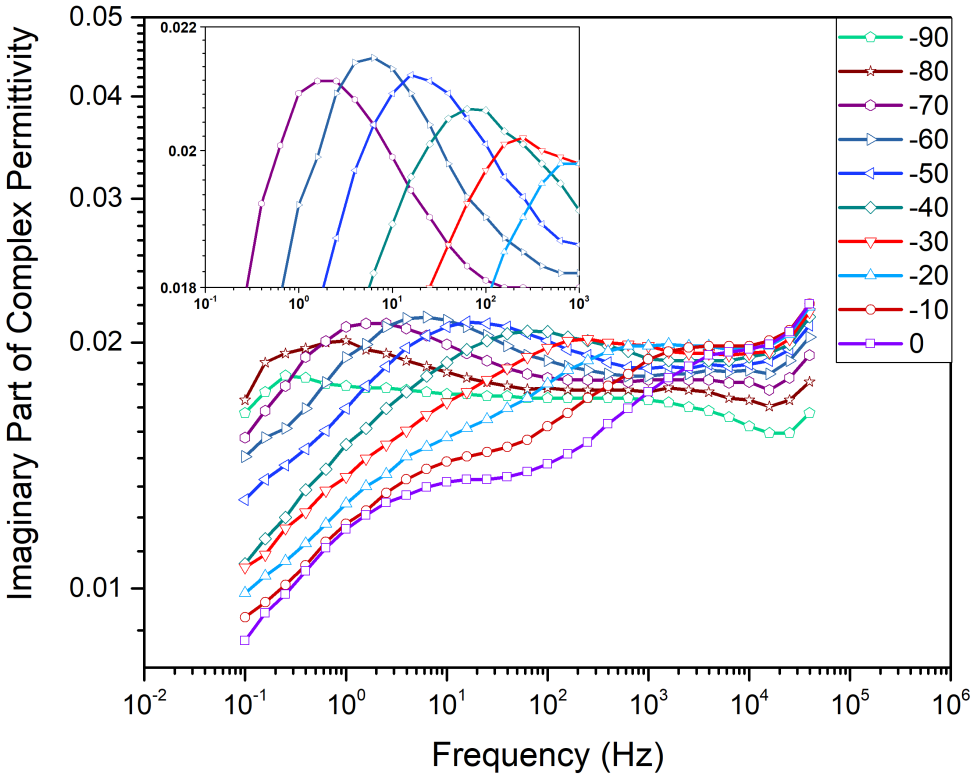

(b) 30AGNPE

Figure 8.19: Plots of the imaginary part of the dielectric permittivity against the frequency as a function of temperatures associate with Process 3 for (a) Neat epoxy and (b) 30AGNPE modified systems. The legend represents the temperature in °C.

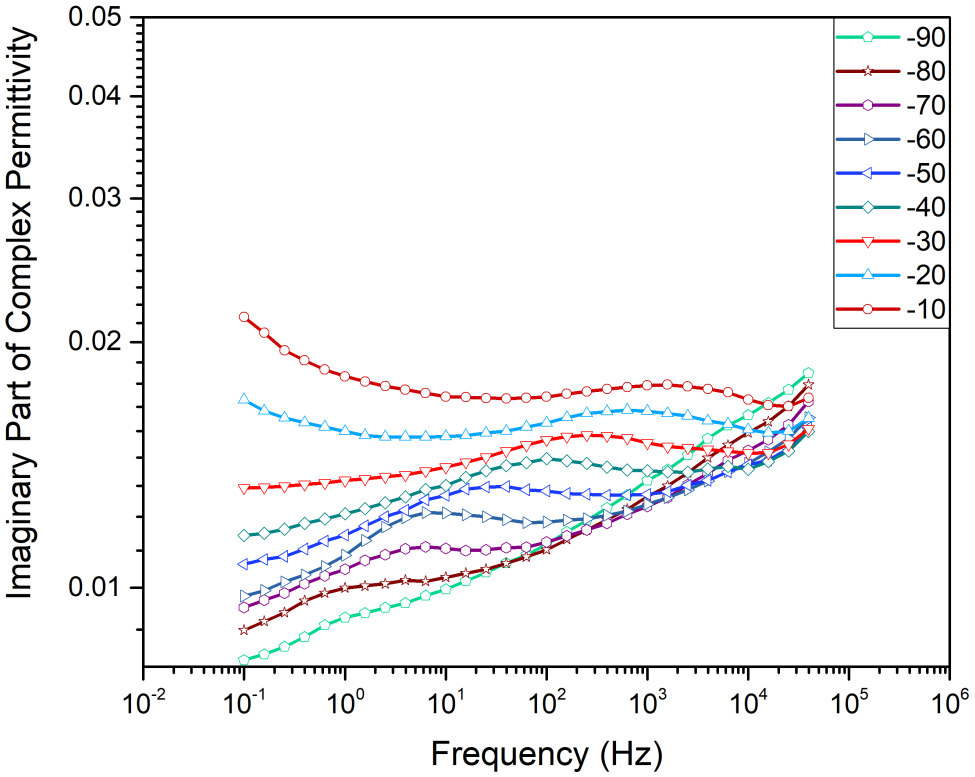

(a) 30AGHE

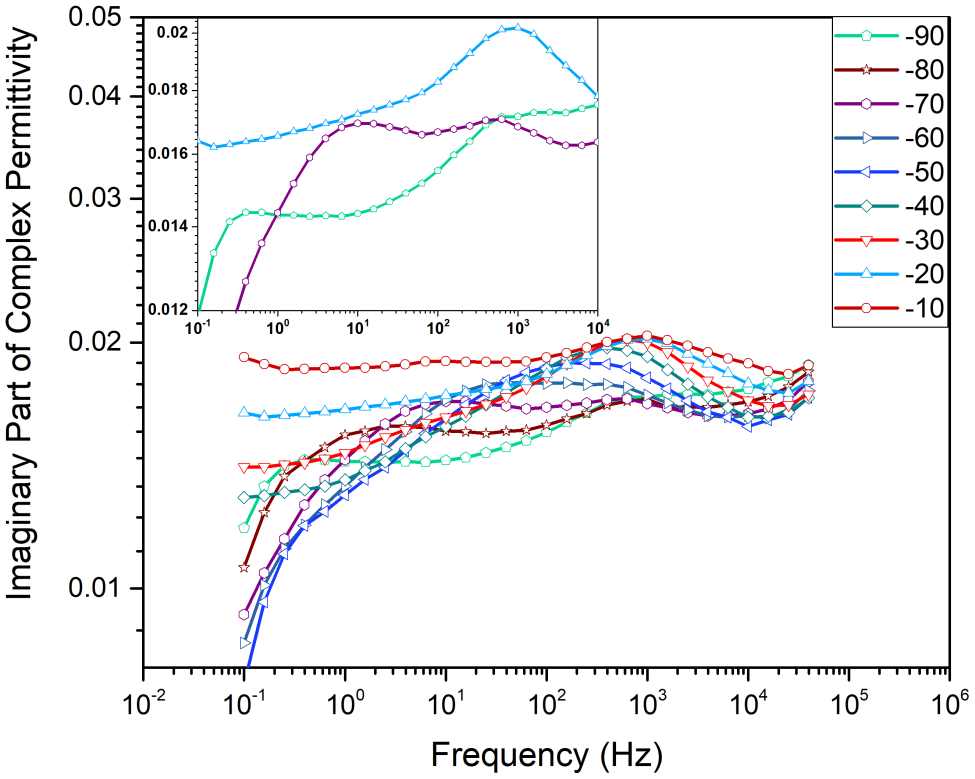

(b) 20AGHE

Figure 8.20: Plots of the imaginary part of the dielectric permittivity against the frequency as a function of temperatures associate with Process 3 for (a) 30AGHE and (b) 20AGHE modified systems. The legend represents the temperature in °C.

8.3.4 Process 4 (γ- relaxation)

The gamma relaxation (process 4 in this study) is related to the motion of dipoles at temperatures way below the glass transition temperature of the material. The gamma process is characterised by a low activation energy required by the polar groups to overcome the potential barrier, compared to the α and β relaxations [1]. To test this claim, the influence of different chain ends on the activation energy of the γ- relaxation along with analysis of the molecular origin of the gamma process is investigated hereafter.

The imaginary part of the complex permittivity of the neat epoxy resin systems (shown in Figure 8.7) illustrates that the γ- relaxation of the neat samples can be observed as a very broad peak across the frequency domain at temperatures from -160 °C to -100 °C. The γ-relaxation for the GNPE modified systems showed similar behaviour to that of the neat epoxy resin, as presented in Figure 8.8. While, the gamma process of the GHE modified systems appears as two separate relaxations, as illustrated in the peaks deconvoluted using Havriliak–Negami fit shown in Figure 8.9 and Figure 8.10.

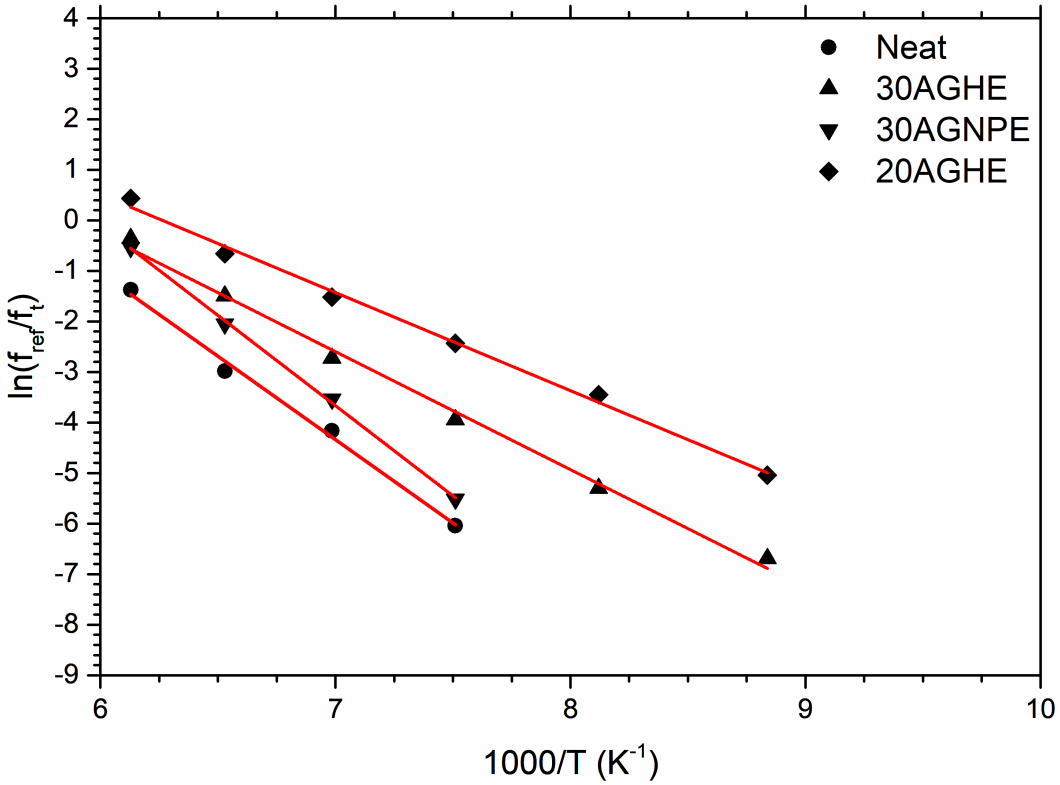

Figure 8.21: Arrhenius plot for process 4 for the study samples

The activation energy of the γ- relaxation determined by the Arrhenius equation from the temperature dependent dielectric measurements of the neat epoxy resin is 0.30 ± 0.02 eV, as depicted in Table 8.2. As anticipated, the introduction of both the GNPE and GHE affected the activation energy of the γ- relaxation. The inclusion of the GNPE resulted in an increase in the activation energy of the γ- relaxation to 0.32 ± 0.04 eV, whereas

the addition of both 30 % and 20 % of the epoxide groups from the GHE resulted in a decrease in the activation energy to 0.20 ± 0.02 eV and 0.17 ± 0.02 eV respectively. Arrhenius plots of γ- relaxation for the reference and modified samples are shown in Figure 8.10. The variation in the activation energy of the γ- relaxation arises from conformational motion of small molecular moieties which could be side groups of the main chain or unreacted retained chains. In the current study, two modifiers were used, which were selected so that their chemical structure comprises of nonreactive end chains which, after curing (bonded to the resins network through their reactive epoxides), become retained in the system, where the consequent effect of the retained groups on the molecular dynamics can be compared and contrasted. The chemical structure of the GHE features a terminal reactive epoxide group, linked to a long chain alkyl group (sixteen carbon atoms $CH_2(CH_2)_{14}CH_3$) through an oxygen bond, while the structure of GNPE comprises of a terminal reactive epoxide group bonded through an ether group to an aromatic ring and an alkyl chain (nine carbon atoms $CH_2(CH_2)_7CH_3$). Alkyl groups and aromatic structures were reported to alter the molecular dynamics of epoxy resins.

In the neat anhydride cured epoxy resin system, the γ- relaxation appears as a broad relaxation. According to Kremer and Schonhals [1], the γ- relaxation is linked to the movement of small dipolar terminal groups and conformational motion of side branches attached to the epoxy network. In anhydride cured structures, these small molecular units correspond to unreacted molecules and retained functional groups or chain ends. In the current case, the modified samples comprised of the GNPE and GHE molecules being added after removing part of the resin. The resin contains an aromatic molecule in addition to an ether group per epoxide groups. The GNPE comprises of a similar structure to that of the resin in addition to a terminal alkyl group, while the chemical structure of GHE features only an ether group per epoxide groups and lacks the aromatic molecule. Consequently, substituting the resin with the GNPE and GHE modifiers resulted in (a) introducing terminal alkyl chains with different lengths into both modified structures, (b) reducing the composition of diphenyl groups in the GHE modified resins.

As mentioned in the chapter 7, the behaviour of the γ process in anhydride cured systems is poorly investigated in the literature. Indeed, Hassan et al [159] have studied the dielectric behaviour of anhydride cured systems, where it was suggested that the γ- relaxation is associated with the flipping motion of aromatic rings between adjacent flexible ether linkages in the DGEBA main chain. Another key study that reported on the behaviour of the γ- relaxation in anhydride cured resins is the investigation conducted by Pogany [226], where the experimental data suggested that the γ relaxation is a product of two separate relaxations. McMaster et al [227] reported that the conformational motion of alkyl groups contributes to the γ- relaxation which is subject to steric hindrance by adjacent environmental structure, while, Pinkus and Lin [228] established an understanding of the conformational motion of alkyl chains based on calculation of

electric dipole moments (separation of negative and positive charges). The study reported that (a) the increases in the length of the alkyl chain rises the conformational freedom of the chain and (b) the presence of aromatic structures increases steric interference, where both affect the dielectric behaviour (temperature and/or activation energy) of the system in different ways.

As can be seen from the above account, the inclusion of the aromatic and the alkyl groups of the FNM impact the characteristics of the gamma relaxation. In the case of the GNPE modified systems, the γ relaxation appears as a broad peak, where the deconvoluted peak of the GNPE modified systems were present at temperatures from -160 °C to 40 °C, while the comparable peaks of the neat system had almost completely disappeared at -20 °C, as illustrated in Figure E.42 and Figure E.19 respectively, which are located in Appendix E. Based on the above discussion, this shift in the temperature of the gamma relaxation can be attributed to the presence of terminal groups in the structure of the GNPE modified systems. The benzene rings connected to a terminal alkyl groups means that the GNPE modified structure contains a higher number of flexible units compared to the structure of the epoxy resin. These links replaced the previously constrained segments of the resin creating a branched network, which facilitates the flipping motion of the aromatic rings while maintaining a similar molecular composition.

In the case of the GHE modified systems, the deconvoluted peaks of the gamma relaxation of the 30AGHE and 20AGHE modified systems are present at temperatures from -160 °C to 0 °C and from -160 °C to -40 °C respectively, as illustrated in Figure E.65 and Figure E.86 respectively. In addition, the deconvoluted peak of the gamma relaxation reveals that the gamma relaxation of the GHE modified systems comprises of two separated peaks, which is inline with the behaviour reported by Pogany [226]. Plots of the deconvoluted Havriliak–Negami fitted temperature dependent bifurcated gamma process for 30AGHE and 20AGHE systems are illustrated in Figure E.65 and Figure E.86 respectively, which are located in Appendix E. The inclusion of the alkyl chains affected the local environment around the relevant dipole, which resulted in shifting the gamma temperature and allowed gamma bifurcation suggesting that the γ- process originates from two set of dipoles. This behaviour was not present in the γ- relaxation process of the neat and the GNPE modified systems. There are two possible explanations for this behaviour. It is likely that the two gamma peaks are very close to each other to an extent that the peaks can only be seen as one broad relaxation. The alternative explanation is that one of the gamma peaks is pronounced more than the other one and probably only one peak is located within the accessible temperature range. In both cases, it may be concluded that the behaviour of the γ- relaxation noticed here is attributed to the presence of unreacted dipolar molecules, the flipping motion of the aromatic groups and the structural environment around the dipoles, i.e. the network topology.

8.4 Summary

This chapter presented a detailed analysis of the dielectric behaviour of neat and modified anhydride cured epoxy resin systems. Differential scanning calorimetry was used to examine the glass transition temperature of the materials. It was anticipated that the inclusion of the GNPE and GHE would shift T_g of the modified systems to lower values. The data reported that the addition of 30 % of the epoxide groups from the GHE and GNPE resulted in shifting T_g to lower temperatures by 66 ± 2 °C and 50 ± 2 °C respectively, compared to that of the reference resin. This effect was associated with the functional groups and presumably on the resulting relaxation of constraints on molecular (dipolar) mobility.

In the case of the electrical conductivity, generally, all the modified systems exhibited higher conductivity values than the unmodified resin. The analysis of the temperature dependent conductivity measurements revealed two different processes in the studied systems, DC conductivity and a transient conductivity. The glass transition temperature of the materials plays a vital role in the transition between the two processes.

In terms of dielectric spectroscopy, the dielectric spectra of the neat and modified systems were collected at temperatures from -160 °C to 180 °C. A three dimensional representation was selected to represent the collected data of the imaginary permittivity against the frequency and the temperature. In addition, Arrhenius plots were used to calculate the activation energy of the accessible relaxations, while Havriliak-Negami fitting was used to fit and deconvolute the data to provide comprehensive understanding of the molecular dynamics. A summary of the Arrhenius plot of all the samples is shown in Figure 8.22.

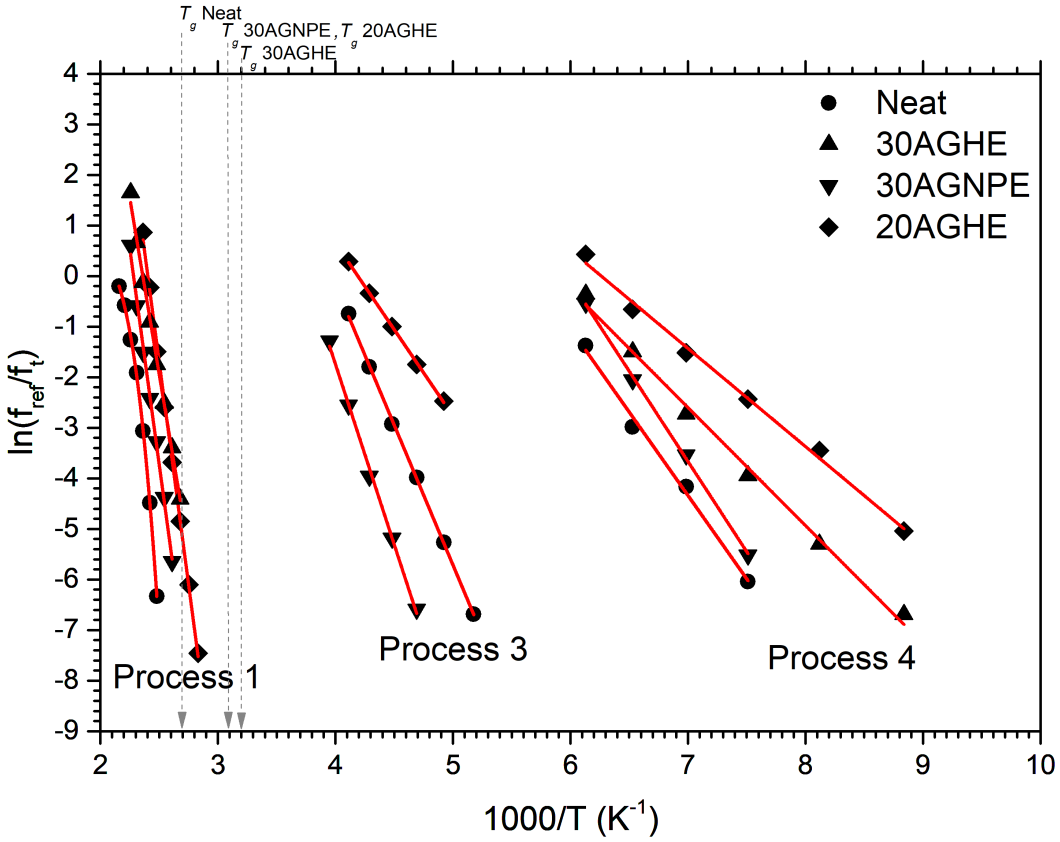

Figure 8.22: Arrhenius plot for the characteristic relaxation frequency relative to that of the reference temperature in neat and modified epoxy resin systems.

Chapter 9

Conclusions and Future Work

9.1 Conclusions

The design of modified dielectric thermosetting material with controlled properties imposes a challenge that varies depending on the considered modifier, host material and the desired properties. The used of functional network modifiers FNM to alter the properties of epoxy resin systems is suggested to be an alternative method to the use of fillers. Improvement in the properties of epoxy resins using nano and micro fillers, are pushed to the limit where the process involved is becoming complicated. On the other hand, modifying the epoxy resin network using FNM is poorly investigated and have shown promising results to become complementary and potential alternative to the used of some fillers. FNM are liquid additives that comprises of reactive groups which react with the hardener in the curing process and become incorporated into the cured resin matrix. As a consequence of the reaction of the FNM with the hardener, the functional groups of the FNM become retained within the epoxy resin structure. For the examined systems, understanding the effect of the different functional groups of the modifiers on the thermal and electrical properties of the system represents a major challenge that needs to be addressed. Therefore, the study initially sets out to investigate the epoxy resin curing mechanisms, the effect of the FNM on the breakdown strength, dielectric properties and thermal behaviour of epoxy resin systems.

In terms of the investigation of the epoxy curing mechanisms, epoxy resin systems cured using two hardeners, namely, amine and anhydride based hardeners were used to provide a comprehensive understanding of the difference between the curing mechanisms to establish the foundation for modifying the systems investigated later. The data revealed that the curing process of an amine system involves reaction between the active group of the hardener with an epoxide group from the resin, while the process for the anhydride cured systems is more complicated, which comprises of anhydride initiation reactions, esterification and possible etherification reactions.

Only a small number of researchers in the literature investigated the impact of functional network modifiers on the electrical properties of epoxy resins systems. In most of these studies the FNM are viewed as fillers without taking into account the ability of the FNM to react and consume the hardener through their epoxide groups i.e. most of the stoichiometric ratios that have been employed are questionable. The stoichiometric ratio is an important parameter in the development of the network structure using FNM, as

it affects the configuration of the network, where the retained functional groups act as a property-altering tool. This study showed that it is possible to alter the architecture of the resin structure using FNM which consequently produced systems with properties different from that of the unmodified material. Adapting the behaviour of some functional groups reported in the literature such as the functional groups present in voltage stabiliser provides a good foundation to establish an understanding of the effect of the selected FNM on the properties of the manufactured systems.

A detailed investigation of the effect of the number of active molecules of the FNM was also considered in this thesis. The study examined two main materials manufactured with stoichiometric ratio calculated using two different methods. Based on the fact that the epoxide groups of the FNM contributes to the curing process, the stoichiometric ratio of one system was calculated so that the epoxide groups of the FNM were compensated by removing equivalent number of epoxide groups from the resin. In the other system, FNM was added as a weight percentage of the total weight without modifying the stoichiometry. The experimental investigation described in chapter 5 has demonstrated that the stoichiometric ratio has a critical influence on the thermal, electrical and dielectric properties of the modified systems. This aligns with hypothesis 1, which states that the effect of the functional network modifiers on the dielectric properties relies on the number of the reactive moieties, which contribute to the chemical curing reactions. Compensated epoxy resin systems have marginal change in the hydroxyl group, while OH groups decreased as the loading of the FNM increased in the uncompensated systems. Also uncompensated structures contained increased number of retained unreacted epoxide groups. By examining the heat flow in the two systems, it was shown that the T_g of the modified systems is influenced by several factors such the structure of the modifier, the influence of the functional group of the modifier on the cross-link density, the network topology and the free volume introduced by the FNM. The experimental results showed that the AC breakdown strength of the compensated system is higher than that of the uncompensated systems and explained that the AC breakdown strength is effected by two main factors: (a) the functional group of the FNM and (b) the modified network topology. Such association clarified that the decreased AC breakdown strength of the uncompensated systems is attributed to the agglomeration of the modifier, which created an inhomogeneous network structure. In terms of the permittivity of the compensated and uncompensated systems, the presence of inorganic components in the FNM altered the real part of the permittivity. On the other hand, the imaginary part of the permittivity indicated increased β relaxation for compensated systems, where the opposite (decrease in the extent of β relaxation) was reported for the uncompensated systems. The dielectric data align with the variation in the epoxide groups and OH molecules evident from the FTIR spectra.

In addition to the investigation of the effect of the stoichiometric ratio of the FNM on the properties of the modified systems, it was necessary to confirm an assumption

made about the number of epoxide groups used to calculate the stoichiometry of the samples. The experimental data of the DSC and dielectric spectroscopy showed that the assumption that each GPOSS contains eight epoxide groups that can contribute to the curing process is valid.

The effect of two different FNMs, namely, GHE and GNPE, on the thermal, electrical and dielectric properties of modified epoxy resins was investigated. This investigation was conducted to tests hypothesis 2, which states that the inclusion of FNM in the resin system leads to changes in the network architecture of an epoxy system and therefore alters the electrical properties in an effect equivalent to the mechanisms by which nanoparticles influence the electrical response of nanocomposites. The data obtained by FTIR proved the presence of the FNM in the cured systems, i.e. the FNM survived the curing and post curing process. The experimental results showed that the glass transition temperature decreases with the increase in the loading of the FNM and that the GHE and GNPE modified systems have altered dielectric permittivity values. Finally, the AC breakdown strength of the modified systems increased up to 4 % loading of the modifier, after which the breakdown strength started to decrease. The impact of the observed effects were found to rely on the selection of the functional group of the FNM. While a comparable technique has previously been used as a means for altering the mechanical properties of epoxy resins, this is the first time to our knowledge that this approach has been explored in depth as a means of integrating different functional groups into a thermosetting polymer in order to effectively customise its properties. While there is no doubt that some types of fillers improved the properties of thermosetting materials, the published literature has highlighted a number of problems associated with dispersion and filler agglomeration. The use of liquid and low-concentration FNM $\sim$4% suggested in the research described in chapter 6 appears to offer a new alternative means of engineering novel materials to meet current and future needs in a simple and adaptable way.

After establishing the basic understanding of the effect of FNM on the different properties of an epoxy resin, it was important to check if the curing mechanisms would impact the generality of the findings reported for the amine cured modified FNM systems. For this purpose, chapter 7 used the FTIR, DSC, DC conductivity and dielectric spectroscopy to examine amine and anhydride cured epoxy resin systems modified using different concentration of a multi terminal epoxide groups FNM (which is TTE). The experimental data showed that the FNM influences the network topology of the resin through the cross-linking reactions, where in anhydride cured systems, TTE promotes esterification and results in a reduction in the probability of etherification mechanism. It was evident from the results that the modifier has influenced the T_g of the amine and anhydride cured systems in a similar way, where in both systems the inclusion of TTE resulted in a steady decrease in T_g as the concentration of the TTE increased. The impact of the TTE on the molecular dynamics revealed that γ relaxation of both

amine and anhydride cured system is associated with the presence of retained dipolar molecules in the TTE modified systems, the rotation of the amino-diphenyl groups, and an increase in molecular mobility facilitated by the incorporation of a higher number of ether links. For the β relaxation, the impact of TTE in the amine cured system was interpreted by the nature of the restrained environments that constrained the movement of the dipoles after the inclusion of the TTE. In the case of the anhydride cured systems, the FTIR data supported the findings that the etherification process that occurred in the anhydride cured systems influenced the strength of the β relaxation. For the electric conductivity experiments, the variation in the DC conductivity was associated with the presence of the functional groups of the FNM, variations in the free volume in the system and the change in the network topology. All these finding aligns with hypothesis 3, which states that changing the type of hardener (amine or anhydride) leads to changes in the curing mechanism, which would significantly affect the dielectric behaviour of the system. This is also the case when the system is altered in a systematic way, using functional network modifiers.

To sum up the impact of FNM on amine and anhydride cured epoxy resin systems, the presence of the functional network modifier has influenced the chemical, thermal and electrical properties of both systems. The reported influence of the FNM is more complex with the anhydride cured materials than in amine cured system, due to the fact that the natural anhydride curing mechanisms involve generation and consumption of hydroxyl groups. The lack of detailed analysis in the literature for the dielectric behaviour of anhydride cured resins made the process challenging for the neat anhydride cured systems, where the addition of the FNM added complexity to a process which is already not well understood. Consequently, this highlighted the importance of a detailed analysis of each relaxation process of the modified anhydride cured systems, where the temperature dependent dielectric tracking of each dynamic molecular relaxation process is acquired, which was the aim of chapter 8.

A detailed investigation of the effect of the FNM on the molecular dynamics of anhydride cured epoxy resin systems was presented in this work. This is to test hypothesis 4, which states that modification of the resin structure affect the molecular dynamics. The γ and β relaxations are associated with terminal groups, while α relaxation is related to segmental movement of main-chains, the consequent dipole relaxation activate charge transport above T_g. The results of chapter 8 discuss the molecular origin of the dipole relaxation and charge transport dynamics in FNM modified epoxy resins systems. To assist the interpretation of the dielectric relaxations, DSC measurements and temperature dependent electrical conductivity was conducted for the studied samples. As anticipated, the T_g of the modified systems is lower than that of the neat epoxy, where the variation in T_g was attributed to the different functional groups of the FNM. For the electrical conductivity, the neat systems showed lower conductivity compared with the conductivity of the modified systems. Analysis of the electrical conductivity

revealed the existence of two different processes. A DC conductivity process appears above the glass transition temperature, while a transient conductivity process was evident at temperatures below the T_g of the system. Regarding the molecular dynamics, the temperature dependent dielectric measurements were represented using a three dimensional representation for the the imaginary permittivity as a function of frequency and the temperature. The activation energy of each molecular relaxation was calculated using Arrhenius plots. It was found that the activation energy of the β and γ relaxations is affected by the functional group of the FNM. This was also clear from the Havriliak-Negami deconvoluted peaks of the molecular relaxations. The temperature dependent dielectric properties along with Havriliak-Negami deconvoluted peaks, the Arrhenius plots and the associated activation energies of the different molecular relaxations proofs that the type of the functional group of the FNM plays a vital role in determining the dielectric properties of the final material.

9.2 Future Work

The work reported in this thesis shows that functional network modifiers constitute a complementary and alternative approach for nanotechnology for designing materials with controlled dielectric properties. The systems researched, combined with the applied research method and the described experimental setup provides a complete guide for future studies to replicate the results and experiment with different FNM combinations. However, additional work is necessary to understand some of the parameters required to take the FNM approach to an industrial scale. Future investigations may therefore include the following:

- It would be worth studying the behaviour of space charge dynamics in neat and FNM modified epoxy resin systems. Investigation of processes such as charge migration, accumulation and decay, may provide more insight into the mechanisms responsible for the improvement in the electrical properties of the modified systems.
- From an industrial and practical point of view, it is necessary to examine the high temperature performance of the mechanical behaviour of the manufactured systems such as the rheology, tensile strength and fatigue behaviour. In addition, understanding the thermal conductivity would help in defining the applications in which each FNM may be used.
- It would be highly useful to investigate the DC breakdown strength of the FNM modified epoxy resin systems. Furthermore, conducting long term AC breakdown measurements provide beneficial information about the practical limits of the different formulations.

- It is recommended to use high resolution electron microscopy such as scanning electron microscopy (SEM) and transmission electron microscopy (TEM). These techniques provide important information about the morphology, structure and crystallisations in the material. Therefore, the use of SEM and TEM assist in understanding the behaviour of the material.

- The work reported in this thesis provides means of modifying the network structure of epoxy resin systems using functional network modifiers, where modified structures with a degree of controlled properties were produced. One of the main conclusions is that the final properties of the modified systems are associated with the chemical structure of the retained functional groups of the modifier. It would be useful to investigate other approaches to incorporate nonreactive functional groups into the epoxy resin network using the hardener. A preliminary investigation of this has already been established. However, all the attempts to cure the resin were unsuccessful because the selected hardener had a low reactivity as all the amine groups were secondary amines and the location of the NH was restricted by the hardener's network structure. It would be worth studying a hardener with an amine hardener with primary terminal amine groups within its chemical structure.

- This study is a qualitative investigation for the effect of the different functional groups on the dielectric, electric breakdown and heat flow in amine and anhydride cured epoxy resin systems. The work here provided a rough estimate for the loading of the FNM which provides improvement in the properties of the resin. According to Bocek et al [229], the optimum POSS loading should be from 1.1 wt% to 6.5 wt%, somewhere else it was suggested to be less than 3 wt% [112]. It would be interesting to find the optimum loading of each functional group.

- It is concluded from this work that the physical properties of the modified epoxy resins are associated with the chemical structure of the resin, hardener and the functional groups of the FNM. Specific functional groups of the FNM impact certain properties. For example, the inclusion of small fraction of alkyl groups is found to improve the breakdown strength and reduce the T_g of the modified systems, while the addition of GPOSS molecules revealed increased breakdown strength without significantly affecting the T_g. Similarly, the in cooperation of aromatic molecules showed positive impact on T_g. FNM with multiple terminal epoxide groups are found to alter the charge transport behaviour through an epoxy network as a results of modifying the network topology. Materials with cyclic structures (Cyclododecene oxide), were also tested but not reported in this thesis, as these FNM showed insignificant effect on the thermal and electrical properties of the modified resins. Finally, it would be worth studying the behaviour of an FNM with chemical structure comprising a halogen (fluorine (F), chlorine (Cl), bromine (Br) and iodine (I)), as they are reported to have high electron affinity, which is the main mechanism associated with the voltage stabilising behaviour of

the alkyl and aromatic structures reported in this work. i.e. increased breakdown strength (discussed in chapter 6).

It can be seen from the above account, that the optimal FNM chemical structure depends on the property of interest. In addition, the material selection process used here was limited by the molecules available in the market. But, in principle, it would be possible to synthesise FNM additives to optimise performance with respect to any given property. Therefore, based on the work reported in this thesis, it is perhaps possible to anticipate that interesting properties may results from the modification of an epoxy resin system using an FNM with chemical structure containing one of the halogens, an aromatic ring and multi terminal epoxide groups connected to the other molecules through ether links. To save time, effort and reduce the cost of the process, it is recommended to utilise a combination of a computer software (as a method simulate the selected FNM candidates), with a synthetic chemistry (to build the modifier) and the approach used in this these to test and verify the properties of the system.

Appendix A

Appendix A

A.1 The Selection Process of The Functional Network Modifiers

Four different functional network modifiers were used in this work. The selection process of these FNM was based on the criteria described in the chart shown in Figure A.1. A summary of the selection process is that, the FNM must be firstly safe to use with no health or environmental hazards. To do so, the safety data sheet SDS of all the possible FNM was checked. Next, intensive search was conducted to read and list any work used functional network modifiers for altering epoxy resin composites available in literature. After searching possible work used the FNM, the flash and boiling point of the FNM were set to be above the curing temperature and below the post curing temperature of the composite. The left materials were divided according to their chemical structure to aliphatic and aromatic. These were subdivided depending on the number of epoxide groups, length of the chain and branches. The remaining FNM were the most promising candidates. By applying the selection process described above, the following FNM were chosen where each one of them contains at least a terminal epoxide group and a functional group. Therefore, the selected five FNM represents all the possible options in terms of the chemical structure. Alkyl groups were represented by 2,3-Epoxypropyl hexadecyl ether modifier, which is the optimum FNM for these functional group which meets the selection criteria and features long chain alkyl group within its molecular structure. This FNM was obtained from Sigma Aldrich which is commercially known as glycidyl hexadecyl ether (GHE). The GHE has molecular weight of 298.50 g mol^{-1}. The Trimethylolpropane triglycidyl ether (TTE) modifier with chemical structure features short chain with multi-epoxide groups, was selected to represent the short chain alkyl groups. The TTE material has molecular weight of 302.36 g mol^{-1} which was also obtained from Sigma Aldrich. For FNM with aromatic structure, Glycidyl 4-Nonylphenyl Ether (GNPE) was chosen. The GNPE modifier obtained from sigma Aldrich has molecular weight of 276.41 g mol^{-1}. Glycidyl POSS (GPOSS) cage mixture obtained from Hybrid Plastics was selected as its features Polyhedral Oligomeric Silsesquioxane (POSS) molecule within its chemical structure. The GPOSS has molecular weight of 1337.88 g mol^{-1}. Finally, to check the effect of epoxy-based reactive modifier with cyclic chemical structure, 1,2-Epoxycyclododecane (ECD) modifier was selected. The ECD modifier has 182.30 g mol^{-1} which was obtained from Sigma Aldrich.

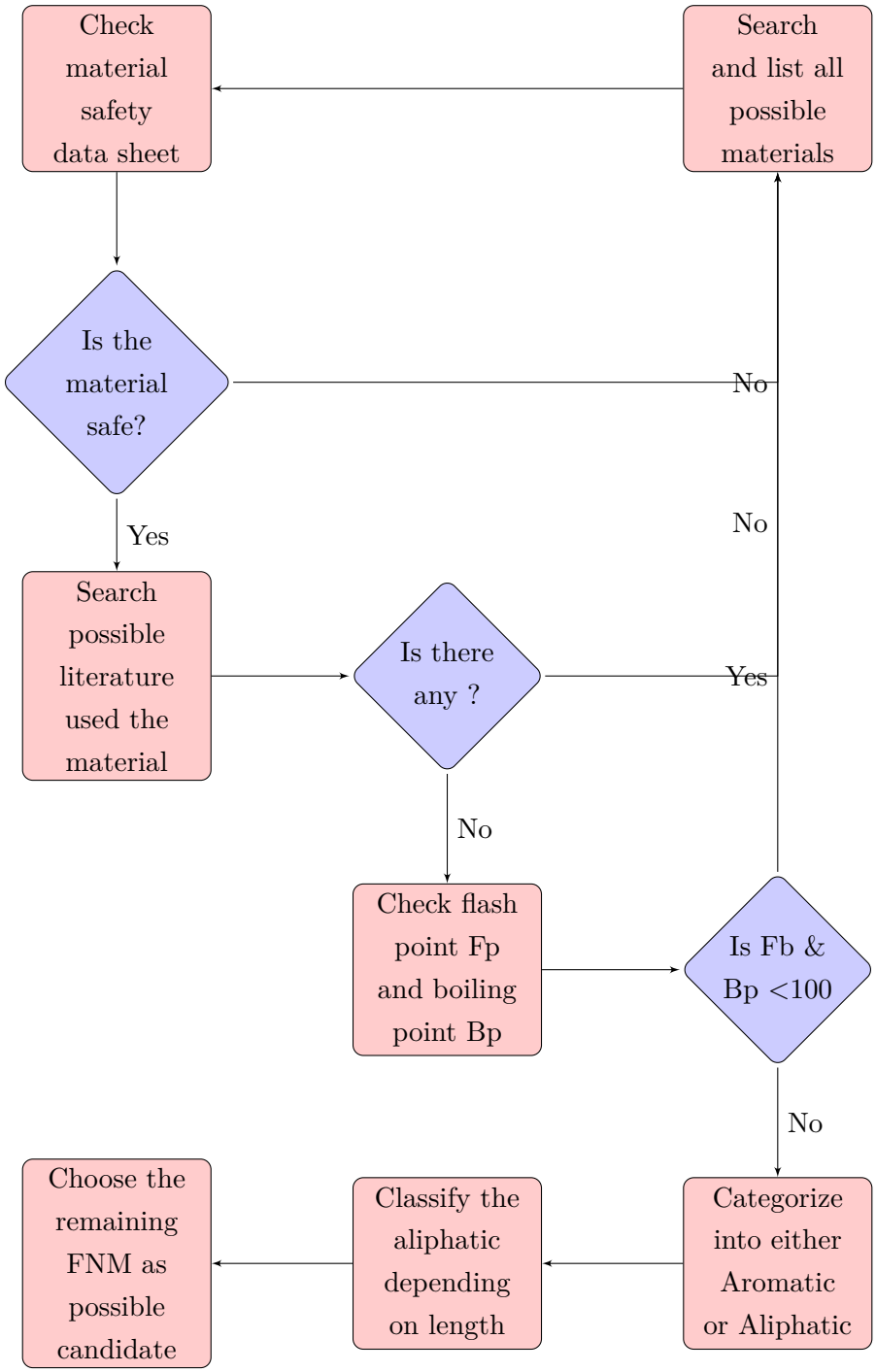

Figure A.1: Flowchart for summarise the selection process of the functional network modifiers.

A.2 Properties of the ECD modified Epoxy resin Systems

The effect of modifying epoxy resins using cyclic epoxy based functional network modifier is discussed in this section. The studied samples were manufactured with 1%, 4%, 10%

and 30% of epoxide groups form the ECD. The following sections illustrates the results of the conducted experiments with data analysis and discussion.

A.2.1 FTIR Spectroscopy

The spectra of the neat and ECD modified epoxy resin systems are shown in Figure A.2. A close look at the CH stretch region at wavenumbers 2980 cm^{-1} and 2820 cm^{-1} is plotted in Figure A.3. The figure indicates that the peak located at 2927 cm^{-1} in the spectra of the neat epoxy increases in intensity as the percentage of the added ECD increase. In addition, the same peak is slightly shifted to a lower wavenumber, from 2927 cm^{-1} in the spectra of the neat epoxy to about 2926 cm^{-1} in the data of the 30ECD. The absorbance peak at 2927 cm^{-1} is associated with the antisymmetric stretch CH_2 groups. The presence of CH_2 groups is reported to increase the absorbance at the region around 2927 cm^{-1} and shift the peak to lower wavenumber [136, 142, 164, 165, 167], which is in good agreement with the effect of the addition of ECD groups reported here. Since the chemicals structure of the ECD comprises of about ten CH_2 groups, the noticed increase in the absorbance spectra (indicated in Figure A.3) is attributed to the presence of ECD groups in the chemical structure of the cured resin.

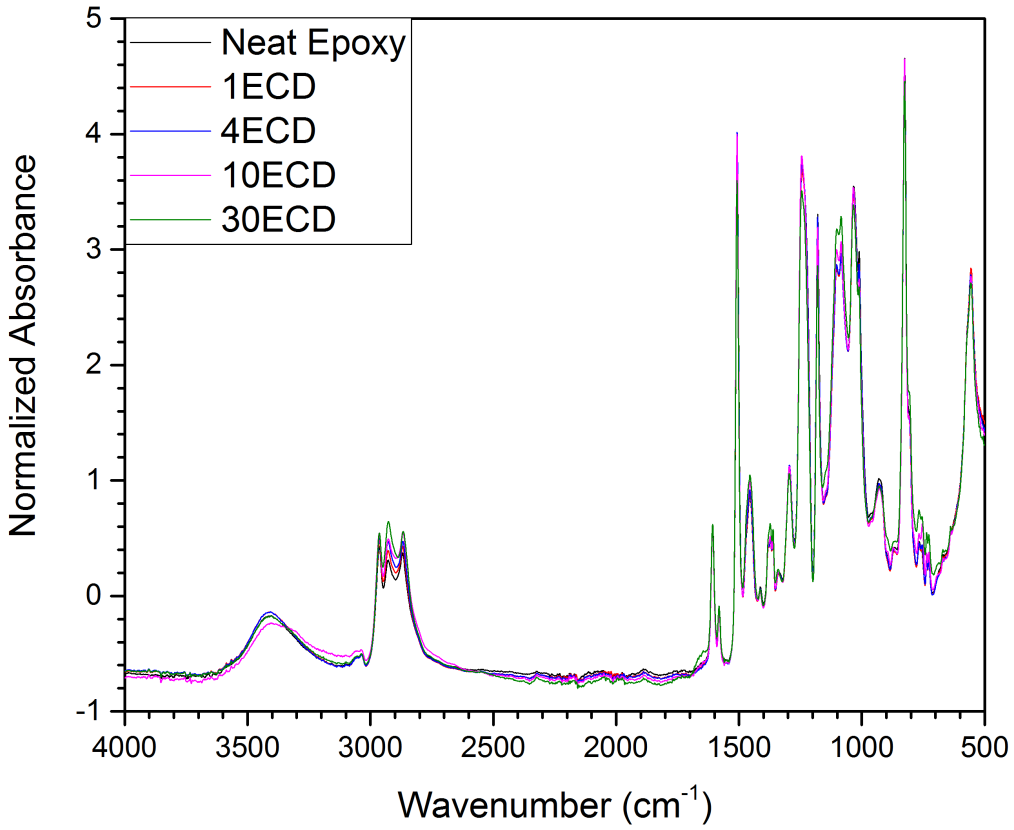

Figure A.2: FTIR spectra of reference and ECD modified systems.

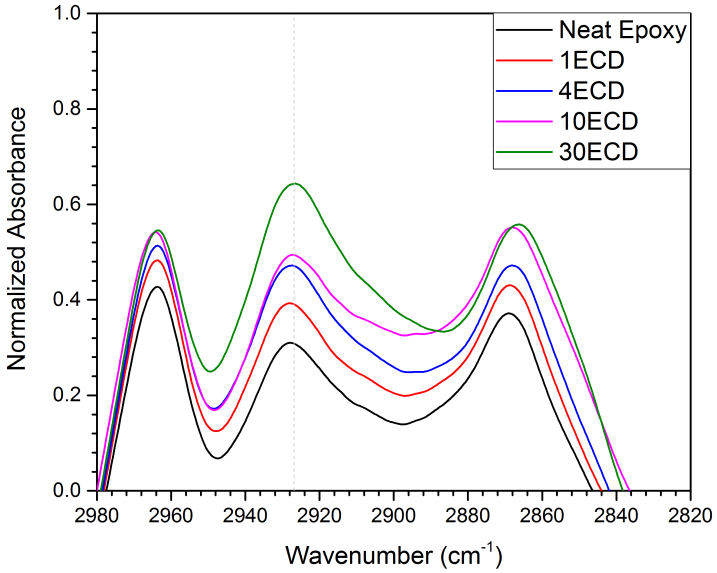

Figure A.3: FTIR spectra of ECD modified epoxy resin systems for wavenumber between 2980 cm^{-1} and 2820 cm^{-1}.

A.2.2 Differential Scanning Calorimetry

The DSC measurements of the neat and ECD modified epoxy resin systems are presented in Figure A.4, while data of the glass transition temperatures are listed in Table A.1. The addition of ECD resulted in shifting the T_g of the modified systems to lower temperatures. As the added percentage of the ECD increased, the glass transition temperature of the modified systems decreased. Modifying the samples by adding 30% of the epoxide groups from the ECD modifier resulted in decrease in T_g from about 85.3 °C for neat epoxy to about 52.4 °C for the 30ECD systems. The effect of ECD on the glass transition temperature of the modified samples could be attributed to the increase in the free volume in the system resulted from the integration of the ECD within the structure of the epoxy resin [130].

Table A.1: DSC measurements for reference and GGPOSS modified systems.

Sample	T_g(°C)
Neat Epoxy	85.3
1ECD	79.8
4ECD	77.0
10ECD	63.4
30ECD	52.4
Error in Tg = ±2 °C	

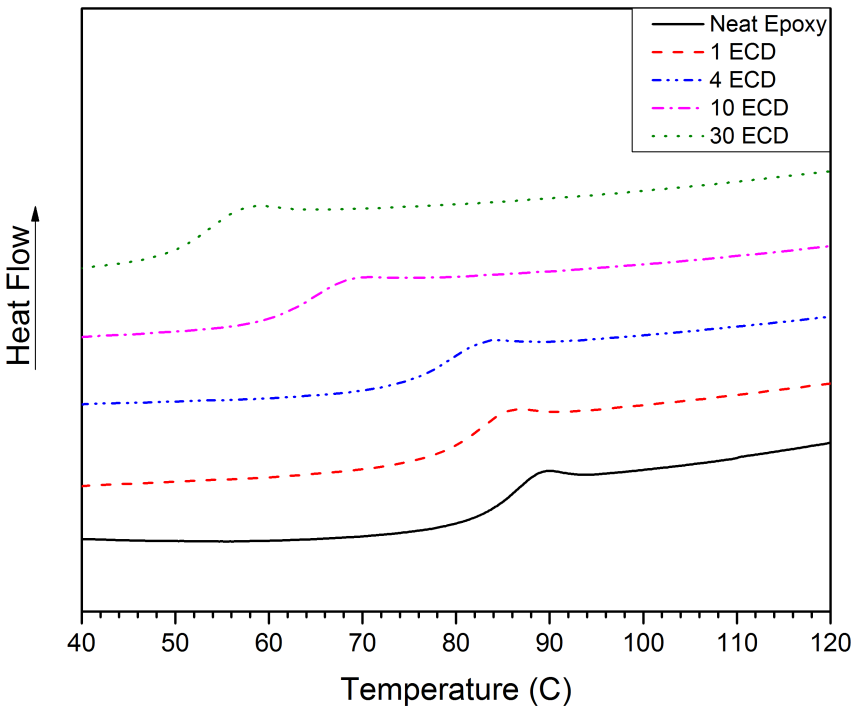

Figure A.4: DSC traces for reference and ECD modified systems.

A.2.3 Dielectric Spectroscopy

The dielectric response of neat and ECD modified epoxy resin systems is shown in Figure A.5. The data of the permittivity indicate that the real part of the complex permittivity decreases as the added percentage of ECD increase, as presented in Figure A.5(a). Similarly, the imaginary part of the permittivity decrease as the loading of the ECD increase, as shown in Figure A.5(b). The peak at the high frequencies end of the imaginary part of the complex permittivity (located at about 10^5 Hz) is associated with β relaxation. The data indicates that the extent of β relaxation decrease, as the added percentage of ECD increase. The extent of β relaxation is associated with the frequency and motion of hydroxyl groups in the system. Therefore, the data suggests that the addition of ECD resulted in producing a system with lower number of hydroxyl groups. In addition, the ECD modifier features a cyclic terminal group, which would have imposed a restriction on the movement of the hydroxyl groups, consequently, reducing the strength of β relaxation.

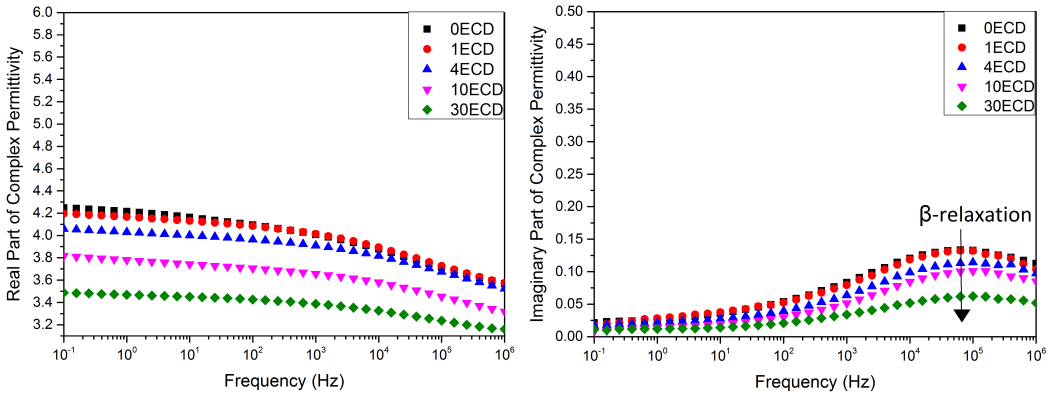

(a) Real part of permittivity of ECD modified epoxy resin systems.

(b) Real part of permittivity of ECD modified epoxy resin systems.

Figure A.5: Real and imaginary part of complex permittivity of reference and ECD modified systems.

A.2.4 AC Breakdown Strength

The cumulative probability of the AC breakdown for the ECD modified epoxy resin systems are shown in Figure A.6. The data suggests that the inclusion of the ECD resulted in limited effect on the breakdown strength. Measurements of the breakdown strength indicated that the maximum increase in the AC breakdown strength is about 3%, which resulted from the addition of 4% - 10% of the epoxide groups from the ECD modifier. The values of the breakdown strength for the neat and ECD modified systems are listed in Table A.2.

A.2.5 Electrical Conductivity

The conductivity measurement of ECD modified epoxy resin systems are illustrated in Table A.2. Samples modified with up to 10% of the epoxide groups from the ECD have increased the conductivity of the modified systems compared to the conductivity of the neat system, but within the same order of magnitude of the neat systems. The addition of 30 parts of the epoxide groups from the ECD resulted in increase in the conductivity of the modified systems by about one order of magnitude, as shown in Table A.2. In addition, the rheology experiment for the modified systems indicated that the addition of ECD affected the viscosity of the neat epoxy resin. Where the viscosity of the modified epoxy was decreased by 66% compared to that of the neat sample. The measured viscosity of the DER332 epoxy was about 0.266 Pa.s, which was decreased to about 0.091 Pa.s for 30ECD systems. The reduction in the viscosity caused by the ECD is the highest compared to the effect on the viscosity resulted from the inclusion of GHE, GNPE and TTE, where the viscosity was reduced by 62%, 49% and 29% respectively. The effect of the ECD on the DC conductivity of the modified systems might be associated with the inclusion of the functional groups of the ECD in

the system, where a branched network is generated. These branches may facilitated charge transport within the system.

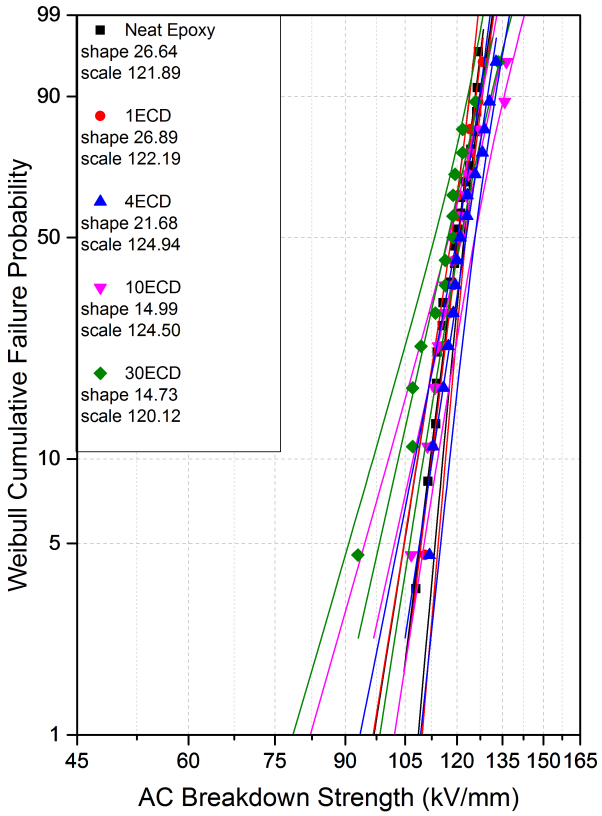

Figure A.6: AC breakdown of reference and ECD modified epoxy resin systems.

Table A.2: DC conductivity and AC breakdown measurements of neat and ECD modified samples.

Sample ID	DC Conductivity (S/cm)	Weibull α (kV/mm)	Weibull β	% BD
Neat Epoxy	$1.03 \times 10^{-17} \pm 1.01 \times 10^{-18}$	121.9 ± 1.7	26.6	100%
1ECD	$1.36 \times 10^{-17} \pm 2.44 \times 10^{-18}$	122.1 ± 3.9	26.8	100.2%
4ECD	$1.86 \times 10^{-17} \pm 3.30 \times 10^{-18}$	124.9 ± 5.4	21.6	103%
10ECD	$3.82 \times 10^{-17} \pm 3.81 \times 10^{-18}$	124.5 ± 7.2	14.9	103%
3ECD	$2.50 \times 10^{-16} \pm 1.54 \times 10^{-17}$	120.1 ± 7.1	14.7	98.2%

Appendix B

Appendix B

The curing and post curing schedule plays a vital role in determining the physical properties of the final epoxy resin material [230]. Time and temperature of both curing and post curing may vary depending on the type of the resin. Therefore, it was very important to investigate the optimum curing and post curing time and temperature for the DER 332/ Jeffamine mixture. Selection of curing time and temperature

Firstly the effect of curing temperature on the physical properties of DER 332 was investigated. Then after selecting the optimum curing temperature, study of the impact of curing time on the electrical and thermal properties at the selected temperature was established. The principle of falling ball viscometer was used to study the effect of the temperature on the epoxy resin [231]. The experimental setup is shown in Figure B.1. Spherical steel ball bearings with a diameter of 6.32 mm and weight of 1.045 g were set to fall free in a cylindrical glass tube, labelled and filled with a 12 grams of a mixture of resin and hardener. The glass tube was placed in a temperature controlled distilled water where a thermometer was used to estimate the resin temperature. Water mixing was done all through the experiment by utilising a magnetic stirrer to ensure even distribution of the heat through the water. After setting the temperature to a required value, the time required for a ball bearing to travel from the start line to the end line indicated in Figure B.1, was recorded. The experiment was repeated for two temperatures, 60 °C and 80 °C.

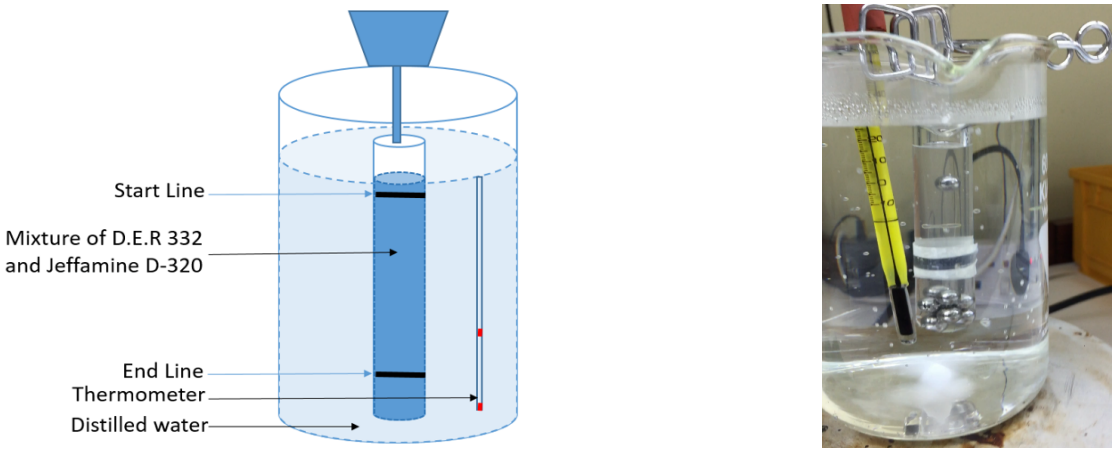

(a) Experiment Setup

(b) Lab Setup

Figure B.1: Setup for falling ball bearing viscosity measurement experiment.

The change in the viscosity was calculated using the following equation [231]:

$$\eta = \frac{2r^2(p_b - p_e)g}{9V_t} \tag{B.1}$$

Where:

η'' is the mixture viscosity. **r** is the radius of the ball bearings.

g is the acceleration due to gravity. V_t is the terminal velocity of ball bearings.

The viscosity measurements at 60 °C and 80 °C are shown in Figure B.2.

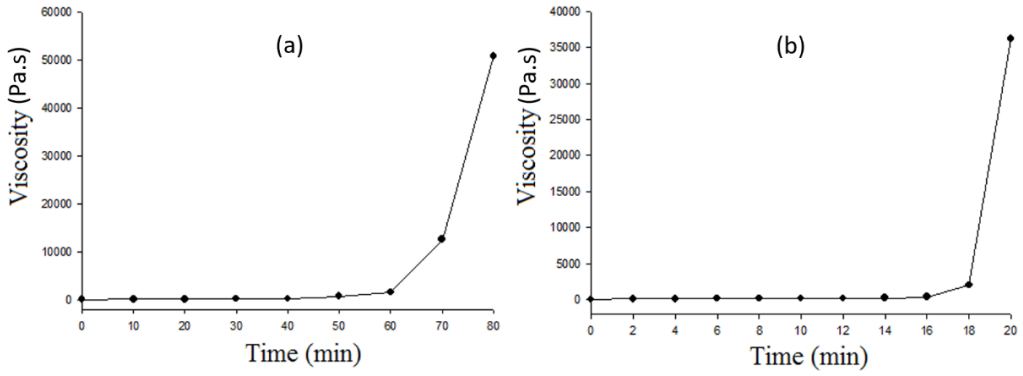

Figure B.2: viscosity measurements at (a) 60 °C and (b) 80 °C.

An ER mixture heated at 80 °C starts the curing process after 20 min, whereas at 60 °C, the mixture takes about 80 min to start curing. It can be seen that at 60 °C the curing process is very slow and the mixture has a long pot life. According to the manufacturer of the amine harder, long time handling of Jeffamine at temperatures above 37 °C in air at atmospheric pressure would give rise to Jeffamine oxidization. Therefore, it can be concluded that the 80 °C could be the recommended curing temperature, because it provided relatively efficient time for the mixture to start curing at appropriate hardener handling. In literature, different temperatures have been used for curing epoxy resin. For example, C. Yeung [232] cured DER 332 epoxy resin mixed with Jeffamine D-230 at 100 °C for 4 hours, which was not justified. The curing temperature recommended by the supplier for DER 332 epoxy cured with amine hardeners was 80 °C. This temperature is in good agreement with the falling ball viscometer experiment. Therefore, 80 °C was used as the temperature for samples curing in this work. After selecting the curing temperature, the effect of curing time on the thermal properties, dielectric response and breakdown strength was investigated. Epoxy resin samples were cured at 80 °C for different curing times. Figure B.4 shows Weibull parameter α (kV/mm) of the AC breakdown strength of epoxy resin samples cured at 80°C, for times ranging from 1 h to 9 h. Unexpectedly, these results indicate that the breakdown strength of samples cured for just 1 h have the highest measured breakdown strength, around 125 kV/mm. The breakdown strength decreased gradually with increasing curing time. After 3 h of curing,

the BDS increase again. Comparing this behaviour with the conductivity shows that the conductivity follows the opposite trend (Figure B.4). Although it is not possible to provide a detailed explanation for this, some speculation is nevertheless possible. Kumar et al. [230] studied the curing behaviour of epoxy resin and showed that the crosslink density is a strong function of the curing time. Therefore, it might be possible that the cross link density could have influenced the variation in the breakdown strength.

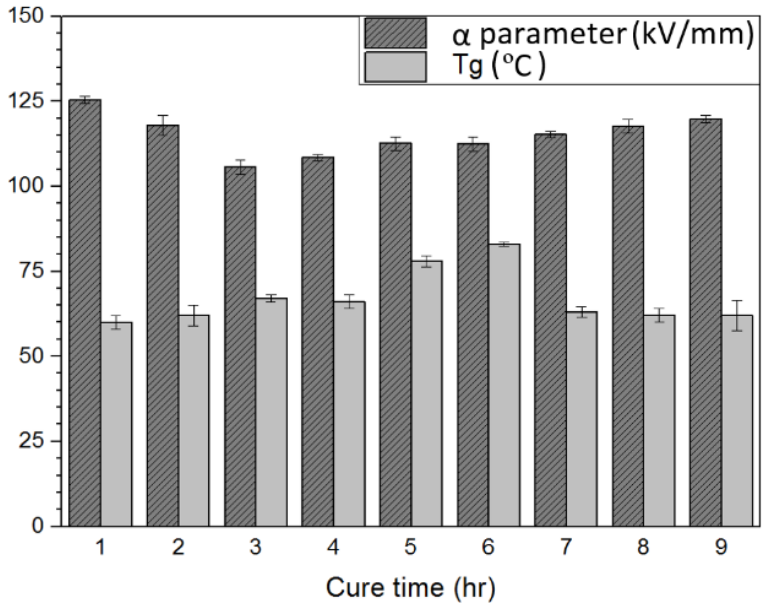

Figure B.3: The effect of curing time on the electrical and thermal properties of neat epoxy resin.

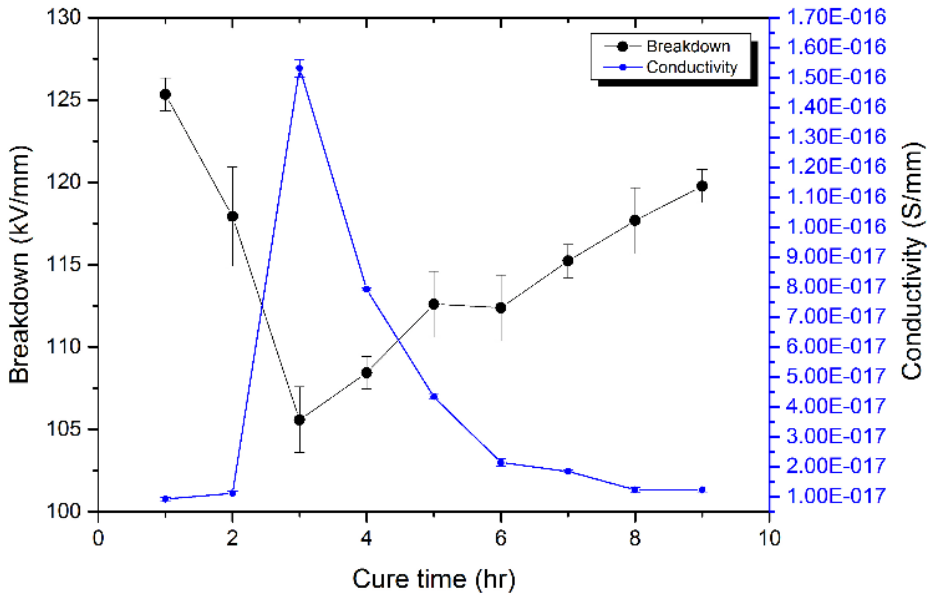

Figure B.4: Weibull parameter α (kV/mm) of the AC Breakdown strength vs conductivity for neat epoxy resin samples cured from 1 - 9 hours at 80 °C.

The behaviour of Tg for the 9 samples is shown in Figure B.3 and Figure B.5. As the curing time increases, T_g shifts to higher values. However, after 6 h of curing, this trend stops. The increased curing time could have resulted in a highly cross linked system. As the cross link density changing, the behaviour of T_g is affected. This behaviour is not anticipated for a homogenous system and is usually expected for inhomogeneous systems [233].

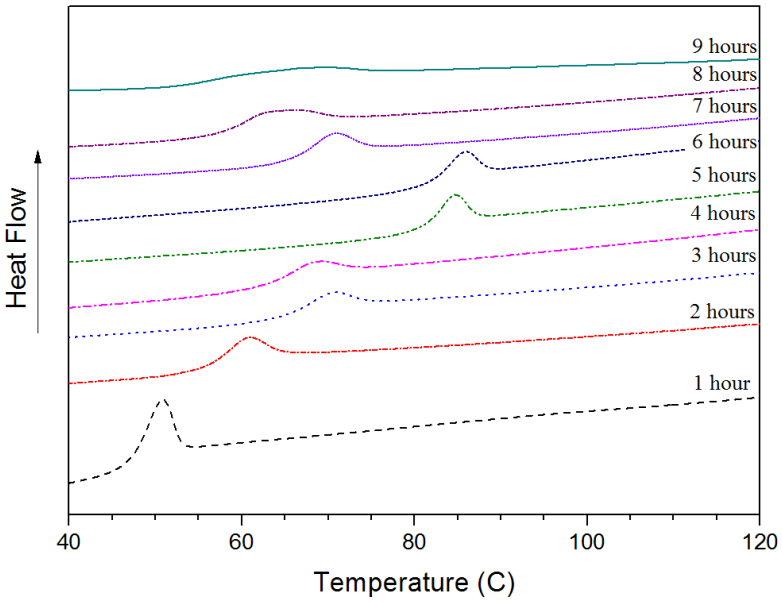

Figure B.5: Differential scanning calorimetry measurements as a function of temperature for epoxy resin systems cured at different curing hours.

The dielectric response of the cured samples is shown in Figure B.6 .The figure indicates strong variation in the both real and imaginary permittivity of cured samples. This behaviour perhaps could be explained by the existence of two factors which are namely the degree of crosslinks (i.e. the extent of reaction) and environmental constraints. As the reaction proceeds, more hydroxyl ether groups are formed but, as the crosslink density increases, they become increasingly constrained. Initially, the degree of crosslinks dominates, where the increased formation of hydroxyl ether groups resulted in rising peak of the dielectric β-relaxation, indicated at the high frequency above 10^4 Hz of imaginary permittivity in Figure B.6. However, later on, it's the environmental constraints which dominates; Therefore, the movement of hydroxyl ether groups become constrained which was reflected by the decreased β-relaxation after 6 hours of curing.

The dielectric α-relaxation at frequency below 100 Hz of imaginary permittivity also change with increasing the curing time as shown in Figure B.6. This behaviour is expected as α-relaxation is linked to T_g [20] and the noted variation in T_g could have resulted in the variation in α-relaxation. Results of the effect of curing time on the electrical properties indicate that 3 hours is a critical curing time, after which the breakdown strength changes significantly. It can be concluded from this experiment that 2 hours of

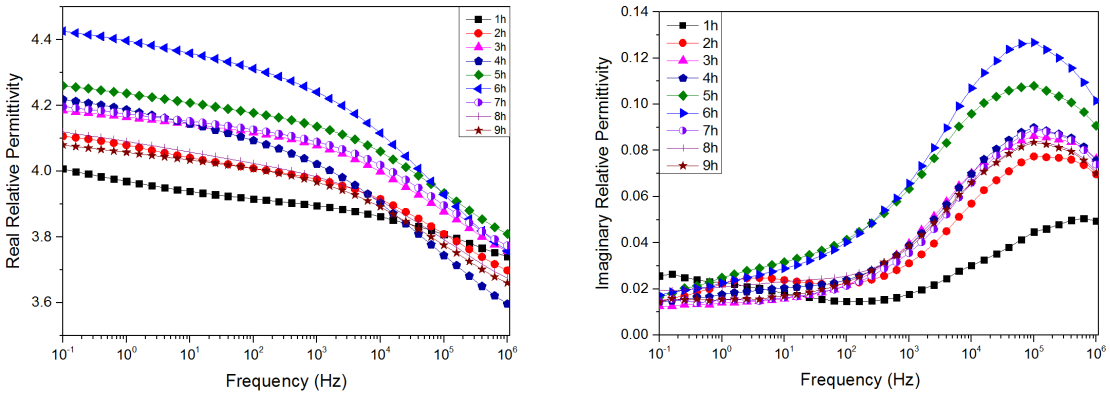

(a) Real part of complex permittivity

(b) Imaginary part of permittivity.

Figure B.6: The effect of curing time on the dielectric response of neat epoxy resin samples

curing could be the optimum curing time in terms of breakdown strength, Tg and the consequent dielectric response. This is consistent with the curing time recommended by the manufacturer. Therefore, the produced samples of this work were cured at 80 °C for 2 h, which was recommended by the manufacturer and confirmed experimentally. Selection of post curing time and temperature

The effect of post curing process on the electrical properties of epoxy resin was studied for different post curing time. All samples were cured at 80 °C for 2 hours, then post cured at 125 °C for 1 - 3 hours. Weibull probability plot of the breakdown strength is shown in Figure B.7. The AC breakdown strength data indicate that after 2 hours of post curing the breakdown increase from 107.8 kV/mm to 121.89 kV/mm, which was further increased to 129.89 kV/mm after 3 hours of post curing. However, the data of the breakdown strength after 3 hours of post curing for low probability of failure (below 50%) overlap with the data of obtained from samples post cured for 2 hours, as shown in Figure B.7. This could indicate that post curing for more than 3 hours result in only limited effect on the breakdown strength.

The real and imaginary parts of complex permittivity for the post cured samples are shown in Figure B.8. The results indicate that post cured systems have relativity lower real permittivity at high frequency compared to not post cured sample. However, post curing time showed limited effect on the real permittivity. In addition. Post cured samples have higher β-relaxation and α-relaxation relative to non-post cured samples. While increasing the post curing time has slightly reduced both relaxation peaks (Figure B.8(b)).

In summary, increasing the post curing time has only a slight effect on the breakdown strength and dielectric behaviour of the samples. As 3 hours of post curing has increased the breakdown strength slightly and altered the dielectric response of the samples, it can be assumed that 3 hours of post curing could be the optimum post curing time.

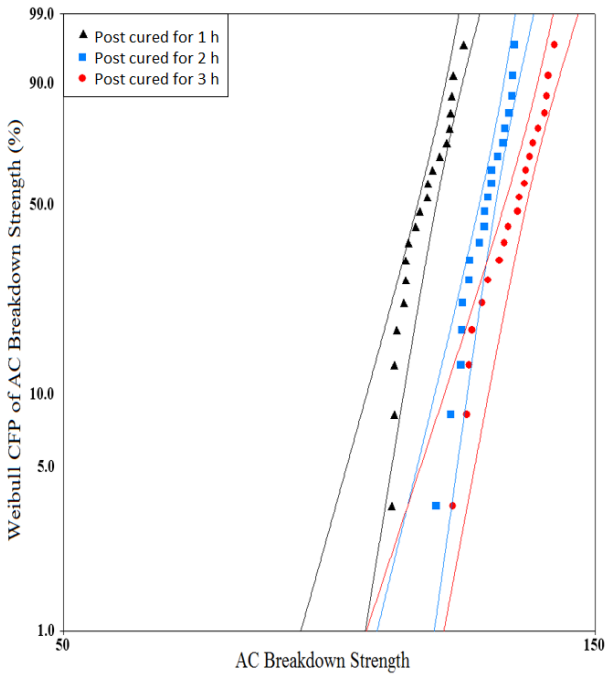

Figure B.7: Weibull plot of breakdown data obtained for neat epoxy resin samples cured from 2 hours at 80 °C then post-cured at 125 °C for 1 - 3 hours.

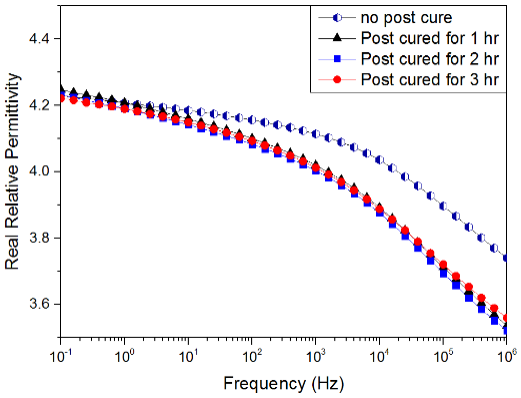

(a) Real permittivity of post-cured epoxy resins.

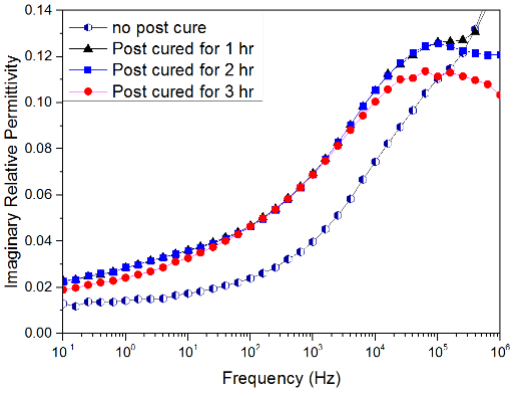

(b) Imaginary permittivity of post-cured epoxy resins.

Figure B.8: Dielectric properties of epoxy resin systems.

According to the manufacturers, it is recommended to post cure the DER 332 samples for a period of 3 hours. As both the manufacturer and the experiment post curing time agree, epoxy resin samples in this work were post cured at 125 °C for 3 hours.

Appendix C

Appendix C

C.1 FTIR Spectroscopy

The complete FTIR spectra for the neat epoxy resin and systems modified using GPOSS modifiers are presented in Figure C.1.

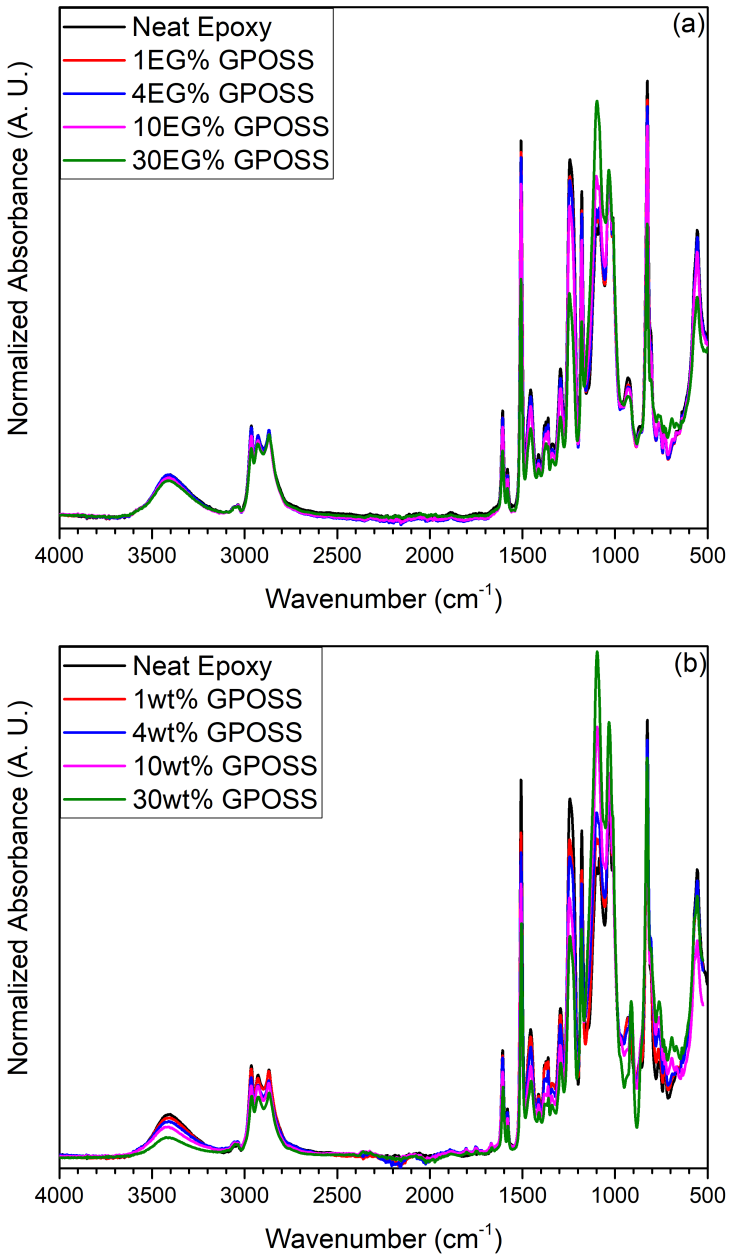

Figure C.1: FTIR spectra of reference and GPOSS modified systems with (a) compensated stoichiometry, and (b) uncompensated stoichiometry.

Appendix D

Appendix D

D.1 FTIR Spectroscopy

The complete FTIR spectra for the reference and amine cured TTE modified epoxy resin samples is shown in Figure D.1. A detailed graph for the FTIR spectra at range from $1800cm^{-1}$ to $600cm^{-1}$ is shown in Figure D.2. It can be seen from Figure D.2 that the introduction of the TTE modified resulted in increase in the ether absorbance peak, which suggests etherification process is promoted by the addition of the TTE. In addition, the figure shows that the introduction of the TTE modifier has insignificant effect on the epoxide groups in the systems.

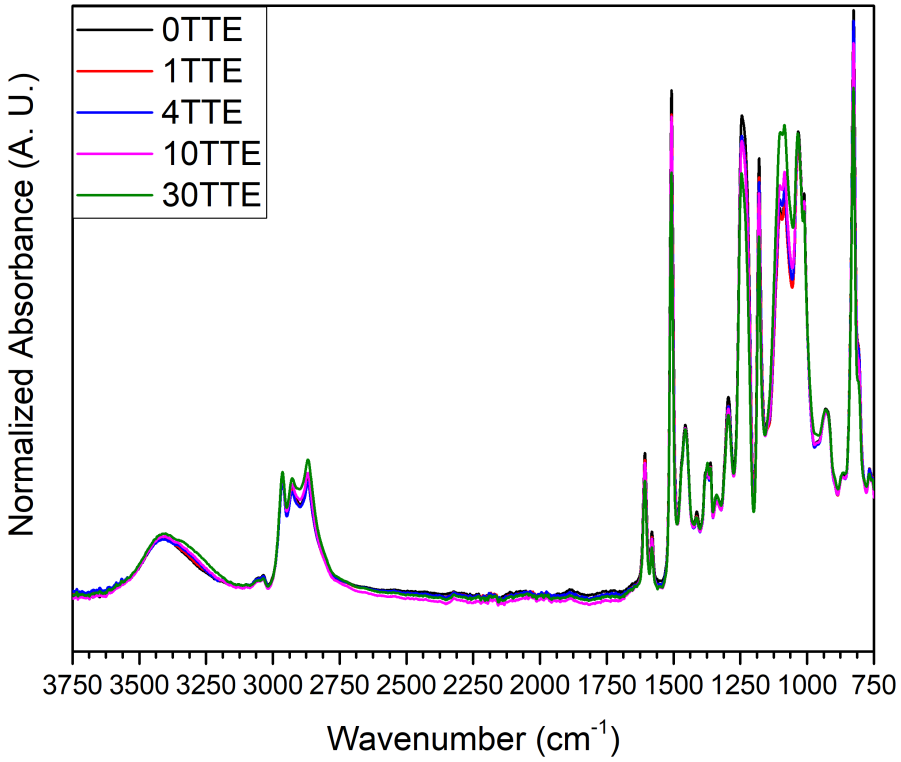

Figure D.1: The complete FTIR spectra for neat and TTE modified epoxy resin samples cured using amine hardener.

The complete FTIR spectra for the reference and anhydride cured TTE modified epoxy resin samples is shown in Figure D.3. A detailed graph for the FTIR spectra at range from $1800cm^{-1}$ to $600cm^{-1}$ is shown in Figure D.4. It can be seen from Figure D.4 that the introduction of the TTE modified resulted in increase in the ester absorbance

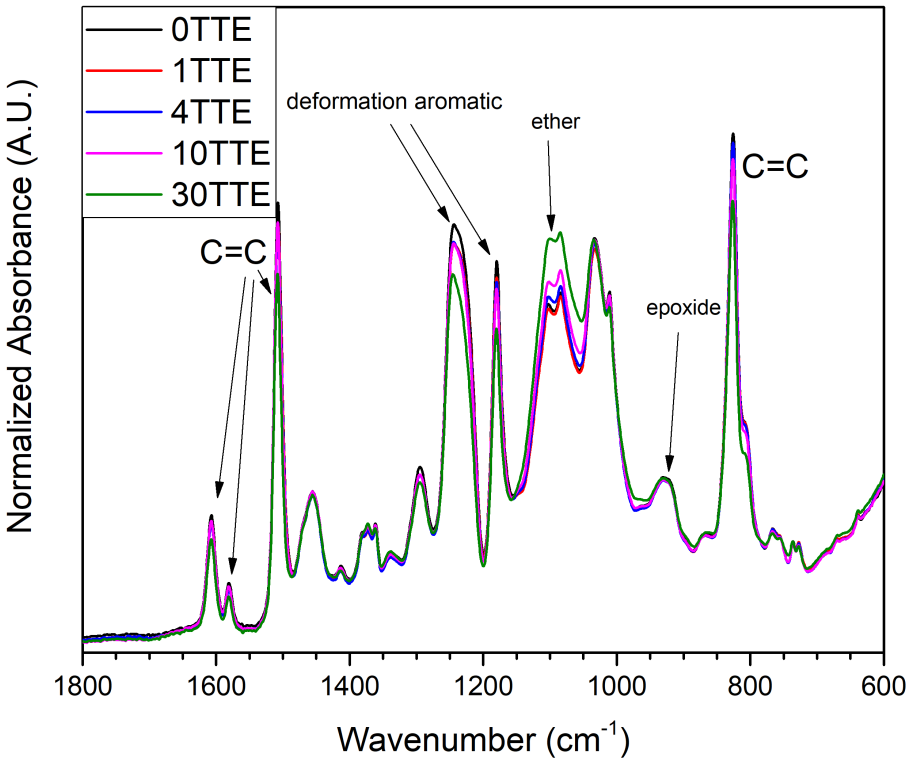

Figure D.2: The FTIR spectra for neat and TTE modified epoxy resin samples cured using amine hardener at range from $1800cm^{-1}$ to $600cm^{-1}$.

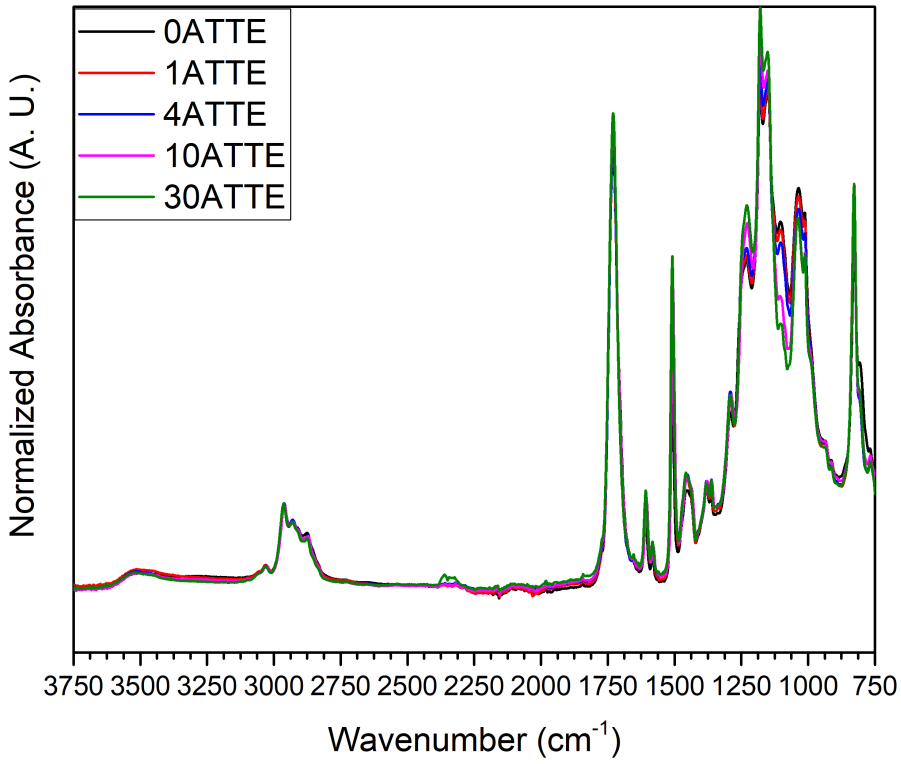

Figure D.3: The complete FTIR spectra for neat and TTE modified epoxy resin samples cured using anhydride hardener.

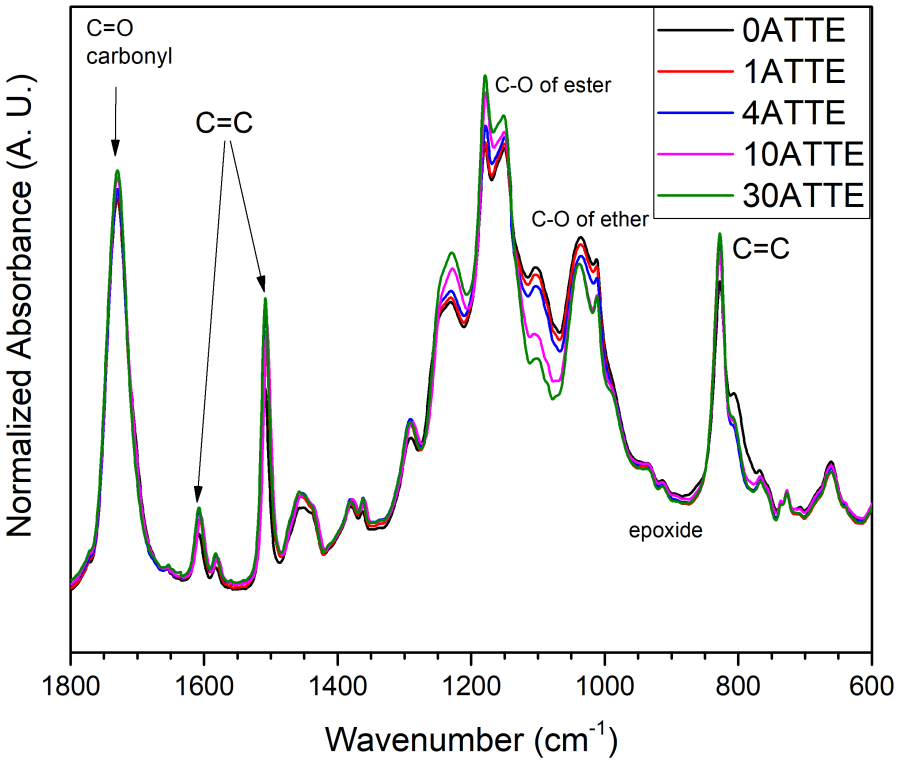

Figure D.4: The FTIR spectra for neat and TTE modified epoxy resin samples cured using anhydride hardener at range from $1800cm^{-1}$ to $600cm^{-1}$.

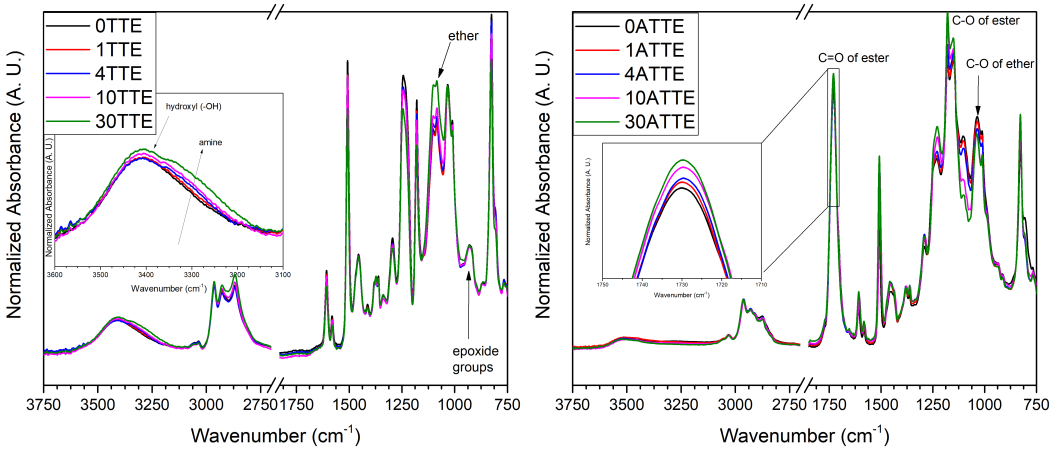

(a) The FT-IR spectra of neat and TTE modified amine cured epoxy resin systems.

(b) The FT-IR spectra of neat and TTE modified anhydride cured epoxy resin systems.

Figure D.5: Comparison between the FTIR spectra of the reference and FNM modified amine and anhydride cured systems.

peak and decrease in the ether absorbance peak. This suggests that the addition of TTE to anhydride cured systems promoted esterification process, while etherfification process become less favourable. In addition, the figure shows that the introduction of the TTE modifier has insignificant effect on the epoxide groups in the systems, as shown in Figure D.4.

D.2 Dielectric spectroscopy

D.2.1 Temperature dependent dielectric spectroscopy of neat and TTE modified amine cured systems

The temperature dependent data of the imaginary part of the complex permittivity of the neat amine cured epoxy resin systems are shown in Figures D.6, D.7 and D.8. While the data of the imaginary permittivity of the 30TTE systems at comparable temperatures are Figures D.9, D.10 and D.11.

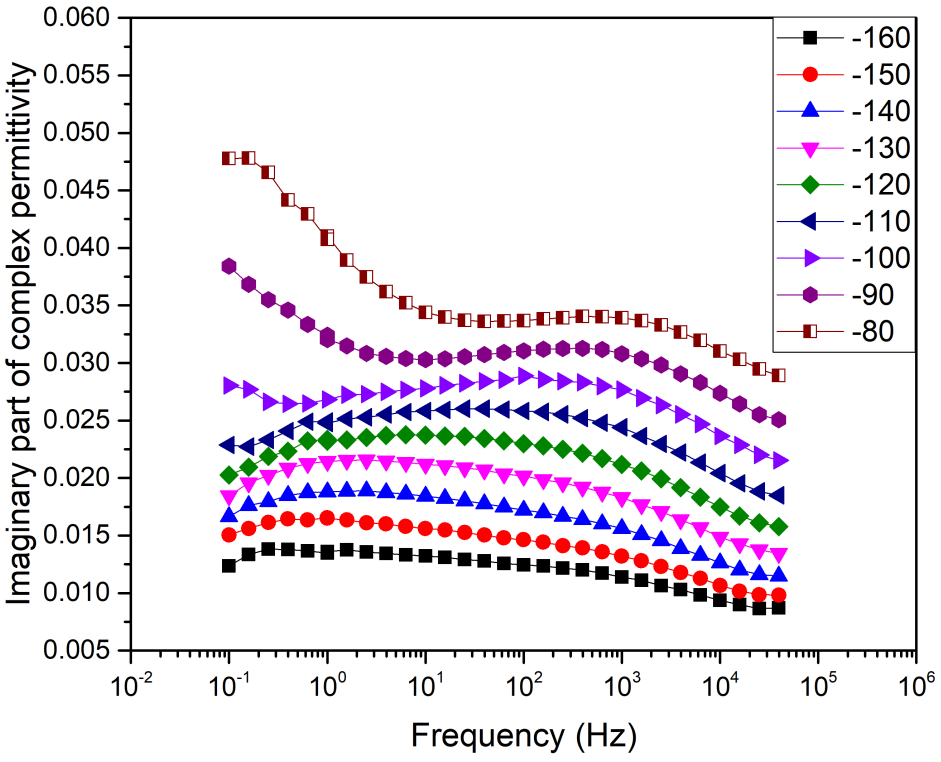

Figure D.6: Dielectric spectroscopy of neat amine cured epoxy resins at temperatures from -160 °C to -80 °C.

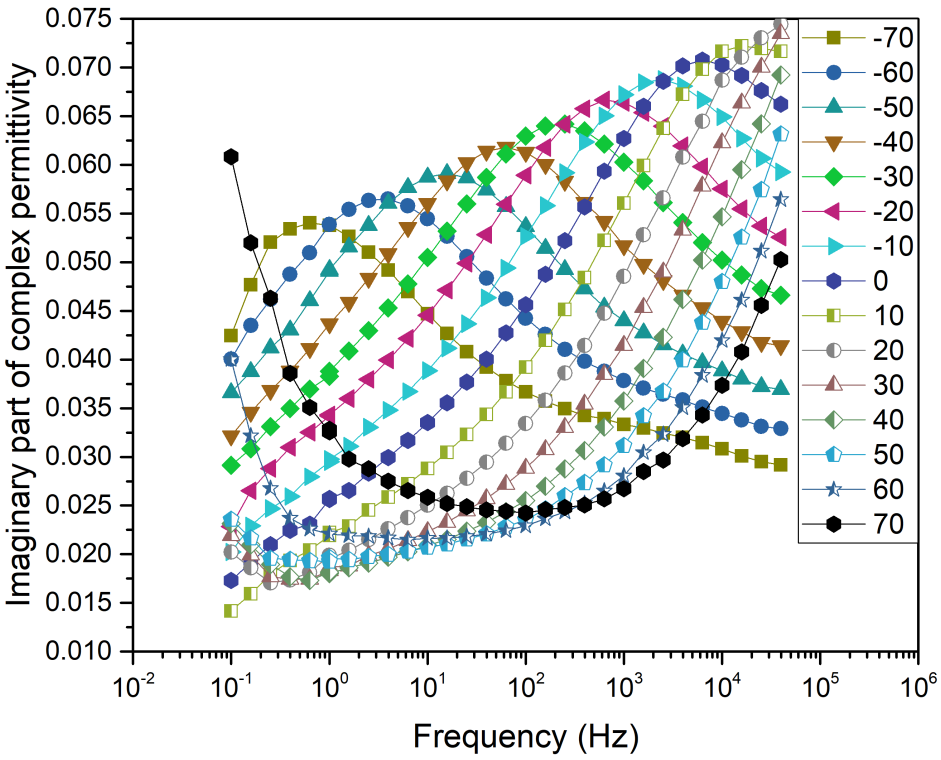

Figure D.7: Dielectric spectroscopy of neat amine cured epoxy resins at temperatures from -70 °C to 70 °C.

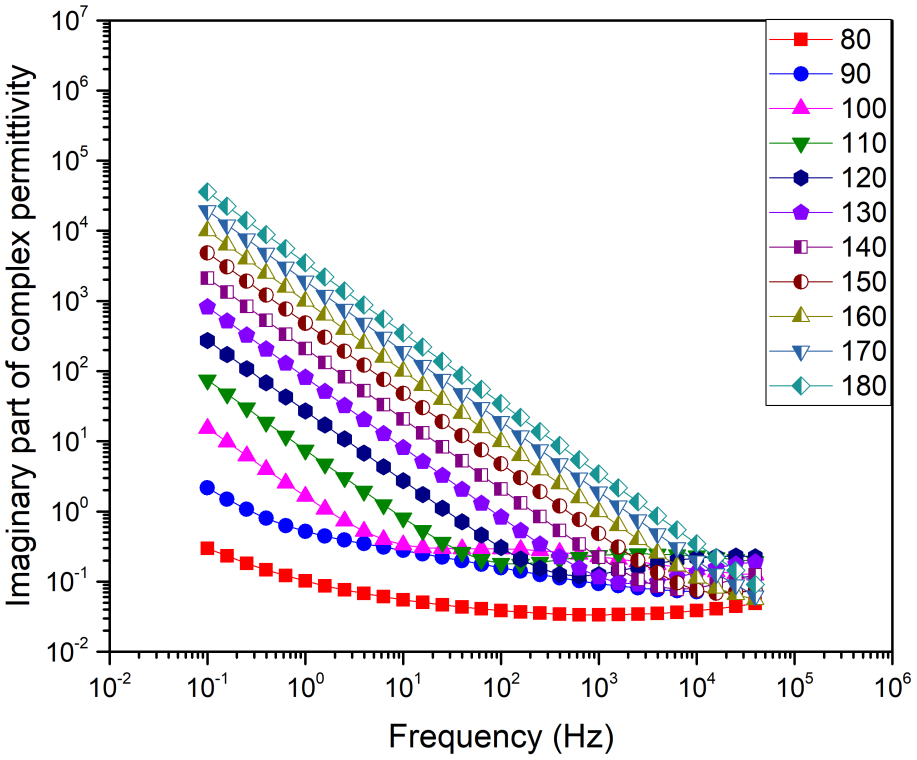

Figure D.8: Dielectric spectroscopy of neat amine cured epoxy resins at temperatures from 80 °C to 180 °C.

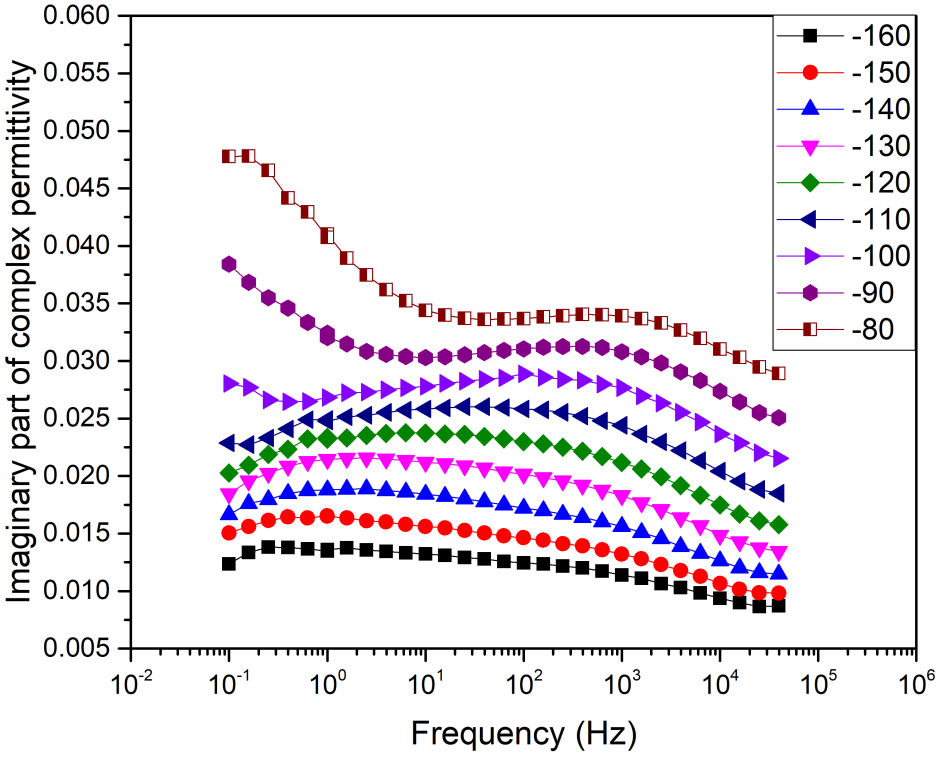

Figure D.9: Dielectric spectroscopy of 30TTE systems at temperatures from -160 °C to -80 °C.

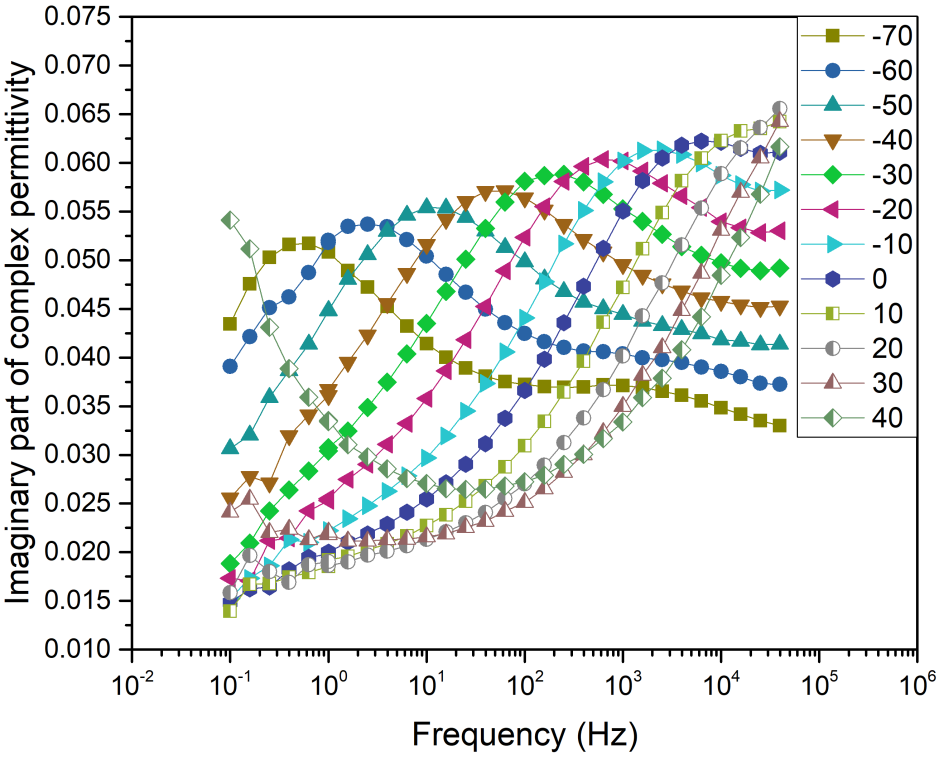

Figure D.10: Dielectric spectroscopy of 30TTE systems at temperatures from -70 °C to 40 °C.

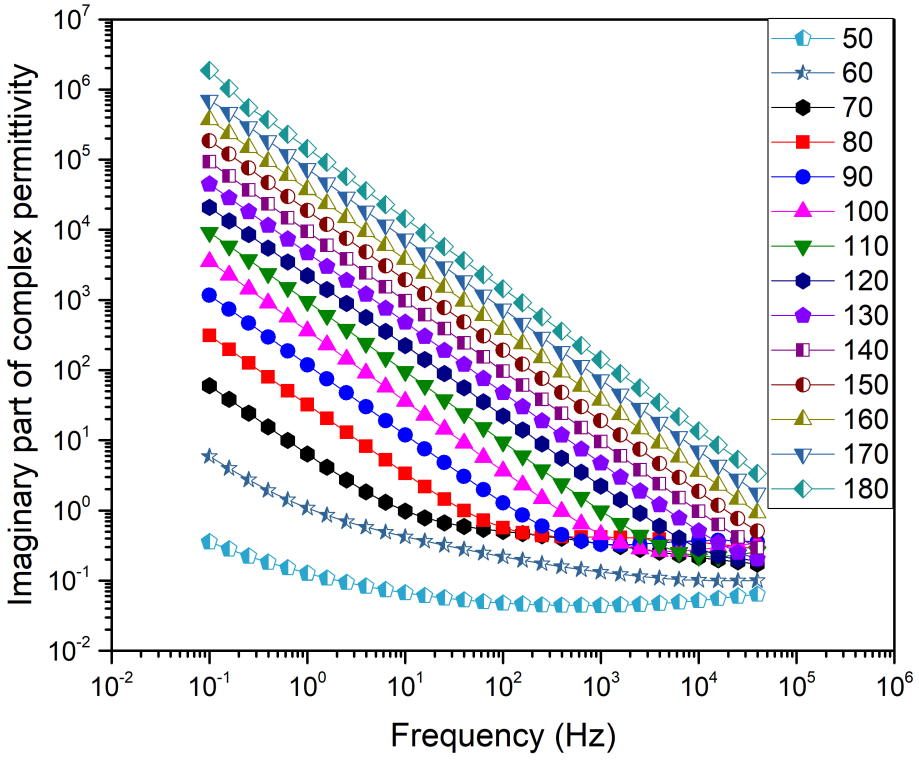

Figure D.11: Dielectric spectroscopy of 30TTE systems at temperatures from 50 °C to 180 °C.

D.2.2 Temperature dependent dielectric spectroscopy of neat and TTE modified anhydride cured systems

The temperature dependent data of the imaginary part of the complex permittivity of the neat anhydride cured epoxy resin systems are shown in Figures D.12, D.13 and D.13. While the data of the imaginary permittivity of the 30ATTE systems at comparable temperatures are Figures D.14, D.15 and D.16.

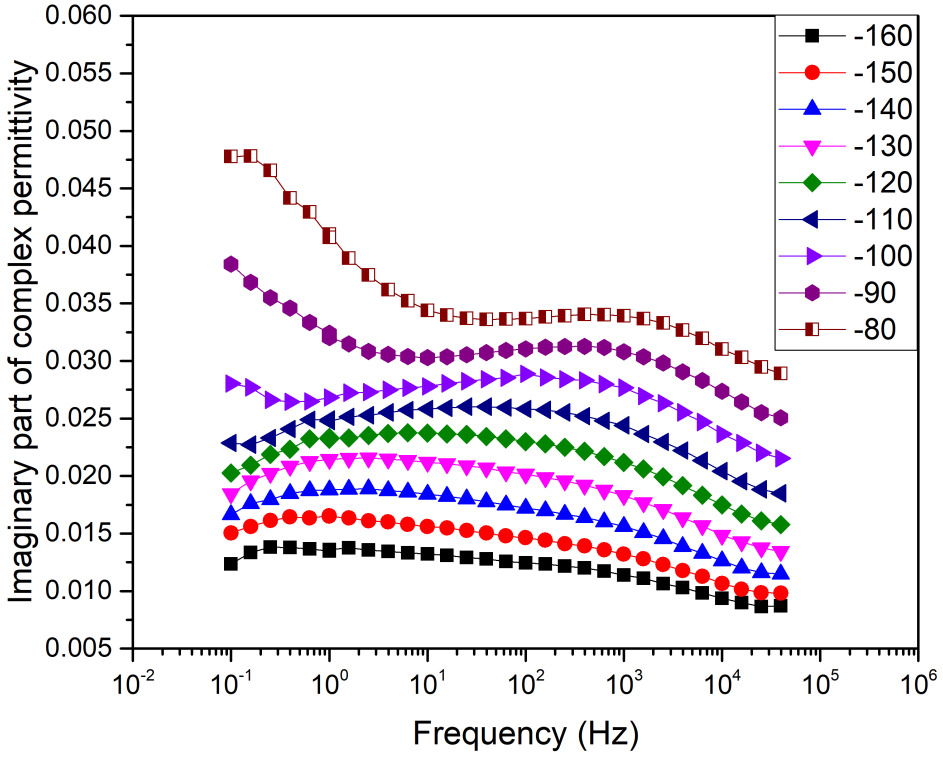

Figure D.12: Dielectric spectroscopy of neat anhydride cured epoxy resins at temperatures from -160 °C to -80 °C.

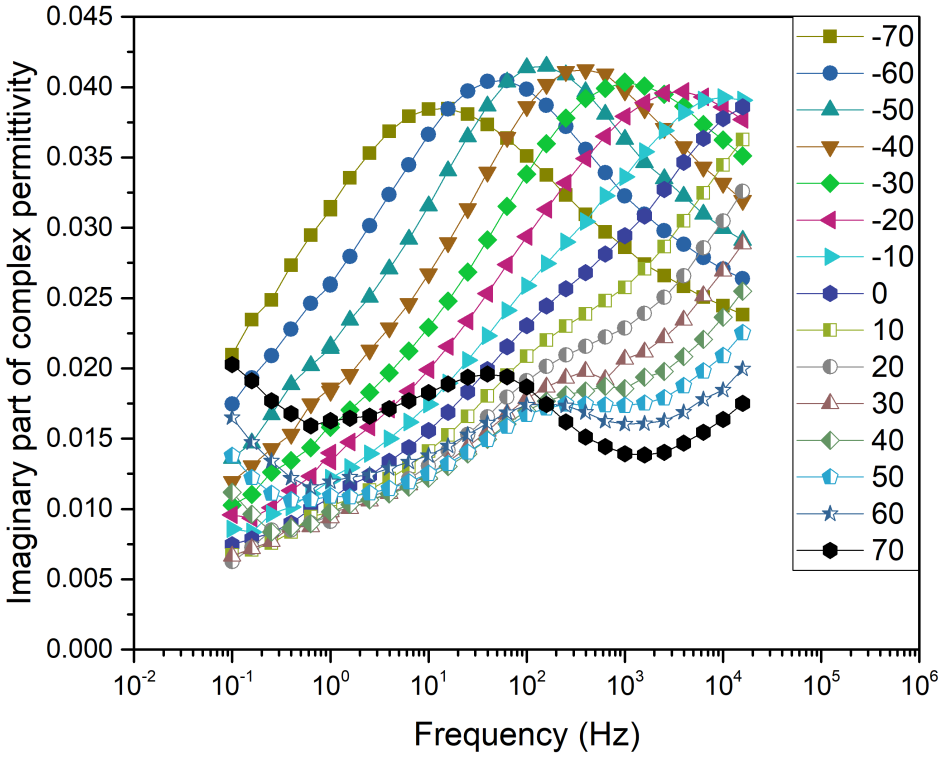

Figure D.13: Dielectric spectroscopy of neat anhydride cured epoxy resins at temperatures from -70 °C to 70 °C.

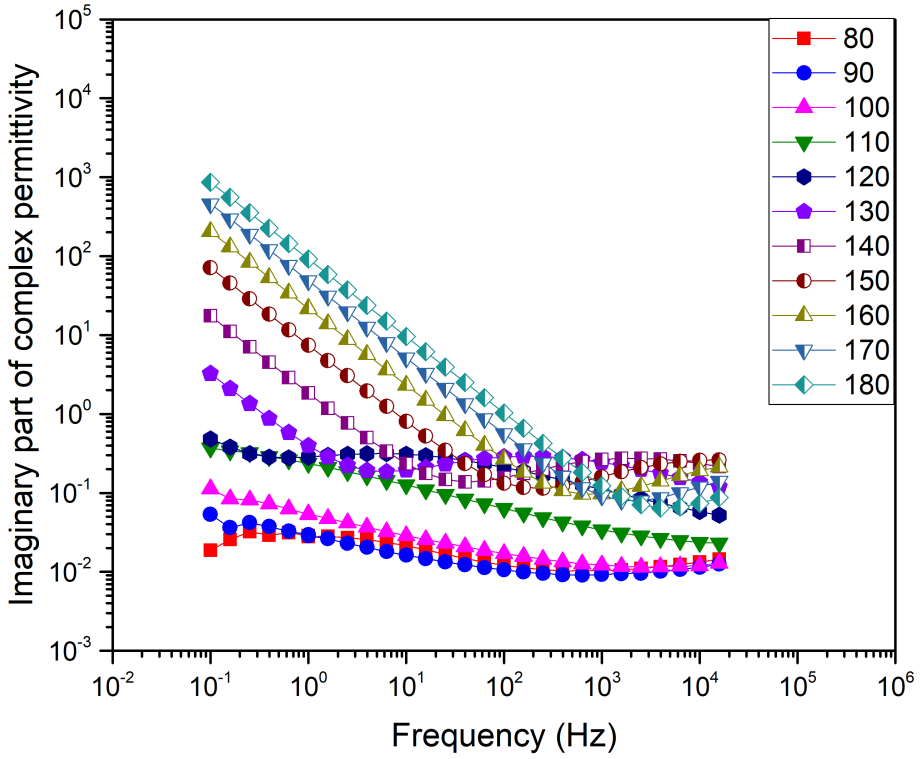

Figure D.14: Dielectric spectroscopy of neat anhydride cured epoxy resins at temperatures from 80 °C to 180 °C.

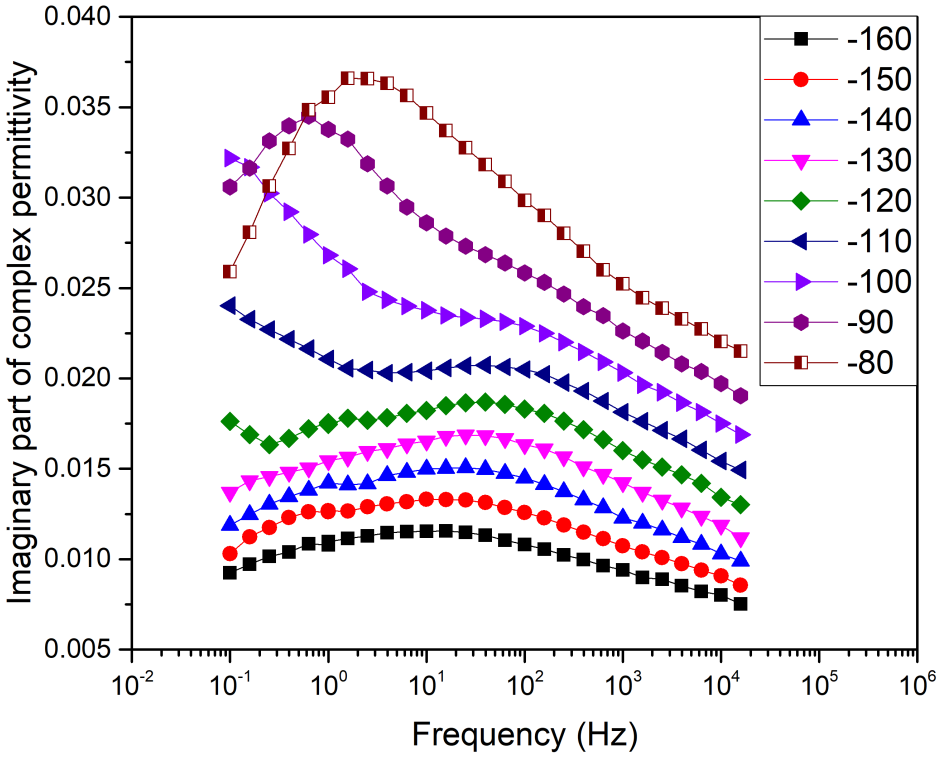

Figure D.15: Dielectric spectroscopy of 30ATTE at temperatures from -160 °C to -80 °C.

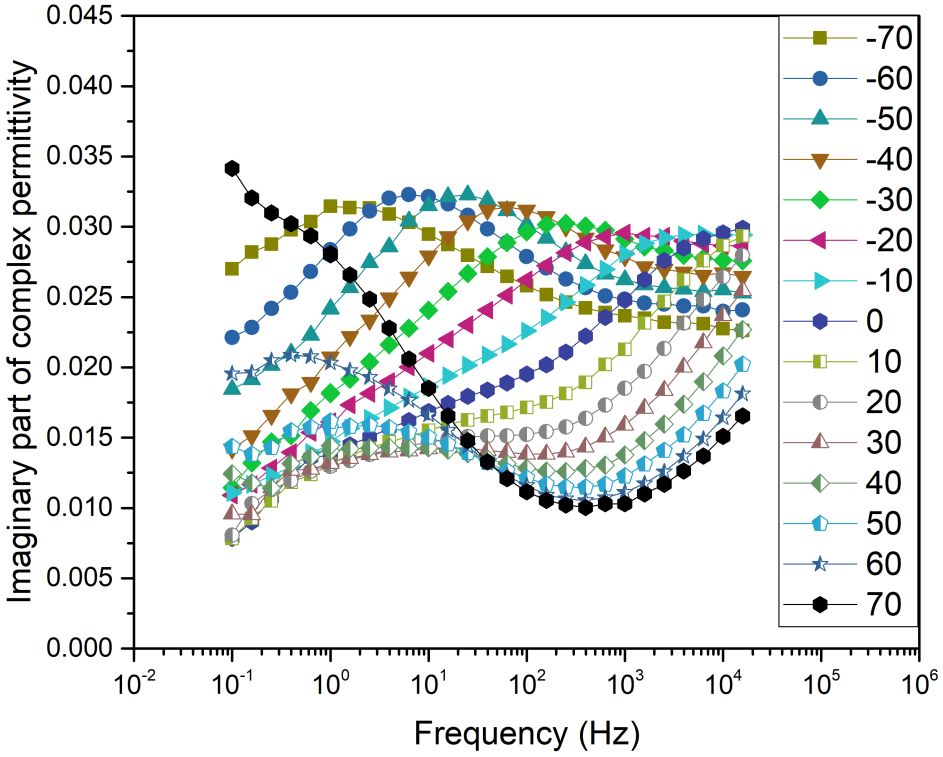

Figure D.16: Dielectric spectroscopy of 30ATTE at temperatures from -70 °C to 70 °C.

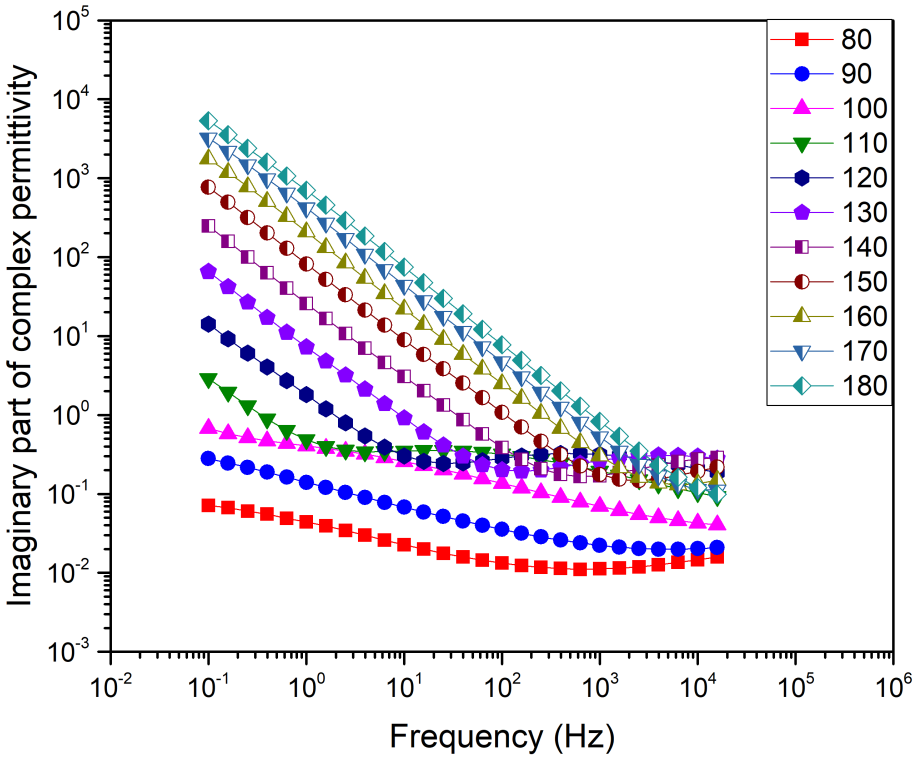

Figure D.17: Dielectric spectroscopy of 30ATTE at temperatures from 80 °C to 180 °C.

D.2.3 Room temperature dielectric spectroscopy of neat and TTE modified systems

The data of the real and imaginary part of the complex permittivity of the neat and samples modified by the inclusion 1%, 4%, 10% and 30% of the TTE modifier are illustrated in Figure D.18, D.19 respectively. While the comparable data acquired for the real and imaginary part of the complex permittivity of the neat and TTE modified anhydride cured systems are shown in Figure D.19, D.20 respectively.

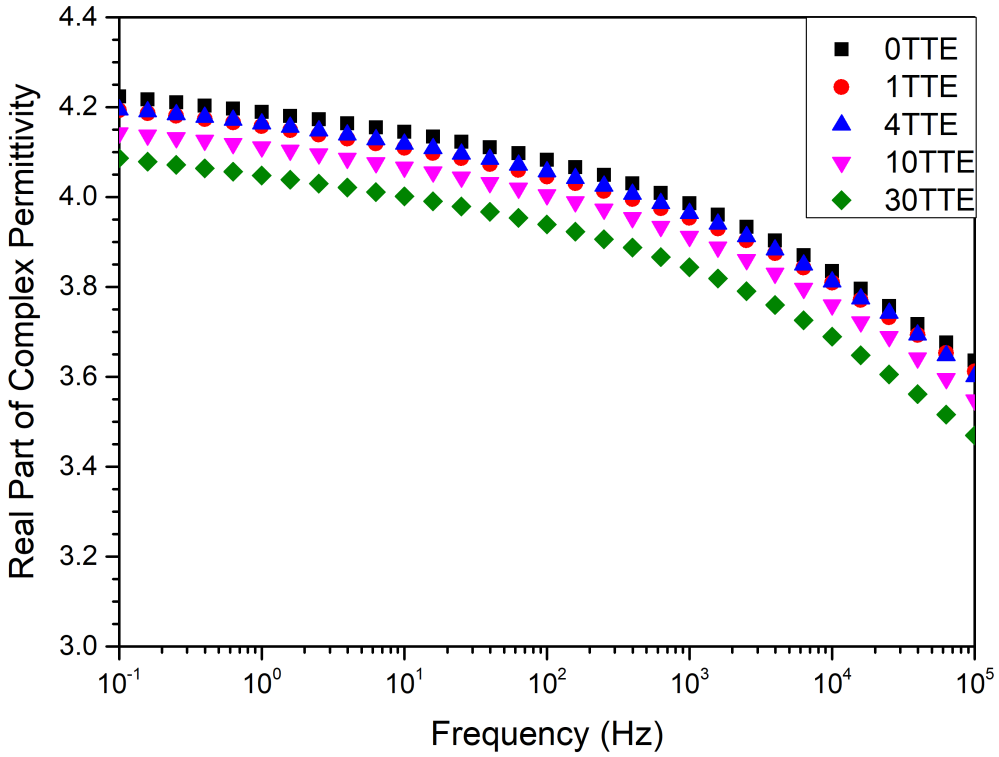

Figure D.18: Real part of complex permittivity for neat and TTE modified, amine cured, epoxy resin systems.

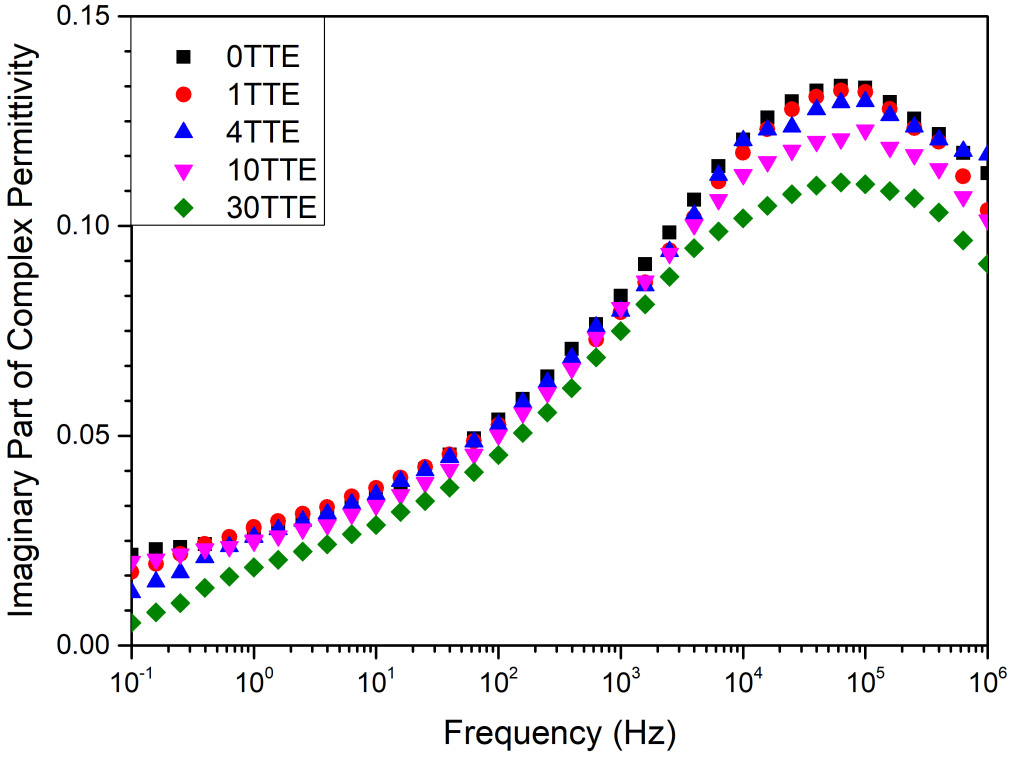

Figure D.19: Imaginary part of complex permittivity for neat and TTE modified, amine cured, epoxy resin systems.

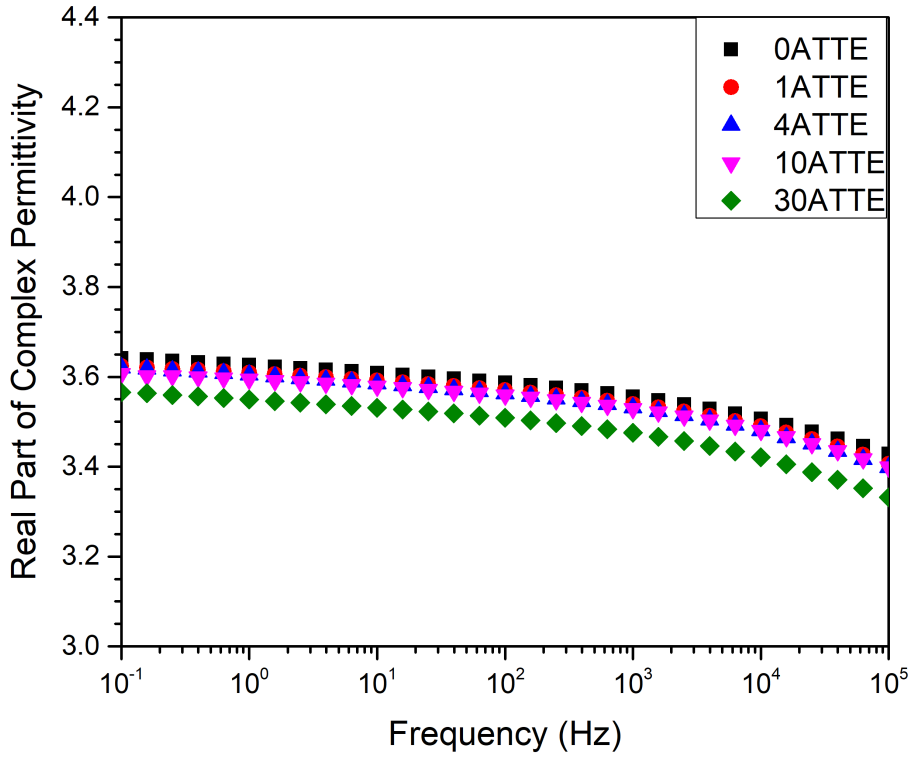

Figure D.20: Real part of complex permittivity for neat and TTE modified, anhydride cured, epoxy resin systems.

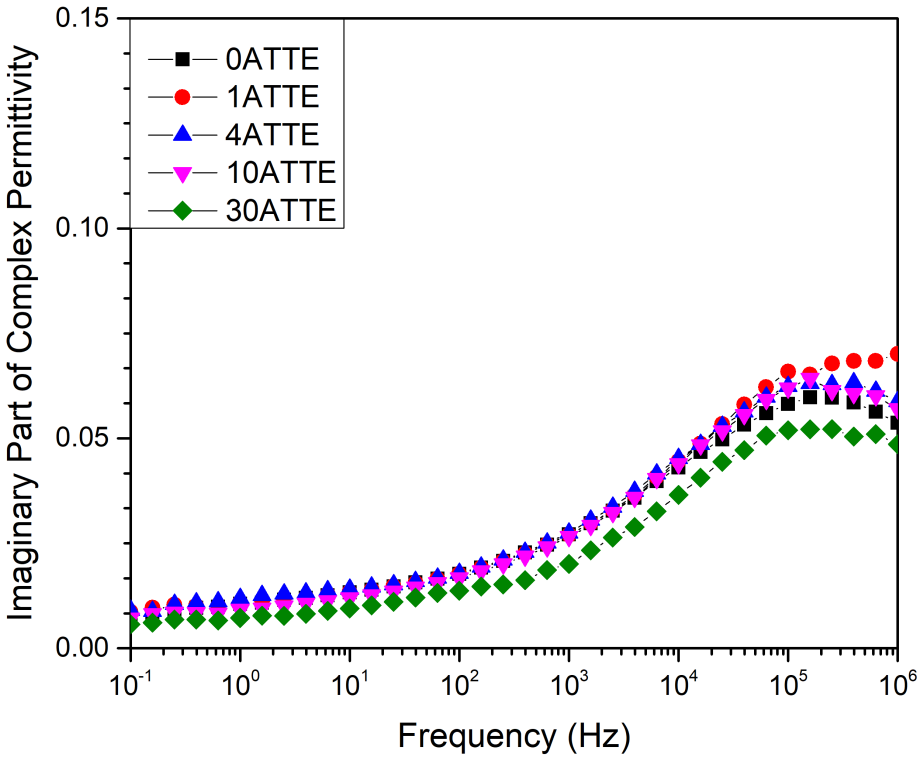

Figure D.21: Imaginary part of complex permittivity for neat and TTE modified, anhydride cured, epoxy resin systems.

Appendix E

Appendix E

The values of the first ten measurements of the electrical conductivity is used to calculate the initial conductivity, referred to as σ_i. The temperature dependent values of σ_i for the neat and modified systems are shown in Figure E.1. The figure illustrates the activation energy for each regime. The behaviour is similar to the one determined for the conductivity after 100 s (σ_{100} shown in Figure 8.3), where the activation energy E_a is low for systems in the glassy state which increase significantly when the material become in a rubbery state.

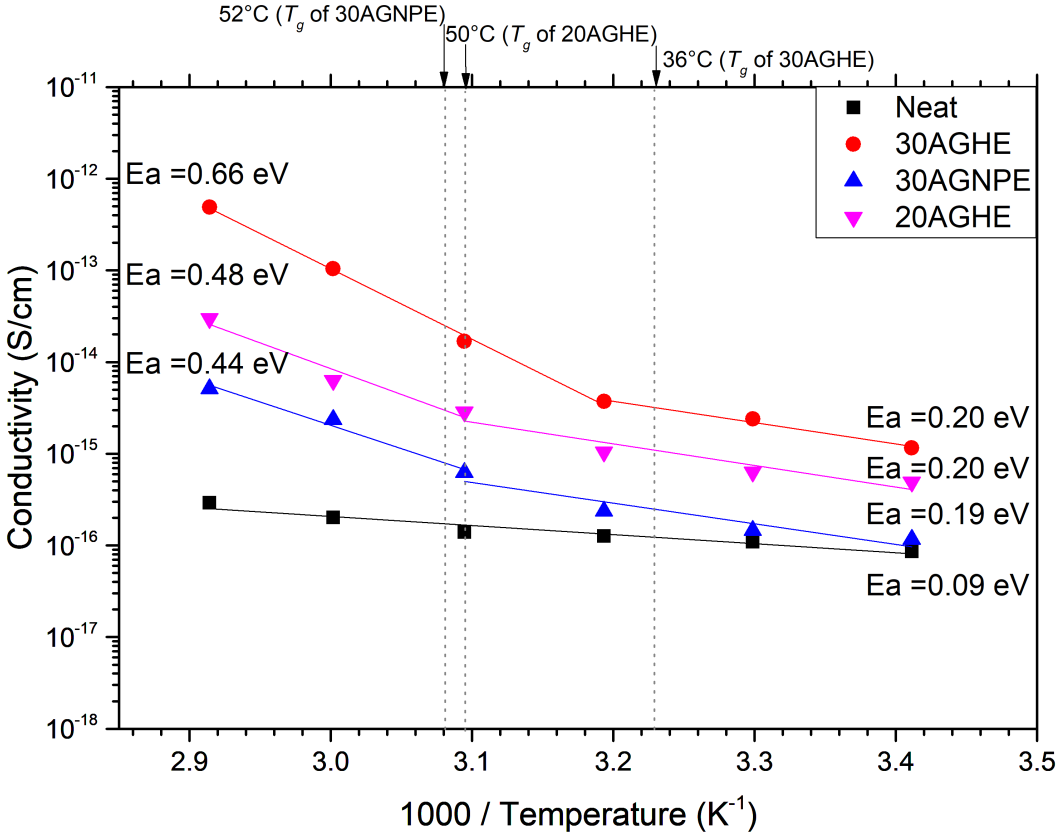

Figure E.1: Variation of the conductivity, as represented by the quantity σ_1, with time at an applied field of 5.5 kV mm^{-1} from 20 °C to 70 °C for the different material formulations.

In order to fit the data of the conductivity, the power law Equation 8.2, was used. To find the values of the parameters a and b of the fitting equation, initially, the values of both parameters were set as free regression parameters. The initial values of parameter

b are shown in Figure E.2. Later, these initial values were used to calculate the limits of parameter b through an iterative procedure, in which, an average value of parameter b was determined. The limits of parameter b are shown as the error bars in Figure E.2. It is important to note that changing the precise values of parameter b has an insignificant effect on parameter a, as was illustrated in Figure 8.4

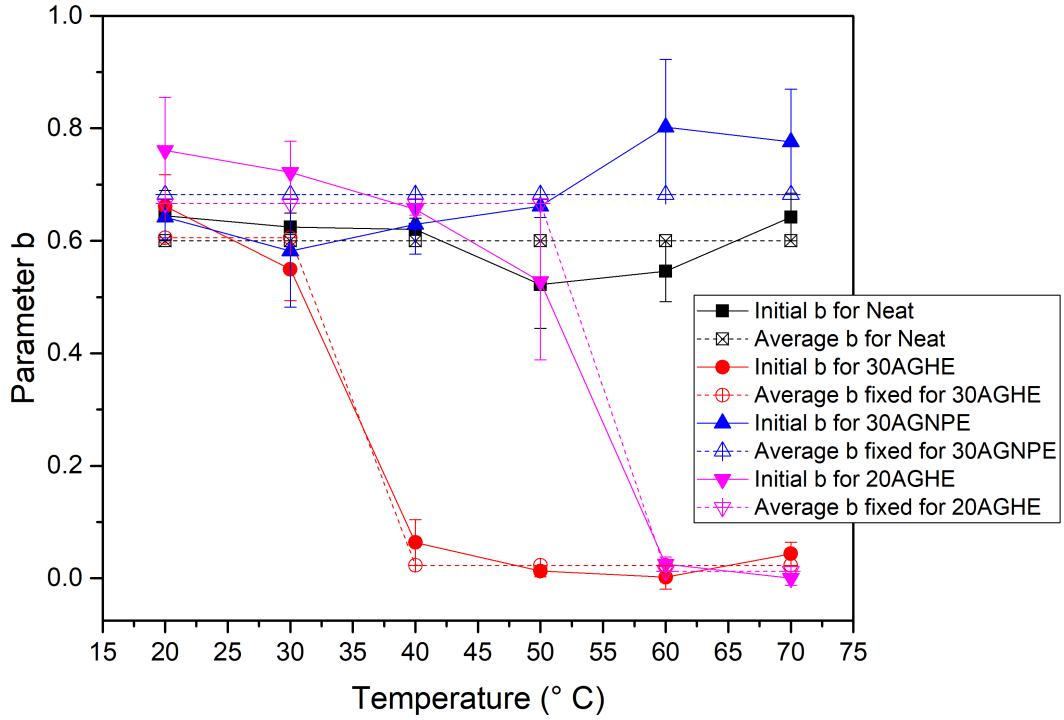

Figure E.2: Sensitivity of parameter b

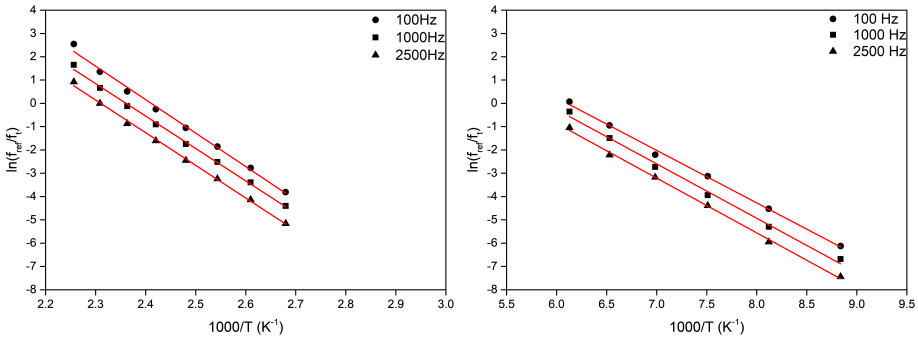

(a) Process 1 (b) Process 4

Figure E.14: Process 1 and 4 for 30AGHE

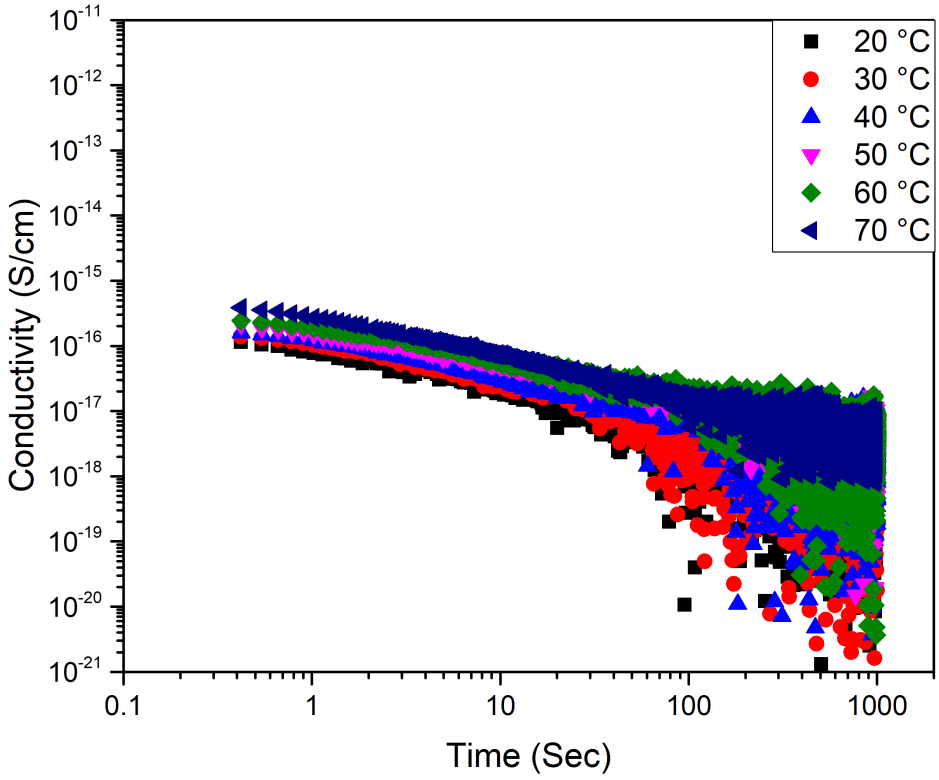

(a) Neat Epoxy

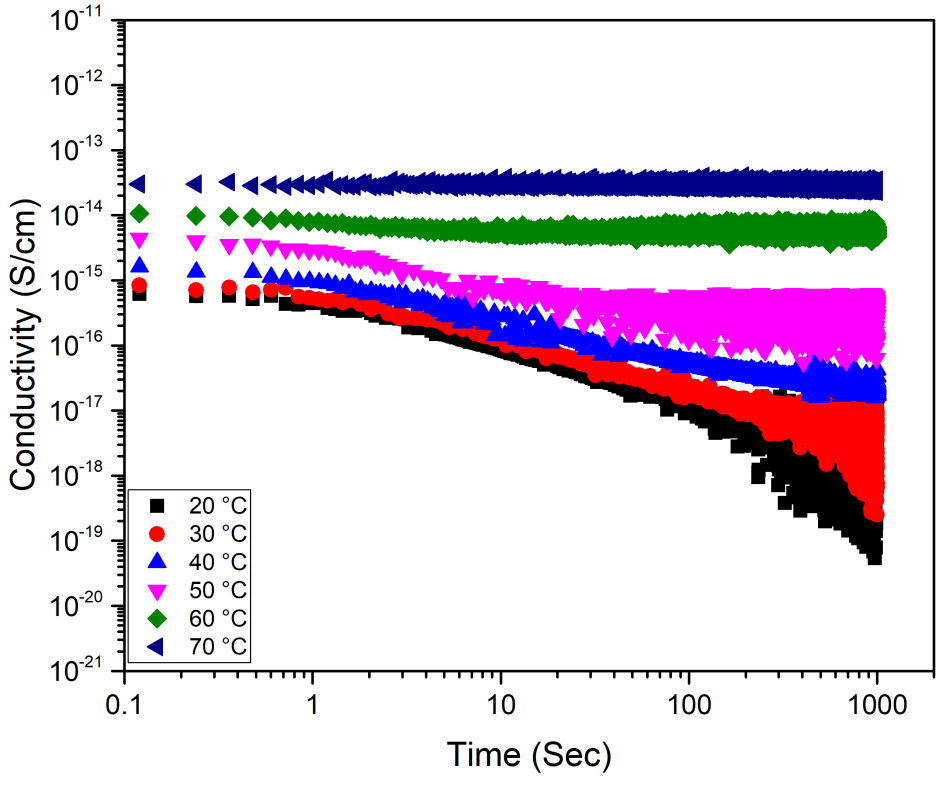

(b) 20AGHE

Figure E.3: Plots of the electrical conductivity measurements conducted for time up to 1000 s.

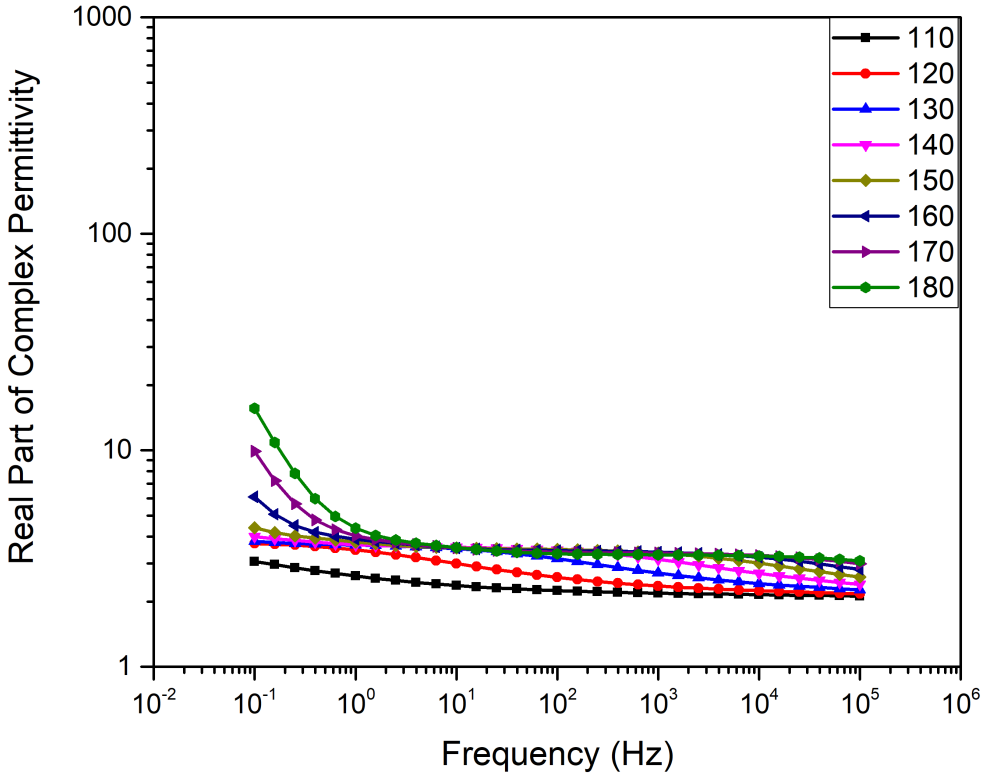

(a) Neat Epoxy

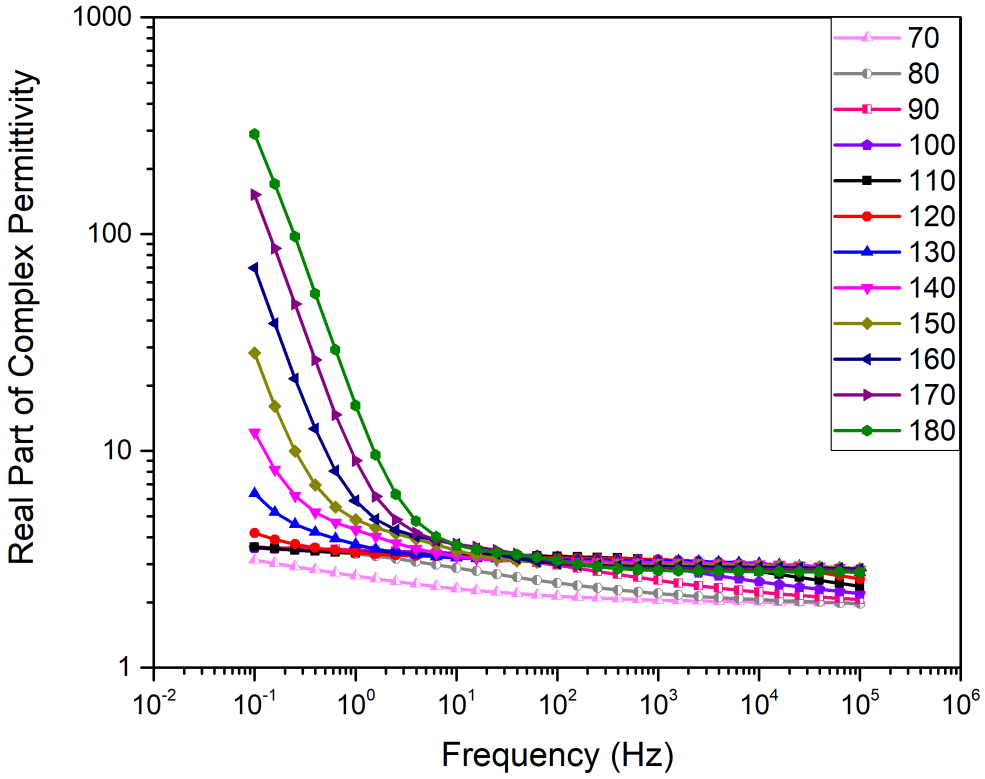

(b) 30AGNPE

Figure E.4: Plots of the real part of the dielectric permittivity against the frequency as a function of temperatures associate with Process 1 for (a) Neat epoxy and (b) 30AGHE modified systems. The legend represents the temperature in °C.

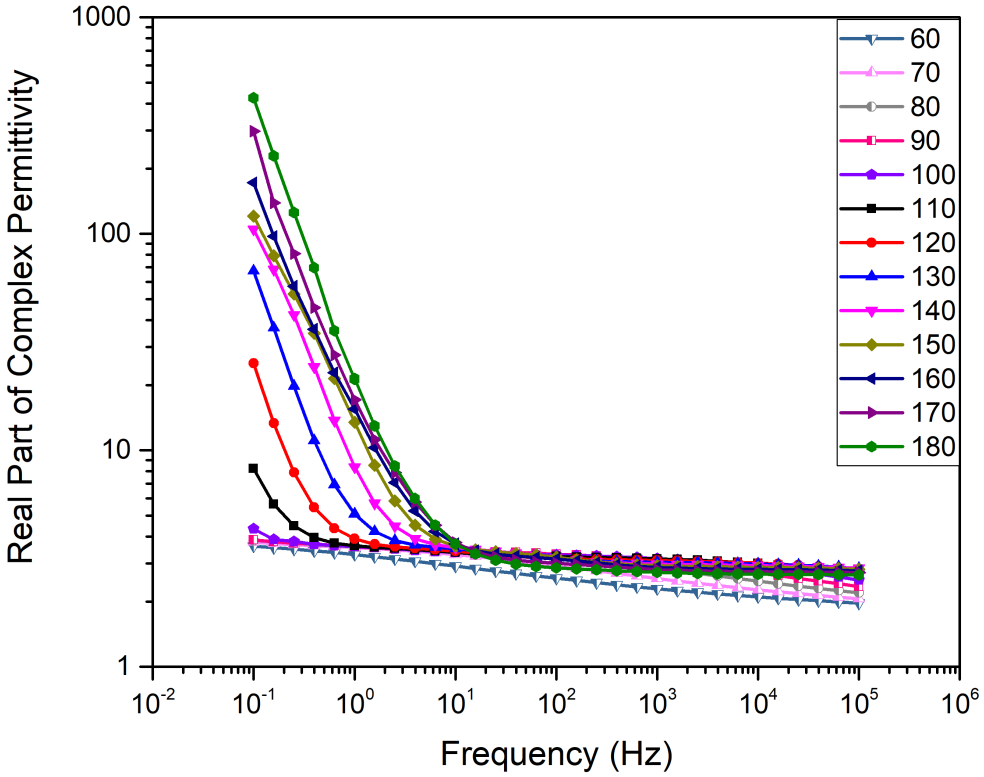

(a) 30AGHE

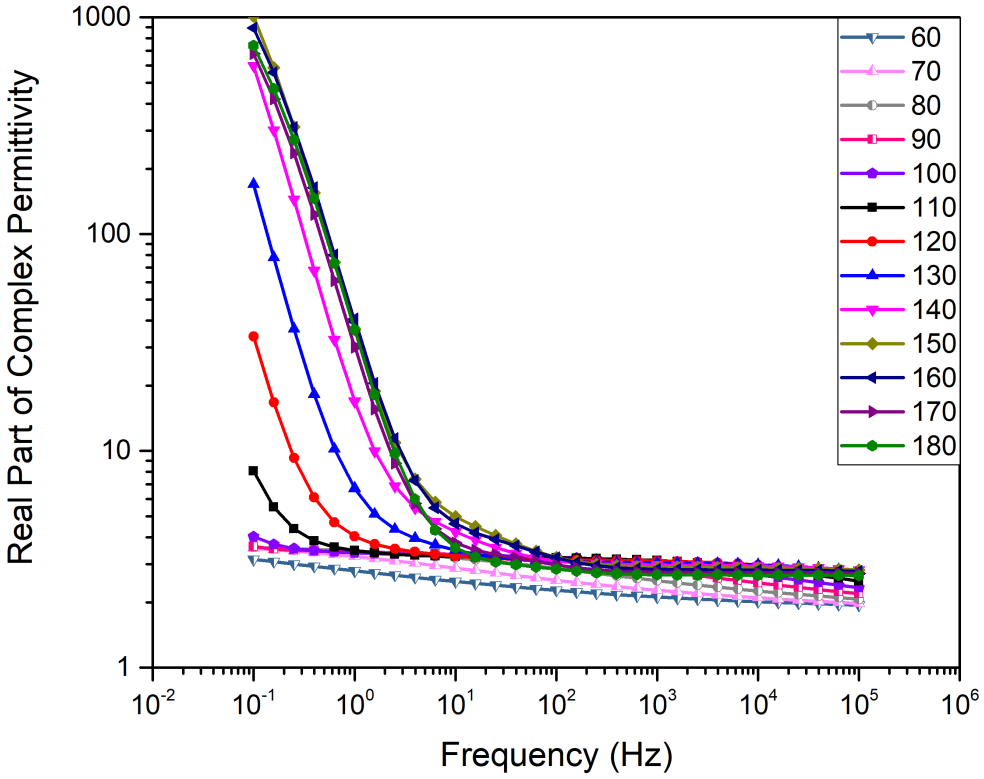

(b) 20AGHE

Figure E.5: Plots of the real part of the dielectric permittivity against the frequency as a function of temperatures associate with Process 1 for (a) 30AGHE and (b) 20AGHE modified systems. The legend represents the temperature in °C.

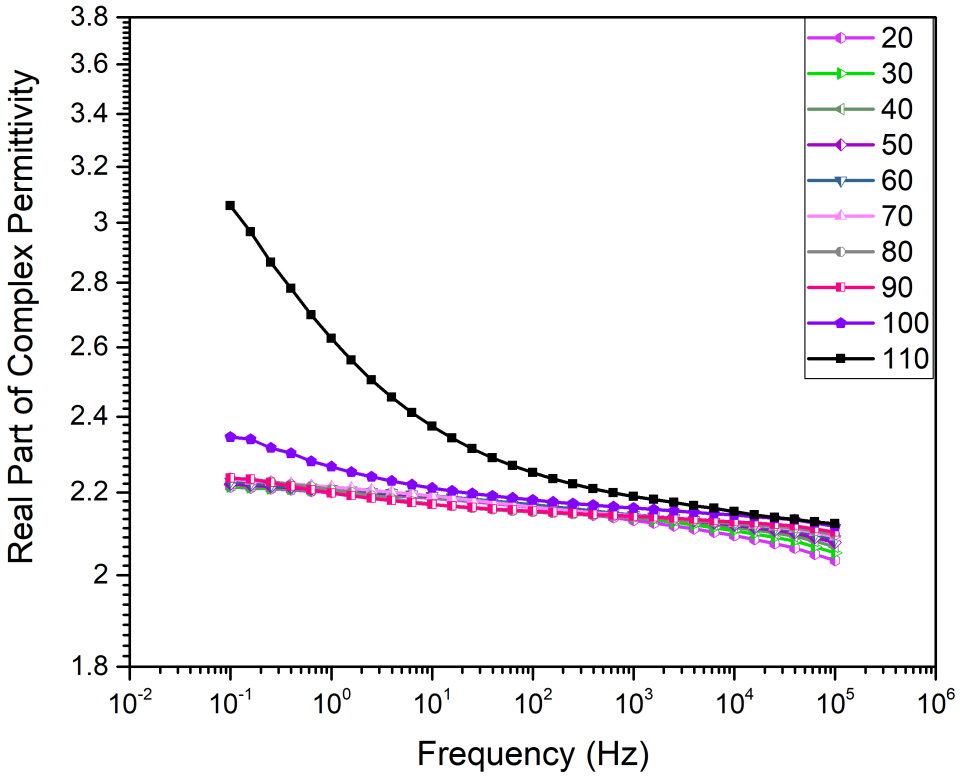

(a) Neat Epoxy

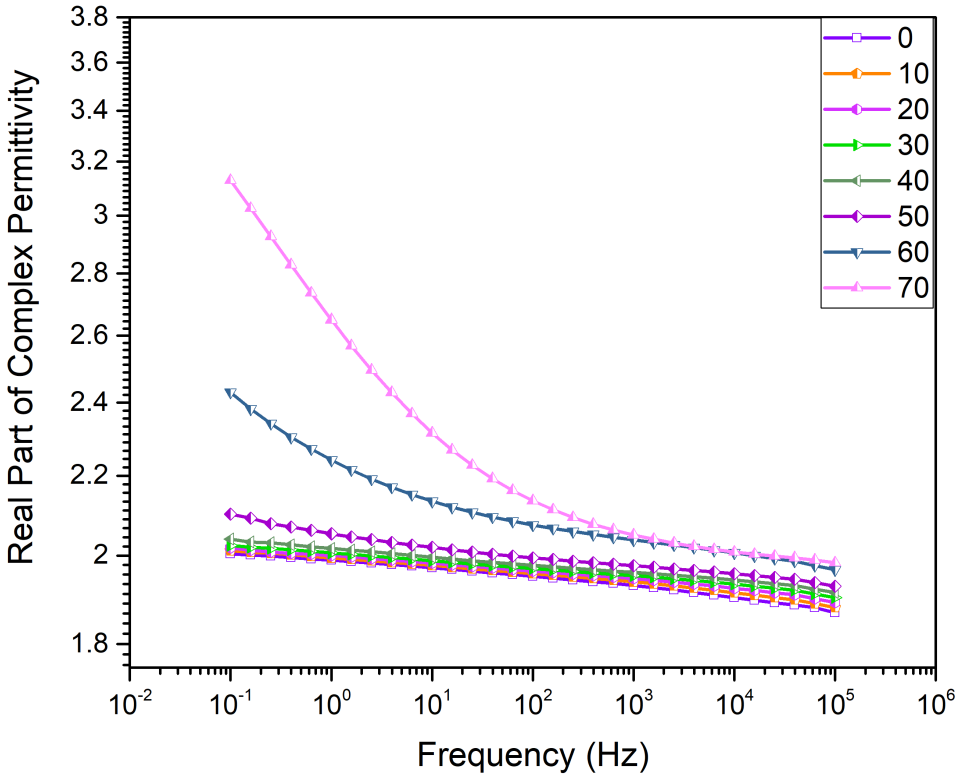

(b) 30AGNPE

Figure E.6: Plots of the real part of the dielectric permittivity against the frequency as a function of temperatures associate with Process 2 for (a) Neat epoxy and (b) 30AGHE modified systems. The legend represents the temperature in °C.

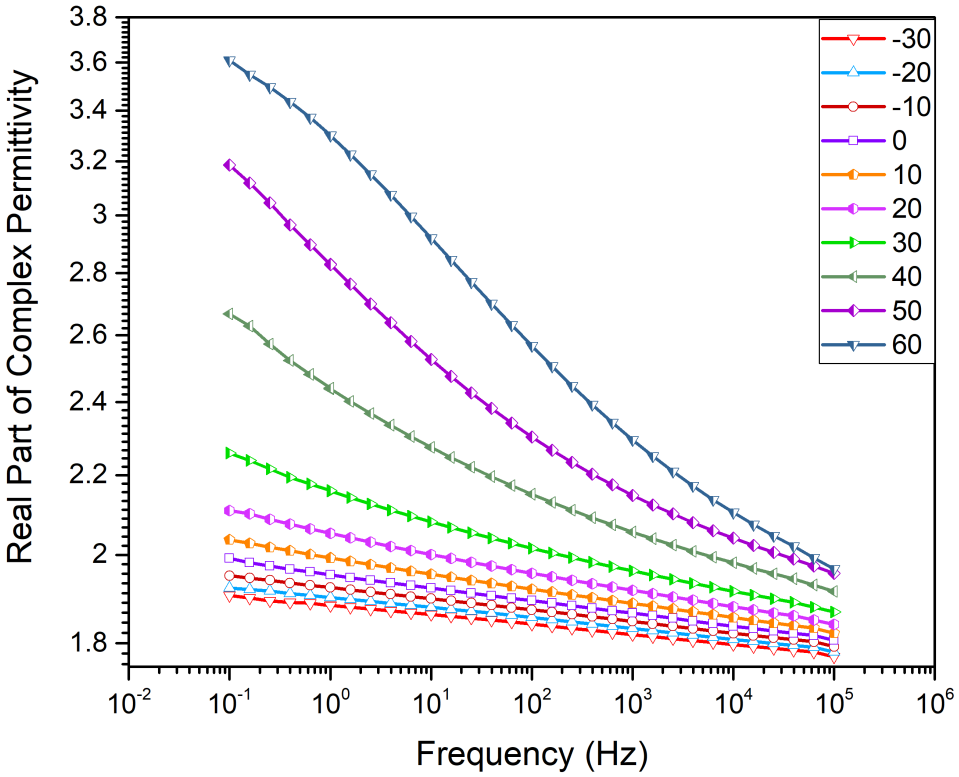

(a) 30AGHE

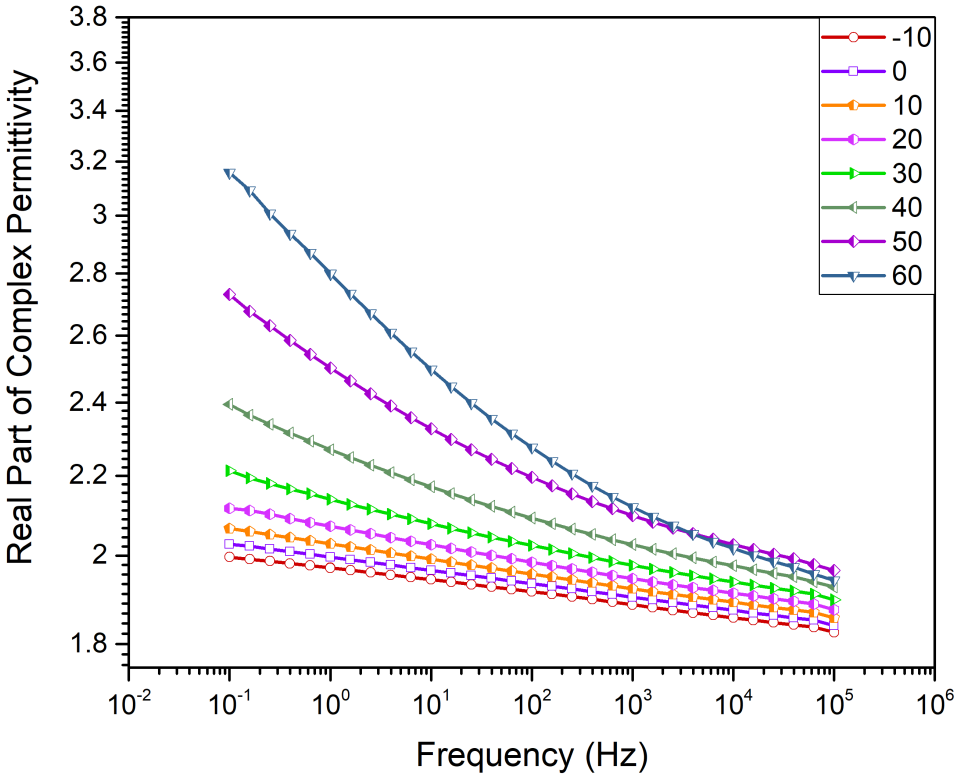

(b) 20AGHE

Figure E.7: Plots of the real part of the dielectric permittivity against the frequency as a function of temperatures associate with Process 2 for (a) 30AGHE and (b) 20AGHE modified systems. The legend represents the temperature in °C.

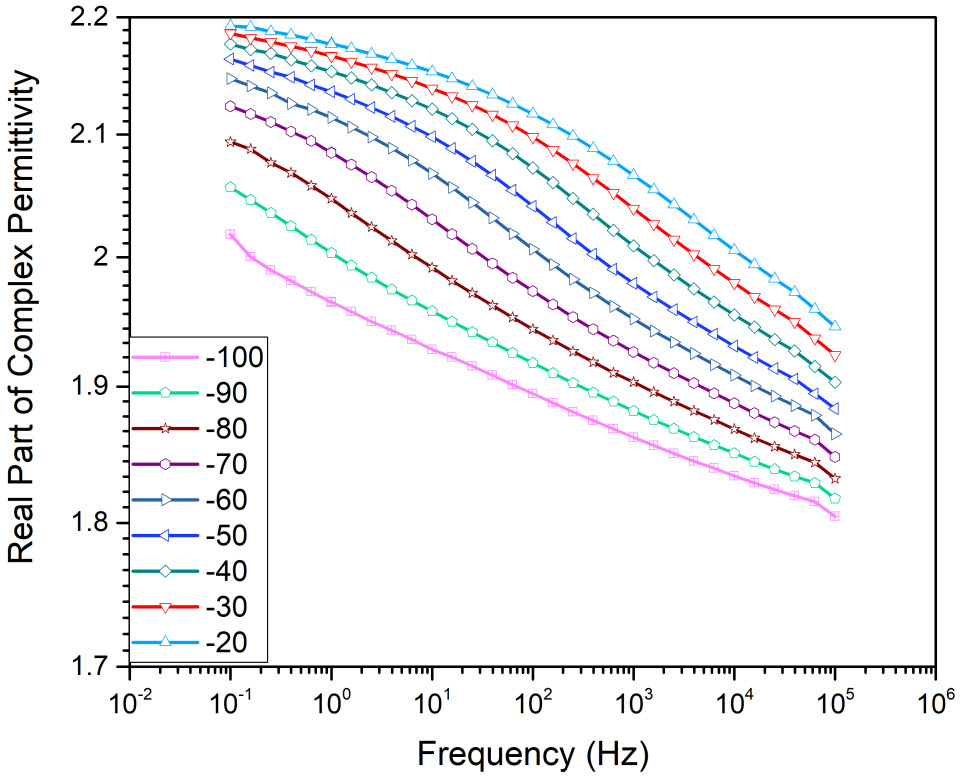

(a) Neat Epoxy

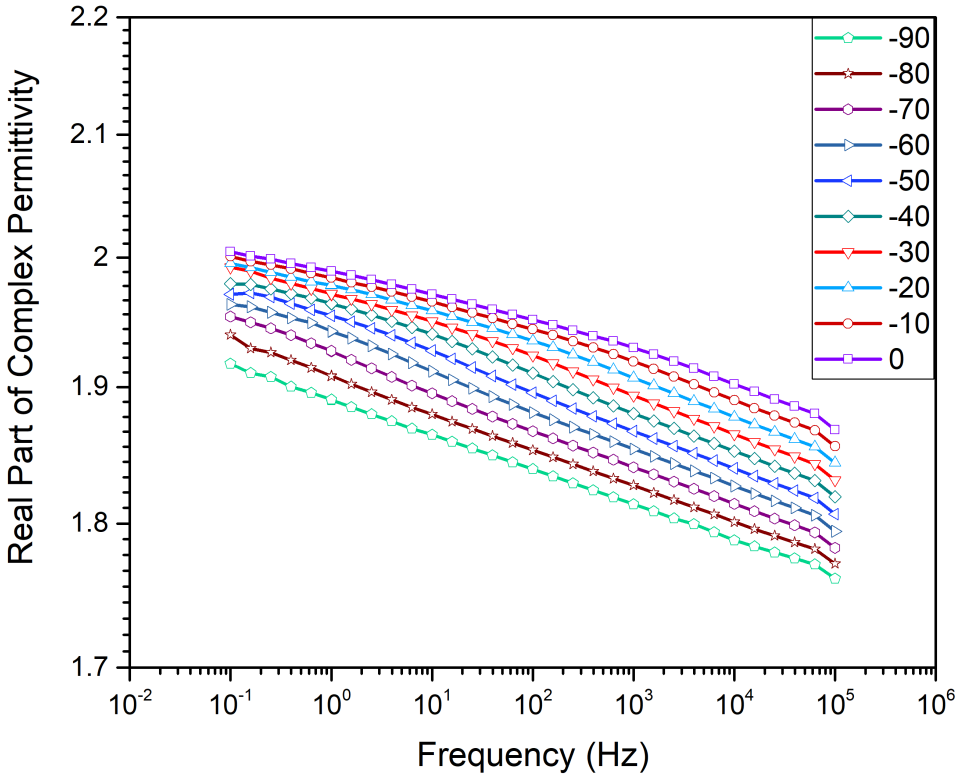

(b) 30AGNPE

Figure E.8: Plots of the real part of the dielectric permittivity against the frequency as a function of temperatures associate with Process 3 for (a) Neat epoxy and (b) 30AGHE modified systems. The legend represents the temperature in °C.

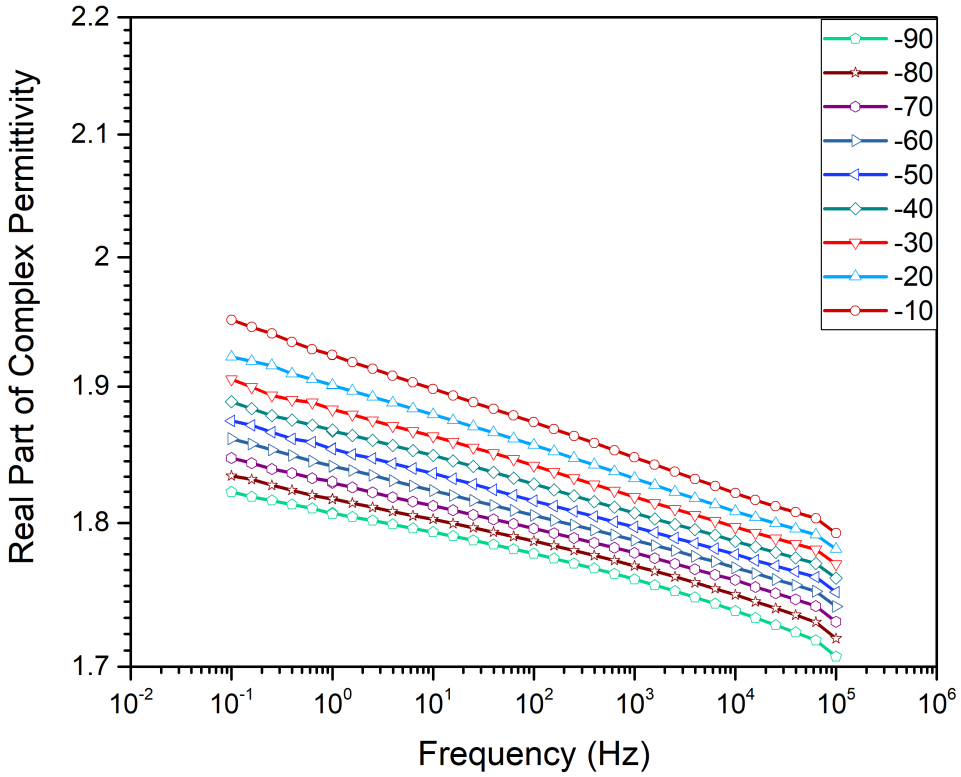

(a) 30AGHE

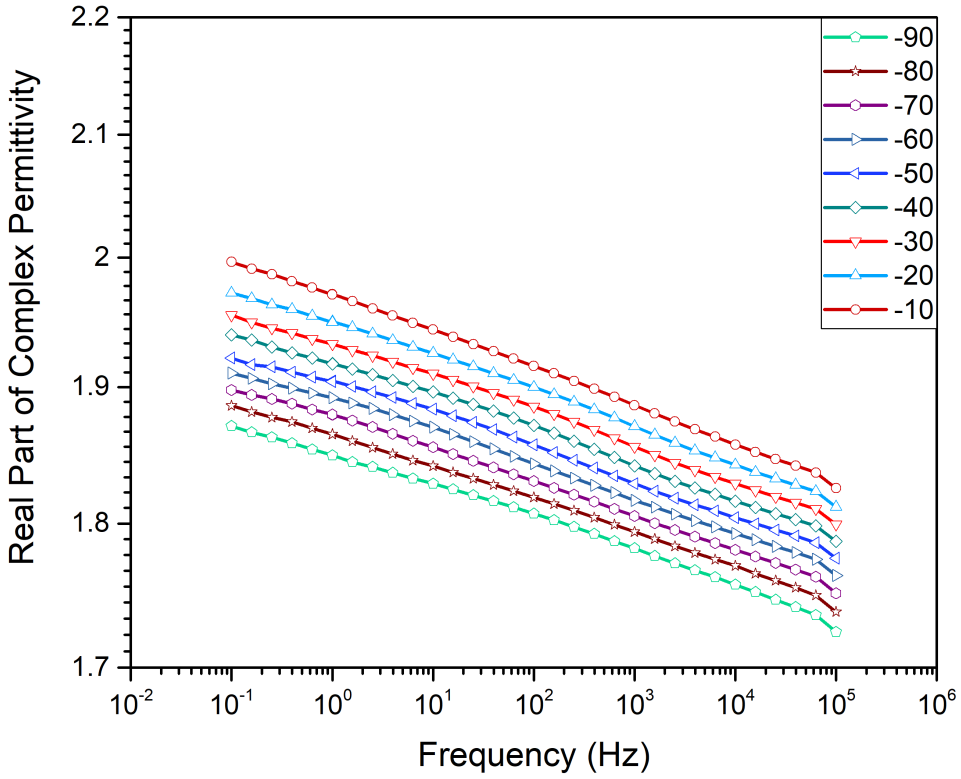

(b) 20AGHE

Figure E.9: Plots of the real part of the dielectric permittivity against the frequency as a function of temperatures associate with Process 3 for (a) 30AGHE and (b) 20AGHE modified systems. The legend represents the temperature in °C.

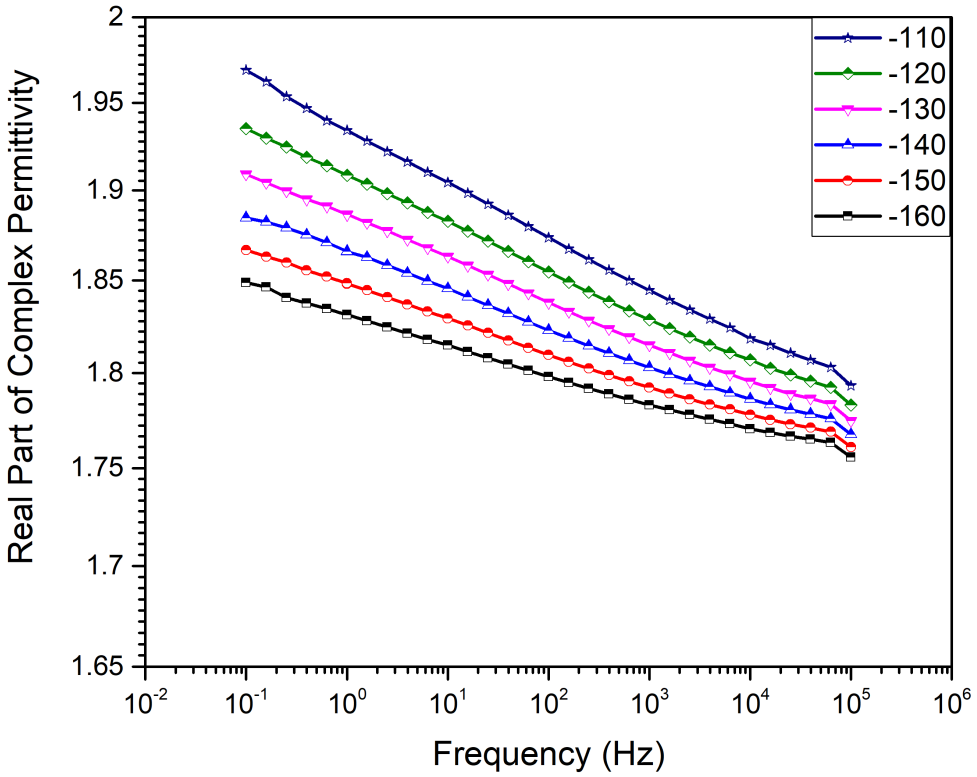

(a) Neat Epoxy

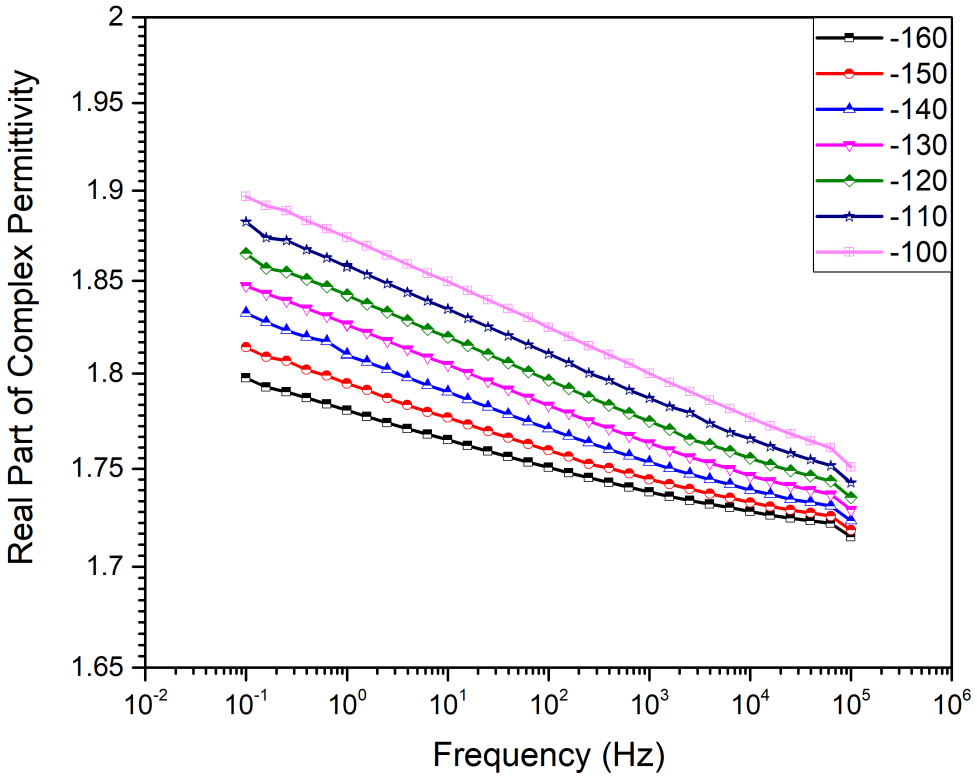

(b) 30AGNPE

Figure E.10: Plots of the real part of the dielectric permittivity against the frequency as a function of temperatures associate with Process 4 for (a) Neat epoxy and (b) 30AGHE modified systems. The legend represents the temperature in °C.

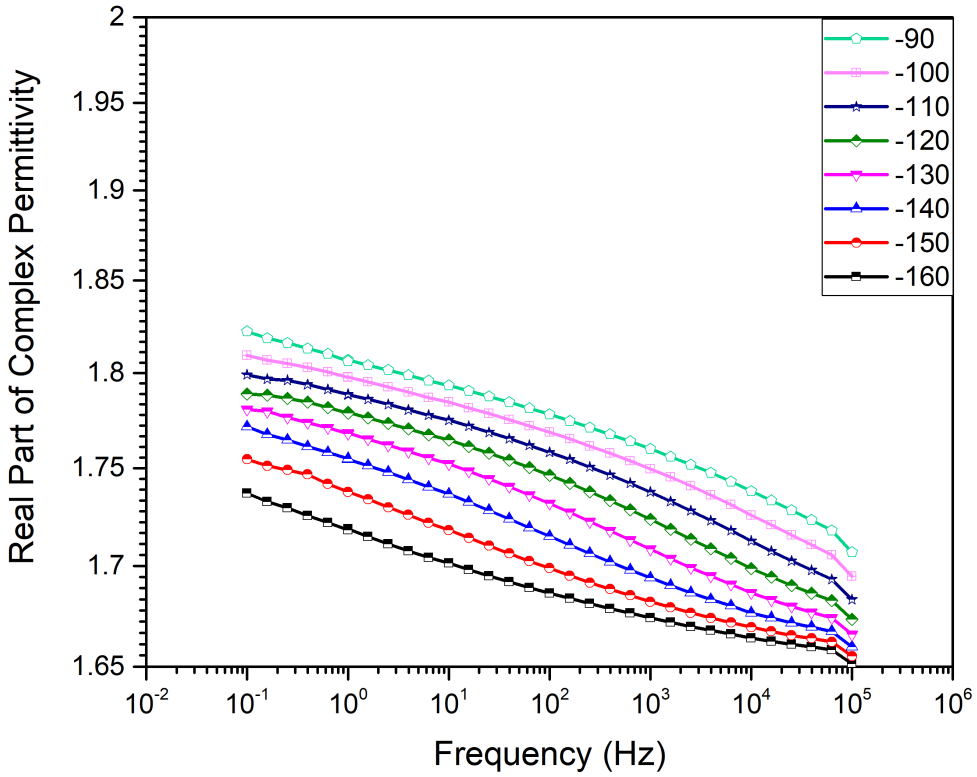

(a) 30AGHE

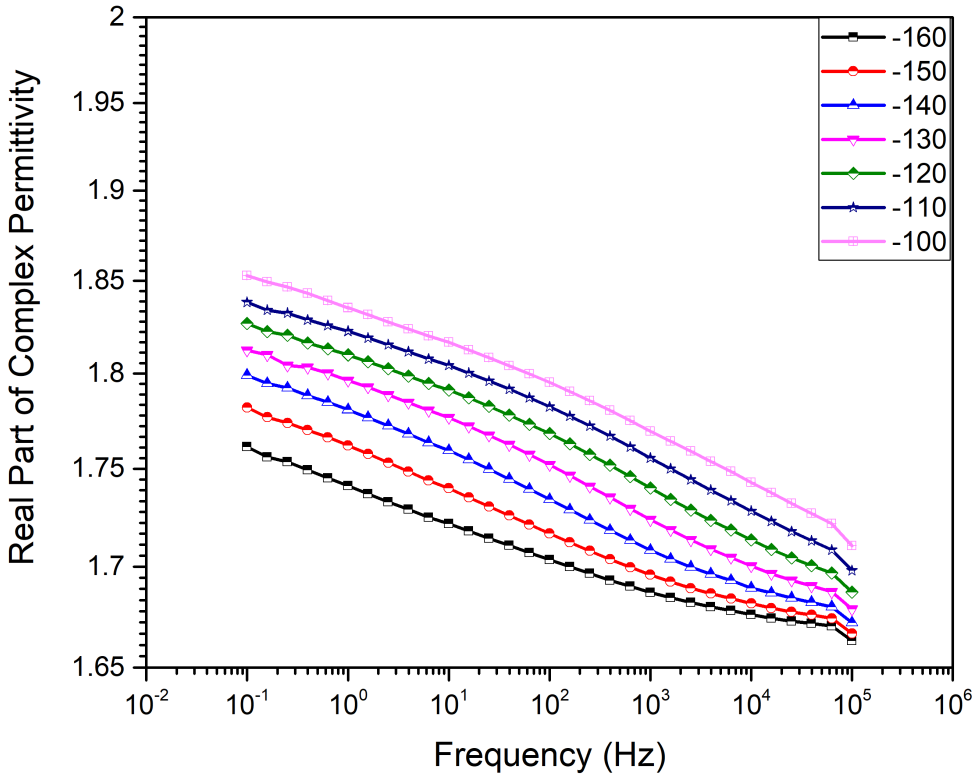

(b) 20AGHE

Figure E.11: Plots of the real part of the dielectric permittivity against the frequency as a function of temperatures associate with Process 4 for (a) 30AGHE and (b) 20AGHE modified systems. The legend represents the temperature in °C.

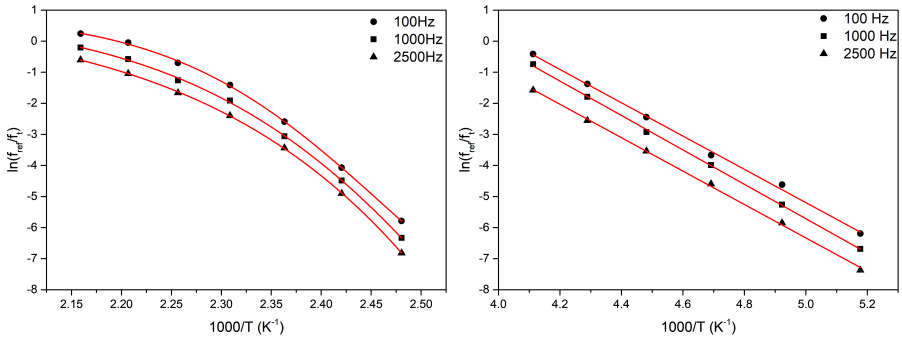

(a) Process 1

(b) Process 3

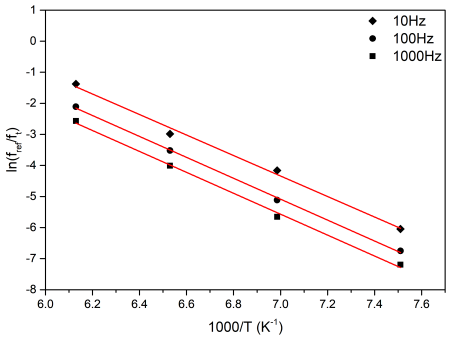

(c) Process 4

Figure E.12: Process 1,3 and 4 for neat epoxy

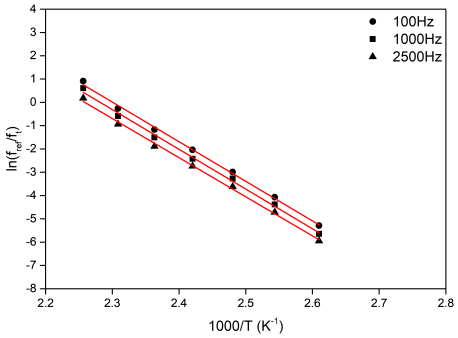

(a) Process 1

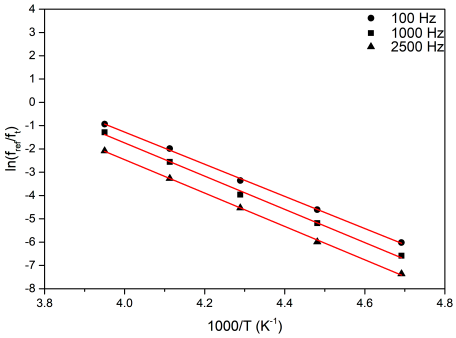

(b) Process 3

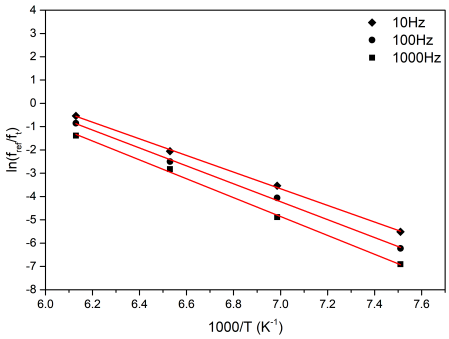

(c) Process 4

Figure E.13: Process 1,3 and 4 for 30AGNPE

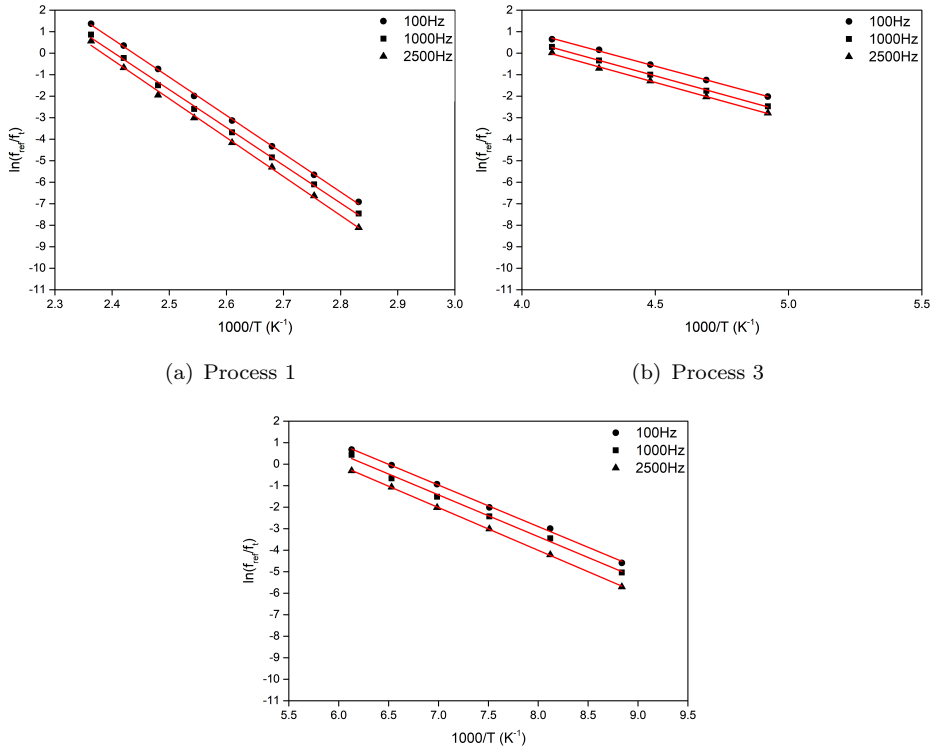

(a) Process 1

(b) Process 3

(c) Process 4

Figure E.15: Process 1,3 and 4 for 20AGHE

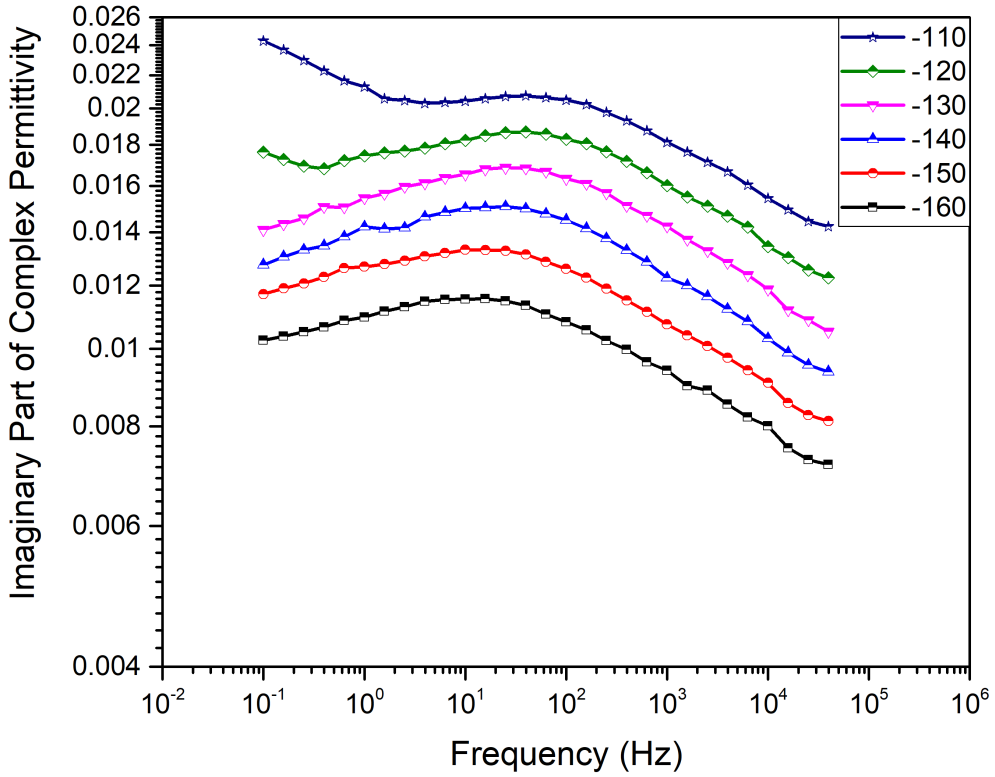

(a) Neat Epoxy

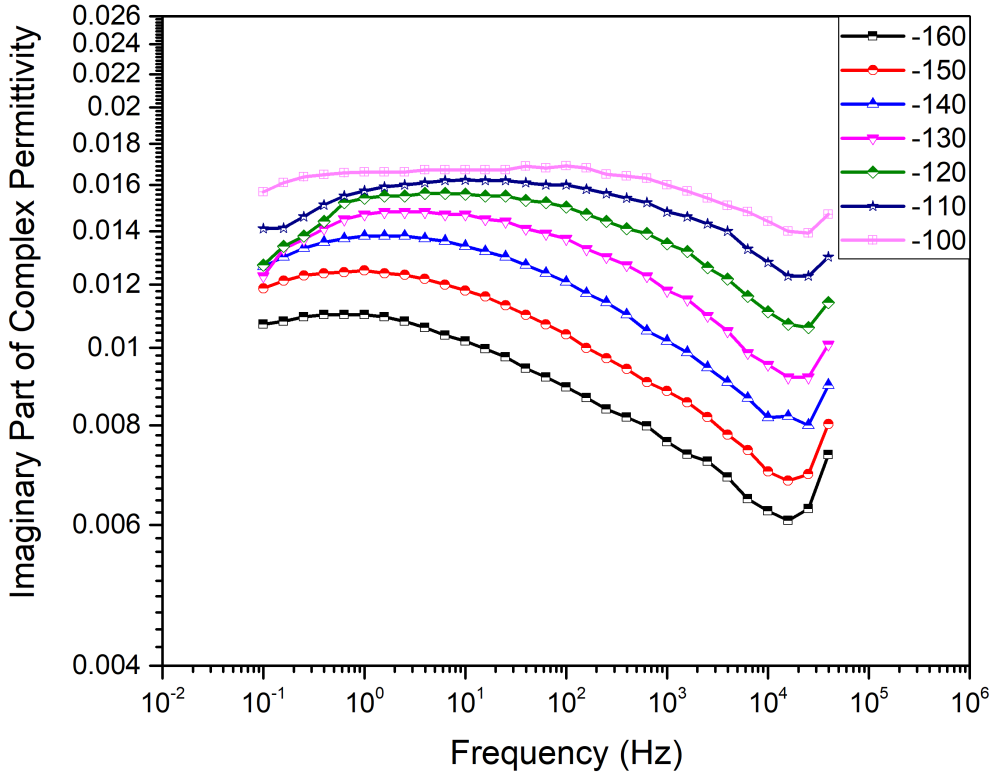

(b) 30AGNPE

Figure E.16: Plots of the imaginary part of the dielectric permittivity against the frequency as a function of temperatures associate with Process 4 for (a) Neat epoxy and (b) 30AGHE modified systems. The legend represents the temperature in °C.

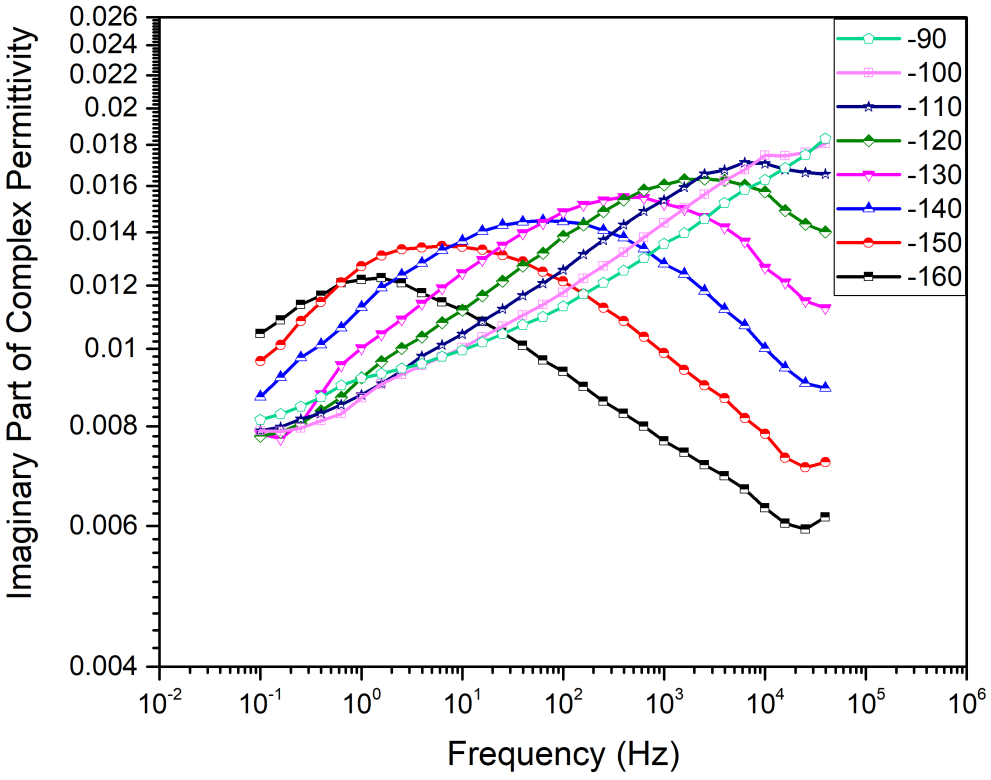

(a) 30AGHE

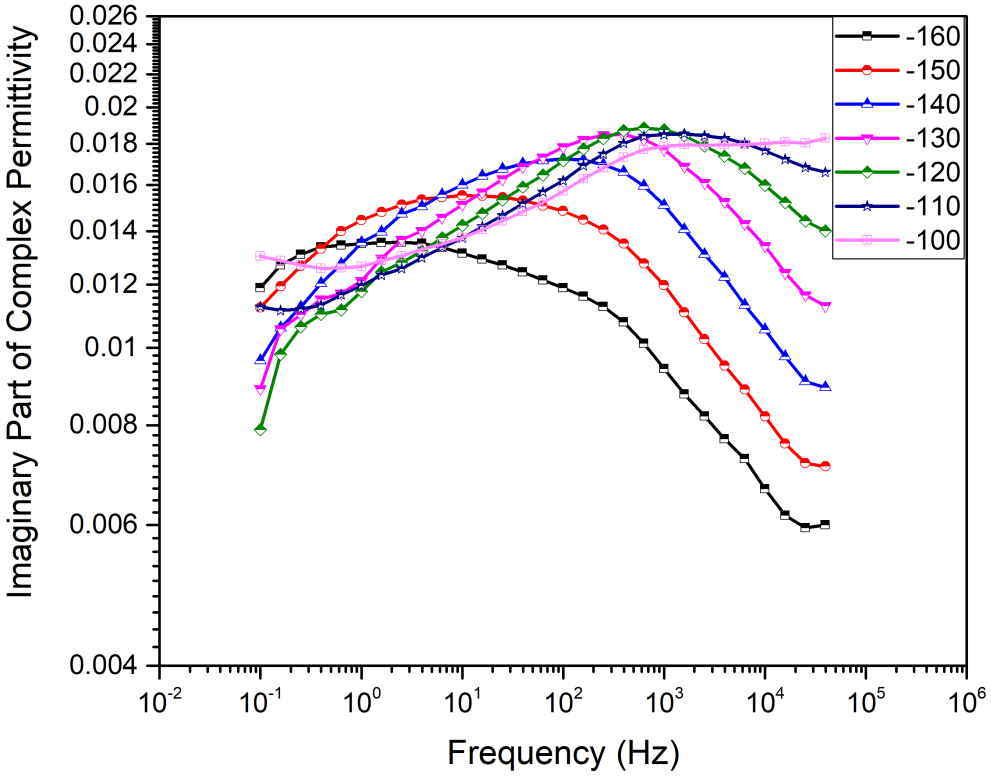

(b) 20AGHE

Figure E.17: Plots of the imaginary part of the dielectric permittivity against the frequency as a function of temperatures associate with Process 4 for (a) 30AGHE and (b) 20AGHE modified systems. The legend represents the temperature in °C.

E.1 Havriliak-Negami relaxation fit function

The Havriliak-Negami fit function is often used to describe the data of the dielectric spectroscopy. The fit equation is a modified version of the Debye, Cole Cole and Cole Davidson functions. The Havriliak-Negami fit equation is shown below [234].

$$\varepsilon(w) = \varepsilon' - \varepsilon'' = -i\left(\frac{\sigma_0}{\varepsilon_0 w}\right)^N + \sum_{k=1}^{\infty}\left[\frac{\Delta\varepsilon_k}{(1+(iw\tau_k)^{\alpha_k})^{\beta_k}} + \varepsilon_{\infty,k}\right]$$

where w is the angular frequency, τ is the characteristic relaxation time, α is the asymmetry, β the broadness of the spectra and ε_0 is the vacuum permittivity. When the exponential parameters α and β reaches unity, the Havriliak-Negami fit is reduces to Debye function, while setting $\beta = 1$ results in Cole-Cole configuration. Finally, the Cole-Davidson function is achieved at $\alpha = 1$. Figure E.18 shows the typical representation of the data used in Havriliak-Negami fit, which is used to represent the data in this study. The next sections will present the temperature dependent Havriliak-Negami fit function for the neat, GNPE and GHE modified systems.

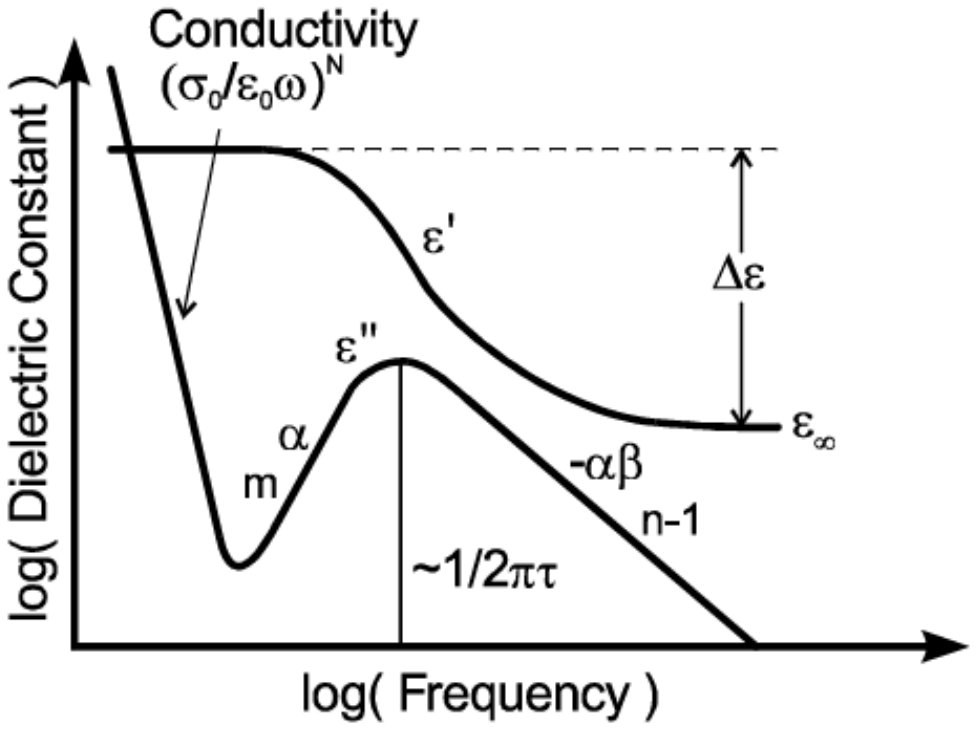

Figure E.18: Representation of the data used in Havriliak-Negami relaxation fit function.

E.2 Havriliak-Negami relaxation fit for the neat epoxy resin system

The dielectric data of the neat epoxy resin system for temperatures from -160 °C to 40 °C was analysed using Havriliak-Negami fit function. The outcome of the analysis is plotted in the figures below from Figure fig. E.21 to fig. E.41. The parameters used in the Havriliak-Negami fit function are listed in Table E.1. To compare the de-convoluted peaks at different temperature, the peaks associated with the β- relaxation, the γ-relaxation, pre-alpha process and the secondary relaxation are plotted in separate figures (Figure E.19 and Figure E.20 respectively.

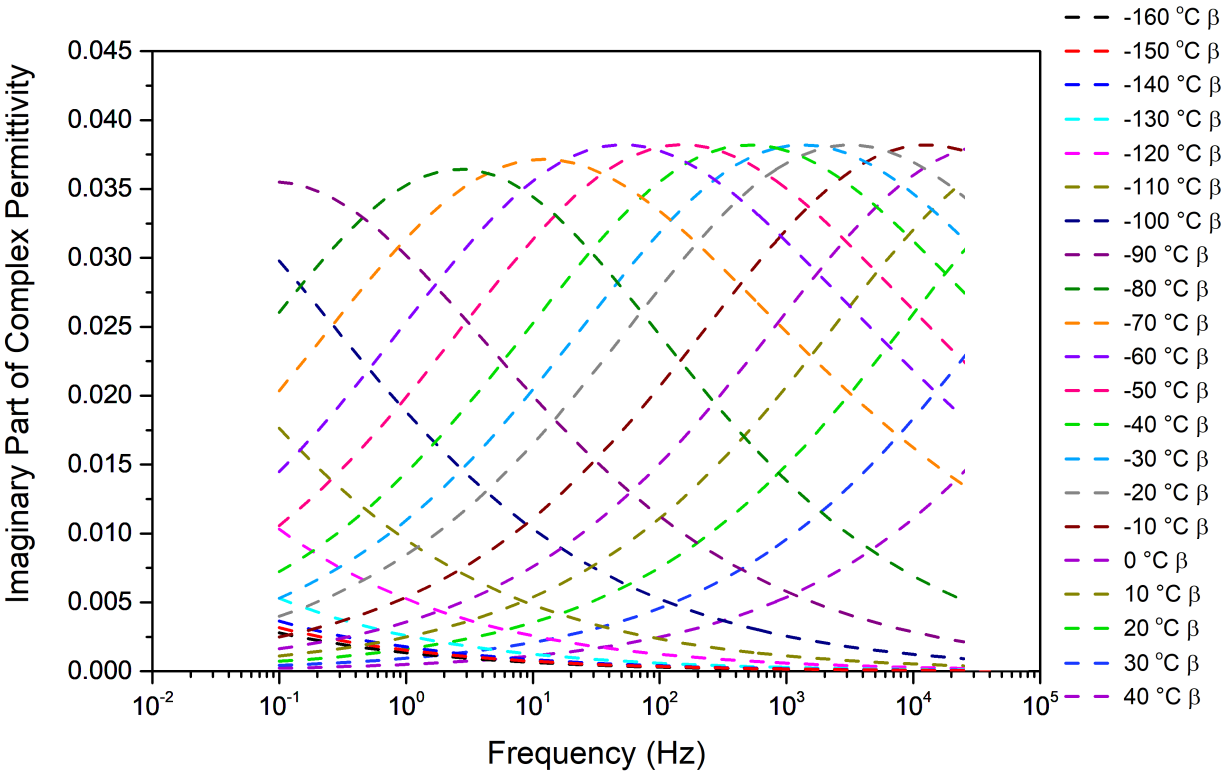

(a) Neat Sample Beta

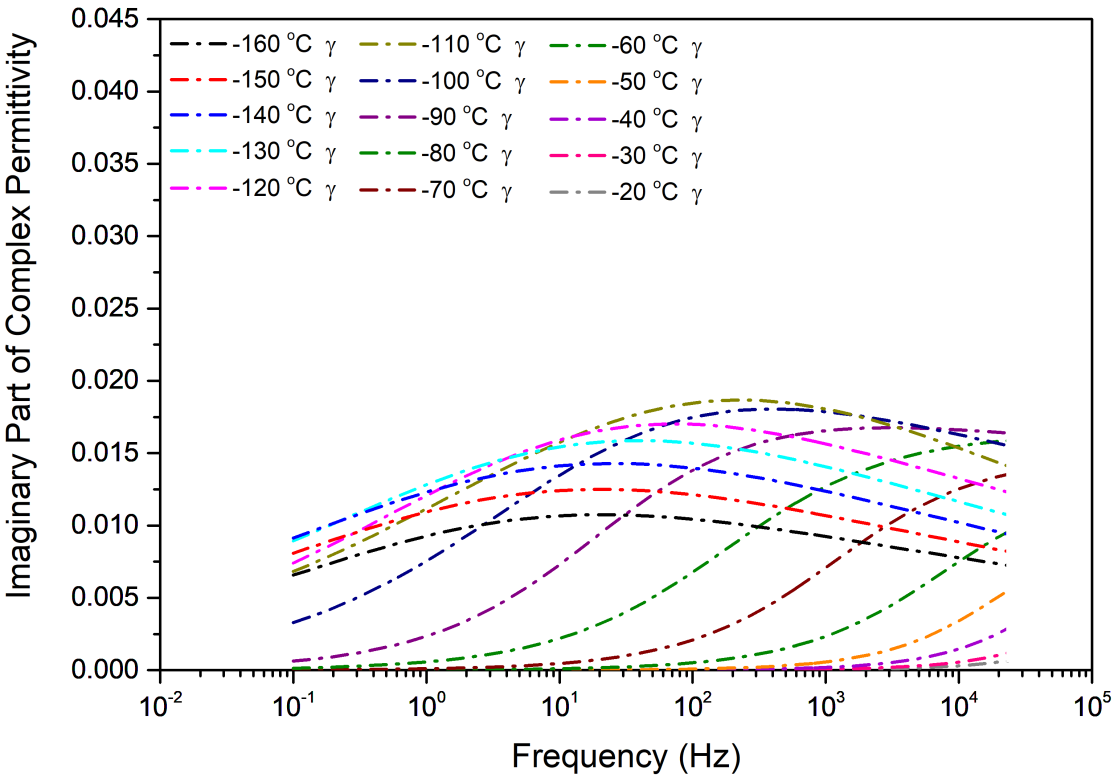

(b) Neat Sample Gamma

Figure E.19: Plots of the deconvoluted temperature dependence of γ and β relaxation peaks using Havriliak-Negami fit for neat sample

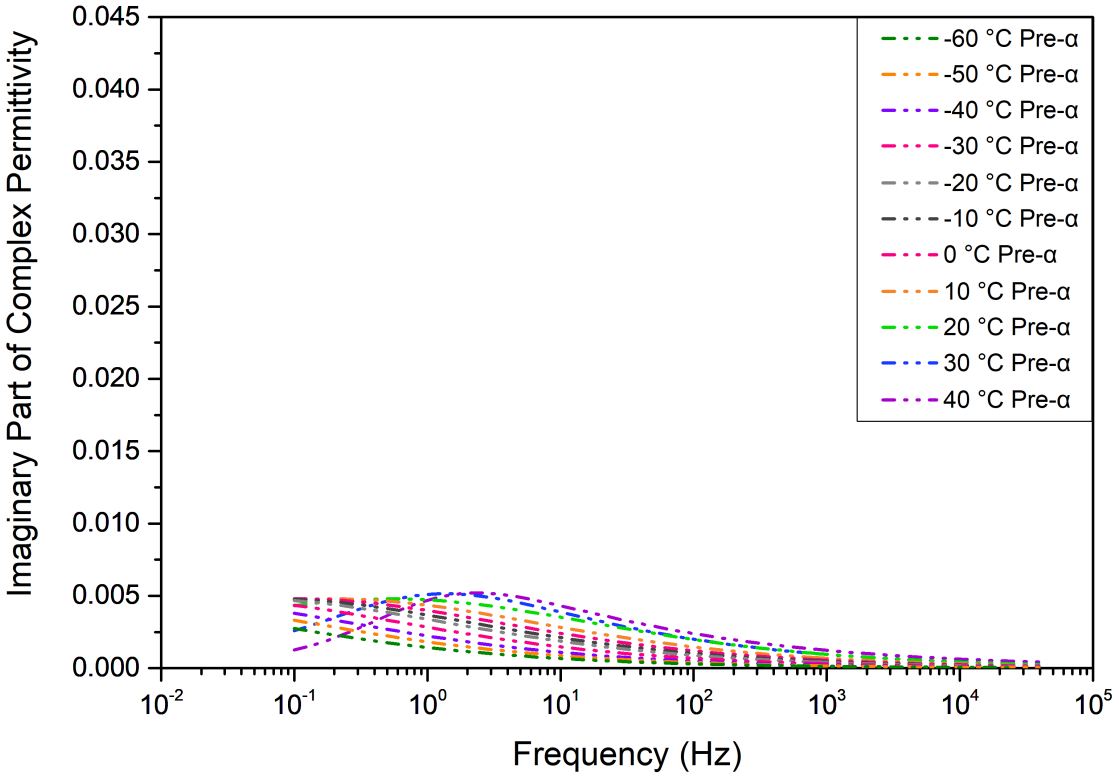

(a) Neat Sample Pre-Alpha

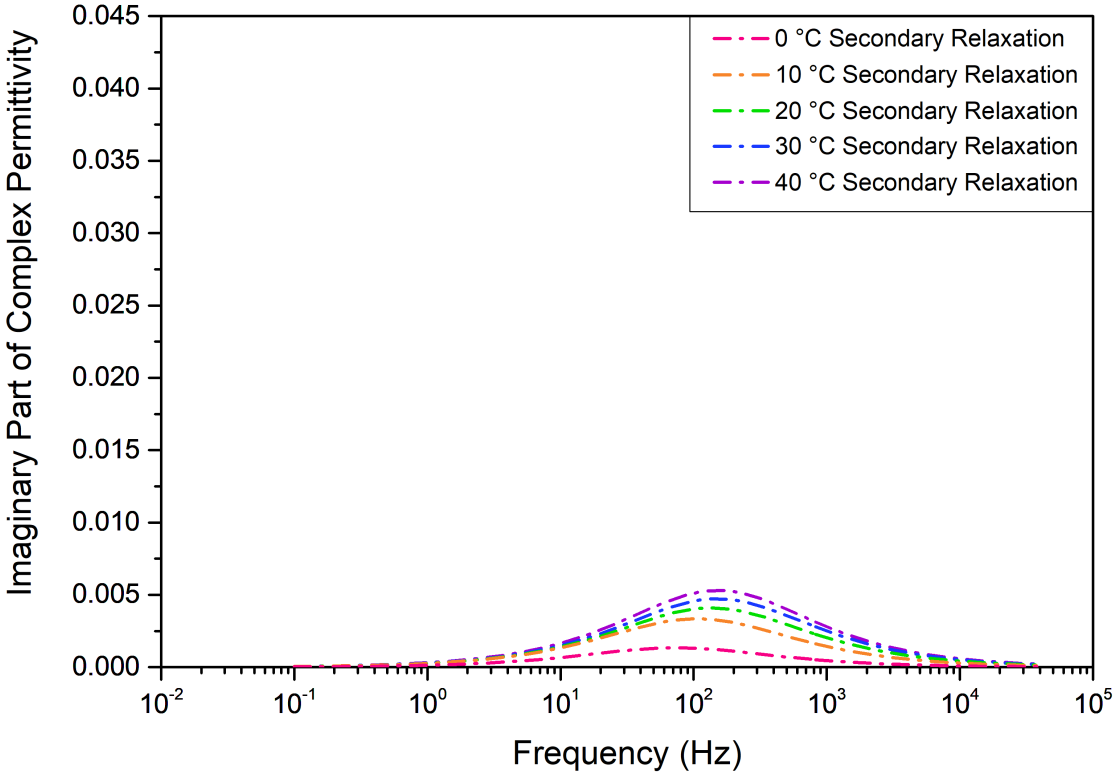

(b) Neat Sample Secondary

Figure E.20: Plots of the deconvoluted temperature dependence of pre alpha and secondary relaxation process using Havriliak-Negami fit for neat sample

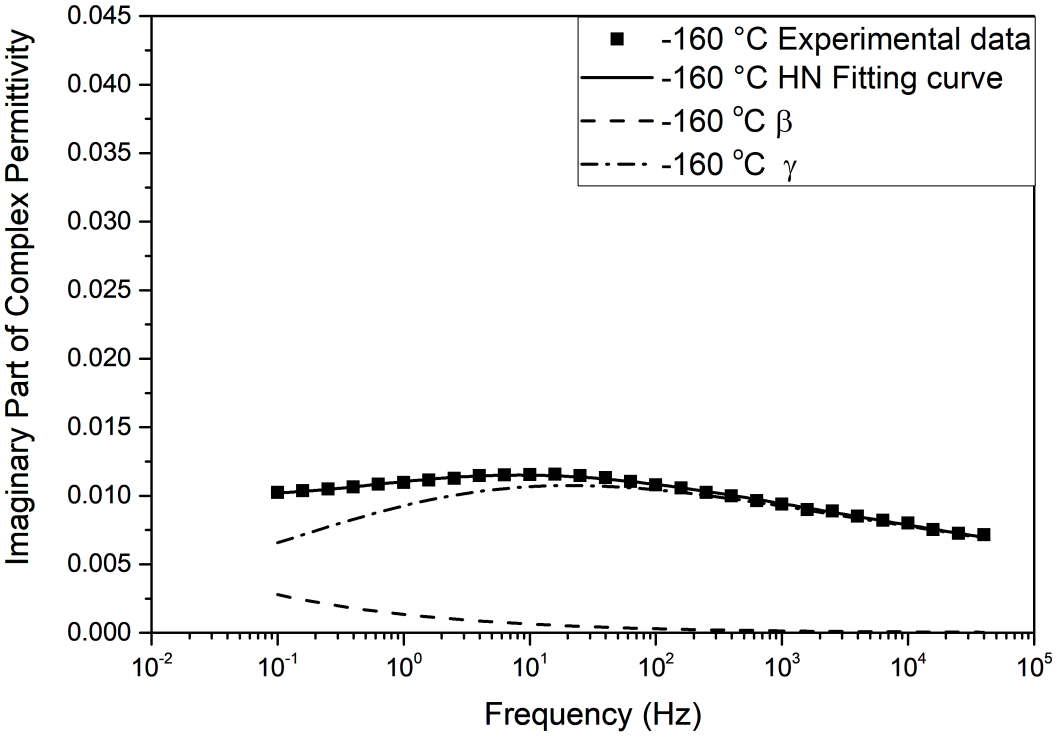

Figure E.21: Havriliak-Negami relaxation fit for neat epoxy resin at -160 °C

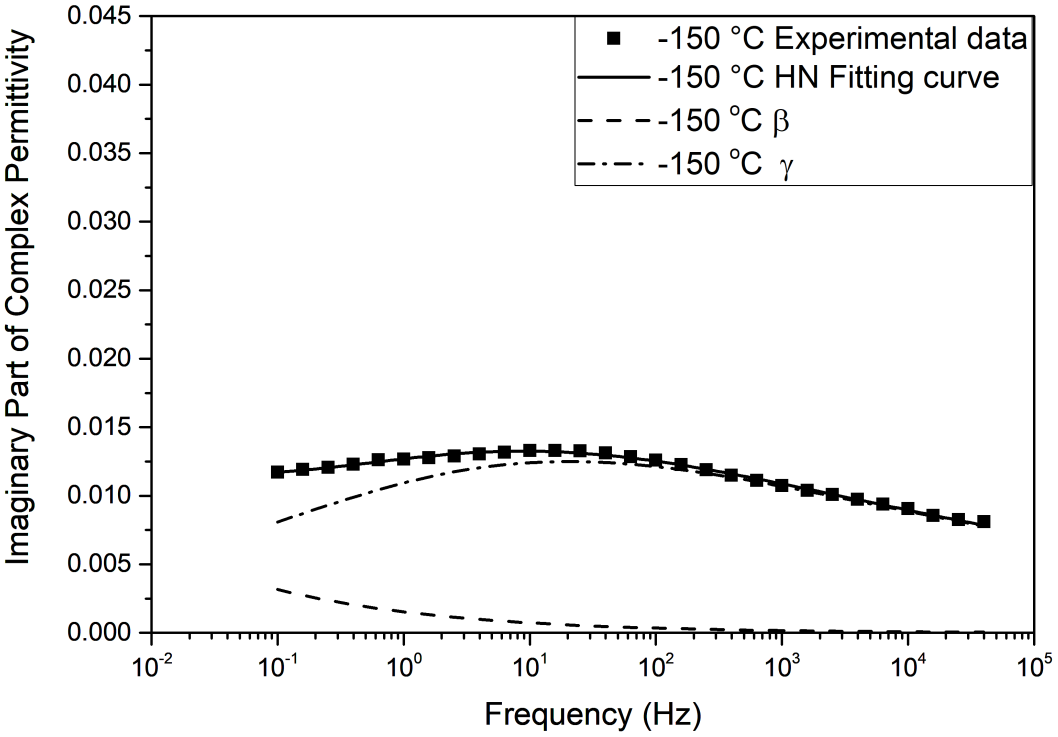

Figure E.22: Havriliak-Negami relaxation fit for neat epoxy resin at -150 °C

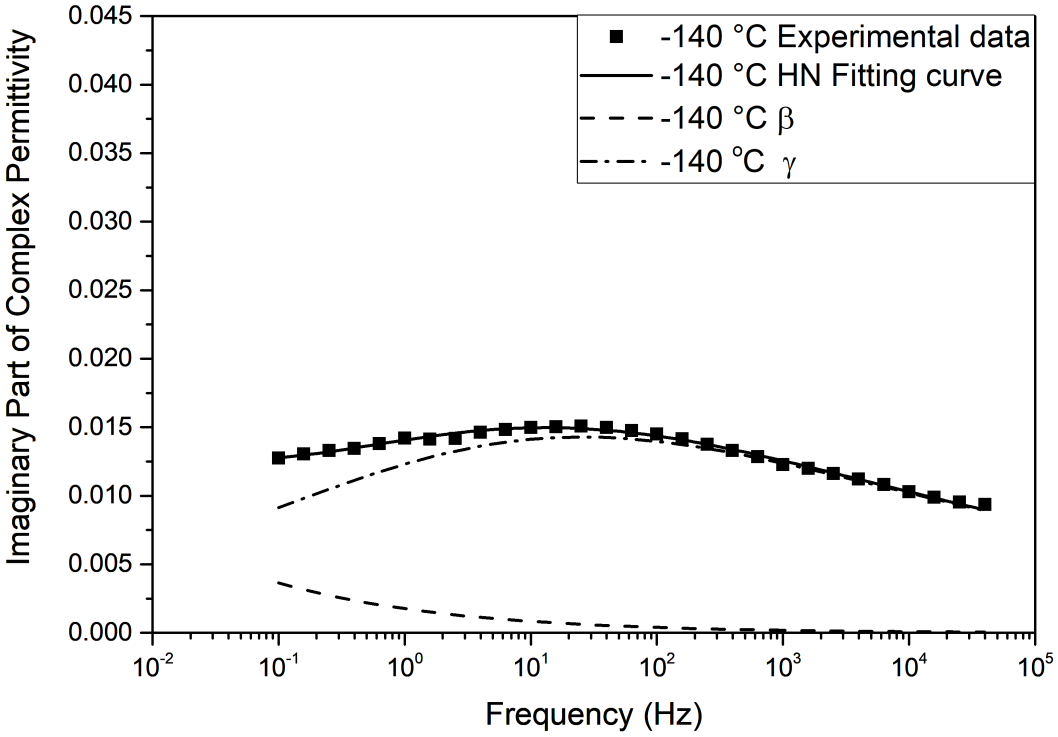

Figure E.23: Havriliak-Negami relaxation fit for neat epoxy resin at -140 °C

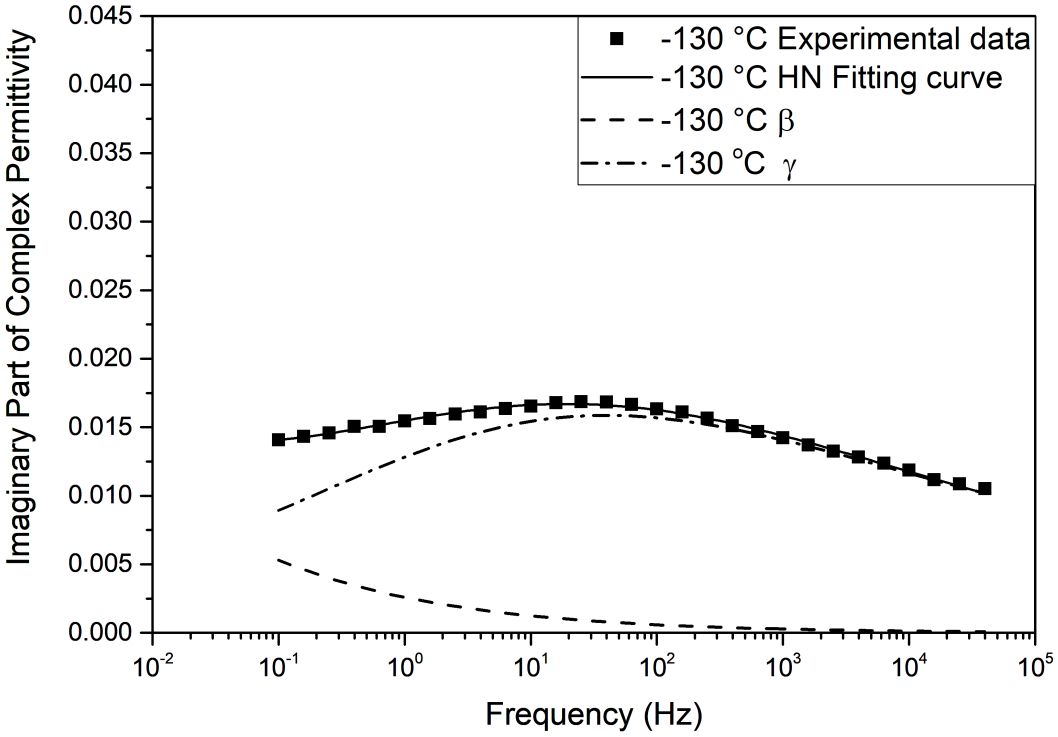

Figure E.24: Havriliak-Negami relaxation fit for neat epoxy resin at -130 °C

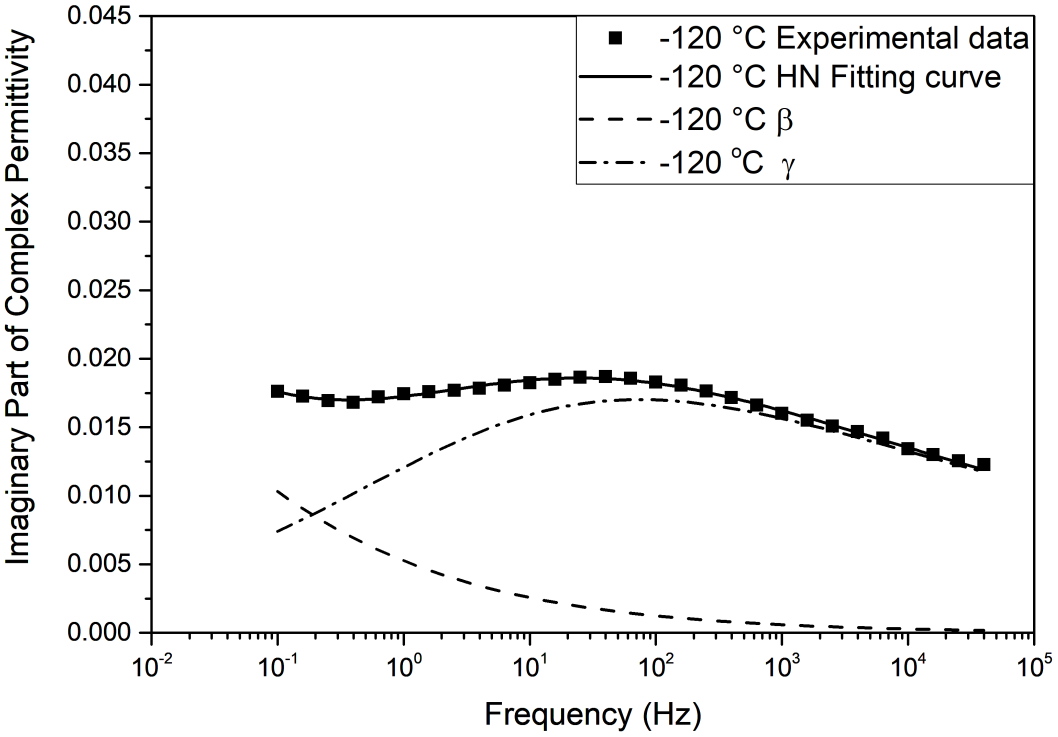

Figure E.25: Havriliak-Negami relaxation fit for neat epoxy resin at -120 °C

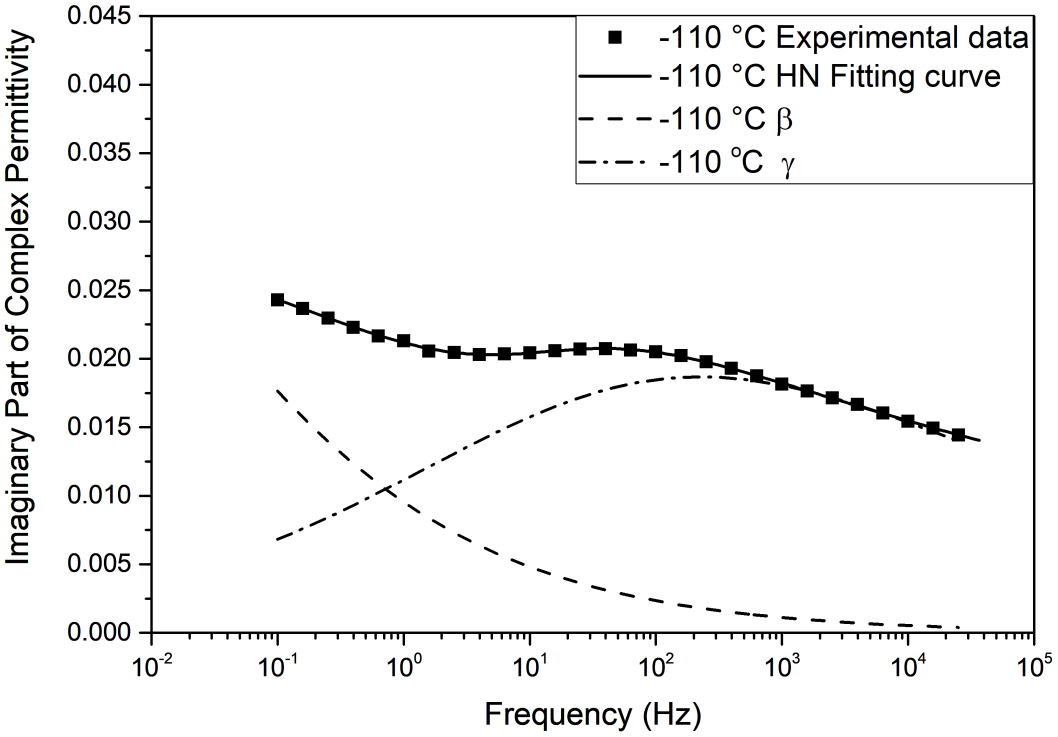

Figure E.26: Havriliak-Negami relaxation fit for neat epoxy resin at -110 °C

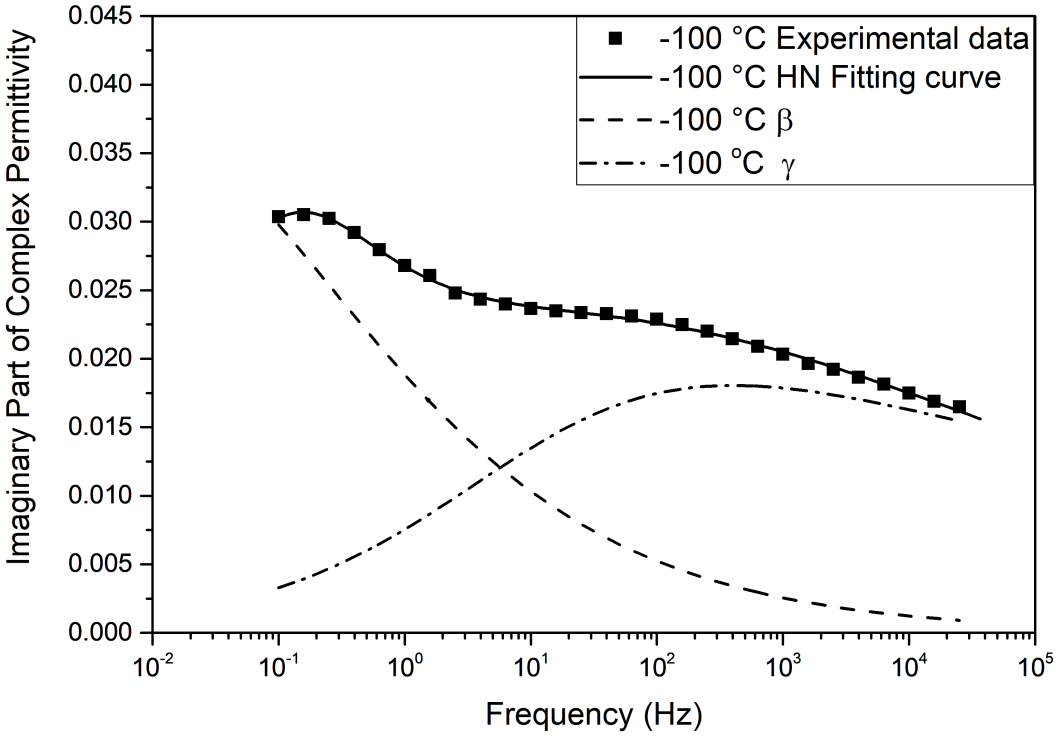

Figure E.27: Havriliak-Negami relaxation fit for neat epoxy resin at -100 °C

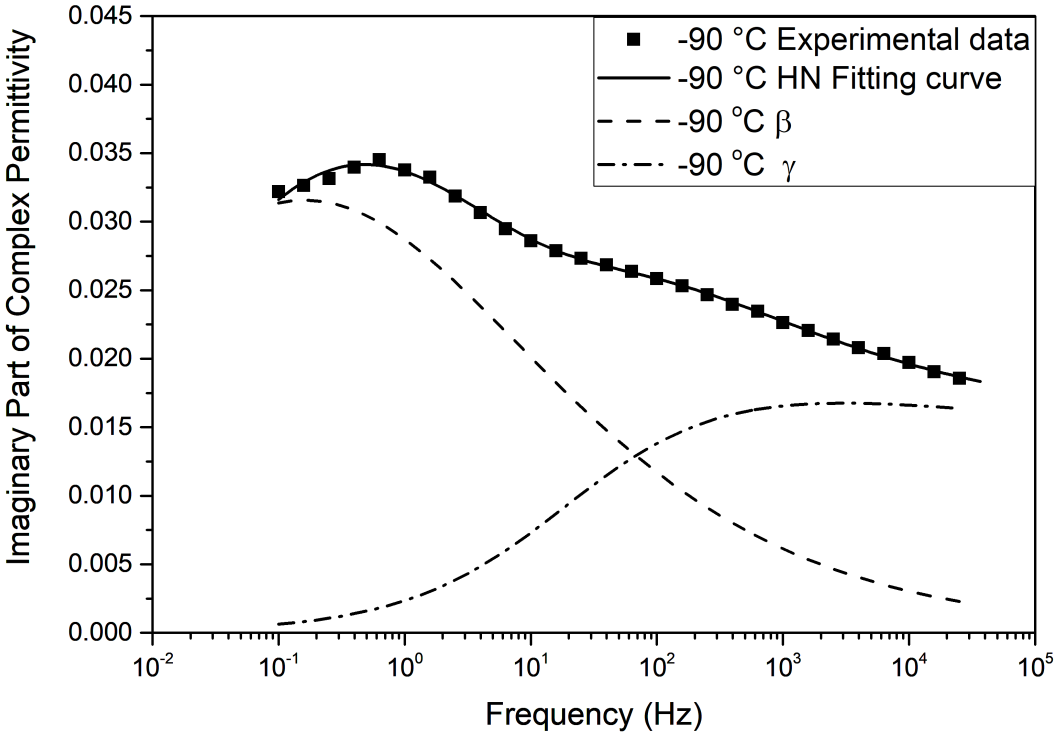

Figure E.28: Havriliak-Negami relaxation fit for neat epoxy resin at -90 °C

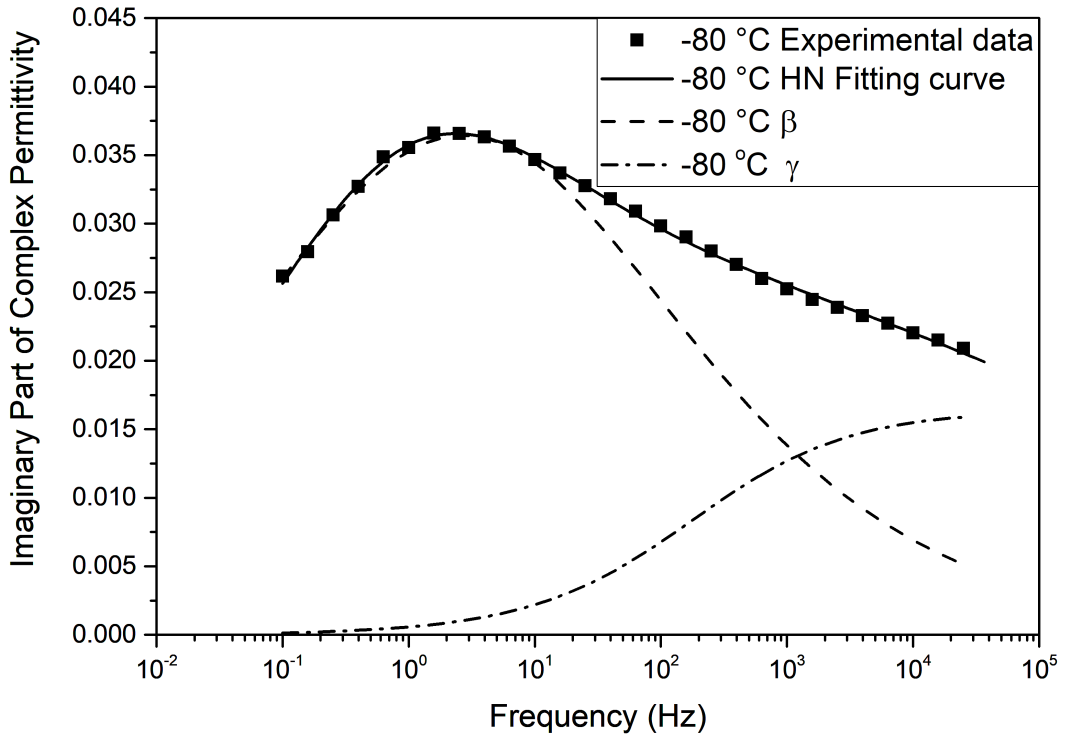

Figure E.29: Havriliak-Negami relaxation fit for neat epoxy resin at -80 °C

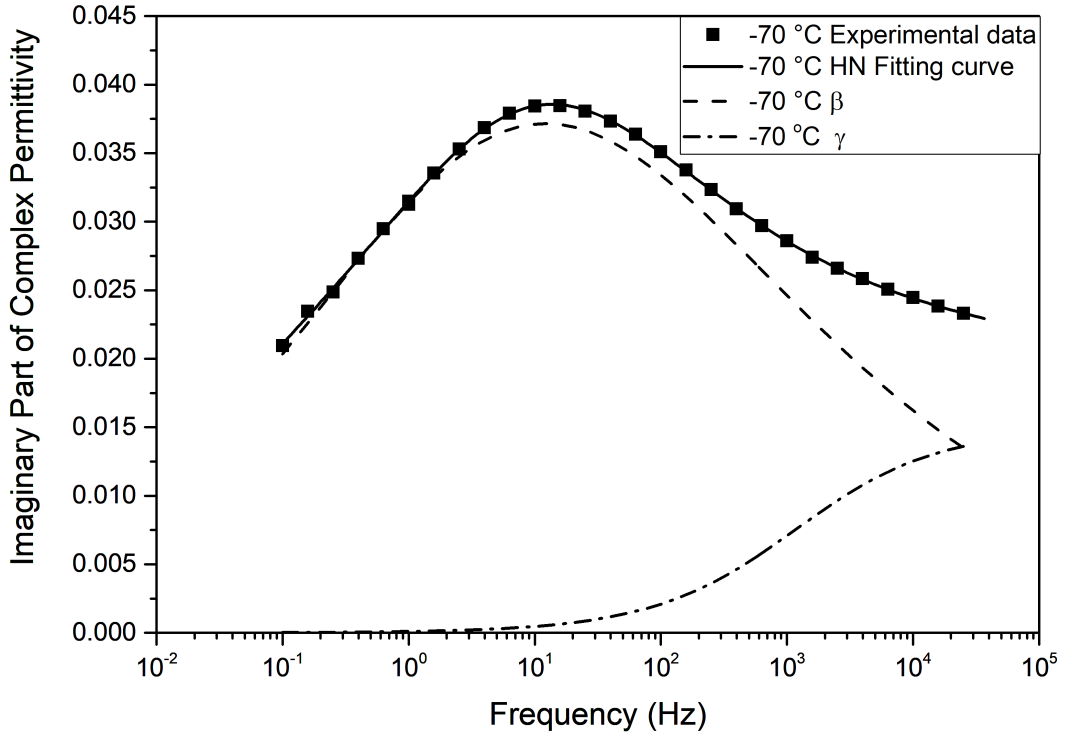

Figure E.30: Havriliak-Negami relaxation fit for neat epoxy resin at -70 °C

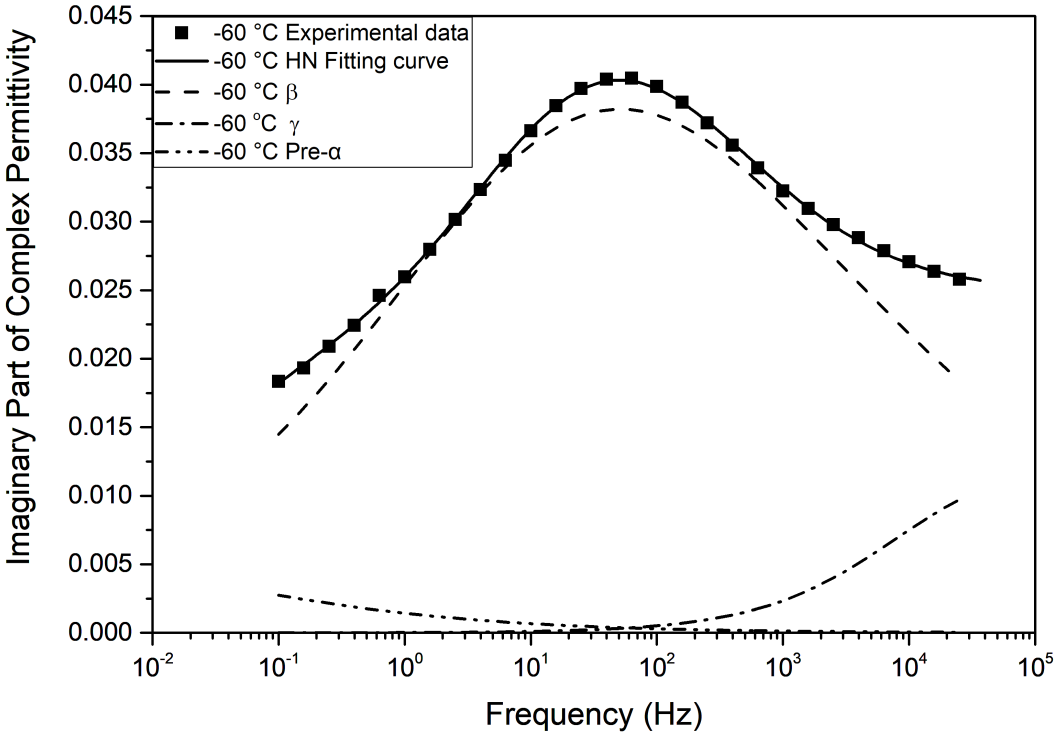

Figure E.31: Havriliak-Negami relaxation fit for neat epoxy resin at -60 °C

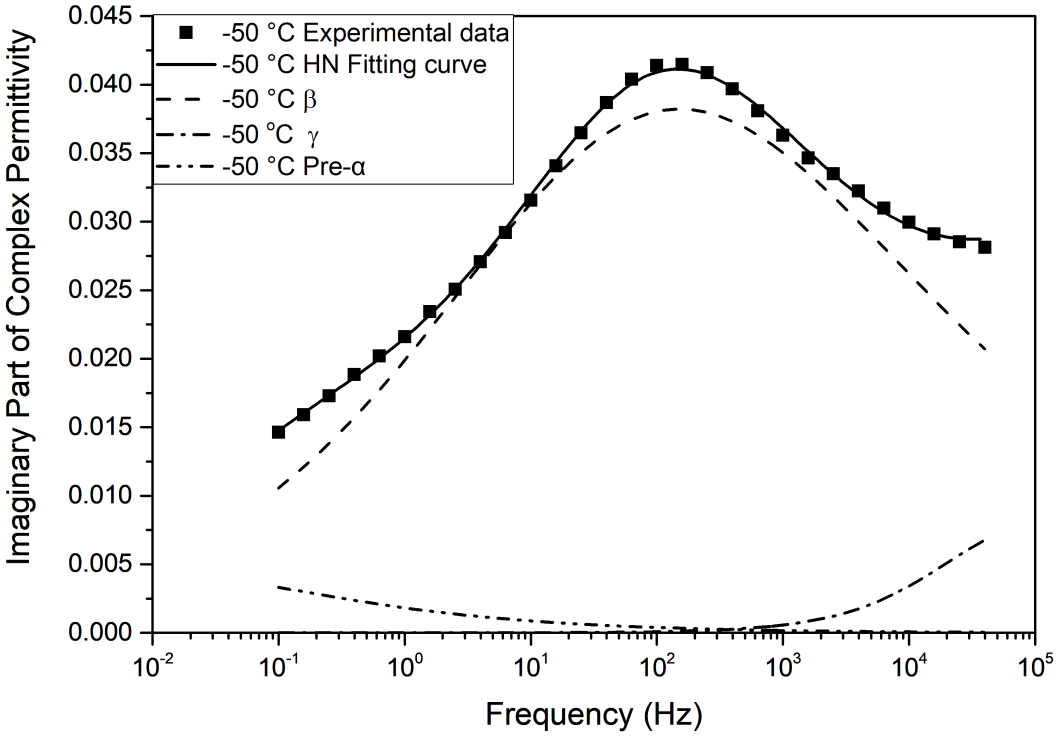

Figure E.32: Havriliak-Negami relaxation fit for neat epoxy resin at -50 °C

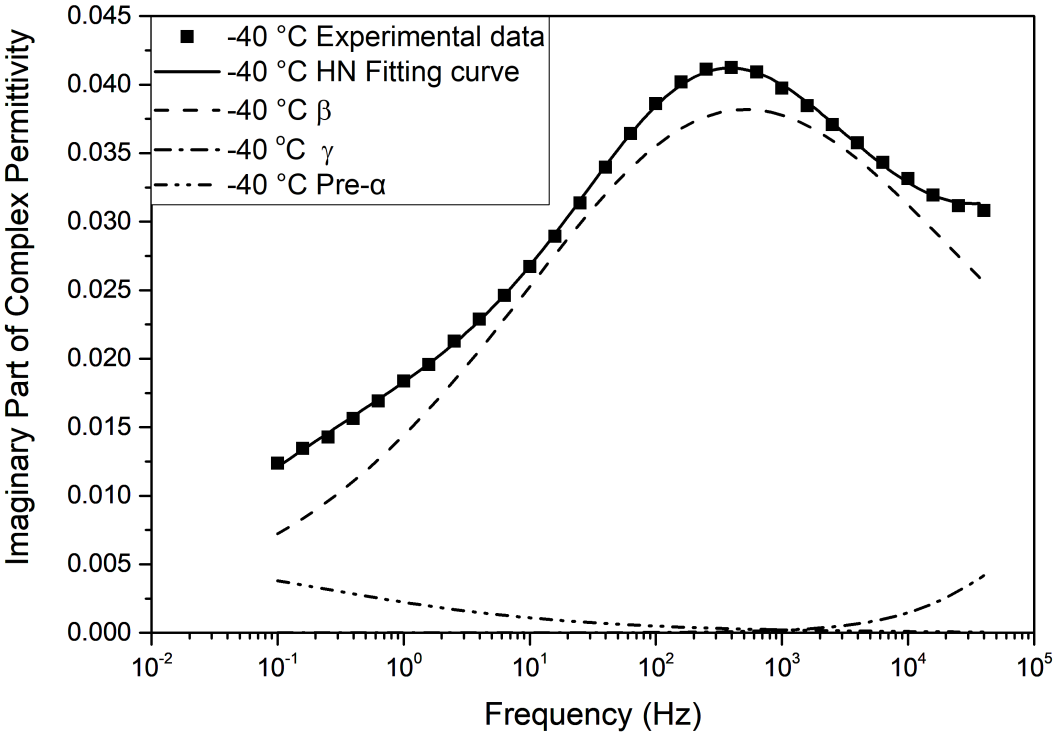

Figure E.33: Havriliak-Negami relaxation fit for neat epoxy resin at -40 °C

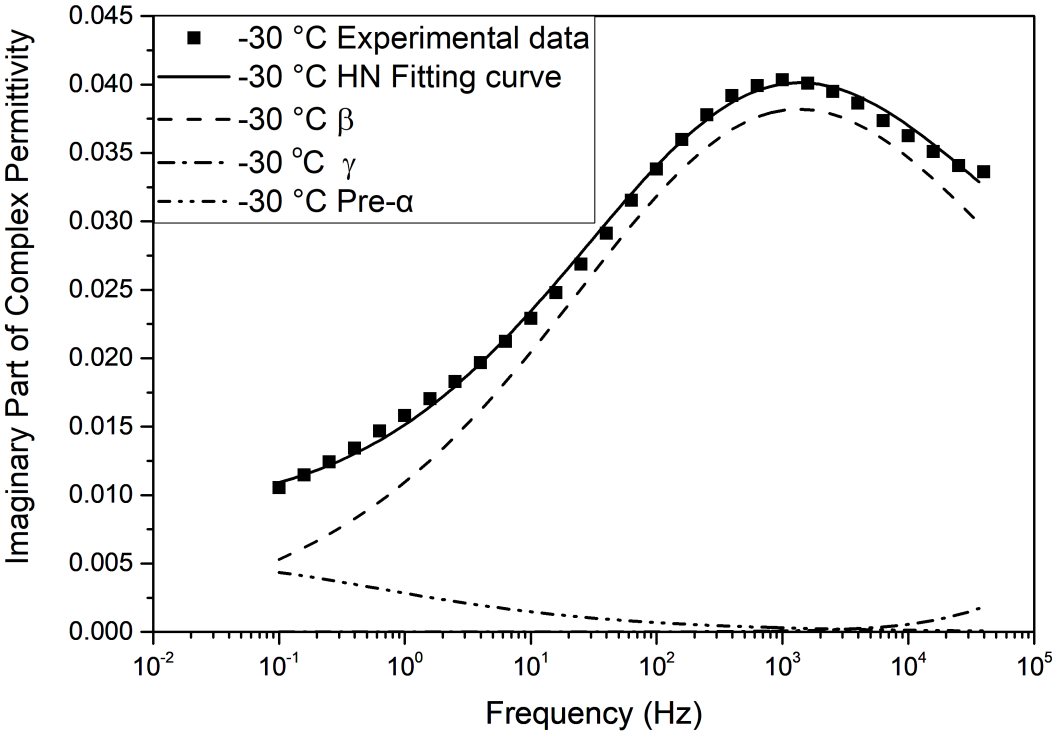

Figure E.34: Havriliak-Negami relaxation fit for neat epoxy resin at -30 °C

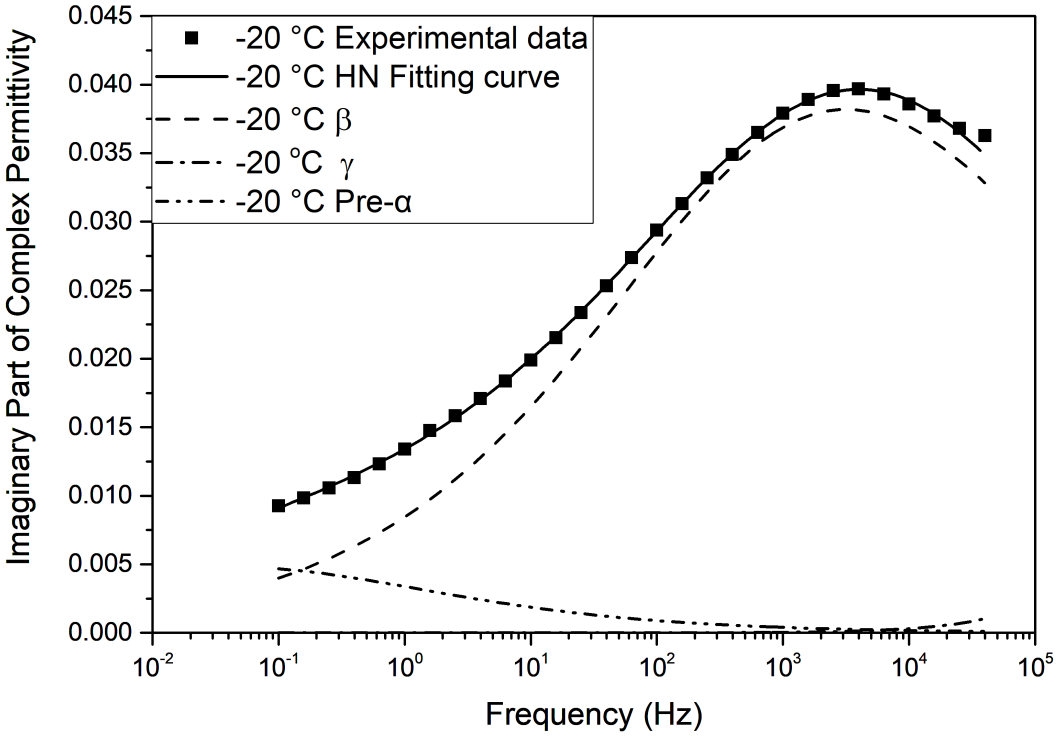

Figure E.35: Havriliak-Negami relaxation fit for neat epoxy resin at -20 °C

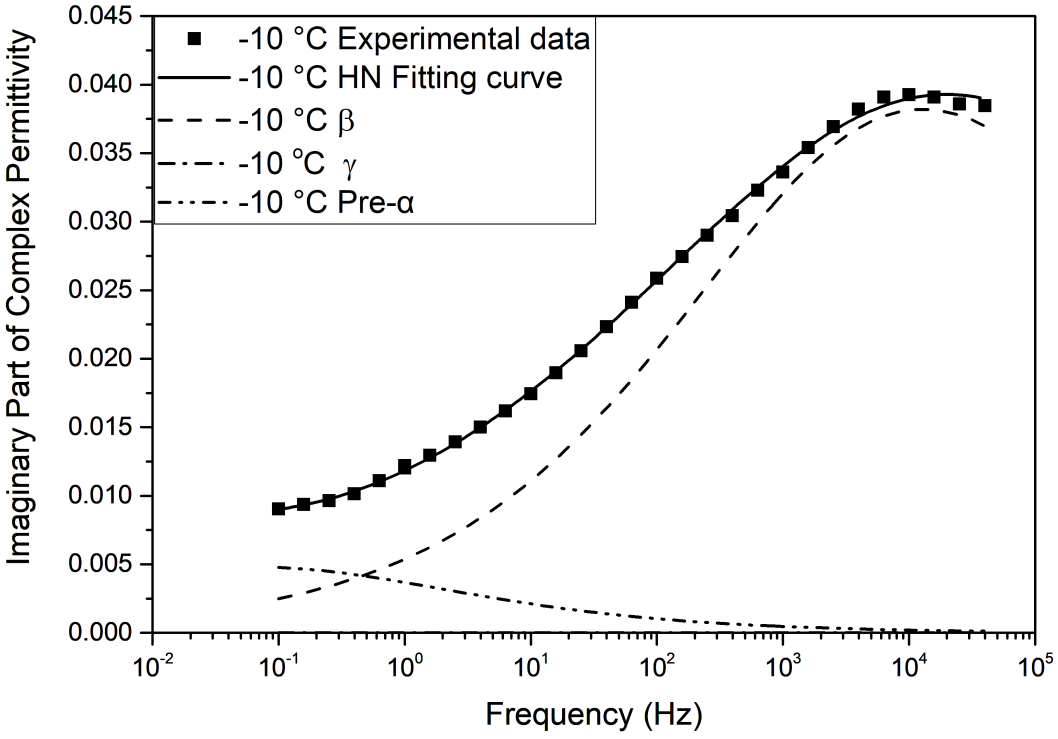

Figure E.36: Havriliak-Negami relaxation fit for neat epoxy resin at -10 °C

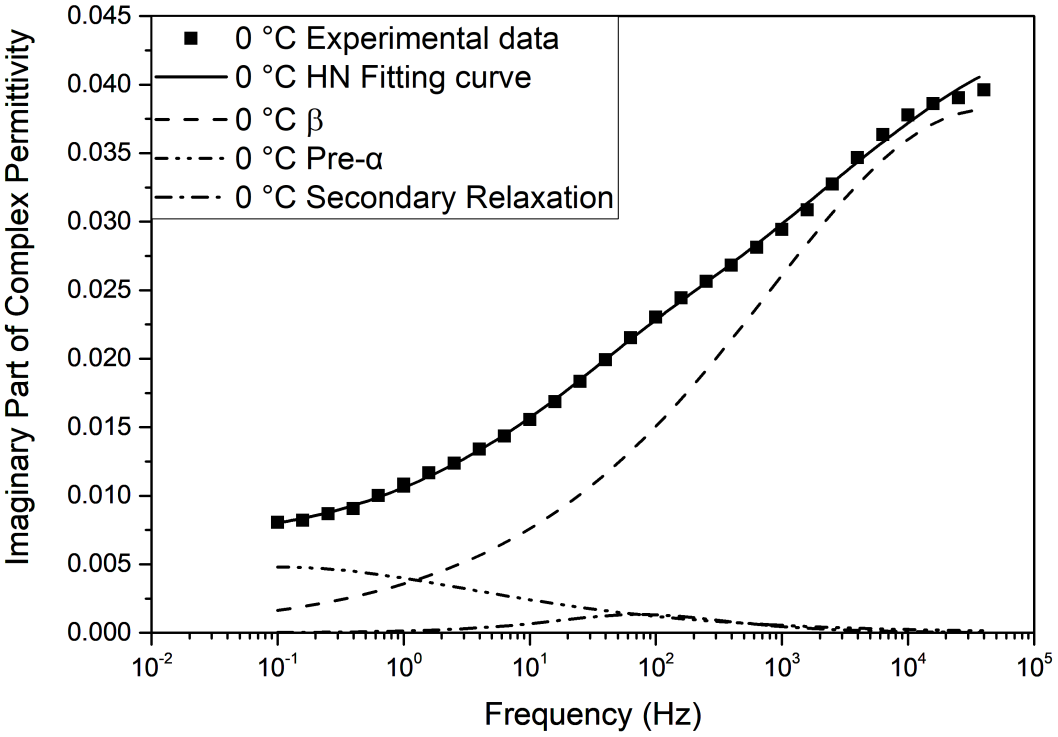

Figure E.37: Havriliak-Negami relaxation fit for neat epoxy resin at 0 °C

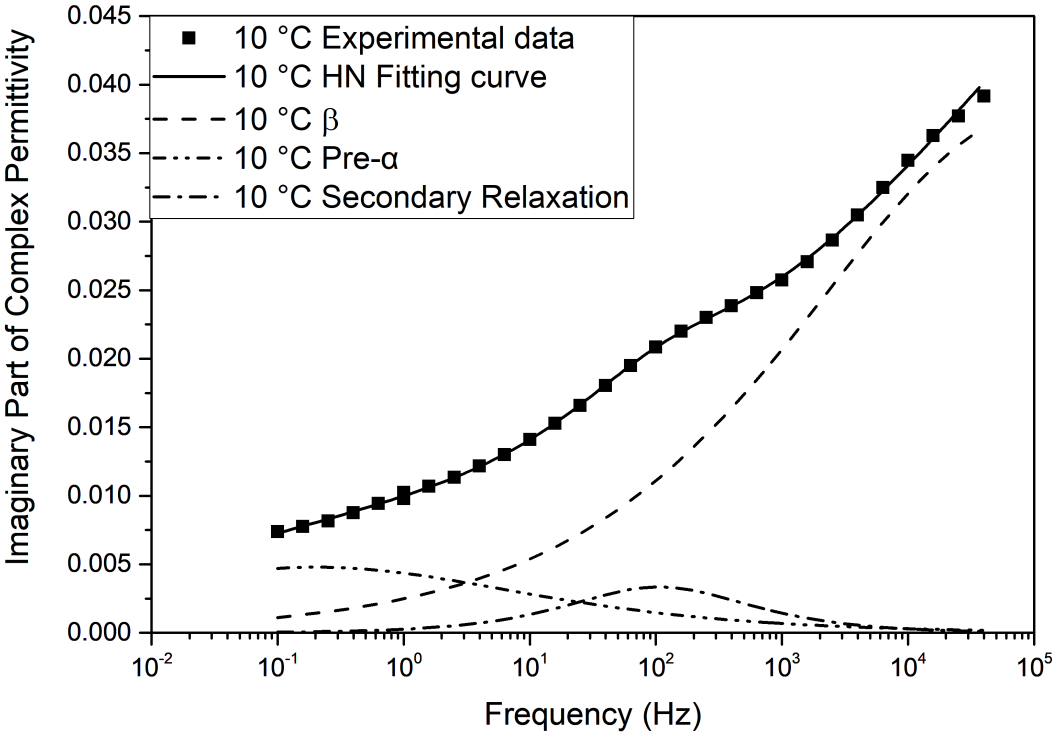

Figure E.38: Havriliak-Negami relaxation fit for neat epoxy resin at +10 °C

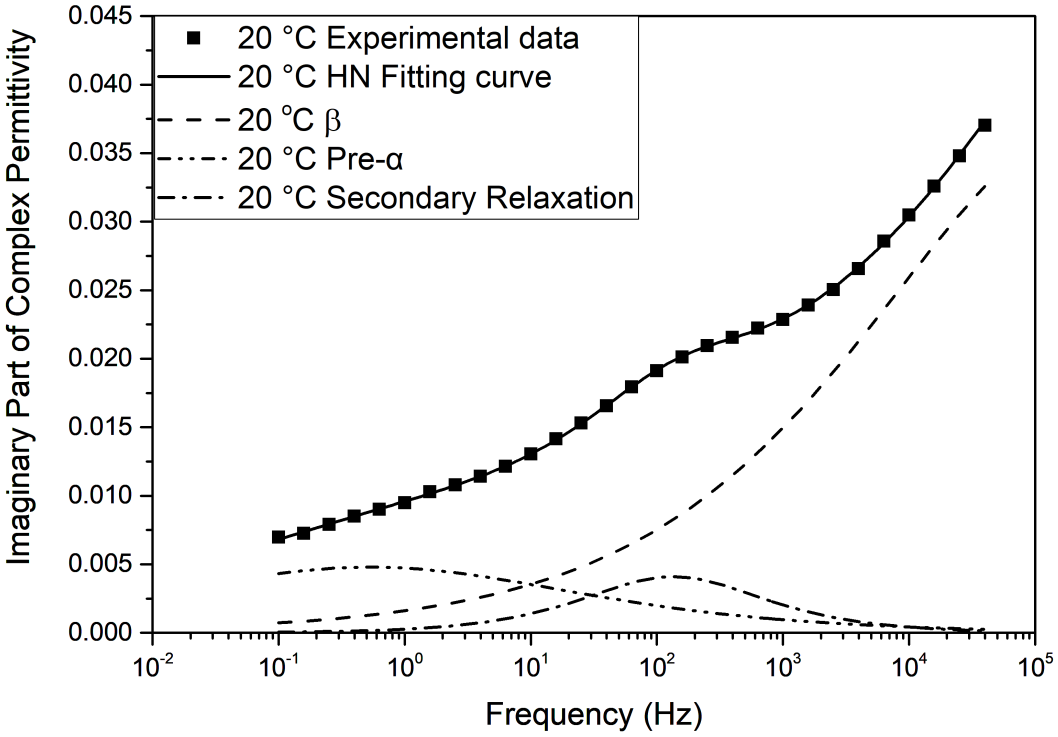

Figure E.39: Havriliak-Negami relaxation fit for neat epoxy resin at +20 °C

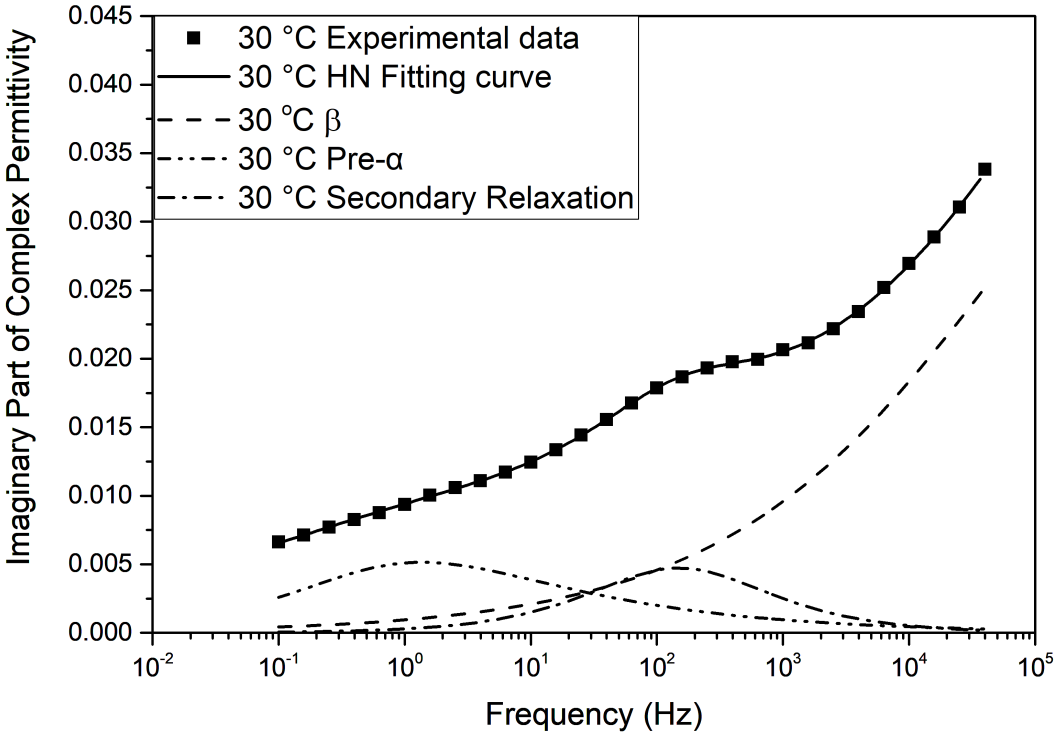

Figure E.40: Havriliak-Negami relaxation fit for neat epoxy resin at +30 °C

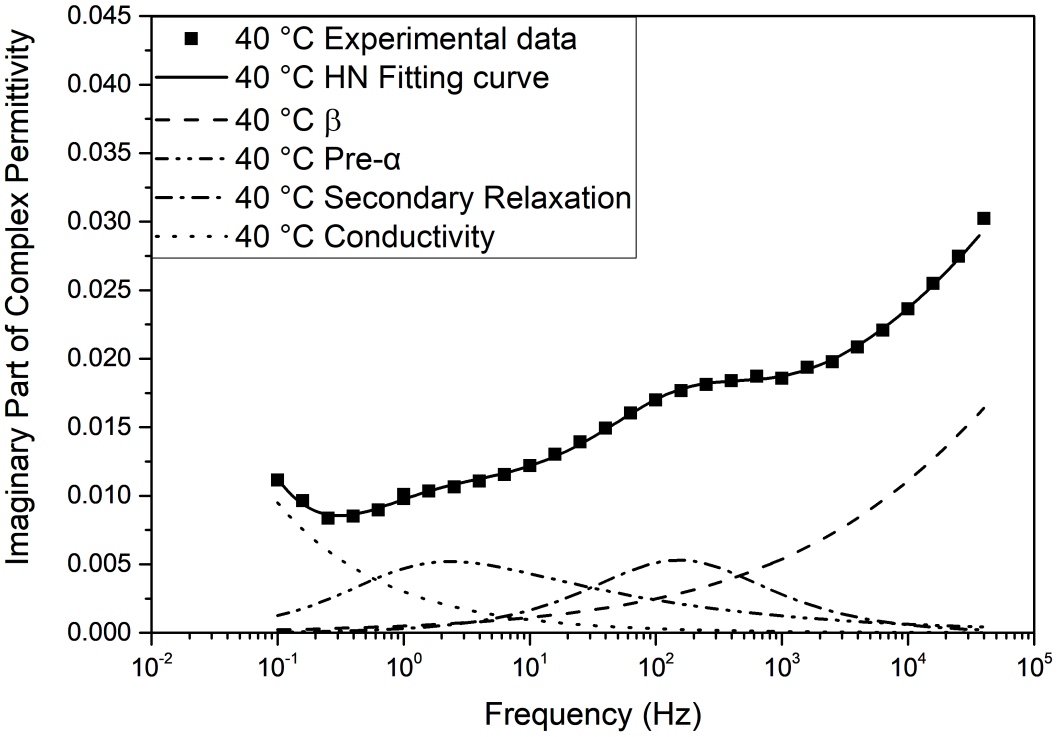

Figure E.41: Havriliak-Negami relaxation fit for neat epoxy resin at +40 °C

E.2.1 Havriliak-Negami fit parameters for neat epoxy resin systems

Table E.1: Havriliak-Negami fit parameters for neat epoxy resin systems

	Process 3				Process 4				Pre Alpha				Secondary Relaxation			
°C	α	β	τ	$\Delta\varepsilon$	α	β	τ	$\Delta\varepsilon$	α	β	τ	$\Delta\varepsilon$	α	β	τ	$\Delta\varepsilon$
-160	0.3272	0.9993	100000	0.22	0.3452	0.2752	0.2986	0.1385	–	–	–	–	–	–	–	–
-150	0.3272	0.9993	100000	0.25	0.3086	0.3563	0.2088	0.1564	–	–	–	–	–	–	–	–
-140	0.3272	0.9993	100000	0.2883	0.2895	0.4197	0.1191	0.1754	–	–	–	–	–	–	–	–
-130	0.3272	0.9993	29770	0.2882	0.3077	0.3922	0.07962	0.1894	–	–	–	–	–	–	–	–
-120	0.3272	0.9993	3219	0.2883	0.3543	0.2962	0.06233	0.2047	–	–	–	–	–	–	–	–
-110	0.3272	0.9993	407.8	0.2883	0.3042	0.5081	0.00625	0.199	–	–	–	–	–	–	–	–
-100	0.3272	0.9993	30.9	0.2883	0.4477	0.1607	0.02045	0.2518	–	–	–	–	–	–	–	–
-90	0.3272	0.9993	1.797	0.2703	0.6093	0.0426	0.007232	0.488	–	–	–	–	–	–	–	–
-80	0.3498	1	0.05926	0.2585	0.6134	0.01	8.56E-04	1.772	–	–	–	–	–	–	–	–
-70	0.35347	0.64097	0.04466	0.30659	0.68	0.009	1.30E-04	0.4068	–	–	–	–	–	–	–	–
-60	0.3535	0.641	0.01066	0.3153	0.7	0.009	2.00E-05	1.4001	0.3764	0.9664	100	0.03173	–	–	–	–
-50	0.3535	0.641	0.0036	0.3153	0.85	0.0086	8.00E-06	0.89	0.3738	0.9665	40	0.03173	–	–	–	–
-40	0.3535	0.641	0.00105	0.3152	0.9	0.007	3.00E-06	1	0.3738	0.9665	20	0.03173	–	–	–	–
-30	0.3535	0.641	4.05E-04	0.3152	0.9	0.007	1.00E-06	1	0.3738	0.9665	8	0.03173	–	–	–	–
-20	0.3535	0.641	1.73E-04	0.3152	0.9	0.007	5.00E-07	1	0.3738	0.9665	3.7	0.03173	–	–	–	–
-10	0.3535	0.641	4.23E-05	0.3152	1	0.9993	1.00E-11	1.00E-09	0.3738	0.9665	2.4	0.03173	–	–	–	–
0	0.3535	0.641	1.23E-05	0.3152	–	–	–	–	0.3738	0.9665	1.5	0.03173	0.7565	1	0.00215	0.00397
10	0.3535	0.641	4.23E-06	0.3152	–	–	–	–	0.3738	0.9965	0.8	0.03173	0.7565	1	0.0015	0.0099
20	0.3535	0.641	1.20E-06	0.3152	–	–	–	–	0.3738	0.9965	0.3	0.03173	0.7565	1	0.00118	0.01213
30	0.3535	0.641	2.60E-07	0.3151	–	–	–	–	0.6738	0.4965	0.3	0.02373	0.7565	1	0.00106	0.01399
40	0.3535	0.641	4.23E-08	0.3151	–	–	–	–	0.8386	0.3484	0.2032	0.02255	0.7602	1	0.00105	0.0156

E.3 Havriliak-Negami relaxation fit for 30AGNPE systems

The dielectric data of the 30AGNPE system for temperatures from -160 °C to 40 °C was analysed using Havriliak-Negami fit function. The outcome of the analysis is plotted in the figures below from Figure fig. E.45 to fig. E.64. The parameters used in the Havriliak-Negami fit function are listed in Table E.2. To compare the de-convoluted peaks at different temperature, the peaks associated with the β- relaxation, the γ- relaxation and pre-alpha process are plotted in separate figures (Figure E.42 and Figure E.43 respectively.

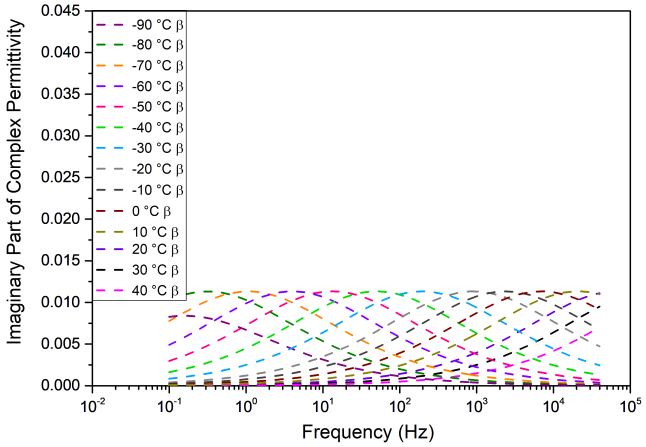

(a) 30AGNPE Sample Beta

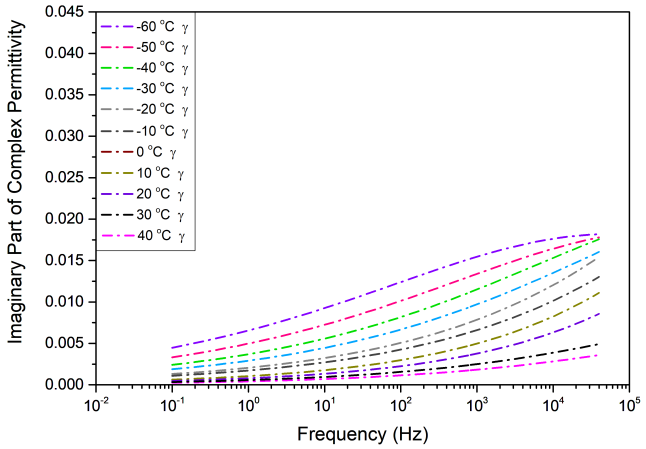

(b) 30AGNPE Sample Gamma part 1

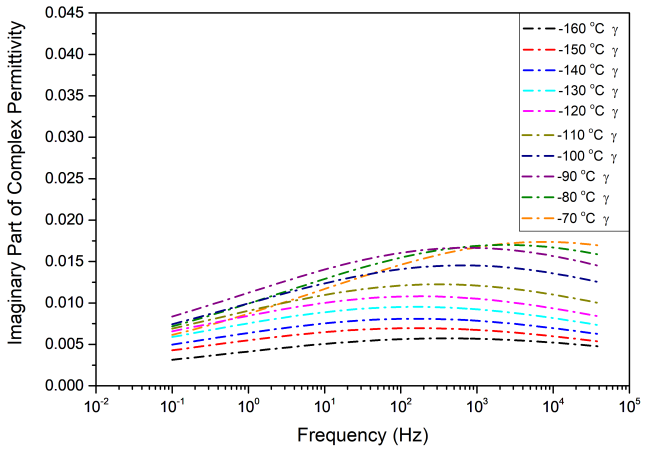

(c) 30AGNPE Sample Gamma part 2

Figure E.42: Plots of the deconvoluted temperature dependence of γ and β relaxation peaks using Havriliak-Negami fit for 30AGNPE sample

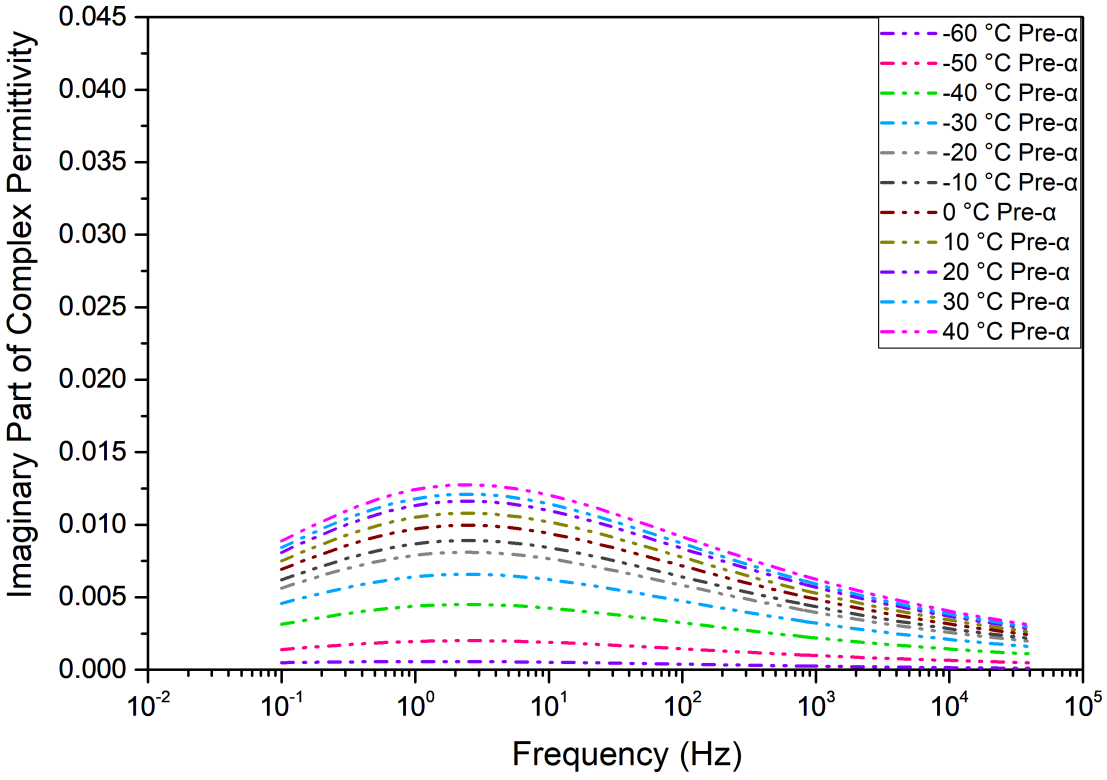

Figure E.43: Plots of the deconvoluted temperature dependence pre alpha process using Havriliak-Negami fit for 30AGNPE sample

E.3.1 Havriliak-Negami fit for 30AGNPE systems

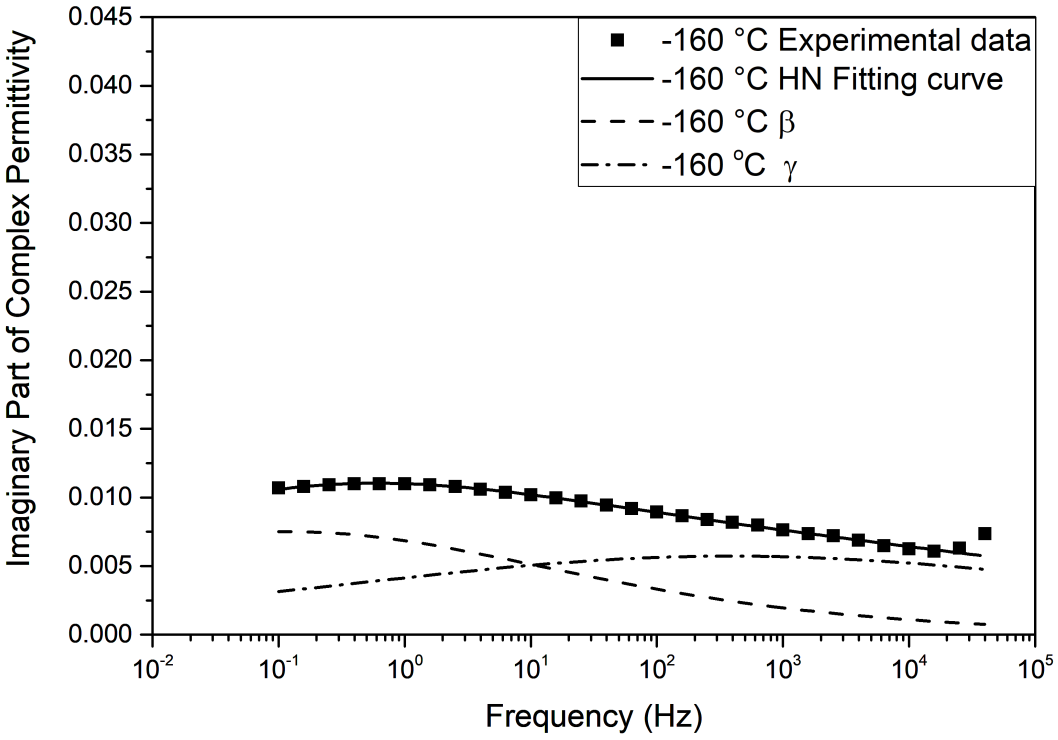

Figure E.44: Havriliak-Negami relaxation fit for 30AGNPE at -160 °C

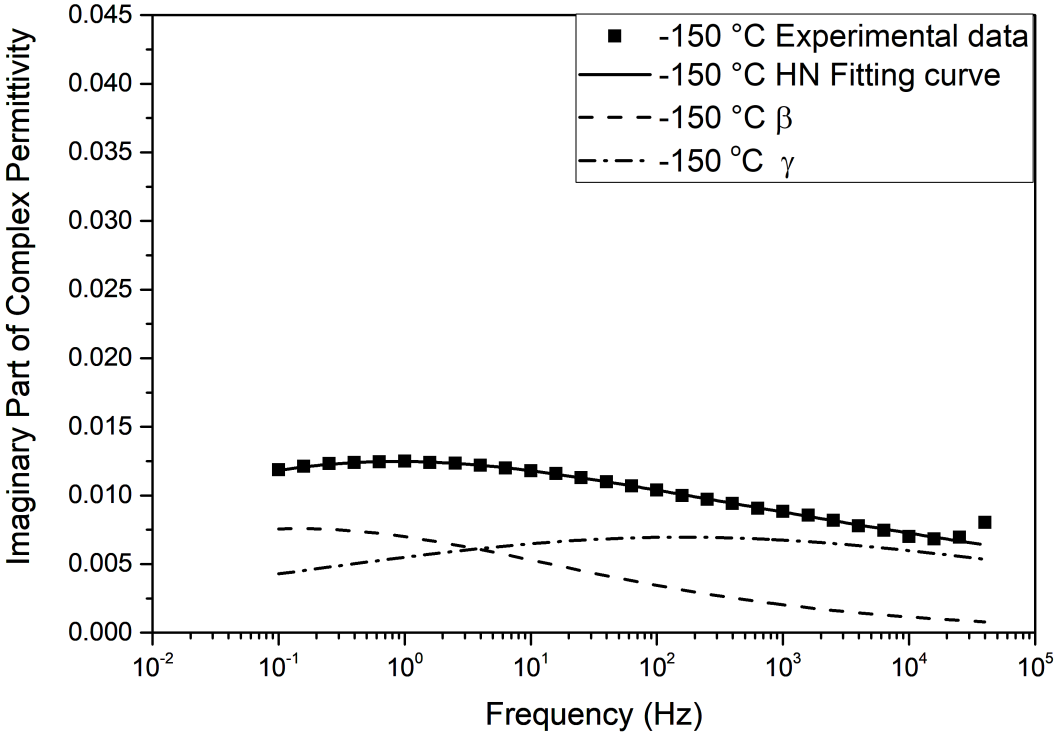

Figure E.45: Havriliak-Negami relaxation fit for 30AGNPE at -150 °C

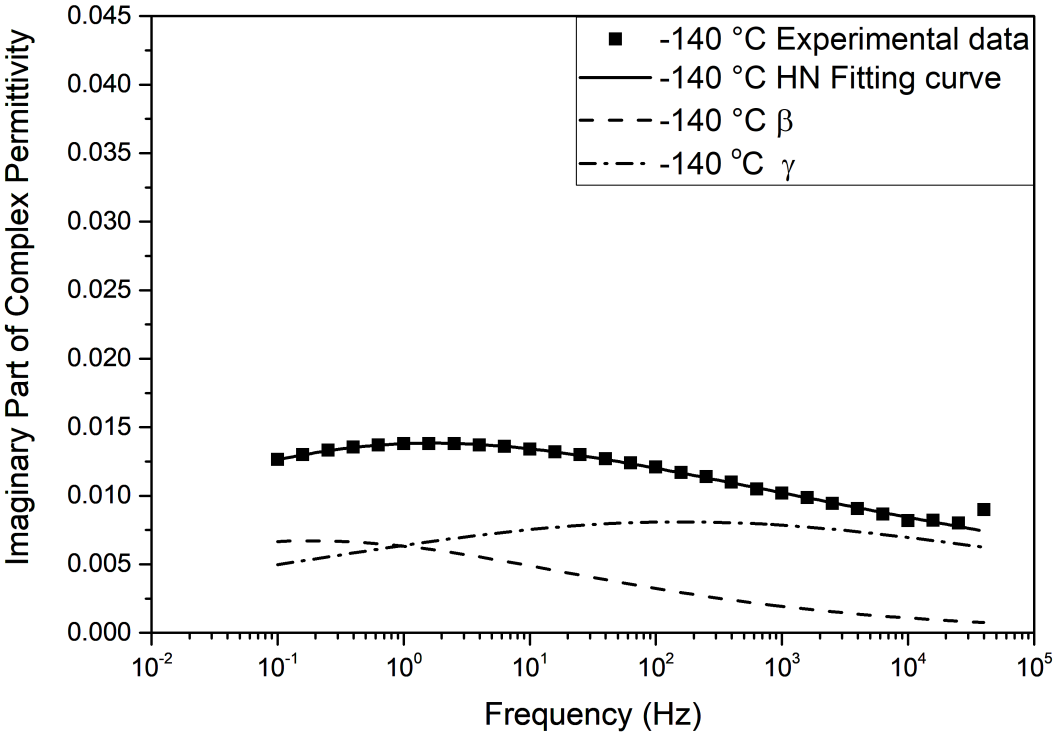

Figure E.46: Havriliak-Negami relaxation fit for 30AGNPE at -140 °C

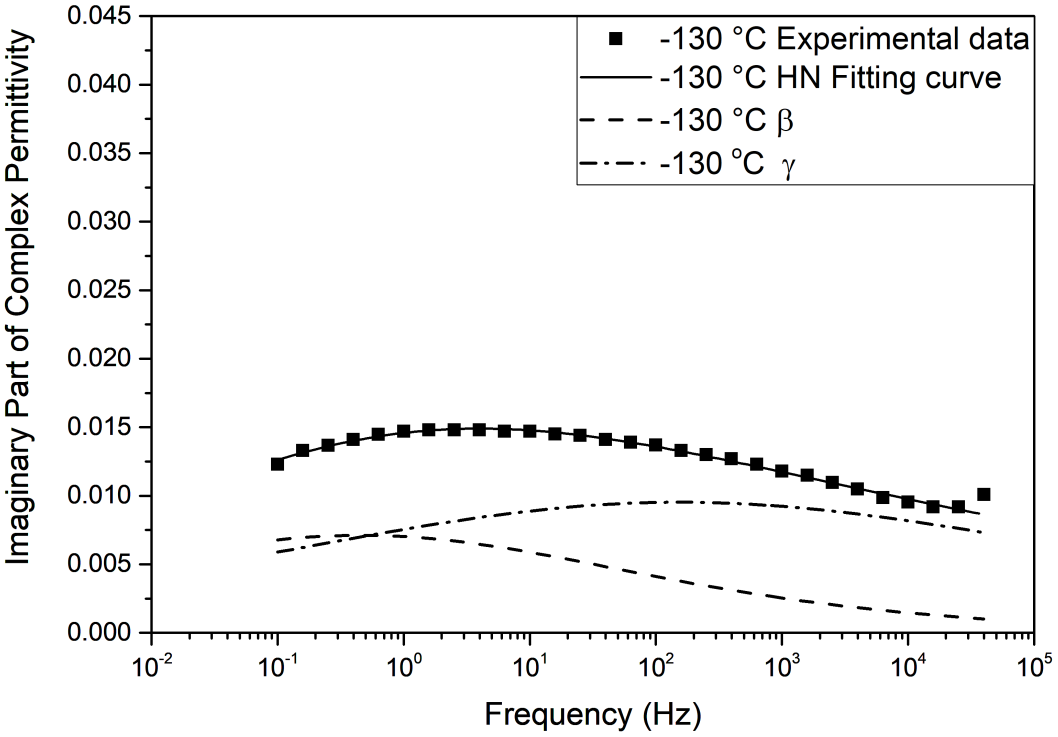

Figure E.47: Havriliak-Negami relaxation fit for 30AGNPE at -130 °C

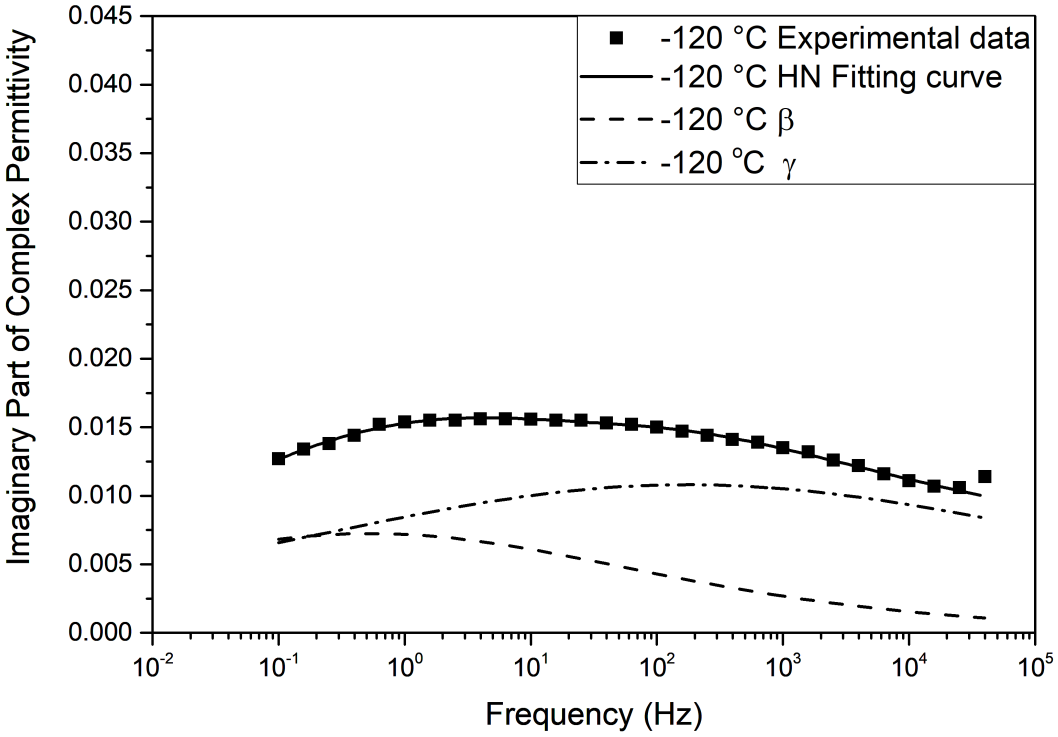

Figure E.48: Havriliak-Negami relaxation fit for 30AGNPE at -120 °C

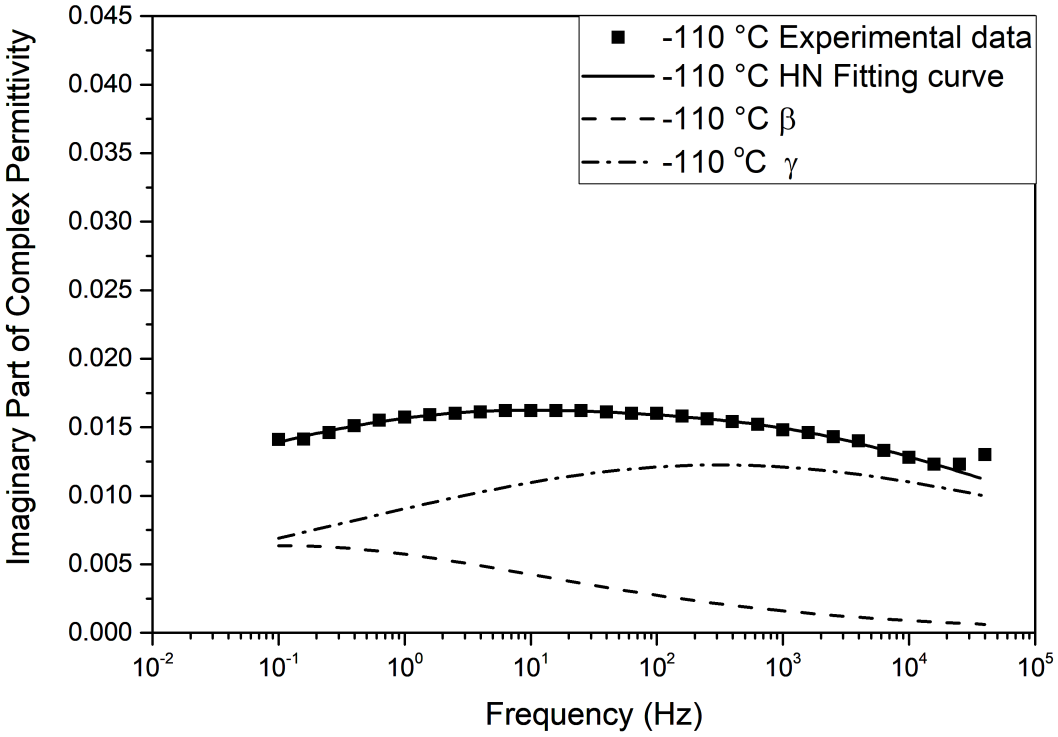

Figure E.49: Havriliak-Negami relaxation fit for 30AGNPE at -110 °C

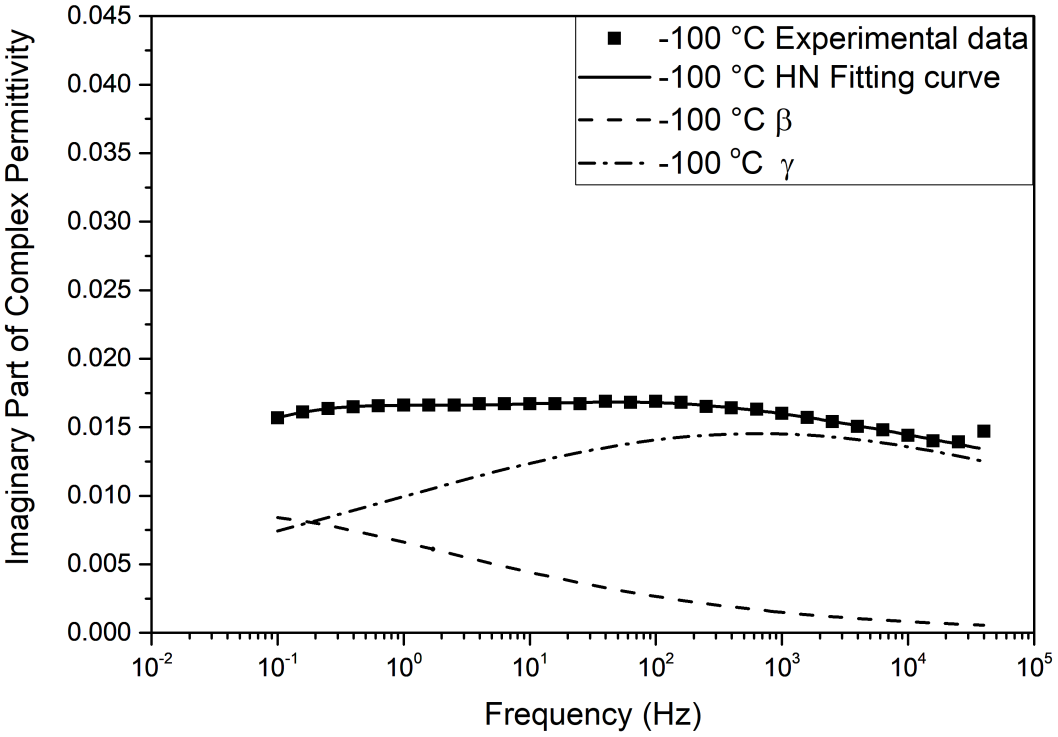

Figure E.50: Havriliak-Negami relaxation fit for 30AGNPE at -100 °C

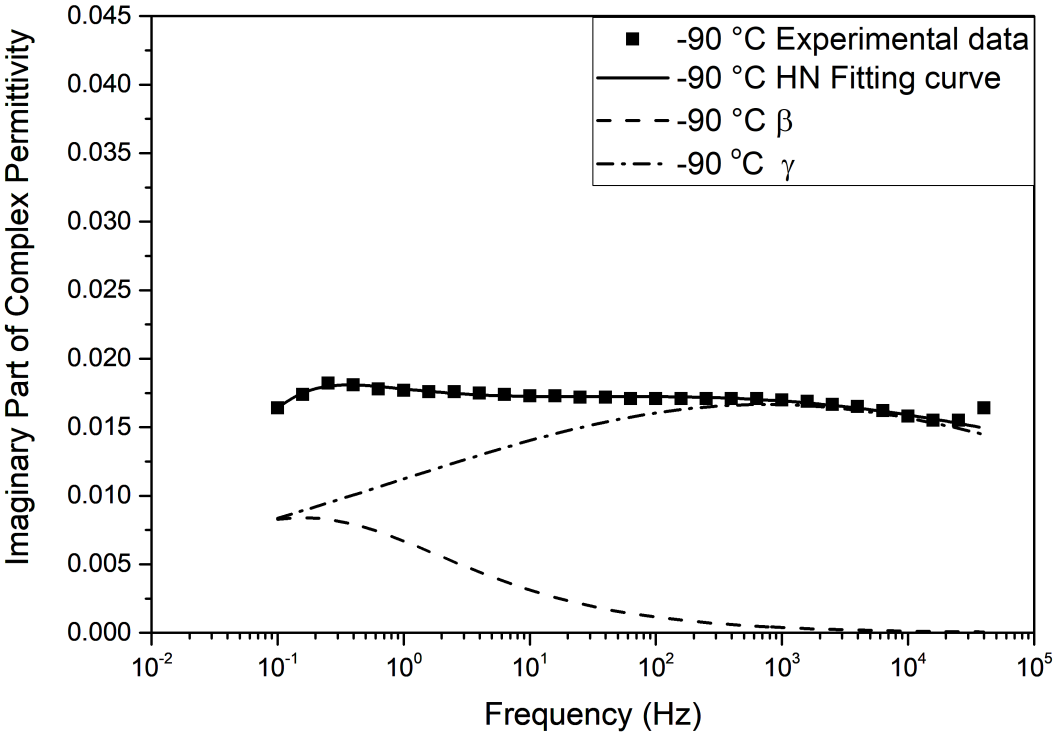

Figure E.51: Havriliak-Negami relaxation fit for 30AGNPE at -90 °C

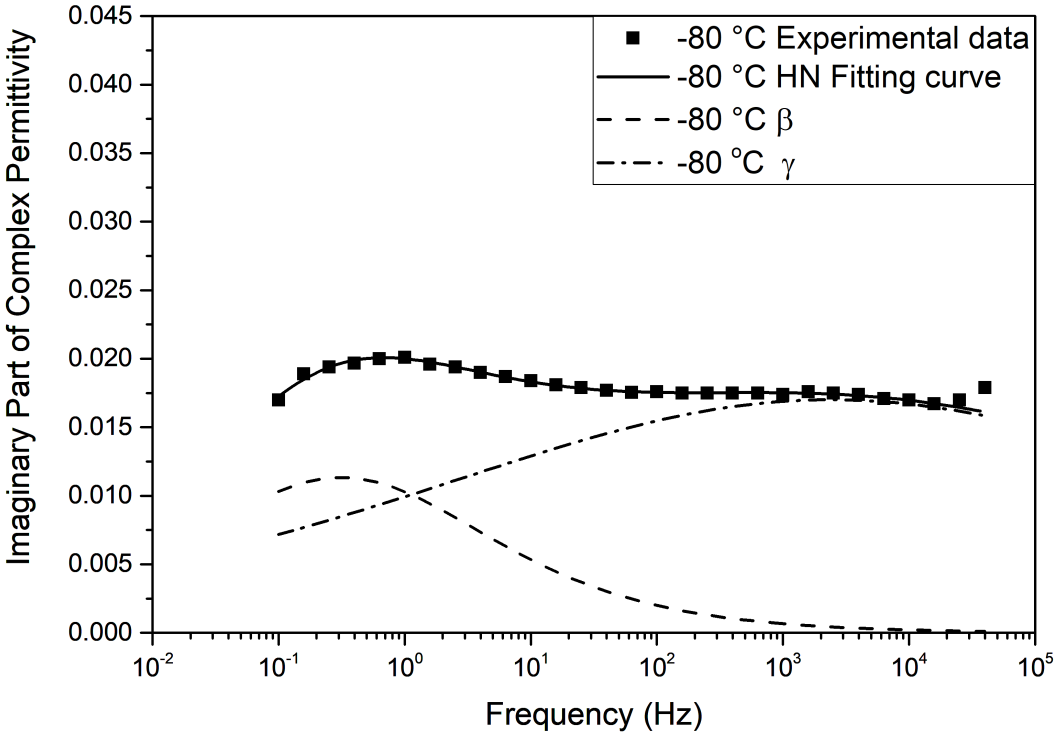

Figure E.52: Havriliak-Negami relaxation fit for 30AGNPE at -80 °C

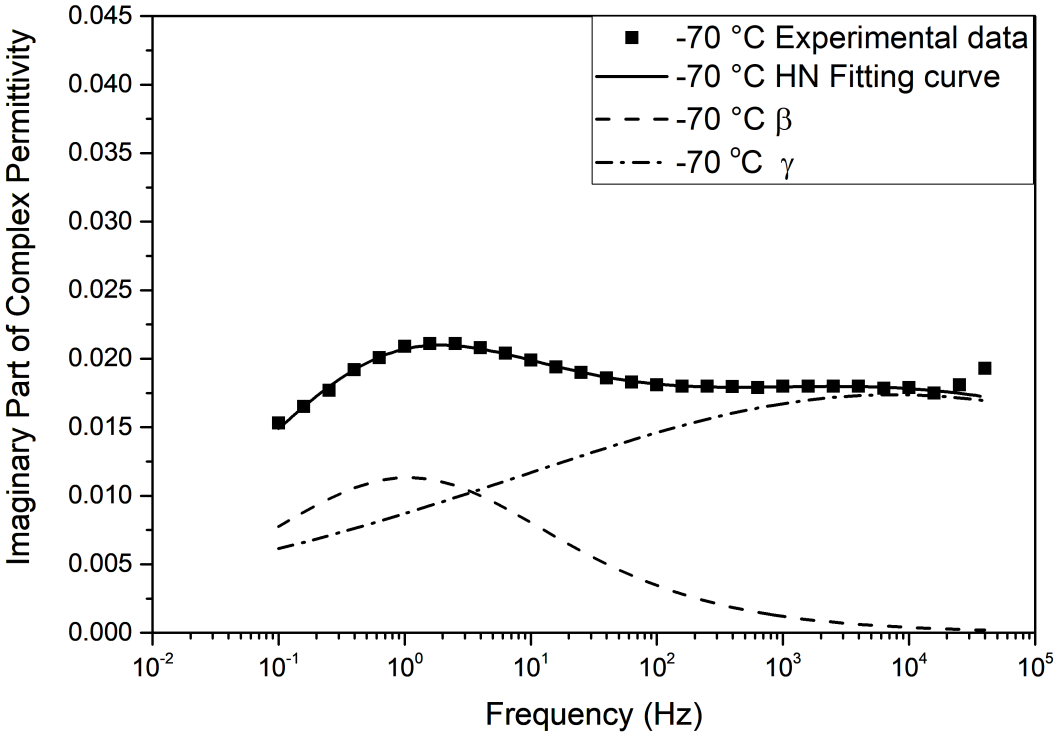

Figure E.53: Havriliak-Negami relaxation fit for 30AGNPE at -70 °C

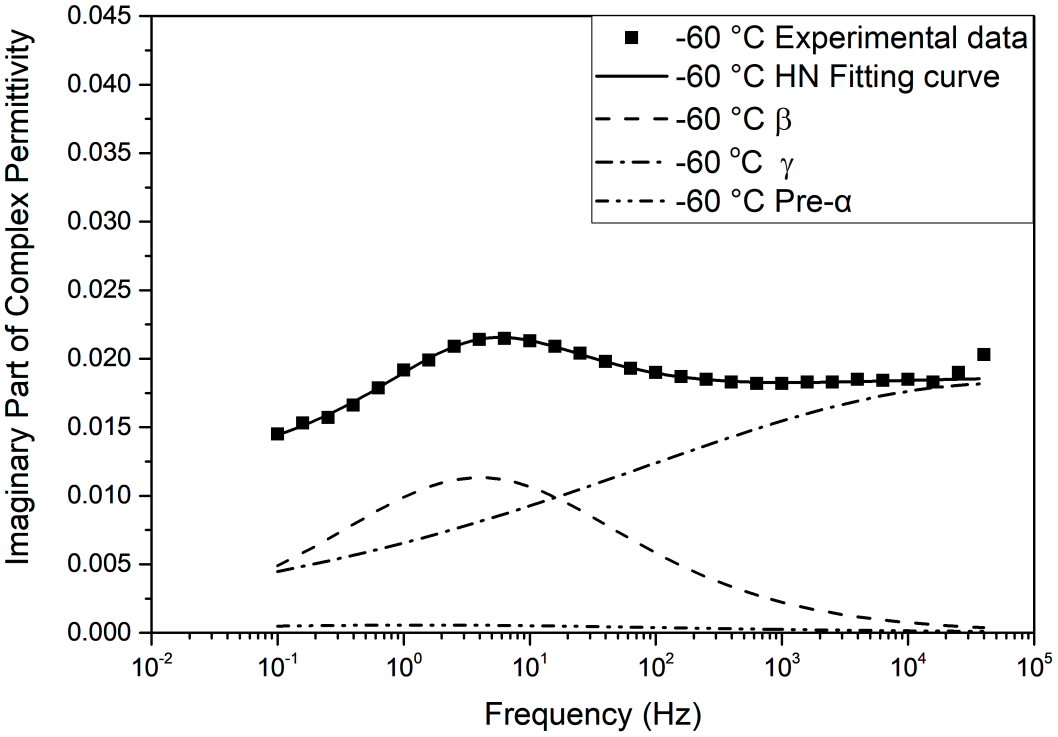

Figure E.54: Havriliak-Negami relaxation fit for 30AGNPE at -60 °C

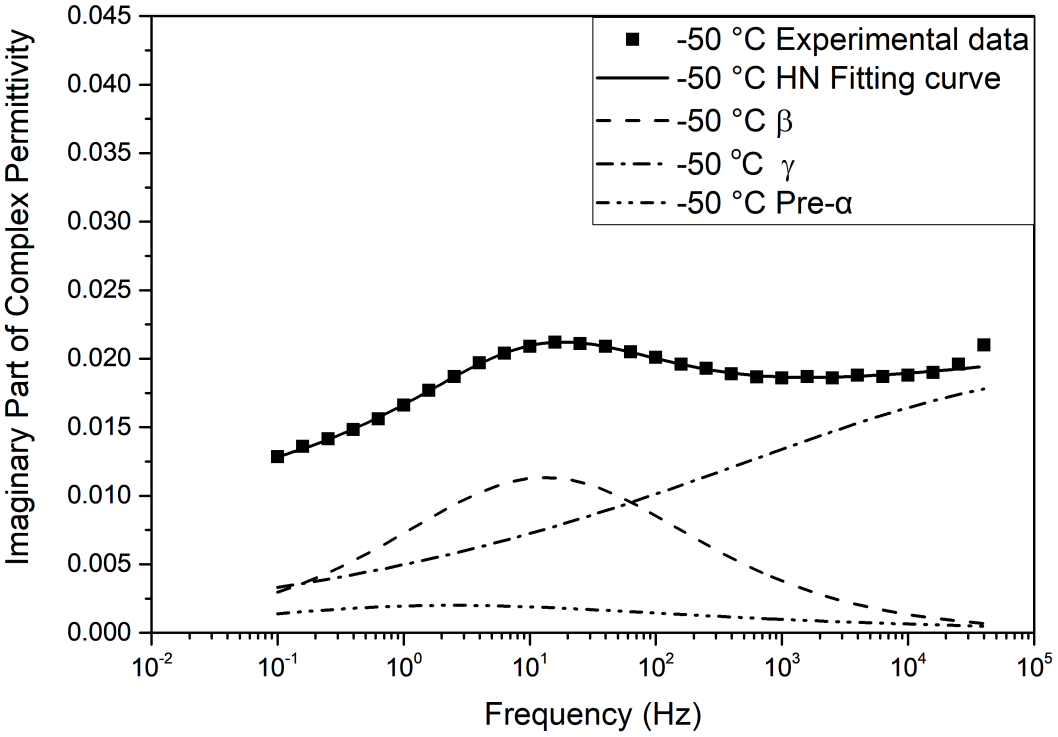

Figure E.55: Havriliak-Negami relaxation fit for 30AGNPE at -50 °C

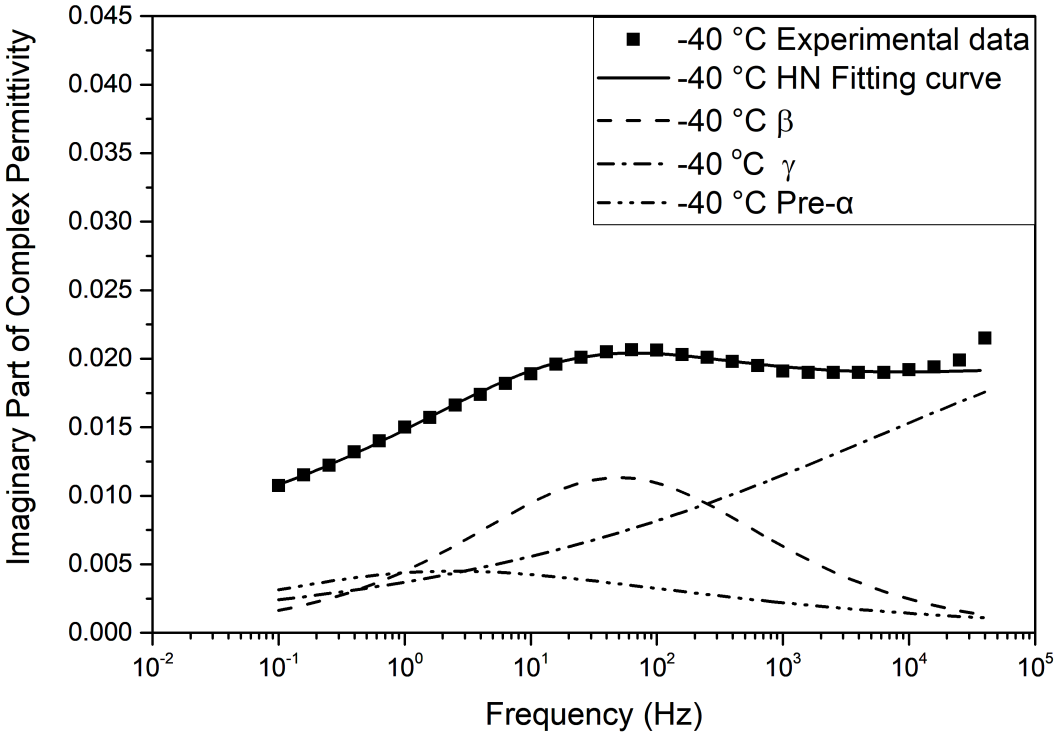

Figure E.56: Havriliak-Negami relaxation fit for 30AGNPE at -40 °C

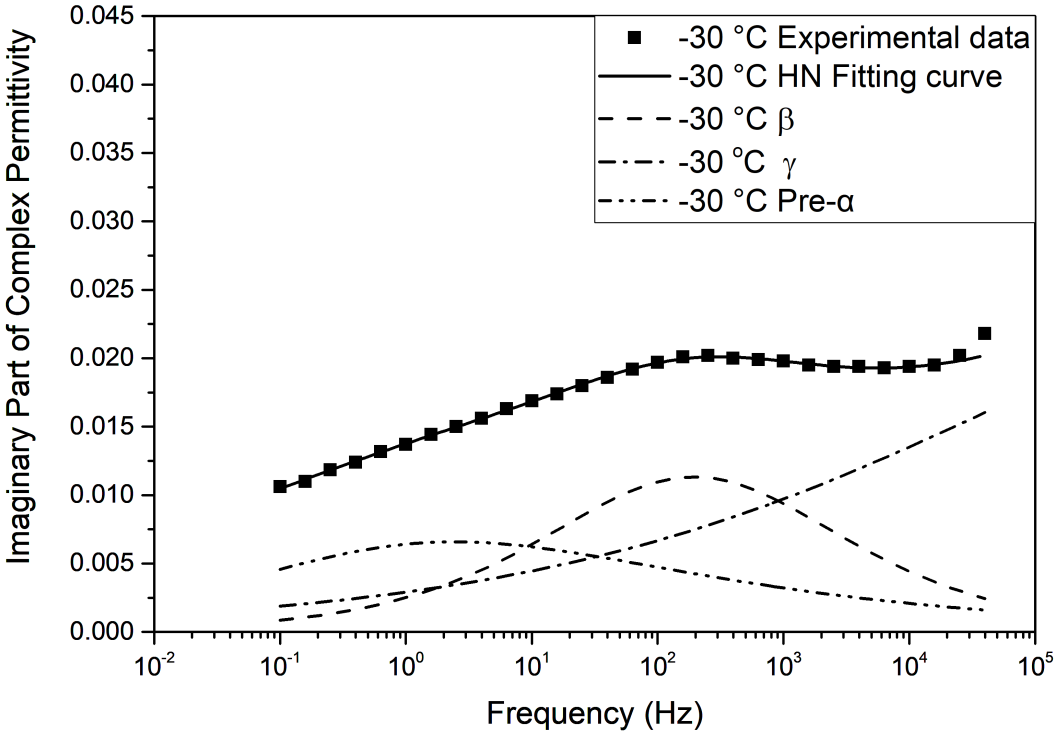

Figure E.57: Havriliak-Negami relaxation fit for 30AGNPE at -30 °C

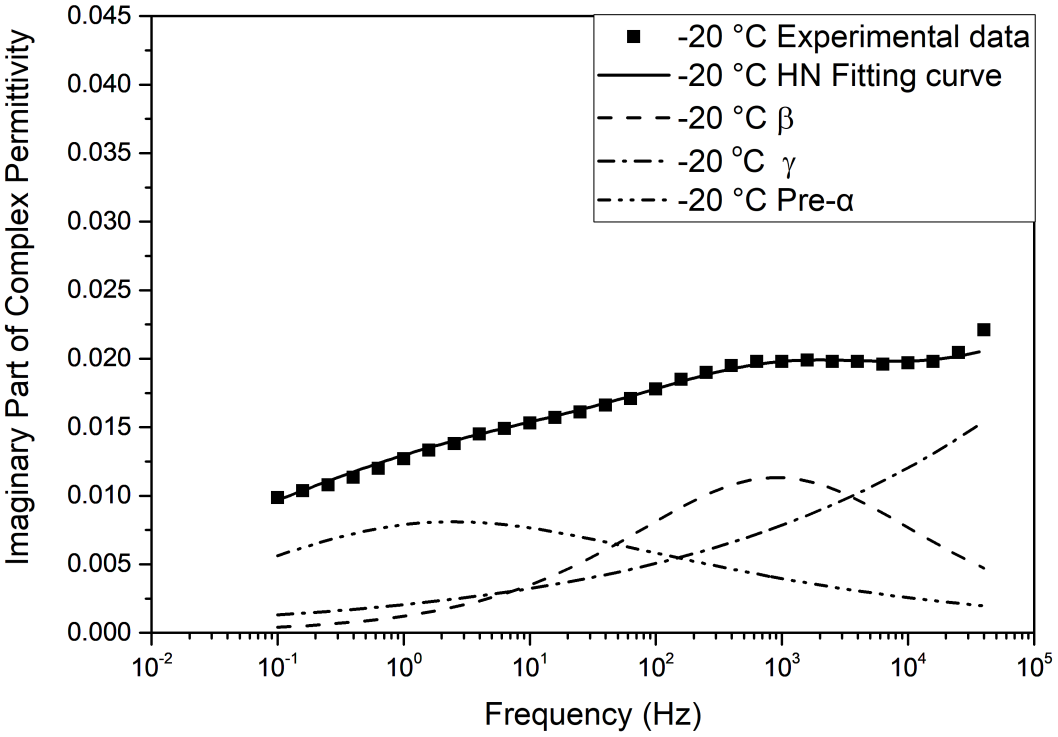

Figure E.58: Havriliak-Negami relaxation fit for 30AGNPE at -20 °C

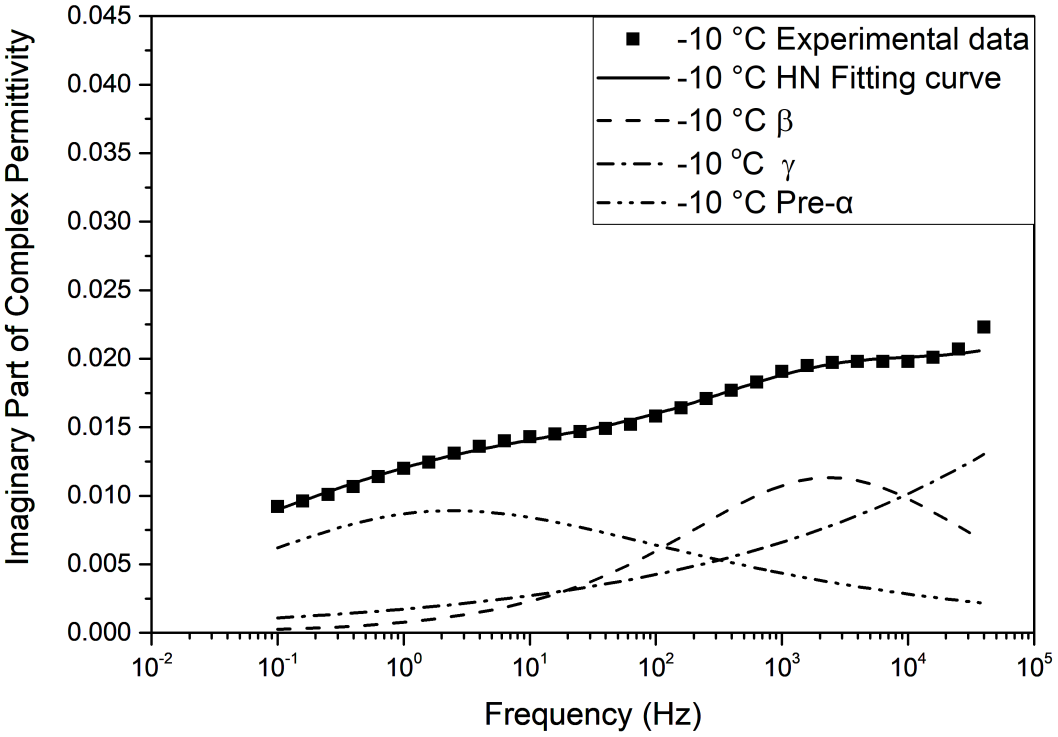

Figure E.59: Havriliak-Negami relaxation fit for 30AGNPE at -10 °C

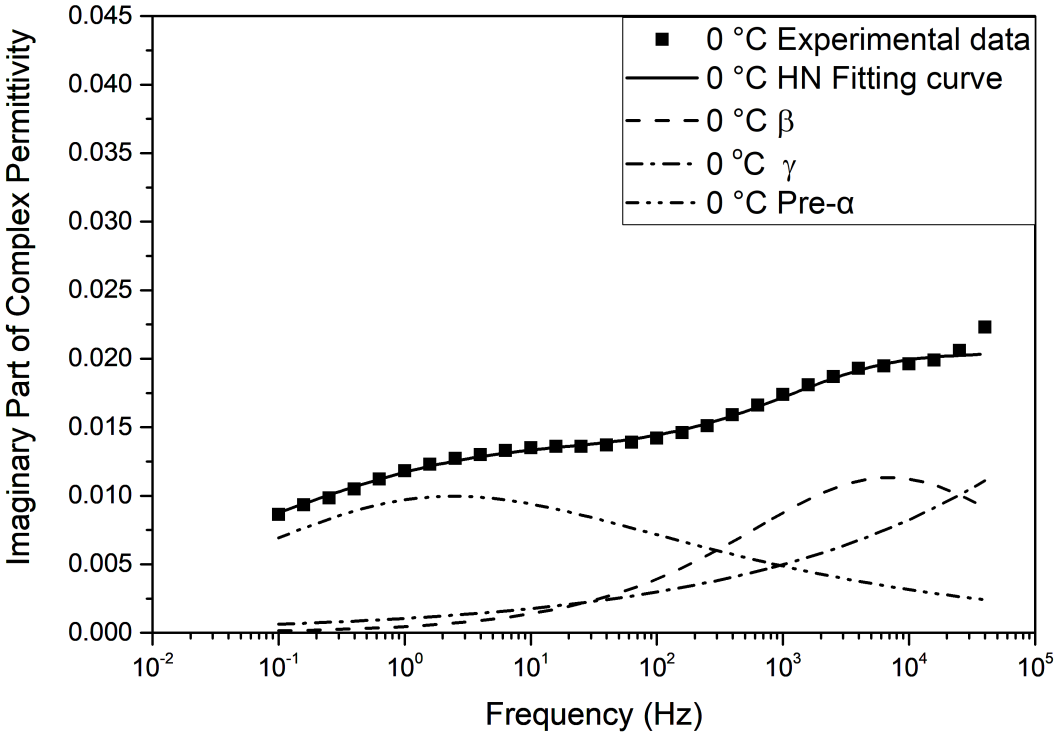

Figure E.60: Havriliak-Negami relaxation fit for 30AGNPE at 0 °C

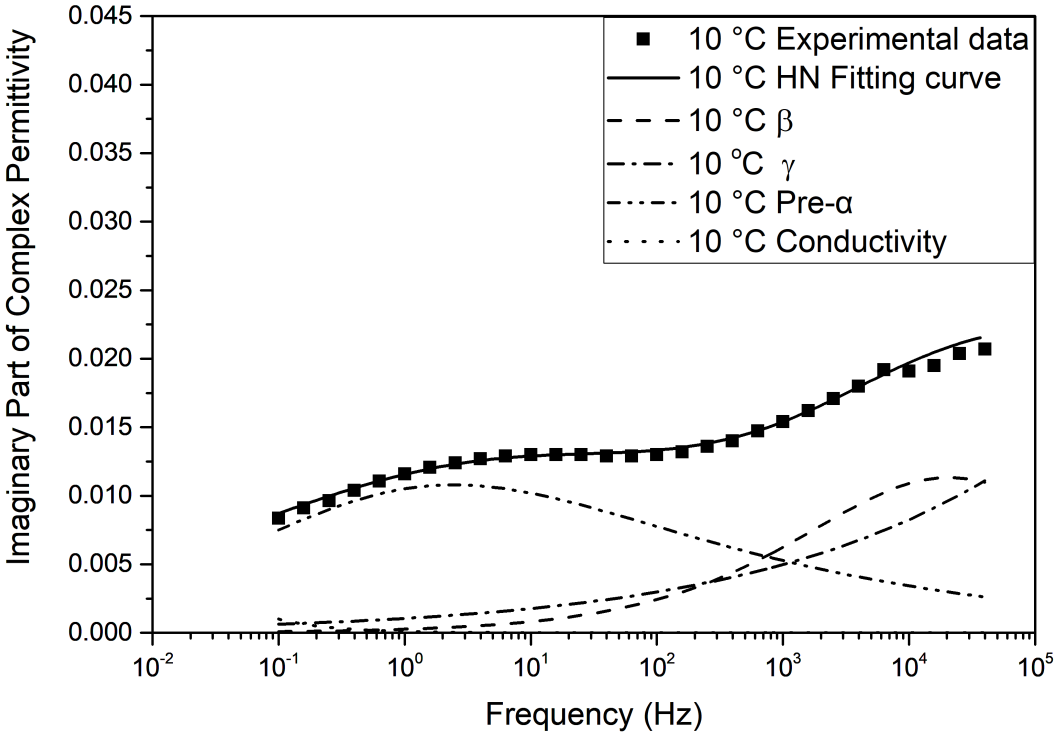

Figure E.61: Havriliak-Negami relaxation fit for 30AGNPE at +10 °C

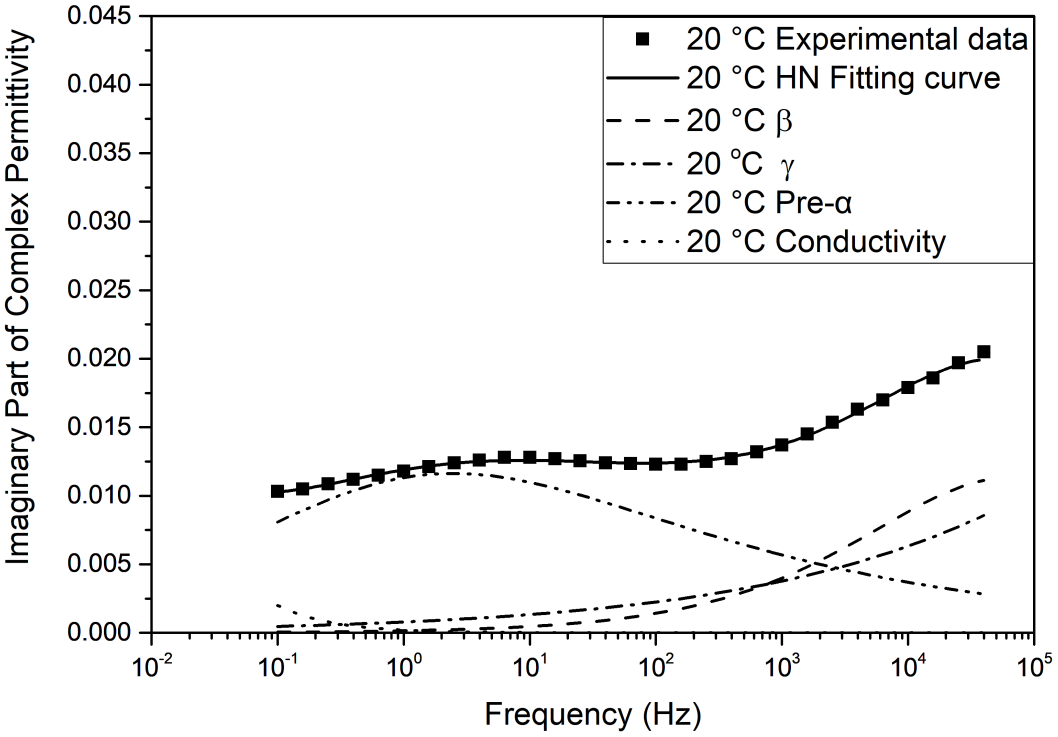

Figure E.62: Havriliak-Negami relaxation fit for 30AGNPE at +20 °C

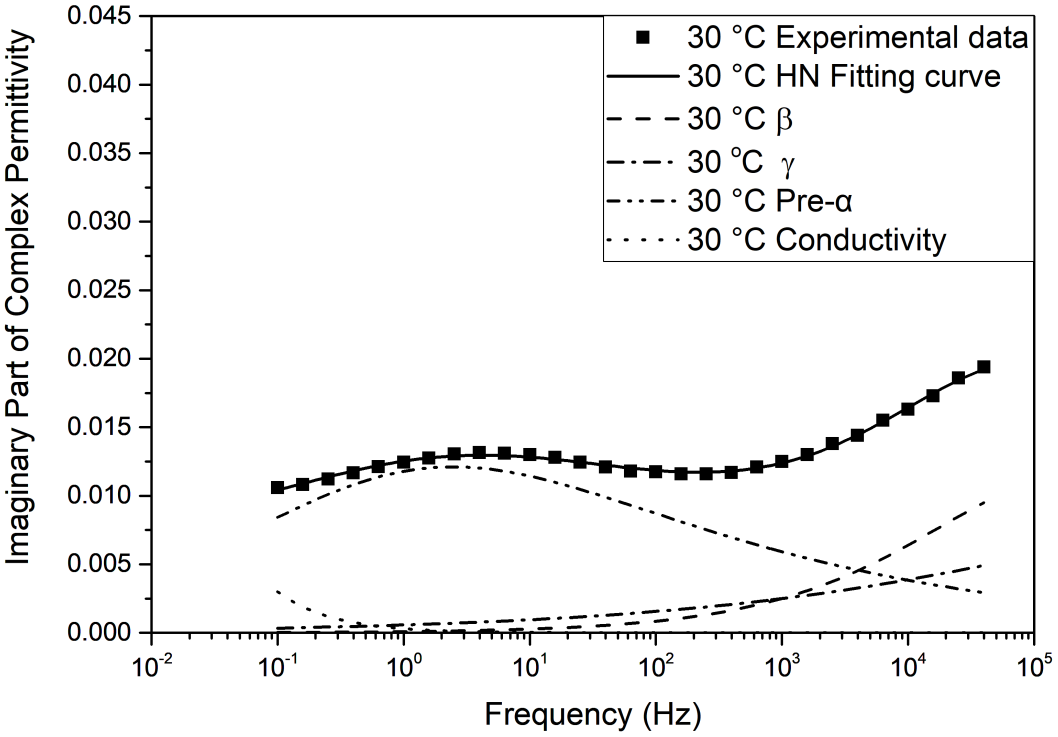

Figure E.63: Havriliak-Negami relaxation fit for 30AGNPE at +30 °C

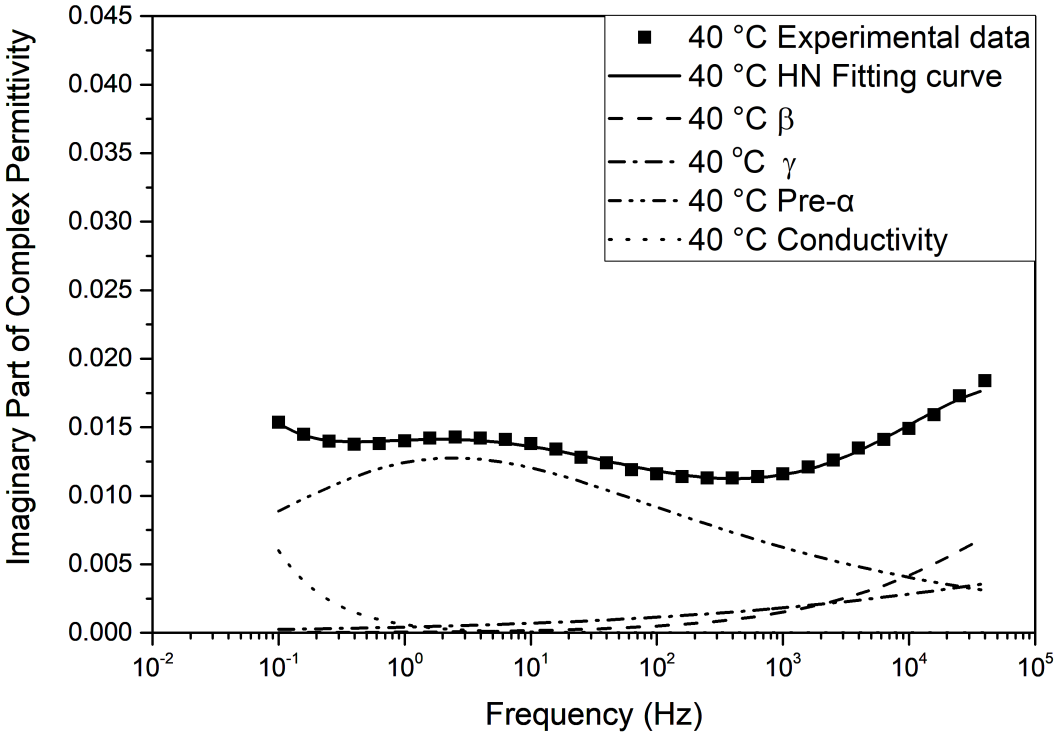

Figure E.64: Havriliak-Negami relaxation fit for 30AGNPE at +40 °C

E.3.2 Havriliak-Negami fit parameters for 30AGNPE systems

Table E.2: Havriliak-Negami fit parameters for 30AGNPE systems

	Process 3				Process 4				Pre Alpha			
°C	α	β	τ	$\Delta\varepsilon$	α	β	τ	$\Delta\varepsilon$	α	β	τ	$\Delta\varepsilon$
-160	0.2821	1	1.32	0.06666	0.2006	0.8294	0.001021	0.07677	–	–	–	–
-150	0.2821	1	1.147	0.06729	0.2006	0.8294	0.00255	0.09317	–	–	–	–
-140	0.2821	1	0.8722	0.05958	0.2006	0.8294	0.0025	0.1084	–	–	–	–
-130	0.2821	1	0.3455	0.06318	0.2006	0.8294	0.002614	0.1276	–	–	–	–
-120	0.2821	1	0.2975	0.0643	0.2006	0.8294	0.00232	0.1447	–	–	–	–
-110	0.2821	1	1.494	0.05646	0.2006	0.8294	0.001278	0.164	–	–	–	–
-100	0.2821	1	7.208	0.07834	0.2006	0.8294	6.24E-04	0.1946	–	–	–	–
-90	0.491	1	1.006	0.04137	0.2006	0.8294	5.43E-04	0.2231	–	–	–	–
-80	0.5	1	0.5074	0.05469	0.2006	0.8294	1.67E-04	0.2277	–	–	–	–
-70	0.5	1	0.1499	0.05469	0.2006	0.8294	5.35E-05	0.2326	–	–	–	–
-60	0.5	1	0.04	0.05469	0.1976	1	2.63E-06	0.2327	0.304	0.881	0.179	0.00487
-50	0.5	1	0.01205	0.05469	0.1976	0.9933	4.21E-07	0.2399	0.4314	0.4625	0.3648	0.01557
-40	0.5	1	0.00322	0.05469	0.2006	0.8294	7.41E-08	0.2954	0.4314	0.4625	0.3648	0.03492
-30	0.5	1	8.21E-04	0.05469	0.2006	0.8294	1.28E-08	0.3207	0.4314	0.4625	0.3648	0.05108
-20	0.5	1	1.75E-04	0.05469	0.2006	0.8294	1.00E-11	0.9054	0.4314	0.4625	0.3648	0.06348
-10	0.5	1	6.73E-05	0.05469	0.2005	0.6975	1.00E-11	0.9001	0.4314	0.4625	0.3648	0.06912
0	0.5	1	2.31E-05	0.05469	0.2289	0.5505	1.00E-11	1.183	0.4314	0.4625	0.3648	0.07723
10	0.5	1	7.64E-06	0.05469	0.2289	0.5505	1.00E-11	1.183	0.4314	0.4625	0.3648	0.0837
20	0.5	1	2.40E-06	0.05469	0.2289	0.5505	1.00E-12	1.5	0.4314	0.4625	0.3648	0.0902
30	0.5	1	8.20E-07	0.05469	0.2289	0.5505	6.87E-09	0.1483	0.4314	0.4625	0.3648	0.0939
40	0.5	1	2.70E-07	0.05469	0.2289	0.5505	6.87E-09	0.1083	0.4314	0.4625	0.3648	0.0989

E.4 Havriliak-Negami relaxation fit for 30AGHE systems

The dielectric data of the 30AGHE system for temperatures from -160 °C to 10 °C was analysed using Havriliak-Negami fit function. The outcome of the analysis is plotted in the figures below from Figure fig. E.69 to fig. E.85. The parameters used in the Havriliak-Negami fit function are listed in Table E.3. To compare the de-convoluted peaks at different temperature, the peaks associated with the β- relaxation, the γ- relaxation, pre-alpha process and the bi-furation of the γ- relaxation are plotted in separate figures (Figure E.65 and Figure E.66, E.67 respectively.

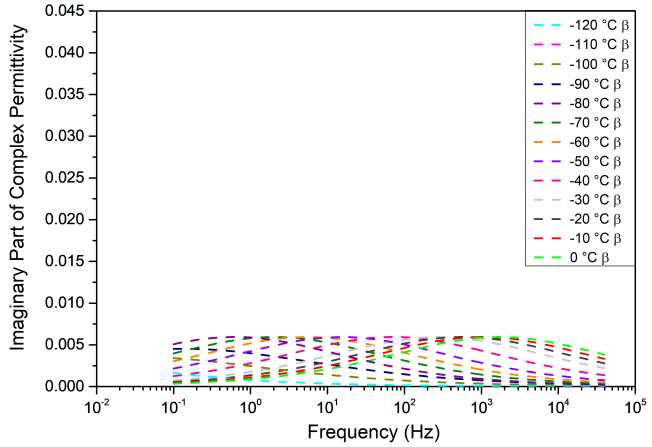

(a) 30AGHE Sample Beta

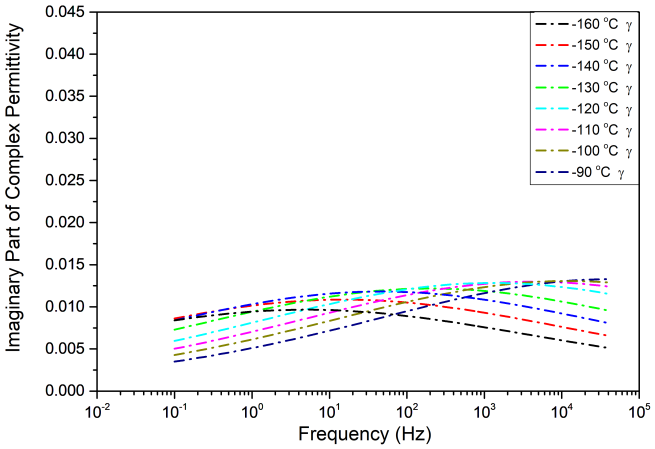

(b) 30AGHE Sample Gamma part 1

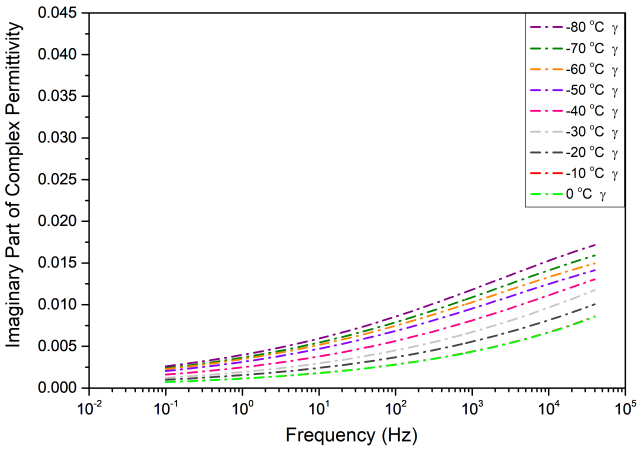

(c) 30AGHE Sample Gamma part 2

Figure E.65: Plots of the deconvoluted temperature dependence of γ and β relaxation peaks using Havriliak-Negami fit for 30AGHE sample

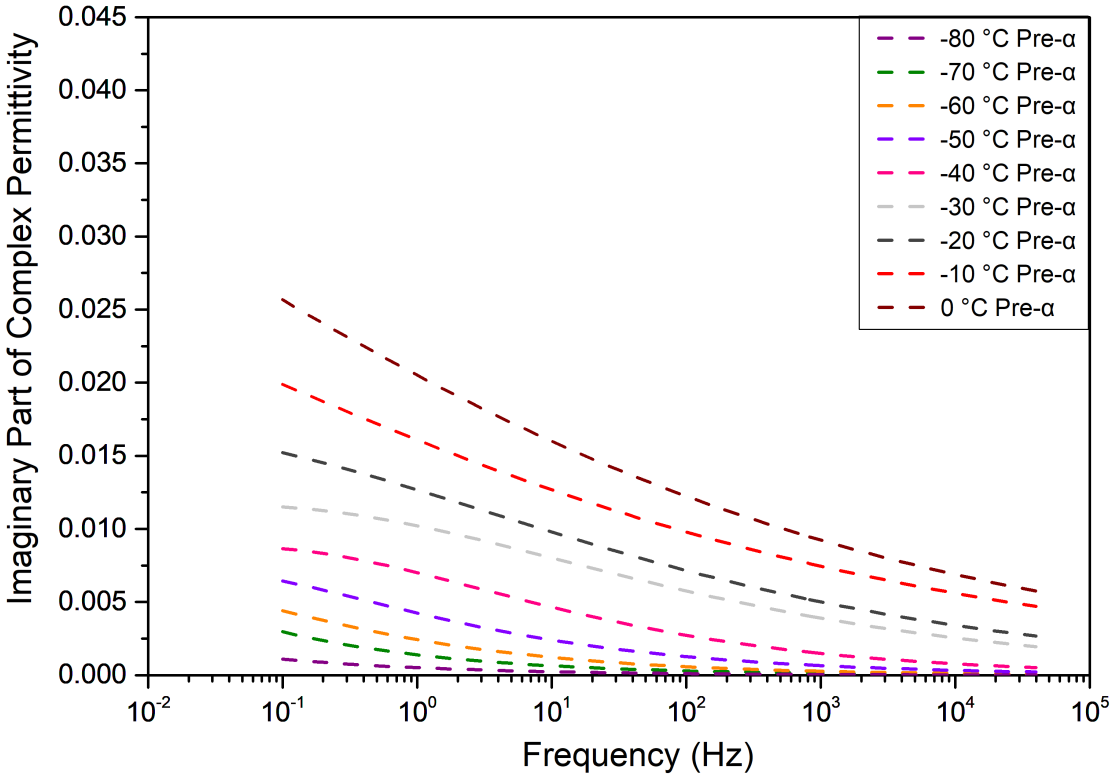

Figure E.66: Plots of the deconvoluted temperature dependence pre alpha process using Havriliak-Negami fit for 30AGHE sample

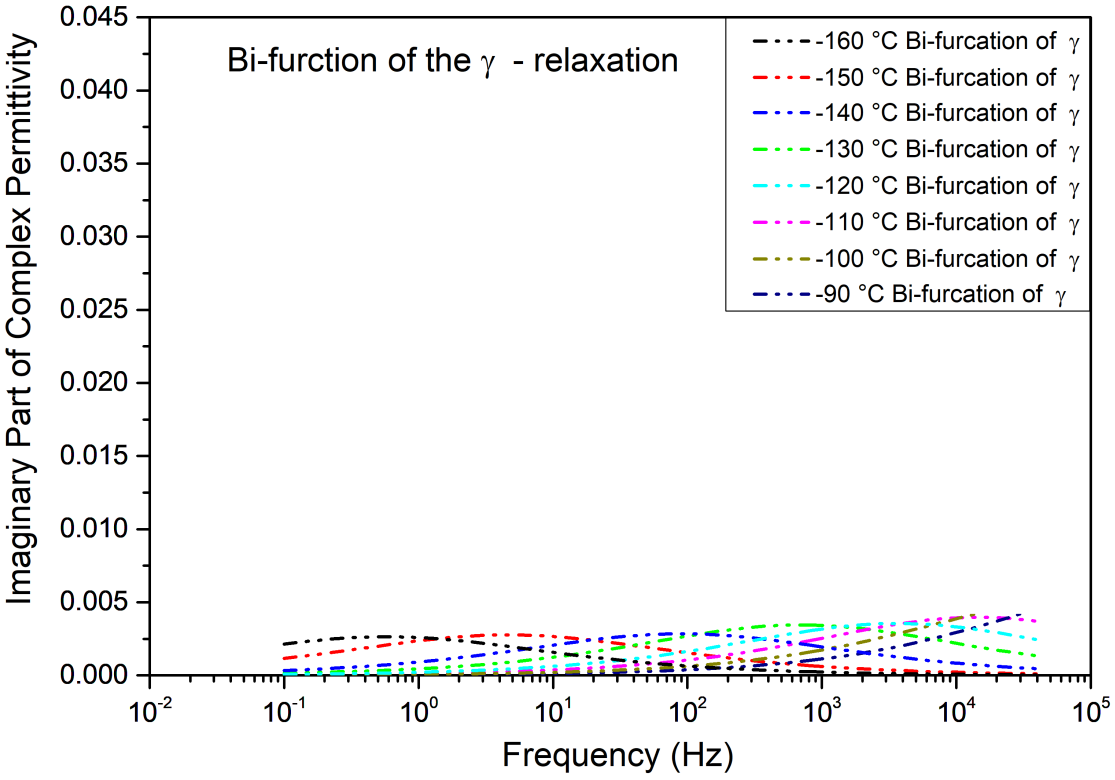

Figure E.67: Plots of the deconvoluted temperature dependence bifurcation of gamma process using Havriliak-Negami fit for 30AGHE sample

E.4.1 Havriliak-Negami fit for 30AGHE systems

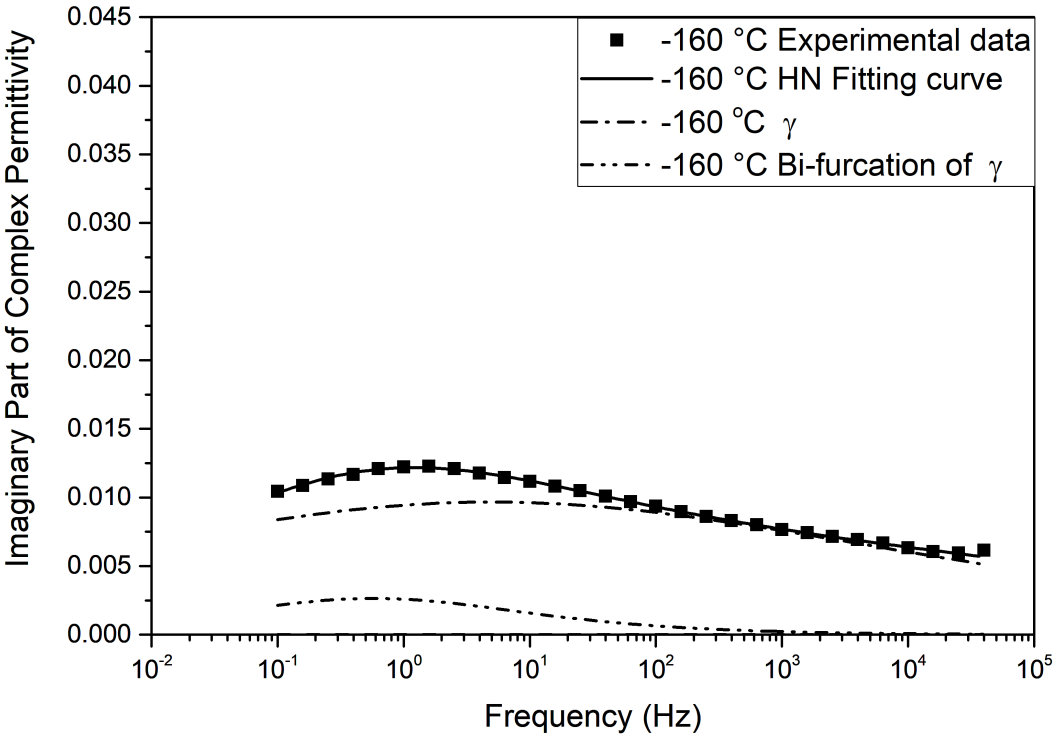

Figure E.68: Havriliak-Negami relaxation fit for 30AGHE system at -160 °C

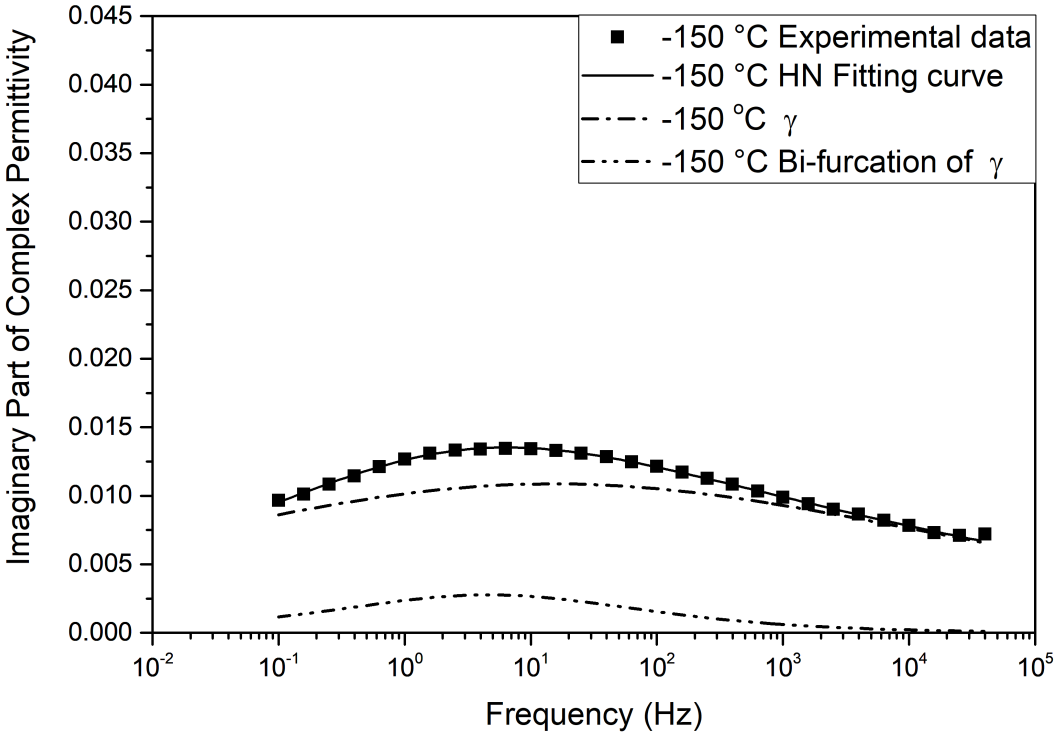

Figure E.69: Havriliak-Negami relaxation fit for 30AGHE system at -150 °C

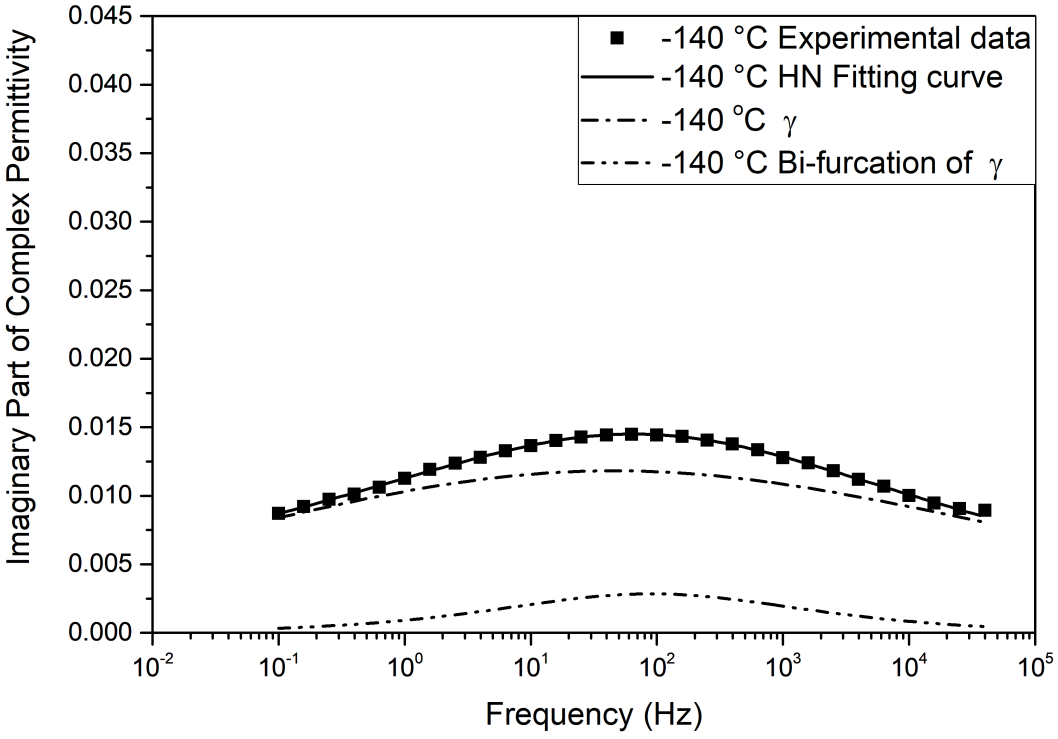

Figure E.70: Havriliak-Negami relaxation fit for 30AGHE system at -140 °C

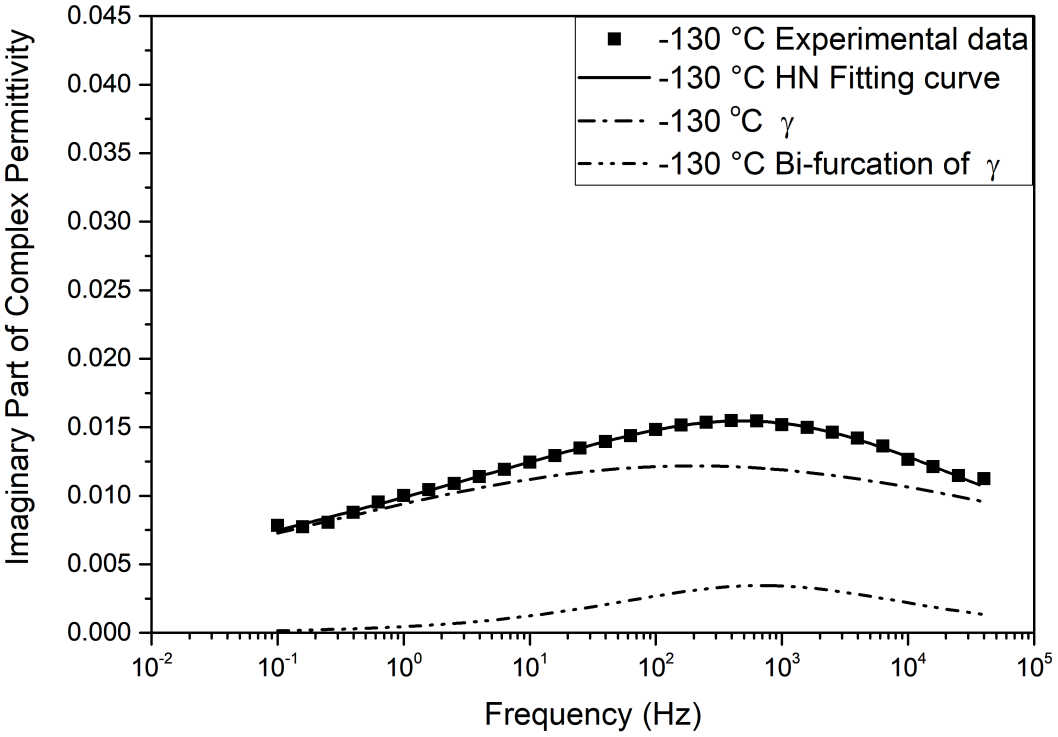

Figure E.71: Havriliak-Negami relaxation fit for 30AGHE system at -130 °C

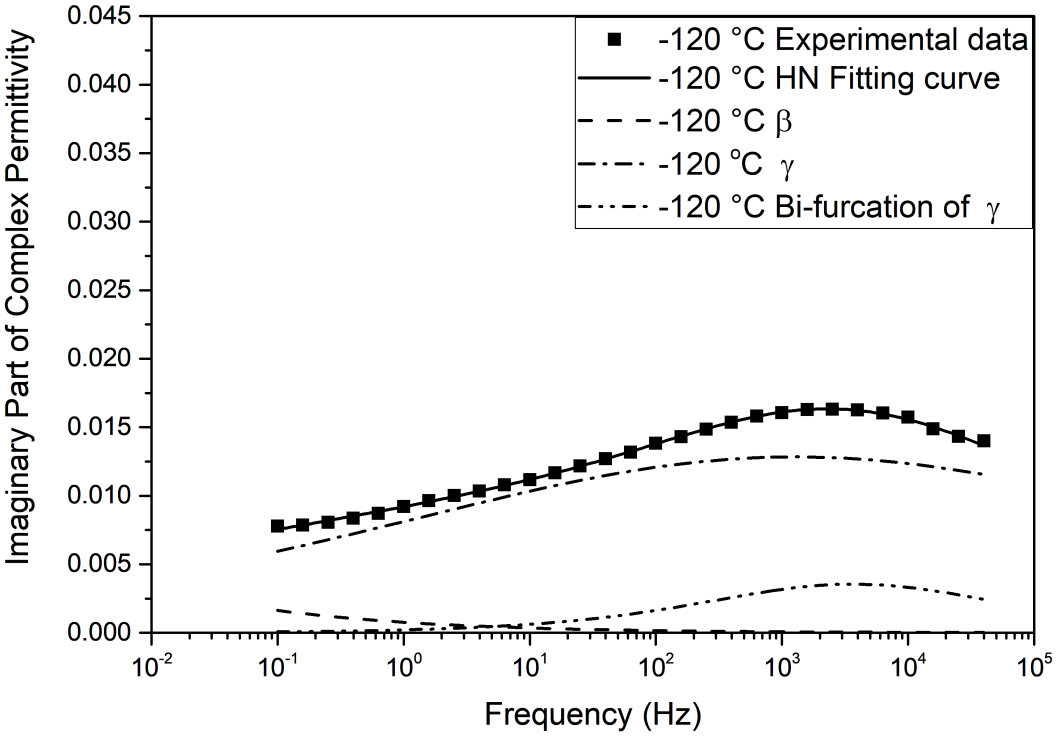

Figure E.72: Havriliak-Negami relaxation fit for 30AGHE system at -120 °C

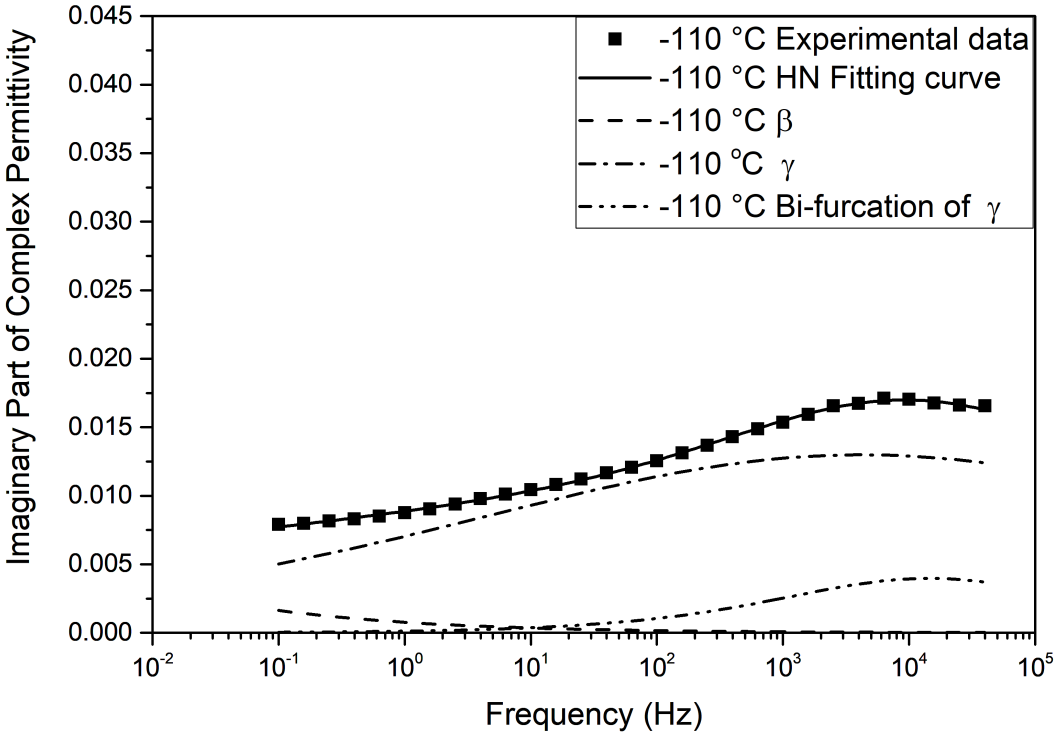

Figure E.73: Havriliak-Negami relaxation fit for 30AGHE system at -110 °C

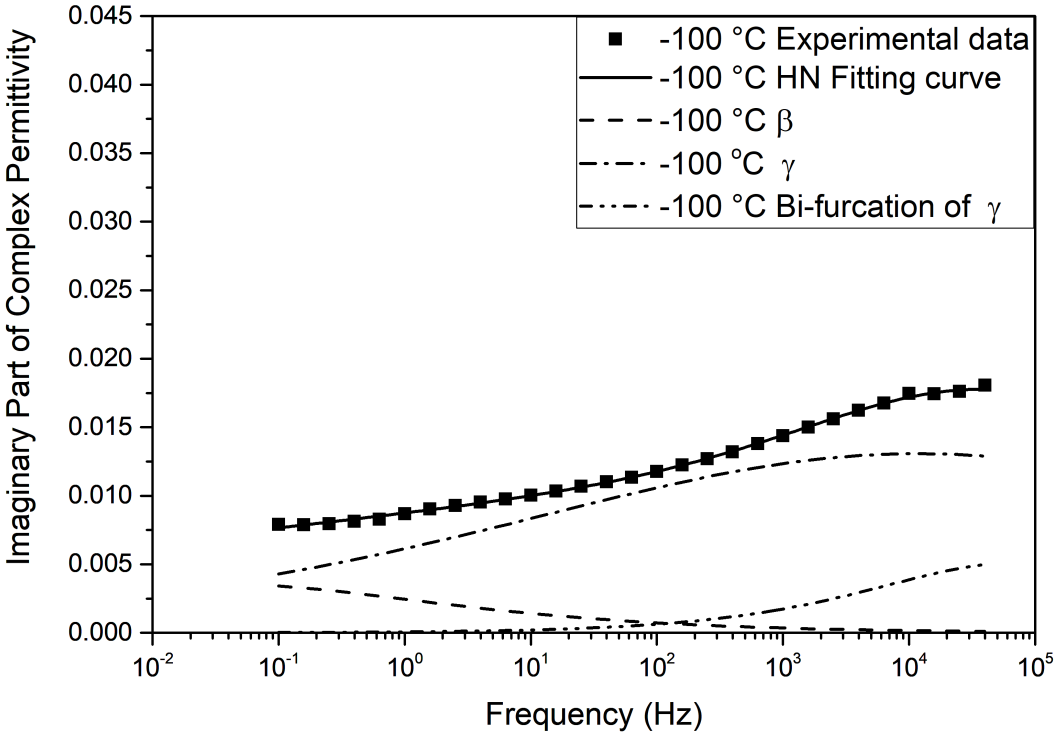

Figure E.74: Havriliak-Negami relaxation fit for 30AGHE system at -100 °C

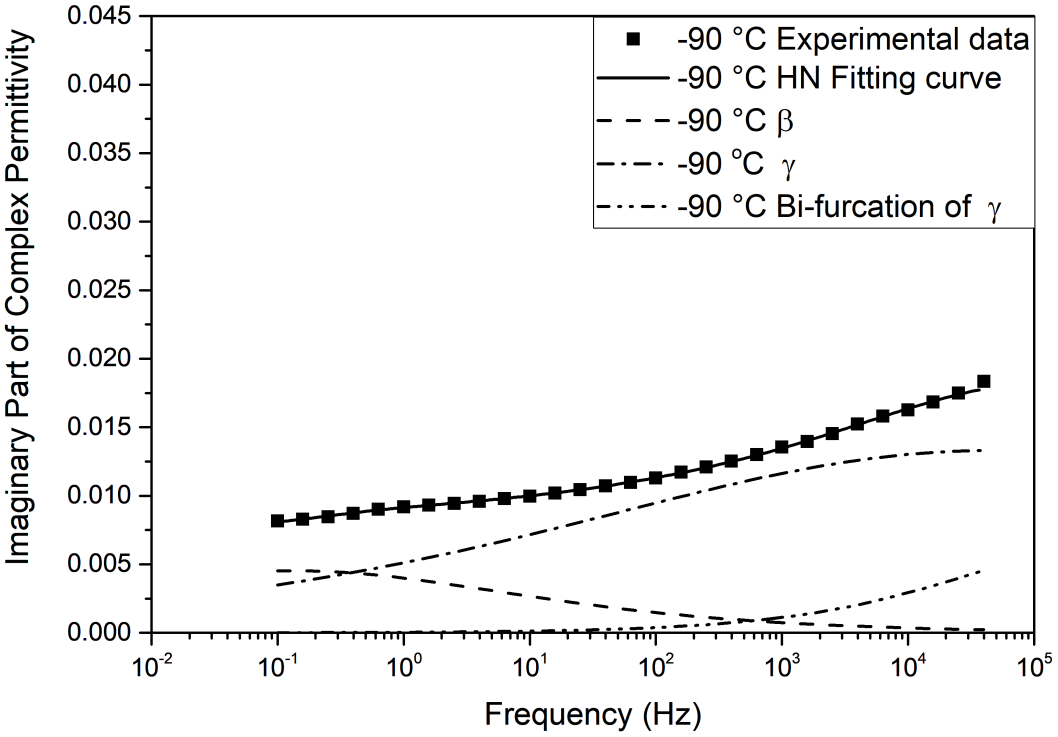

Figure E.75: Havriliak-Negami relaxation fit for 30AGHE system at -90 °C

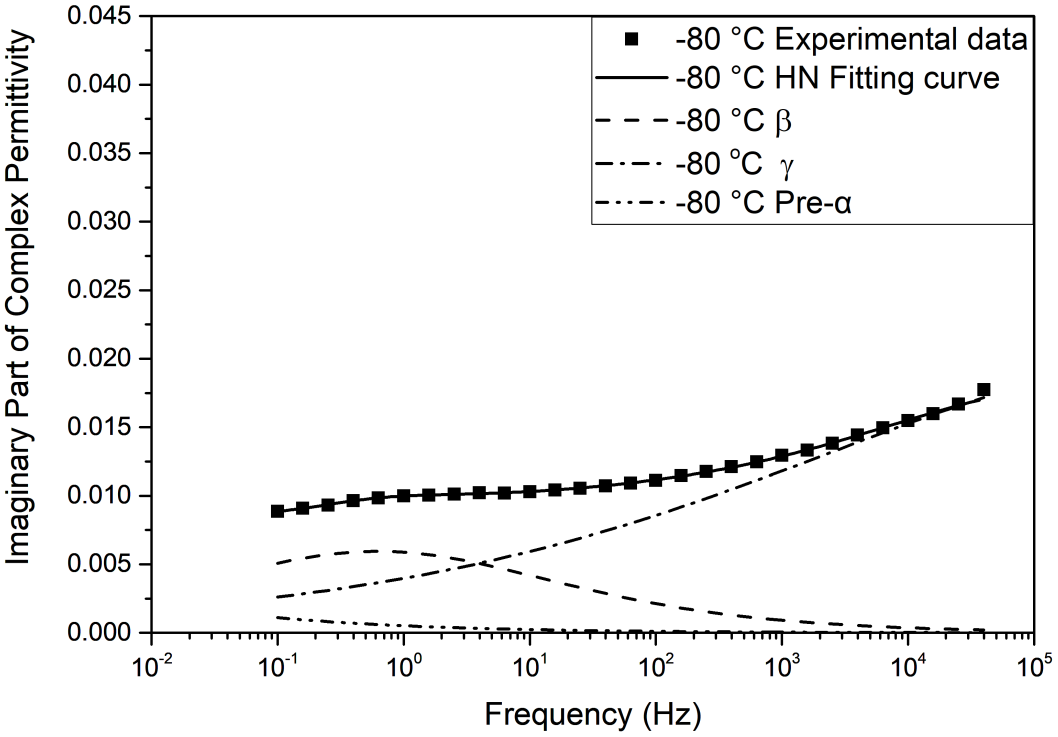

Figure E.76: Havriliak-Negami relaxation fit for 30AGHE system at -80 °C

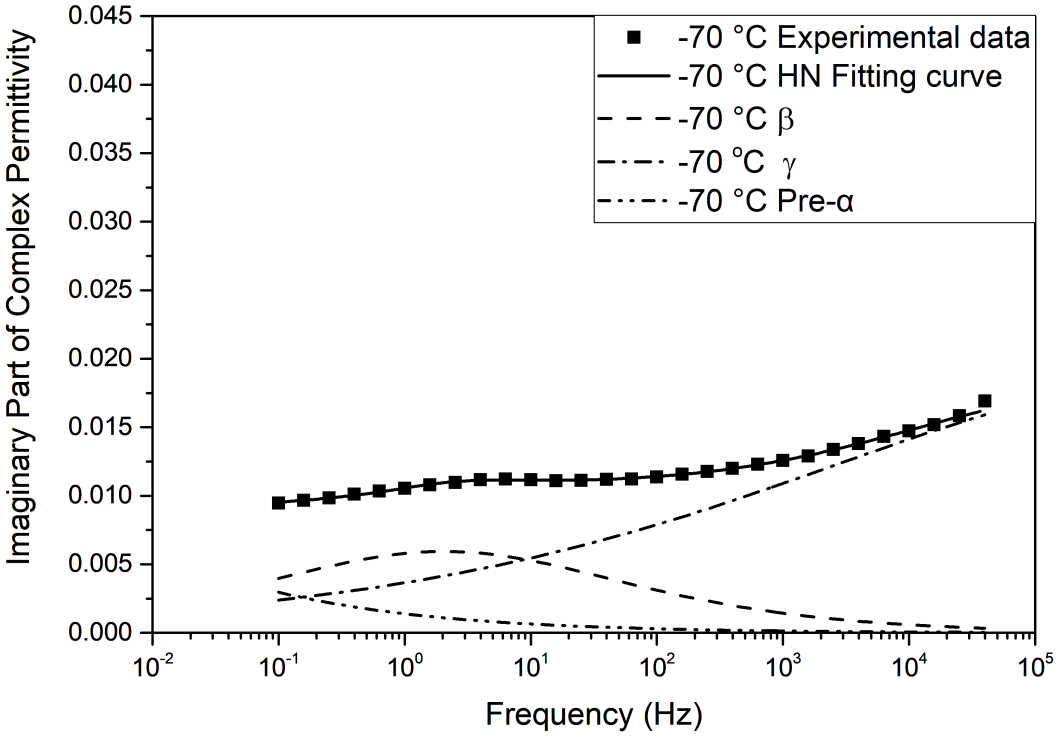

Figure E.77: Havriliak-Negami relaxation fit for 30AGHE system at -70 °C

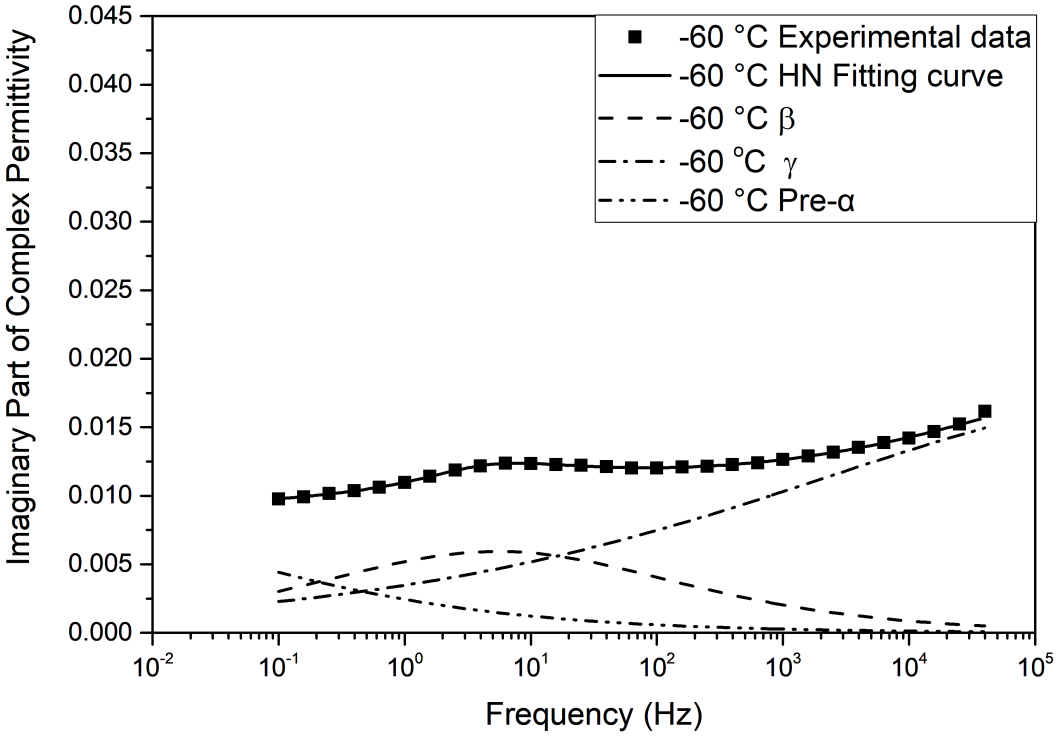

Figure E.78: Havriliak-Negami relaxation fit for 30AGHE system at -60 °C

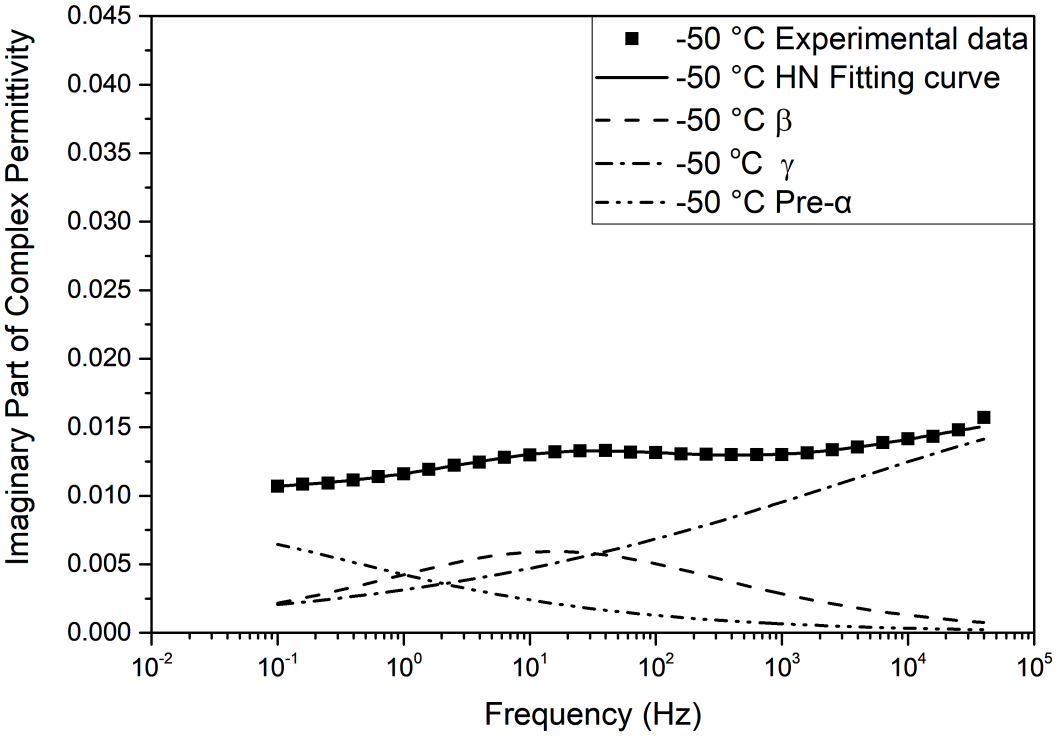

Figure E.79: Havriliak-Negami relaxation fit for 30AGHE system at -50 °C

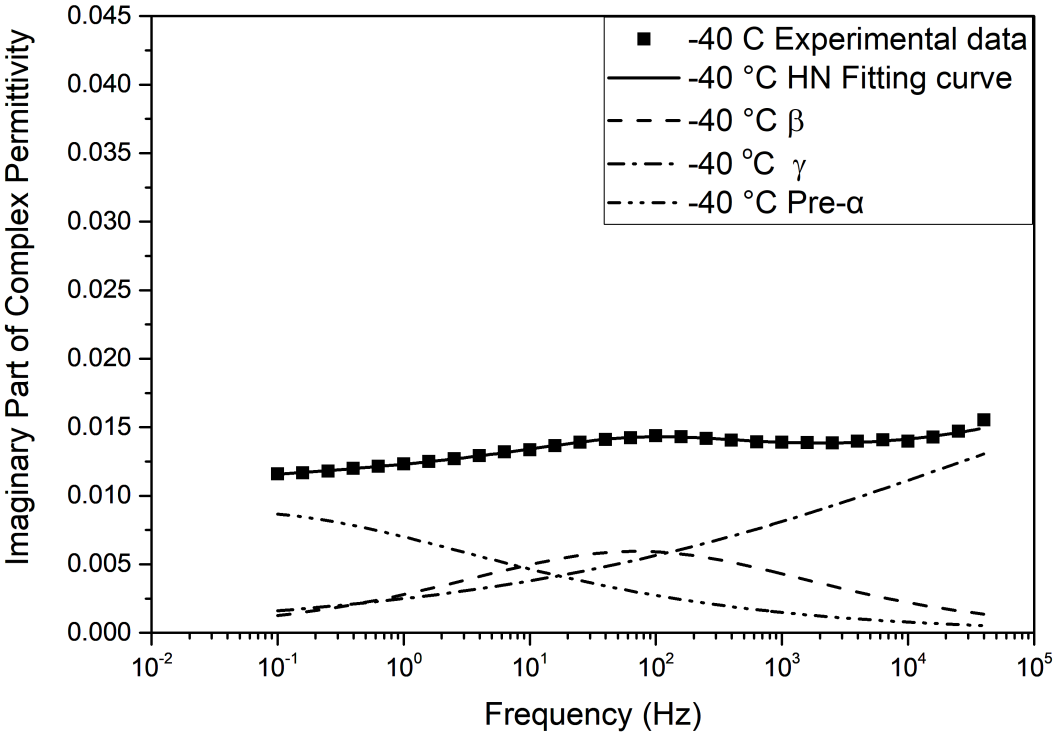

Figure E.80: Havriliak-Negami relaxation fit for 30AGHE system at -40 °C

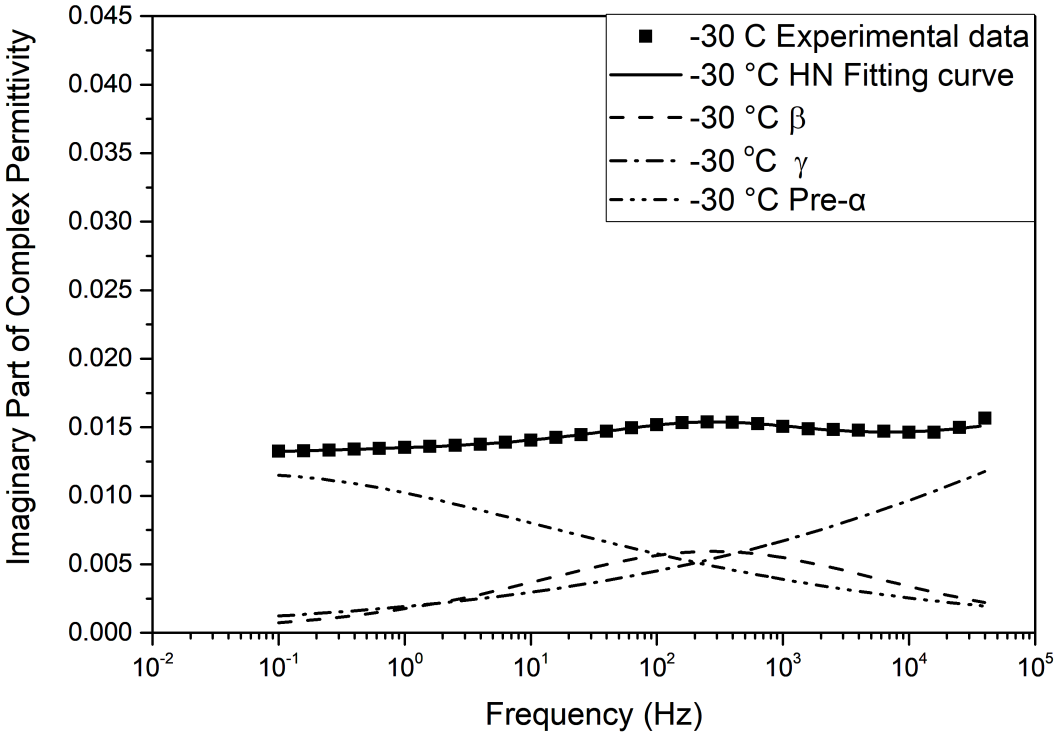

Figure E.81: Havriliak-Negami relaxation fit for 30AGHE system at -30 °C

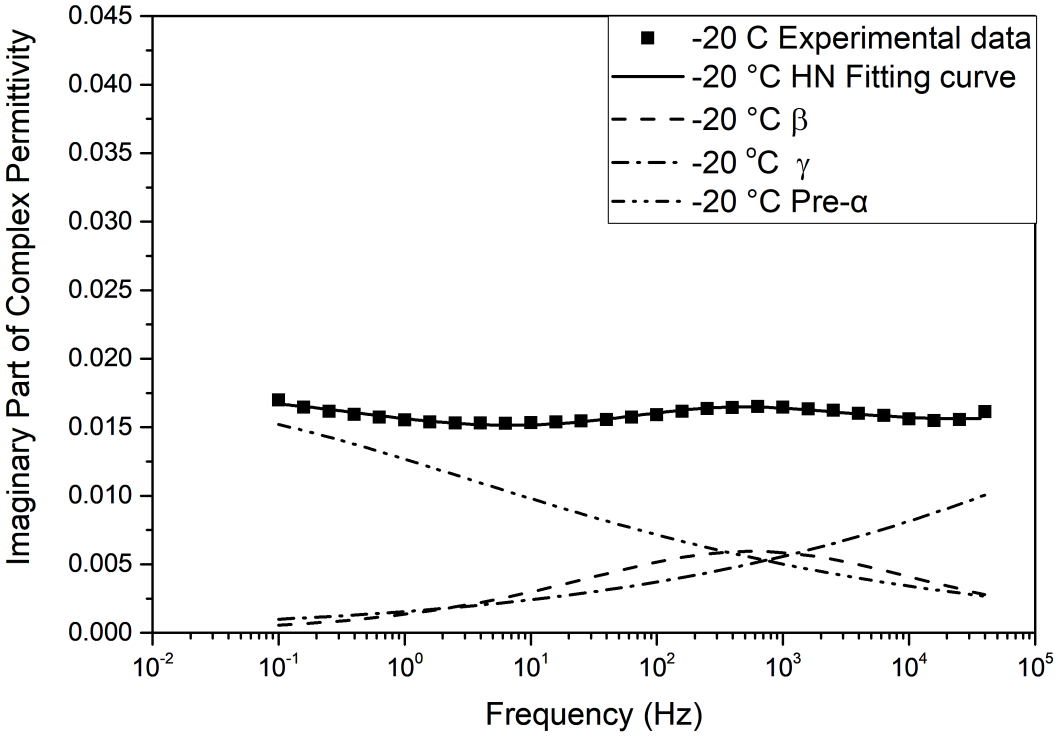

Figure E.82: Havriliak-Negami relaxation fit for 30AGHE system at -20 °C

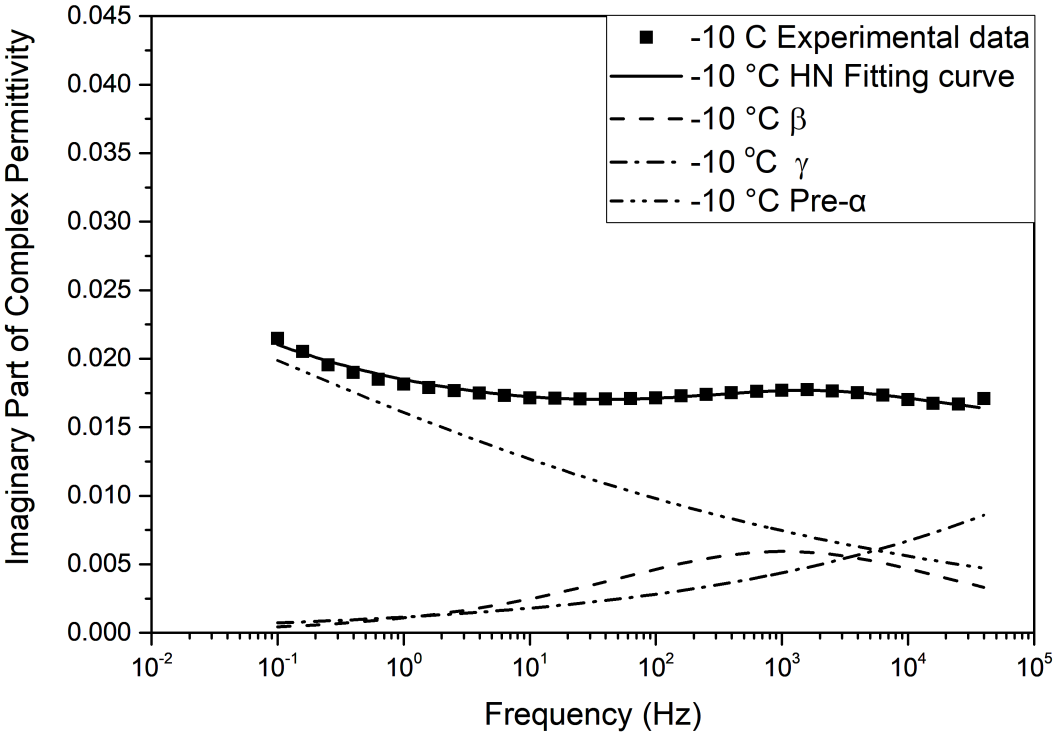

Figure E.83: Havriliak-Negami relaxation fit for 30AGHE system at -10 °C

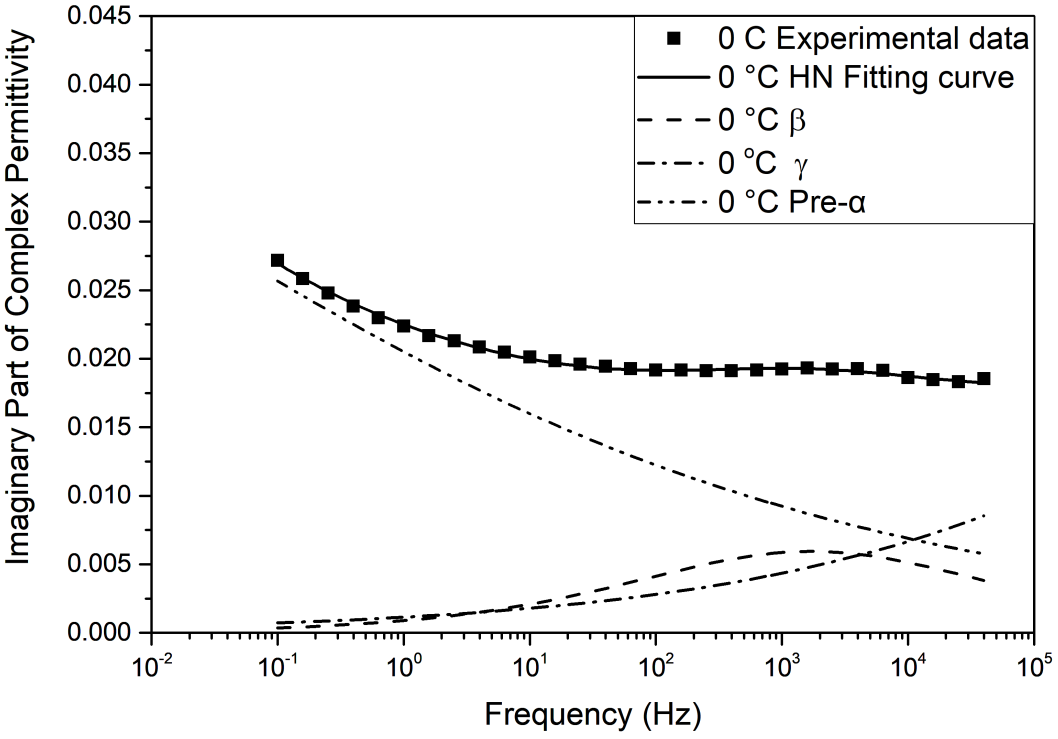

Figure E.84: Havriliak-Negami relaxation fit for 30AGHE system at 0 °C

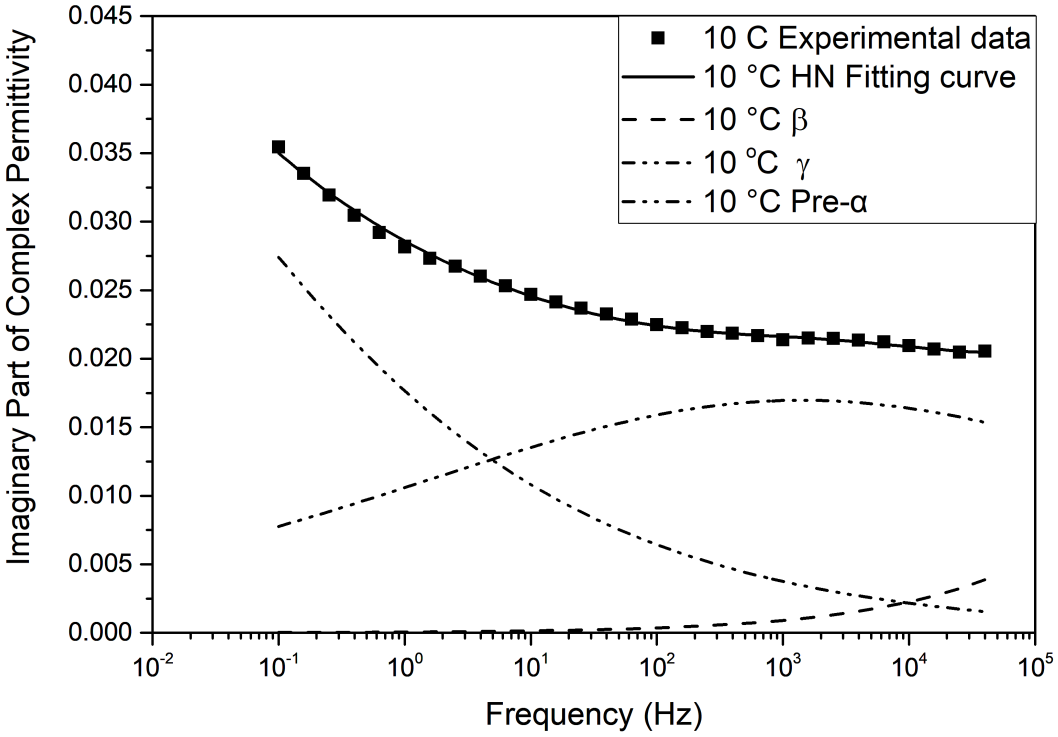

Figure E.85: Havriliak-Negami relaxation fit for 30AGHE system at +10 °C

E.4.2 Havriliak-Negami fit parameters for 30AGHE systems

E.5 Havriliak-Negami relaxation fit for 20AGHE systems

The dielectric data of the 20AGHE system for temperatures from -160 °C to 10 °C was analysed using Havriliak-Negami fit function. The outcome of the analysis is plotted in the figures below from Figure fig. E.89 to fig. E.106. The parameters used in the Havriliak-Negami fit function are listed in Table E.4. To compare the de-convoluted peaks at different temperature, the peaks associated with the β- relaxation, the γ-relaxation, pre-alpha process, the secondary relaxation and the bi-furcation of the γ-relaxation are plotted in separate figures (Figure E.86 and Figure E.87, E.88 respectively.

Table E.3: Havriliak-Negami fit parameters for 30AGHE systems

	Bi-furcation of Gamma				Process 3				Process 4				Pre Alpha			
	α	β	τ	$\Delta\varepsilon$	α	β	τ	$\Delta\varepsilon$	α	β	τ	$\Delta\varepsilon$	α	β	τ	$\Delta\varepsilon$
160	0.491	1	0.2764	0.013	0.2006	0.8294	0.08098	0.1294	0.8	0.8	1.00E-11	1.00E-06				
150	0.491	1	0.0344	0.01365	0.2006	0.8294	0.02669	0.1455	0.8	0.8	1.00E-11	1.00E-06	–	–	–	–
140	0.491	1	0.001774	0.014	0.2006	0.8294	0.008777	0.1583	0.8	0.8	1.00E-11	1.00E-06	–	–	–	–
130	0.491	1	2.29E-04	0.017	0.2006	0.8294	0.002019	0.1631	0.8	0.8	1.00E-11	1.00E-06	–	–	–	–
120	0.491	1	4.36E-05	0.01751	0.2006	0.8294	3.15E-04	0.1719	0.339	1	33560	0.1	–	–	–	–
110	0.491	1	1.12E-05	0.01957	0.2006	0.8294	9.49E-05	0.1739	0.339	1	33560	0.1	–	–	–	–
100	0.491	1	1.97E-06	0.02547	0.2006	0.8294	3.39E-05	0.175	0.339	1	6.62	0.02672	–	–	–	–
90	0.491	1	4.89E-07	0.03	0.2006	0.8294	9.06E-06	0.178	0.339	1	1.243	0.03323	–	–	–	–
80	–	–	–	–	0.2006	0.8294	1.93E-07	0.2658	0.4166	1	0.2553	0.035	0.339		1	100000	0.09555
70	–	–	–	–	0.2006	0.8294	1.77E-07	0.2479	0.4166	1	0.07806	0.035	0.339		1	100000	0.2579
60	–	–	–	–	0.2006	0.8294	1.96E-07	0.2313	0.4166	1	0.02936	0.035	0.339		1	141.7	0.05674
50	–	–	–	–	0.2006	1	7.38E-08	0.2087	0.4166	1	0.01043	0.035	0.3996	0.7395	24.55	0.0508
40	–	–	–	–	0.2006	0.8294	2.41E-08	0.2436	0.4166	1	0.002283	0.035	0.3066	0.9666	4.057	0.07246
30	–	–	–	–	0.2006	0.8294	2.41E-09	0.29	0.4166	1	5.81E-04	0.035	0.2481	0.8342	6.682	0.1246
20	–	–	–	–	0.2006	0.8294	8.87E-10	0.2848	0.4166	1	2.81E-04	0.035	0.1933	0.9901	46.73	0.2212
10	–	–	–	–	0.2006	0.8294	1.00E-11	0.5043	0.4166	1	1.56E-04	0.035	0.1419	0.9683	49790	0.5746
0	–	–	–	–	0.2006	0.8294	1.00E-11	0.5015	0.4166	1	9.30E-05	0.035	0.1419	0.9864	88670	0.7905
10	–	–	–	–	0.2006	0.8294	2.84E-04	0.2272	0.4	1	2.11E-10	0.35	0.2451		1	2019	0.5684

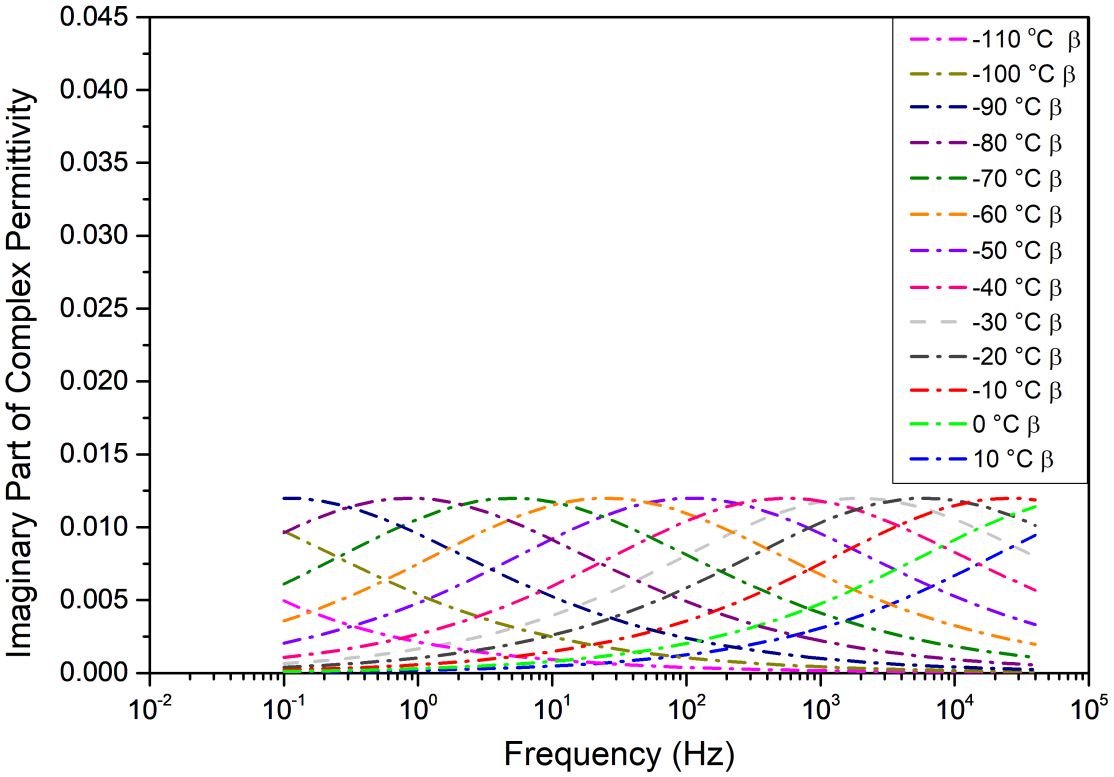

(a) 20AGHE Sample Beta

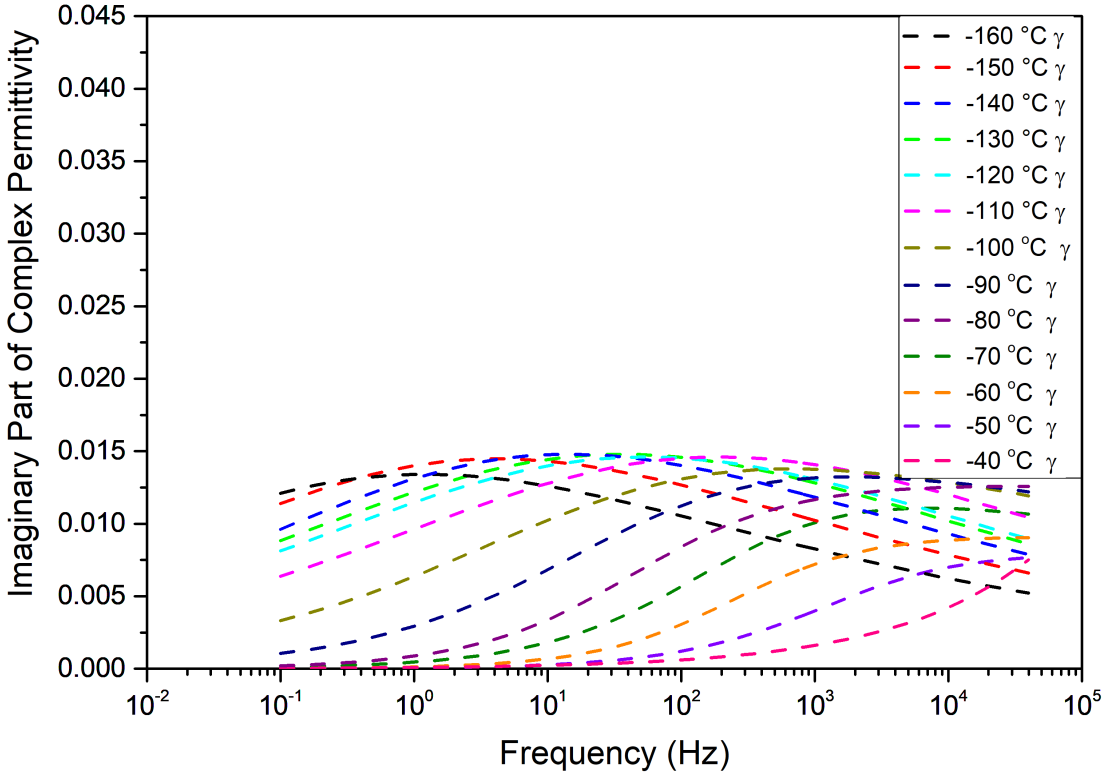

(b) 20AGHE Sample Gamma

Figure E.86: Plots of the deconvoluted temperature dependence of γ and β relaxation peaks using Havriliak-Negami fit for 20AGHE sample

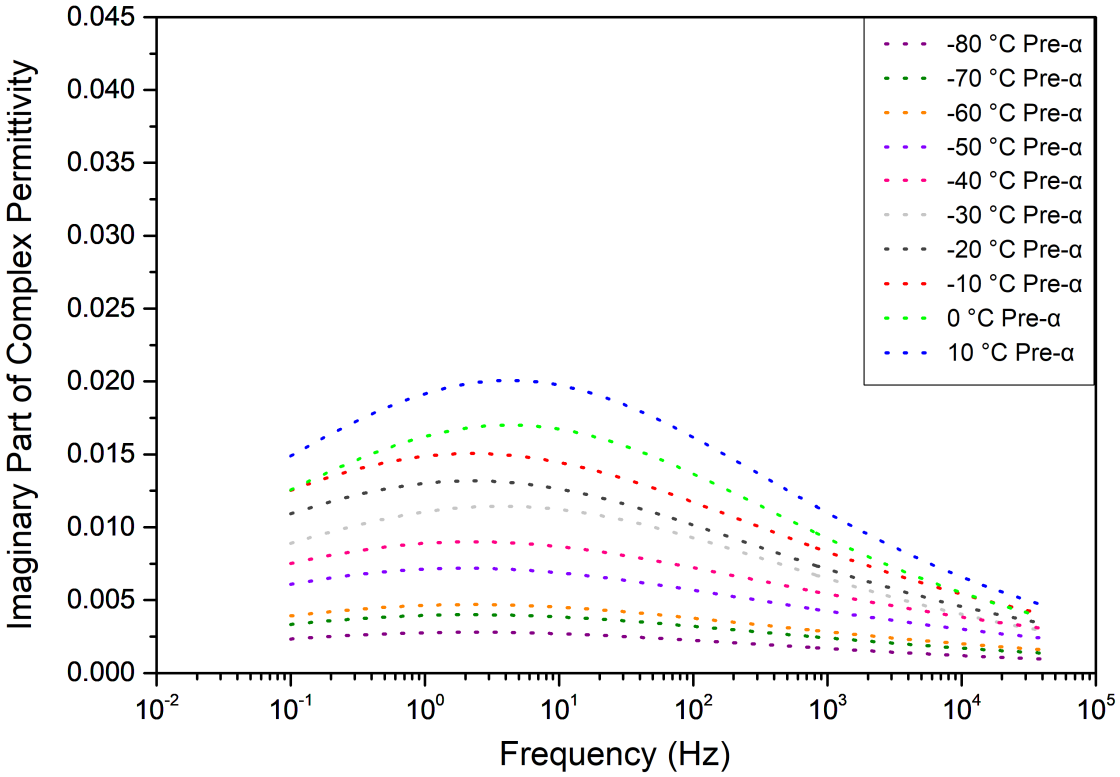

(a) 20AGHE Sample Pre-Alpha

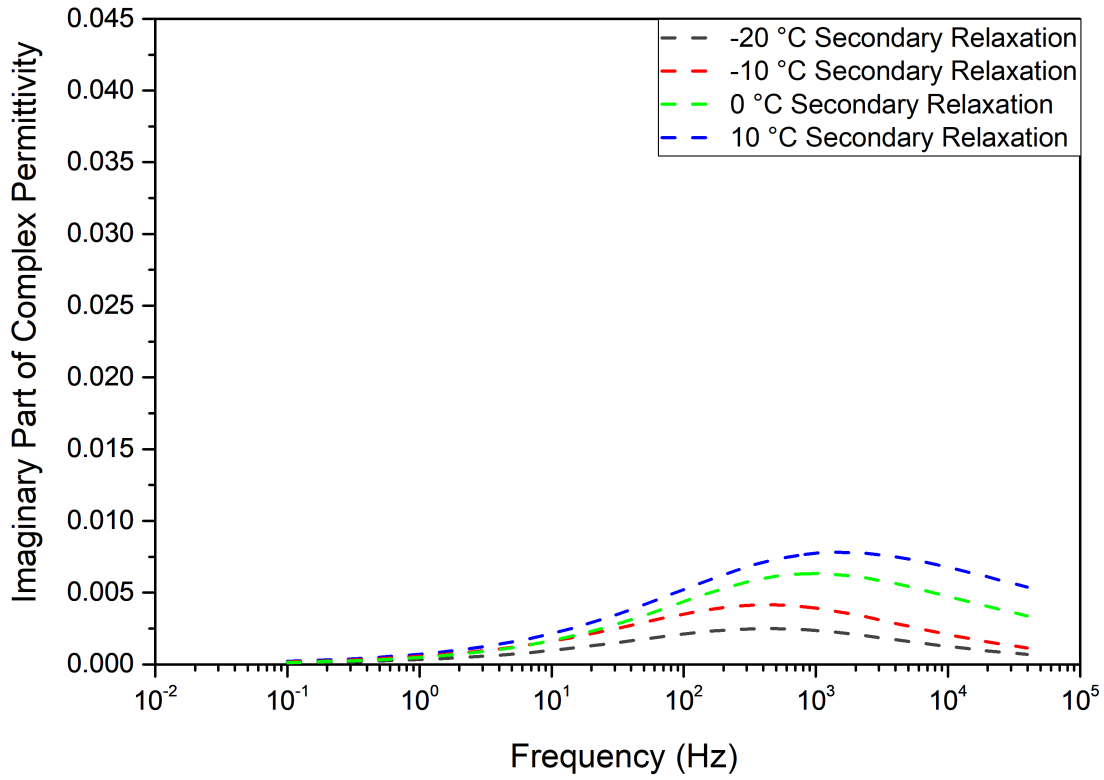

(b) 20AGHE Sample Secondary

Figure E.87: Plots of the deconvoluted temperature dependence of pre alpha and secondary relaxation process using Havriliak-Negami fit for neat sample

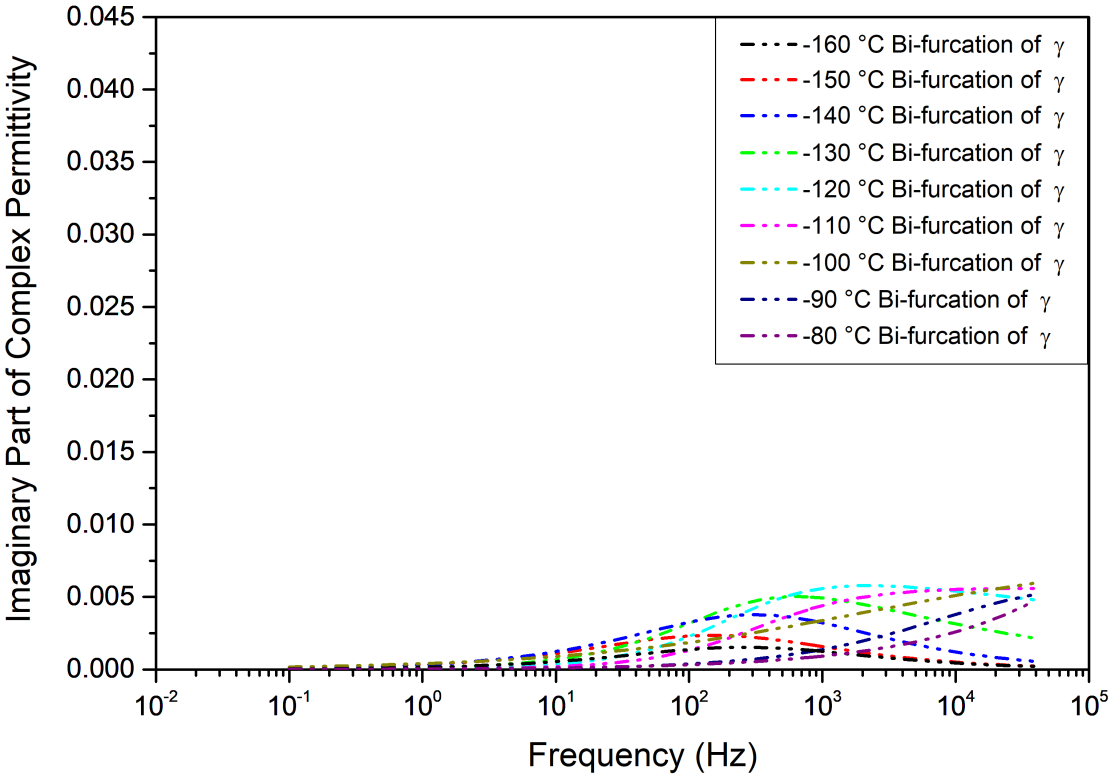

Figure E.88: Plots of the deconvoluted temperature dependence bifurcation of gamma process using Havriliak-Negami fit for 20AGHE sample

E.5.1 Havriliak-Negami fit for 20AGHE systems

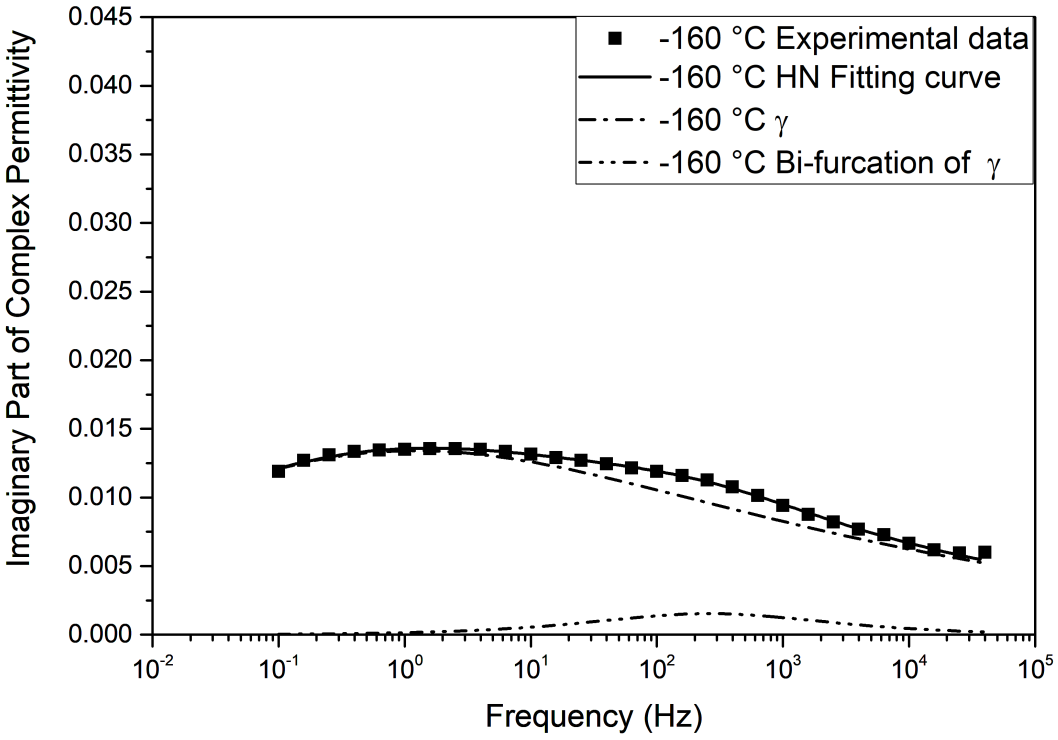

Figure E.89: Havriliak-Negami relaxation fit for 20AGHE at -160 °C

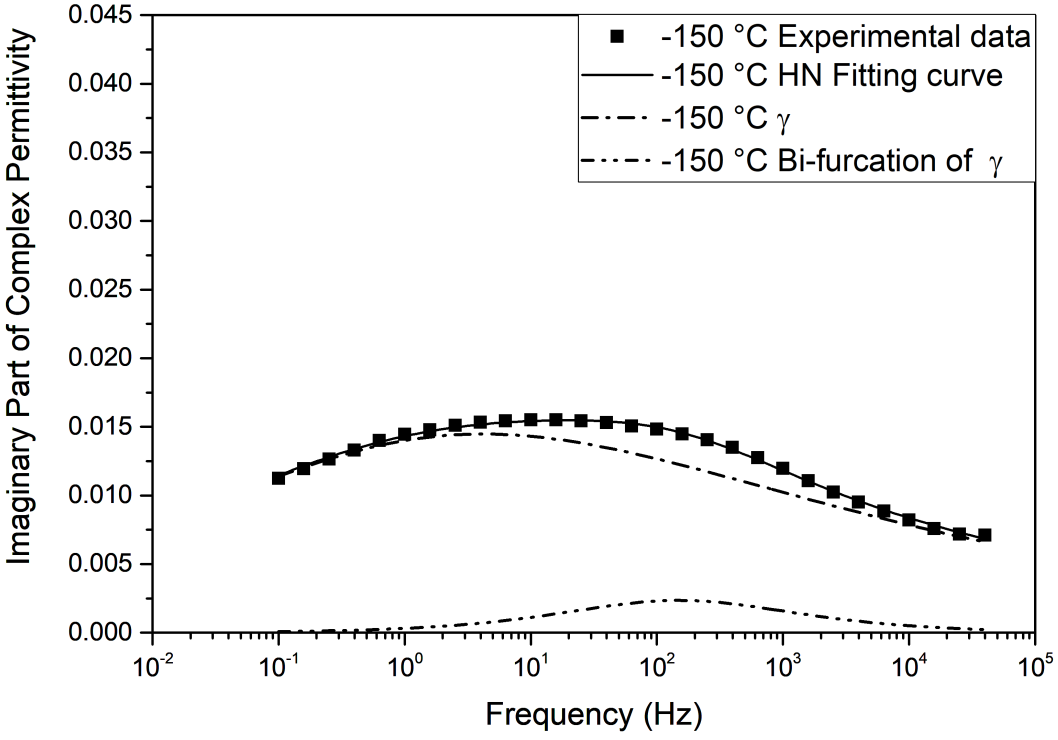

Figure E.90: Havriliak-Negami relaxation fit for 20AGHE at -150 °C

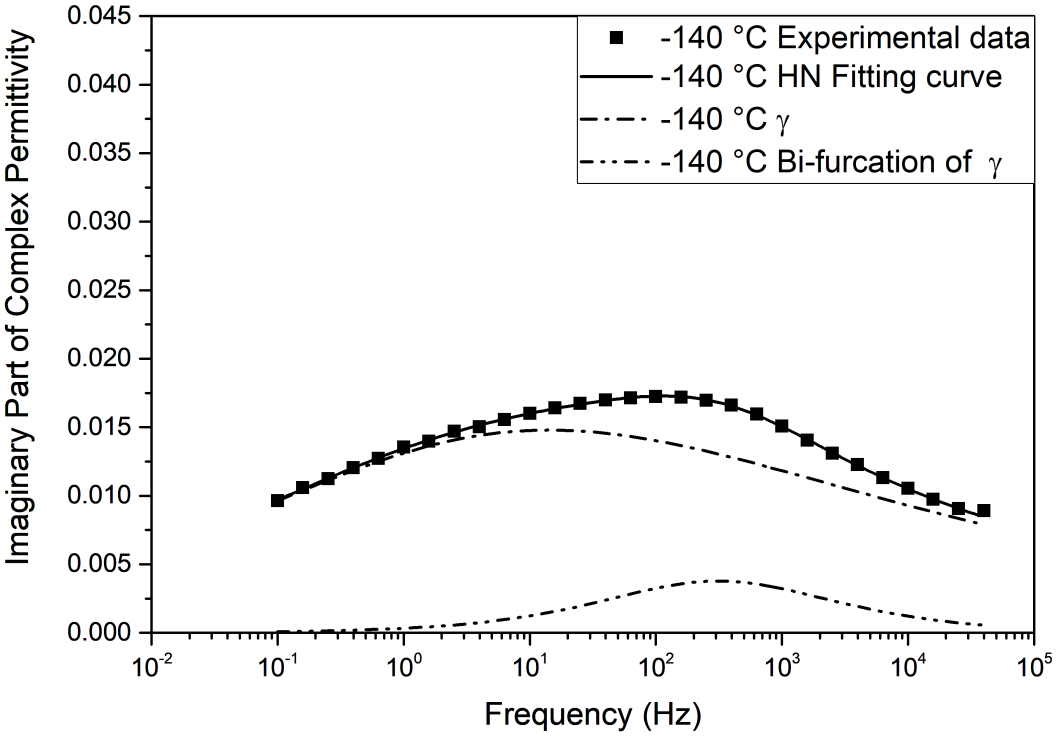

Figure E.91: Havriliak-Negami relaxation fit for 20AGHE at -140 °C

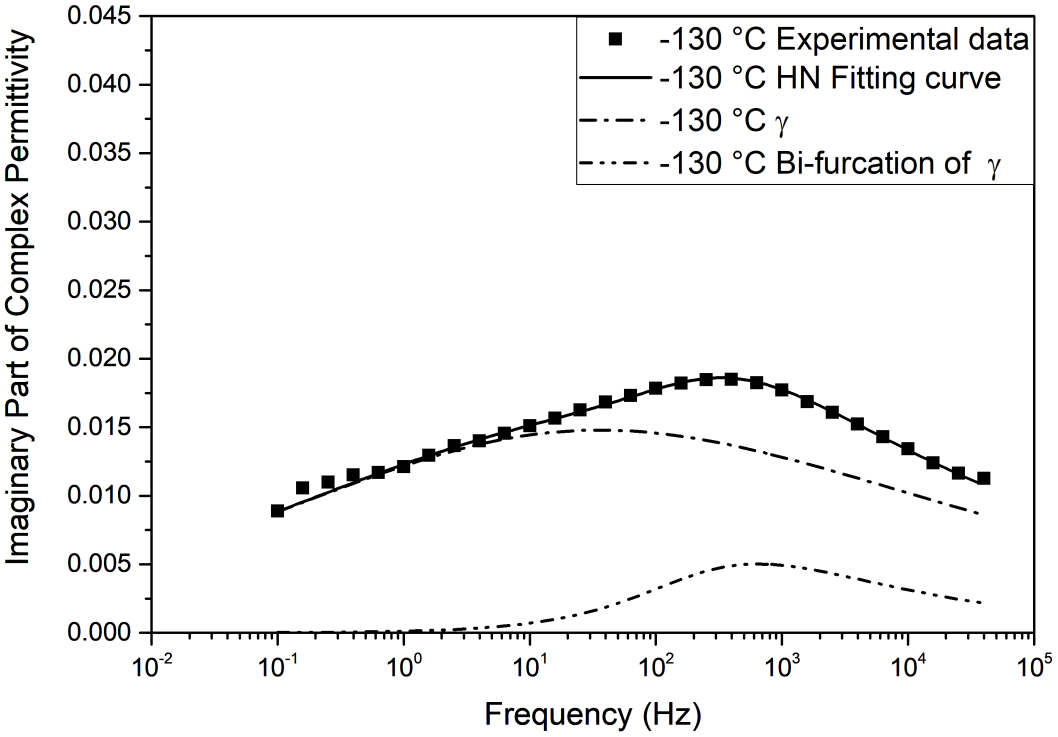

Figure E.92: Havriliak-Negami relaxation fit for 20AGHE at -130 °C

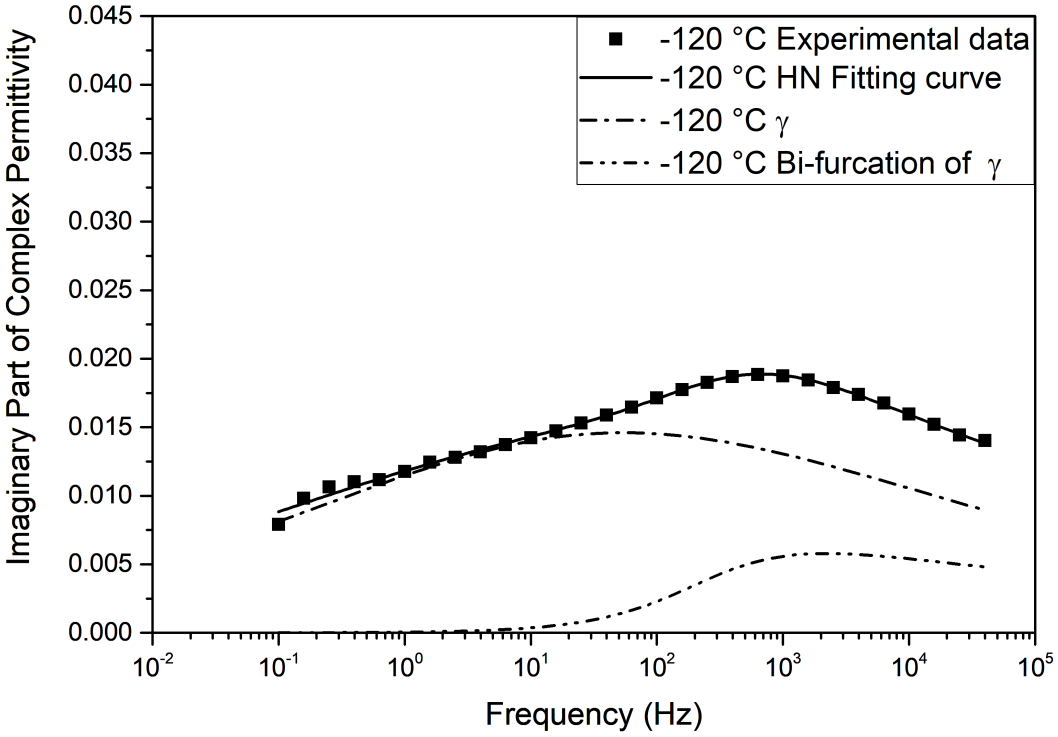

Figure E.93: Havriliak-Negami relaxation fit for 20AGHE at -120 °C

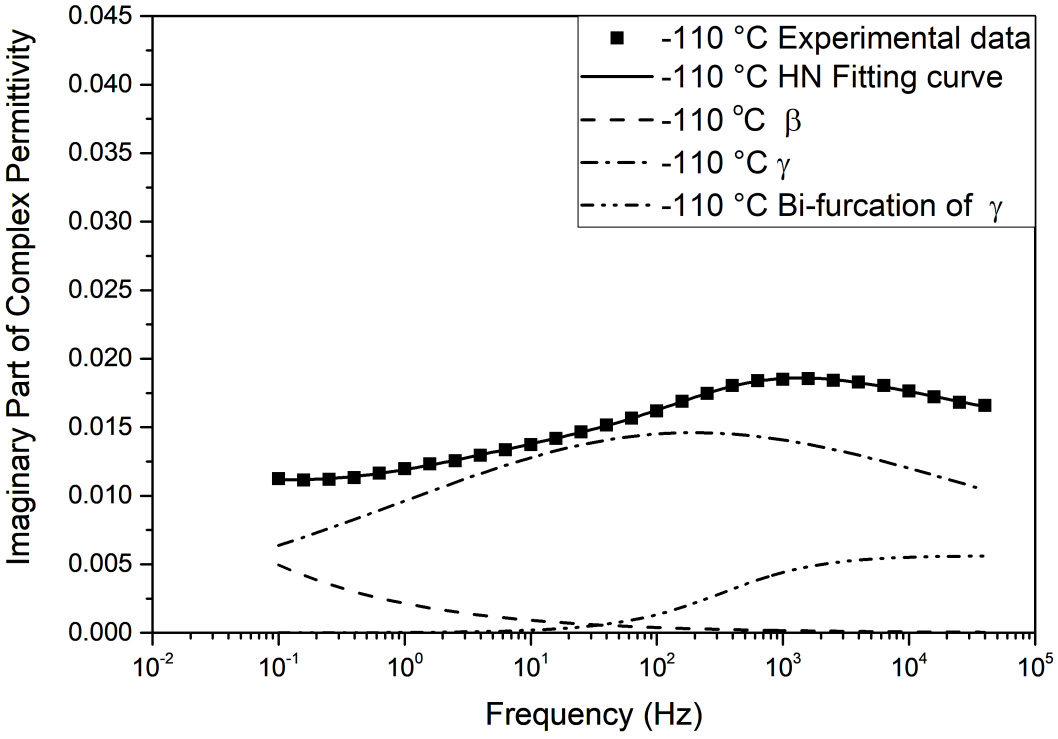

Figure E.94: Havriliak-Negami relaxation fit for 20AGHE at -110 °C

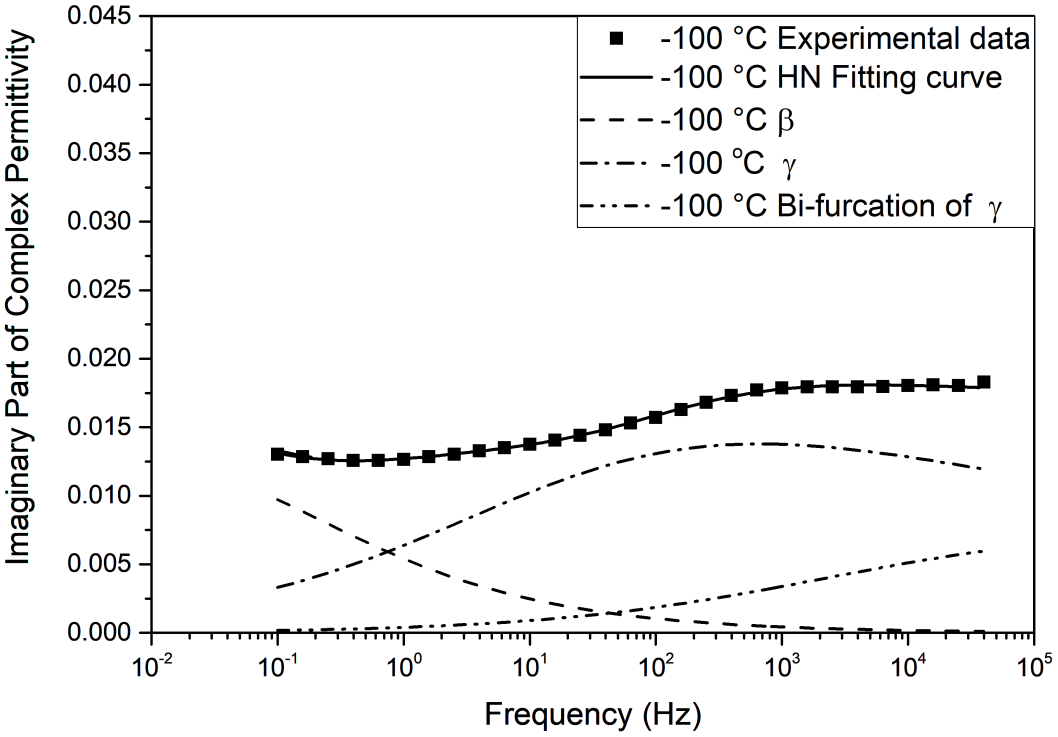

Figure E.95: Havriliak-Negami relaxation fit for 20AGHE at -100 °C

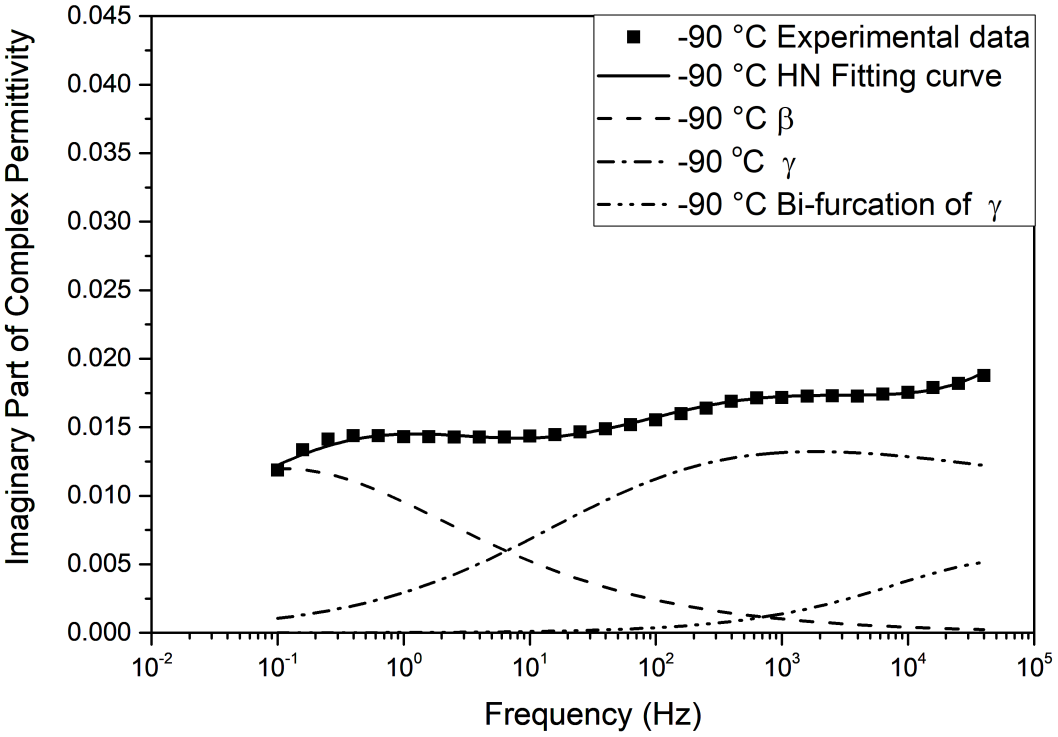

Figure E.96: Havriliak-Negami relaxation fit for 20AGHE at -90 °C

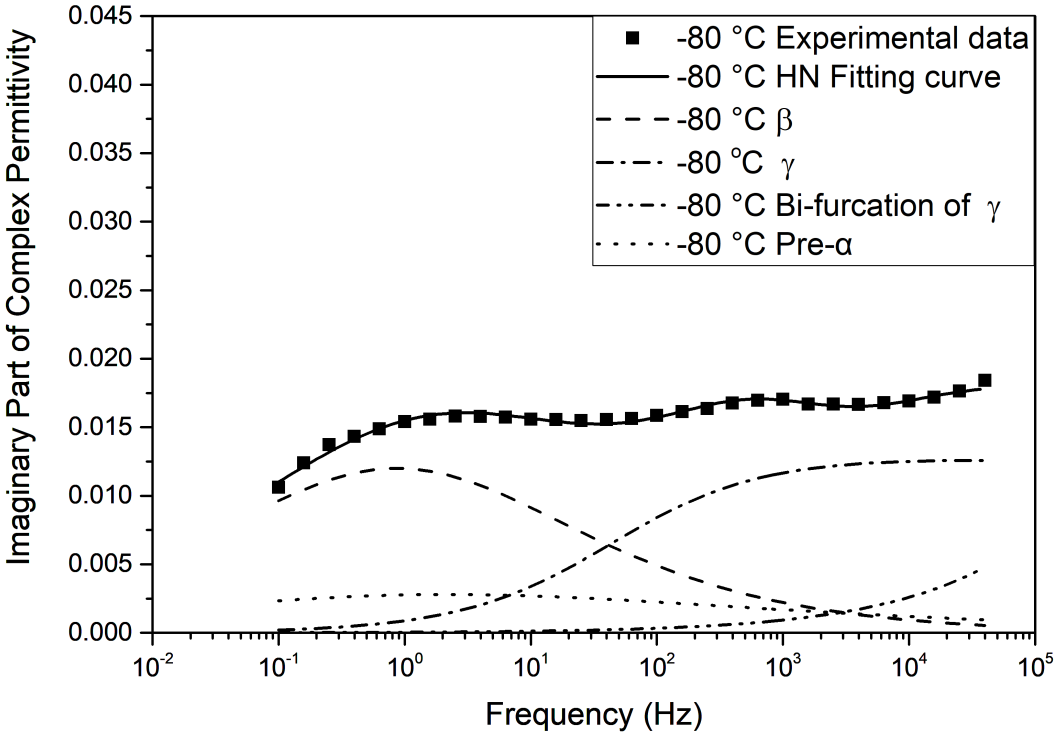

Figure E.97: Havriliak-Negami relaxation fit for 20AGHE at -80 °C

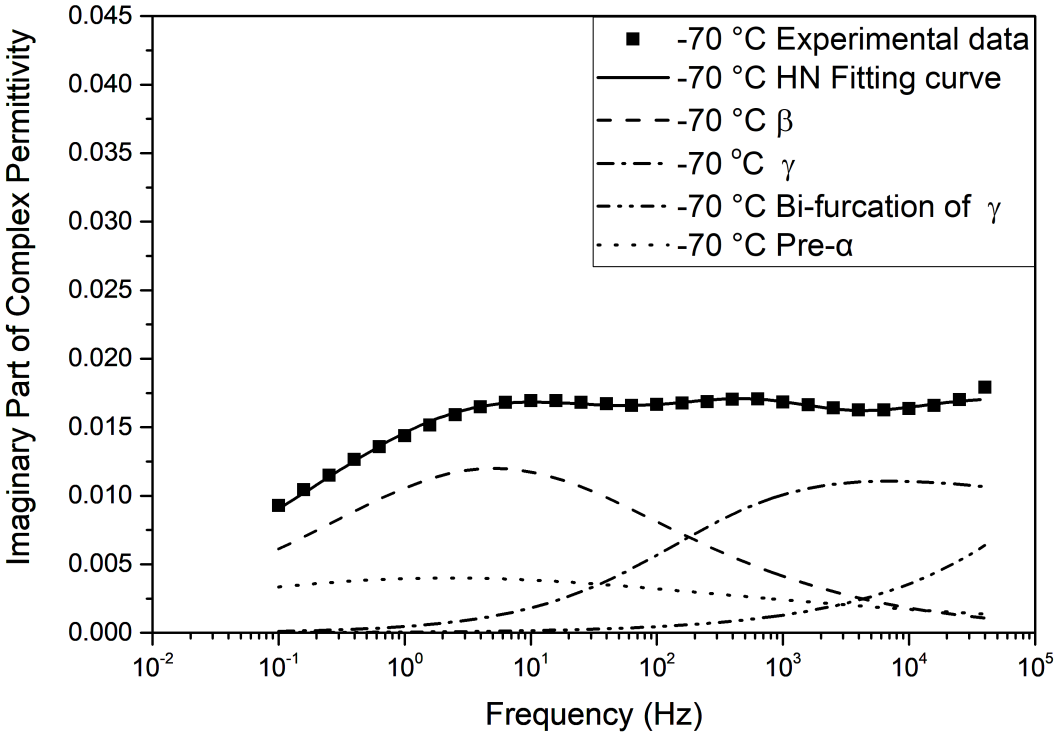

Figure E.98: Havriliak-Negami relaxation fit for 20AGHE at -70 °C

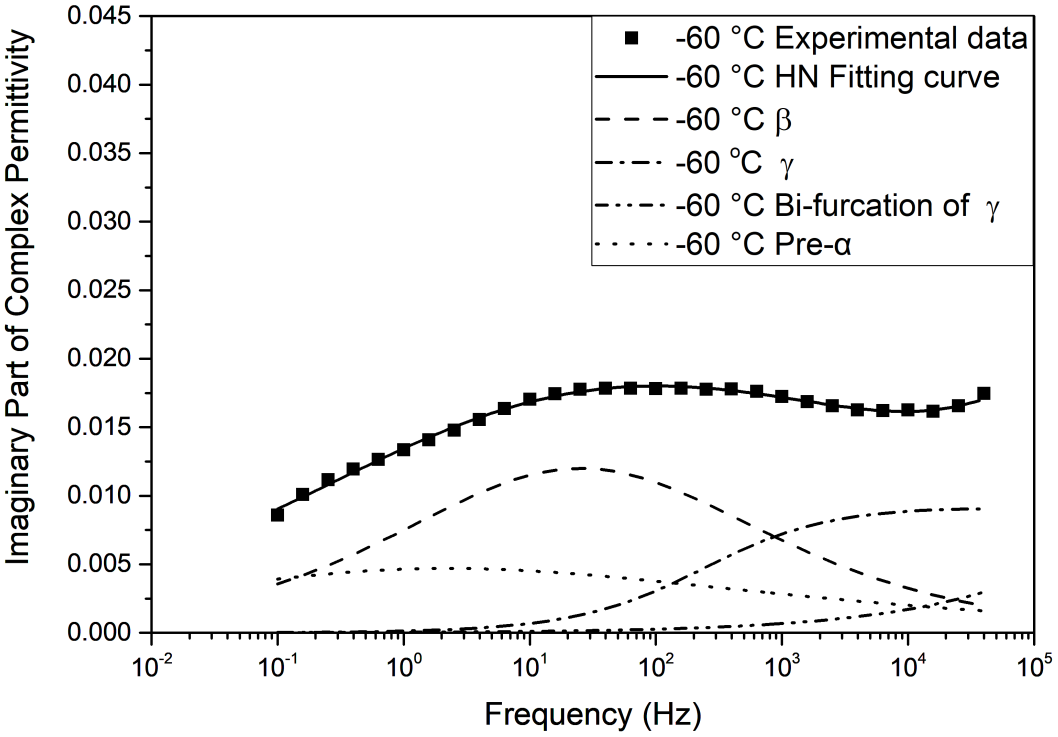

Figure E.99: Havriliak-Negami relaxation fit for 20AGHE at -60 °C

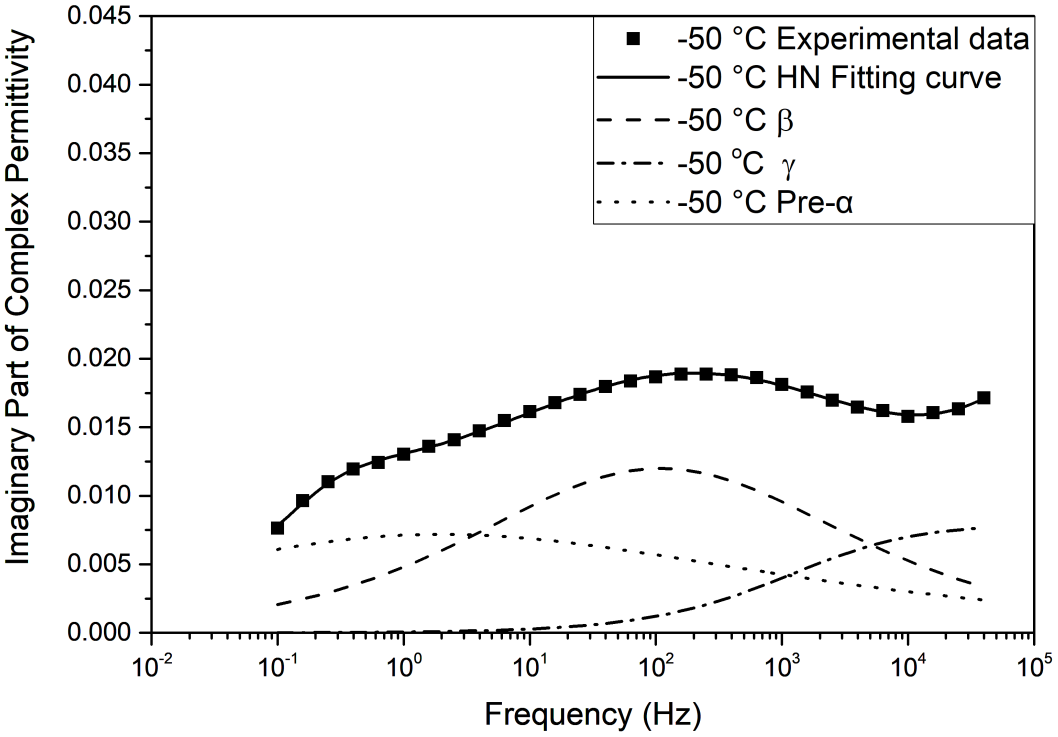

Figure E.100: Havriliak-Negami relaxation fit for 20AGHE at -50 °C

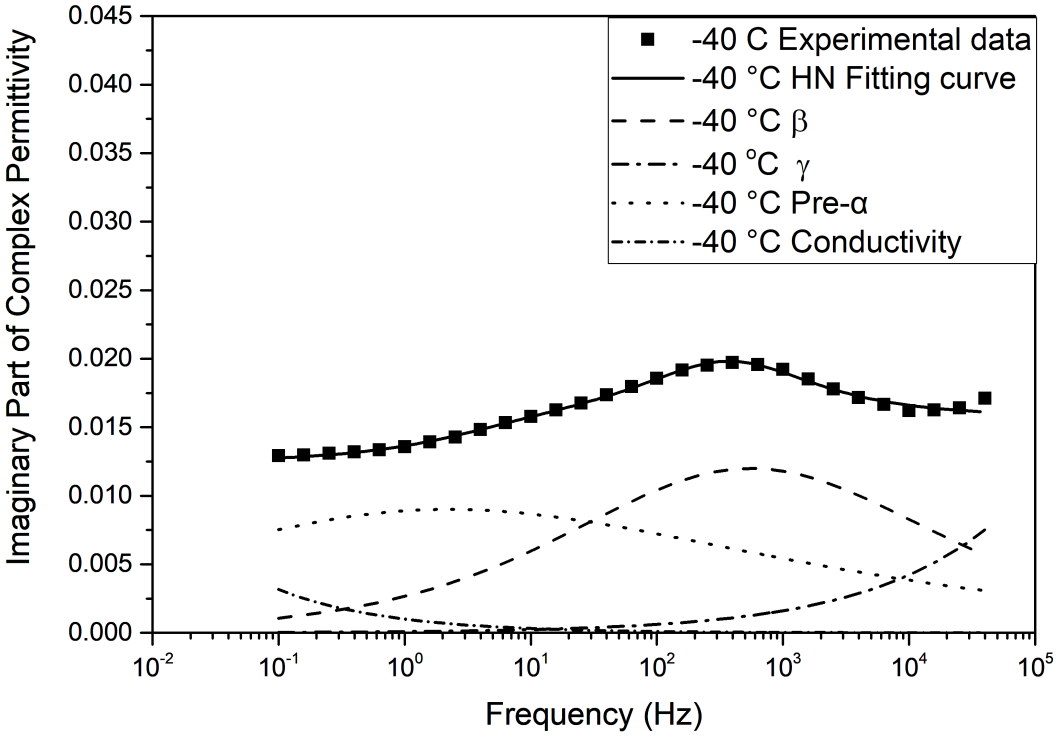

Figure E.101: Havriliak-Negami relaxation fit for 20AGHE at -40 °C

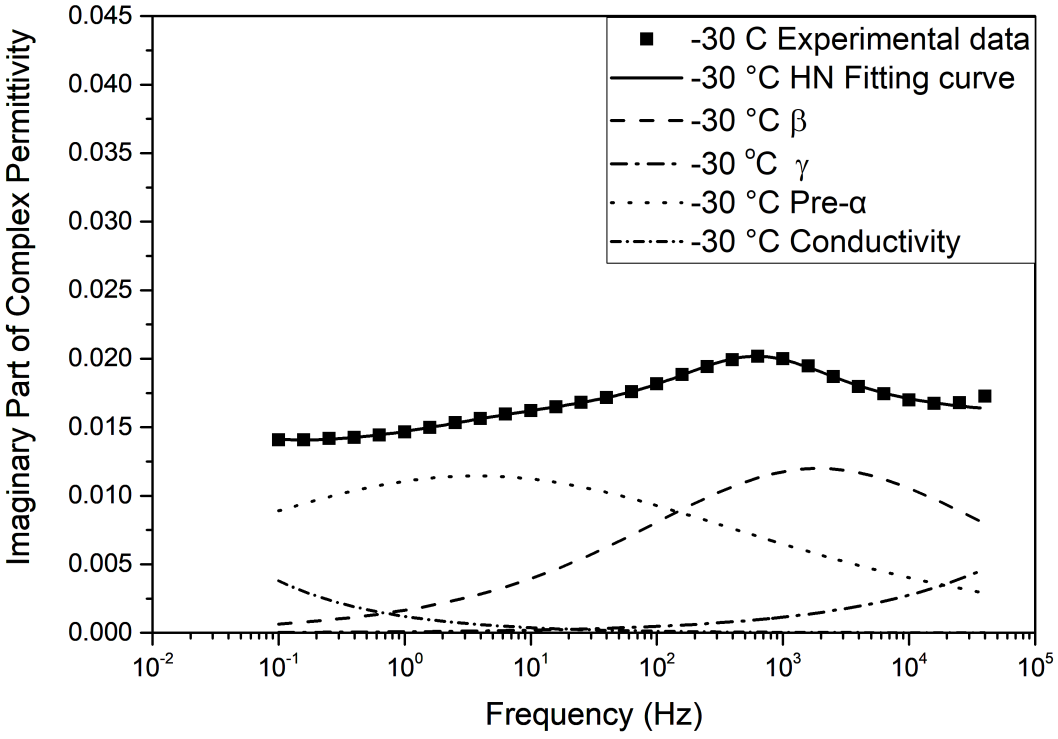

Figure E.102: Havriliak-Negami relaxation fit for 20AGHE at -30 °C

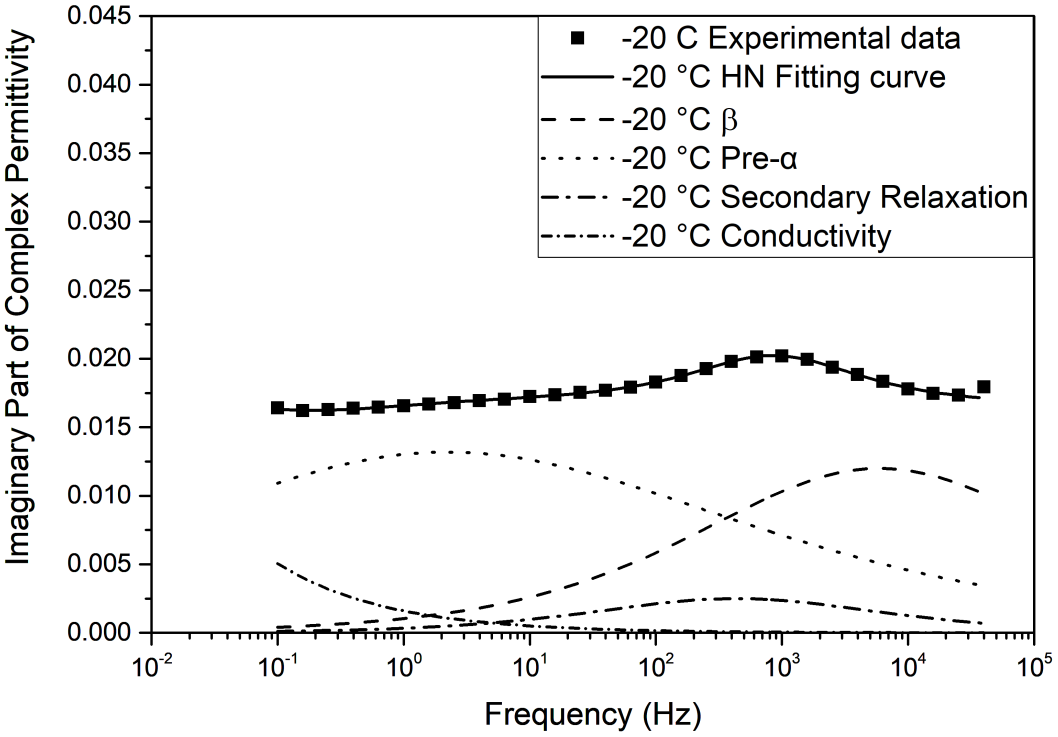

Figure E.103: Havriliak-Negami relaxation fit for 20AGHE at -20 °C

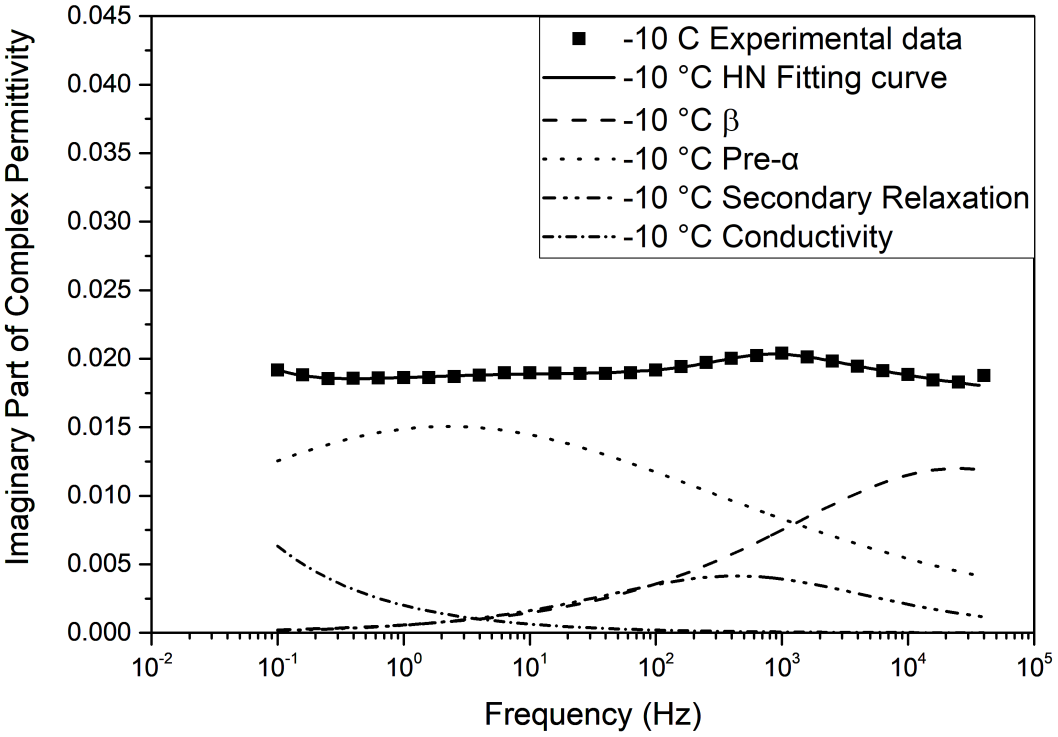

Figure E.104: Havriliak-Negami relaxation fit for 20AGHE at -10 °C

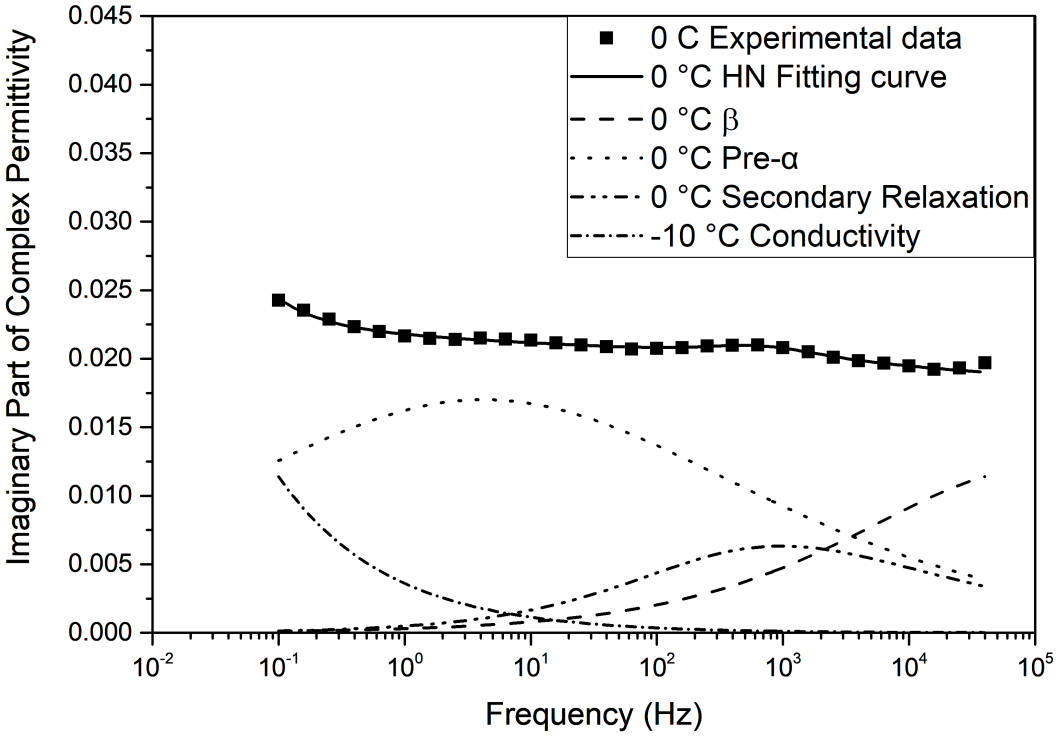

Figure E.105: Havriliak-Negami relaxation fit for 20AGHE at 0 °C

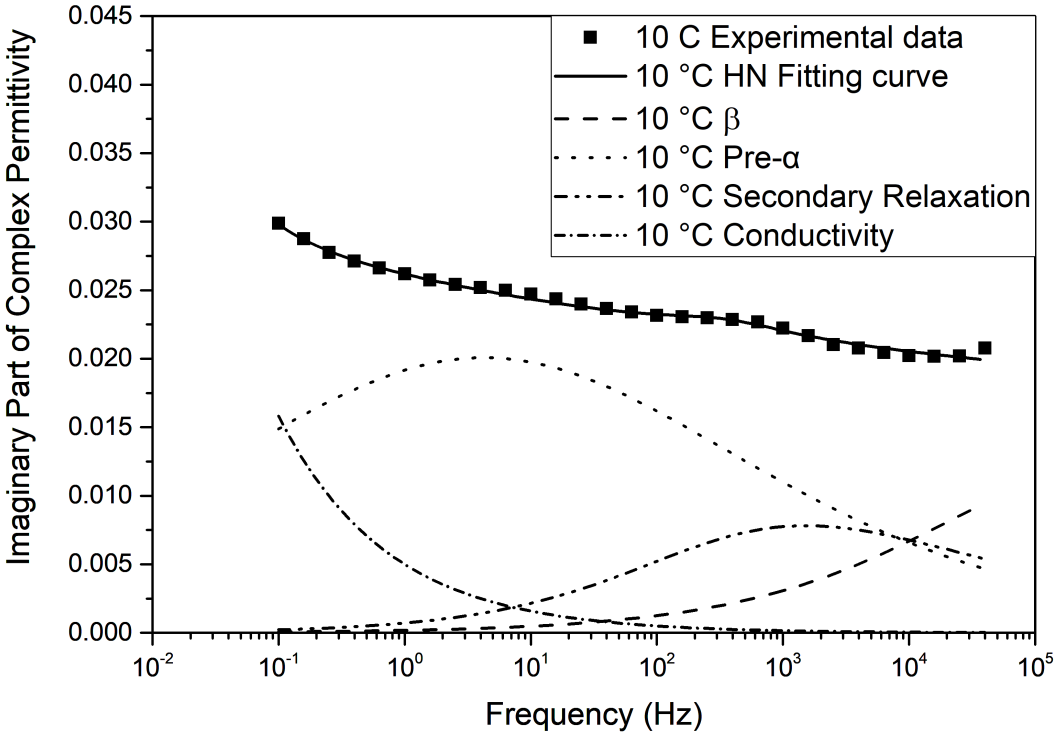

Figure E.106: Havriliak-Negami relaxation fit for 20AGHE at +10 °C

E.5.2 Havriliak-Negami fit parameters for 20AGHE systems

Table E.4: Havriliak-Negami fit parameters for 20AGHE systems

°C	Process 3				Process 4				Bi-furcation of Gamma				pre alpha				Secondary Relaxation			
	α	β	τ	$\Delta\varepsilon$	α	β	τ	$\Delta\varepsilon$	α	β	τ	$\Delta\varepsilon$	α	β	τ	$\Delta\varepsilon$	α	β	τ	$\Delta\varepsilon$
160	1	0.7006	1.01E-10	1.00E-06	0.3122	0.4416	1.739	0.1487	0.6168	1	6.11E-04	0.00583	–	–	–	–	–	–	–	–
150	1	0.7006	1.01E-10	1.00E-06	0.3122	0.4416	0.5	0.1605	0.6168	1	0.00106	0.00895	–	–	–	–	–	–	–	–
140	1	0.7006	1.01E-10	1.00E-06	0.3122	0.4416	0.1449	0.164	0.6168	1	5.13E-04	0.01436	–	–	–	–	–	–	–	–
130	1	0.7006	1.01E-10	1.00E-06	0.2724	0.6012	0.02783	0.164	0.7829	0.3705	7.58E-04	0.02281	–	–	–	–	–	–	–	–
120	1	0.7006	1.01E-10	1.00E-06	0.2724	0.6012	0.01844	0.1619	0.8601	0.1179	6.45E-04	0.05115	–	–	–	–	–	–	–	–
110	0.3712	1	99220	0.5564	0.2724	0.6012	0.00515	0.1619	0.8723	0.01005	4.78E-04	0.4283	–	–	–	–	–	–	–	–
100	0.4255	0.9291	15.945	0.07081	0.3725	0.2073	0.01472	0.1957	0.375	0.01	7.13E-05	1.365	–	–	–	–	–	–	–	–
90	0.4255	0.9291	1.756	0.07081	0.4921	0.1126	0.00619	0.2166	0.6087	0.2689	9.43E-06	0.04009	–	–	–	–	–	–	–	–
80	0.4255	0.9291	0.2174	0.07081	0.652	0.01	0.00352	1.297	0.4486	0.516	5.41E-10	0.7942	0.3031	0.5876	0.398	0.02809	–	–	–	–
70	0.4255	0.9291	0.03687	0.07081	0.6277	0.09027	8.50E-04	0.1675	0.4587	0.0681	6.20E-08	1.078	0.3031	0.5876	0.398	0.04015	–	–	–	–
60	0.4255	0.9291	0.007455	0.07081	0.7349	0.01371	6.27E-04	0.6134	0.4087	0.9689	4.43E-10	0.2199	0.3031	0.5876	0.398	0.04714	–	–	–	–
50	0.4255	0.9291	0.001737	0.07081	0.6676	0.0448	1.16E-04	0.1968	–	–	–	–	0.3031	0.5876	0.4522	0.07212	–	–	–	–
40	0.4255	0.9291	3.38E-04	0.07081	0.4189	0.02053	4.42E-11	71.81	–	–	–	–	0.3031	0.5876	0.398	0.09035	–	–	–	–
30	0.4255	0.9291	9.89E-05	0.07081	0.3837	0.03249	1.00E-11	36.03	–	–	–	–	0.2772	1	0.04285	0.1035	–	–	–	–
20	0.4255	0.9291	3.17E-05	0.07081	–	–	–	–	–	–	–	–	0.2877	0.8298	0.1353	0.1221	0.521	1	3.70E-04	0.01153
10	0.4255	0.9291	7.46E-06	0.07081	–	–	–	–	–	–	–	–	0.2825	0.8298	0.1353	0.1421	0.521	1	3.70E-04	0.01913
0	0.4255	0.9291	1.69E-06	0.07081	–	–	–	–	–	–	–	–	0.2941	1	0.03759	0.1447	0.5675	0.5484	4.42E-04	0.03375
10	0.4255	0.9291	4.96E-07	0.07081	–	–	–	–	–	–	–	–	0.2941	1	0.03759	0.172	0.5256	0.4498	4.42E-04	0.0498

References

[1] F. Kremer and A. Schönhals, *Broadband Dielectric Spectroscopy*. Springer Science and Business Media, 2012.

[2] W. G. Potter, *Epoxide resins*. London, United Kingdom: The plastics institute, 1970.

[3] K. Neville and H. Lee, *Handbook of epoxy resins*. Michigan, USA: MacGraw-Hill, 1967.

[4] EIA, "The international energy outlook 2016 (ieo2016)," https://www.eia.gov/outlooks/ieo/ Retrieved 04.04.2019.

[5] International renewable energy agency IRENA, "Renewable energy policy brief uruguay," Retrieved 04.04.2019. [Online]. Available: http://www.irena.org/

[6] BP Global, "Bp statistical review of world energy june 2017," Retrieved 04.04.2019. [Online]. Available: https://www.bp.com/

[7] C. Ng and L. Ran, *Offshore wind farms: Technologies, design and operation*. Cambridge, UK: Woodhead Publishing, 2016.

[8] T. Letcher, *Wind Energy Engineering: A Handbook for Onshore and Offshore Wind Turbines*. London: Elsevier, 2017.

[9] T. J. Lewis, "Nanometric dielectrics," *IEEE Transactions on Dielectrics and Electrical Insulation*, vol. 1, no. 5, pp. 812–825, 1994.

[10] H. Gu, S. Tadakamalla, X. Zhang, Y. Huang, Y. Jiang, H. A. Colorado, Z. Luo, S. Wei, and Z. Guo, "Epoxy resin nanosuspensions and reinforced nanocomposites from polyaniline stabilized multi-walled carbon nanotubes," *Journal of Materials Chemistry C*, vol. 1, no. 4, pp. 729–743, 2013.

[11] O. Becker, R. Varleyb, and G. Simon, "Morphology, thermal relaxations and mechanical properties of layered silicate nanocomposites based upon high-functionality epoxy resins," *Polymer*, vol. 43, no. 16, pp. 4365–4373, 2002.

[12] L.-Z. Guan, Y.-J. Wan, L.-X. Gong, D. Yan, L.-C. Tang, L.-B. Wu, J.-X. Jiang, and G.-Q. Lai, "Toward effective and tunable interphases in graphene oxide/epoxy composites by grafting different chain lengths of polyetheramine onto graphene oxide," *Journal of Materials Chemistry A*, vol. 2, no. 36, pp. 15 058–15 069, 2014.

[13] J. Wei, T. Vo, and F. Inam, "Epoxy/graphene nanocomposites–processing and properties: a review," *RSC Advances*, vol. 5, no. 90, pp. 73 510–73 524, 2015.

[14] X. Qian, L. Song, B. Yu, B. Wang, B. Yuan, Y. Shi, Y. Hu, and R. K. Yuen, "Novel organic–inorganic flame retardants containing exfoliated graphene: preparation and their performance on the flame retardancy of epoxy resins," *Journal of Materials Chemistry A*, vol. 1, no. 23, pp. 6822–6830, 2013.

[15] S. Vaisakh, K. Mahesh, S. Balanand, R. Metz, M. Hassanzadeh, and S. Anantha kumar, "Max phase ternary carbide derived 2-d ceramic nanostructures [cdcn] as chemically interactive functional fillers for damage tolerant epoxy polymer nanocomposites," *RSC Advances*, vol. 5, no. 21, pp. 16 521–16 531, 2015.

[16] Y. Y. Sun, Z. Q. Zhang, K. S. Moon, and C. P. Wong, "Glass transition and relaxation behavior of epoxy nanocomposites," *Journal of Polymer Science, Part B: Polymer Physics*, vol. 42, no. 21, pp. 3849–3858, 2004.

[17] Z. Elimat, A. Zihlif, and G. Ragosta, "Study of ac electrical properties of aluminium–epoxy composites," *Journal of Physics D: Applied Physics*, vol. 41, no. 16, p. 165408, 2008.

[18] Y. Li, M. Tian, Z. Lei, and J. Zhang, "Effect of nano-silica on dielectric properties and space charge behavior of epoxy resin under temperature gradient," *Journal of Physics D Applied Physics*, vol. 51, no. 12, p. 125309, 2018.

[19] J. Nelson and Y. Hu, "Nanocomposite dielectrics—properties and implications," *Journal of Physics D: Applied Physics*, vol. 38, no. 2, pp. 213 – 222, 2005.

[20] G. Belijar, S. Diaham, Z. Valdez-Nava, and T. Lebey, "Online optical and dielectric monitoring of anisotropic epoxy/batio3 composite formation tailored by dielectrophoresis," *Journal of Physics D: Applied Physics*, vol. 49, no. 4, p. 045501, 2015.

[21] S. S. Ghoneim, N. A. Sabiha, M. M. Hessien, and A. Alahmadi, "Evaluation of dielectric breakdown strength of transformer oil with batio 3 and nife 2 o 4 nanoparticles," *Electrical Engineering*, vol. 101, no. 2, pp. 369–377, 2019.

[22] A. Thabet, M. Allam, and S. Shaaban, "Assessment of individual and multiple nanoparticles on electrical insulation of power transformers nanofluids," *Electric Power Components and Systems*, vol. 47, no. 4-5, pp. 420–430, 2019.

[23] S. Zeb, I. Ullah, A. Karim, W. Muhammad, N. Ullah, M. Khan, and W. Komal, "A review on nanotechnology applications in electric components," *eleyon nanoscale reports*, pp. 32–38, 2019.

[24] M. P. Bahrman and B. K. Johnson, "The abcs of hvdc transmission technologies," *IEEE power and energy magazine*, vol. 5, no. 2, pp. 32–44, 2007.

[25] L. Zhe, K. Okamoto, Y. Ohki, and T. Tanaka, "Role of nano-filler on partial discharge resistance and dielectric breakdown strength of micro-Al2O3/ epoxy composites," in *2009 IEEE 9th International Conference on the Properties and Applications of Dielectric Materials*, no. July, 2009, pp. 753–756.

[26] S. Siddabattuni, T. P. Schuman, and F. Dogan, "Improved polymer nanocomposite dielectric breakdown performance through barium titanate to epoxy interface control," *Materials Science and Engineering: B*, vol. 176, no. 18, pp. 1422–1429, 2011.

[27] P. Preetha and M. J. Thomas, "AC Breakdown Characteristics of Epoxy Nanocomposites," *IEEE Transactions on Dielectrics and Electrical Insulation*, vol. 18, no. 5, pp. 1526–1534, 2011.

[28] Z. Li, G. Sheng, X. Jiang, and T. Tanaka, "Effects of inorganic fillers on withstanding short-time breakdown and long-time electrical aging of epoxy composites," *IEEJ Transactions on Electrical and Electronic Engineering*, vol. 12, no. S2, 2017.

[29] S. Singha and M. J. Thomas, "Dielectric properties of epoxy nanocomposites," *IEEE Transactions on Dielectrics and Electrical Insulation*, vol. 15, no. 1, 2008.

[30] T. Imai, F. Sawa, T. Ozaki, Y. Inoue, T. Shimizu, and T. Tanaka, "Comparison of insulation breakdown properties of epoxy nanocomposites under homogeneous and divergent electric fields," *IEEE Conference on Electrical Insulation and Dielectric Phenomena*, pp. 306–309, 2006.

[31] X. Huang, Z. Ma, Y. Wang, P. Jiang, Y. Yin, and Z. Li, "Polyethylene/aluminum nanocomposites: improvement of dielectric strength by nanoparticle surface modification," *Journal of applied polymer science*, vol. 113, no. 6, pp. 3577–3584, 2009.

[32] H. Yang, Q. Zhang, M. Guo, C. Wang, R. Du, and Q. Fu, "Study on the phase structures and toughening mechanism in pp/epdm/sio2 ternary composites," *Polymer*, vol. 47, no. 6, pp. 2106–2115, 2006.

[33] J. Kruenate, R. Tongpool, T. Panyathanmaporn, and P. Kongrat, "Optical and mechanical properties of polypropylene modified by metal oxides," *Surface and Interface Analysis: An International Journal devoted to the development and application of techniques for the analysis of surfaces, interfaces and thin films*, vol. 36, no. 8, pp. 1044–1047, 2004.

[34] S. Maiti and B. Lopez, "Tensile properties of polypropylene/kaolin composites," *Journal of applied polymer science*, vol. 44, no. 2, pp. 353–360, 1992.

[35] K. Lau, A. Vaughan, G. Chen, and I. Hosier, "Polyethylene nanodielectrics: The effect of nanosilica and its surface treatment on electrical breakdown strength," in *2012 Annual Report Conference on Electrical Insulation and Dielectric Phenomena*. IEEE, 2012, pp. 21–24.

[36] T. Lewis, "Interfaces are the dominant feature of dielectrics at the nanometric level," *IEEE transactions on dielectrics and electrical insulation*, vol. 11, no. 5, pp. 739–753, 2004.

[37] T. Tanaka, M. Kozako, N. Fuse, and Y. Ohki, "Proposal of a multi-core model for polymer nanocomposite dielectrics," *IEEE Transactions on Dielectrics and Electrical Insulation*, vol. 12, no. 4, pp. 669 – 681, 2005.

[38] S. Li, D. Min, and G. Wang, Weiwang Chen, "Linking traps to dielectric breakdown through charge dynamics for polymer nanocomposites," *IEEE Transactions on Dielectrics and Electrical Insulation*, vol. 23, no. 5, pp. 1070–9878, 2016.

[39] T. Tanaka, "Roles of quantum dot like multi-functional traps in electrical conduction of polymer nanocomposites," in *1st International Conference on Electrical Materials and Power Equipment (ICEMPE)*, Xi'an, 2017, pp. 61–70.

[40] U. S. Energy Information Administration, "Early release: Annotated summary of two cases," Washington, D.C, 2016.

[41] F. Gojny, M. Wichmann, B. Fiedler, and K. Schulte, "Influence of different carbon nanotubes on the mechanical properties of epoxy matrix composites–a comparative study," *Composites Science and Technology*, vol. 65, no. 15, pp. 2300–2313, 2005.

[42] A. Allaoui, S. Bai, H. Cheng, and J. Bai, "Mechanical and electrical properties of a MWNT/epoxy composite," *Composites Science and Technology*, vol. 62, no. 15, pp. 1993–1998, 2002.

[43] R. Thomas, D. Yumei, H. Yuelong, Y. Le, P. Moldenaers, Y. Weimin, T. Czigany, and S. Thomas, "Miscibility, morphology, thermal, and mechanical properties of a DGEBA based epoxy resin toughened with a liquid rubber," *Polymer*, vol. 49, no. 1, pp. 278–294, 2008.

[44] K. D. Kumar and B. Kothandaraman, "Modification of (DGEBA) epoxy resin with maleated depolymerised natural rubber," *Express Polymer Letters*, vol. 2, pp. 302–311, 2008.

[45] W. Liu, S. Ma, Z. Wang, C. Hu, and C. Tang, "Morphologies and mechanical and thermal properties of highly epoxidized polysiloxane toughened epoxy resin composites," *Macromolecular research*, vol. 18, no. 9, pp. 853–861, 2010.

[46] H. Shengshu, C. Yenpin, and C. Chengkuang, "Function and performance of silicone copolymer. Part IV Curing behavior and characterization of epoxy-siloxane co-polymers blended with diglycidyl ether of bisphenol-A," *Polymer*, vol. 41, pp. 3263–3270, 2000.

[47] B. Ellis, *Chemistry and technology of epoxy resins.* Hall, UK: Springer, 1993.

[48] C. A. May, *Epoxy resins: Chemistry and technology.* New York: Marcel Dekker., 1988.

[49] I. Isarn, F. Gamardella, X. Fernàndez-Francos, À. Serra, and F. Ferrando, "Thermal conductive composites prepared by addition of several ceramic fillers to thermally cationic curing cycloaliphatic epoxy resins," *Polymers*, vol. 11, no. 1, p. 138, 2019.

[50] J. M. Tomasi, J. A. King, A. S. Krieg, I. Miskioglu, and G. M. Odegard, "Thermal, electrical, and mechanical properties of talc-and glass microsphere-reinforced cycloaliphatic epoxy composites," *Polymer Composites*, vol. 39, no. S3, pp. E1581–E1588, 2018.

[51] H. Panda, *Epoxy Resins Technology Handbook.* Asia pacific business press Inc., 2016. [Online]. Available: https://books.google.co.uk/books?id=D0gtDQAAQBAJ

[52] M. J. Yoo, S. H. Kim, S. D. Park, W. S. Lee, J.-W. Sun, J.-H. Choi, and S. Nahm, "Investigation of curing kinetics of various cycloaliphatic epoxy resins using dynamic thermal analysis," *European Polymer Journal*, vol. 46, no. 5, pp. 1158–1162, 2010.

[53] E. Dogan and A. E. Acar, "The use of anhydride linkages to increase the glass transition temperatures of polymers containing carboxyl end groups: a perspective in powder coatings," *Progress in Organic Coatings*, vol. 76, no. 2-3, pp. 513–518, 2013.

[54] J. Nakka, K. Jansen, and L. Ernst, "Tailoring the viscoelasticity of epoxy thermosets," *Journal of Applied Polymer Science*, vol. 128, no. 6, pp. 3794–3806, 2013.

[55] G. C. Stevens, "Cure kinetics of a low epoxide/hydroxyl group-ratio bisphenol a epoxy resin–anhydride system by infrared absorption spectroscopy," *Journal of Applied Polymer Science*, vol. 26, no. 12, pp. 4259–4278, 1981.

[56] B. Steinmann, "Investigations on the curing of epoxy resins with hexahydrophthalic anhydride," *Journal of applied polymer science*, vol. 37, no. 7, pp. 1753–1776, 1989.

[57] Y. Tanaka and H. Kakiuchi, "Study of epoxy compounds. part vi. curing reactions of epoxy resin and acid anhydride with amine, acid, alcohol, and phenol as

catalysts," *Journal of Polymer Science Part A: General Papers*, vol. 2, no. 8, pp. 3405–3430, 1964.

[58] O. Vryonis, T. Andritsch, A. Vaughan, and P. Lewin, "Improved lightning protection of carbon fiber reinforced polymer wind turbine blades: Epoxy/graphene oxide nanocomposites," in *Electrical Insulation and Dielectric Phenomena (CEIDP)*, 2016, pp. 635–638.

[59] F. Ardente, M. Beccali, M. Cellura, and V. L. Brano, "Energy performances and life cycle assessment of an Italian wind farm," *Renewable and Sustainable Energy Reviews*, vol. 12, no. 1, pp. 200–217, 2008.

[60] D. C. Blackley, *Polymer Latices: Science and Technology Volume 3: Applications of Latices*. Springer Science & Business Media, 2012.

[61] J. Njuguna, F. Ansari, S. Sachse, H. Zhu, and V. Rodriguez, "Nanomaterials, nanofillers, and nanocomposites: types and properties," in *Health and Environmental Safety of Nanomaterials*. Elsevier, 2014, pp. 3–27.

[62] J. Jordan, K. I. Jacob, R. Tannenbaum, M. A. Sharaf, and I. Jasiuk, "Experimental trends in polymer nanocomposites—a review," *Materials science and engineering: A*, vol. 393, no. 1-2, pp. 1–11, 2005.

[63] T. Andritsch, "Epoxy Based Nanodielectrics for High Voltage DC Applications: Synthesis, Dielectric Properties and Space Charge Dynamics," Ph.D. dissertation, Doctoral dissertation, Delft University of Technology, 2010.

[64] T. Hanemann and D. V. Szabó, "Polymer-nanoparticle composites: from synthesis to modern applications," *Materials*, vol. 6, no. 3, pp. 3468–3517, 2010.

[65] M. Xanthos, *Functional fillers for plastics*. John Wiley & Sons, 2010.

[66] M. Frounchi, M. Mehrabzadeh, and M. Parvary, "Toughening epoxy resins with solid acrylonitrile–butadiene rubber," *Polymer international*, vol. 49, no. 2, pp. 163–169, 2000.

[67] A. C. Garg and Y. W. Mai, "Failure mechanisms in toughened epoxy resins—A review," *Composites Science and Technology*, vol. 31, no. 3, pp. 179–223, 1988.

[68] T. Imai, F. Sawa, T. Nakano, T. Ozaki, T. Shimizu, M. Kozako, and T. Tanaka, "Effects of nano-and micro-filler mixture on electrical insulation properties of epoxy based composites," *IEEE Transactions on Dielectrics and Electrical Insulation*, vol. 13, no. 2, pp. 319–326, 2006.

[69] E. Tuncer, I. Sauers, D. R. James, A. R. Ellis, M. P. Paranthaman, T. Aytuğ, S. Sathyamurthy, K. L. More, J. Li, and A. Goyal, "Electrical properties of epoxy resin based nano-composites," *Nanotechnology*, vol. 18, no. 2, p. 025703, 2006.

[70] M. Donnay, S. Tzavalas, and E. Logakis, "Boron nitride filled epoxy with improved thermal conductivity and dielectric breakdown strength," *Composites Science and Technology*, vol. 110, pp. 152–158, 2015.

[71] S. Virtanen, T. M. Krentz, J. K. Nelson, L. S. Schadler, M. Bell, B. Benicewicz, H. Hillborg, and S. Zhao, "Dielectric breakdown strength of epoxy bimodal-polymer-brush-grafted core functionalized silica nanocomposites," *IEEE Transactions on Dielectrics and Electrical Insulation*, vol. 21, no. 2, pp. 563–570, 2014.

[72] I. A. Tsekmes, R. Kochetov, P. H. F. Morshuis, and J. J. Smit, "AC Breakdown Strength of Epoxy-Boron Nitride Nanocomposites : Trend & Reproducibility," in *2015 IEEE Electrical Insulation Conference (EIC)*, no. June, 2015, pp. 446–449.

[73] T. Andritsch, R. Kochetov, Y. T. Gebrekiros, P. H. Morshuis, and J. J. Smit, "Short term dc breakdown strength in epoxy based bn nano-and microcomposites," in *2010 10th IEEE International Conference on Solid Dielectrics*. IEEE, 2010, pp. 1–4.

[74] S. Siddabattuni, S. H. Akella, A. Gangula, S. Belliraj, and L. A. A. Chunduri, "Dielectric properties study of surface engineered nanotio2 tio2 epoxy composites," *Bulletin of Materials Science*, vol. 41, no. 13, pp. 1–9, february 2018.

[75] G. Iyer, R. S. Gorur, R. Richert, A. Krivda, and L. E. Schmidt, "Dielectric properties of epoxy based nanocomposites for high voltage insulation," *IEEE Transactions on Dielectrics and Electrical Insulation*, vol. 18, no. 3, pp. 659–666, June 2011.

[76] Y. Sun, Z. Zhang, and C. P. Wong, "Influence of interphase and moisture on the dielectric spectroscopy of epoxy/silica composites," *Polymer*, vol. 46, no. 7, pp. 2297–2305, 2005.

[77] J. K. Nelson and J. C. Fothergill, "Internal Charge Behaviour of Nanocomposites." *Nanotechnology*, vol. 15, no. 5, pp. 1–28, 2004.

[78] P. Maity, P. K. Poovamma, S. Basu, V. Parameswaran, and N. Gupta, "Dielectric spectroscopy of epoxy resin with and without nanometric alumina fillers," *IEEE Transactions on Dielectrics and Electrical Insulation*, vol. 16, no. 5, pp. 1481–1488, 2009.

[79] S. Nishanth, M. Kaviarasu, and N. Mallireddy, "Thermal Properties of Modified Epoxy Nano Composite," *International Journal of Engineering Research & Technology (IJERT).*, vol. 3, no. 3, pp. 304–305, 2014.

[80] T. V. Kosmidou, A. Vatalis, C. Delides, E. Logakis, P. Pissis, and G. Papanicolaou, "Structural, mechanical and electrical characterization of epoxy-amine/carbon black nanocomposites," *eXPRESS Polymer Letters*, vol. 2, no. 5, pp. 364–372, 2008.

[81] J. Brown, I. Rhoney, and R. A. Pethrick, "Epoxy resin based nanocomposites: 1. diglycidylether of bisphenol a (dgeba) with triethylenetetramine (teta)," *Polymer International*, vol. 53, no. 12, pp. 2130–2137, 2004.

[82] K. Yang and M. Gu, "The effects of triethylenetetramine grafting of multi walled carbon nanotubes on its dispersion, filler matrix interfacial interaction and the thermal properties of epoxy nanocomposite," *Polymer Engineering & Science*, vol. 49, no. 11, pp. 2158–2167, 2009.

[83] P. Peyser and W. D. Bascom, "Effect of filler and cooling rate on the glass transition of polymers," *Journal of Macromolecular Science, Part B: Physics*, vol. 13, no. 4, pp. 597–610, 1977.

[84] R. J. Andrews and E. A. Grulke, "Glass transition temperatures of polymers," *The Wiley Database of Polymer Properties*, 2003.

[85] L. M. McGrath, R. S. Parnas, S. H. King, J. L. Schroeder, D. A. Fischer, and J. L. Lenhart, "Investigation of the thermal, mechanical, and fracture properties of alumina-epoxy composites," *Polymer*, vol. 49, no. 4, pp. 999–1014, 2008.

[86] K. Radford, "The mechanical properties of an epoxy resin with a second phase dispersion," *Journal of Materials Science*, vol. 6, no. 10, pp. 1286–1291, 1971.

[87] N. Suprapakorn, S. Dhamrongvaraporn, and H. Ishida, "Effect of CaCO3 on the mechanical and rheological properties of a ring-opening phenolic resin: Polybenzoxazine," *Polymer Composites*, vol. 19, no. 2, pp. 126–132, 1998.

[88] S. H. Lim, K. Y. Zeng, and C. B. He, "Morphology, tensile and fracture characteristics of epoxy-alumina nanocomposites," *Materials Science and Engineering A*, vol. 527, no. 21-22, pp. 5670–5676, 2010.

[89] Y. Nakamura, M. Yamaguchi, M. Okubo, and T. Matsumoto, "Effect of particle size on mechanical properties of epoxy resin filled with angular-shaped silica," *Journal of applied polymer*, vol. 44, no. 1, pp. 151–158, 1992.

[90] R. A. Pearson and A. F. Yee, "Toughening mechanisms in thermoplastic-modified epoxies: 1. Modification using poly(phenylene oxide)," *Polymer*, vol. 34, no. 17, pp. 3658–3670, 1993.

[91] I. Hamerton, *Recent developments in epoxy resins*, 91st ed. Shrewsbury: iSmithers Rapra Publishing, 1996.

[92] F. Mustata and C. N. Cascaval, "Rheological and Thermal Behaviour of an Epoxy Resin Modified With Reactive Diluents," *Journal of Polymer Engineering*, vol. 17, no. 6, pp. 491–506, 1997.

[93] R. M. Wang, S. R. Zheng, and Y. G. Zheng, *Polymer Matrix Composites and Technology*. Oxford: Woodhead Publishing, 2011.

[94] Y. H. Liao, O. Marietta-Tondin, Z. Liang, C. Zhang, and B. Wang, "Investigation of the dispersion process of SWNTs/SC-15 epoxy resin nanocomposites," *Materials Science and Engineering A*, vol. 385, no. 1-2, pp. 175–181, 2004.

[95] M. R. Loos, L. A. F. Coelho, S. H. Pezzin, and S. C. Amico, "The effect of acetone addition on the properties of epoxy," *Polímeros*, vol. 18, no. 1, pp. 76–80, 2008.

[96] S. G. Hong and C. S. Wu, "DSC and FTIR analysis of the curing behaviors of epoxy/DICY/solvent open systems," *Thermochimica Acta*, vol. 316, no. 2, pp. 167–175, 1998.

[97] H. Harani, S. Fellahi, and M. Bakar, "Toughening of epoxy resin using hydroxyl-terminated polyesters," *Journal of Applied Polymer Science*, vol. 71, no. 1, pp. 29–38, 1999.

[98] B. Tang, X. Liu, X. Zhao, and J. Zhang, "Highly efficient in situ toughening of epoxy thermosets with reactive hyperbranched polyurethane," *Journal of Applied Polymer Science*, vol. 131, no. 16, pp. 1–9, 2014.

[99] D. Gui, X. Gao, J. Hao, and J. Liu, "Preparation and Characterization of Liquid Crystalline Polyurethane-Imide Modified Epoxy Resin Composites," *Polymer engineering and science*, vol. 54, no. 7, pp. 1704–1711, 2014.

[100] M. Bakar, R. Duk, M. Przybylek, and M. Kostrzewa, "Mechanical and Thermal Properties of Epoxy Resin Modified with Polyurethane," *Journal of Reinforced Plastics and Composites*, vol. 28, no. 17, pp. 2107–2118, 2009.

[101] J. A. Dougherty and F. J. Vara, "Solvent resistant irradiation curable coatings," United States, pp. 3–7, 1989.

[102] J. P. Pan, G. Y. Shiau, and K. M. Chen, "Novel effect of barbituric acid on glass transition temperature of bismaleimide–epoxy resin systems," *Journal of Applied Polymer Science*, vol. 44, no. 3, pp. 467–476, 1992.

[103] T. Y. Juang, J. K. Liu, C. C. Chang, S. M. Shau, M. H. Tsai, S. A. Dai, W. C. Su, C. H. Lin, and R. J. Jeng, "A reactive modifier that enhances the thermal mechanical properties of epoxy resin through the formation of multiple hydrogen-bonded network," *Journal of Polymer Research*, vol. 18, no. 5, pp. 1169–1176, 2011.

[104] J. Chen, X. Nie, Z. Liu, Z. Mi, and Y. Zhou, "Synthesis and application of polyepoxide cardanol glycidyl ether as biobased polyepoxide reactive diluent for epoxy resin," *ACS Sustainable Chemistry and Engineering*, vol. 3, no. 6, pp. 1164–1171, 2015.

[105] C. Li, M.-H. Liu, Z.-Y. Liu, M.-L. Qing, and G. Wang, "DSC and curing kinetics of epoxy resin using cyclohexanediol diglycidyl ether as active diluents," *Journal of Thermal Analysis and Calorimetry*, vol. 116, no. 1, pp. 411–416, 2014.

[106] L. Nunez-Regueira, M. Villanueva, and I. Fraga-Rivas, "Effect of a reactive diluent on the curing and dynamomechanical properties of an epoxy-diamine system," *Journal of Thermal Analysis and Calorimetry*, vol. 86, no. 2, pp. 463–468, 2006.

[107] S. Montserrat, G. Andreu, P. Cortes, Y. Calventus, P. Colomer, J. M. Hutchinson, and Malek, "Addition of a reactive diluent to a catalyzed epoxy-anhydride system .I. Influence on the cure kinetics," *Journal of Applied Polymer Science*, vol. 61, no. 10, pp. 1663–1674, 1996.

[108] A. F. E. Pineda, F. G. Garcia, A. Z. Simoes, and E. L. da Silva, "Mechanical properties, water absorption and adhesive properties of diepoxy aliphatic diluent-modified DGEBA/Cycloaliphatic amine networks on 316L stainless steel," *International Journal of Adhesion and Adhesives*, vol. 68, pp. 205–211, 2016.

[109] T. Heid, M. Frechette, and E. David, "Enhanced electrical and thermal performances of nanostructured epoxy/POSS composites," *IEEE Transactions on Dielectrics and Electrical Insulation*, vol. 23, no. 3, pp. 1732–1742, 2016.

[110] T. Heid, M. Fréchette, and E. David, "Nanostructured epoxy/POSS composites: enhanced materials for high voltage insulation applications," *IEEE Transactions on Dielectrics and Electrical Insulation*, vol. 22, no. 3, pp. 1594–1604, 2015.

[111] C. Ramírez, M. Rico, A. Torres, L. Barral, J. López, and B. Montero, "Epoxy/-POSS organic–inorganic hybrids: ATR-FTIR and DSC studies," *European Polymer Journal*, vol. 44, no. 10, pp. 3035–3045, 2008.

[112] M. Takala, M. Karttunen, J. Pelto, P. Salovaara, T. Munter, M. Honkanen, T. Auletta, and K. Kannus, "Thermal, Mechanical and Dielectric Properties of Nanostructured Epoxy-polyhedral Oligomeric Silsesquioxane Composites," *IEEE Transactions on Dielectrics and Electrical Insulation*, vol. 15, no. 5, pp. 1224–1235, 2008.

[113] F. N. Alhabill, R. Ayoob, T. Andritsch, and A. S. Vaughan, "Effect of resin/hardener stoichiometry on electrical behavior of epoxy networks," *IEEE Transactions on Dielectrics and Electrical Insulation*, vol. 24, no. 6, pp. 3739–3749, 2017.

[114] V. Nguyen, A. Vaughan, P. Lewin, and A. Krivda, "The effect of resin stoichiometry and nanoparticle addition on epoxy/silica nanodielectrics," *IEEE Transactions on Dielectrics and Electrical Insulation*, vol. 22, no. 2, pp. 895–905, 2015.

[115] Y. Liu, A. S. Vaughan, I. L. Hosier, C. Yeung, and T. Andritsch, "On epoxy network structure and dielectric performance," in *Electrical Insulation and Dielectric Phenomena (CEIDP), IEEE Conference*, 2015, pp. 114–117.

[116] I. Hosier, A. Vaughan, and S. Swingler, "Structure–property relationships in polyethylene blends: the effect of morphology on electrical breakdown strength," *Journal of Materials Science*, vol. 32, no. 17, pp. 4523–4531, 1997.

[117] S. Dodd, J. Champion, Y. Zhao, A. Vaughan, S. Sutton, and S. Swingler, "Influence of morphology on electrical treeing in polyethylene blends," *IEE Proceedings-Science, Measurement and Technology*, vol. 150, no. 2, pp. 58–64, 2003.

[118] L. Martinotto, F. Peruzzotti, and M. Del Brenna, "Cable, in particular for transport or distribution of electrical energy and insulating composition," *U.S. Patent No. 6,696,154*, 2004.

[119] A. C. Ashcraft, R. M. Eichhorn, and R. G. Shaw, "Laboratory studies of treeing in solid dielectrics and voltage stabilization of polyethylene," *EEE Intern Sympos Electr Insul*, vol. 213–218, no. 6, 1976.

[120] M. Jarvid, "Voltage stabilizers: From design to synthesis, processing and electrical characterization," Thesis, Chalmers University of Technology, Department of Chemical and Biological Engineering, 2014.

[121] M. Takahashi, A. Ito, Y. Igarashi, S. Kawada, J. Ogura, and R. Ito, "Dielectric polyolefin compositions," *United States patent No. 3,933,772*, Jan 1976.

[122] V. Englund, R. Huuva, S. Gubanski, and T. Hjertberg, "Synthesis and efficiency of voltage stabilizers for xlpe cable insulation," *IEEE Transactions on Dielectrics and Electrical Insulation*, vol. 16, no. 5, pp. 1455–1461, 2009.

[123] V. Englund, R. Huuva, S. M. Gubanski, and T. Hjertberg, "High efficiency voltage stabilizers for XLPE cable insulation," *Polymer Degradation and Stability*, vol. 94, no. 5, pp. 823–833, 2009.

[124] M. Jarvid, A. Johansson, J. M. Bjuggren, H. Wutzel, V. Englund, S. Gubanski, C. Muller, and M. R. Andersson, "Tailored side-chain architecture of benzil voltage stabilizers for enhanced dielectric strength of cross-linked polyethylene," *Journal of Polymer Science, Part B: Polymer Physics*, vol. 52, no. 16, pp. 1047–1054, 2014.

[125] M. Jarvid, A. Johansson, V. Englund, A. Lundin, S. Gubanski, C. Müller, and M. R. Andersson, "High electron affinity: a guiding criterion for voltage stabilizer design," *J. Mater. Chem. A*, vol. 3, no. 14, pp. 7273–7286, 2015.

[126] I. A. Saeedi, A. S. Vaughan, T. Andritsch, and S. Virtanen, "The effect of curing conditions on the electrical properties of an epoxy resin," in *Electrical Insulation and Dielectric Phenomena (CEIDP)*, 2016, pp. 461–464.

[127] B. H. Stuart, *Infrared Spectroscopy: Fundamentals and Applications*. John Wiley & Sons, 2004.

[128] J. Workman Jr and A. Springsteen, *Applied spectroscopy: a compact reference for practitioners*. Academic Press, 1998.

[129] R. Böhmer, G. Diezemann, F. Kremer, and A. Schönhals, *Broadband Dielectric Spectroscopy*. Springer-Verlag Berlin Heidelberg GmbH, 2001.

[130] J. D. Menczel and R. B. Prime, Eds., *Thermal Analysis of Polymers: Fundamentals and Applications*. New Jersey: John Wiley & Sons, 2009.

[131] M. Reading, "An investigation into the structure and properties of polyethylene oxide nanocomposites," Ph.D. dissertation, University of Southampton, 2010.

[132] O. Vryonis, S. Virtanen, T. Andritsch, A. Vaughan, and P. Lewin, "Understanding the cross-linking reactions in highly oxidized graphene/epoxy nanocomposite systems," *Journal of Materials Science*, pp. 1–17, 2018.

[133] J. C. Fothergill, "Estimating the cumulative probability of failure data points to be plotted on Weibull and other probability paper,"," *IEEE Transactions on Electrical Insulation*, vol. 25, no. June, pp. 489–492, 1990.

[134] W. Weibull *et al.*, "A statistical distribution function of wide applicability," *Journal of applied mechanics*, vol. 18, no. 3, pp. 293–297, 1951.

[135] D. L. Pavia, G. M. Lampman, G. S. Kriz, and J. A. Vyvyan, *Introduction to spectroscopy*. Cengage Learning, 2008.

[136] J. B. Lambert, H. F. Shurvell, D. A. Lightner, and R. G. Cooks, *Organic Structural Spectroscopy*. New Jersey: Prentice Hall, 1998.

[137] L. J. Bellamy, *The Infra-red Spectra of Complex Molecules*. London, Uk: Springer, 1975.

[138] C. Zhang, F. Babonneau, C. Bonhomme, R. M. Laine, C. L. Soles, H. A. Hristov, and A. F. Yee, "Highly porous polyhedral silsesquioxane polymers. synthesis and characterization," *Journal of the American Chemical Society*, vol. 120, no. 33, pp. 8380–8391, 1998.

[139] K. Nakanishi *et al.*, *Infrared absorption spectroscopy, practical*. Emerson-Adams Press, 1962.

[140] Y. Ma and L. He, "Poss-pendanted in epoxy chain inorganic-organic hybrid for highly thermo-mechanical, permeable and hydrothermal-resistant coatings," *Materials Chemistry and Physics*, vol. 201, pp. 120–129, 2017.

[141] C.-M. Leu, Y.-T. Chang, and K.-H. Wei, "Synthesis and dielectric properties of polyimide-tethered polyhedral oligomeric silsesquioxane (poss) nanocomposites via poss-diamine," *Macromolecules*, vol. 36, no. 24, pp. 9122–9127, 2003.

[142] P. Pasbakhsh, H. Ismail, M. A. Fauzi, and A. A. Bakar, "Epdm/modified halloysite nanocomposites," *Applied Clay Science*, vol. 48, no. 3, pp. 405–413, 2010.

[143] H. Liu, W. Zhang, and S. Zheng, "Montmorillonite intercalated by ammonium of octaaminopropyl polyhedral oligomeric silsesquioxane and its nanocomposites with epoxy resin," *Polymer*, vol. 46, no. 1, pp. 157–165, 2005.

[144] J. Mijović and S. Andjelić, "Monitoring of reactive processing by remote mid infrared spectroscopy," *Polymer*, vol. 37, no. 8, pp. 1295–1303, 1996.

[145] M. G. González, J. C. Cabanelas, and J. Baselga, "Applications of ftir on epoxy resins-identification, monitoring the curing process, phase separation and water uptake," *Infrared Spectroscopy-Materials Science, Engineering and Technology*, vol. 2, no. 261–284, 2012.

[146] D. S. Achilias, M. M. Karabela, E. A. Varkopoulou, and I. D. Sideridou, "Cure kinetics study of two epoxy systems with fourier tranform infrared spectroscopy (ftir) and differential scanning calorimetry (dsc)," *Journal of Macromolecular Science, Part A*, vol. 49, no. 8, pp. 630–638, 2012.

[147] J. Mijovic and S. Andjelic, "A study of reaction kinetics by near-infrared spectroscopy. 1. comprehensive analysis of a model epoxy/amine system," *Macromolecules*, vol. 28, no. 8, pp. 2787–2796, 1995.

[148] J. Mijović, S. Andjelić, and J. M. Kenny, "In situ real-time monitoring of epoxy/amine kinetics by remote near infrared spectroscopy," *Polymers for Advanced Technologies*, vol. 7, no. 1, pp. 1–16, 1996.

[149] J. D. Menczel and R. B. Prime, *Thermal analysis of polymers: fundamentals and applications*. USA: John Wiley & Sons, 2014.

[150] P. Pissis and D. Fragiadakis, "Dielectric studies of segmental dynamics in epoxy nanocomposites." *Journal of Macromolecular Science Part B: Physics*, pp. 119–136, 2007.

[151] N. Hao, M. Böhning, H. Goering, and A. Schönhals, "Nanocomposites of polyhedral oligomeric phenethylsilsesquioxanes and poly (bisphenol a carbonate) as investigated by dielectric spectroscopy," *Macromolecules*, vol. 40, no. 8, pp. 2955–2964, 2007.

[152] K. N. Raftopoulos and K. Pielichowski, "Segmental dynamics in hybrid polymer/-poss nanomaterials," *Progress in Polymer Science*, vol. 52, pp. 136–187, 2016.

[153] X. Huang, Y. Li, F. Liu, P. Jiang, T. Iizuka, K. Tatsumi, and T. Tanaka, "Electrical properties of epoxy/poss composites with homogeneous nanostructure," *IEEE Transactions on Dielectrics and Electrical Insulation*, vol. 21, no. 4, pp. 1516–1528, 2014.

[154] A. Lee and J. D. Lichtenhan, "Viscoelastic responses of polyhedral oligosilsesquioxane reinforced epoxy systems," *Macromolecules*, vol. 31, no. 15, pp. 4970–4974, 1998.

[155] N. Florea, A. Lungu, P. Badica, L. Craciun, M. Enculescu, D. Ghita, C. Ionescu, R. Zgirian, and H. Iovu, "Novel nanocomposites based on epoxy resin/epoxy-functionalized polydimethylsiloxane reinforced with poss," *Composites Part B: Engineering*, vol. 75, pp. 226–234, 2015.

[156] I. Bacosca, E. Hamciuc, M. Bruma, and I. A. Ronova, "Study of aromatic polyimides containing cyano groups," *High Performance Polymers*, vol. 22, no. 6, pp. 703–714, 2010.

[157] E. Donth, "The size of cooperatively rearranging regions at the glass transition," *Journal of Non-Crystalline Solids*, vol. 53, no. 3, pp. 325–330, 1982.

[158] J. Horwath, D. Schweickart, G. Garcia, D. Klosterman, M. Galaska, A. Schrand, and L. Walko, "improved electrical properties of epoxy resin with nanometer-sized intorganic fillers," in *Power Modulator Symposium, 2006.Conference Record of the 2006 Twenty-Seventh International. IEEE*, 2006.

[159] M. K. Hassan, S. J. Tucker, A. Abukmail, J. S. Wiggins, and K. A. Mauritz, "Polymer chain dynamics in epoxy based composites as investigated by broadband dielectric spectroscopy," *Arabian Journal of Chemistry*, vol. 9, no. 2, pp. 305–315, 2016.

[160] W. Jilani, N. Mzabi, N. Fourati, C. Zerrouki, O. Gallot-Lavallée, R. Zerrouki, and H. Guermazi, "A comparative study of structural and dielectric properties of diglycidyl ether of bisphenol a (dgeba) cured with aromatic or aliphatic hardeners," *Journal of Materials Science*, vol. 51, no. 17, pp. 7874–7886, 2016.

[161] G. Mikolajczak, J. Cavaille, and G. Johari, "Dynamic mechanical behaviour and its dependence on preparation method of structural epoxide resin," *Polymer*, vol. 28, no. 12, pp. 2023–2031, 1987.

[162] I. A. Saeedi, T. Andritsch, and A. S. Vaughan, "On the dielectric behavior of amine and anhydride cured epoxy resins modified using multi-terminal epoxy functional network modifier," *Polymers*, vol. 11, no. 8, p. 1271, 2019.

[163] A. K. Sharma, R. Sloan, R. Ramakrishnan, S. I. Nazarenko, and J. S. Wiggins, "Structure-property relationships in epoxy hybrid networks based on high mass fraction pendant poss incorporated at molecular level," *Polymer*, vol. 139, pp. 201–212, 2018.

[164] G. Nikolic, S. Zlatkovic, M. Cakic, S. Cakic, C. Lacnjevac, and Z. Rajic, "Fast fourier transform IR characterization of epoxy GY systems crosslinked with aliphatic and cycloaliphatic EH polyamine adducts," *Sensors*, vol. 10, no. 1, pp. 684–696, 2010.

[165] H. Alamri and I. M. Low, "Effect of water absorption on the mechanical properties of n-SiC filled recycled cellulose fibre reinforced epoxy eco-nanocomposites," *Polymer Testing*, vol. 31, no. 6, pp. 810–818, 2012.

[166] P. Pasbakhsh, H. Ismail, M. N. A. Fauzi, and A. A. Bakar, "EPDM/modified halloysite nanocomposites," *Applied Clay Science*, vol. 48, no. 3, pp. 405–413, 2010.

[167] J. B. Lambert, H. Shurvell, L. Verbit, R. Cooks, and G. Stout, *Organic structural analysis*. New York: Macmillan Publishing Co., 1976.

[168] C. A. Daniels, *Polymers: Structure and Properties*, 1st ed. CRC Press, 1989.

[169] T. Takahama and P. Geil, "The β relaxation behavior of bisphenol-type resins," *Journal of Polymer Science: Polymer Physics Edition*, vol. 20, no. 11, pp. 1979–1986, 1982.

[170] J. K. Nelson, *Dielectric polymer nanocomposites*. New York, USA: Springer, 2010.

[171] E. Riande and R. Diaz-Calleja, *Electrical Properties of Polymers*. U.S.A.: CRC Press, 2004.

[172] R. Casalini, D. Fioretto, A. Livi, M. Lucchesi, and P. A. Rolla, "Influence of the glass transition on the secondary relaxation of an epoxy resin," *PHYSICAL REVIEW B*, vol. 56, no. 6, pp. 3016–3021, 1997.

[173] F. Tian and Y. Ohki, "Charge transport and electrode polarization in epoxy resin at high temperatures," *Journal of Physics D: Applied Physics*, vol. 47, no. 4, p. 045311, 2013.

[174] Y. Wang, K. Wu, D. Cubero, and N. Quirke, "Molecular modeling and electron transport in polyethylene," *IEEE Transactions on Dielectrics and Electrical Insulation*, vol. 21, no. 4, pp. 1726 – 1734, 2014.

[175] Y. Wang, D. MacKernan, D. Cubero, D. F. Coker, and N. Quirke, "Single electron states in polyethylene," *Journal of Chemical Physics*, vol. 140, no. 15, p. 154902, 2014.

[176] L. Xie, K.-Y. Chan, and N. Quirke, "Poly (ethylene glycol)(peg) in a polyethylene (pe) framework: A simple model for simulation studies of a soluble polymer in an open framework," *Langmuir*, vol. 33, no. 42, pp. 11 746–11 753, 2017.

[177] G. H. Hunt, "Voltage stabilized polyolefin dielectric compositions using liquid-aromatic compounds and voltage stabilizing additives," *U.S. Patent No. 3,542,684*, 1970.

[178] P. G. Babayevsky and J. Gillham, "Epoxy thermosetting systems: dynamic mechanical analysis of the reactions of aromatic diamines with the diglycidyl ether of bisphenol a," *Journal of Applied Polymer Science*, vol. 17, no. 7, pp. 2067–2088, 1973.

[179] M. Meunier and N. Quirke, "Molecular modeling of electron trapping in polymer insulators," *Journal of Chemical Physics*, vol. 113, no. 1, pp. 369–376, 2000.

[180] D. Cubero and N. Quirke, "Computer simulations of localized small polarons in amorphous polyethylene," *Journal of chemical physics*, vol. 120, no. 16, pp. 7772–7778, 2004.

[181] M. Meunier and N. Quirke, "Molecular modeling of electron traps in polymer insulators: Chemical defects and impurities," *The Journal of Chemical Physics*, vol. 115, no. 6, pp. 2876–2881, 2001.

[182] S.-G. Hong and C.-S. Wu, "Dsc and ftir analysis of the curing behaviors of epoxy/dicy/solvent open systems," *Thermochimica Acta*, vol. 316, no. 2, pp. 167–175, 1998.

[183] G. Rajagopalan, K. Immordino, J. Gillespie Jr, and S. McKnight, "Diffusion and reaction of epoxy and amine in polysulfone studied using fourier transform infrared spectroscopy: experimental results," *Polymer*, vol. 41, no. 7, pp. 2591–2602, 2000.

[184] M. Finzel, "Bulk-phase kinetics and physical properties of epoxy/amine systems," *Michigan State University. Department of Chemical Engineering*, 1991.

[185] D. Foix, Y. Yu, A. Serra, X. Ramis, and J. M. Salla, "Study on the chemical modification of epoxy/anhydride thermosets using a hydroxyl terminated hyperbranched polymer," *European Polymer Journal*, vol. 45, no. 5, pp. 1454–1466, 2009.

[186] M. Flores, X. Fernández-Francos, X. Ramis, and A. Serra, "Novel epoxy-anhydride thermosets modified with a hyperbranched polyester as toughness enhancer. i. kinetics study," *Thermochimica acta*, vol. 544, pp. 17–26, 2012.

[187] O. Vryonis, S. Virtanen, T. Andritsch, A. Vaughan, and P. Lewin, "Understanding the cross-linking reactions in highly oxidized graphene/epoxy nanocomposite systems," *Journal of Materials Science*, vol. 54, no. 4, pp. 3035–3051, 2019.

[188] B. Romão, M. F. Diniz, M. F. Azevedo, V. L. Lourenço, L. C. Pardini, R. C. Dutra, and F. Burel, "Characterization of the curing agents used in epoxy resins with tg/ft-ir technique," *Polímeros*, vol. 16, no. 2, pp. 94–98, 2006.

[189] V. Ollier-Dureault and B. Gosse, "Photooxidation of anhydride-cured epoxies: Ftir study of the modifications of the chemical structure," *Journal of applied polymer science*, vol. 70, no. 6, pp. 1221–1237, 1998.

[190] D. Lin-Vien, N. B. Colthup, W. G. Fateley, and J. G. Grasselli, *The handbook of infrared and Raman characteristic frequencies of organic molecules*. Elsevier, 1991.

[191] S.-Y. Lin, W.-T. Cheng, Y.-S. Wei, and H.-L. Lin, "Dsc-ftir microspectroscopy used to investigate the heat-induced intramolecular cyclic anhydride formation between eudragit e and pva copolymer," *Polymer journal*, vol. 43, no. 6, p. 577, 2011.

[192] F. N. Alhabill, R. Ayoob, T. Andritsch, and A. S. Vaughan, "Influence of filler/matrix interactions on resin/hardener stoichiometry, molecular dynamics, and particle dispersion of silicon nitride/epoxy nanocomposites," *Journal of materials science*, vol. 53, no. 6, pp. 4144–4158, 2018.

[193] R. J. Morgan, F.-M. Kong, and C. M. Walkup, "Structure-property relations of polyethertriamine-cured bisphenol-a-diglycidyl ether epoxies," *Polymer*, vol. 25, no. 3, pp. 375–386, 1984.

[194] M. Ochi, M. Okazaki, and M. Shimbo, "Mechanical relaxation mechanism of epoxide resins cured with aliphatic diamines," *Journal of polymer science: polymer physics edition*, vol. 20, no. 4, pp. 689–699, 1982.

[195] M. Ochi, H. Iesako, and M. Shimbo, "Relaxation mechanism of epoxide resin cured with acid anhydrides. iii. effect of alkyl side chains on mechanical and dielectric β relaxations," *Journal of Polymer Science Part B: Polymer Physics*, vol. 24, no. 6, pp. 1271–1282, 1986.

[196] E. Cuddihy and J. Moacanin, "Dynamic mechanical properties of epoxies' beta-transition mechanism," *Journal of Polymer Science Part A-2: Polymer Physics*, 1970.

[197] M. K. Hassan, S. J. Tucker, A. Abukmail, J. S. Wiggins, and K. A. Mauritz, "Polymer chain dynamics in epoxy based composites as investigated by broadband dielectric spectroscopy," *Arabian Journal of Chemistry*, vol. 9, no. 2, pp. 305–315, 2016.

[198] M. Shimbo, M. Ochi, and H. Iesako, "Mechanical relaxation mechanism of epoxide resins cured with acid anhydrides," *Journal of Polymer Science Part B: Polymer Physics*, vol. 22, no. 8, pp. 1461–147, 1984.

[199] H. Van Hoorn, "A dynamic mechanical study of the effect of chemical variations on the internal mobility of linear epoxy resins (polyhydroxyethers)," *Journal of Applied Polymer Science*, vol. 12, no. 4, pp. 871–888, 1968.

[200] F. Dammont and T. Kwei, "Dynamic mechanical properties of aromatic, aliphatic, and partially fluorinated epoxy resins," *Journal of Polymer Science Part A-2: Polymer Physics*, vol. 5, no. 4, pp. 761–769, 1967.

[201] M. Ochi, H. Iesako, S. Nakajima, and M. Shimbo, "Mechanical relaxation mechanism of epoxide resins cured with acid anhydrides. ii. effect of the chemical structure of the anhydrides on the β relaxation mechanism," *Journal of Polymer Science Part B: Polymer Physics*, vol. 24, no. 2, pp. 251–261, 1986.

[202] M. B. Mangion and G. Johari, "Relaxations in thermosets. 7. dielectric effects during the curing and postcuring of an epoxide by mixed amines," *Macromolecules*, vol. 23, no. 15, pp. 3687–3695, 1990.

[203] V. Varshney, S. S. Patnaik, A. K. Roy, and B. L. Farmer, "A molecular dynamics study of epoxy-based networks: cross-linking procedure and prediction of molecular and material properties," *Macromolecules*, vol. 41, no. 18, pp. 6837–6842, 2008.

[204] H. B. Fan and M. M. Yuen, "Material properties of the cross-linked epoxy resin compound predicted by molecular dynamics simulation," *Polymer*, vol. 48, no. 7, pp. 2174–2178, 2007.

[205] C. Wu and W. Xu, "Atomistic molecular modelling of crosslinked epoxy resin," *Polymer*, vol. 47, no. 16, pp. 6004–6009, 2006.

[206] S. Yang and J. Qu, "Computing thermomechanical properties of crosslinked epoxy by molecular dynamic simulations," *Polymer*, vol. 53, no. 21, pp. 4806–4817, 2012.

[207] E.-A. McGonigle, J. H. Daly, S. D. Jenkins, J. J. Liggat, and R. A. Pethrick, "Influence of physical aging on the molecular motion and structural relaxation in poly (ethylene terephthalate) and related polyesters," *Macromolecules*, vol. 33, no. 2, pp. 480–489, 2000.

[208] S. Verot, P. Battesti, and G. Perrier, "Semi-empirical calculations and dielectric spectrometry of molecular units in peek," *Polymer*, vol. 40, no. 10, pp. 2605–2617, 1999.

[209] A. Leonardi, E. Dantras, J. Dandurand, and C. Lacabanne, "Dielectric relaxations in peek by combined dynamic dielectric spectroscopy and thermally stimulated current," *Journal of thermal analysis and calorimetry*, vol. 111, no. 1, pp. 807–814, 2013.

[210] J. Rault, "Origin of the vogel–fulcher–tammann law in glass-forming materials: the α–β bifurcation," *Journal of Non-Crystalline Solids*, vol. 271, no. 3, pp. 177–217, 2000.

[211] D. Cubero, N. Quirke, and D. F. Coker, "Electronic transport in disordered n-alkanes: From fluid methane to amorphous polyethylene," *The Journal of chemical physics*, vol. 119, no. 5, pp. 2669–2679, 2003.

[212] A. M. P. Schwartz and W. James, *Surface active agents.* New York: Interscience Publishers, Inc.; New York, 1949.

[213] I. A. H. Saeedi, A. S. Vaughan, and T. Andritsch, "Functional design of epoxy-based networks: tailoring advanced dielectrics for next-generation energy systems," *Journal of Physics D: Applied Physics*, 2019.

[214] A. Thielen, J. Niezette, G. Feyder, and J. Vanderschueren, "Characterization of polyester films used in capacitors. i. transient and steady-state conductivity," *Journal of applied physics*, vol. 76, no. 8, pp. 4689–4695, 1994.

[215] C. Guillermin, P. Rain, and S. W. Rowe, "Transient and steady-state currents in epoxy resin," *Journal of Physics D: Applied Physics*, vol. 39, no. 3, p. 515, 2006.

[216] B. Hamon, "An approximate method for deducing dielectric loss factor from direct-current measurements," *Proceedings of the IEE-Part IV: Institution Monographs*, vol. 99, no. 3, pp. 151–155, 1952.

[217] X. Liang and Y. Gao, "Application of the dissado-hill model in the analysis of dielectric response," in *Proceedings of the CSEE*, vol. 36, 2016, pp. 6002–6011.

[218] G. Niklasson, "Fractal aspects of the dielectric response of charge carriers in disordered materials," *Journal of applied physics*, vol. 62, no. 7, pp. R1–R14, 1987.

[219] S. Dodd, N. Chalashkanov, L. Dissado, and J. Fothergill, "Influence of absorbed moisture on the dielectric properties of epoxy resins," in *2010 Annual Report Conference on Electrical Insulation and Dielectic Phenomena.* IEEE, 2010, pp. 1–4.

[220] J. Medina, R. Prosmiti, and J. Alemán, "The role of the havriliak-negami relaxation in the description of local structure of kohlrausch's function in the frequency domain. part i," *arXiv preprint arXiv:1509.07893*, 2015.

[221] M. Ochi, S. Zhu, and M. Shimbo, "Mechanical relaxation properties of spiro-type epoxide resins cured with acid anhydrides," *Polymer*, vol. 27, no. 10, pp. 1569–1573, 1986.

[222] C. Zhang and G. C. Stevens, "The dielectric response of polar and non-polar nanodielectrics," *IEEE Transactions on Dielectrics and Electrical Insulation*, vol. 15, no. 2, pp. 606–617, 2008.

[223] H. Zhao and R. K. Li, "Effect of water absorption on the mechanical and dielectric properties of nano-alumina filled epoxy nanocomposites," *Composites Part A: Applied Science and Manufacturing*, vol. 39, no. 4, pp. 602–611, 2008.

[224] C. May, *Epoxy resins: chemistry and technology.* Routledge, 2018.

[225] P. Moy and F. Karasz, "Epoxy-water interactions," *Polymer Engineering & Science*, vol. 20, no. 4, pp. 315–319, 1980.

[226] G. Pogany, "Gamma relaxation in epoxy resins and related polymers," *Polymer*, vol. 11, no. 2, pp. 66–78, 1970.

[227] M. S. McMaster, T. E. Yilmaz, A. Patel, A. Maiorana, I. Manas-Zloczower, R. Gross, and K. D. Singer, "Dielectric properties of bio-based diphenolate ester epoxies," *ACS applied materials & interfaces*, vol. 10, no. 16, pp. 13 924–13 930, 2018.

[228] A. Pinkus and E. Y. Lin, "Electric dipole moment studies of carboxylic ester conformations: alkyl acetates, benzoates, 2, 4, 6-trimethyl-benzoates and 2, 3, 5, 6-tetramethylbenzoates," *Journal of Molecular Structure*, vol. 24, no. 1, pp. 9–26, 1975.

[229] J. Boček, L. Matějka, V. Mentlík, P. Trnka, and M. Šlouf, "Electrical and thermo-mechanical properties of epoxy-poss nanocomposites," *European Polymer Journal*, vol. 47, no. 5, pp. 861–872, 2011.

[230] D. S. Kumar, M. J. Shukla, K. K. Mahato, D. K. Rathore, R. K. Prusty, and B. C. Ray, "Effect of post-curing on thermal and mechanical behavior of GFRP composites," *IOP Conference Series: Materials Science and Engineering*, vol. 75, no. 1, 2015.

[231] T. Cameron, L. Y. Alexander, and F. John, Eds., *Springer Handbook of Experimental Fluid Mechanics, Volume 1.* Berlin: Springer, 2007.

[232] C. Yeung, "Spectroscopic Analysis of Nanodielectric Interfaces," PhD diss, Doctoral dissertation, University of Southampton, 2013.

[233] M. M. Coleman, P. C. Painter, and J. F. Graf, *Specific interaction and the miscibility of polymer blends.* Pennsylvania: CRC Press, 1995.

[234] S. Havriliak and S. Negami, "A complex plane representation of dielectric and mechanical relaxation processes in some polymers," *Polymer*, vol. 8, pp. 161–210, 1967.